Silylene: Application as an Alluring Ligand in Transition Metals and Catalysis

A thesis submitted in partial fulfillment of the requirements for the degree

of

Doctor of Philosophy

By

Nasrina Parvin

ID: 20153368

IISER PUNE

Indian Institute of Science Education and Research, Pune

2020

Dedicated to...

My Family

Indian Institute of Science Education and Research (IISER), Pune

Certificate

It is hereby certified that the work described in this thesis entitled *"Silylene: Application as an Alluring Ligand in Transition Metals and Catalysis"* submitted by **Ms. Nasrina Parvin** was carried out by the candidate, under my supervision. The work presented here or any part of it has not been included in any other thesis submitted previously for the award of any degree or diploma from any other university or institution.

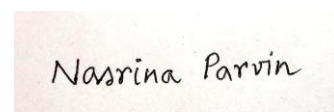Date: 13.10.2020

Dr. Shabana Khan

Research Supervisor

Email: shabana@iiserpune.ac.in

Contact No.: +91 (20) 2590-8137

Declaration

I declare that this written submission represents my ideas in my own words and wherever other's ideas have been included; I have adequately cited and referenced the original sources. I also declare that I have adhered to all principles of academic honesty and integrity and have not misrepresented or fabricated or falsified any idea/data/fact/source in my submission. I understand that violation of the above will cause for disciplinary action by the Institute and can also evoke penal action from the sources which have thus not been properly cited or from whom proper permission has not been taken when needed.

Date: 13.10.2020

Nasrina Parvin

ID: 20153368

Acknowledgment

First and foremost, I would like to thank the supreme power Almighty God for guiding me to work on the right path of life.

I would like to express my deepest and sincere gratitude to my research supervisor Prof. Dr. Shabana Khan for being warmly welcomed to her working group and for the trust she has placed on me. She is the person of ethics, compassion, forgiveness, and motivation. I would also like to thank for her continuous encouragement, numerous suggestions, productive and pleasant discussions at the regular meeting throughout my PhD tenure. Her immense knowledge, enthusiasm, and inspiring guidance energized me every time, promoted my research and helped me to find out a way to solve any difficulties. I always feel fortunate to have her as my PhD mentor.

I feel honoured to be a part of Indian Institute of Science Education and Research (IISER), Pune. I would like to thank each and every one related to IISER Pune to build such a wonderful institute with world-class research facilities. Thanks to the former director Prof. K. N. Ganesh for establishing such as excellent institute with outstanding research facilities, funding, and an excellent interdisciplinary research atmosphere. I would also like to acknowledge the present director Prof. Jayant B. Udgaonkar for continuing the same.

I am grateful to my Research Advisory committee (RAC) members Dr Sujit K. Ghosh (IISER Pune) and Dr. Samir H. Chikkali (National Chemical Laboratory Pune) for their indispensable views and thoughtful suggestions during the annual meetings. I would like to convey my gratitude to my collaborators Dr. Parameswaran Pattiyil (National Institute of Technology, Calicut), Prof. Santiago Alvarez (Universitat de Barcelona, Spain) and Prof. Swapan K. Pati (Jawaharlal Nehru Centre for Advanced Scientific Research, Bangalore) for carrying out the theoretical calculations and precious suggestions to understand the deep insight of the research results obtained of this thesis. I am grateful to Prof. Srinivas Hotha (IISER Pune) and his co-workers Bijoyananda Mishra and Mahesh Neralkar for their collaboration and contribution regarding the glycosidation reactions. I would like to give special thanks to Dr. Sakya S. Sen (National Chemical Laboratory Pune) for his insightful suggestions with positive feedback during various stages of my Ph.D.

I am thankful to Prof. Dr. Evamarie Hey-Hawkins for giving me the opportunity to work in her laboratory in Leipzig University.

Rome, Italy. Along with this, MTIC-2017 and IFC-2018 conference organizer have provided me the opportunity to present my work in the oral and poster form. I am thankful to Erasmus Exchange programme for giving me the opportunity to work in Universität Leipzig for a short period of time.

Moreover, I would like to thank American Chemical Society (ACS), Royal Sciety of Chemistry (RSC), John Wiley & Sons for publishing research articles during the course of my research.

Thank you all for your help and support and would like to say…It was indeed a great and wonderful journey…

Contents

Synopsis

The thesis entitled *"Silylene: Application as an Alluring Ligand in Transition Metals and Catalysis"* is primarily focused upon comprehensive experimental investigations of silylene stabilized transition metal complexes mainly with coinage metals in a way to gain better insights into the structure and bonding property. In fact, such systems are aimed at the development in homogeneous catalysis reactions by introducing silylene as ligands which are still underdeveloped. To sum up, we seek to flourish novel silylene-based transition metal mediated catalysis with high catalytic efficiency in various organic transformation reactions.

"Chemistry without catalysis, would be a sword without a handle, a light without brilliance, a bell without sound."

Alwin Mittasch (1869-1953), co-inventor of the Haber-Bosch process

Suitable, highly effective catalysts are required everywhere in laboratory experiments to industrially relevant chemical processes. In contrast to superior heterogeneous catalysis, homogenously catalyzed processes are gradually blooming due to the mild reaction conditions and higher chemo- and stereo-selectivity. Chemical refinement of the ligands to foster efficient catalysts is the fundamental interest in metal-mediated catalytic reactions. During my entire Ph.D tenure, a considerable effort has been put upon the design, synthesis, and experimental investigation of unstable Si=E (E= O, S, and Se) complexes through Lewis acid-base adduct formation and a number of Si(II)-transition metal complexes with the diverse catalytic applications. In the quest of navigating such chemical functionalities and their crucial influence on the structural property, extensively recorded experimental findings have been methodically analysed herein and correlating them with theoretical insights.

Chapter 1: Introduction

"We have considered all the known types of organic derivatives of silicon and we see how few are their number in comparison with the purely organic compounds. Since the few which are known are very limited in their reactions, the prospect of any immediate and important advance in this section of chemistry does not seem very hopeful."

Organosilicon pioneer Frederic S. Kipping, 1934, Bakerian Lecture Royal Society.

However, recent advanced studies on silicon chemistry changed this perspective with an impressive transition from initially unrecognized to easily accessible organosilicon compounds with enormous applications in basic science to an industrial level. Benefitted with most stable +IV oxidation state, silicon is also an emerging member in the field of low-valent main group chemistry, regardless of its transient stability and high synthetic difficulties. One such class of low valent silicon compounds are divalent Si(II) species i.e. silylenes possessing a lone pair of electrons and a vacant p-orbital and can be accessible by proper thermodynamic and kinetic stabilization. From the last three decades, the burgeoning of silylene chemistry has been achieved by isolating plenty of fascinating structures with potential application as ligands for small molecule activation, and metal-mediated catalysis reactions. Based on the relevance of this milestone to this thesis, we are mainly focusing on four-membered donor stabilized silylenes as ligands in transition-metal mediated homogeneous catalytic transformations such as C-C bond formation, C-X bond formation, and reduction reactions of olefins and ketones.

Chapter 2: Synthesis of Si(II)=E (E= O, S, Se) complexes and their Lewis acid−base adducts.

2A. Unique Approach to Cu(I) Silylene-Chalcogenone complexes

Until three decades ago, it was assumed that the heavier double-bonded compounds between silicon and chalcogens (Si=S/Se/Te) are elusive species due to their higher reactivity and relatively poor pπ-pπ overlap between silicon and chalcogens atoms. These Si-chalcogenones can further be used as ligands in transition metal chemistry. However, unlike aldehyde and ketones, Si=E (E = S, Se, Te) bonded compounds were not explored for such complexation with transition metals. In this chapter, I will discuss systematically the synthesis and characterization of Si chalcogenones (Si=S and Si=Se) and their transition-metal-based Lewis acid−base adducts of composition Si=E→LA (E = S, Se) where electron-deficient CuX (X = Cl, Br) were used as Lewis acid (LA). In addition, we also prepared thione and their corresponding Lewis acid−base adducts from sterically hindered carbene to compare them with their silicon analogs. Further, we obtained Si=E →LA adducts from the reaction of dimeric silylene copper complexes with chalcogens;

however, this route does not work for the carbene copper complex. The dichotomy was rationalized by theoretical calculations, which reveal that carbene-S→CuBr formation is 51.6 kcal/mol more endergonic than silylene-S→CuBr formation. According to DFT calculation, the Si→CuBr (WBI=0.68) bond is much weaker compared to Si=S (WBI=1.55) bond that renders the thermodynamic driving force for the aforementioned process.
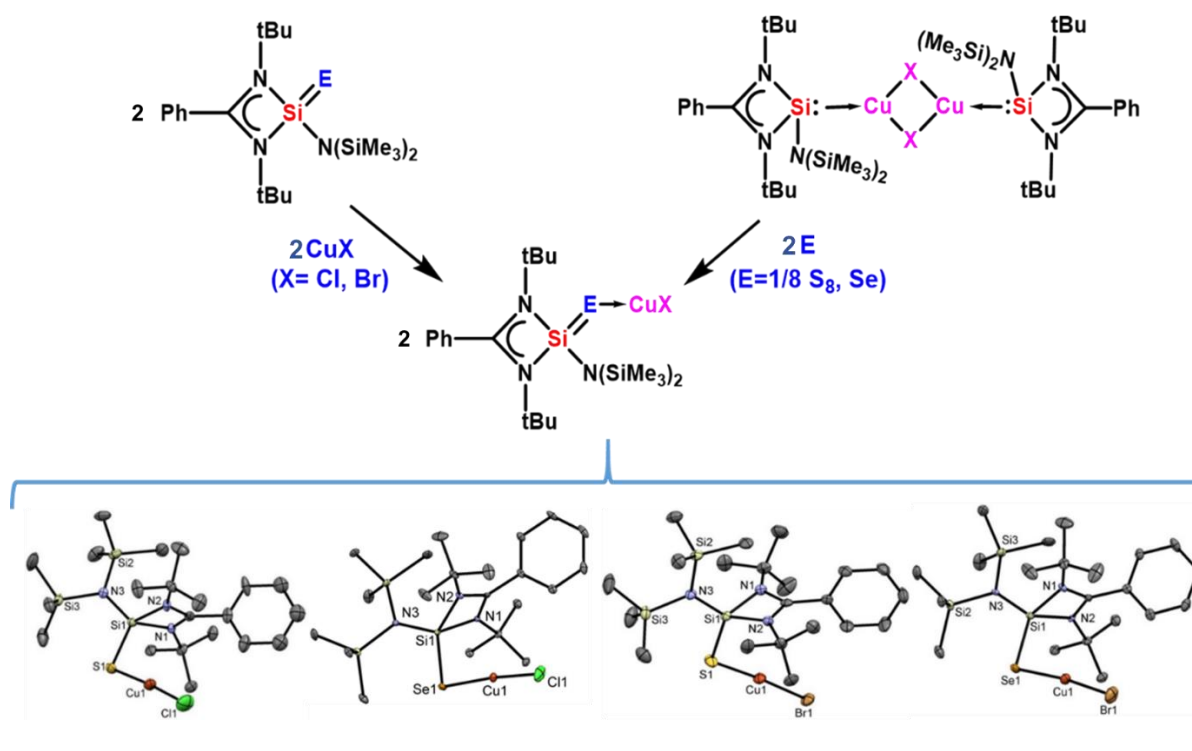
2B. Convenient access to compounds with silicon/germanium-oxygen double bond

The silicon analogue of ketone (Si=O), a transient species, since the days of organosilicon pioneer Frederic S. Kipping, has mesmerized silicon chemists. Isolation and stabilization of E=O (E= Si, Ge, Sn, Pb) species are very difficult due to their oligomeric or polymeric nature and the reason can be attributed to the strong polarization of $Si^{\delta+}-O^{\delta-}$ bond as well as unfavourable $p_\pi(E)$ and $p_\pi(O)$ orbitals overlapping. Recently, considering the donor-acceptor concept, scientists are able to stabilize Si/Ge=O species. Hence, the convenient access of silicon and germanium analogue of acetamide featuring silicon/germanium-oxygen double bond compounds are discussed. These are the first example of benzamidinato sila-acetamide and germa-acetamide. We are able to stabilize such Si/Ge=O moieties by the adduct formation with Lewis acid BF_3. Analogues reaction with

stannylene did not afford stana-acetamide instead led to the formation of fluorinated Sn(IV) compound due to the poor orbital overlap between tin and oxygen atoms.
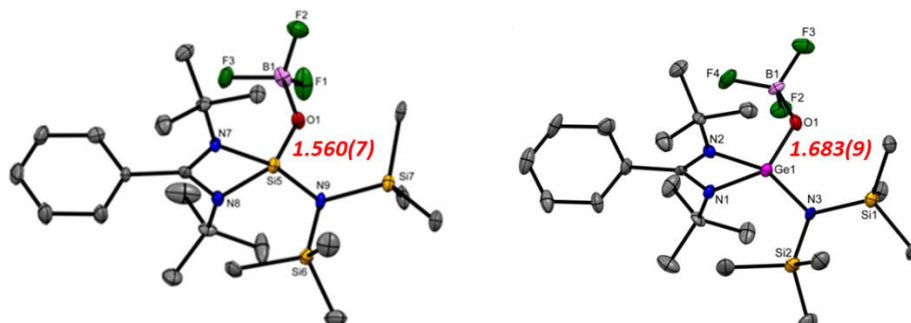
Chapter 3: N-heterocyclic silylene stabilized monocordinated Cu(I)-arene cationic complexes and their application in Click chemistry.

Theoretical and experimental results suggested that $[Cu(C_6H_6)]^+$ prefers the η^1/η^2 mode over the η^6 mode due to the enhanced repulsion between the benzene ring and metal d-electrons. Thus isolation of copper cation bound to the benzene ring in an unsupported η^6 mode poses a formidable synthetic challenge and has only been observed in the gas phase but never realized under laboratory conditions. In this work, we have successfully isolated and characterized the first elusive $[Cu(\eta^6\text{-}C_6H_6)]^+$ moiety stabilized by silylene. An analogous reaction was observed with hexamethyl benzene which also displayed η^6 coordination mode. DFT calculations revealed that the positive charge on silylene favours back-donation from Cu→Si(II) atom, which is the key factor to stabilize such moiety by releasing the repulsions between the benzene π-system and the Cu d-electrons. Thus in order to stabilize η^6 coordination mode, the complementary ligands must have π-acceptor character. This work is fundamentally very important to understand the bonding of silylene with Cu(I) and their further effect on the coordination of arenes.

Subsequently, we have isolated silylene supported monocoordinated Cu(I)-unsymmetrical arene cations and their reactivities with σ-donor ligands such as MeCN, NHC, NHSi. We have utilized the copper-toluene cationic complex for the click chemistry. Although the weak bonding between copper and free arene is the synthetic obstacle, it constitutes a major driving force for the catalysis reaction by easy substitution of an arene

with the substrates. Hence, we have carried out the click reaction for the synthesis of a series of triazoles by using copper-toluene cationic complex. Low catalyst loading and less reaction time is the important feature of the catalyst. We observed that 0.5 mol% catalyst loading is sufficient for different types of azides and alkynes under ambient conditions, which afforded the desired triazoles in good to excellent yields. It is important to note that we have utilized first-time naphthylmethyl azide in homogeneous click chemistry for the formation of triazole which is otherwise only be accessed in a heterogeneous manner.
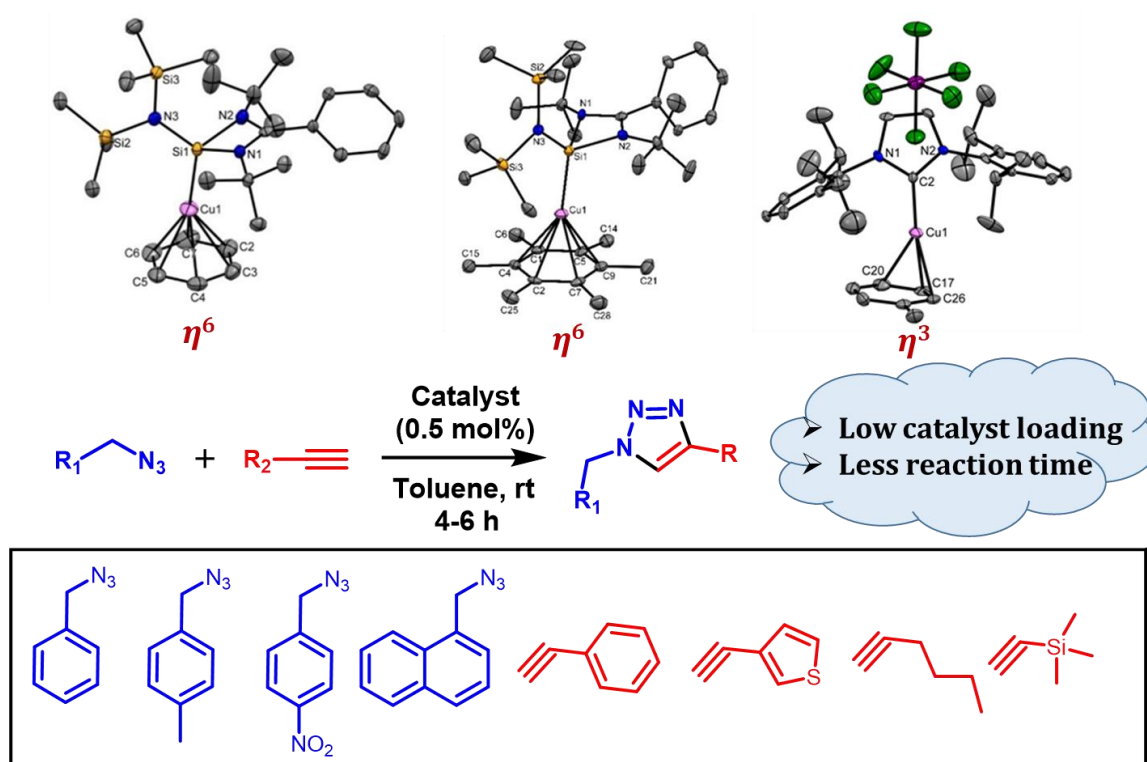
Chapter 4: Ligand on Demand: Carbene/Silylene/Germylene supported Nearly Naked Au(I)-Arene Complexes and Their Applications in Glycosidation

It has been proposed that in the Au catalyzed transformation reactions, true catalysts are the cationic Au(I) complexes [LAu$^+$], which are prepared in situ from the gold halide precursors. The naked Au(I) cation [LAu$^+$] is very unstable due to high Lewis acidic nature and hence not isolable. A closest related complex of the naked Au cation could be the [Au-(arene)]$^+$ complexes as the binding of gold with arene is significantly weaker than

alkyne/alkene. In silylene chemistry, the examples of silylene-Au(I) complexes are scarce and not explored in the catalytic application. Hence, we have introduced well-defined [Au-arene]$^+$ complexes using N-heterocyclic silylene, germylene, and carbene as a σ-donor ligand and were probed the first time for glycoside synthesis. For glycosidation reaction, the ligand is limited to phosphines/phosphites only, and the catalysts are usually not well-defined and generated in situ. Therefore, we explored the well-characterized Au cations in disaccharide synthesis and observed to be superior over Au(III) salt, even better than NHC- and phosphite-Au(I) complexes for the activation of propargyl 1,2-orthoester donors. When it comes for the activation of carbonate donors, NHC-Au(I) complex is the most efficient. It is noted that the weak arene-Au(I) interaction reduces the decay of the catalyst. DFT studies are provided further insights into the mechanism. The practical application of the catalysts was achieved by the synthesis of the branched pentamannan core of the HIV-gp120 envelope under mild conditions.
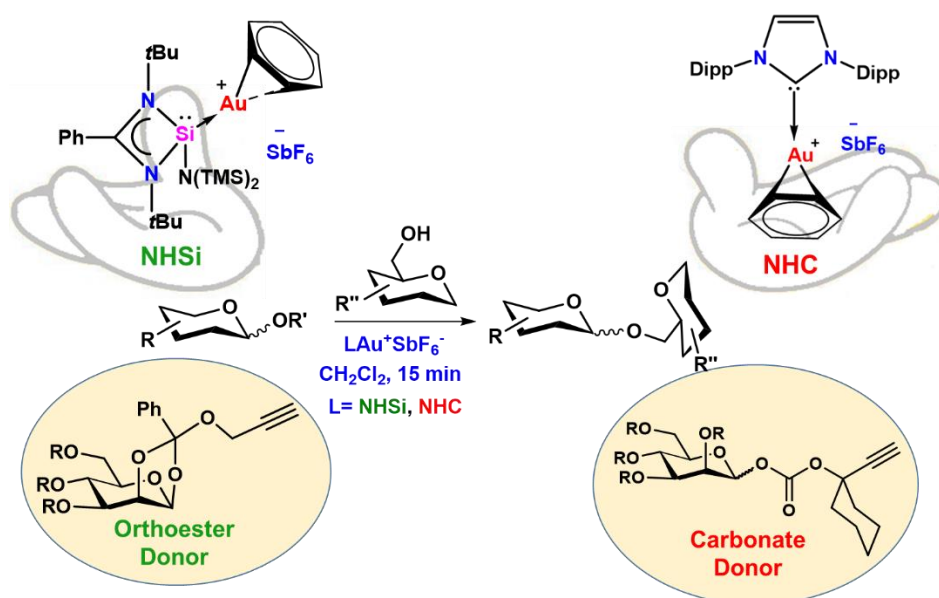
Chapter 5: C-N Cross-Coupling Reactions of Bulky Primary Anilines with Aryl Halides Using Pd/NHSi System

Recent development in N-heterocyclic silylenes as ligands for metal-mediated homogeneous catalysis is due to their strong σ-donor and π-acceptor ability. In silylene chemistry, Pd-catalyzed C-N cross-coupling reactions are not explored. Recent studies on

amination reactions of sterically hindered groups motivated us to develop new ligands where the coupling of such a bulky system with electron-deficient substituent are very challenging. Hence, we investigated the potential application of a bidentate ligand (SiNP) bearing Si(II) and P(III) coordination site with Pd(dba)$_2$ salt for Buchwald-Hartwig amination reactions of enormously bulky primary anilines with bulky aryl bromide containing electron-donating and withdrawing substituents with broad substrate scope by the conventional method as well as under the microwave technique (10-15 min). It is worth to mention that the SiNP/Pd(dba)$_2$ system showed outstanding performance (~90-99%), even better than reported phosphines and carbenes. The remarkable potential of the SiNP/Pd(dba)$_2$ system may be elucidated due to the presence of two strong donor sites, Si(II) and P(III). The theoretical calculation also revealed that the strong Si-Pd bond plays a key role in the catalytic process. We believe that these studies will be worthwhile because of the lack of general studies on these bulky class of substrates where the yields are very low (~30–70%) (*vide infra*).

- First NHSi/Pd system in C-N cross coupling reaction
- Coupling between extremely bulky primary anilines with electron-donating and withdrawing aryl halides
- Broad substrate scope
- > 90% yield of coupling products

*****
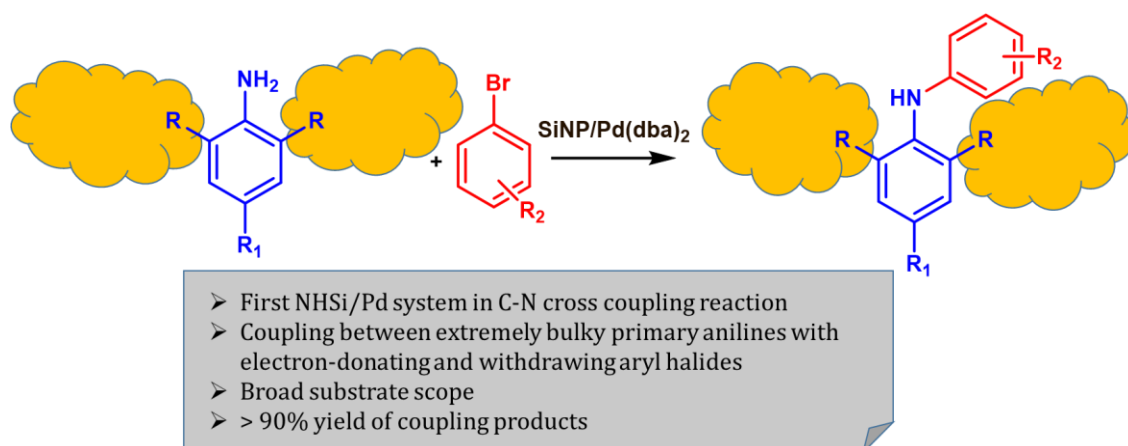
Abbreviations

Anal.	Analysis	MAOS	microwave-assisted organic synthesis
BINAP	2,2′-bis(diphenylphosphino)-1,1′-binaphthyl	min	Minutes
BippyPhos	5-[Bis(1-adamantyl)phosphino]-1′,3′,5′-triphenyl-1,4′-bi-1H-pyrazole	MALDI	Matrix-Assisted Laser Desorption/Ionization
Calcd.	Calculated	mmol	Millimoles
CCDC	Cambridge Crystallographic Data Centre	NMR	Nuclear Magnetic Resonance
CIF	Crystallographic Information file	ppm	Parts per million
C_6D_6	Deuterated benzene	RT	Room Temperature
$CDCl_3$	Deuterated chloroform	TM	Transition metal
cod	cyclooctadiene	Xantphos	4,5-Bis(diphenylphosphino)-9,9-dimethylxanthene
DCM	Dichloromethane	XRD	X-ray Diffraction
DFT	Density Functional Theory		
Dipp	2,6-diisopropylaniline		
DPEphos	Bis[(2-diphenylphosphino)phenyl] ether		
dppf	1,1′-Ferrocenediyl-bis(diphenylphosphine)		
dppp	1,3-Bis(diphenylphosphino)propane		
HRMS	High-Resolution Mass Spectroscopy		
Hz	Hertz		
IR	Infrared spectroscopy		
*i*Pr	Isopropyl		

Publications

Publications included in Thesis

1. **Parvin, N.**; Pal, S.; Khan, S.;* Das, S.; Pati, S. K.;* Roesky, H. W.* Unique Approach to Copper(I) Silylene Chalcogenone Complexes, *Inorganic Chemistry* **2017** , *56*, 1706–1712.

2. **Parvin, N.**; Dasgupta, R.; Pal, S.; Sen, S. S.;* Khan, S.* Strikingly Diverse Reactivity of Structurally Identical Silylene and Stannylene, *Dalton Transaction* **2017**, *46*, 6528-6532.

3. **Parvin, N.**; Pal, S.; Echeverría, J.; Alvarez, S.;* Khan, S.* Taming Monomeric [Cu(η^6-C$_6$H$_6$)]$^+$ Complex with Silylene, *Chemical Science* **2018** , *9*, 4333-4337. (Selected as ChemSci Pick of the Week, selected as collection of 100 women in Chemistry and highlighted in Chemistry World).

4. **Parvin, N.**; Hossain, J.; George, A., Parameswaran, P.;* Khan, S.* N-heterocyclic Silylene Stabilized Monocordinated Copper(I)–Arene Cationic Complexes and Their Application in Click Chemistry, *Chem. Comm.* **2020,** *56*, 273-276.

5. **Parvin, N.**; Mishra, B.; George, A.; Neralkar, M.; Hossain, J;. Parameswaran, P.;* Hotha, S.;* Khan, S.* N-Heterocyclic Silylene/Germylene Ligands in Au(I) Catalysis, *Chem. Comm.* **2020**, *56*, 7625-7628.

6. **Parvin, N.**; Khan, S.* Convenient Access to Compounds with Silicon/ Germanium-Oxygen Double Bond. (*Manuscript under preparation*)

7. **Parvin, N.**; Khan, S.* C-N Cross-Coupling Reactions of Bulky Primary Anilines with Aryl Halides Using Pd/NHSi System. (*Manuscript under preparation*)

Publications not included in Thesis

8. Khan, S. ;* Ahirwar, S. K. ; Pal, S. ; **Parvin, N.**; Kathewad, N. Silicon(II) Bis(trimethylsilyl)amide (LSiN(SiMe$_3$)$_2$, L = PhC(NtBu)$_2$) Supported Copper, Silver, and Gold Complexes, *Organometallics* **2015**, *34*, 5401–5406.

9. **Parvin, N.**; Pal, S.; Rojisha, V. C.; De, S.; Parameswaran, P.;* Khan, S.* Comparing Nucleophilicity of Heavier Heteroleptic Amidinato-Amido Tetrelylenes: An Experimental and Theoretical Study, *ChemistrySelect* **2016**, *1*, 1991–1995.

10. Swamy, V. S. V. S. N.; **Parvin, N.**; Raj, K. V.; Vanka, K.;* Sen, S. S.* C(sp3)–F, C(sp2)–F and C(sp3)–H Bond Activation at Silicon(II) Center, *Chem. Comm.* **2017**, *53*, 9850 – 9853.

11. Kathewad, N.; Anagha, M. C.; **Parvin, N.**; Parambath, S.; Parameswaran, P.;* Khan, S.* Facile Buchwald–Hartwig coupling of Sterically Encumbered Substrates Effected by PNP Ligands, *Dalton Transaction* **2019**, *48*, 2730-2734.

Chapter 1

A Brief Introduction on Low-Valent

Silicon(II) Compounds

1.1.   The elemental silicon and organosilicon compounds

The name of *silicon* is derived from the Latin word *silex* or *silicis*, which means "flint" or "hard stone". Although silicon was first identified in 1787 by Antoine Lavoisier, the first amorphous elemental silicon was uncovered by a Swedish chemist, Jöns Jacob Berzelius in 1824.[1] Due to the semiconducting nature, the influence of the elemental silicon into our daily lives has widened gradually with manufacturing the microchip, processor, transistor, and photovoltaic cells' production.[2] Recent application of metallurgical grade silicon with 98-99.99% purity is directly applied as an alloying component and deoxidant in the steel industry or as the prerequisite component for chlorosilane synthesis or solar and semiconductor technologies. "Siemens process" is the most commonly used methodology for trichlorosilane and polycrystalline silicon. Whereas the "Czochralski process" has been used for monocrystalline semiconductor silicon (>99.99% purity).[3]

Carbon has been considered as "carrier of life" due to its enormous application in all living organisms to fossil fuels owing to their stable single and multiple bond formation with numerous elements in the periodic table. Silicon, the next heavier carbon component,, is the second most abundant element (27%)[4] in the lithosphere boosts the evolution of silicon-based life formation.[5] In comparison to a stable alkane (CH_4), the higher analogue silane (SiH_4) is flammable in air and vigorously reacts with halogen. Another limitation of silicon as a hypothetical life source is the minimal overlapping of s and p-orbitals to reduce the formation of multiple bonds with itself and other elements.[6,7]

In 1901 Frederic S. Kipping accidentally came across the polysiloxanes [(-Si-O-Si-)$_n$], speciously termed as "silicones", when he was willing to discover the silicon analogues of ketones (Si=O). The formation of Si-O-Si single bond in polysiloxanes can be attributed to the presence of strong polarization of $Si^{\delta+}-O^{\delta-}$ bond and high liability for polymerization.[8,9] Significant industrial application of Kipping's discovery had been recognized after 1940 with the isolation of silicone precursor Me_2SiCl_2 in a commercial process by R. Müller and E. Rochow independently.[10] Since then, the increasing demand for silicones, organochlorosilanes, and high-molecular polysiloxanes has been fulfilled by well-established "Direct Synthesis" or "Müller-Rochow Process".[10]

Along with the most stable +IV oxidation states of silicon, another still growing field is low-valent organosilicon chemistry. The reduced coordination numbers and lower oxidation states, which were once considered to be elusive species and highly challenging to synthesize are being realized in the laboratories. However, the recent achievements of silicon compounds with lower oxidation states have changed the scenario as an emerging field of research.[11]

1.2. Brief Overview on Low-Valent Silicon Chemistry

Until the last two decades of the twentieth century, the chemistry of heavier main group elements was not much explored due to their limited number of obtainable oxidation states compared to the d-block transition metals. Nonetheless, several recent discoveries have disclosed that heavier main-group compounds can mimic transition-metals with divergent intrinsic electronic properties than their lighter analogue.[12] Discoveries of such main group compounds consisting of non-preferred electronic environments have a propensity to go for oligomerization or decomposition due to their highly reactive nature. Hence, thermodynamic and kinetic stabilization is necessary to access such heavier low-valent main group compounds e.g. multiply bonded compounds of Al, Si, P or their heavier congeners, stable low-valent derivatives with open coordination sites, heavier main-group elements possessing radical etc.[13]

Heavier group 14 elements, Si, Ge, Sn and Pb, have contrasting physical and chemical properties with novel structural features compared to their lighter analogue carbon. Recently, low-valent silicon chemistry has received a lot of attention and studied well to understand their fundamental electronic properties and nature of bonding. Low-valent silicon compounds consisting of unfavourable oxidation states are varied from 0 to +III. Few selected examples of low-valent silicon compounds are summarized in Chart 1.1. The wander of stable low-valent silicon compounds started with the first isolation of disilene **1.1**, a Si=Si double-bonded compound in 1981, where both the silicon atoms present in +II oxidation states.[14] West and co-workers stabilized the disilene kinetically using sterically bulky substituents (Mes$_2$Si=SiMes$_2$, Mes = 2,4,6-Me$_3$C$_6$H$_2$). After that, a lot of progress has been made in the π bonded compounds between two silicon atoms[15] such as utilization of the masked disilenes for the polymerization,[16] and synthesis of functionalized disilene with organic and inorganic substrates.[17]

From the last two decades, numerous kinds of low-valent silicon compounds have been successfully obtained by providing thermodynamic and kinetic stability. For example, In
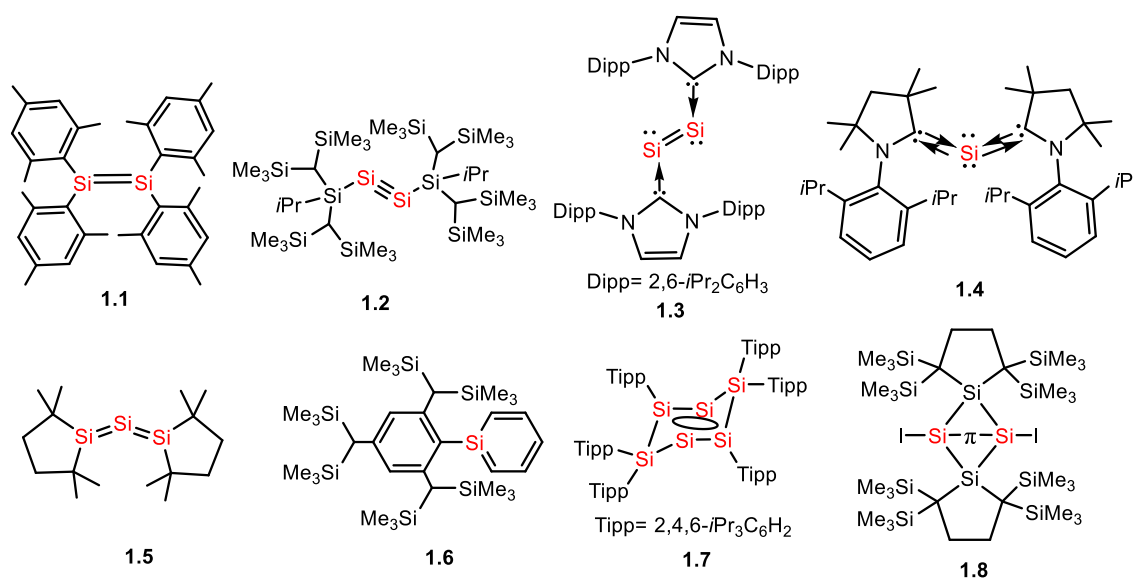
Chart 1.1. *Selected reported examples of low-valent silicon compounds.*

2004 Sekiguchi group reported a disilyne (R-Si≡Si-R), **1.2**, a silicon analogue of an alkyne, where they have used two large silyl substituents to provide kinetic and thermodynamic stabilization.[18] In 2008, N-heterocyclic carbene stabilized bis-silylene (L:Si=Si:L) (**1.3**) was obtained by the Robinson group, where both the silicon atom present in the formal oxidation state of zero.[19a] Whereas, Roesky and co-workers isolated CAAC carbene stabilized monomeric Si(0) complex (**1.4**).[19b] Kira and Sekiguchi group isolated *sp*-hybridized trisilaallene (**1.5**) which is significantly bent in structure, unlike its carbon analogue.[20] On the other hand, Tokitoh group isolated a stable aromatic silabenzene (**1.6**) stabilized by a bulky substituent.[21] New feathers were added in silicon chemistry by isolating a novel hexasilabenzene (**1.7**)[22] having dismutational aromaticity and Si-Si π single bonded compound (**1.8**),[23] where a π bond is not accompanied by a σ bond and the bond length is longer than the Si-Si σ bond. Additionally, cationic Si(II) species (RSi⁺) have introduced another class of low valent silicon compounds.[24] On the top of above, silylenes (a divalent silicon atom) are the most vigorously explored low valent silicon compounds. Hence, details studies on silylenes such as their electronic and bonding properties, reactivity with small molecules and metal-mediated catalytic application will be the centre of discussion of this chapter.

1.3. Silylenes: Fundamental Electronic and Bonding Properties

In general, group 14 elements possess $(ns)^2(np)^2$ electronic configuration with four valence electrons. A divalent carbon species, termed as carbene, usually form sp^2-hybrid orbital and display in triplet ground state with $\Delta E_{S,T}$ = –14 kcal/mol having two unpaired electrons with parallel spin.[25] It is to be noted that the less propensity of hybridization was observed for heavier analogues of carbon because of the larger atomic radius and minimal s- and p-orbital overlapping,[26] which enhances the $\Delta E_{S,T}$ energy gap down the group. For that reason, the heavier tetrylenes generally acquire a singlet ground state. Hence, the HOMO of heavier tetrylenes shows a high s-character, while LUMO has a high p-character. It was observed that the stability of the divalent tetrylenes (M(II), M= Si, Ge, Sn, Pb) increases down the group with increasing the HOMO-LUMO gap.
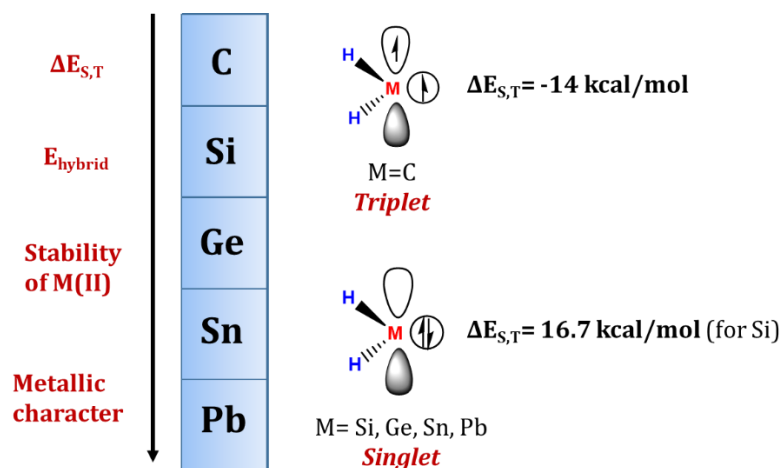
Figure 1.1. General trends of Group 14 elements and schematic representation of tetrylenes (C, Si, Ge, Sn, Pb).

Silylenes, the silicon analogue of carbene, is present in +II oxidation states with molecular formula $R_1R_2Si(II)$, where R_1 and R_2 should be σ or π coordinating ligands or bidentate chelating ligands. They are mononuclear, neutral, species with singlet ground state having a higher HOMO-LUMO gap ($\Delta E_{S,T}$= 16.7 kcal/mol) (in comparison to carbene). Hence, the paired electrons of silylene occupy the low lying HOMO orbital and the energetically higher p-orbital remains vacant. Owing to the presence of an electron pair and a highly Lewis acidic vacant p-orbital, silylenes are extremely reactive short-lived

species, such that isolation and handling of the species are very difficult. Until two decades ago, synthesis of the elusive silylenes could only be possible in cryogenic matrices at -196°C[27] and above this temperature, they have a tendency to undergo dimerization or polymerization.[28] The two important key factors that play a very important role in stabilizing the silylene at ambient temperature are thermodynamic and kinetic stabilizations. Thermodynamic stabilization could be provided by introducing heteroatom based ligand via the mesomeric effect and the intramolecular
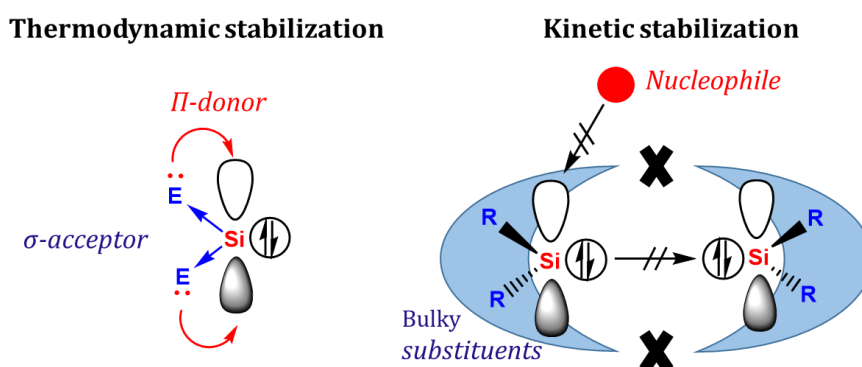
Figure 1.2. *Thermodynamic (π-donor and σ-acceptor) and kinetic (bulky substituents) stabilization of silylenes.*

coordination of the heteroatoms. Ligands containing nitrogen, sulphur, phosphorous accepts the electron density from the silicon centre and stabilize the HOMO which increases its s-character and favouring the singlet state. Further, they reduce the electrophilicity at the Si(II) centre by donating the lone pair of electrons from electronegative heteroatoms leading to an increase in the HOMO-LUMO gap.[29] Contrastingly electron-withdrawing substituents containing silyl and boryl groups or alkali metals reduce the HOMO-LUMO gap to encourage highly reactive triplet state.[30a] Thus they tend to undergo dimerization and such kind of triplet silylenes ((t-Bu$_3$Si)$_2$Si(II) and (t-Bu$_3$Si)MSi(II); M = Li, Na, K) were obtained *via* EPR experiments in frozen hydrocarbon matrices.[30b,c] Another important strategy is introducing sterically hindered substituents, which will provide enough kinetic stabilization to prevent self-dimerization or interaction by external nucleophiles. In principle, excessive steric hindrance may

increase the ligands repulsion leading to an expansion of the bonding angle that favours a triplet state.[30a,31]

1.4. Historic landmark in the timeline of monomeric silylenes

Blooming of silylene chemistry from the last three decades has been achieved by isolating plenty of fascinating structures with the impressive transition from once transient species to a readily available ligand for small molecule activation, stoichiometric transformation, and catalysis. The journey started in 1964 by the generation of dimethylsilylene (SiMe$_2$:) as a transient species in the gas phase by Skell and Goldstein via the reduction of dimethyldichlorosilane with sodium-potassium vapour at 260°C.[32] Several photochemical and thermal experiments were carried out to isolate a transient silylene, but due to the highly reactive nature, they were only observed in gas phase or hydrocarbon matrices at low temperature (≤ 77K). Growth of silicon chemistry was accelerated one step further in 1986 by Jutzi *et al.* through the isolation of first monomeric Si(II) compound **1.9** at ambient temperature-stabilized by two cyclopentadienyl group akin to the sandwich compound.[33] Owing to the hypercoordination of two cyclopentadienyl rings, the resultant highly nucleophilic silylene cannot be considered true silylene by definition. Finally, in 1994, West and Denk isolated the long-awaited room temperature stable, divalent and dicoordinated monomeric silylene, **1.10a**,[34] termed as N-heterocyclic silylene (NHSi). Reduction of the corresponding dichlorosilane to generate thermally stable unsaturated silylene **1.10a** as a crystalline solid, stabilized by two adjoining electron-donating bulky amino group giving both thermodynamic and kinetic protection. After this breakthrough, few more examples of unsaturated NHSis have been isolated by changing the R group attached to the N-centre along with their saturated version.[47] An interesting dialkylsilylene, 2,2,5,5-tetrakis(trimethylsilyl)silacyclopentane-1,1-diyl (**1.11**), was introduced by Kira *et al.* in 1999, which was stabilized by kinetic protection only and least distressed electronically.[35] Four bulky SiMe$_3$ groups have been used for steric shielding, diminishing π-donor ligand's requirement, and turning out to be an electrophilic silylene with highly downfield shifted ^{29}Si NMR (δ 567.4 ppm). Although **1.11** is stable at 0°C in solid-state and decomposed at room temperature to form the corresponding silaethene. In 2003, West and co-workers established a formidable acyclic bis(amino)silylene (**1.12**) from the respective dibromo Si(IV) species but the crystal structure could not be isolated.[36] **1.12**

can only be persisted at -20˚C for more than 12 h and undergoes rapid decomposition at room temperature and reason can be attributed to the insufficient kinetic stabilization. Furthermore, a conjugated *β*-diketiminato ligand stabilized NHSi (**1.13a**) was introduced by Driess and co-workers in 2006, which enriched the class of N-heterocyclic silylenes.[37] In the same year, the Roesky group reported a three-coordinate four-membered N-heterocyclic silylene (**1.14a**) stabilized by amidinato ligand via base induced reduction of HCl from its respective chlorohydridosilicon(IV) complex.[38] After that the chemistry of
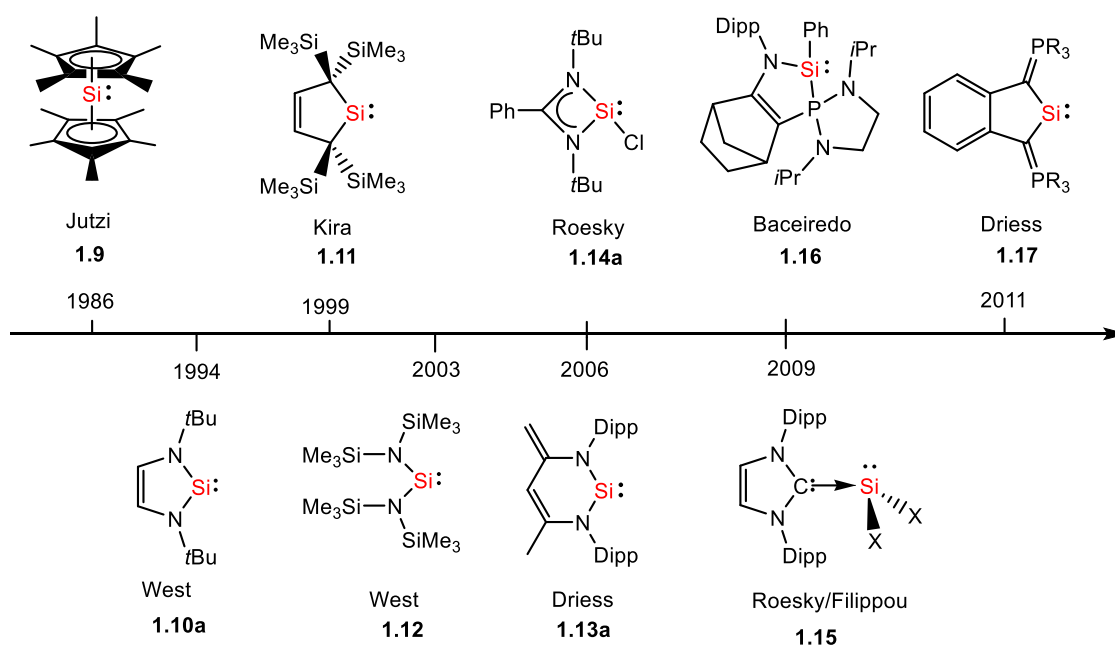
Chart 1.2. *Historical landmarks of isolable monomeric silylenes (**1.9**-**1.17**).*

stable silylene has been polished with relatively new fascinating features. Based on the essential pillar of the thesis, synthesis and reactivity of **1.14a** are addressed in details in the next section of this chapter. Roesky and co-workers have attained a significant breakthrough in 2009 by synthesizing a miraculous NHC-stabilized dichlorosilylene (**1.15**) via trichlorosilane reduction with N-heterocyclic carbene (2 equiv.) which is the replica of highly reactive elusive dichlorosilylene and an important component during the synthesis of elemental silicon in the industrial level.[39a] Filippou group also utilized a similar methodology to synthesize the analogous dibromo- and diiodosilylene.[39b,c] A phosphine stabilized silylene (**1.16**) is obtained by the groups of Berceiredo and Kato, which undergoes a reversible reaction with ethylene gas.[40] Another carbocyclic silylene

1.17 has been developed by Driess and co-workers in 2011 which is stabilized by introducing a zwitterionic phosphonium ylide PR₃⁺-C⁻ to increase the π-donor strength at the carbon centre.[41a] In contrast to Kira's carbocyclic silylene, **1.17** is stable at room temperature, even no decomposition was observed at 60°C for
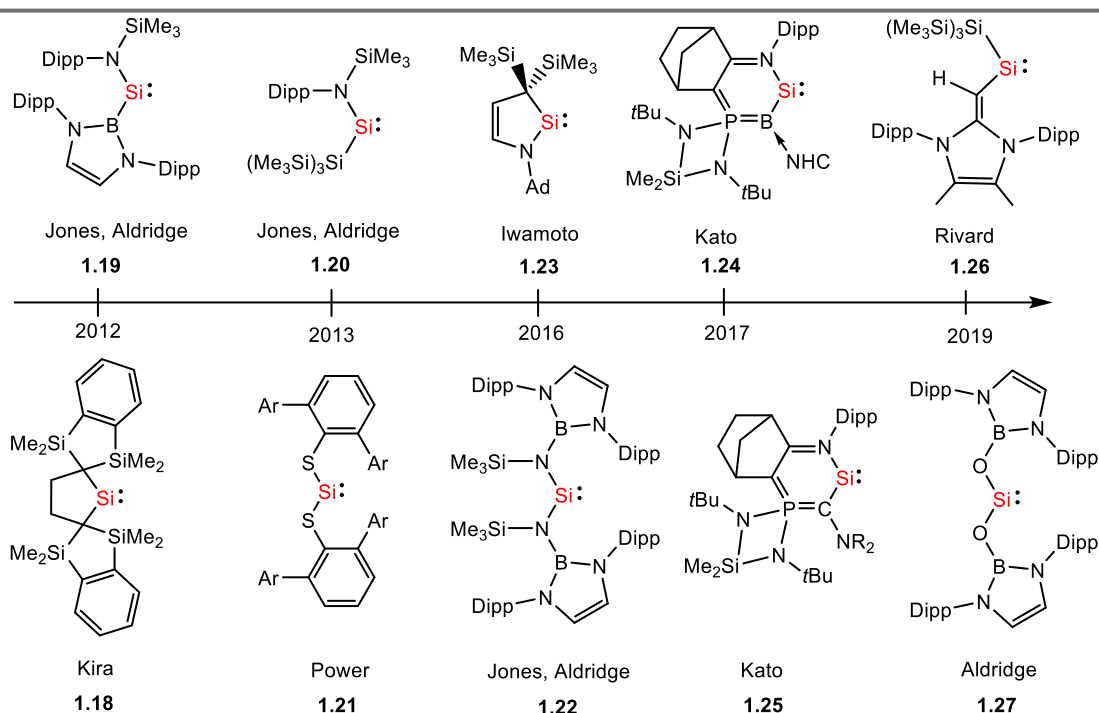
Chart 1.3. *Historic landmarks of isolable monomeric silylenes (**1.18**-**1.27**).*

several days. Following this, Kira *et al.* introduced a third example of carbocyclic silylene **1.18** by modifying the R group attached to the carbon centre of its parent compound **1.11**.[41b] Incorporation of sterically hindered flexible 1,3-disilaindane functional group stabilizes **1.18** at ambient temperature and enable it to present in equilibrium with its dimeric form in the solution state. The holy grail to isolate more flexible room temperature stable acyclic silylene has been accomplished in 2012 by Jones and Aldridge group and separately by Power group. This landmark discovery stops the long-awaited credence about short-lived elusive acyclic silylenes, which are considered useful candidates for small molecule activation due to their small HOMO-LUMO gaps. The Power group utilized arylthiolato ligand on each side of the Si(II) centre to generate **1.21** with an S-Si-S bond angle of 90.5°.[42a] Whereas, the groups of Jones and Aldridge introduced a strong π-donor amino group as well as an electropositive σ-donating boryl or silyl group to reduce HOMO-LUMO difference and increases the Lewis acidity at the Si(II) centre

(**1.19**: δ 439.7 ppm and **1.20**: δ 438.2/467.4 ppm).[42b,c] Hence higher triplet silylene character is observed for **1.19** and **1.20** due to the obtuse inter ligand angle (N–Si–B 109.7° and N–Si–Si 116.9°, respectively). **1.19** and **1.20** have been fortunately able to activate H$_2$ under mild conditions[42b,c] due to their definite electronic properties.[43] Iwamoto group isolated another type of two coordinated cyclic silylene (**1.23**) in 2016, which is stabilized by the amino group and alkyl group, termed as cyclic alkyl(amino) silylene (CAASi), having a downfield shifted ^{29}Si NMR (δ 274.7 ppm).[44] Electronic properties of **1.23** are intermediate to NHSi and cyclic dialkyl silylene and along with the high thermal stability (stable for 2 days at 150℃). It readily undergoes cyclization reactions with alkynes, Si-H insertions, intramolecular C-H insertion reactions and dehydrogenation reactions. Baceiredo and Kato's group recently introduced two coordinated cyclic silylenes **1.24** and **1.25** where they utilized π-donating phosphonium or bora-ylide ligand, respectively along with the amino group.[45] Owing to the phosphorous or boron centre, their electronic properties are akin to **1.23** with ^{29}Si NMR shifts of δ 202.2 ppm (**1.24**) and 295.5 ppm (**1.25**). Further, the same group implemented **1.24** and **1.25** to discover "Kipping's" long-awaited dream *i.e.* a stable silicon analogue of ketone (Si=O) at ambient temperature.[46] In 2019, Rivard and co-workers isolated first time a vinylic olefin stabilized acyclic silylene (**1.26**), which is highly reactive towards small molecules such as P$_4$.[42f] In the same year Aldridge group obtained N-heterocyclic boryloxy (NHBO) ligand stabilized acyclic silylene, **1.27**, which is the first example of acyclic dioxysilylene.[42g] In comparison to the carbene chemistry, the examples of isolated silylene structures are still very limited. This field needs further research to study the structures of new silylenes in the novel, precisely designed chemical environments to understand their bonding and further applications.

1.5.   N-heterocyclic silylenes (NHSis)

1.5.1. Isolable five- and six-membered NHSis

Since the first isolation of "Ardueugo type" five-membered silylene by West and Denk, a series of unsaturated five-membered NHSis (**1.10a-1.10f**, Chart 1.4a) stabilized by alkyl and aryl substituted N donor atoms were isolated.[47] Subsequently, the same group obtained more reactive saturated NHSi (**1.28a**, Chart 1.4b) which tends to undergo reversible oligomerization to disilene in the solid state or in concentrated solutions. Afterwards, several research group introduced bulky group at the ring carbon to prevent

oligomerization and able to synthesize room temperature stable saturated five-membered NHSis (**1.28b-1.28e**, Chart 1.4b).[47] Along with these, another type of isolable five membered NHSis fused by benzo or pyrido ring are summarized in Chart 1.4c.[47]

The chemistry of six membered NHSis was established by Driess and cowokers with the help of *β*-diketiminate ligand and was further enhanced by changing the substituent of ligand backbone or substituent attached to the Si(II) centre or extra stabilization provided by a donor NHC (**1.13**, **1.30-1.33**, Chart 1.4d).[48]
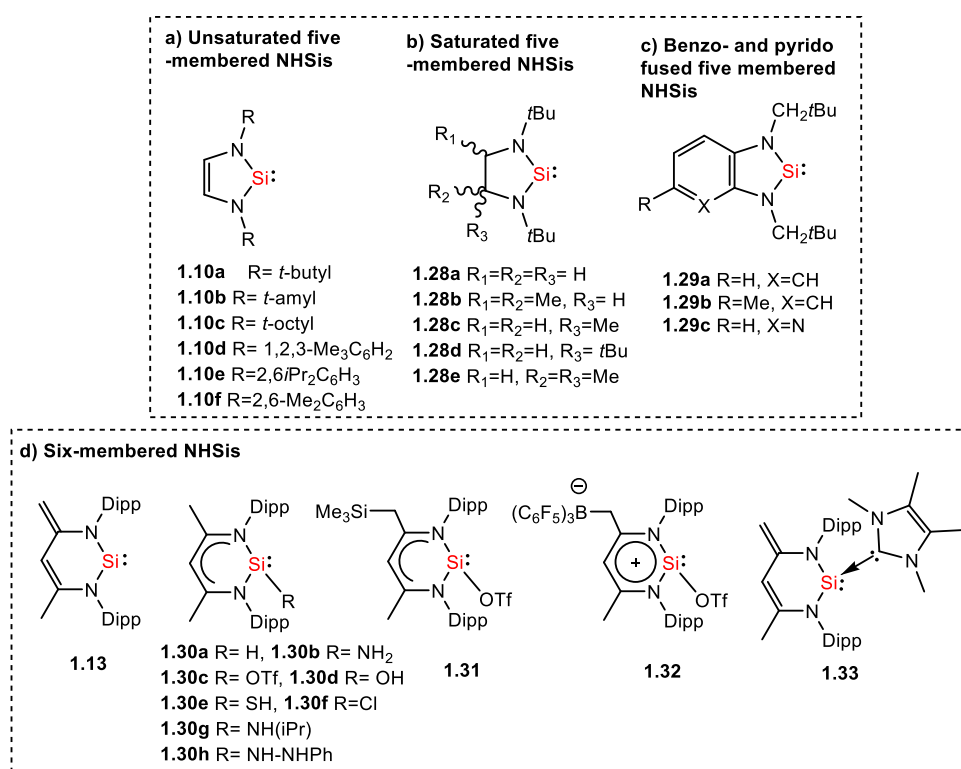
Chart 1.4. *Selected reported examples of five- and six-membered NHSis*

1.5.2. Isolable four-membered NHSis

Isolation of four-membered NHSi (**1.14a**) in 2006 by Roesky and co-workers set a landmark discovery in silylene chemistry with the extensive utilization as a ligand or functional group in small molecule activation and catalytic or stoichiometric transformations with transition metals. **1.14a** was first synthesized from the reduction of the respective trichlorosilane precursor with very low isolated yield (only 10%). Afterward, in 2009, the same group modified the procedure to improve the product
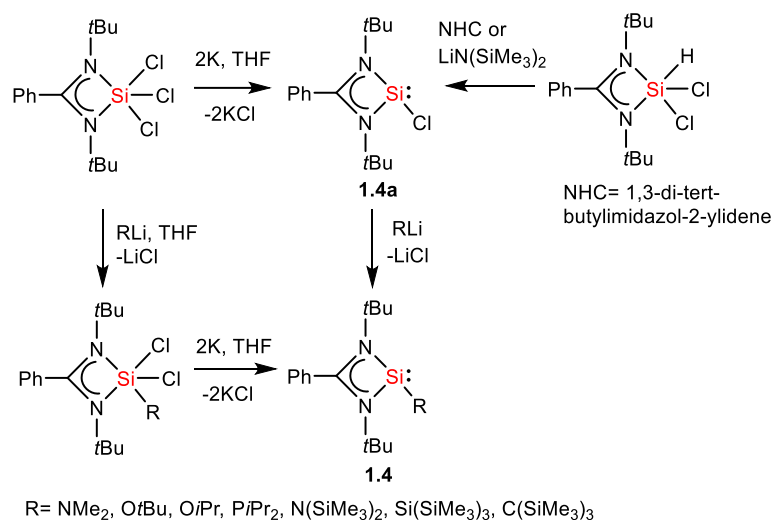
Scheme 1.1. *Synthesis of the four-membered amidinato ligand stabilized NHSis.*

conversion via base induced removal of HCl from its corresponding chlorohydridosilane using $LiN(SiMe_3)_2$ or NHC as the reducing agent and observed 90% isolated yield with $LiN(SiMe_3)_2$ and 35% with NHC (Scheme 1.1). Subsequently, the chlorine attached to the Si(IV) centre could be substituted by NMe_2, O*t*Bu, O*i*Pr or P*i*Pr$_2$, $N(SiMe_3)_2$ groups followed by the reduction with potassium afforded **1.14b-1.14m** (Chart 1.5a).[49] Of late, **1.14a** has been implemented as the precursor for a bunch of functionalized monosilylenes (**1.14b**, **1.14d**, **1.14m**, **1.35**-**1.39**) (Chart 1.5a)[49] and bissilylenes (**1.40**-**1.45**) (Chart 1.5b)[50] in a chelating scaffold via salt elimination method. A series of guanidinato ligand stabilized four-membered NHSis (**1.34a**-**1.34c**) are reported by Tacke and co-workers.[49h,i,j]

1.6. Reactivity of NHSis with small molecules

From the last few decades, significant development has been achieved in silylene chemistry in terms of facile activation of small molecules by taking advantage of small HOMO–LUMO energy gap and ambiphilic nature of divalent Si centres, mimicking transition-metal complexes.[51] In the following chapter, our discussion would be focused

exclusively on small molecule activation of monodentate four membered NHSis. Among them, **1.14** has received a substantial concentration in the area of metal-free bond activation with P_4, H_2O, H_2 etc (Chart 1.5).[51]

For living organism, phosphorous is a very crucial element and the important feature of the phosphorous-containing compounds has been noticed in organic synthesis to optoelectronic materials. It is to be noted that the advantage of the isolation of silylene mediated phosphorous compounds are mild reaction condition and easy purification methods which are otherwise prepared via dangerous multi-step process.
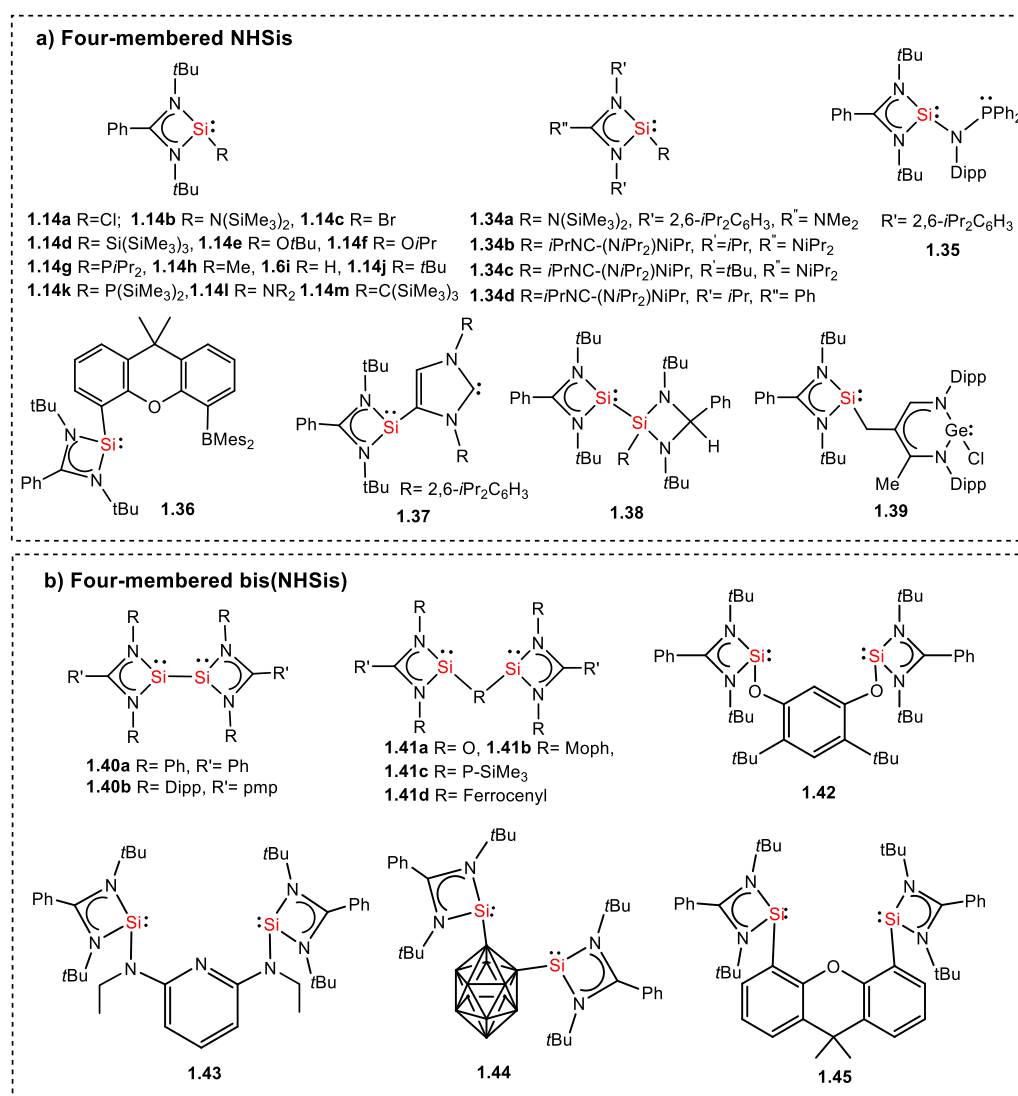
Chart 1.5. *Selected reported examples of four-membered mono(NHSis) and bis(NHSis)*

In 2011, the Roesky group reported P_4 activation by **1.14a** afforded Si-P-Si-P four-membered ring compound **1.46** (Chart 1.6a) with a positive charge on the silicon centres whereas phosphorous centres have partial negative charges.[52a] Contrastingly, a neutral acyclic Si=P–P=P–P=Si chain compound (**1.47**) featuring a diphosphine and two phosphasilene units could be obtained from the reaction of bis(trimethylsilyl)amido silylene (**1.14b**) with P_4 (Chart 1.6a).[52b] Similar reaction with As_4 furnished an unprecedented As_{10} cage compound (**1.48**) with exocyclic Si=As bond (Chart 1.6a).[53]

Water activation is usually observed in a series of hydrolase enzymes and fundamentally important to the industrial work for the development of new productive and ecologically feasible sources of dihydrogen. Although, such examples to form dihydrogen compounds from H_2O activation is scarce. Monochlorosilylene (**1.14a**) reacted with $H_2O \cdot B(C_6F_5)_3$ in the presence of NHC [1,3-bis(2,6-diisopropylphenyl)-imidazol-2-ylidene] to impart an acid anhydride of silicon (**1.49**) presenting an O=Si–O–Si=O moiety via the formation of intermediate silaformaldehyde and silacarboxylic acid.[54a] Into the bargain, Driess group reported an intramolecular silylene borane FLP complex **1.36** and experienced a silanone–borane adduct (**1.50**) from the metal-free dehydrogenation reaction with H_2O through the initial oxidation of O-H to the silicon centre (Chart 1.5b).[54b] Identical Si=O→BR_3 adduct (**1.50**) was also obtained from the activation of O_2, CO_2, and N_2O by **1.36**.

CO_2 and N_2O activation has become a fascinating area of research in terms of environmental aspects. Owing to the higher oxophilic property, silylenes can react very productively with CO_2 and N_2O to form thermodynamically stable species. Hence, the reaction of bis(amidinato)silylene with an excess of N_2O and CO_2 at low temperatures afforded the dinuclear complex **1.51a**-**1.51c** and mononuclear Si(IV) species **1.54a**, respectively through the formation of an intermediate five-coordinate silanone species.[40d,55] In parallel, bis(guanidinato)silylene imparted **1.52**, **1.53** and **1.54b**, **1.55** from the reaction with N_2O and CO_2, respectively, at low temperature (Chart 1.6c and 1.6d).[56]

Further, the Driess group reported the reaction of N-heterocyclic silylene-borane adduct (**1.36**) with H_2 and D_2 to produce a silane borane adduct (**1.56**) analogous to FLP chemistry due to the presence of a Lewis acidic boryl group which is otherwise not

observed for the electronically similar N,N'-di-tertbutyl(phenylamidinato) phenylsilylene (Chart 1.6e).[54b]

Nowadays, the fixation of nitrogen and further conversion to ammonia, hydrazine, and other fundamental nitrogen-containing chemicals by main group elements are discussed. Literature study disclosed that the crucial factor for the successful N_2 fixation is back
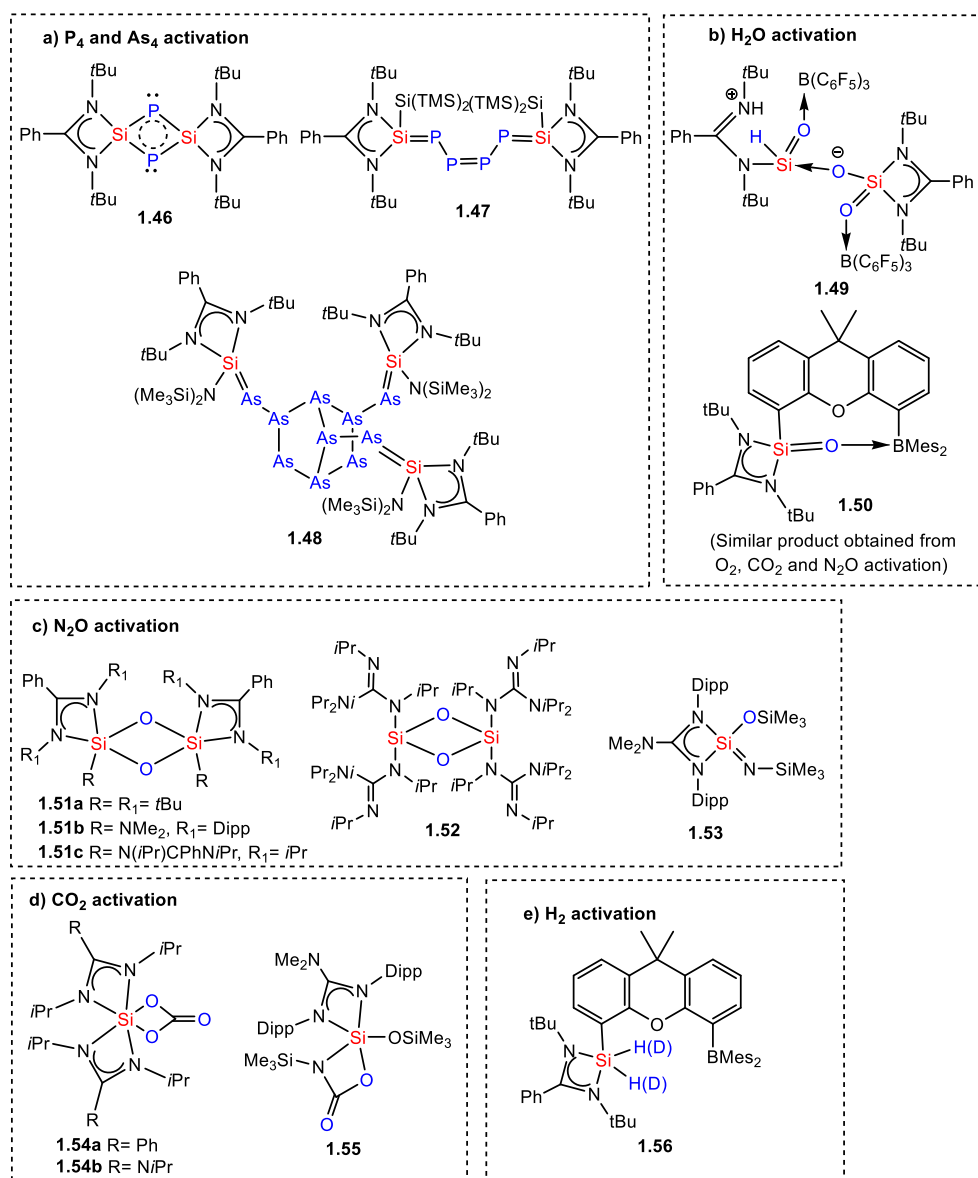
Chart 1.6. *Selected examples of small molecule activation by four-membered NHSis.*

bonding. Hence, crowning achievement will be accomplished by modifying silylene with filled and vacant orbital to activate nonpolar strong triple bonded N_2 in low valent silicon chemistry.

1.7.   N-heterocyclic Silylenes: Potent Ligands in Homogeneous Catalysis

In transition metal-mediated catalysis, utilization of new ligands is an important feature to regulate the reactivity, selectivity, and efficiency of the catalyst. It is well noticeable from the literature that various types of N-donor, P-donor (phosphines, phosphates, etc), O-donor ligands, and NHCs have received considerable attention in homogeneous catalysis due to the presence of powerful donating atoms. Szilvási group theoretically showed that several silylenes could challenge or even outshine classical carbenes and phosphines ligands in terms of σ-donation and π-accepting ability, ligand-to-metal charge transfer, and steric properties.[49f] Further, Driess group investigated σ-donor strengths of *β*-diketiminato silylenes by examining the CO stretching frequency of the corresponding isoelectronic $Ni(CO)_3$ complexes.[57] It is to be noted that four membered base stabilized NHSis are superior σ-donor than phosphines manifested experimentally by our group in 2016 where a bidentate ligand containing a four-membered amidinato NHSi and a P(III) centre reacted with AuCl to afford a monomeric Si(II)→Au(I) coordination complex while P(III) remains uncoordinated.[58]

NHSi has been exhibited as marvelous ligands for transition metals after 1977 when Welz and Schmid isolated the first NHSi-iron complex.[59] As compared to five- and six-membered NHSis, chemical refinements of four-membered N,N-di(tertbutyl)amidinato silylene (**1.14a**) is more flexible. Plenty of mono- and bis-(amidinato silylenes) have been evolved and demonstrated as monodentate (Chart 1.5a) and bidentate or tridentate (Chart 1.5b) chelating ligands in transition-metal mediated homogeneous catalytic transformations including (1) carbon-carbon (C-C) bond formation reactions, (2) carbon-heteroatom (C-X) bond formation reactions, and (3) reduction reactions with olefins and ketones, which will be discussed in detail in the following sections.[60,50b]

1.7.1. C-C bond formation

C-C cross-coupling reactions such as Suzuki coupling, Heck coupling, Kumada-Tamao-Corriu coupling, Negishi coupling, Sonogashira coupling are the most versatile and

convenient methodology to synthesize functional organic compounds in laboratory research as well as in industrial application. Several Si(II)-TM complexes have been utilized for the C-C bond formation, summarized in Chart 1.7. Fürstner and co-workers first did the inauguration of an NHSi complex in a catalytic process in 2001 through the
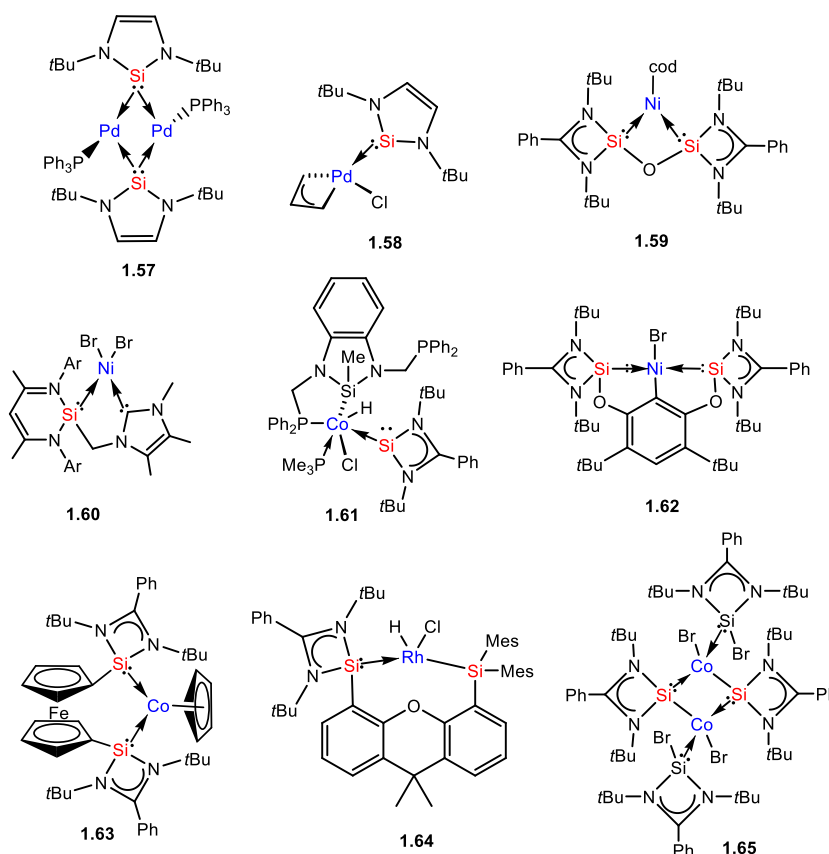
Chart 1.7. *Reported examples of NHSi-transition metal complexes for C-C bond formation reactions.*

isolation of a novel dinuclear μ^2-bridged NHSi-Pd complex (**1.57**) which is effectively employed in the Suzuki cross-coupling reaction (Scheme 1.2a).[61] After seven long years, Roesky and co-workers reported the second example of a catalytically active Pd-based NHSi complex (**1.58**) having η^3-C_3H_5 moiety for the Heck coupling of styrene and bromoacetophenone with the quantitative yield of the coupling product at 140°C and investigated the effect of the substituent in the catalytic performance (Scheme 1.2b).[62] Inoue and co-workers incorporated the first chelating bis(NHSi)-Ni complex (**1.59**) as pre-catalyst for Kumada-Tamao-Corriu and Negishi coupling reactions of R'-MgBr

(Grignard reagents) and R'-ZnBr (organozinc reagents) with aryl halides, respectively (Scheme 1.2c and 1.2d).[63a] Subsequently, independent work by Driess and co-workers and Li and Sun group for the isolation of bis(NHSi) supported Ni (**1.60**)[63b] and Co (**1.61**)[63c] complexes, respectively, played an important role in the similar cross-coupling reactions (Kumada-Tamao-Corriu coupling and Negishi coupling). Moreover, **1.60** is highly efficient with 99% product conversion in Kumada-Tamao-Corriu coupling
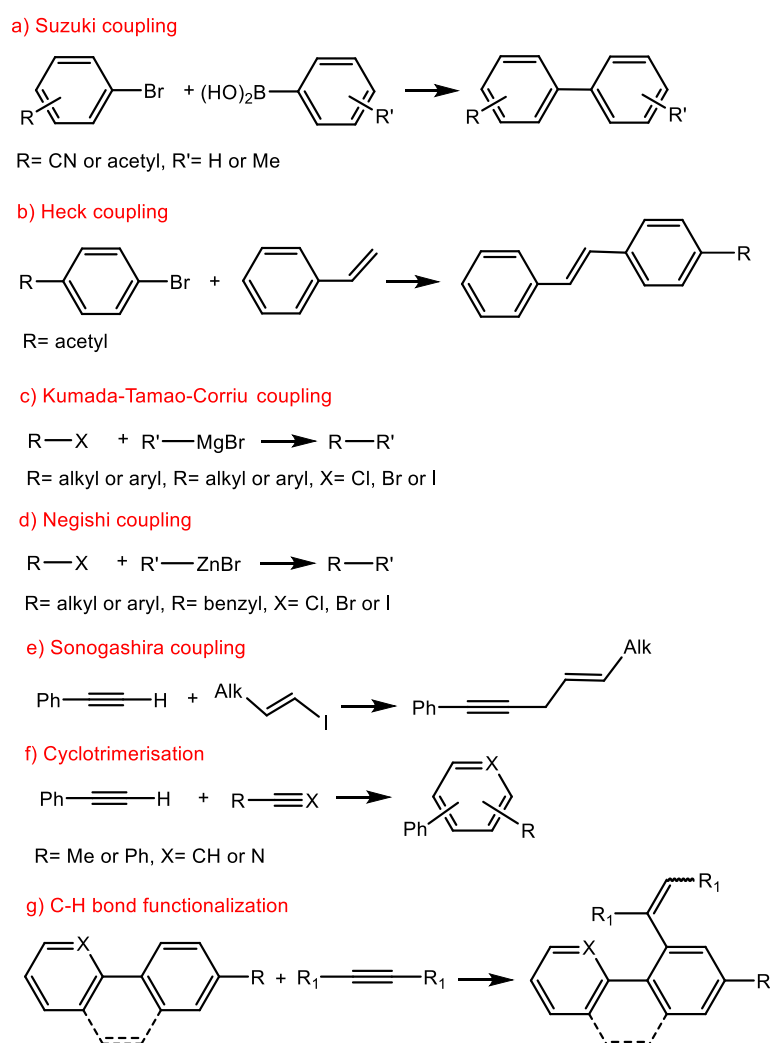
Scheme 1.2. *General scheme of Si(II)-transition metal-catalyzed C-C bond formation reactions.*

reactions. Another bis(NHSi)-stabilized Ni complex (**1.62**) reported by Driess and Hartwig group implemented as an active pre-catalyst for the Sonogashira coupling reaction of phenylacetylene with 1-iodo-1-octene and isolated an unusual

heterobimetallic intermediate. This intermediate contains both nickel and copper centre, where copper is coordinated to the alkyne π-system (Scheme 1.2e).[64] Beside the cross-coupling reactions, the Driess group also performed the cyclotrimerization and hydroformylation reaction by NHSi-TM complexes for C-C bond formation. They utilized the Co(I) Complex (**1.63**) effectively to synthesize triphenylbenzene and substituted pyridine via cyclotrimerization of phenylacetylene and the reaction of acetonitrile with phenyl acetylene, respectively (Scheme 1.2f).[65] Group of Driess and So separately carried out C-H bond functionalization by NHSi supported Rh and Co complexes **1.64** and **1.65**, respectively (Scheme 1.2g).[66]

1.7.2. C-X bond formation reaction

Mono- and bis-(NHSi) supported transition metal complexes including Ir, Co, Ni and Pt have been functionalized for C-X bond formation such as C-B, C-D, C-N bonds. Examples of the catalysts are listed in Chart 1.8 which are prepared via C-H oxidative addition
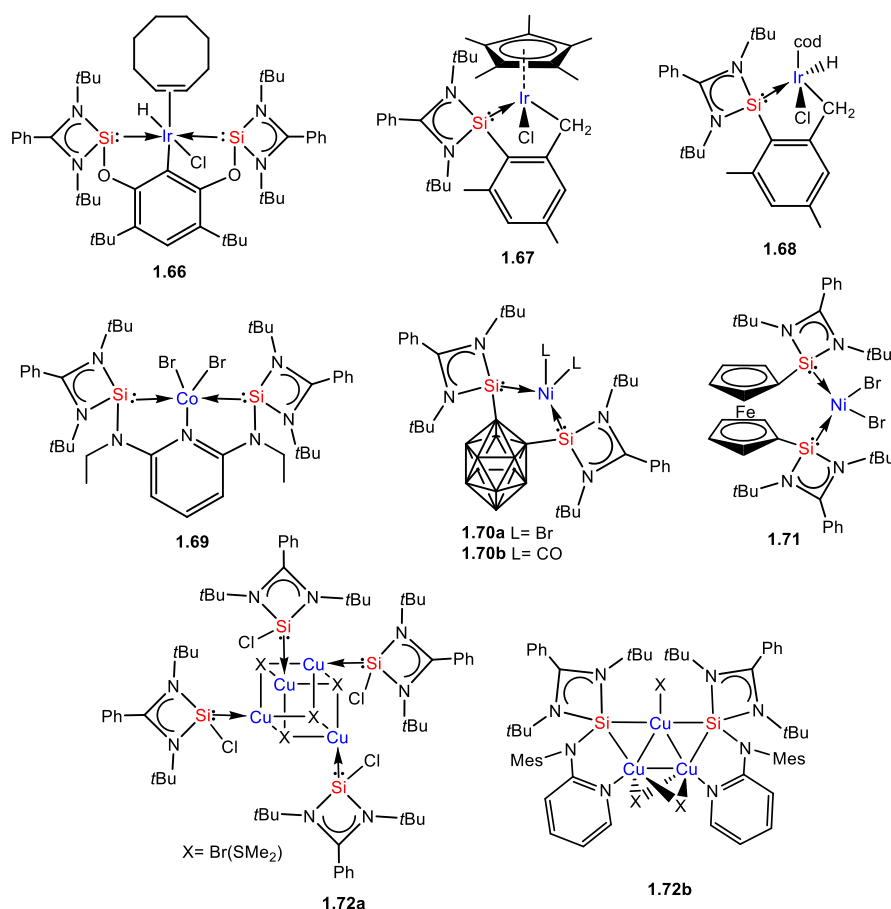
Chart 1.8. *Reported examples of NHSi-transition metal complexes for C-X (X= B, H/D, N) bond formation reactions.*

or direct coordination reaction or ligand exchange reaction or reduction under CO atmosphere of silylenes with the corresponding transition metals.

Borylation of arenes such as benzene, toluene, fluorinated arenes and heterocycles with pinacolborane is well-familiar for the generation of C-B bond formation and several research groups including Driess and Hartwig, Cabeza and García-Alvarez and Cui added new catalysts **1.66**, **1.68**, and **1.69**, respectively for such reactions (Scheme 1.3a).[67] Very recently, a group of Cabeza reported a silylene-Ir complex **1.67** for the C-D bond formation reaction of styrene and 1,3,5-trimethoxybenzene with CD_3OD via H/D-exchange (Scheme 1.3b).[67b]

The C-N cross-coupling reactions, termed as Buchwald-Hartwig amination reactions, have emerged as a general tool for the preparation of N-containing compounds with extensive applications in basic science and applied chemistry. Pd-salts are very useful metals for this reaction. Using bis(NHSi), the Driess group obtained Ni complexes **1.70a**,
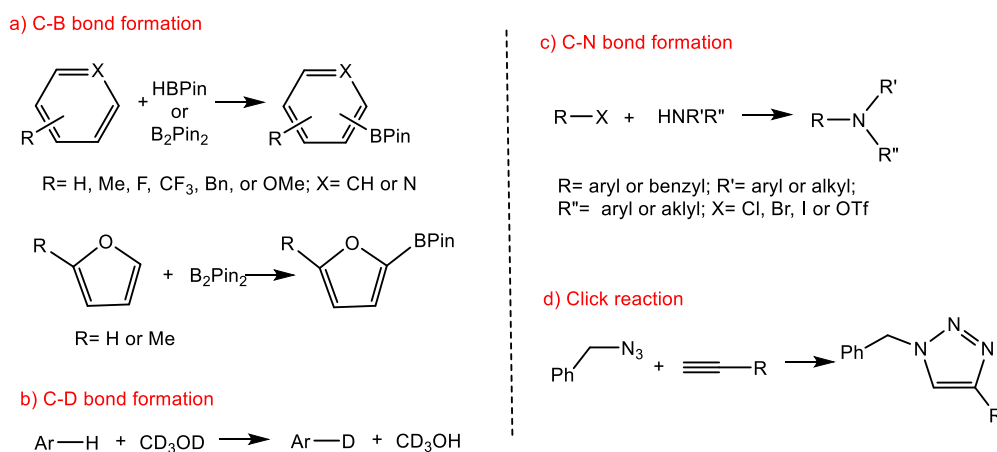
Scheme 1.3. *NHSi-transition metal-catalyzed C-X bond formation reactions.*

1.70b, and **1.71** and used them as efficient catalysts for C-N bond formation reaction of aryl halides with secondary amines in the presence of $AgBPh_4$ and KOtBu (1.3c).[68a]

Another C-N bond-forming reaction is the click reaction where two C-N bonds are generated to form a triazole ring. Very recently, the Stalke group utilized multinuclear NHSi-Cu(I) complexes (**1.72a** and **1.72b**) for azide-alkyne cycloaddition reactions (Scheme 1.3d).[68b]

1.7.3. Reduction reactions

Reduction reactions such as hydrosilylation of ketones, hydrogenation of olefins and carbonyl compounds, amide reduction and silylation of dinitrogen are of great significance in pharmaceuticals and fine organic molecules. NHSi-TM catalysts used for the reduction reactions are summarized in Chart 1.9. Driess group exploited NHSi supported Fe(0) complexes **1.73** and **1.74** for hydrosilylation of carbonyl compounds with good functional group tolerance towards discrete substituents in high yields (Scheme 1.4a).[69]
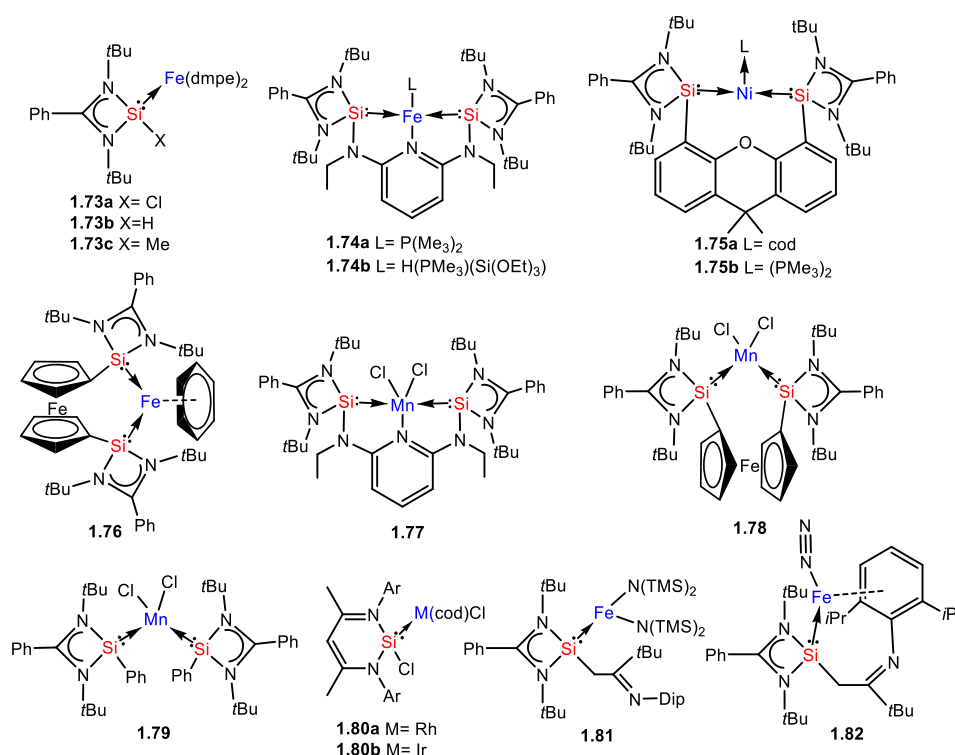
Chart 1.9. *Reported examples of NHSi-transition metal complexes for reduction reactions.*

The active catalyst **1.74b** displayed a different hydrosilylation mechanism where its coordinative saturation and steric effects prohibit Fe center involvement in the catalytic cycle.[69c] Surprisingly, the Lewis acidic Si(IV) centre attached to the Fe(II) atom plays a crucial role in activating the carbonyl compounds followed by a peripheral mechanism.

The same group in 2017 generated a xanthene based bis(NHSi) coordinated Ni(cod) (cod= cyclooctadiene) (**1.75a**) complex for the hydrogenation of olefins with excellent catalytic performance under mild reaction conditions (Scheme 1.4b).[70] Complex **1.75b** bearing the same ligand backbone with Ni(PMe$_3$)$_2$ was observed to be less productive. Hydrogenation of a series of ketones having electron-donating and -withdrawing substituents, bulkier, and unactivated aliphatic ketones by bis(NHSi) supported Fe(0) complex (**1.76**) coordinated with η^6-arene is reported by Oestreich and Driess groups to afford moderate to good product conversion (Scheme 1.4c).[71] Further development in the hydrogenation of unsaturated hydrocarbons was achieved by Driess and co-workers using NHSi stabilized Mn complexes **1.77**, **1.78** and **1.79** with different ligand backbones. Among them, the best result was obtained by **1.77** for the semi-hydrogenation reactions of various alkynes to afford E-alkenes selectively using NH$_3$BH$_3$ (Scheme 1.4d).[72]

In 2013, reduction of amides by six-membered NHSi supported Rh(I) (**1.80a**) and Ir(I) (**1.80b**) catalysts yielded selectively the C–O cleavage product (for **1.80a**)

a) Hydrosilylation of ketones
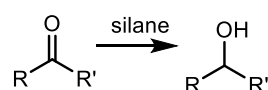
R= aryl or alkyl; R'= aryl or alkyl;
silane= (OEt)$_3$SiH or Ph$_2$SiH$_2$

b) Hydrogenation of olefins
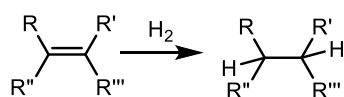
c) Hydrogenation of carbonyl compounds
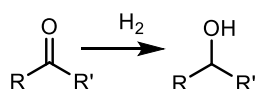
d) Semi hydrogenation of alkynes
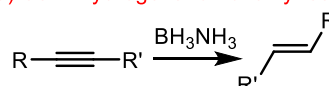
R= aryl; R'= aryl, alkyl or silyl

e) Amide reduction

f) Silylation of dinitrogen

N$_2$ + 6 TMSCl + 6 KC$_8$ $\xrightarrow{\text{-6 KCl}}$ 2 N(TMS)$_3$
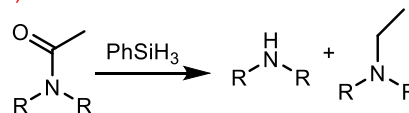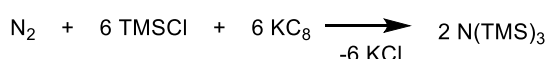
Scheme 1.4. *NHSi-transition metal-catalyzed reduction reactions.*

and both C–O and C–N cleavage products (for **1.80b**) (Scheme 1.4e). It was observed that the conversion rate is significantly higher for **1.80b** than the standard [Ir(Cl)cod]$_2$ complexes owing to the strong coordination with NHSi ligand.[73] Later, Cui and co-workers realized impressive progress by introducing three coordinated Fe(II) silylamido NHSi→Fe[N(SiMe$_3$)$_2$]$_2$ (**1.81**) and Fe(0) dinitrogen NHSi→Fe-N$_2$ (**1.82**) complexes for silylation of dinitrogen to furnish N(SiMe$_3$)$_3$ under N$_2$ (1 atm) atmosphere at the ambient condition with high TONs (Scheme 1.4f).[74]
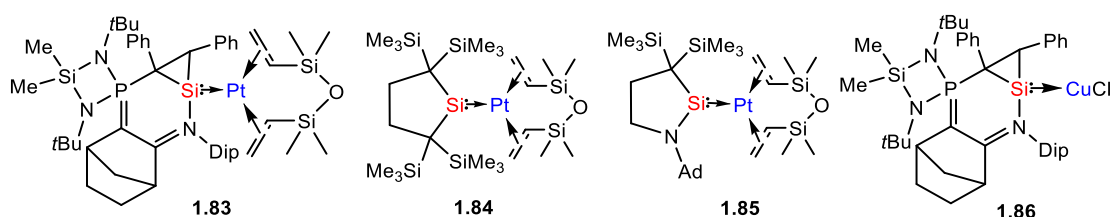
Chart 1.10. *Reported Silylene-TM (other than NHSis) complexes for homogeneous catalysis.*

Other than NHSi, few silylene-transition metals complexes used as catalyst for hydrosilylation of olefins and ketones (Chart 1.10). The groups of Baceiredo and Kato and the group of Iwamoto independently reported hydrosilylation of olefins such as 1-octene and functionalized terminal alkenes by utilizing Si(II)-Pt(0) complexes **1.83**, **1.84**, and **1.85** with high conversion rate.[75] Additionally, base stabilized Si(II)-Cu(I) complex (**1.86**) has been employed for hydrosilylation of bulky ketones.[75a]

The utilization of silylenes in transition-metal mediated organic transformation reactions are still in the primitive level and there is an open area to flourish them as a ligand in various homogeneous catalysis reactions.

1.8. Motivation and Objectives

The coinage metal (d^{10}) (Cu, Ag and Au) chemistry has attracted considerable attention in the last few decades due to their structural diversities, metallophilicity, rich photophysical properties, and catalytic applications. A variety of carbenes and phosphines and many more N, O, S donor ligand scaffolds are utilized to form a wide range of structural motifs combined with coinage metals and found to display efficient catalytic performance in various organic transformations over many years. As pointed out in section 1.6 of this chapter, silylenes can be a good competitor of phosphines and

NHCs due to their strong σ-donation and π-acceptance properties. However, the development of silylenes with transition metals (Mn, Fe, Ni, Co, Rh, Ir, Pd and Pt) as a catalyst is not that much scrutinized compared to phosphines and NHCs. In the case of coinage metals, the examples of silylene–Cu(I)/Ag(I)/Au(I) complexes are very limited and have hardly been explored in catalysis. Currently, there are only two available reports on the utilization of Si(II)-Cu(I) complexes in homogeneous catalysis such as hydrosilylation of ketones by the groups of Baceiredo and Kato,[75a] and alkyne–azide cycloaddition reaction by Stalke and co-workers.[68b] Whereas, NHSi-Au(I)/Ag(I) as a catalyst is still untouched in silylene chemistry. The underdeveloped field of silylene-coinage metal complexes motivate us to close the gap and flourish their fundamental bonding and catalytic applications.

Therefore, the first objective to achieve the goal is the stabilization of elusive double-bonded compound between Si and E (E= O, S, and Se) atom, which tend to undergo complexation reactions with Lewis acids such as CuX (X= Cl, Br) and BF$_3$ to form Lewis-acid base adducts due to the presence of a lone pair of electrons at the E centre. It is to be noted that the isolation of compounds containing Si=E group is very difficult due to easy polymerization and unfavourable orbital overlapping of Si and E atom. Particularly for oxygen (E= O), synthesis of the silicon analogue of acetamide (N-Si=O) can be achievable by utilizing the above Lewis acid-base adduct concept which is otherwise a challenging task due to the presence of an extremely reactive Si=O moiety.

Another objective of my doctoral research is to generate highly Lewis acidic Cu(I) or Au(I) cationic centre which will enhance the catalyst activity by interaction with olefins in the catalytic cycle. According to theoretical calculations, binding of Cu(I)/Au(I) with arene is significantly weaker than olefins and will generate a closest related complex of the naked [Cu/Au-(arene)]$^+$. Hence, our target is first to synthesize nearly naked NHSi stabilized mono-coordinate Cu(I)-arene and Au(I)-arene cationic complexes and investigate their fundamental bonding and coordination pattern with free arene ring in an acuity way. The weakly bound Cu(I)/Au(I)- free arene is the major driving force to activate the substrates in the catalytic cycle. Hence, the NHSi stabilized [Cu/Au-(arene)]$^+$ complexes can be employed as potential catalysts in various organic transformation reactions such as click reaction and glycosidaytion reaction. Such novel catalysts and their catalytic reactions will take one step ahead in silicon chemistry.

As discussed in section 1.6, NHSi-Pd complexes are employed in the C-C cross-coupling reaction and have never been explored for the C-N cross-coupling reaction. Hence, there is an open area of research on palladium-catalyzed C-N cross-coupling reactions using silylene as a ligand. Hence, we intend to introduce a bidentate ligand bearing two strong nucleophilic centres, Si(II) and P(III), which will boost the catalytic efficiency with Pd-salt in Buchwald-Hartwig amination reactions with broad substrate scope especially with the bulky class of substrates. The paucity of studies on the bulky substrate of amination reactions is another motivation of the work.

1.9.   References

1. Berzelius, J. J. *The Philosophical Magazine and Journal*. **1825**, *65*, 254–267.

2. Heywang, W.; Zaininger, K. H. Silicon Evolution and Future of a Technology. Springer-Verlag Berlin Heidelberg **2004**. *doi: 10.1007/978-3-662-09897-4.*

3. (a) Wiberg, N. *Lehrbuch der anorganischen Chemie*. 102. ed.; de Gruyter: Berlin, **2007**. (b) Brook, M. A., *Silicon in Organic, Organometallic, and Polymer Chemistry*. 1. ed.; John Wiley & Sons: Hoboken, **2000**. (c) Riedel, E.; Janiak, C., *Anorganische Chemie*. de Gruyter: Berlin, **2007**.

4. Periodictable   "Abundance   in   Earth's   Crust   of   the   elements". *http://periodictable.com/Properties/A/CrustAbundance.an.html* (04.01.2018).

5. Astrobio "Possibility of silicon-based life grows". *https://www.astrobio.net/news-exclusive/possibility-silicon-based-life-grows/* (04.01.2018).

6. Fischer, R. C.; Power, P. P. *Chem. Rev.* **2010**, *110*, 3877-3923.

7. (a) Wiberg, N. *Lehrbuch der anorganischen Chemie.* 102. ed.; de Gruyter: Berlin, **2007**. (b) Brook, M. A. *Silicon in Organic, Organometallic, and Polymer Chemistry.* 1. ed.; John Wiley & Sons: Hoboken, **2000**. (c) Riedel, E.; Janiak, C. *Anorganische Chemie.* de Gruyter: Berlin, **2007**.

8. Kipping, F. S.; Lloyd, L. L. *J. Chem. Soc.* **1901**, *79*, 449-459.

9. (a) Avakyan, V. G.; Sidorkin, V. F.; Belogolova, E. F.; Guselnikov, S. L.; Gusel'nikov, L. E. *Organometallics* **2006**, *25*, 6007-6013. (b) Kudo, T.; Nagase, S. *J. Am. Chem. Soc.* **1985**, *107*, 2589-2595.

10. Burkhard, C. A.; Rochow, E. G.; Booth, H. S.; Hartt, J. *Chem. Rev.* **1947**, *41*, 97-149.

11. (a) Gehrhus, B.; Lappert, M. F. *J. Organomet. Chem.* **2001**, *617-618*, 209-223. (b) Hill, N. J.; West, R. *J. Organomet. Chem.* **2004**, *689*, 4165-4183.

12. Power, P. P. *Nature.* **2010**, *463*, 171-177.

13. Power, P. P. *Chem. Rev.* **1999**, *99*, 3463–3503. (b) Gaspar, P. P.; West, R. *Silylene Chemistry of Organic Silicon Compounds 2,* Part 3 (eds Rappoport, Z. & Apeloig, Y.) **1998**, 2463–2568. (c) Mizuhata, Y.; Sasamori, T.; Tokitoh, N. *Chem. Rev.* **2009**, *109*, 3479–3511. (d) Linti, G.; Schnöckel, H. *Coord. Chem. Rev.* **2000**, *206–207*, 285–319. (e) Power, P. P. *Chem. Rev.* **2003**, *103*, 739–809. (f) Hicks, R. G. *Org. Mol. Biochem* **2007**, *5*, 1321–1338. (f) Ya. L. V.; Nakamoto, M.; Sekiguchi, A. *Chem. Lett.* **2008**, *37*, 128–133.

14. West, R.; Fink, M. J.; Michl, J. *Science* **1981**, *214*, 1343-1344.

15. (a) Matsuo, T.; Hayakawa, N. *Sci. Technol. Adv. Mater.* **2018**, *19*, 108 -129. (b) Fischer, R. C.; Power, P. P. *Chem. Rev.* **2010,** *110,* 3877–3923.

16. Sakamoto, K.; Obata, K.; Hirata, H.; Nakajima, M.; Sakurai, H. *J. Am. Chem. SOC.* **1989**, *111*, 7641-7643.

17. (a) Scheschkewitz, D. *Angew. Chem., Int. Ed.* **2004**, *43*, 2965. (b) Nguyen, T.; Scheschkewitz, D. *J. Am. Chem. Soc.* **2005**, *127*, 10174. (c) Abersfelder, K.; Güclü, D.; Scheschkewitz, D. *Angew. Chem., Int. Ed.* **2006**, *45*, 1643. (d) Scheschkewitz, D. *Angew. Chem., Int. Ed.* **2005**, *44*, 2954. (e) Inoue, M. Ichinohe, S.; Sekiguchi, A. *Angew. Chem., Int. Ed.* **2007**, *46*, 3346. (f) Bejan, I.; Güclü, D.; Inoue, S.; Ichinohe, M.; Sekiguchi, A.; Scheschkewitz, D. *Angew. Chem., Int. Ed.* **2007**, *46*, 3349. (g) Bejan, I.; Scheschkewitz, D. *Angew. Chem., Int. Ed.* **2007**, *46*, 5783.

18. Sekiguchi, A.; Kinjo, R.; Ichinohe, M. *Science* **2004**, *305*, 1755-1757.

19. (a) Wang, Y.; Xie, Y.; Wei, P.; King, R. B.; Schaefer, H. F., III; Schleyer, P. V. R.; Robinson, G. H. *Science* **2008**, *321*, 1069-1071. (b) Mondal, K. C.; Roesky, H. W.; Schwarzer, M. C.; Frenking, G.; Niepoetter, B.; Wolf, H.; Herbst-Irmer, R.; Stalke, D. *Angew. Chem., Int. Ed.* **2013**, *52*, 2963-2967.

20. (a) Ishida, S.; Iwamoto, T.; Kabuto, C.; Kira, M. *Nature.* **2003**, *421,* 725–727. (b) Tanaka, H.; Inoue, S.; Ichinohe, M.; Driess, M.; Sekiguchi, A. *Organometallics.* **2011**, *30*, 3475–3478.

21. (a) Wakita, K.; Tokitoh, N.; Okazaki, R.; Nagase, S. *Angew. Chem. Int. Ed.* **2000**, *39*, 364–636. (b) Kinjo, R.; Ichinohe, M.; Sekiguchi, A.; Takagi, N.; Sumimoto, M.; Nagase, S. *J. Am. Chem. Soc.* **2007**, *129*, 7766–7767. (c) Han, J. S.; Sasamori, T.; Mizuhata, Y.; Tokitoh, N. *Dalton Trans*. **2010**, *39*, 9238–9240.

22. Abersfelder, K.; White, A. J. P.; Rzepa, H. S.; Scheschkewitz, D. *Science.* **2010**, *327*, 564–566.

23. (a) Nukazawa, T.; Iwamoto, T. *J. Am. Chem. Soc.* **2020**, *142*, 9920–9924. (b) Yildiz, C. B.; Leszczyńska, K. I.; González-Gallardo, S.; Zimmer, M.; Azizoglu, A.; Biskup, T.; Kay, C. W. M.; Huch, V.; Rzepa, H. S.; Scheschkewitz, D. *Angew. Chem. Int. Ed. https://doi.org/10.1002/anie.202006283,* **2020**.

24. Jutzi, P.; Mix, A.; Rummel, B.; Schoeller, W. W.; Neumann, B.; Stammler, H.-G. *Science* **2004**, *305*, 849-851.

25. Mizuhata, Y.; Sasamori, T.; Tokitoh, N., *Chem. Rev.* **2009**, *109*, 3479-3511.

26. (a) Gaspar, P. P.; Xiao, M.; Pae, D. H.; Berger, D. J.; Haile, T.; Chen, T.; Lei, D.; Winchester, W. R.; Jiang, J. P. *J. Organomet. Chem.* **2002**, *646*, 68–79. (b) Apeloig, Y.; Pauncz, R.; Karni, M.; West, R.; Steiner, W.; Chapman, D. *Organometallics* **2003**, *22*, 3250–3256. (c) Mizuhata, Y.; Sasamori, T.; Tokitoh, N. *Chem. Rev.* **2009**, *109*, 3479–3511.

27. (a) Drahnak, T. J.; Michl, J.; West, R. *J. Am. Chem. Soc.* **1979**, 101, 5427–5428. (b) Weidenbruch, M. *Coord. Chem. Rev.* **1994**, 130, 275–300.

28. West, R.; Fink, M. J.; Michl, J. *Science* **1981**, *214*, 1343–1344.

29. Driess, M.; Grützmacher, H. *Angew. Chem., Int. Ed.* **1996**, *108*, 900-929.

30. (a) Grev, R. S.; Schaefer, H. F.; Gaspar, P. P. *J. Am. Chem. Soc.* **1991**, *113*, 5638-5643. (b) Sekiguchi, A.; Tanaka, T.; Ichinohe, M.; Akiyama, K.; Tero-Kubota, S. *J. Am. Chem. Soc.* **2003**, *125*, 4962-4963. (c) Sekiguchi, A.; Tanaka, T.; Ichinohe, M.; Akiyama, K.; Gaspar, P. P. *J. Am. Chem. Soc.* **2008**, *130*, 426-427.

31. Pae, D. H.; Xiao, M.; Chiang, M. Y.; Gaspar, P. P., *J. Am. Chem. Soc.* **1991**, *113*, 1281-1288.

32. Skell, P. S.; Goldstein, E. J., *J. Am. Chem. Soc.* **1964**, *86*, 1442-1443.

33. Jutzi, P.; Kanne, D.; Kruger, C., *Angew. Chem., Int. Ed.* **1986**, *25*, 164-165.

34. Denk, M.; Lennon, R.; Hayashi, R.; West, R.; Belyakov, A. V.; Verne, H. P.; Haaland, A.; Wagner, M.; Metzler, N., *J. Am. Chem. Soc.* **1994**, *116*, 2691-2692.

35. Kira, M.; Ishida, S.; Iwamoto, T.; Kabuto, C. *J. Am. Chem. Soc.* **1999**, *121*, 9722-9723.

36. Lee, G.-H.; West, R.; Müller, T. *J. Am. Chem. Soc.* **2003**, *125*, 8114-8115.

37. Driess, M.; Yao, S.; Brym, M.; Van Wuellen, C.; Lentz, D., *J. Am. Chem. Soc.* **2006**, *128*, 9628-9629.

38. (a) So, C.-W.; Roesky, H. W.; Magull, J.; Oswald, R. B. *Angew. Chem., Int. Ed.* **2006**, *45*, 3948–3950. (b) Sen, S. S.; Roesky, H. W.; Stern, D.; Henn, J.; Stalke, D. *J. Am. Chem. Soc.* **2010**, *132*, 1123–1126.

39. (a) Ghadwal, R. S.; Roesky, H. W.; Merkel, S.; Henn, J.; Stalke, D., *Angew. Chem., Int. Ed.* **2009**, *48*, 5683-5686. (b) Filippou, A. C.; Chernov, O.; Schnakenburg, G., *Angew. Chem.,*

Int. Ed. **2009**, *48*, 5687-5690. (c) Filippou, A. C.; Lebedev, Y. N.; Chernov, O.; Strassmann, M.; Schnakenburg, G., *Angew. Chem., Int. Ed.* **2013**, *52*, 6974-6978.

40. (a) Gau, D.; Kato, T.; Saffon-Merceron, N.; Cossío, F. P.; Baceiredo, A. *J. Am. Chem. Soc.* **2009**, *131*, 8762–8763. (b) Gau, D.; Kato, T.; Saffon-Merceron, N.; de Cózar, A.; Cossío, F. P.; Baceiredo, A. *Angew. Chem., Int. Ed.* **2010**, *49*, 6585–6588. (c) Gau, D.; Rodriguez, R.; Kato, T.; Saffon-Merceron, N.; de Cózar, A.; Cossío, F. P.; Baceiredo, A. *Angew. Chem., Int. Ed.* **2011**, *50*, 1092–1096. (d) Rodriguez, R.; Gau, D.; Contie, Y.; Kato, T.; Saffon-Merceron, N.; Baceiredo, A. *Angew. Chem., Int. Ed.* **2011**, *50*, 11492–11495.

41. (a) Asay, M.; Inoue, S.; Driess, M. *Angew. Chem., Int. Ed.* **2011**, *50*, 9589-9592. (b) Abe, T.; Tanaka, R.; Ishida, S.; Kira, M.; Iwamoto, T. *J. Am. Chem. Soc.* **2012**, *134*, 20029-20032.

42. (a) Rekken, B. D.; Brown, T. M.; Fettinger, J. C.; Tuononen, H. M.; Power, P. P. *J. Am. Chem. Soc.* **2012**, *134*, 6504−6507. (b) Protchenko, A. V.; Birjkumar, K. H.; Dange, D.; Schwarz, A. D.; Vidovic, D.; Jones, C.; Kaltsoyannis, N.; Mountford, P.; Aldridge, S. *J. Am. Chem. Soc.* **2012**, *134*, 6500−6503. (c) Protchenko, A. V.; Schwarz, A. D.; Blake, M. P.; Jones, C.; Kaltsoyannis, N.; Mountford, P.; Aldridge, S. *Angew. Chem., Int. Ed.* **2013**, *52*, 568−571. (d) Hadlington, T. J.; Abdalla, J. A. B.; Tirfoin, R.; Aldridge, S.; Jones, C. *Chem. Commun.* **2016**, *52*, 1717−1720. (e) Wendel, D.; Porzelt, A.; Herz, F. A. D.; Sarkar, D.; Jandl, C.; Inoue, S.; Rieger, B. *J. Am. Chem. Soc.* **2017**, *139*, 8134–8137. (f) Roy, M. M. D.; Ferguson, M. J.; McDonald, R.; Zhou, Y.; Rivard, E. *Chem. Sci.* **2019**, *10*, 6476–6481. (g) Loh, Y.; Ying, L.; Fuentes, M. Á.; Do, D. C. H.; Aldridge, S. *Angew. Chem., Int. Ed.* **2019**, *58*, 4847–4851.

43. Wang, Y.; Ma, J. *J. Organomet. Chem.* **2009**, *694*, 2567-2575.

44. Kosai, T.; Ishida, S.; Iwamoto, T.*Angew. Chem., Int. Ed.* **2016**, *128*, 15783-15787.

45. (a) Alvarado-Beltran, I.; Baceiredo, A.; Saffon-Merceron, N.; Branchadell, V.; Kato, T. *Angew. Chem., Int. Ed.* **2016**, *55,* 16141-16144. (b) Rosas-Sanchez, A.; Alvarado-Beltran, I.; Baceiredo, A.; Saffon-Merceron, N.; Massou, S.; Branchadell, V.; Kato, T. *Angew. Chem., Int. Ed.* **2017**, *56*, 10549-10554.

46. (a) Alvarado-Beltran, I.; Rosas-Sánchez, A.; Baceiredo, A.; Saffon-Merceron, N.; Branchadell, V.; Kato, T. *Angew. Chem., Int. Ed.* **2017**, *56*, 10481-10485. (b) Rosas-Sánchez, A.; Alvarado-Beltran, I.; Baceiredo, A.; Saffon-Merceron, N.; Massou, S.; Hashizume, D.; Branchadell, V.; Kato, T. *Angew. Chem., Int. Ed.* **2017**, *129*, 16132-16136.

47. For the five-membered unsaturated NHSis, see: (a) Mitra, A.; Brodovitch, J.-C.; Krempner, C.; Percival, P. W.; Vyas, P.; West, R. *Angew. Chem., Int. Ed.* **2010**, *49*, 2893–2895. (b) Kong, L.; Zhang, J.; Song, H.; Cui, C. *Dalton Trans.* **2009**, 5444–5446. (c) Zark, P.; Schäfer, A.; Mitra, A.; Haase, D.; Saak, W.; West, R.; Müller, T. *J. Organomet. Chem.* **2010**, *695*, 398–408. For the five-membered saturated NHSis, see: (d) West, R.; Denk, M. *Pure Appl. Chem.* **1996**, *68*, 785–788. (e) Schmedake, T. A.; Haaf, M.; Apeloig, Y.; Mueller, T.; Bukalov, S.; West, R. *J. Am. Chem. Soc.* **1999**, *121*, 9479–9480. (f) Li, W.; Hill, N. J.; Tomasik, A. C.; Bikzhanova, G.; West, R. *Organometallics* **2006**, *25*, 3802–3805. (g) Tomasik, A. C.; Mitra, A.; West, R. *Organometallics* **2009**, 28, 378–381. For the benzo and pyrido-fused five-membered NHSis, see: (h) Gehrhus, B.; Lappert, M. F.; Heinicke, J.; Boese, R.; Blaeser, D. *J. Chem. Soc., Chem. Commun.* **1995**, 1931–1932. (i) Heinicke, J.; Oprea, A.; Kindermann, M. K.; Karpati, T.; Nyulaszi, L.; Veszpremi, T. *Chem. Eur. J.* **1998**, 4, 541–545. (j) Gehrhus, B.; Hitchcock, P. B.; Lappert, M. F. *Z. Anorg. Allg. Chem.* **2005**, *631*, 1383–1386.

48. (a) Driess, M.; Yao, S.; Brym, M.; van Wuellen, C. *Angew. Chem., Int. Ed.* **2006**, *45*, 6730–6733. (b) Wang, R. -H.; Su, M. -D. *J. Phys. Chem. A* **2008**, *112*, 7689–7698. (c) Yao, S.; Brym, M.; van Wüllen, C.; Driess, M. *Angew. Chem., Int. Ed.* **2007**, *46*, 4159–4162.

49. (a) So, C.-W.; Roesky, H. W.; Gurubasavaraj, P. M.; Oswald, R. O.; Gamer, M. T.; Jones, P. G.; Blaurock, S. *J. Am. Chem. Soc.* **2007**, *129*, 12049–12054. (b) Yeong, H.-X.; Lau, K.-C.; Xi, H.-W.; Lim, K. H.; So, C.-W. *Inorg. Chem.*, **2010**, *49*, 371–373. (c) Zhang, S.-H.; Yeong, H.-X.; Xi, H.-W.; Lim, K. H.; So, C.-W. *Chem. Eur. J.*, **2010**, *16*, 10250–10254. (d) Sen, S. S.; Hey, J.; Herbst-Irmer, R.; Roesky, H. W.; Stalke, D. *J. Am. Chem. Soc.,* **2011**, *133*, 12311–12316. (e) Sarish, S. P.; Sen, S. S.; Roesky, H. W.; Objartel, I.; Stalke, D. *Chem. Commun.*, **2011**, *47*, 7206–7208. (f) Benedek, Z.; Szilvási, T. *RSC Adv.* **2015**, *5*, 5077–5086. (g) Azhakar, R.; Ghadwal, R. S.; Roesky, H. W.; Wolf, H.; Stalke, D. *Chem. Commun.,* **2012**, *48*, 4561–4563. (h) Mück, F. M.; Junold, K.; Baus, J. A.; Burschka, C.; Tacke, R. *Eur. J. Inorg. Chem.* **2013**, 5821 –5825. (i) Mück, F. M.; Kloß, D.; Baus, J. A.; Burschka, C.; Tacke, R. *Chem. Eur. J.* **2014**, *20*, 9620 –9626. (j) Mück, F. M.; Kloß, D.; Baus, J. A.; Burschka, C.; Bertermann, R.; Poater, Fonseca Guerra, J. C.; Bickelhaupt, F. M.; Tacke, R. *Chem. Eur. J.* **2015**, *21*, 14011–14021. (k) Rottschäfer, D.; Blomeyer, S.; Neumann, B.; Stammler, H.-G.; Ghadwal, R. S. *Chem. Eur. J.* **2018**, *24*, 380 –387. (l) Khan, S.; Pal, S.; Kathewad, N.; Purushothaman, I.; Deb, S.; Parameswaran, P. *Chem. Commun.* **2016**, *52*, 3880-3882.

50. (a) Sen, S. S.; Jana, A.; Roesky, H. W.; Schulzke, C. *Angew. Chem., Int. Ed.* **2009**, *48*, 8536–8538. (b) Zhou, Y.-P.; Driess, M. *Angew. Chem. Int. Ed.* **2019**, *58*, 3715 – 3728.

51. Shan, C.; Yao, S.; Driess, M. *Chem. Soc. Rev.* **2020**, *49*, 6733-6754.

52. (a) Sen, S. S.; Khan, S.; Roesky, H. W.; Kratzert, D.; Meindl, K.; Henn, J.; Stalke, D.; Demers, J. P.; Lange, A. *Angew. Chem., Int. Ed.* **2011**, *50*, 2322–2325. (b) Khan, S.; Michel, R.; Sen, S. S.; Roesky, H. W.; Stalke, D. *Angew. Chem., Int. Ed.* **2011**, *50*, 11786–11789.

53. Seitz, A. E.; Eckhardt, M.; Sen, S. S.; Erlebach, A.; Peresypkina, E. V.; Roesky, H. W.; Sierka, M.; Scheer, M. *Angew. Chem., Int. Ed.* **2017**, *56*, 6655–6659.

54. (a) Ghadwal, R. S.; Azhakar, R.; Roesky, H. W.; Propper, K.; Dittrich, B.; Klein, S.; Frenking, G. *J. Am. Chem. Soc.* **2011**, *133*, 17552–17555. (b) Mo, Z.; Szilvasi, T.; Zhou, Y. P.; Yao, S.; Driess, M. *Angew. Chem., Int. Ed.* **2017**, *56*, 3699–3702.

55. (a) Junold, K.; Nutz, M.; Baus, J. A.; Burschka, C.; Guerra, C. F.; Bickelhaupt, F. M.; Tacke, R. *Chem. Eur. J.* **2014**, *20*, 9319–9329. (b) Tacke, R.; Kobelt, C.; Baus, J. A.; Bertermann, R.; Burschka, C. *Dalton Trans.* **2015**, *44*, 14959–14974.

56. (a) Junold, K.; Nutz, M.; Baus, J. A.; Burschka, C.; Guerra, C. F.; Bickelhaupt, F. M.; Tacke, R. *Chem. Eur. J.* **2014**, *20*, 9319–9329. (b) Mück, F. M.; Baus, J. A.; Nutz, M.; Burschka, C.; Poater, J.; Bickelhaupt, F. M.; Tacke, R. *Chem. Eur. J.* **2015**, *21*, 16665–16672. (c) Mück, F. M.; Kloss, D.; Baus, J. A.; Burschka, C.; Bertermann, R.; Poater, J.; Guerra, C. F.; Bickelhaupt, F. M.; Tacke, R. *Chem. Eur. J.* **2015**, *21*, 14011–14021.

57. Meltzer, A.; Inoue, S.; Präsang, C.; Driess, M. *J. Am. Chem. Soc.* **2010**, *132*, 3038–3046.

58. Parvin, N.; Mishra, B.; George, A.; Neralkar, M.; Hossain, J.; Parameswaran, P.; Hotha, S.; Khan, S. *Chem. Commun.*, **2020**, *56*, 7625-7628.

59. Schmid, G.; Welz, E. *Angew. Chem.* **1977**, *89*, 823; *Angew. Chem., Int. Ed. Engl.* **1977**, *16*, 785.

60. (a) Raoufmoghaddam, S.; Zhou, Y.-P.; Wang, Y.; Driess, M. *Journal of Organometallic Chemistry* **2017**, *829*, 2-10. (b) Schmidt, M.; Blom, B.; Szilvási, T.; Schomäcker, R.; Driess, M. *Chem. Eur. J.* **2013**, *19,* 40–62.

61. Fgrstner, A.; Krause, H.; Lehmann, C. W. *Chem. Commun.* **2001**, 2372–2373.

62. Zhang, M.; Liu, X.; Shi, C.; Ren, C.; Ding, Y.; Roesky, H. W. *Z. Anorg. Allg. Chem.* **2008**, *634*, 1755–1758.

63. (a) Someya, C. I.; Haberberger, M.; Wang, W.; Enthaler, S.; Inoue, S.; *Chem. Lett.* **2013**, *42*, 286–288. (b) Tan, G.; Enthaler, S.; Inoue, S.; Blom, B.; Driess, M. *Angew. Chem. Int.*

Ed. **2015**, *54*, 2214–2218. (c) Qi, X.; Sun, H.; Li, X.; Fuhr, O.; Fenske, D. *Dalton Trans.* **2018**, *47*, 2581–2588.

64. D. Gallego, A. Brgck, E. Irran, F. Meier, M. Kaupp, M. Driess, J. F. Hartwig, *J. Am. Chem. Soc.* **2013**, *135*, 15617 –15626.

65. Wang, W.; Inoue, S.; Enthaler, S.; Driess, M. *Angew. Chem. Int. Ed.* **2012**, *51*, 6167–6171.

66. (a) Khoo, S.; Cao, J.; Yang, M.-C.; Shan, Y.-L.; Su, M.-D.; So, C.-W. *Chem. Eur. J.* **2018**, *24,* 14329–14334. (b) Mo, Z.; Kostenko, A.; Zhou, Y. P.; Yao, S.; Driess, M. *Chem. Eur.J.* **2018**, *24,* 14608 –14612.

67. (a) Brgck, A.; Gallego, D.; Wang, W.; Irran, E.; Driess, M.; Hartwig, J. F. *Angew. Chem. Int. Ed.* **2012**, *51*, 11478–11482. (b) Cabeza, J. A.; García-Álvarez, P.; González-Álvarez, L. *Chem. Commun.* **2017**, *53*, 10275–10278. (c) Ren, H.; Zhou, Y.-P.; Bai, Y.; Cui, C.; Driess, M. *Chem. Eur. J.* **2017**, *23*, 5663–5667.

68. (a) Zhou, Y.-P.; Raoufmoghaddam, S.; Szilvási, T.; Driess, M. *Angew. Chem. Int. Ed.* **2016**, *55*, 12868 –12872. (b) Paesch, A. N.; Kreyenschmidt, A.-K.; Herbst-Irmer, R.; Stalke, D. *Inorg. Chem.* **2019**, *58*, 7000–7009.

69. (a) Blom, B.; Enthaler, S.; Inoue, S.; Irran, E.; Driess, M. *J. Am. Chem. Soc.* **2013**, *135*, 6703–6713. (b) Gallego, D.; Inoue, S.; Blom, B.; Driess, M. *Organometallics* **2014**, *33*, 6885–6897. (c) Metsnen, T. T.; Gallego, D.; Szilvási, T.; Driess, M.; Oestreich, M. *Chem. Sci.* **2015**, *6*, 7143–7149.

70. Wang, Y.; Kostenko, A.; Yao, S.; Driess, M. *J. Am. Chem. Soc.* **2017**, *139*, 13499–13506.

71. Luecke, M.-P.; Porwal, D.; Kostenko, A.; Zhou, Y. P.; Yao, S.; Keck, M.; Limberg, C.; Oestreich, M.; Driess, M. *Dalton Trans.* **2017**, *46*, 16412–16418.

72. Zhou, Y. P.; Mo, Z.; Luecke, M. P.; Driess, M. *Chem. Eur. J.* **2018**, *24*, 4780–4784.

73. Stoelzel, M.; Präsang, C.; Blom, B.; Driess, M.; *Aust. J. Chem.* **2013**, *66*, 1163–1170.

74. Bai, Y.; Zhang, J.; Cui, C. *Chem. Commun.* **2018**, *54*, 8124–8127.

75. (a) Troadec, T.; Prades, A.; Rodriguez, R.; Mirgalet, R.; Baceiredo, A.; Saffon-Merceron, N.; Branchadell, V.; Kato, T. *Inorg. Chem.* **2016**, *55*, 8234–8240. (b) Iimura, T.; Akasaka, N.; Iwamoto, T. *Organometallics* *2016*, *35*, 4071–4076. (c) Iimura, T.; Akasaka, N.; Kosai, T.; Iwamoto, T. *Dalton Trans.* **2017**, *46*, 8868–8874.

*****

Chapter 2

Synthesis and Characterization of Lewis acid–base adducts Si(II)=E→LA (E= O, S, Se; LA= CuCl, CuBr, BF$_3$)

Chapter 2A

Unique Approach to Cu(I) Silylene

Chalcogenone Complexes

2A.1. Introduction

Ketones are one of the most important functional groups in organic chemistry. However it was assumed for many years that the heavier double-bonded compounds between silicon and chalcogen would not exist as stable species due to their higher reactivity and relatively poor pπ-pπ overlap between chalcogens and silicon atoms. [1] In 1989, Corriu et al. reported the first stable diaryl-Si-thiones and diaryl-Si-selones **2A.Ia-2A.Ic** (Chart 2A.1a).[2] Subsequently, Tokitoh, Okazaki, and their coworkers synthesized and characterized a series of kinetically stable heavier diaryl-Si-chalcogenones **2A.IIa-2A.IId** using sterically hindered aromatic groups.[3] Since then numerous examples of compounds containing a Si chalcogen double bond have been reported, thanks to extensive work from the groups of Kira (**2A.III**), West (**2A.IV**), Driess (**2A.V** and **2A.VI**), and others.[4] With these compounds in hand, one can envisage to use these Si-chalcogenones as ligands in transition metal chemistry. It has also been known for some time that aldehydes and ketones can serve as ligands in transition metal complexes.[5] In fact, the frequent use of acetone often led to serendipitous acetone complexes such as $[(\eta^5\text{-}C_5H_5)Re(NO)(PPh_3)(\eta^1\text{-}(CH_3)_2C{=}O)]^+PF_6^-$ or $[Fe(C_{19}H_{25}N_5)(C_3H_6O)(H_2O)_2](BF_4)_2 \cdot 2C_3H_6O$.[6] There are several reports where Si=O double-bonded compounds were isolated as adducts with transition metals;[7] however, other Si=E (E = S, Se, Te) bonded compounds were not explored for such complexation. The only available report on Si=S→LA type (LA= Lewis acid) linkage is observed in a monomeric silicon disulfide (SiS_2) **2A.VII**[8a] stabilized by the Lewis acid $GaCl_3$ (Chart 2A.1b). The same ligand system was further used to isolate the germanium analogue of **2A.VII.**[8b]

In 2007, we synthesized and characterized a silicon thioester with the Si(=S)-S skeleton by using benzamidinato-chlorosilylene $[PhC(N{t}Bu)_2SiCl]$.[9] Furthermore this silylene was utilized for preparing the functionalized silylene $[PhC(N{t}Bu)_2SiN(SiMe_3)_2]$[10] (**1.14b**) in high yield. However, **1.14b** is yet to be explored for preparing Si-chalcogenones. The first aim of our investigation focused on the reactivity of **1.14b** towards chalcogens (E= S, Se). When we observed that compound **1.14b** can smoothly afford the formation of silylene-S-thione (**2A.2**) and silylene-Se-selone (**2A.3**), we investigated the donating abilities of the Si-chalcogenones toward transition metals. The reaction of CuCl and CuBr resulted in the monomeric Lewis acid-base adducts **2A.4**, **2A.5**, **2A.6,** and **2A.7** respectively.

It must be noted here that this is the first report on a sterically encumbered silicon-based chalcogenone donor ligand for the synthesis of low-coordinate transition metal complexes. Moreover, the present study pointed to a distinctly superior donating ability of silylene-chalcogenones over silylenes as the latter were found to form dimeric complexes with transition metals from analogous reactions.
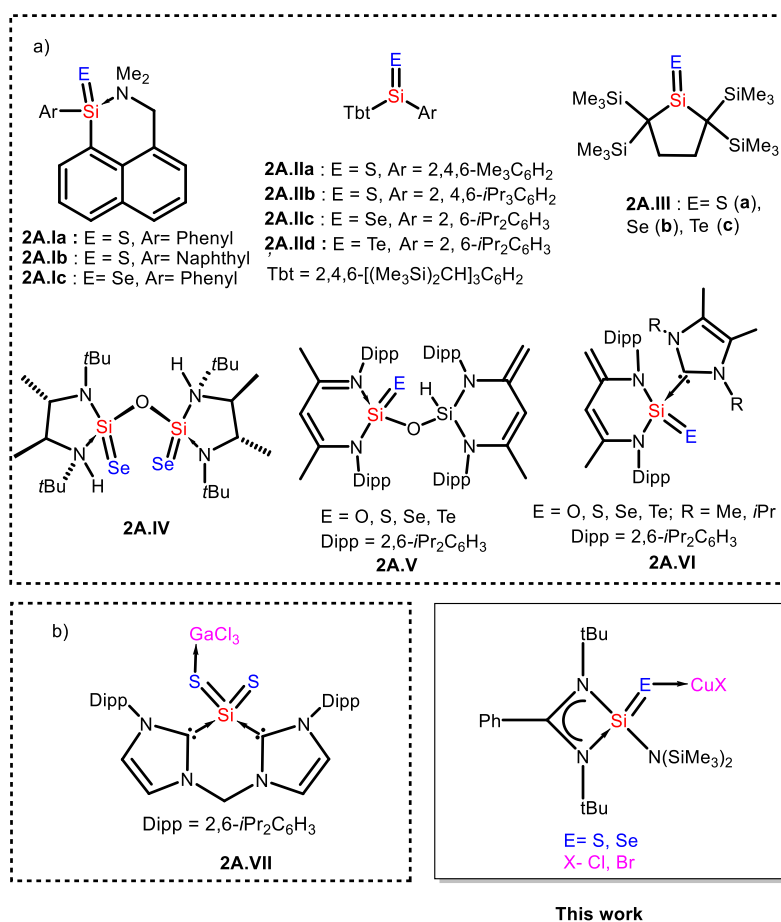
Chart 2A.1. *a) Reported compounds with a double bond involving chalcogens and silicon atoms. b) Lewis acid-base adduct with Si-bisthione.*

2A.2. Experimental Section

2A.2.1. General Remarks

All experiments were carried out under dry oxygen free dinitrogen using standard Schlenk techniques and in a dinitrogen filled MBRAUN MB 150-G1 glovebox. The solvents used were purified by MBRAUN solvent purification system MB SPS-800. The starting material **1.14b, 2A.8, 2A.9, 2A.10** and **2A.12** were prepared by literature method. All

other chemicals purchased from Aldrich were used without further purification. ^{1}H, ^{13}C, ^{29}Si and ^{77}Se NMR spectra were recorded in CDCl$_3$ using Bruker 400 MHz spectrometer with an external standard (SiMe$_4$ for ^{1}H, ^{13}C, ^{29}Si and SeMe$_2$ for ^{77}Se). Concentrated solutions of the samples in CDCl$_3$ were sealed off in an NMR tube for measurement. All the heteronuclear NMRs are proton decoupled. Mass spectra were recorded using AB Sciex, 4800 plus MALDI TOF/TOF and HRMS.

2A.2.2. Synthesis of **2A.2-2A.9, 2A.11, 2A.13- 2A.15**

Synthesis of 2A.2: Toluene (40 mL) was added to the mixture **1.14b** (0.210 g, 0.5 mmol) and 1/8th equivalent of S$_8$ (0.016g, 0.5 mmol) in a 100 mL Schlenk flask and the solution of the reaction mixture became pale yellow after 2 h. It was stirred overnight at room temperature and the solution was filtered, concentrated to 10 mL and kept it at 0 °C to afford colorless crystals of **2A.2** suitable for single crystal X-ray analysis. Yield: 66% (0.148 g). Mp: 193-196 °C. ^{1}H NMR (400 MHz, CDCl$_3$, 298K): δ 0.41 (*s*, 9H, Si*Me$_3$*), 0.55 (*s*, 9H, Si*Me$_3$*), 1.30 (s, 18H, C*Me$_3$*), 7.41-7.58 (*m*, 5H, Ph) ppm. ^{13}C {^{1}H} NMR (100.613 MHz, CDCl$_3$, 298 K): δ 5.15 (Si*Me$_3$*), 6.56 (Si*Me$_3$*), 31.02 (C*Me$_3$*), 55.31 (*C*Me$_3$), 127.32, 127.59, 128.07, 128.18, 130.08, 130.66 (Ph-*C*), 173.93 (N*C*N) ppm. ^{29}Si {^{1}H} NMR (79.495 MHz, CDCl$_3$, 298 K): δ 6.26 (*Si*Me$_3$), 1.69 (*Si*Me$_3$), -16.82 (*Si*N(SiMe$_3$)$_2$). HRMS *m/z* (C$_{21}$H$_{41}$N$_3$Si$_3$S): 452.2405 (100%) [M]$^+$. Anal. Calcd: C, 55.82; H, 9.15; N, 9.30; S, 7.09. Found: C, 55.95; H, 8.92; N, 9.67; S, 6.79.

Synthesis of 2A.3: 40 mL toluene was added to a 100 mL Schlenk flask containing mixture of **1.14b** (0.210 g, 0.5 mmol) and Se powder (0.039 g, 0.5 mmol) and the solution of the reaction mixture became colorless after 4 h. It was stirred overnight at room temperature and the solution was filtered, concentrated to 10 mL and kept it at 0 °C to afford colorless crystals of **2A.3**. Yield: 70% (0.175 g). Mp: 220-223 °C. ^{1}H NMR (400 MHz, CDCl$_3$, 298K): δ 0.43 (*s*, 9H, Si*Me$_3$*), 0.60 (*s*, 9H, Si*Me$_3$*), 1.34 (*s*, 18H, C*Me$_3$*), 7.42-7.59 (*m*, 5H, Ph). ^{13}C {^{1}H} NMR (100.613 MHz, CDCl$_3$, 298 K): δ 5.31 (Si*Me$_3$*), 6.89 (Si*Me$_3$*), 31.08 (C*Me$_3$*), 55.60 (*C*Me$_3$), 127.46, 128.03, 128.12, 130.11, 130.71 (Ph-*C*), 173.26 (N*C*N). ^{29}Si {^{1}H} NMR (79.495 MHz, CDCl$_3$, 298 K): δ 8.40 (*Si*Me$_3$), 2.78 (*Si*Me$_3$), -20.22 (*Si*N(SiMe$_3$)$_2$). ^{77}Se {^{1}H} NMR (76.311 MHz, CDCl$_3$, 298): δ -458.42 ppm. HRMS *m/z* (C$_{21}$H$_{41}$N$_3$Si$_3$Se): 500.1852 (100%) [M]$^+$. Anal. Calcd: C, 50.57; H, 8.29; N, 8.42. Found: C, 50.75; H, 8.22; N, 8.91.

Synthesis of 2A.4: Toluene (40 mL) was added to the mixture **2A.2** (0.225 g, 0.5 mmol) and CuCl (0.050g, 0.5 mmol) in a 100 mL Schlenk flask and the solution of the reaction

mixture became colorless after overnight stirring at room temperature. Then the reaction mixture was filtered, reduced the volume under vaccuo and kept it at 0 °C to afford colorless crystals of **2A.4**. Yield: 60% (0.165g). Mp: 191-194 °C. ^{1}H NMR (400 MHz, CDCl$_3$, 298K): δ 0.47 (*s*, 9H, Si*Me$_3$*), 0.53 (*s*, 9H, Si*Me$_3$*), 1.37 (*s*, 18H, C*Me$_3$*), 7.38-7.67 (*m*, 4H, Ph), 8.36-8.43 (*m*, 1H, Ph) ppm. ^{13}C {^{1}H} NMR (100.613 MHz, CDCl$_3$, 298 K): δ 5.17 (Si*Me$_3$*), 6.09 (Si*Me$_3$*), 31.48 (C*Me$_3$*), 56.43 (*C*Me$_3$), 126.30, 127.83, 128.27, 128.58, 129.13, 131.35 (Ph-*C*), 177.59 (N*C*N) ppm. ^{29}Si {^{1}H} NMR (79.495 MHz, CDCl$_3$, 298 K): δ 10.74 (*Si*Me$_3$), 4.63 (*Si*Me$_3$), -14.96 (*Si*N(SiMe$_3$)$_2$). HRMS *m/z* (C$_{21}$H$_{41}$N$_3$Si$_3$SCuCl): 550.4680 (100%) [M]$^+$. Anal Calcd: C, 45.79; H, 7.50; N, 7.63. Found: C, 45.56; H, 7.67; N, 7.33.

Synthesis of 2A.5: Toluene (40 mL) was added to the mixture **2A.2** (0.225 g, 0.5 mmol) and CuBr (0.074 g, 0.5 mmol) in a 100 mL Schlenk flask and the solution of the reaction mixture became colorless after overnight stirring at room temperature. Then the reaction mixture was filtered using frit and concentrated to 10 mL and kept it at 0 °C to afford colorless crystals of **2A.5**. Yield: 58% (0.172g). Mp: 174-176 °C. ^{1}H NMR (400 MHz, CDCl$_3$, 298K): δ 0.47 (*s*, 9H, Si*Me$_3$*), 0.53 (*s*, 9H, Si*Me$_3$*), 1.37 (*s*, 18H, C*Me$_3$*), 7.39-7.44 (*m*, 1H, Ph), 7.46-7.53 (*m*, 1H, Ph), 7.55-7.67 (*m*, 2H, Ph), 8.39-8.45 (*m*, 1H, Ph) ppm. ^{13}C {^{1}H} NMR (100.613 MHz, CDCl$_3$, 298 K): δ 5.19 (Si*Me$_3$*), 6.12 (Si*Me$_3$*), 31.52 (C*Me$_3$*), 56.43 (*C*Me$_3$), 126.31, 127.87, 128.22, 128.77, 129.03, 131.37 (Ph-*C*), 177.53 (N*C*N) ppm. ^{29}Si {^{1}H} NMR (79.495 MHz, CDCl$_3$, 298 K): δ 11.09 (*Si*Me$_3$), 2.61 (*Si*Me$_3$), -17.19 (*Si*N(SiMe$_3$)$_2$). HRMS *m/z* (C$_{21}$H$_{41}$N$_3$Si$_3$SCuBr): 452.2406 [M-CuBr]$^+$. Anal Calcd: C, 42.37; H, 6.94; N, 7.06, S, 5.39. Found: C, 42.57; H, 7.10; N, 6.77; S, 5.23.

Synthesis of 2A.6: Toluene (40 mL) was added to the mixture **2A.3** (0.250 g, 0.5 mmol) and CuCl (0.050g, 0.5 mmol) in a 100 mL Schlenk flask and the solution of the reaction mixture became colorless after overnight stirring at room temperature. Then the reaction mixture was filtered and concentrated to 15 mL and kept it at 0 °C to afford colorless crystals of **2A.6**. Yield: 61% (0.182 g). Mp: 178-182 °C. ^{1}H NMR (400 MHz, CDCl$_3$, 298K): δ 0.48 (*s*, 9H, Si*Me$_3$*), 0.57 (*s*, 9H, Si*Me$_3$*), 1.40 (*s*, 18H, C*Me$_3$*), 7.39-7.52 (*m*, 2H, Ph), 7.54-7.70 (*m*, 2H, Ph), 8.48 (*d*, *J*= 7.6 Hz, 1H, Ph). ^{13}C {^{1}H} NMR (100.613 MHz, CDCl$_3$, 298 K): δ 5.36 (Si*Me$_3$*), 6.42 (Si*Me$_3$*), 31.52 (C*Me$_3$*), 56.67 (*C*Me$_3$), 126.44, 127.78, 128.32, 128.62, 129.17, 131.37 (Ph-*C*), 177.03 (N*C*N). ^{29}Si {^{1}H} NMR (79.495 MHz, CDCl$_3$, 298 K): δ 11.37 (*Si*Me$_3$), 5.57 (*Si*Me$_3$), -19.79 (*Si*N(SiMe$_3$)$_2$). ^{77}Se {^{1}H} NMR (76.311 MHz, CDCl$_3$, 298): δ -466.68 ppm. HRMS *m/z* (C$_{21}$H$_{41}$N$_3$Si$_3$SeCuCl): 598.3542 (100%) [M]$^+$. Anal Calcd: C, 42.19; H, 6.91; N, 7.03. Found: C, 41.96; H, 6.69; N, 7.58.

Synthesis of 2A.7: Toluene (40 mL) was added to the mixture **2A.3** (0.250 g, 0.5 mmol) and CuBr (0.074g, 0.5 mmol) in a 100 mL Schlenk flask and the solution of the reaction mixture became colorless after overnight stirring at room temperature. Then the reaction mixture was filtered and concentrated to 15 mL and kept it at 0 °C to afford colorless crystals of **2A.7**. Yield: 55% (0.176 g). Mp: 195-197 °C. ^{1}H NMR (400 MHz, CDCl$_3$, 298K): δ 0.48 (*s*, 9H, Si*Me$_3$*), 0.57 (*s*, 9H, Si*Me$_3$*), 1.40 (*s*, 18H, C*Me$_3$*), 7.40-7.45 (*m*, 1H, Ph), 7.46-7.52 (*m*, 1H, Ph), 7.56-7.68 (*m*, 2H, Ph), 8.49(*d*, *J*= 7.6 Hz, 1H, Ph). ^{13}C {^{1}H} NMR (100.613 MHz, CDCl$_3$, 298 K): δ 5.39(Si*Me$_3$*), 6.46 (Si*Me$_3$*), 31.56 (C*Me$_3$*), 56.68 (*C*Me$_3$), 126.46, 127.87, 128.27, 128.83, 129.04, 131.41 (Ph-*C*), 176.98 (N*C*N). ^{29}Si {^{1}H} NMR (79.495 MHz, CDCl$_3$, 298 K): δ 11.34 (*Si*Me$_3$), 5.59 (*Si*Me$_3$), -19.92 (*Si*N(SiMe$_3$)$_2$). ^{77}Se {^{1}H} NMR (76.311 MHz, CDCl$_3$, 298): - 454.80 ppm. MALDI-MS *m/z* (C$_{21}$H$_{41}$N$_3$Si$_3$SeCuBr): 642.67 (20%) [M]$^+$. Anal Calcd: C, 39.27; H, 6.43; N, 6.54. Found: C, 39.09; H, 6.31; N, 7.10.

Synthesis of 2A.8: Compound **1.14b** (0.419 g, 1 mmol) and CuCl (0.100g, 1 mmol) were taken in a 100 mL Schlenk flask and 40 mL toluene was added to it. The solution became colorless after 7 hour stirring at room temperature. Then it was filtered, concentrated, and stored at 0 °C overnight to afford colorless crystals of **2A.8**. Yield: 65% (0.350 g). Mp: 110-114 °C. ^{1}H NMR (400 MHz, CDCl$_3$, 298K): δ 0.23 (*s*, 18H, Si*Me$_3$*), 0.46 (*s*, 18H, Si*Me$_3$*), 1.18 (*s*, 36H, C*Me$_3$*), 7.06-7.13 (*m*, 2H, *Ph*), 7.22-7.27 (*m*, 2H, Ph), 7.29-7.35 (*m*, 2H, Ph), 7.39-7.45 (*m*, 4H, Ph) ppm; ^{13}C {^{1}H} NMR (100.613 MHz, CDCl$_3$, 298 K): δ 3.57 (Si*Me$_3$*), 4.97 (Si*Me$_3$*), 30.83 (C*Me$_3$*), 53.68 (*C*Me$_3$), 124.28, 126.22, 127.12, 127.20, 127.37, 128.01, 129.73, 130.00, 131.31, 136.84 (Ph-*C*), 167.40 (N*C*N) ppm. ^{29}Si {^{1}H} NMR (79.495 MHz, CDCl$_3$, 298 K): δ 4.79 (*Si*N(SiMe$_3$)$_2$); 6.78 (*Si*Me$_3$); 7.17 (*Si*Me$_3$) ppm. MALDI: *m/z* (C$_{42}$H$_{82}$Cu$_2$Cl$_2$N$_6$Si$_6$): 1035.43 [M+H]$^+$. Anal. Calcd. C, 48.62; H, 7.97; N, 8.10. Found: C, 48.49; H, 7.78; N, 8.08.

Synthesis of 2A.9: 40 mL toluene was added into the mixture of compound **1.14b** (0.419 g, 1 mmol) and CuBr (0.145 g, 1 mmol) in a 100 mL Schlenk flask. After 30 min the solution became colorless. It was stirred overnight at room temperature and was filtered and concentrated. Colorless crystals of **2A.9** were found at 0 °C. Yield: 65% (0.400 g). Mp: 145-150 °C. ^{1}H NMR (400 MHz, CDCl$_3$, 298K): δ 0.24 (*s*, 18H, Si*Me$_3$*), 0.46 (*s*, 18H, Si*Me$_3$*), 1.19 (*s*, 36H, C*Me$_3$*), 7.07-7.13 (*m*, 3H, Ph), 7.23-7.29 (*m*, 2H, Ph), 7.36-7.49 (*m*, 5H, Ph) ppm. ^{13}C {^{1}H} NMR (100.613 MHz, CDCl$_3$, 298 K): δ 3.56 (Si*Me$_3$*), 4.92 (Si*Me$_3$*), 30.81 (C*Me$_3$*), 53.67 (*C*Me$_3$), 124.28, 126.36, 127.12, 127.18, 127.20, 128.01, 129.69, 130.05, 136.84 (Ph-*C*); 167.25 (N*C*N) ppm. ^{29}Si {^{1}H} NMR (79.495 MHz, CDCl$_3$, 298 K): δ 5.72

(*Si*N(SiMe$_3$)$_2$); 6.80 (*Si*Me$_3$); 7.15 (*Si*Me$_3$) ppm. HRMS: *m/z* (C$_{42}$H$_{82}$Cu$_2$Br$_2$N$_6$Si$_6$): 1122.6686 [M]$^+$. Anal. Calcd. C, 44.78; H, 7.34; N, 7.46. Found: C, 44.76; H, 7.54; N, 7.64.

Synthesis of 2A.11: 60 mL toluene was added to the mixture of **2A.10** (0.460 g, 0.5 mmol) and 1/8th equivalent of S$_8$ (0.016 g, 0.5 mmol) and it was stirred overnight. The pale brown colored solution was filtered off and partially reduced in vaccuo. Storage of the solution at 0 °C afforded colorless crystals of **2A.11**. Yield: 80% (0.380 g). Mp: 326-331°C. ^{1}H NMR (400 MHz, CDCl$_3$, 298K): δ 2.24 (*s*, 6H, C*H*$_3$), 5.30 (s, 2H, *H*$_{Im}$), 5.47 (*s*, 4H, C*H*Ph$_2$), 6.82-6.92 (*m*, 12H, Ph), 7.07-7.38 (*m*, 44H, Ph) ppm. ^{13}C {^{1}H} NMR (100.613 MHz, CDCl$_3$, 298 K): δ 21.84 (*C*H$_3$), 51.71 (*C*HPh$_2$), 118.74 (*C*H$_{Im}$), 125.29, 126.24, 126.38, 128.08, 128.20, 129.03, 129.35, 129.98, 130.24, 133.12, 139.28, 141.70, 142.76, 143.50 (Ph-*C*), 165.47 (*C*$_{carbene}$) ppm. HRMS *m/z* (C$_{69}$H$_{56}$N$_2$S): 945.4424 (100%) [M]$^+$. Anal Calcd: C, 87.67; H, 5.97; N, 2.96; S, 3.39. Found: C, 87.30; H, 5.99; N, 2.68; S, 3.38.

Synthesis of 2A.13: 60 mL toluene was added to the mixture of **2A.11** (0.475g, 0.5 mmol) and CuCl (0.074g, 0.5 mmol) and it was stirred overnight. The pale brown colored solution was filtered and partially reduced to ~10 ml in vaccuo. Storage of the solution at 0 °C afforded colorless crystals of **2A.13**. Yield: 75% (0.410 g). Mp: 316-320 °C. ^{1}H NMR (400 MHz, CDCl$_3$, 298K): δ 2.24 (*s*, 6H, C*H*$_3$), 5.30 (*s*, 2H, *H*$_{Im}$), 5.48 (*s*, 4H, C*H*Ph$_2$), 6.83-6.90 (*m*, 12H, Ph), 7.08-7.27 (*m*, 35H, Ph), 7.30-7.38 (*m*, 9H, Ph) ppm. ^{13}C {^{1}H} NMR (100.613 MHz, CDCl$_3$, 298 K): δ 21.84 (*C*H$_3$), 51.71 (*C*HPh$_2$), 118.74 (*C*H$_{Im}$), 125.30, 126.25, 126.38, 128.08, 128.20, 129.03, 129.35, 129.99, 130.25, 133.12, 137.87, 139.29, 141.70, 142.76, 143.51 (Ph-*C*), 165.47 (*C*$_{carbene}$) ppm. MALDI *m/z* (C$_{69}$H$_{56}$N$_2$SCuBr): 1007.39 [M-Br]$^+$. Anal Calcd: C, 76.12; H, 5.18; N, 2.57; S, 2.94. Found: C, 76.42; H, 5.97; N, 2.57; S, 2.95.

Synthesis of 2A.14: 50 mL toluene was added to the mixture of **2A.12** (0.500 g, 0.5 mmol) and CuBr (0.074g, 0.5 mmol) and it was stirred overnight. The pale brown colored solution was filtered off and concentrated to reduce the volume in vaccuo. Storage of the solution at 0 °C afforded colorless crystals of **2A.14**. Yield: 70% (0.400 g). Mp: 320-325 °C. ^{1}H NMR (400 MHz, CDCl$_3$, 298K): δ 2.21 (*s*, 6H, C*H*$_3$), 5.16 (*s*, 2H, *H*$_{Im}$), 5.40 (*s*, 4H, C*H*Ph$_2$), 6.74-6.86 (*m*, 15H, Ph), 7.03-7.20 (*m*, 34H, Ph), 7.32-7.40 (*m*, 7H, Ph) ppm. ^{13}C {^{1}H} NMR (100.613 MHz, CDCl$_3$, 298 K): δ 21.97 (*C*H$_3$), 51.79 (*C*HPh$_2$), 120.90 (*C*H$_{Im}$), 125.38, 126.36, 126.52, 128.16, 128.27, 129.12, 129.43, 130.15, 130.40, 131.68, 133.86, 139.53, 141.58, 142.83, 143.46 (Ph-*C*), 166.05 (*C*$_{carbene}$) ppm. ^{77}Se {^{1}H} NMR (76.311 MHz, CDCl$_3$, 298): δ -276.84 ppm. MALDI *m/z* (C$_{69}$H$_{56}$N$_2$SeCuBr): 1055.13 [M-Br]$^+$.

Synthesis of 2A.15: 60 mL toluene was added to the mixture of **2A.10** (0.460 g, 0.5 mmol) and CuBr (0.074 g, 0.5 mmol) and it was stirred overnight. The colorless solution was filtered off using frit and partially reduced in vaccuo. Storage of the solution at 0 °C afforded colorless crystals of **2A.15**. Yield: 79% (0.420 g). Mp: 288-290 °C. ^{1}H NMR (400 MHz, CDCl$_3$, 298K): δ 2.16 (*s*, 6H, C*H*$_3$), 5.13 (*s*, 4H, C*H*Ph$_2$), 5.79 (*s*, 2H, *H*$_{Im}$), 6.35-7.64 (*m*, 53H, Ph) ppm. ^{13}C {^{1}H} NMR (100.613 MHz, CDCl$_3$, 298 K): δ 21.74 (*C*H$_3$), 51.09 (*C*HPh$_2$), 123.13 (*C*H$_{Im}$), 126.51, 126.58, 128.30, 128.55, 129.32, 129.48, 130.11, 134.04, 139.98, 140.81, 142.21, 142.97 (Ph-*C*), 160.51 (*C*$_{carbene}$) ppm. MALDI *m/z* (C$_{69}$H$_{56}$N$_2$CuBr) 975.23 [M-Br]$^+$. Anal Calcd: C, 78.43; H, 5.34; N, 2.65. Found: C, 78.19; H, 5.36; N, 2.68.

2A.2.3. X-ray crystallographic Details

Single crystals of suitable size, were coated with paraffin oil was mounted for all the complexes. Crystal data for all the complexes were collected on a Bruker Smart Apex Duo diffractometer at 100 K using Mo Kα radiation (λ = 0.71073 A). Collected data were integrated by using SAINT and then absorption correction was done by multi-scan method using SADABS program All the structures were solved by direct methods and refined by fullmatrix least-squares methods against F2 (SHELXL-2014/6).

2A.2.4 Computational details

Molecular geometries of all model complexes are optimized using the Becke's three-parameter hybrid exchange and Lee‑Young‑Parr correlation functional (B3LYP). The Stuttgart/Dresden effective core potential along with the SDD basis set is used on Cu atom. For all the other atoms, the 6‑31G(d) basis set is employed. Each optimized structure is characterized by harmonic vibrational frequency analysis. For accurate energy predictions, single point energy calculations are performed on the B3LYP/(SDD,6-31G(d)) optimized structures at the M06/(SDD,6-311+G(d,p)) level of theory. All thermochemical data are estimated within the ideal gas rigid-rotor-harmonic oscillator approximation at 293.15 K. Solvent effects (toluene) are taken into account within SMD solvation model. Due to large molecular size, the *t*Bu groups in [{PhC(N*t*Bu)$_2$}Si{N(SiMe$_3$)$_2$}] (**1.14b**) are replaced by methyl groups. This does not impose any major structural changes as found in our initial test calculations involving the full structures of a few selected silylene complexes. Thus, [{PhC(NMe)$_2$}Si{N(SiMe$_3$)$_2$}] is used to model the silylene ligand. Similarly, 1,3-bis(2,4,6-trimethylphenyl)imidazol-2-ylidine is used to model the carbene ligand. All calculations are performed using

Gaussian09 suite of S13 programs. Natural population analysis (NPA) is performed by employing NBO 3.1 program included in Gaussian program package.

2A.3. Result and Discussion

Our efforts began by exploring the reactivity of **1.14b** with chalcogens (E= S, Se). Treatment of **1.14b** in toluene with 1/8th equivalent of S_8 at room temperature for 12 h afforded a pale yellow colored solution of **2A.2** in 66% yield (Scheme 2A.1). Similarly, **2A.3** was synthesized in 70% yield by reacting **1.14b** with one equivalent of selenium powder. (Scheme 2A.1). The color of the reaction mixture changed from yellow to colorless. Products **2A.2** and **2A.3** were isolated as colorless crystalline solids with good solubility in toluene, THF, and dichloromethane.
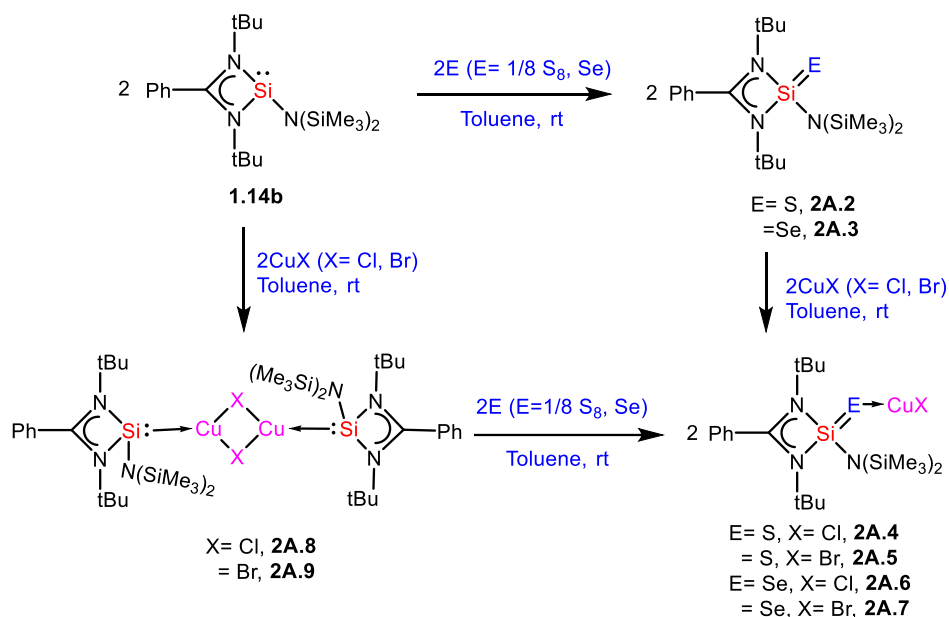
Scheme 2A.1. *Reactions of* **1.14b** *with chalcogens (S, Se) and copper halides (CuCl, CuBr).*

After the isolation of **2A.2** and **2A.3**, we explored the donor properties of the Si-chalcogenones. We were able to prepare the Lewis acid-base adducts [{PhC(NtBu)$_2$}Si(=S→CuX)N(SiMe$_3$)$_2$] [X= Cl (**2A.4**) and Br (**2A.5**)], [{PhC(NtBu)$_2$}Si(=Se→CuX)N(SiMe$_3$)$_2$] [X= Cl (**2A.6**) and Br (**2A.7**)] by using Si-chalcogenones **2A.2** and **2A.3**. Alternatively, the reactions of silylene-copper complexes [{PhC(NtBu)$_2$}Si{N(SiMe$_3$)$_2$}]$_2$Cu$_2$X$_2$ [X= Cl (**2A.8**) and Br (**2A.9**)] with chalcogens also resulted in the formation of products **2A.4**-**2A.7**.

The ^{1}H NMR spectra of **2A.2** and **2A.3** display each a sharp singlet at δ 1.30 and 1.34 ppm for 18 *t*Bu protons, which are shifted downfield when compared to those of **1.14b** [10] (δ 1.23 ppm). The ^{29}Si NMR spectra of both **2A.2** and **2A.3** display three resonances (**2A.2**: δ = -16.82, 1.69, 6.26 ppm; **2A.3**: δ = -20.22, 2.78, 8.40 ppm). The resonances at δ -16.82 and -20.22 ppm for **2A.2** and **2A.3**, respectively, correspond to the central silicon atom, which are upfield shifted when compared with that of **1.14b** (δ -8.07 ppm). The other two resonances for both **2A.2** and **2A.3** are assigned to the two SiMe$_3$ groups. A sharp resonance is exhibited at δ -458.42 ppm for **2A.3** in the ^{77}Se NMR spectrum. In the HRMS spectrum, the most abundant ion was observed at *m/z* 452.2405 for **2A.2** and 500.1852 for **2A.3** with the highest relative intensity (100%).

The ORTEP diagrams of **2A.2** and **2A.3** are shown in Figures 2A.1 with their structural parameters. **2A.2** crystallizes in the monoclinic space group *P*2$_1$/*c* whereas **2A.3** crystallizes in the triclinic space group *P*-1.[12] Both crystals were obtained in toluene at -30 °C in a freezer. The silicon center in both **2A.2** and **2A.3** is four coordinate and each exhibits a distorted tetrahedral geometry. The two sites are occupied by the N atoms from the amidinato ligand, one site is occupied by the N atom of the N(TMS)$_2$ moiety, and the other site is connected with the chalcogens (S; **2A.2**, Se; **2A.3**). The Si=S double bond length in **2A.2** is 1.987(2) Å which is in good agreement with the previously reported [{PhC(N*t*Bu)$_2$}Si(S)S*t*Bu] (1.984(8) Å).[9] The Si=S bond length in **2A.2** is slightly longer than in **IIIa** and **IIa-b** (1.957(2) Å, 1.948(4) and 1.952(4) Å respectively)[3a-b,4a] but shorter than that of the base stabilized Si-thione **Ia**[2] (2.013(3) Å). Similarly, the Si=Se bond distance in **2A.3** is 2.1369(9) Å, which is longer than those of **III** and **V** (2.096(1) Å and 2.117(1) Å) but shorter than those of **IV** and **VI** (2.153(1) Å and 2.146(1) Å). The average Si-S-N bond angle is 116.50° that matches with an average Si-Se-N bond angle (116.52°).

The reactions of **2A.2** and **2A.3** with 1 equivalent of CuCl in toluene afforded colorless crystalline solids of **2A.4** and **2A.6** with approximately 60-61% yield (Scheme 2A.1) where S and Se donate a lone pair of electrons each to the Cu center. The coordination of the Si- chalcogens is accompanied by the shift in the respective ^{29}Si NMR spectrum while the resonance for the central Si atom is exhibited at δ -14.96 and -19.79 ppm for **2A.4** and **2A.6,** respectively. These resonances are downfield shifted when compared with their parent compounds **2A.2** and **2A.3**. The ^{77}Se NMR spectrum of **2A.6** shows a sharp singlet at δ -466.68 ppm, which is upfield shifted when compared to **2.3** (δ -458.42 ppm).
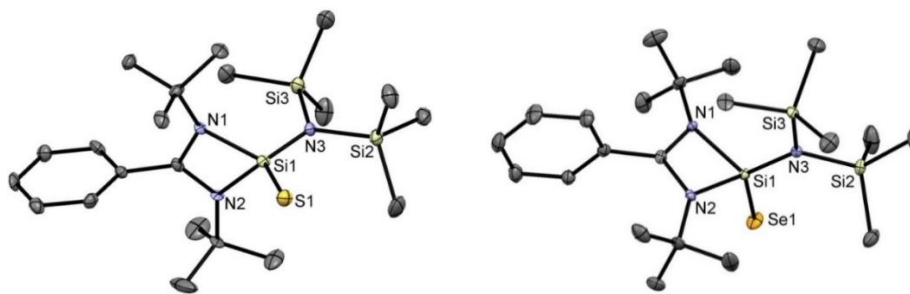
Figure 2A.1. *Molecular structure of **2A.2** (left) and **2A.3** (right) with anisotropic displacement parameters depicted at the 50% probability level. Hydrogen atoms are not shown for clarity. Selected bond lengths (Å) and bond angles (deg) for **2A.2**: Si1-S1- 1.987(2), Si1-N3 1.716(4), Si1-N2 1.816(4), Si1-N1 1.834(4); N3-Si1-S1 119.04(17), N2-Si1-S1 117.13(14), N1-Si1-S1 113.32(16); Selected bond lengths (Å) and bond angles (deg) for **2A.3**: Se1-Si1 2.1369(9), N3-Si1 1.715(2), N2-Si1 1.815(2), N1-Si1 1.827(2); N3-Si1-Se1 121.86(8), N2-Si1-Se1 113.23(8), N1-Si1-Se1 114.48(8).*

Compounds **2A.4** and **2A.6** were further characterized by single crystal X-ray diffraction analysis shown in Figure 2A.2 and selected bond parameters are listed in the legend of the figures. Both complexes crystallize in the orthorhombic space group *Pbca*. The silicon center is tetra-coordinate for compounds **2A.4** and **2A.6**. In both cases, the chalcogens are dicoordinate, one site is connected with the silicon center and the other site is coordinated with the copper center of the CuCl moiety. In **2A.4**, the Si=S bond length is 2.039(2) Å, which is quite longer than that of **2A.2** due to coordination with the Lewis acid CuCl and also closely matches with that of the previously reported **2A.VII** (2.106(2) Å),[7a] where S donates its lone pair of electrons to the Lewis acid of $GaCl_3$. The S→Cu bond length is 2.1260(18) Å. The S-Cu-Cl exhibits an angle of 175.00(9)° while the Si-S-Cu angle is 99.64(9)°. Similarly, in the case of **2A.6**, the Si=Se bond length is 2.1903(8) Å, which is slightly longer than that of the precursor. The Se→Cu bond length is 2.2412(5) Å. Here, like in the previous case the Se, Cu and Cl are arranged in the same plane with a bond angle of 174.15(4)°.

Furthermore, compounds **2A.5** and **2A.7** were obtained in good yield (60-62%) from the reaction of **2A.2** and **2A.3** with 1 equivalent of CuBr in toluene at room temperature (Scheme 2A.1). The ^{1}H and ^{29}Si NMR spectra of **2A.5** and **2A.7** reflect the coordination of S and Se center via one of its lone pair of electrons to the CuBr moiety. The resonances
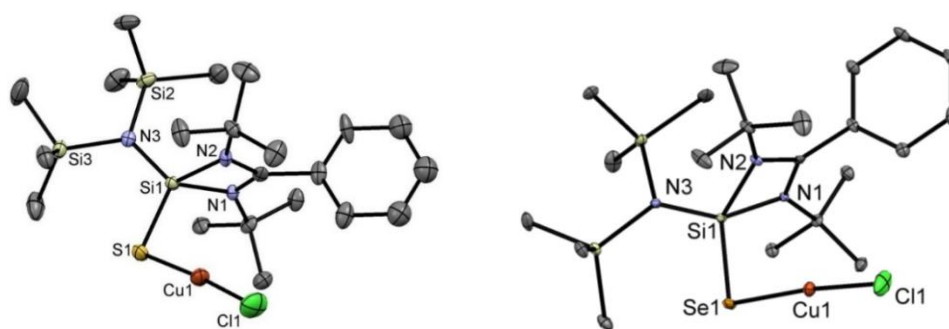
Figure 2A.2. *Molecular structure of **2A.4** (left) and **2A.6** (right) with anisotropic displacement parameters depicted at the 50% probability level. Hydrogen atoms are not shown for clarity. Selected bond lengths (Å) and bond angles (deg) for **2A.4**: Si1-S1- 2.039(2), Cu1-S1- 2.1260(18), Cu1-Cl1 2.092(2), Si1-N3 1.692(5), Si1-N2 1.819(5), Si1-N1 1.804(5); Cl1-Cu1-S1 175.00(9), Si1-S1-Cu1 99.64(9), N3-Si1-S1 115.13(19), N2-Si1-S1 115.83(18), N1-Si1-S1 112.66(18); Selected bond lengths (Å) and bond angles (deg) for **2A.6**: Si1-Se1 2.1903(8), Cu1-Se1 2.2412(5), Cu1-Cl1 2.0953(9), Si1-N3 1.694(2), Si1-N2 1.821(2), Si1-N1 1.808(2); Cl1-Cu1-Se1 174.15(4), Si1-Se1-Cu1 98.96(2), N3-Si1-Se1 115.14(8), N2-Si1-Se1 115.22(8), N1-Si1-Se1 113.20(8).*

for the silicon center were observed at δ -17.19 ppm (**2A.5**) and δ -19.93 ppm (**2A.7**). The slight upfield shift in the resonance of **2A.5** is unexpected as there should be an electron density shift from Si to S upon coordination with the Lewis acid (CuX). However, this unusual behavior can be attributed to the domination of Si-S σ-bonding MO which was previously reported for the Si=S→GaCl$_3$ compound (**2A.VII**).[7a] The solid state structures of **2A.5** and **2A.7** are the bromide analogs of **2A.4** and **2A.6** (Figure 2A.3). **2A.5** crystalizes in the monoclinic space group *P*21/*c* and **2A.7** crystallizes in the orthorhombic space group *Pbca.*[12] Here also each of the silicon centers is tetra-coordinate and forms a double bond between the chalcogen and the silicon atom. Furthermore each of the dicoordinate chalcogen atoms is bound to the Lewis acid CuBr. Compounds **2A.5** and **2A.7** show Si=E (E= S and Se) bond lengths of 2.0491(10) and 2.1902(18) Å, respectively. The E→Cu (E= S, Se) bond lengths are 2.1304(8) Å and 2.2460(11) Å for **2A.5** and **2A.7,** respectively. The S1-Cu1-Br1 angle of 175.79(3)° in **2A.5** and the Se1-Cu1-Br1 angle of 173.22(5)° in **2A.7** indicate that Cu, Cl, E (S and Se) are arranged in the same plane.

Compounds **2A.4**, **2A.5**, **2A.6,** and **2A.7** can also be prepared by the insertion of E (=S and Se) into the Si→Cu bond of the complexes [PhC(N*t*Bu)$_2$SiN(SiMe$_3$)$_2$CuCl]$_2$ (**2A.8**) and PhC(N*t*Bu)$_2$SiN(SiMe$_3$)$_2$CuBr]$_2$ (**2A.9**), respectively. Complexes **2A.8** and **2A.9** can be

furnished by the treatment of silylene **1.14b** with one molar equivalent of CuBr and CuCl in toluene at room temperature (Scheme 2A.1) with downfield shifted ^{29}Si NMR
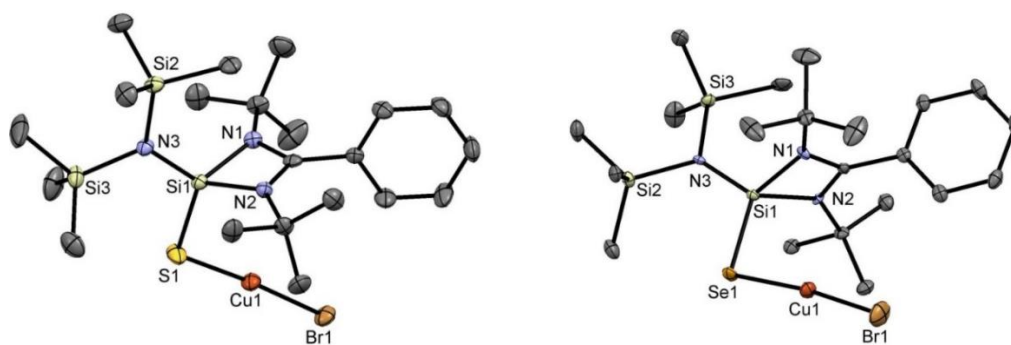

Figure 2A.3. *Molecular structure of **2A.5** (left) and **2A.7** (right) with anisotropic displacement parameters depicted at the 50% probability level. Hydrogen atoms are not shown for clarity. Selected bond lengths (Å) and bond angles (deg) for **2A.5**: Si1-S1 2.0491(10), S1-Cu1 2.1304(8), Cu1-Br1 2.2316(4), Si1-N3 1.702(2), Si1-N2 1.814(2), Si1-N1 1.816(2); S1-Cu1-Br1 175.79(3), Si1-S1-Cu1 105.79(4), N3-Si1-S1 115.00(8), N2-Si1-S1 112.80(8), N1-Si1-S1 114.64(8). Selected bond lengths (Å) and bond angles (deg) for **2A.7**: Se1-Si1 2.1901(18), Se1-Cu1 2.2460(11), Cu1-Br1 2.2194(11), Si1-N3 1.696(5), Si1-N2 1.811(5), Si1-N1 1.817(5); Se1-Cu1-Br1 173.22(5), Si1-Se1-Cu1 99.55(6), N3-Si1-Se1 114.93(19), N2-Si1-Se1 113.32(18), N1-Si1-Se1 115.38(18).*

resonance (**2A.8**: δ 5.72 and **2A.9**: δ 4.79 ppm) in comparison to **1.14b** (δ −8.07 ppm) but upfield with respect to that of [{PhC(NtBu)$_2$}Si{N(SiMe$_3$)$_2$}]$_2$Cu$_2$I$_2$ (δ 16.85 ppm).[11a] The corresponding structural parameters of **2A.8** and **2A.9** are very much alike and the noticeable alterations of the bond lengths and angles are attributed to the different halides. Both **2A.8** and **2A.9** crystallize in the triclinic space group *P-1* [12] and consist of a four-membered Cu$_2$X$_2$ (X=Cl, Br) core, where each silylene ligand is coordinated to a Cu atom. A two-fold symmetry axis passes through the centroid of the four-membered Cu$_2$X$_2$ ring, which is almost planar. Each Si(II) center in **2A.8** and **2A.9** is four coordinate and exhibits a slightly distorted tetrahedral geometry (Figure 2A.4). The Si→Cu bond lengths in **2A.8** are 2.221(2) and 2.222(2) Å, while in **2A.9** the bond lengths are 2.197(2) and 2.203(2) Å. These bond lengths are in good accordance with the previously reported Si–Cu bond lengths in [{PhC(NtBu)$_2$}Si{N(SiMe$_3$)$_2$}]$_2$Cu$_2$I$_2$ (2.243(3) and 2.250(3) Å)[11a] and other reported Si–Cu bond lengths [2.1981(12)–2.289(4) Å].[11]

The reactions of complexes **2A.8** and **2A.9** with chalcogens (E= S, Se) resulted in the Lewis acid-base adducts **2A.4**, **2A.5**, **2A.6,** and **2A.7** respectively. This is another useful route to synthesize Lewis acid-base adducts from the Si(II)→CuX (X= Cl, Br) coordination
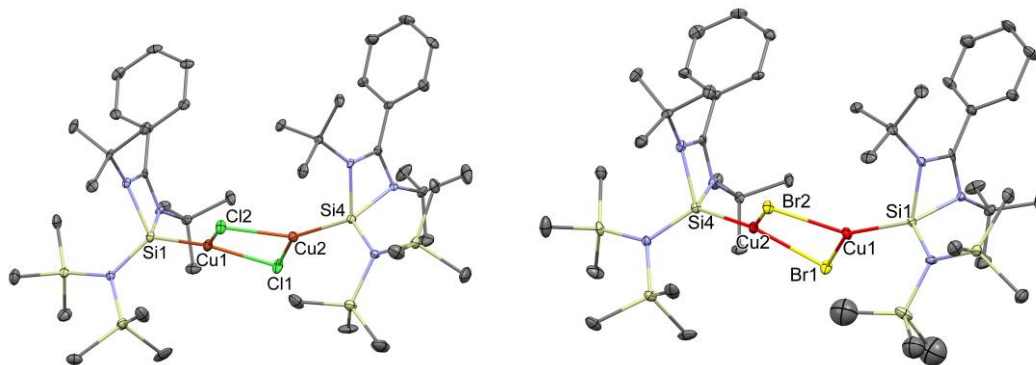

Figure 2A.4. *Molecular structures of **2A.8** (left) and **2A.9** (right) with anisotropic displacement parameters depicted at the 50% probability level. Hydrogen atoms are not shown for clarity. Selected bond lengths (Å) and bond angles (°):* ***2A.8****: Cu1-Cu2 3.1378(9), Cu1–Si1 2.1986(13), Cu1– Cl1 2.3003(11), Cu1–Cl2 2.3542(11), Cu2–Si4 2.2027(13), Cu2–Cl1 2.3022(11), Cu2–Cl2 2.3450(11); Si1– Cu1–Cl1 134.41(4), Si1–Cu1–Cl2 131.00(4), Cl1–Cu1–Cl2 94.20(4), Si4–Cu2–Cl1 136.75(4), Si4– Cu2–Cl2 128.81(4), Cl1–Cu2–Cl2 94.39(4), Cu2–Cl2–Cu1 83.79(4), and Cu1–Cl1–Cu2 85.97.* ***2A.9****: Cu1–Si1 2.222(2), Cu2–Si4 2.221(2), Cu1-Cu2 3.255(1), Cu1–Br1 2.4297(12), Cu1–Br2 2.4828(12), Cu2–Br1 2.4360(12), Cu2–Br2 2.4822(11); Si1–Cu1–Br1 135.79(7), Si1–Cu1–Br2 128.08(7), Si4– Cu2–Br1 133.62(7), Si4–Cu2–Br2 130.21(7), Cu1–Br1–Cu2 83.96(4), Cu2–Br2–Cu1 81.92(4), Br1– Cu1–Br2 95.99(4), and Br1–Cu2–Br2 95.84(4).*

complexes. DFT calculation reveals that the Si→CuBr (WBI=0.68) bond is much weaker compared to Si=S (WBI=1.55) bond. Therefore, the formation of a stronger Si-S (Si-Se) bond is at the expense of a weaker Si-Cu bond that renders the thermodynamic driving force for the aforementioned process.

For comparison reason we further investigated the reactivity of N-heterocyclic carbene instead of silylene with chalcogens to explore their coordination behavior. For this purpose, we prepared the previously reported sterically demanding N-heterocyclic carbene 1,3-bis(2,6-bis(diphenylmethyl)-4-methylphenyl)imidazol-2-ylidene (**2A.10**).[13] Treating **2A.10** with the sulfur and selenium afforded the thione **2A.11** and a previously reported selenone **2A.12**,[14] respectively. Subsequently, these chalcogenones act as a Lewis base to form adducts **2A.13** and **2A.14** (Scheme 2A.2). We have also prepared the carbene-CuBr complex (**2A.15**) and subsequently attempted to react the latter with

chalcogens (E = S, Se). However, unlike **2A.8** and **2A.9**, no reaction between **2A.15** and chalcogens was observed. Therefore, this synthetic protocol did not lead to the formation of **2A.13** and **2A.14**, which was explained by density functional theory (DFT) calculation. Theoretical study was performed using isodesmic reactions and comparison of the solvent-corrected Gibbs free energies of these isodesmic reactions shows that carbene-S→CuBr formation is 51.6 kcal/mol more endergonic than silylene-S→CuBr formation. Compounds **2A.11**, **2A.13-2A.15** were characterized by state of the art spectroscopic tools and single crystal X-ray diffraction analysis. Although X-ray diffraction on a single crystal unambiguously established the connectivity of **2A.11**, **2A.13**, **2A.14** and **2A.15,** we refrain from the discussion of bonding parameters because of the low quality of the data (Figure 2A.A.1, see Appendix for crystal structures).
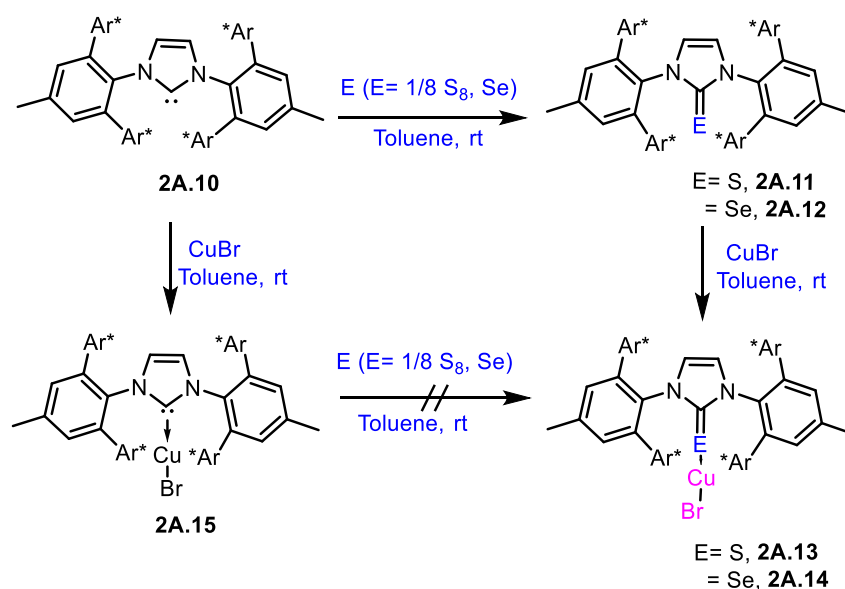
Scheme 2A.2. *Reaction of* **2A.10** *with chalcogens and CuBr; [Ar*= 4- Me-C$_6$H$_2$-2,6-(CHPh$_2$)$_2$].*

In order to obtain a deeper insight into the electronic structure of the silicon-chalcogen double bonds, we have carried out density functional theory (DFT) calculations on model compounds [PhC(NMe)$_2$Si(=S)N(SiMe$_3$)$_2$] (**2A.2m**) and [PhC(NMe)$_2$Si(=Se)N(SiMe$_3$)$_2$] (**2A.3m**). The calculated structural parameters are fairly consistent with the crystallographic data and the geometry optimized structures of **2A.2m** is shown in Figure 2A.5. The Si=S bond length in **2A.2m** is found to be 1.997 Å, which is close to the experimentally measured value of 1.987 Å in **2A.2**. The Wiberg bond index (WBI) for the Si=S bond is found to be 1.55, which indicates that the Si=S bond has a multiple bonding

character as well as there is a contribution from the charge separated canonical forms (*vide infra* NPA calculation). An inspection of the molecular orbitals (MOs) confirms the bonding picture. MO analysis shows both σ and π-bonding interaction between the Si and the S atoms. As illustrated in Figure 2A.5a, the HOMO and HOMO-1 of **2A.2m** are π-type bonding orbitals (concentrated on the Si-S bond), while HOMO-4 clearly shows the σ-bonding interaction between the Si and S. NBO analysis suggests that the Si-S sigma bonding orbital is polarized toward the S atom (64% of NBO density on S). The calculated NPA charges on Si and S atoms are 1.829 and -0.802, consistent with a polarized Si-S bond. Furthermore, at the second-order perturbation level, a donor–acceptor interaction is found between the lone pairs of S atom and the empty *p* orbitals of Si (interaction energy sums up to 105.8 kcal/mol), which is in support of the backbonding picture. The bonding situation in **2A.3m** is found to be similar to **2A.2m** with a calculated WBI of 1.59. MO analysis shows that both σ and π-bonding interactions are present in the Si=Se bond (Figure 2A.5b). The Si=Se σ-bonding orbital is polarized toward the Se atom (60.5% of NBO density on Se). However, as expected from relatively smaller electronegativity of the Se compared to S, the Si=Se bond is slightly less polarized than the Si=S bond; the NPA
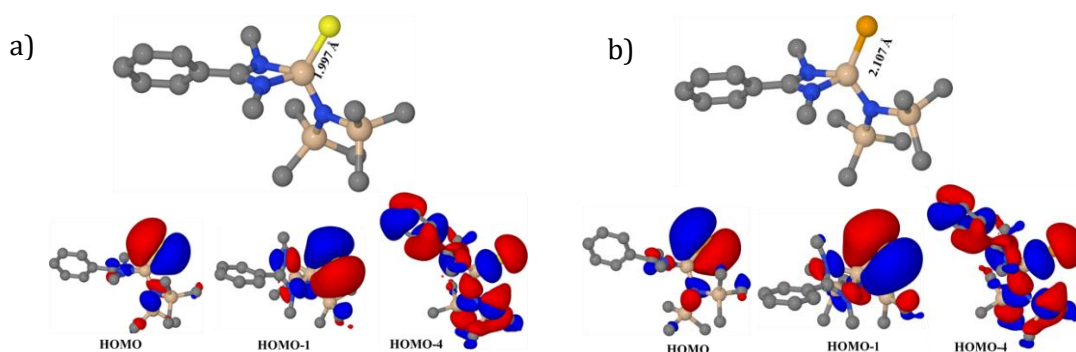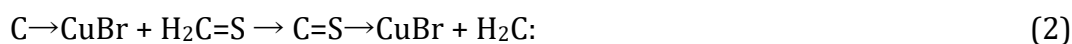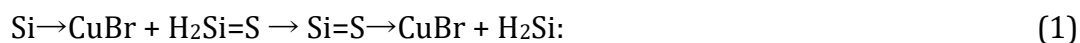

Figure 2A.5. *Molecular Geometry optimized structure and relevant molecular orbitals of a)* **2A.2m** *(left) and b)* **2A.3m** *(right).*

charges on Si and Se atoms are 1.747 and -0.709 (Δq=2.456 *vs.* 2.631 in **2A.2m**). Furthermore, the Se→Si back-donation is confirmed by NBO analysis, which suggests a donor-acceptor interaction between the lone pairs of Se and the empty *p* orbitals of Si. The coordinate bonded 1:1 complexes between Si-chalcogenones and CuX (X=Cl, Br) are also subjected to computational analysis. Geometry optimized structures of these

complexes (**2A.4m-2A.7m**) are depicted in Figure 2A.A.2 (see Appendix). Our results indicate that in all the complexes, silicon-chalcogen double bonds are elongated compared to those in the Si-chalcogenones. For example, the Si=S bond in **2A.5m** is elongated to 2.064 Å (computed 1.997 Å in **2A.2m**), while the WBI is reduced to 1.22 (1.55 in **2A.2m**). This can be explained by the electron donation from S to Cu. In fact, NBO analysis shows a significant donor-acceptor interaction between a lone pair of S atom and an empty *s* orbital in Cu. (at the second-order perturbation level the interaction energy amounts to 104.9 kcal/mol).

Apart from the bonding analysis, we also posed few questions which we tried to answer from DFT calculations. For example, silylene copper halide complexes **2A.8** and **2A.9** are dimeric, while silachalcogenone copper halides complexes **2A.4**−**2A.7** are monomeric. The free energy of dimerization of Si=S→CuBr (**2A.5m**) is endergonic by 7.4 kcal/mol, while dimerization of Si→CuBr is almost thermoneutral in toluene. It is also interesting to note that sulfur and selenium insert into the Si−Cu bond but not into the C−Cu bond. To rationalize this observation of why **2A.13** and **2A.14** cannot be afforded from **2A.15**, we have formulateda couple of isodesmic reactions through which we aim to examine the propensity of the formation of (silylene/carbene)-S→CuBr complexes from (silylene/carbene)-CuBr complexes. For construction of the isodesmic equations, H_2Si: and H_2C: are used as reference molecules and the equations are

$$Si\rightarrow CuBr + H_2Si=S \rightarrow Si=S\rightarrow CuBr + H_2Si: \tag{1}$$

$$C\rightarrow CuBr + H_2C=S \rightarrow C=S\rightarrow CuBr + H_2C: \tag{2}$$

A comparison of the solvent-corrected Gibbs free energies of these isodesmic reactions show that the carbene-S→CuBr formation is 51.6 kcal/mol more endergonic than the silylene-S→CuBr formation. This result is consistent with the experimental findings.

2A.4. Conclusion

In summary, we have done a systematic study of the synthesis and characterization of Si chalcogenones **2A.2** and **2A.3** and their transition-metal-based Lewis acid−base adducts **2A.4**−**2A.7** of composition Si=E→LA (E = S, Se) with electron-deficient CuX (X = Cl, Br). In addition to the Si=S/Se-based complexes **2A.4**−**2A.7**, we also prepared thione **2A.11** and

their Lewis acid−base adducts **2A.13** and **2A.14** from sterically hindered carbene **2A.10** to compare them with their silicon analogues. On comparison, we observed that Si chalcogen based Lewis acid−base adducts **2A.4**−**2A.7** can also be obtained from the reaction of silylene copper complexes **2A.8** and **2A.9** with chalcogens; however, this route does not work for the carbene copper complex **2A.15**, as the latter does not react with chalcogens to form **2A.13** and **2A.14**. The dichotomy was rationalized by theoretical calculations, which reveal that carbene-S→CuBr formation is 51.6 kcal/mol more endergonic than silylene-S→CuBr formation.

2A.5. References

1. (a) Pitzer, K. S. *J. Am. Chem. Soc.* **1948**, *70*, 2140. (b) Barrau, J.; Escudie, J.; Satgé, J. *Chem. Rev*. **1990**, *90*, 283–319. (c) Okazaki, R.; Tokitoh, N. *Acc. Chem. Res*. **2000**, *33*, 625–630. (d) Okazaki, R.; Tokitoh, N. *Adv. Organomet. Chem.* **2001**, *47*, 121–166. (e) Xiong, Y.; Yao, S.; Inoue, S., Irran, E.; Driess, M. *Angew. Chem. Int. Ed.* **2012**, *51*, 10074 –10077. (f) Yao, S.; Brym, M.; van Wüllen C.; Driess, M. *Angew. Chem. Int. Ed.* **2007**, *46*, 4159 –4162. (g) Tan, G.; Xiong, Y.; Inoue, S.; Enthaler, S.; Blom, B.; Epping, J. D.; Driess, M. *Chem. Commun.* **2013**, *49*, 5595—5597. For stable germanium-chalcogen doubly bonded compounds, see: (h) Tokitoh, N.; Matsumoto, T.; Manmaru, K.; Okazaki, R. *J. Am. Chem. Soc.* **1993**, *115*, 8855. (i) Matsumoto, T.; Tokitoh, N.; Okazaki, R. *Angew. Chem. Int. Ed. Engl.* **1994**, *33*, 2316. (j) Tokitoh, N.; Matsumoto, T.; Okazaki, R. *J. Am. Chem. Soc.* **1997**, *119*, 2337. (k) Tokitoh, N.; Matsumoto, T.; Okazaki, R. *Bull. Chem. Soc. Jpn.* **1999**, *72*, 1665. (l) Matsumoto, T.; Tokitoh, N.; Okazaki, R. *J. Am. Chem. Soc*. **1999**, *121*, 8811. For stable tin-chalcogen doubly bonded compounds, see: (m) Tokitoh, N.; Saito, M.; Okazaki, R. *J. Am. Chem. Soc.* **1993**, *115*, 2065. (n) Saito, M.; Tokitoh, N.; Okazaki, R. *Organometallics* **1996**, *15*, 4531. (o) M. Saito, N. Tokitoh and R. Okazaki, *J. Am. Chem. Soc.* 1997, **119**, 11124; (p) R. Okazaki, M. Saito and N.Tokitoh, *Phosphorus, Sulfur Silicon Relat. Elem.* 1997, **363**, 124-125; (q) M. Saito, N. Tokitoh and R. Okazaki, *J. Am. Chem. Soc* 2004, **126,** 15572.

2. Arya, P.; Boyer, J.; Carré´, F.; Corriu, R.; Lanneau, G.; Lapasset, J.; Perrot, M.; Priou, C. *Angew. Chem. Int. Ed. Engl.* **1989**, *28*, 1016.

3. (a) Suzuki, H.; Tokitoh, N.; Nagase, S.; Okazaki, R. *J. Am. Chem. Soc.* **1994**, *116*, 11578. (b) Suzuki, H.; Tokitoh, N.; Okazaki, R.; Nagase, S.; Goto, M. *J. Am. Chem. Soc.* **1998**, *120*,

11096. (c) Tokitoh, N.; Sadahiro, T.; Hatano, K.; Sasaki, T.; Takeda, N.; Okazaki, R. *Chem. Lett.* **2002**, *31*, 34-35.

4. (a) Iwamoto, T.; Sato, K.; Ishida, S.; Kabuto, C.; Kira, M. *J. Am. Chem. Soc.* **2006,** *128,* 16914–16920. (b) Mitra, A.; Wojcik, J. P.; Lecoanet, D.; Müller, T.; West, R. *Angew. Chem. Int. Ed*. **2009**, *48***,** 4069–4072. (c) Yao, S.; Xiong, Y.; Brym, M.; Driess, M. *J. Am. Chem. Soc.,* **2007**, *129*, 7268-7269. (d) Yao, S.; Xiong, Y.; Brym, M.; Driess, M. *Chem. Asian J.* **2008**, *3*, 113 – 118. (e) Yao, S.; Xiong, Y.; Driess, M. *Chem. Eur. J.* **2010**, *16*, 1281 – 1288.

5. (a) Lee, H.; Knobler, C. B.; Hawthorne, M. F. *J. Am. Chem. Soc.* **2001**, *123*, 8543-8549. (b) Motoyama, Y.; Okano, M.; Narusawa, H.; Makihara, N.; Aoki, K.; Nishiyama, H. *Organometallics* **2001**, *20*, 1580-1591. (c) Munakata, M.; Kuroda-Sowa, T.; Maekawa, M.; Nakamura, M.; Akiyama, S.; Kitagawa, S. *Inorg. Chem.* **1994**, *33*, 1284-1291. (d) Sun, Y.; Piers, W. E.; Yap, G. P. A. *Organometallics* **1997**, *16*, 2509-2513. (e) Fernández, J. M.; Emerson, K.; Lamen, R D.; Gladysz, J. A. *J. Am. Chem. Soc.* **1986**, *108*, 8268-8270.

6. (a) Huang, Y.-H.; Gladysz, J. A. *J. Chem. Educ.* **1988**, *65*, 298-303. (b) Kilner, C. A.; Halcrow, M. A. *Acta Cryst.* **2006**, *C62*, m437-m439.

7. (a) Xiong, Y.; Yao, S.; Driess, M. *Dalton Trans.* **2010**, *39*, 9282–9287. (b) Muraoka, T.; Abe, K.; Haga, Y.; Nakamura, T.; Ueno, K. *J. Am. Chem. Soc.* **2011**, *133*, 15365–15367. (c) Fukuda, T.; Hashimoto, H.; Sakaki, S.; Tobita, H. *Angew. Chem., Int. Ed.* **2016**, *55*, 188–192. (d) Muraoka, T.; Abe, K.; Kimura, H.; Haga, Y.; Ueno, K.; Sunada, Y. *Dalton Trans.* **2014**, *43*, 16610–16613.

8. (a) Xiong, Y.; Yao, S.; Müller, R.; Kaupp, M.; Driess, M. *Angew. Chem. Int. Ed.* **2015**, *54*, 10254 –10257. (b) Xiong, Y.; Yao, S.; Karni, M.; Kostenko, A.; Burchert, A.; Apeloig, Y.; Driess, M. *Chem. Sci.* **2016**, *7*, 5462–5469.

9. Sinhababu, S.; Yadav, D.; Karwasara, S.; Sharma, M. K.; Mukherjee, G.; Rajaraman, G.; Nagendran, S. *Angew. Chem. Int. Ed.* **2016**, *55*, 7742 –7746.

10. So, C.-W.; Roesky, H. W.; Oswald, R. B.; Pal, A.; Jones, P. G. *Dalton Trans.* **2007**, 5241–5244.

11. Sen, S. S.; Hey, J.; Herbst- Irmer, R.; Roesky, H. W.; Stalke, D. *J. Am. Chem. Soc.* **2011**, *133*, 12311–12316.

12. (a) Khan, S.; Ahirwar, S. K.; Pal, S.; Parvin, N.; Kathewad, N. *Organometallics*, **2015**, *34*, 5401–5406. (b) Inagawa, Y.; Ishida, S.; Iwamoto, T.; *Chem. Lett.*, **2014**, *43*, 1665–1667. (c) Avert, A. G.; Gehrhus, B.; Hitchcock, P. B.; Lappert, M. F.; Maciejewski, H.; *J. Organomet. Chem.*, **2003**, *686*, 321–331. (c) Tan, G.; Blom, B.; Gallego, D.; Driess, M. *Organometallics*, **2014**, *33*, 363–369. (d) Chen, M.; Wang, Y.; Xie, Y.; Wei, P.; Gilliard Jr., R. J.; Schwartz, N. A.; Schaefer III, H. F.; Schleyer, P. v. R.; Robinson, G. H. *Chem. Eur. J.*, **2014**, *20*, 9208–9211.

13. (a) Kottke, T.; Stalke, D. *J. Appl. Crystallogr.* **1993**, *26*, 615-619. (b) Stalke, D. *Chem. Soc. Rev.* **1998**, *27*, 171-178. (c) Sheldrick, G. M. *Acta Crystallogr.* **2015**, *71*, 3-8. (d) Schulz, T.; Meindl, K.; Leusser, D.; Stern, D.; Ruf, M.; Sheldrick, G. M.; Stalke, D. *J. Appl. Crystallogr.* **2009**, *42*, 885-891. (e) Krause, L.; Herbst-Irmer, R.; Sheldrick, G. M.; Stalke, D. *J. Appl. Crystallogr.* **2015**, *48*, 3-10.

14. Berthon-Gelloz, G.; Siegler, M. A.; Spek, A. L.; Tinant, B.; Reek, J. N. H.; Marko, I. E. *Dalton Trans.* **2010**, *39*, 1444.

15. Nelson, D. J.; Collado, A.; Manzini, S.; Meiries, S.; Slawin, A. M. Z.; Cordes, D. B.; Nolan, S. P. *Organometallics* **2014**, *33*, 2048–2058.

*****

Chapter 2B

Convenient access to compounds with silicon/ germanium-oxygen double bond

---

2B.1. Introduction

Unlike ketones, their higher homologues (E=O, E: Si-Pb) are oligomeric or polymeric in nature due to the unfavourable overlapping between $p_\pi(E)$ and $p_\pi(O)$ orbitals as well as large electronegativity difference between the E and O atoms.[1] Frederic S. Kipping observed a similar phenomenon in 1901, when first time attempted to discover silicon analogue of ketones (Si=O) but coincidentally observed the polymeric siloxane *i.e.* silicones.[2] Therefore, the isolation and stabilization of silicon-oxygen or germanium-oxygen doubly bonded compounds is very laborious. Recently such compounds have been attracting a great deal of attention to flourish fundamental inorganic chemistry. To harness the reactivity of Si=O or Ge=O bonds, the synthetic chemists devised the donor-acceptor concept and reported a good number of compounds featuring a Si=O/Ge=O double bond, where an additional donor like N-heterocyclic carbene (NHC) or 4-(dimethylamino)pyridine (4-DMAP) is coordinated to the silicon/germanium atom.[3] Coordination of these Lewis bases lower the electrophilicity of the Si/Ge atom and, thereby stabilize the E=O functionality. The entrée of the first *bonafide* heavy ketone was noted by the isolation of a germanone (**2B.VII**) (Chart 2B.1b) by Tamao and coworkers,[4] who used an immensely bulky ligand, 1,1,3,3,5,5,7,7-octaethyl-s-hydrindacen-4-yl (Eind) to provide the kinetic and thermodynamic stabilization to the Ge=O double bond. Subsequently, Filippou et al. isolated a stable cationic metallasilanone containing a Si=O double bond with a three coordinate silicon atom (**2B.I**).[5] A dialkyl silanone, persistent at -80°C in solution, is reported by Iwamoto and co-workers (characterized by NMR and IR spectroscopy).[6] Shortly afterwards, the group of Kato obtained fairly stable (amino)(ylide)silanones (**2B.II**) with $t_{1/2}$= 5h.[7a] The most remarkable breakthrough in silanone chemistry has come very recently when the groups of Inoue and Rieger reported an acyclic three-coordinate silanone (**2B.IV**) with a half-life of 4 days in acetonitrile.[8] At the same time Kato group disclosed another room temperature stable cyclic silanone, **2B.III**, stabilized by bulky amino and strong electron-donating phosphonium bora-ylide substituent.[7b] In 2019, Iwamoto and co-workers modified the previous unstable dialkyl silanone by increasing the bulkiness of the substituent and generated the first genuine room temperature stable silanone **2B.V**, which is neither stabilized by Lewis acids and bases nor by
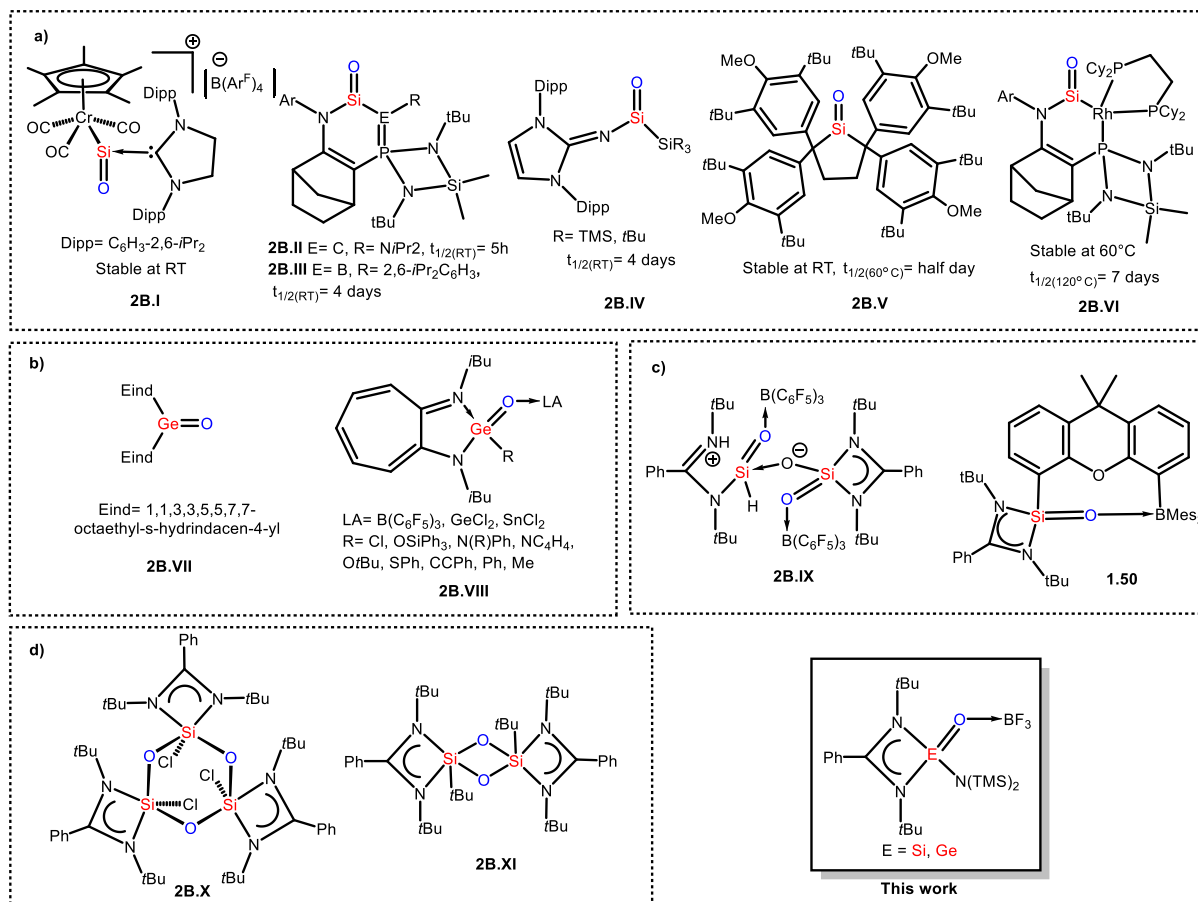
Chart 2B.1. *a) Selected examples of silanones (**2B.I-2B.VI**); b) germanone (**2B.VII, 2B.VIII**); c) Amidinato silylene based Si=O multiply bound compounds (**2B.IX** and **1.50**); d) Amidinato silylene based Si$_x$O$_y$ (x= y= 2, 3) cyclic compounds (**2B.X, 2B.XI**) (unsuccessful attempts to synthesize Si=O).*

electron-donating substituent.[9] In 2020, Kato and co-workers introduced a most stable N-hetero-Rh(I)-metallacyclic silanone (**2B.VI**) with high dimerization energy (ΔG=+86.2 kcalmol^{-1}) and persisted in solution up to 60°C.[10] Half-life of **2B.VI** is 7 days at 120°C. Nagendran and co-workers utilized aminotroponiminate ligand for the synthesis of germanium analogues of acid chloride, esters, and related compounds (**2B.VIII**, Chart 2B.1b).[11]

The classical synthetic strategy aimed towards the isolation of Si=O/Ge=O compound is the oxygenation of the corresponding silylene. A class of silylene that has enjoyed a lot of attraction in recent years in this regard is the benz-amidinato silylenes.[12] Due to the presence of the functionalized Si-X bond, they were deemed as suitable precursors for making silicon analogues of several organic

functionalities. For example, taking advantage of this ligand, Roesky and coworkers prepared the silicon analogue of acid anhydride (**2B.IX**).[13] The same group also reported the isolation of a sila-formaldehyde.[14] Previous unavailing attempts to isolate benz-amidinato ligand stabilized Si=O ended up with the trimeric six-membered Si_3O_3 ring (**2B.X**) and dimeric four-membered Si_2O_2 ring (**2B.XI**).[15] After that in 2017, Driess and coworkers have reported a silanone (**1.50**) featuring Si=O→BMes$_2$ interaction supported by 9,9-dimethylxanthene spacer.[16] Unlike benz-amidinato silylene, the benz-amidinato germylene did not render any multiply bound germanium compounds. In this paper, we report the convenient access towards compounds with silicon/germanium-oxygen double bonds starting from the reaction of amidinate silylene/germylene with NOBF$_4$, which can be deemed as analogues of acetamide. NO$^+$BF$_4^-$ is well known for an efficient nitrosating agent or fluorinating agent.[17] It is to be noted that here it is behaving as an oxygenating agent to form Si/Ge=O in the coordination with BF_3 via Lewis acid-base adduct formation.

2B.2. Experimental Section

2B.2.1. General Remarks

All experiments were carried out under an atmosphere of dry argon or in vaccuo using standard Schlenk technique and in a dinitrogen filled MBRAUN MB 150-G1 glovebox. The solvents used were purified by MBRAUN solvent purification system MB SPS-800. The starting materials **1.14b**, **2B.1** and **2B.6** were prepared as reported in the literature. All other chemicals purchased from Aldrich were used without further purification. ^{1}H, ^{13}C, ^{29}Si, ^{11}B and ^{19}F NMR spectra were recorded with Bruker 400 MHz spectrometer, using C_6D_6 as solvent with an external standard (SiMe$_4$ for ^{1}H, ^{13}C, ^{29}Si and CHF$_3$ for ^{19}F). Concentrated solution of the samples in C_6D_6 were sealed off in a NMR tube for measurement. All the heteronuclear NMRs are proton decoupled. Mass spectra were recorded using AB Sciex, 4800 plus MALDI TOF/TOF.

2B.2.2 Synthesis of **2B.2-2B.7**

Synthesis of 2B.2 and 2B.4 mixture:

30 mL toluene was added into the mixture of **1.14b** (E= Si) (0.210g, 0.5 mmol) and NOBF$_4$ (0.058g, 0.5 mmol) in a 100 mL schlenk flask. After 24h stirring at room temperature, the

pale yellow colored solution was filtered off and the volume was reduced to 15 mL and kept it at 0 °C. The colorless crystals suitable for X-ray analysis was obatined wthin 24h. ^{1}H NMR (400 MHz, CDCl$_3$, 298K): δ 0.39 (*s*, 18H, Si*Me$_3$*), 0.66 (*s*, 18H, Si*Me$_3$*), 1.25 (*s*, 36H, C*Me$_3$*), 6.95-6.99 (*m*, 3H, Ph), 7.02-7.06 (*m*, 2H, Ph), 7.15-7.18 (*m*, 3H, Ph), 7.26 (*s*, 2H, Ph) ppm. ^{13}C {^{1}H} NMR (100.613 MHz, CDCl$_3$, 298 K): δ 1.02 (Si*Me$_3$*), 4.79 (Si*Me$_3$*), 30.72 (*C*Me$_3$), 31.20 (*C*Me$_3$), 53.86 (C*Me$_3$*), 57.09 (C*Me$_3$*), 126.87, 127.83, 128.17, 128.38, 129.62, 130.01, 132.47, 133.01(Ph-*C*), 166.54 (N*C*N) ppm. ^{29}Si {^{1}H} NMR (79.495 MHz, CDCl$_3$, 298 K): δ 9.52 (*Si*Me$_3$), 0.87 (*Si*Me$_3$), 13.39 (*Si*Me$_3$), -60.35 (*Si*N(SiMe$_3$)$_2$), -62.70 (*Si*N(SiMe$_3$)$_2$). ^{19}F {^{1}H} NMR (376.49 MHz, CDCl$_3$, 298): δ -109.66 and -148.75 ppm. ^{11}B {^{1}H} NMR (128.387 MHz, CDCl$_3$, 298 K): δ -0.84 (*s*), 3.02 (*m*)   MALDI: *m/z* [C$_{21}$H$_{41}$N$_3$Si$_3$OBF$_3$]: 485.07 [M-F]; *m/z* [C$_{21}$H$_{41}$N$_3$Si$_3$F$_2$]: 387.39 [M-SiMe$_3$].

Synthesis of 2B.3 and 2B.5 mixture:

30 mL toluene was added into the mixture of **2B.1** (E= Ge) (0.232g, 0.5 mmol) and NOBF$_4$ (0.058g, 0.5 mmol) in a 100 mL schlenk flask. After 24h stirring at room temperature, the reaction mixture was filtered and concentrated. The colorless crystals suitable for X-ray analysis were obatined wthin 24 hrs at 0 °C. ^{1}H NMR (400 MHz, CDCl$_3$, 298K): δ 0.28 (*m*, 36H, C*Me$_3$*), 0.52-0.56 (*m*, 18H,), 1.10-1.13 (*m*, 18H, Si*Me$_3$*), 6.83-6.95 (*m*, 4H, Ph), 6.99-7.05 (*m*, 2H, Ph), 7.10-7.15 (*m*, 3H, Ph), 7.68-7.76 (*s*, 1H, Ph) ppm. ^{13}C {^{1}H} NMR (100.613 MHz, CDCl$_3$, 298 K): δ 2.74 (Si*Me$_3$*), 3.29 (Si*Me$_3$*), 3.29 (Si*Me$_3$*), 3.80 (Si*Me$_3$*), 4.21 (Si*Me$_3$*), 4.73 (Si*Me$_3$*), 29.30 (*C*Me$_3$), 29.79 (*C*Me$_3$), 30.37 (C*Me$_3$*), 31.03 (C*Me$_3$*), 52.60 (C*Me$_3$*), 53.90 (C*Me$_3$*), 55.54 (C*Me$_3$*), 126.33, 127.37, 127.68, 127.87, 128.17, 128.63, 129.95, 131.34, 135.09 (Ph-*C*), 169.71(N*C*N), 175.97 (N*C*N) ppm. ^{29}Si {^{1}H} NMR (79.495 MHz, CDCl$_3$, 298 K): δ 11.40 (*Si*Me$_3$), 4.21 (*Si*Me$_3$), 2.33 (*Si*Me$_3$) ppm. ^{19}F {^{1}H} NMR (376.49 MHz, CDCl$_3$, 298): δ -105.68 and -142.56 ppm. ^{11}B {^{1}H} NMR (128.387 MHz, CDCl$_3$, 298 K): δ -0.14 (*dd, J*= 22.4, 11.2 *Hz*)   MALDI: *m/z* [C$_{21}$H$_{41}$N$_3$Si$_2$GeOBF$_3$]: 511.41 [M-2F]$^+$.

Synthesis of 2B.7:

30 mL toluene was added into the mixture of **2B.6** (E= Sn) (0.255g, 0.5 mmol) and NOBF$_4$ (0.058g, 0.5 mmol) in a 100 mL schlenk flask. After 24h stirring at room temperature, the solution was filtered through frit. Colorless crystals were obtained upon supersaturation. ^{1}H NMR (400 MHz, CDCl$_3$, 298K): δ 0.35-0.37 (*m*, 15H, Si*Me$_3$*), 1.01 (*s*, 3H, Si*Me$_3$*), 1.10-1.14 (*m*, 18H, C*Me$_3$*), 7.26-7.28 (*m*, 1H, Ph), 7.31-7.48 (*m*, 4H, Ph) ppm. ^{13}C {^{1}H} NMR (100.613 MHz, CDCl$_3$, 298 K): δ 1.03 (Si*Me$_3$*), 3.23 (Si*Me$_3$*), 4.43 (Si*Me$_3$*), 4.86 (Si*Me$_3$*), 30.77 (*C*Me$_3$), 31.96 (*C*Me$_3$), 32.12 (C*Me$_3$*), 32.14 (C*Me$_3$*), 32.27 (C*Me$_3$*), 55.05 (C*Me$_3$*),

55.69 (C*Me₃*), 125.29, 127.67, 127.84, 128.34, 128.65, 129.02, 129.24, 129.59, 129.79, 129.89, 132.65, 137.64 (Ph-*C*), 169.03 (N*C*N), 170.57 (N*C*N) ppm. ^{29}Si {^{1}H} NMR (79.495 MHz, CDCl₃, 298 K): δ 4.35 (*Si*Me₃), 4.69 (*Si*Me₃), ppm. ^{119}Sn {^{1}H} NMR (149.18MHz, CDCl₃, 298): δ -387.33 (*d*, *J*=2984.8 Hz) ppm. ^{19}F {^{1}H} NMR (376.49 MHz, CDCl₃, 298): δ -94.92 and -137.83 ppm. HRMS: *m/z* [C₂₁H₄₁N₃Si₂SnF₂]: 572.16 [M+Na]$^+$.

2B.2.3. X-Ray Crystallographic Details

Single crystals of suitable size, coated with paraffin oil was mounted for all the complexes. Crystal data for all the complexes were collected on a Bruker Smart Apex Duo diffractometer at 100 K using Mo Kα radiation (λ = 0.71073 Å). Collected data were integrated by using SAINT and then absorption correction was done by multi-scan method using SADABS program. All the structures were solved by direct methods and refined by full-matrix least-squares methods against F^2 (SHELXL-2014/6). Crystallographic Information File (CIF) for the structures has been deposited to the Cambridge Crystallographic Data Centre as supplementary publication nos. 1907152 (**2B.2**), 1907153 (**2B.3**), 1907154 (**2B.4**), 1907155 (**2B.5**), 1907156 (**2B.7**). These CIF can be obtained free of charge from The Cambridge Crystallographic Data Centre via www.ccdc.cam.ac.uk/data_request/cif.

2B.2.4. Computational Methods

All the geometries were optimized at the DFT level of theory BP86[1] comprising the exchange functional of Becke in conjunction with the correlation functional of Perdew using Gaussian 09 program package.[2] The basis set def2-SVP[3], a double ζ-quality augmented with one set of polarization functions, is used for the geometry optimization. The single point calculations were performed using meta-GGA exchange correlation functional M06[4] with basis set having triple ζ-quality augmented by two sets of polarization functions (def2-TZVPP).[3] The natural bond orbital analysis (NBO)[5] were carried out at the M06/def2-TZVPP//BP86/def2-SVP level of theory. Energy Decomposition Analysis (EDA)[6] of **2B.2'** and **2B.3'** was carried out at the BP86/TZ2P level of theory with a frozen-core approximation for the core electrons using ADF 2016.01 program.[7] It focuses on the instantaneous interaction energy (ΔE_{int}) of a bond

between two fragments in the frozen geometry of the compound. ΔE_{int} is again divided into three chemically meaningful terms: Electrostatic interaction (ΔE_{elstat}), Pauli's repulsion (ΔE_{Pauli}) and Orbital interactions (ΔE_{orb}).

$$\Delta E_{int}= \Delta E_{elstat}+ \Delta E_{Pauli}+ \Delta E_{orb}$$

The electronic state which leads to lowest ΔE_{orb} is considered as the best bonding description. EDA-NOCV analysis is an extension of EDA analysis which decomposes the ΔE_{orb} term into the contributions from different natural orbitals of chemical valence (NOCV).[8] The EDA-NOCV calculations provide pairwise energy contributions for each pair of interacting orbitals to the total bond energy.

2B.3. Results and discussion

The reaction of silylene, [PhC(NtBu)$_2$SiN(SiMe$_3$)$_2$] (**1.14b**),[18] with NOBF$_4$ in toluene afforded the formation of [{PhC(NtBu)$_2$SiN(SiMe$_3$)$_2$}OBF$_3$] (**2B.2**) and [PhC(NtBu)$_2$SiF$_2$N(SiMe$_3$)$_2$] (**2B.4**) with the concomitant elimination of N$_2$O and BF$_3$ (Scheme 2B.1). Monitoring the reaction mixture by the ^{19}F NMR spectroscopy shows two signals at δ -148.75 and -109.66 ppm, indicating the formation of **2B.2** and **2B.4**, respectively. The ^{29}Si NMR spectrum of **2B.2** shows a signal at δ −13.39 ppm for the Si=O bond, which is consistent with the four-coordinated silicon atom.[19] The ^{29}Si NMR spectrum of **2B.4** displays a doublet resonance at −61.55 ppm with the $^1J_{Si-F}$ coupling constant of 227.2 Hz. The upfield shift is consistent with the increase of the coordination number around the Si center.

Analogous reaction with [PhC(NtBu)$_2$GeN(SiMe$_3$)$_2$][20] (**2B.1**) also led to the formation of the Ge=O doubly bound compound [{PhC(NtBu)$_2$GeN(SiMe$_3$)$_2$}OBF$_3$] (**2B.3**) and the oxidative addition product, [PhC(NtBu)$_2$GeF$_2$N(SiMe$_3$)$_2$] (**2B.5**) (Scheme 2B.1). As seen before, the ^{19}F NMR spectrum of the reaction mixture displays two resonances at δ −142.56 and −105.68 ppm for **2B.3** and **2B.5**, respectively. The ^{11}B NMR of **2B.2** and **2B.3** show multiplet at δ 3.02 and −0.14 ppm, respectively.
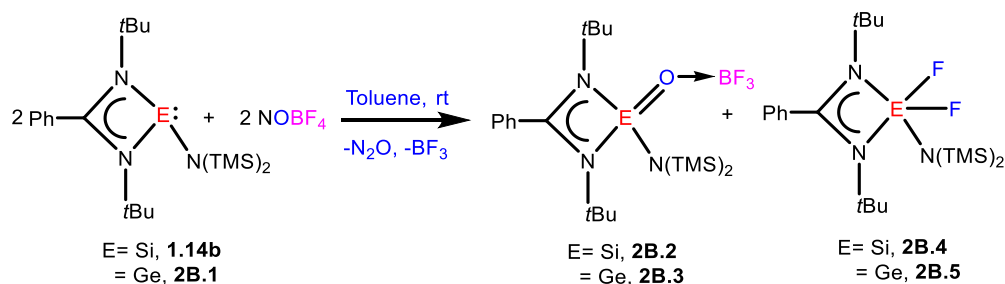
Scheme 2B.1. *Syntheses of complexes 2B.2-2B.5*

2B.2 crystallizes in the monoclinic space group *Pn*, where the central silicon atom is four coordinated featuring a distorted tetrahedral geometry containing two nitrogen atoms from the amidinate ligand, one nitrogen atom of the N(TMS)$_2$ moiety and one oxygen atom (Figure 2B.1). The Si-O bond length in **2B.2** is 1.560(7) Å, which is slightly longer than those in **2B.I** (1.523(3) Å),[5a] **2B.II** (1.533(1) Å)[7a] and **2B.IV** (1.537(3) Å),[8] but well comparable with the Lewis acid stabilized silanone, **1.50**(1.5568(14) Å).[16] **2B.3** also crystallizes in the monoclinic space group *Pn* and is shown in Figure 2B.1. The Ge-O bond length is of 1.683(9) Å, which is slightly longer than that in **2B.VII** (1.6468(5) Å),[4] but matching well with Lewis acid/base stabilized germanones (**2B.VIII**, 1.67-1.71 Å).[3g-i,11] Notwithstanding the coordination of the oxygen atom to the BF$_3$, the B–O bond lengths in **2B.2** (1.43(1) Å) and **2B.3** (1.49(2) Å) are significantly shorter than typical B–O single bond (~ 1.5 Å).[21]
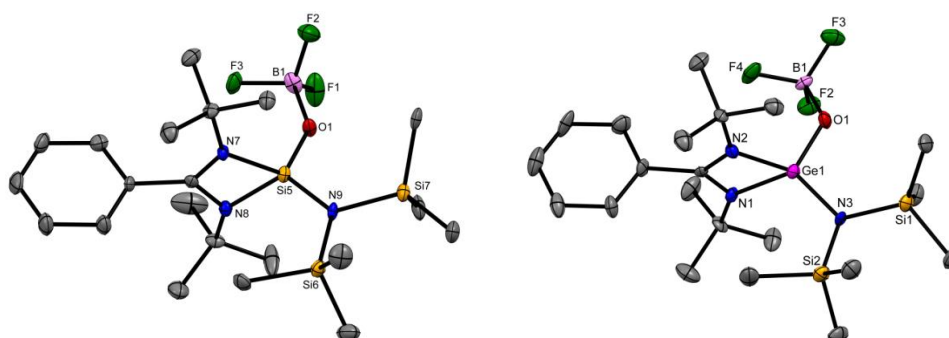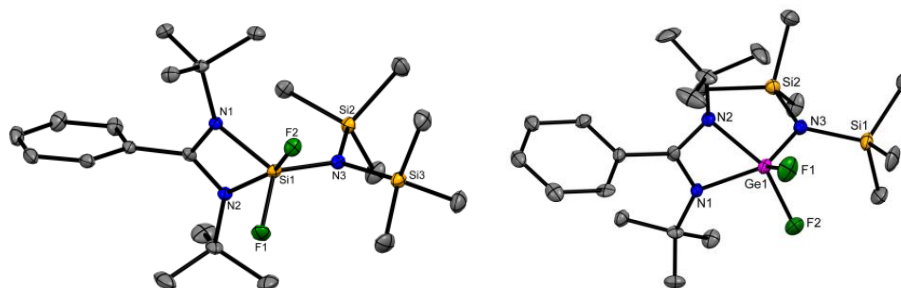

Figure 2B.1. *The molecular structure of 2B.2 (left) and 2B.3 (right) (ellipsoids are shown at the probability level of 30%). Hydrogen atoms are omitted for clarity. Selected bond lengths (Å) and bond angles (deg) for 2B.2: Si5-N71.800(8), Si5-N8 1.803(7), Si5-N9 1.685(7), Si5-O1 1.560(7), O1-B1 1.43(1), B1-F1 1.36(1), B1-F21.37(1), B1-F31.43(1); N8-Si5-O1 113.5(3),*

*N7-Si5-O1 113.5(3), Si5-O1-B1 140.8(6), O1-B1-F1110.9(9), O1-B1-F2 110.7(9), O1-B1-F3 108.7(8). Selected bond lengths (Å) and bond angles (deg) for **2B.3**: Ge1-N11.88(1), Ge1-N2 1.92(1), Ge1-N3 1.794(9), Ge1-O1 1.683(9), O1-B1 1.49(2), B1-F2 1.38(2), B1-F31.36(2), B1-F41.38(2); N1-Ge1-O1 116.7(4), N2-Ge1-O1 113.3(4), Ge1-O1-B1 127.2(8), O1-B1-F2109(1), O1-B1-F3 108(1), O1-B1-F4 110(1).*

2B.4 crystallizes in the monoclinic space group $P2_1/c$, where the central Si or Ge atom is five coordinated acquiring distorted trigonal bipyramidal geometry. The Si-F bond distances are 1.612(2) and 1.647(2) Å, which is well matched with [{PhC(N*t*Bu)$_2$SiFN(SiMe$_3$)$_2$}C$_6$F$_4$(CF$_3$)] (1.640(3) Å)[22] and [{PhC(N*t*Bu)$_2$SiFCl}C$_6$F$_4$(CF$_3$)] (1.633(3)Å).[23] Despite several attempts, we obtained only poor quality crystals of **2B.5**. Although the single crystal X-ray studies confirm the constitution unequivocally (Figure 2B.2), we abstain from discussing the bonding parameters of **2B.5**.

We have carried out quantum mechanical calculations at the M06/def2-TZVPP//BP86/def2-SVP level of theory to explore the stability of the compounds **2B.2**

Figure 2B.2. *The molecular structure of **2B.4** (left) and **2B.5** (right) (ellipsoids are shown at the probability level of 30%). Hydrogen atoms are omitted for clarity. Selected bond lengths (Å) and bond angles (deg) for **2B.4**:N1-Si1 1.796(2), N2-Si1 1.997(2), N3-Si1 1.725(2), Si1-F1 1.612(2), Si1-F2 1.647(2); F1-Si1-F2 90.92(8), N1-Si1-N2 68.45(8), N2-Si1-F1 86.42(8), F1-Si1-N3 117.52(9), N3-Si1-F2 98.28(9), F2-Si1-N1 95.20(8), N1-Si1-N3 123.05(9), N2-Si1-N3 100.83(9).*

and **2B.3** as compared to the hypothetical compounds without the Lewis acid BF$_3$ (**2B.2'** and **2B.3'**).[24] The calculated geometrical parameters of compounds **2B.2** and **2B.3** are in

good agreement with the experimental values (Figure 2B.A.1, see Appendix). The Si–O and Ge–O bond in **2B.2′** (1.573 Å) and **2B.3′** (1.680 Å) are slightly shortened as compared to those in sila- and germa-acetamide **2B.2** (1.608Å) and **2B.3** (1.733 Å), while the Si–N1 and Si–N2 bond in **2B.2′** (1.896 Å and 1.895 Å) and **2B.3′** (2.016 Å) are elongated as compared to those in **2B.2** (1.860 Å and 1.851 Å) and **2B.3** (1.961 Å and 1.969 Å). These differences in geometrical parameters can be attributed to the differing hyperconjugative interactions from the lone pair of oxygen to the Si–N antibonding σ-orbitals. NBO analysis indicate that the compounds **2B.2′** and **2B.3′** show significant hyperconjugative donor-acceptor interactions (66.2 kcal/mol and 67.0 kcal/mol respectively) from the lone pair of oxygen to the Si–N σ* orbitals as compared to those present in **2B.2** (25.9 kcal/mol) and **2B.3** (22.24 kcal/mol). The high positive charge on E (2.45 e in Si and 2.32 e in Ge) and a high negative charge on the oxygen atom (-1.17 e - -1.13 e) indicate a highly polarized E–O bond in compounds **2B.2** and **2B.3** (Table 2B.A.2, see Appendix).

The EDA-NOCV analysis (Table 2B.A.4) indicate that the Si–O and Ge–O bond in **2B.2′**and **2B.3′** can be best represented by charge separated electron sharing Si^+–O^- and Ge^+–O^- σ-bonds (ΔE_1). The lone pair of electrons from oxygen atoms involves in hyperconjugative interaction with the antibonding Si–N σ-MOs. The corresponding stabilization energies are -67.7 kcal/mol ($\Delta\rho_2 + \Delta\rho_3$) for **2B.2′** and -51.9 kcal/mol ($\Delta\rho_2 + \Delta\rho_3$) for **2B.3′** (Table

a

$\Delta_{\rho 1}$ (ΔE_1 = -196.9)
(Isosurface value = 0.002)

$\Delta_{\rho 2}$ (ΔE_2 = -35.3)
(Isosurface value = 0.001)

$\Delta_{\rho 3}$ (ΔE_3 = -32.4)
(Isosurface value = 0.001)

b

$\Delta_{\rho 1}$ (ΔE_1 = -161.9)
(Isosurface value = 0.003)

$\Delta_{\rho 2}$ (ΔE_2 = -28.7)
(Isosurface value = 0.001)

$\Delta_{\rho 3}$ (ΔE_3 = -23.2)
(Isosurface value = 0.001)
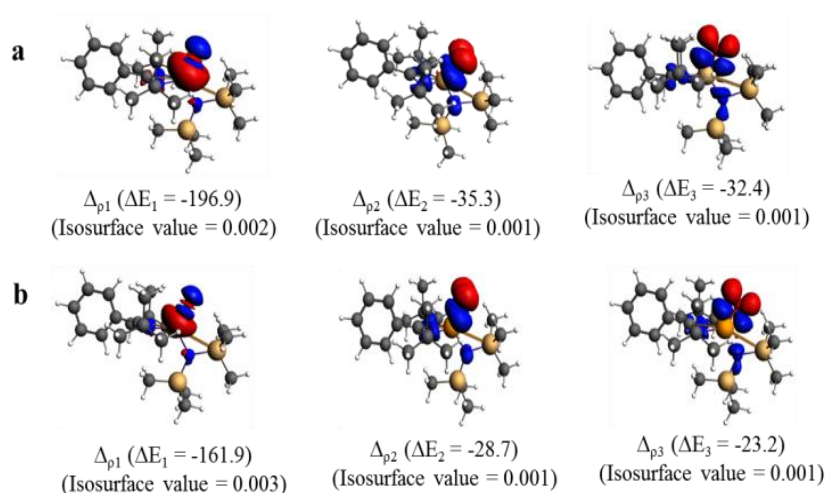
Figure 2B.3. *Plots of deformation densities $\Delta\rho_n$ and the associated orbital stabilization energies ΔE of **a)** 2B.2 (left) and **b)** 2B.3 (right) (in kcal/mol) at the BP86/TZ2P level of theory*

2B.A.5 and Figure 2B.A.2, see Appendix). The EDA-NOCV analysis is in agreement with the NBO and MO analyses indicating a partial multiple bond character of the Si−O and Ge−O bonds.

The MESP analysis of **2B.2′** and **2B.3′** show a global minimum (-59.0 kcal/mol and -57.2 kcal/mol) in the direction of lone pair of oxygen atom, indicating its high nucleophilicity (Figure 2B.A.3, see Appendix). The MESP values on the van der Waals surface of oxygen atom in **2B.2′** and **2B.3′** are -52.9 kcal/mol and -51.7 kcal/mol respectively, whereas it is decreased to -32.9 kcal/mol and -35.3 kcal/mol in **2B.2** and **2B.3** respectively (Table 2B.A.6). This indicates that the reactivity of oxygen atom in **2B.2′** and **2B.3′** is getting reduced on coordination with the Lewis acid BF_3 and hence, stabilizes the sila- and germa- acetamide **2B.2′** and **2B.3′**. This is well supported by high exothermic reaction energy for the formation of BF_3 adduct from **2B.2′** (-40.3 kcal/mol) and **2B.3′** (-40.8 kcal/mol) (Table 2B.A.7, see Appendix). The charge separated E^+-O^- bonds results in the high nucleophilicty at oxygen atoms which in turn is stabilized by adduct formation with BF_3.

When we performed the analogous reaction with $[PhC(NtBu)_2SnN(SiMe_3)_2]$[25] (**2B.6**), we were able to obtain only the difluorostannane $[PhC(NtBu)_2SnF_2N(SiMe_3)_2]$ (**2B.7**), which is analogous to **2B.4** and **2B.5** (Scheme 2B.2). Monitoring the reaction by ^{19}F NMR spectroscopy shows two signals at δ −137.83 and −94.92 ppm. The latter signal implies the formation of a Sn=O multiply bound compound, however, no such compound could be isolated. The large electronegativity difference between Sn and O as well as size mismatch could be attributed to the instability of Sn=O compound isolation. The ^{119}Sn NMR of **2B.7** exhibits a doublet at δ −387.33 ppm with a coupling constant of 2784.8 Hz, which is in agreement with the Sn-F coupling constant of 3100 Hz reported for LSnF [L=HC{CMeN(2,6-*i*Pr$_2$-C$_6$H$_3$)}].[26] Similar to **2B.5**, we could not obtain good quality crystals of **2B.7** suitable for single crystal X-ray studies The molecular structure of **2B.7** is given in Scheme 2B.2. The low MESP value of -6.4 kcal/mol in the direction of lone pair on Sn in stannylene **2B.6** as compared to that on Si in **1.14b** (-29.2 kcal/mol) and Ge in **2B.1** (-18.8 kcal/mol) indicates lesser nucleophilicity at the Sn atom (Figure 2B.A.4, see Appendix). Accordingly, the reaction energy for the oxygenation at Sn in **2B.6** is less exothermic (-68.5 kcal/mol, Table S5) as compared to the oxygenation at Si in **1.14b** and Ge in **2B.1**.
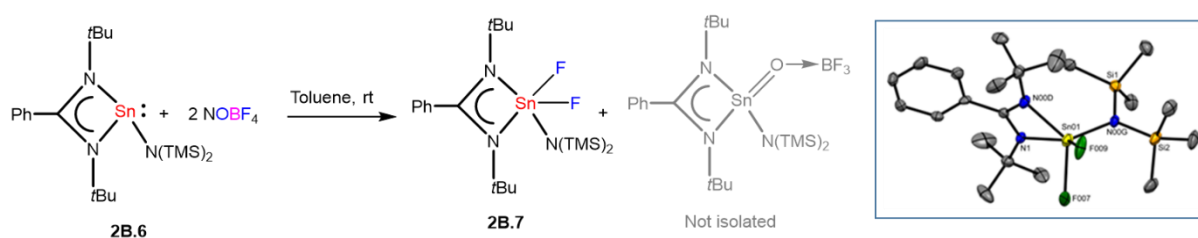
Scheme 2B.2. *Formation of **2B.7**.*

2B.4. Conclusions

In summary, we report the Lewis acid stabilized benzamidinatosila- (**2B.2**) and germa-acetamide (**2B.3**) from the reaction of **1.14b** and **2B.1** with NOBF$_4$. Single crystal X-ray studies on **2B.2** and **2B.3** confirm the formation of the Si=O, Ge=O doubly bound compounds. The theoretical calculations on the hypothetical sila- (**2B.2′**) and germa- (**2B.3′**) acetamide supports the high reactivity of oxygen atoms which in turn stabilized by the adduct formation with Lewis acid BF$_3$. The reaction of analogous stannylene did not afford stana-acetamide instead led to the formation of fluorinated Sn(IV) compound (**2B.7**). This difference of the reactivity of stannylene could be attributed to the poor orbital overlap between tin and oxygen atoms.

2B.5. References

1. (a) Avakyan, V. G.; Sidorkin, V. F.; Belogolova, E. F.; Guselnikov, S. L.; Gusel'nikov, L. E. *Organometallics* **2006**, *25*, 6007-6013. (b) Kudo, T.; Nagase, S. *J. Am. Chem. Soc.* **1985**, *107*, 2589-2595.

2. Kipping, F. S.; Lloyd, L. L. *J. Chem. Soc.* 1901, *79*, 449-459.

3. Hyper-coordinated silanone: (a) Xiong, Y.; Yao, S.; Driess, M. *J. Am. Chem. Soc.* **2009**, *131*, 7562. (b) Xiong, Y.; Yao, S.; Müller, R.; Kaupp, M.; Driess, M. *Nat. Chem.* **2010**, *2*, 577. (c) Gau, D.; Rodriguez, R.; Kato, T.; Saffon-Merceron, N.; deCózar, A.; Cossío, F. P.; Baceiredo, A. *Angew. Chem. Int. Ed.* **2011**, *50*, 1092. (d) Rodriguez, R.; Troadec, T.; Gau, D.; Saffon-Merceron, N.; Hashizume, D.; Miqueu, K.; Sotiropoulos, J.-M.; Baceiredo, A.; Kato, T. *Angew. Chem. Int. Ed.* **2013**, *52*, 4426. (e) Ghadwal, R. S.; Azhakar, R.; Roesky, H. W.; Pröpper, K.; Dittrich, B.; Klein, S.; Frenking, G. *J. Am. Chem. Soc.* **2011**, *133*,

17552. (f) Xiong, Y.; Yao, S.; Driess, M. *Angew. Chem. Int. Ed.* **2013**, *52*, 4302. HypercoordinatedGermanone: (g) Sinhababu, S.; Yadav, D.; Karwasara, S.; Sharma, M. K.; Mukherjee, G.; Rajaraman, G.; Nagendran, S. *Angew. Chem., Int. Ed.*, **2016**, *55*, 7742–7746. (h) Yao, S.; Xiong, Y.; Driess, M. *Chem. Commun.,* **2009**, 6466. (i) Yao, S.; Xiong, Y.; Wang, W.; Driess, M. *Chem. Eur., J.* **2011**, *17*, 4890.

4. Li, L.; Fukawa, T.; Matsuo, T.; Hashizume, D.; Fueno, H.; Tanaka, K.; Tamao, K. *Nat. Chem.* **2012**, *4*, 361-365.

5. (a) Filippou, A. C.; Baars, B.; Chernov, O.; Lebedev, Y. N.; Schnakenburg, G. *Angew. Chem., Int. Ed.* **2014,** *53*, 565. (b) Sen, S. S. *Angew. Chem., Int. Ed.* **2014**, *53*, 8820–8822.

6. Ishida, S.; Abe, T.; Hirakawa, F.; Kosai, T.; Sato, K.; Kira. M.; Iwamoto, T. *Chem. Eur. J.,* **2015**, *21*, 15100.

7. Alvarado-Beltran, I.; Rosas-Sanchez, A.; Baceiredo, A.; Saffon-Merceron, N.; Branchadell, V.; Kato, T. *Angew. Chem. Int. Ed.*, **2017**, *56*, 10481–10485. (b) Rosas-Sánchez, A.; Alvarado-Beltran, I.; Baceiredo, A.; Saffon-Mer-ceron, N.; Massou, S.; Hashizume, D.; Branchadell, V.; Kato, T. *Angew. Chem. Int. Ed.* **2017**, *56*, 15916 – 15920.

8. Wendel, D.; Reiter, D.; Porzelt, A.; Altmann, P. J.; Inoue, S.; Reiger, B. *J. Am. Chem. Soc.*, **2017**, *139*, 17193–17198.

9. Kobayashi, R.; Ishida, S.; Iwamoto, T. *Angew. Chem. Int. Ed.* **2019**, *58*, 9425 –9428.

10. Takahashi, S.; Nakaya, K.; Frutos, M.; Baceiredo, A.; Saffon-Merceron, N.; Massou, S.; Nakata, N.; Hashizume, D.; Branchadell, V.; Kato, T. *Angew. Chem. Int. Ed.* **2020**, *59*, 15937 –15941.

11. Kumar Sharma, M.; Sinhababu, S.; Mahawar, P.; Mukherjee, G.; Pandey, B.; Rajaraman, G.; Nagendran, S. *Chem. Sci.,* **2019**, *10*, 4402-4411.

12. (*a*) Sen. S. S.; Khan, S.; Nagendran, S.; Roesky, H. W. *Acc. Chem. Res.,* **2012**, *45*, 578–587; (*b*) Sen, S. S.; Khan, S.; Samuel, P. P.; Roesky, H. W. *Chem. Sci.,* **2012**, *3*, 659–682.

13. Ghadwal, R. S.; Azhakar, R.; Roesky, H. W.; Pröpper, K.; Dittrich, B.; Klein, S.; Frenking, G. *J. Am. Chem. Soc.*, **2011**, *133*, 17552–17555.

14. Ghadwal, R. S.; Azhakar, R.; Roesky, H. W.; Pröpper, K.; Dittrich, B.; Goedecke, C.; Frenking, G. *Chem. Commun.,* **2012**, *48*, 8186.

15. (a) Jana, A.; Azhakar, R.; Sarish, S. P.; Samuel, P. P.; Roesky, H. W.; Schulzke, C.; Koley, D. *Eur. J. Inorg. Chem.,* **2011**, 5006–5013. (b) Azhakar, R.; Ghadwal, R. S.; Roesky, H. W.; Wolf, H.; Stalke, D. *Chem. Commun.,* **2012**, *48*, 4561–4563.

16. Mo, Z.; Szilvási, T.; Zhou, Y.-P.; Yao, S.; Driess, M. *Angew. Chem., Int. Ed.*, **2017**, *56*, 3699–3702.

17. (a) Olah, G. A.; Prakash, G. K. S.; Wang, Q.; Li, X.-y. *Nitrosonium Tetrafluoroborate* University of Southern California, Los Angeles, CA, USA. (b) Williams, D. L. H. *Nitrosation* Cambridge University Press: Cambridge, *1988*. (c) Olah, G. A. Aldrichim. Acta **1979**, *12*, 43. (d) Olah, G. A. *Acc. Chem. Res.* **1980**, *13*, 330. (e) Kitamuraa, Y.; Matsumuraa, M.; Murataa, Y.; Yamadaa, M.; Kakusawab, N.; Tanakaa, M.; Okabec, H.; Nakac, H.; Obataa, T.; Yasuike, S. *Journal of Fluorine Chemistry* **2017**, *199*, 1–6. (f) Gusev, D.; Llamazares, A.; Artus, G.; Jacobsen, H.; Berke, H. *Organometallics* **1999,** *18,* 75-89.

18. Sen, S. S.; Hey, J.; Herbst-Irmer, R.; Roesky, H. W.; Stalke, D. *J. Am. Chem. Soc.*, **2011**, *133*, 12311–12316.

19. Khan, S.; Sen, S. S.; Kratzert, D.; Tavčar, G.; Roesky, H. W.; Stalke, D. *Chem. Eur. J.*, **2011**, *17*, 4283–4290 and references therein.

20. Samuel, P. P.; Singh, A. P.; Sarish, S. P.; Matussek, J.; Objartel, I.; Roesky, H. W.; Stalke, D. *Inorg. Chem.*, **2013**, *52*, 1544–1549.

21. Theuergarten, E.; Bannenberg, T.; Walter, M. D.; Holschumacher, D.; Freytag, M.; Daniliuc, C. G.; Jones, P. G.; Tamm, M. *Dalton Trans.*, **2014**, *43*, 1651–1662.

22. Swamy, V. S. V. S. N.; Parvin, N.; Raj, K. V.; Vanka, K.; Sen, S. S. *Chem. Commun.*, **2017**, *53*, 9850-9853.

23. Jana, A. ; Samuel, P. P.; Tavčar, G.; Roesky, H. W.; Schulzke, C. *J. Am. Chem. Soc.*, **2010**, *132*, 10164–10170.

24. See the Appendix for the details of computational methodology.

25. Sen, S. S.; Kritzler-Kosch, M. P.; Nagendran, S.; Roesky, H. W.; Beck, T.; Pal, A.; Herbst-Irmer, R. *Eur. J. Inorg. Chem.*, **2010**, 5304–5311.

26. Jana, A.; Roesky, H. W.; Schulzke, C.; Döring, A.; Beck, T.; Pal, A.; Herbest-Irmer, R. *Inorg. Chem.*, **2009**, *48*, 193-197.

*****

Chapter 3

N-heterocyclic silylene stabilized monocordinated Cu(I)-arene cationic complexes and their application in Click chemistry

---

3.1. Introduction:

Coinage metal π-complexes are important due to the catalytic functionalization of the π-substrates. Owing to their highly reactive nature it is very challenging to isolate them in monocoordinated form. Synthetic chemists often find fascination in isolating a compound that has been theoretically predicted as well as observed in the gas phase but never realized under laboratory condition. However, access to such compounds often poses formidable synthetic challenge. One such moiety is $[Cu(\eta^6\text{-}C_6H_6)]^+$. It is well evident from literature that group 11 metal–arene complexes strongly prefer the η^2 binding mode (**3.I** and **3.II**, Chart 3.1).[1,2] Armentrout and coworkers reasoned that the preference of η^2 bonding mode over η^6 is due to the increase of repulsion between the metal d-electrons and the benzene ligand in the latter.[3] Cu-arene complexes with η^6 bonding mode have also been reported albeit in small number, when using tethered arene rings in order to create cavity between the two arene rings by diminishing the repulsion.[4] These experimental results were further computationally supported by Guo and co-workers, who found that in the gas phase free Cu+ may form η^6 type of complexation with benzene but in the condensed phase the propensity of Cu+ to form η^2 complexes with benzene drastically increases in presence of a counter-anion.[5]
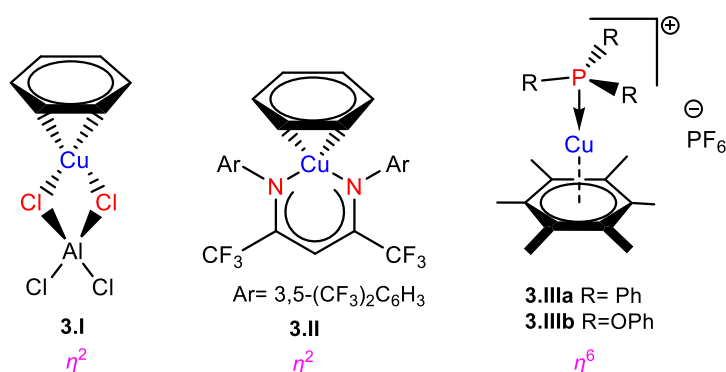
Chart 3.1. *Reported examples of Cu-η^2-C_6H_6 (**3.I** and **3.II**) and Cu-η^6-C_6Me_6 (**3.IIIa** and **3.IIIb**)*

A major breakthrough in this research was recently achieved by Hayton and coworkers, who isolated two half sandwich complexes $[(\eta^6\text{-}C_6Me_6)Cu(PR_3)][PF_6]$ (R=Ph, OPh) where the C_6Me_6 ring is bound to the Cu ion in η^6 coordination mode (**3.IIIa** and **3.IIIb**, Chart 3.1).[6] However, they have also theoretically showed that when benzene is employed

instead of hexamethylbenzene as an arene, η^2 mode is preferred, and hence surmised that the preference for η^6 mode over η^2 mode is exclusively due to steric repulsion between Me groups and PR_3 units. Additionally, they calculated the relative energies for $[Cu(C_6H_6))]^+$ in gas as well as condensed phases and found the preference for η^2 mode in both phases but more in condensed phase, as previously predicted by Guo et al. These studies consequently lead to the question: Is it even possible to isolate $[Cu(\eta^6\text{-}C_6H_6)]^+$ in the condensed phase?

It is apparent now that one of the main factors responsible for the success or failure in the synthesis of $[Cu(\eta^6\text{-arene})]^+$ is the ligand with appropriate substituent. Being better σ-donor than phosphines, silylenes are recently found to gain widespread interest as ligands for transition metals.[7] For this challenging work, we turned our attention towards $[PhC(NtBu)_2SiN(SiMe_3)_2]$[8] supported copper bromide complex, $[\{PhC(NtBu)_2\}Si\{N(SiMe_3)_2\}]_2Cu_2Br_2$ (**2A.9**).[9] An appealing facet of $[PhC(NtBu)_2SiN(SiMe_3)_2]$ (**1.14b**) is that it accepts electron density from the metal as evidenced in its coinage metal complexes.[9,10] We postulate that such back-donation can diminish the electrostatic repulsion between metal d-electrons and arene rings that may facilitate the formation of η^6 mode. This potential has been duly realized through the isolation and characterization of an unprecedented $[\{PhC(NtBu)_2SiN(SiMe_3)_2\}Cu(\eta^6\text{-}C_6H_6)]^+[SbF_6]^-$ (**3.2**) complex, which is the first example of $[Cu(\eta^6\text{-}C_6H_6)]^+$. For a direct systematic comparison, we carried out the same reactions with *N*-heterocyclic carbene, but unlike silylene it forms $[IPr \cdot Cu(\eta^2\text{-}C_6H_6)]^+[SbF_6]^-$ (**3.5**) containing η^2 coordination with C_6H_6 ring.

In light of the synthetic advances concerning Cu(I) arene complexes, a thorough study on other common arenes, especially unsymmetrical arenes such as toluene and *m*-xylene, is anticipated as no structural evidence exists for N-heterocyclic carbene (NHC)/silylene (NHSi) Cu(I) cations with such unsymmetrical arenes. To fill this void, we synthesized $[\{PhC(NtBu)_2SiN(SiMe_3)_2\}Cu(\eta^3\text{-}C_7H_8)]^+[SbF_6]^-$ (**3.6**), $[\{PhC(NtBu)_2SiN(SiMe_3)_2\}Cu(\eta^2\text{-}Me_2C_6H_4)]^+[SbF_6]^-$ (**3.7**), $[IPr\_Cu(\eta^3\text{-}C_7H_8)]^+[SbF_6]^-$ (**3.8**) and $[IPr\_Cu(\eta^2\text{-}Me_2C_6H_4)]^+[SbF_6]^-$ (**3.9**) complexes. Further we explored the reactivity of **3.6** and **3.8** with strong donor ligands i.e., MeCN, $[PhC(NtBu)_2SiN(SiMe_3)_2]$ and IPr. The synthetic difficulties to isolate weakly bound Cu(I)-free arene constitutes a major thrust for the catalysis reactions by

easy substitution of an arene with the substrates. Hence, we explored the Cu-arene complexes as catalysts for click reactions which is the cycloaddition reactions of azides and terminal alkynes. The use of Cu(I) metal in click reaction is well known and such reactions are widely used in organic synthesis, materials sciences, polymer chemistry, and pharmaceutical sciences. In this study we examined **3.6** as catalyst in copper-catalyzed azide–alkyne cycloaddition (CuAAC) reactions. Our results are reported herein.

3.2. Experimental Section

3.2.1. General Remarks

All experiments were carried out under an atmosphere of dry argon or in vaccuo using standard Schlenk technique and in a dinitrogen filled MBRAUN MB 150-G1 glovebox. The solvents used were purified by MBRAUN solvent purification system MB SPS-800. The starting materials **2.9** and **3.3** were prepared as reported in the literature.[9,11] All other chemicals purchased from Aldrich were used without further purification. ^{1}H, ^{13}C, ^{19}F and ^{29}Si NMR spectra were recorded with Bruker 400 MHz spectrometer, using $CDCl_3$ and CD_2Cl_2 as solvent with an external standard ($SiMe_4$ for ^{1}H, ^{13}C and ^{29}Si and trifluorotoluene for ^{19}F). All the heteronuclear NMRs are proton decoupled. Mass spectra were recorded using AB Sciex, 4800 plus MALDI TOF/TOF.

3.2.2 Synthesis of **3.1, 3.2, 3.4, 3.5, 3.6, 3.7, 3.8, 3.9, 3.10, 3.11, 3.12:**

Synthesis of 3.1:

30 mL CH_2Cl_2 was added to a 100 mL Schlenk flask containing mixture of **2.9** (0.281g, 0.25 mmol), $AgSbF_6$ (0.171g, 0.5 mmol) and C_6Me_6 (0.081 g, 0.5 mmol). After overnight stirring, AgBr was separated out from the reaction mixture by filtration and colorless block shaped crystals were observed in CH_2Cl_2-pentane mixture at 0 °C. Yield: 0.280g (64%). Mp: 130 °C (decomposition). ^{1}H NMR (400 MHz, CD_2Cl_2, 298K): δ 0.20 (*s*, 9H, Si*Me₃*), 0.27 (*s*, 9H, Si*Me₃*), 1.06 (*s*, 18H, C*Me₃*), 2.34 (*s*, 18H, C_6Me_6), 7.31-7.36 (*m*, 1H, Ph), 7.42-7.56 (*m*, 4H, Ph) ppm. ^{13}C {^{1}H} NMR (100.613 MHz, CD_2Cl_2, 298 K): δ 4.59 (Si*Me₃*), 5.15 (Si*Me₃*), 17.59 (C_6Me₆), 31.54 (C*Me₃*), 54.61 (*C*Me₃), 126.11, 127.92, 128.47, 128.87, 129.89, 130.56, 131.32 (Ph-*C*), ppm. ^{29}Si {^{1}H} NMR (79.495 MHz, $CDCl_3$, 298 K): δ 7.83 (*Si*Me₃), 7.09 (*Si*Me₃), 0.02 (*Si*N(SiMe₃)₂). ^{19}F {^{1}H} NMR (376.49 MHz, $CDCl_3$, 298K): δ -

176.70 (br) ppm. MALDI: *m/z* [C$_{33}$H$_{59}$N$_3$Si$_3$Cu]$^+$: 482.47 [M-C$_6$Me$_6$]$^+$. Anal Calcd: C, 44.97; H, 6.75; N, 4.77. Found: C, 44.89; H, 6.64; N, 4.82.

Synthesis of 3.2:

AgSbF$_6$ (0.171g, 0.5 mmol) was dissolved in CH$_2$Cl$_2$ (15 mL) and added to the solution of **2.9** (0.280g, 0.25 mmol) in benzene (15 mL). It was stirred overnight at room temperature. After that, AgBr was separated out from the reaction mixture by filtration and reduced the volume to 15 mL and kept it at 0 °C. Colorless block shaped crystals suitable for X-ray analysis were observed after one day. Yield: 0.260 g (65 %). Mp: 112 °C (decomposition). ^{1}H NMR (400 MHz, CDCl$_3$, 298K): δ 0.24 (*s*, 9H, Si*Me$_3$*), 0.39 (*s*, 9H, Si*Me$_3$*), 1.15 (*s*, 18H, C*Me$_3$*), 7.22-7.32 (*m*, 1H, Ph), 7.33-7.43 (*m*, 2H, Ph), 7.46 (*s*, 6H, C$_6$*H$_6$*) 7.47-7.69 (*m*, 2H, Ph) ppm. ^{13}C {^{1}H} NMR (100.613 MHz, CDCl$_3$, 298 K): δ 3.51 (Si*Me$_3$*), 4.87 (Si*Me$_3$*), 30.72 (C*Me$_3$*), 53.91 (*C*Me$_3$), 126.55, 126.67, 126.92, 127.82, 129.23, 129.86, 130.08 (Ph-*C*), 168.91 (N*C*N) ppm. ^{29}Si {^{1}H} NMR (79.495 MHz, CDCl3, 298 K): δ 7.65 (*Si*Me$_3$), 7.21 (*Si*Me$_3$), 4.41 (*Si*N(SiMe$_3$)$_2$). ^{19}F {^{1}H} NMR (376.49 MHz, CDCl$_3$, 298K): δ -173.64 (br) ppm. MALDI: *m/z* [C$_{27}$H$_{47}$N$_3$Si$_3$Cu]$^+$: 482.84 [M-C$_6$H$_6$]$^+$. Anal Calcd: C, 40.68; H, 5.94; N, 5.27. Found: C, 40.57; H, 6.05; N, 5.37.

Synthesis of 3.4:

30 mL CH$_2$Cl$_2$ was added to a 100 mL Schlenk flask containing mixture of **3.3** (0.266g, 0.5 mmol), AgSbF$_6$ (0.171g, 0.5 mmol) and C$_6$Me$_6$ (0.081 g, 0.5 mmol). After overnight stirring, AgBr was separated out from the reaction mixture by filtration and it was crystallized in saturated CH$_2$Cl$_2$ solution. Yield: 0.300g (70%). Mp: 175 °C (decomposition). ^{1}H NMR (400 MHz, CDCl$_3$, 298K): δ 1.10 (*dd*, 24H, *J*= 9.7, 6.9 Hz, CH(C*H$_3$*)$_2$), 1.80 (*s*, 18H, C$_6$*Me$_6$*), 2.20- 2.30 (*m*, 4H, C*H*(CH$_3$)$_2$), 7.29 (*d*, 4H, *J*= 7.8 Hz, Ph), 7.52 (*t*, 2H, *J*= 7.8 Hz, Ph) ppm. ^{13}C {^{1}H} NMR (100.613 MHz, CDCl$_3$, 298 K): δ 16.21, 22.81, 23.19, 27.67, 123.34, 123.54, 128.27, 129.82, 133.62, 144.34, 175.90 ppm. ^{19}F {^{1}H} NMR (376.49 MHz, CDCl$_3$, 298K): δ -174.02 (br) ppm. MALDI: *m/z* [C$_{39}$H$_{54}$N$_2$Cu]$^+$: 613.43 [M]$^+$. Anal Calcd: C, 55.10; H, 6.40; N, 3.30. Found: C, 55.22; H, 6.60; N, 3.24.

Synthesis of 3.5:

AgSbF$_6$ (0.171g, 0.5 mmol) was dissolved in CH$_2$Cl$_2$ (15 mL) and added to the solution of **3.3** (0.266g, 0.5 mmol) in benzene (15 mL). After overnight stirring, AgBr was separated out from the reaction mixture by filtration and reduced the volume to 15 mL and kept it at 0 °C. Colorless block shaped crystals suitable for X-ray analysis was observed after one day. Yield: 0.275g (72%). Mp: 228 °C

(decomposition). ^1H NMR (400 MHz, CD_2Cl_2, 298K): δ 1.14 (*dd*, 24H, *J*= 8.9, 7.0 Hz, CH(C*H₃*)₂), 2.25-2.32 (*m*, 4H, C*H*(CH₃)₂), 7.11 (*br*, 4H, C_6H_6), 7.18 (*s*, 2H, C_6H_6), 7.31 (*d*, 4H, *J*= 7.8 Hz, Ph), 7.53 (*t*, 2H, *J*= 7.8 Hz, Ph) ppm. ^{13}C {^1H} NMR (100.613 MHz, CD_2Cl_2, 298 K): δ 23.01, 23.68, 27.94, 123.62, 123.68, 130.25, 133.13, 144.74 ppm. ^{19}F {^1H} NMR (376.49 MHz, $CDCl_3$, 298K): δ -173.64 (br) ppm. MALDI: *m/z* [$C_{33}H_{42}N_2Cu$]$^+$: 451.19 [M -C_6H_6]$^+$. Anal Calcd: C, 51.74; H, 5.53; N, 3.66. Found: C, 51.62; H, 5.40; N, 3.57.

Synthesis of 3.6:

AgSbF₆ (0.171g, 0.5 mmol) was dissolved in DCM and added to the solution of **2.9** (0.295g, 0.25 mmol) in toluene. It was stirred for overnight at room temperature. AgBr was precipitated out from the reaction mixture was filtered off and the volume was reduced to 15 mL and kept it at 0 °C. The colorless, block shaped crystals suitable for x-ray analysis was observed after one day. Yield: 0.252g (61%). Mp: 134-139 °C. ^1H NMR (400 MHz, $CDCl_3$, 298K): δ 0.29 (*s*, 9H, Si*Me₃*), 0.41 (*s*, 9H, Si*Me₃*), 1.19 (*s*, 18H, C*Me₃*), 2.51 (*s*, 3H, C*H₃*,toluene), 7.32-7.38 (*m*, 2H, Ph), 7.46-7.53 (*m*, 4H, Ph), 7.55-7.60 (*m*, 3H, Ph), 7.66-7.70 (*m*, 1H, Ph) ppm. ^{13}C {^1H} NMR (100.613 MHz, $CDCl_3$, 298 K): δ 4.56 (Si*Me₃*), 5.93 (Si*Me₃*), 21.62 (*C*H₃, toluene), 31.70 (C*Me₃*), 54.93 (*C*Me₃), 121.33, 121.62, 125.20, 125.41, 127.30, 127.48, 128.05, 128.12, 128.18, 129.16, 129.76, 131.21 (Ph-*C*), 170.01 (N*C*N) ppm. ^{29}Si {^1H} NMR (79.495 MHz, $CDCl_3$, 298 K): δ 7.52 (*Si*Me₃), 6.72 (*Si*Me₃), 2.28 (*Si*N(SiMe₃)₂) ppm. ^{19}F {^1H} NMR (376.49 MHz, $CDCl_3$, 298): δ -162.88 ppm. MALDI: *m/z* [$C_{29}H_{52}CuN_3Si_3$]$^+$: 482.20 [M-MeC₆H₅]. Anal Calcd: C, 42.15; H, 6.34; N, 5.09. Found: C, 42.24; H, 6.44; N, 5.27.

Synthesis of 3.7:

AgSbF₆ (0.171g, 0.5 mmol) was dissolved in DCM and added to the solution of **2.9** (0.295g, 0.25 mmol) in *m*-xylene. It was stirred overnight at room temperature. The solution was filtered to separate AgBr, concentrated to 10 mL and kept it at 0 °C overnight to afford colorless crystals of **3.8**. Yield: 0.280g (67%). Mp: 108-113 °C. ^1H NMR (400 MHz, $CDCl_3$, 298K): δ 0.29 (*s*, 9H, Si*Me₃*), 0.47 (*s*, 9H, Si*Me₃*), 1.25 (*s*, 18H, C*Me₃*), 2.28 (*s*, 6H, C*H₃*, *m*-xylene), 6.94-7.02 (*m*, 2H, Ph), 7.37-7.53 (m, 7H, Ph) ppm. ^{13}C {^1H} NMR (100.613 MHz, $CDCl_3$, 298 K): δ 3.83 (Si*Me₃*), 5.22 (Si*Me₃*), 20.33 (*Me₂*C₆H₄), 30.86 (C*Me₃*), 53.80 (*C*Me₃), 125.58, 126.55, 127.23, 127.51, 127.71, 127.89, 128.16, 128.95, 129.23, 129.99, 130.35 (Ph-*C*), 167.68 (N*C*N) ppm.

^{29}Si {^{1}H} NMR (79.495 MHz, CDCl$_3$, 298 K): δ 7.49 (*Si*Me$_3$) (marched two SiMe$_3$ peak to give a broad peak), 2.80 (*Si*N(SiMe$_3$)$_2$) ppm. ^{19}F {^{1}H} NMR (376.49 MHz, CDCl$_3$, 298): δ -178.35 (br) ppm. MALDI: *m/z* [C$_{30}$H$_{54}$CuN$_3$Si$_3$]$^+$: 482.25 [M-Me$_2$C$_6$H$_4$]. Anal Calcd: C, 42.88; H, 6.48; N, 5.00. Found: C, 42.92; H, 6.62; N, 4.93.

Synthesis of 3.8:

AgSbF$_6$ (0.171g, 0.5 mmol) was dissolved in DCM and added to the solution of **3.3** (0.266g, 0.5 mmol) in toluene. Immediately AgBr was precipitaed out. After overnight stirring, AgBr was separated out from the reaction mixture by filtration and reduced the volume to 15 mL and kept it at 0 °C. Colorless block shaped crystals suitable for X-ray analysis was observed after one day. Yield: 0.295g (74%). Mp: more than 200 °C. ^{1}H NMR (400 MHz, CDCl$_3$, 298K): δ 1.23-1.26 (*m*, 24H, CH(C*H*$_3$)$_2$), 2.05 (*s*, 3H, C*H*$_3$, toluene), 2.40-2.50 (*m*, 4H, C*H*(CH$_3$)$_2$), 6.74-6.81 (*m*, 1H, Ph), 6.87-7.01 (*m*, 1H, Ph), 7.08-7.18 (*m*, 1H, Ph), 7.27 (*s*, 1H, Ph), 7.35-7.37 (*s*, 5H, Ph) 7.55-7.59 (*m*, 2H, Ph) ppm. ^{13}C {^{1}H} NMR (100.613 MHz, CDCl$_3$, 298 K): δ 21.07, 23.99, 24.59, 28.72, 124.20, 124.45, 131.12, 133.83, 137.91, 145.40 ppm. ^{19}F {^{1}H} NMR (376.49 MHz, CDCl$_3$, 298): δ -183.43 (br) ppm. MALDI: *m/z* [C$_{35}$H$_{47}$CuN$_2$]+: 451.02 [M-MeC$_6$H$_5$]. Anal Calcd: C, 52.87; H, 5.96; N, 3.52. Found: C, 52.72; H, 5.80; N, 3.57.

Synthesis of 3.9:

AgSbF$_6$ (0.171g, 0.5 mmol) was dissolved in DCM and added to the solution of **3.3** (0.266g, 0.5 mmol) in *m*-xylene. Immediately AgBr was precipitaed out. After overnight stirring, AgBr was separated out from the reaction mixture by filtration and reduced the volume to 10 mL and kept it at 0 °C. Colorless block shaped crystals suitable for X-ray analysis was observed after one day. Yield: 0.315g (78%). Mp: 170 °C (decomposed). ^{1}H NMR (400 MHz, CDCl$_3$, 298K): δ 1.20-1.22 (*m*, 24H, CH(C*H*$_3$)$_2$), 2.02 (*s*, 6H, C*H*$_3$,*m*-xylene), 2.25-2.41 (*m*, 4H, C*H*(CH$_3$)$_2$), 6.74-6.76 (*m*, 2H, Ph), 6.86-6.90 (*m*, 1H, Ph), 6.94 (*s*, 1H, Ph), 7.37 (*s*, 4H, *J*= 7.8Hz, Ph) 7.60 (*t*, 2H, *J*= 7.8Hz, Ph) ppm. ^{13}C {^{1}H} NMR (100.613 MHz, CDCl$_3$, 298 K): δ 21.04, 24.07, 24.38, 28.65, 124.37, 124.44, 131.13, 134.03, 137.93, 145.43 ppm. ^{19}F {^{1}H} NMR (376.49 MHz, CDCl$_3$, 298): δ -160.86 (br) ppm. MALDI: *m/z* [C$_{36}$H$_{49}$CuN$_2$]$^+$: 451.35 [M-Me$_2$C$_6$H$_4$]. Anal Calcd: C, 53.44; H, 6.10; N, 3.46. Found: C, 53.42; H, 6.14; N, 3.57.

Synthesis of 3.10:

Acetonitrile (0.05 mL) was added into the solution of **3.6** (0.413g, 0.5 mmol) in 20 mL DCM. After overnight stirring, the reaction mixture was dried completely and crystallized in DCM/pentane mixture and kept it at 0 °C. Colorless block shaped crystals suitable for X-ray analysis was observed after one day. Yield: 0.270g (47%). MP: 110 °C. ^{1}H NMR (400 MHz, CDCl$_3$, 298K): δ 0.32 (*s*, 6H, Si*Me$_3$*), 0.34 (*s*, 6H, Si*Me$_3$*), 0.37 (*s*, 6H, Si*Me$_3$*), 0.45 (*s*, 6H, Si*Me$_3$*), 0.47 (*s*, 6H, Si*Me3*),0.55 (*s*, 6H, Si*Me$_3$*), 1.24 (*s*, 12H, C*Me$_3$*), 1.26 (*s*, 12H, C*Me$_3$*), 1.30 (*s*, 12H, C*Me$_3$*), 2.21 (acetonitrile), 7.17-7.19 (*m*, 1H, Ph), 7.36-7.39 (*m*, 1H, Ph), 7.44-7.47 (*m*, 1H, Ph), 7.52-7.63 (*m*, 7H, Ph) ppm. ^{13}C {^{1}H} NMR (100.613 MHz, CDCl$_3$, 298 K): δ 4.54, 4.69, 4.85, 5.69, 5.87, 5.92, 6.25, 31.66, 31.84, 31.88, 54.74, 54.81, 55.10, 116.88, 116.93, 125.28, 126.57, 127.64, 127.70, 127.83, 127.97, 128.21, 128.28, 128.48, 128.77, 129.03, 130.26, 130.53, 130.81, 131.02, 131.37 ppm. ^{29}Si {^{1}H} NMR (79.495 MHz, CDCl$_3$, 298 K): δ 10.22 (*Si*Me$_3$) (br), 7.09 (*Si*Me$_3$) (br), 5.53 (*Si*N(SiMe$_3$)$_2$),4.11 (*Si*N(SiMe$_3$)$_2$) ppm. Anal Calcd: C, 44.29; H, 7.26; N, 7.38. Found: C, 44.32; H, 7.21; N, 7.46.

Synthesis of 3.11:

IPr carbene (0.194g, 0.5 mmol) was dissolved in toluene and added to the solution of **3.6** (0.413g, 0.5 mmol) in toluene. After overnight stirring, the reaction mixture was filtered and dried completely. Further the reaction mixture was crystallized in DCM/pentane mixture and kept it at 0 °C. Colorless block shaped crystals suitable for X-ray analysis was observed after one day. Yield: 0.320g (58%). Mp: 185 °C (decomposed). ^{1}H NMR (400 MHz, CDCl$_3$, 298K): δ0.03 (*s*, 9H, Si*Me$_3$*), 0.21 (*s*, 9H, Si*Me$_3$*), 0.90 (*s*, 18H, C*Me$_3$*), 1.22 (*d*, *J*= 6.8, 12H, CH(C*H$_3$*)$_2$), 1.35 (*d*, *J*= 6.8, 12H, CH(C*H$_3$*)$_2$), 2.65-2.76 (*m*, 4H, C*H*(CH$_3$)$_2$), 6.90-6.97 (*m*, 1H, Ph), 7.25-7.26 (*m*, 1H, Ph), 7.32-7,35 (*m*, 5H, Ph), 7.43-7.59 (*m*, 6H, Ph) ppm. ^{13}C {^{1}H} NMR (100.613 MHz, CDCl$_3$, 298 K): δ 4.81, 5.41, 24.53, 24.64, 28.82, 31.52, 54.19, 124.48, 124.94, 127.90, 128.29, 128.62, 129.99, 131.03, 131.30, 134.98, 145.38, 169.88 ppm. ^{29}Si {^{1}H} NMR (79.495 MHz, CDCl$_3$, 298 K): δ 4.24 (*Si*Me$_3$), 3.97 (*Si*Me$_3$), 3.60 (*Si*N(SiMe$_3$)$_2$) ppm. ^{19}F {^{1}H} NMR (376.49 MHz, CDCl$_3$, 298): δ - 179.02 (br) ppm. MALDI: *m/z* [C$_{48}$H$_{77}$CuN$_5$Si$_3$]$^+$: 871.60 [M]$^+$. Anal Calcd: C, 52.05; H, 7.01; N, 6.32. Found: C, 52.24; H, 7.17; N, 6.39.

Synthesis of 3.12:

Acetonitrile (0.05 mL) was added into the solution of **3.8** (0.397g, 0.5 mmol) in 20 mL DCM. After overnight stirring, the reaction mixture was dried completely and crystallized in DCM/pentane mixture and kept it at 0 °C. Colorless triangle shaped crystals suitable for X-ray analysis was observed after one day. Yield: 0.260g (67%). Mp: 121°C. ^{1}H NMR (400 MHz, CDCl$_3$, 298K): δ 1.26 (dd, *J*= 6.8, 3.6, 24H, CH(C*H*$_3$)$_2$), 2.07 (*s*, 6H, C*H*$_3$, *acetonitrile*), 2.46-2.57 (*m*, 4H, C*H*(CH$_3$)$_2$), 7.16-7.21 (*m*, 2H, C*H*$_{Imidazole}$), 7.36 (*d*, 4H, *J*= 7.8 Hz, Ph), 7.57 (*t*, *J*= 7.8Hz, 2H, Ph) ppm. ^{13}C {^{1}H} NMR (100.613 MHz, CDCl$_3$, 298 K): δ 21.46, 23.91, 24.69, 28.72, 123.78, 124.31, 125.29, 128.22, 129.03, 130.83, 137.87, 145.60 ppm. ^{19}F {^{1}H} NMR (376.49 MHz, CDCl$_3$, 298): δ 179.39 (br) ppm. MALDI: *m/z* [C$_{31}$H$_{42}$CuN$_4$]$^+$: 533.29 [M]$^+$. Anal Calcd: C, 48.36; H, 5.50; N, 7.28. Found: C, 48.42; H, 5.34; N, 7.19.

3.2.3. General reaction procedure and optimization table for triazole synthesis:

Catalyst (0.5 mol%) was taken in a catalysis tube inside the glove box and 2 mL dry toluene was added into this. Azide (0.2 mmol) and substituted terminal acetylene (0.2 mmol) were added into the catalysis tube and the reaction mixture was stirred at 25^{0}C for 5 hours. After 5 hours, the solvent was evaporated by using rota and solid product was obtained.

Table 3.1. *Optimization of reaction conditions for CuAAC reaction using catalyst 3.6.[a]*

Entry	Catalyst (mol%)	Solvent	Temp.	Time	Conversion yield (%)[b]
1.	1	THF	25	10	93
2.	0.5	THF	25	10	92
3.	1	Toluene	25	10	>98
4.	0.5	Toluene	25	10	98
5.	**0.5**	**Toluene**	**25**	**5**	**98**
6.	0.5	Toluene	25	3	82
7.	0.5	Toluene	25	1	60
8.	0.5	Toluene	50	3	>99
9.	0.5	Toluene	50	1	80

3.2.4. NMR spectroscopic data of the catalysis products:

3.13a[3.6]. ^{1}H NMR (400 MHz, CDCl$_3$): δ 5.58 (*s*, 2H), 7.33-7.29 (*m*, 3H), 7.42-7.36 (*m*, 5H), 7.66 (*s*, 1H), 7.81-7.78 (*m*, 2H).
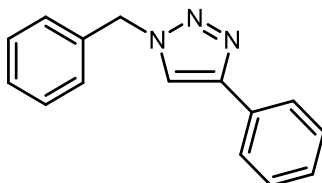
1-benzyl-4-phenyl-1H-1,2,3-triazole

3.13b[3.6]. ^{1}H NMR (400 MHz, CDCl$_3$): δ 5.55 (s, 2H), 7.30-7.28 (m, 2H), 7.42-7.34 (m, 5H), 7.56 (s, 1H), 7.65-7.64 (m, 1H).
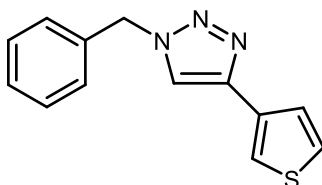
1-benzyl-4-(thiophen-3-yl)-1H-1,2,3-triazole

3.13c[3.6]. ^{1}H NMR (400 MHz, CDCl$_3$): δ 0.93-0.89 (*t*, 3H), 1.40-1.31 (*m*, 2H), 1.66-1.58 (*m*, 2H), 2.68 (*t*, 2H), 5.49 (*s*, 2H), 7.18 (*s*, 1H), 7.26-7.24 (*m*, 2H), 7.38-7.34 (*m*, 3H).
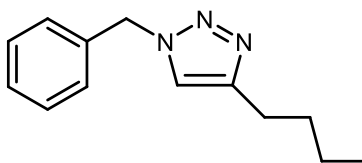
1-benzyl-4-butyl-1H-1,2,3-triazole

3.13d[3.6]. ^{1}H NMR (400 MHz, CDCl$_3$): δ 0.29 (*s*, 9H), 5.55 (*s*, 2H), 7.33-7.33 (*m*, 1H), 7.39-7.36 (*m*, 4H), 7.42 (*s*, 1H).
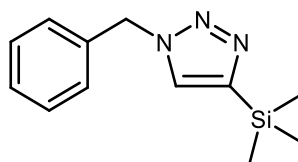
1-benzyl-4-(trimethylsilyl)-1H-1,2,3-triazole

3.13e[3.6]. ^{1}H NMR (400 MHz, CDCl$_3$): δ 6.01 (*s*, 2H), 7.31-7.28 (*m*, 1H), 7.39-7.35 (*m*, 2H), 7.56-7.47 (*m*, 5H), 7.77-7.75 (*m*, 2H), 7.94-7.91 (*m*, 2H), 8.04-8.02 (*m*, 1H).
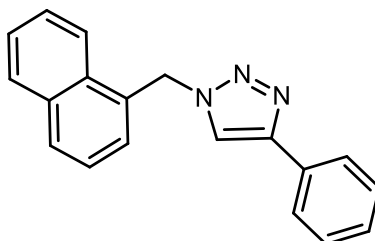
1-(naphthalen-1-ylmethyl)-4-phenyl-1H-1,2,3-triazole

3.13f[3.6]. ^{1}H NMR (400 MHz, CDCl3): δ 5.97 (*s*, 2H), 7.30-7.28 (*m*, 1H), 7.35-7.33 (*m*, 1H), 7.53-7.42 (*m*, 5H), 7.58-7.57 (*m*, 1H), 7.92-7.88 (*m*, 2H), 8.00-7.98 (*m*, 1H).
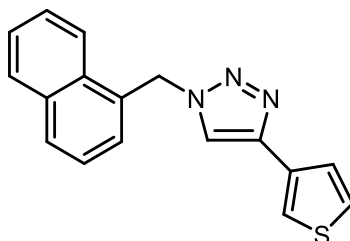
1-(naphthalen-1-ylmethyl)-4-(thiophen-3-yl)-1H-1,2,3-triazole

3.13g[3.6]. ^{1}H NMR (400 MHz, CDCl$_3$): δ 5.94 (*s*, 2H), 7.39-7.61 (*m*, 5H), 7.87-7.92 (*m*, 2H), 8.03-8.06 (*d*, 1H).
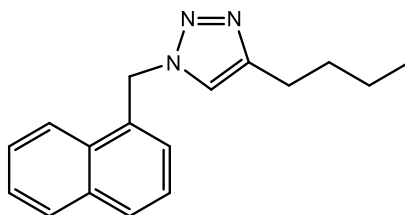
4-butyl-1-(naphthalen-1-ylmethyl)-1H-1,2,3-triazole

3.13h[3.6]. ^{1}H NMR (400 MHz, CDCl$_3$): δ 6.01 (*s*, 2H), 7.40-7.51 (*m*, 3H), 7.53-7.61 (*m*, 2H), 7.86-7.92 (*m*, 2H), 8.03-8.06 (*d*, 1H).
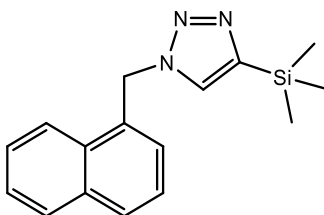
1-(naphthalen-1-ylmethyl)-4-(trimethylsilyl)-1H-1,2,3-triazole

3.13i[3.6]**.** ¹H NMR (400 MHz, CDCl₃): δ 2.36 (s, 3H), 5.52 (*s*, 2H), 7.18-7.22 (*m*, 4H), 7.29-7.32
(*m*, 1H), 7.37-7.41 (*m*, 2H), 7.64 (*s*, 1H), 7.78-7.80 (*d*, 2H).
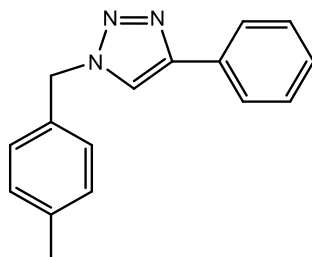
1-(4-methylbenzyl)-4-phenyl-1H-1,2,3-triazole

3.13j[3.6]**.** ¹H NMR (400 MHz, CDCl₃): δ 2.35 (*s*, 3H), 5.51 (*s*, 2H), 7.17-7.21 (*m*, 4H), 7.33-7.35 (*m*, 1H), 7.40-7.41 (*m*, 1H), 7.54 (*s*, 1H), 7.63-7.64 (*d*, 1H).
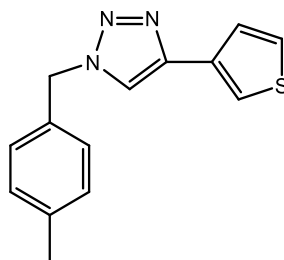
1-(4-methylbenzyl)-4-(thiophen-3-yl)-1H-1,2,3-triazole

3.13k[3.6]**.** ¹H NMR (400 MHz, CDCl₃): δ 5.69 (*s*, 2H), 7.38-7.44 (m, 2H), 7.47-7.49 (d, 1H), 7.54-7.56 (*d*, 1H), 7.79-7.81 (*d*, 2H), 8.19-8.23 (*m*, 4H).
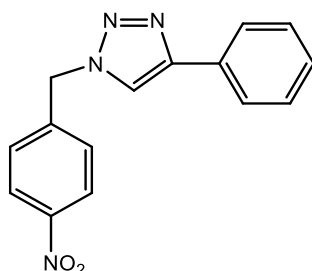
1-(4-nitrobenzyl)-4-phenyl-1H-1,2,3-triazole

3.13l[3.6]**.** ¹H NMR (400 MHz, CDCl₃): δ 5.68 (*s*, 2H), 7.22-7.44 (*m*, 1H), 7.48-7.50 (*d*, 1H), 7.55-7.57 (d, 1H), 7.67-7.69 (*m*, 1H), 8.19-8.24 (*m*, 4H).
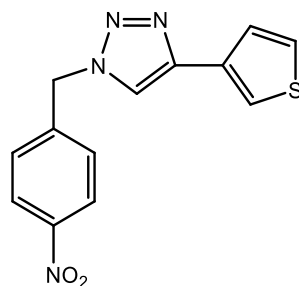
1-(4-nitrobenzyl)-4-(thiophen-3-yl)-1H-1,2,3-triazole

3.2.5. X-ray crystallographic Details

Single crystals of suitable size, coated with paraffin oil was mounted for all the complexes. Crystal data for all the complexes were collected on a Bruker Smart Apex Duo diffractometer at 100 K using Mo Kα radiation (λ = 0.71073 Å). Collected data were integrated by using SAINT and then absorption correction was done by multi-scan method using SADABS program. All the structures were solved by direct methods and refined by full-matrix least-squares methods against F2 (SHELXL-2014/6). CCDC No.: 1540046 (**3.1**), 1540047 (**3.2**), 1547791 (**3.4**), 1547792 (**3.5**), 1896663 (**3.6**), 1896664 (**3.7**), 1896665 (**3.8**), 1886948 (**3.9**), 1896666 (**3.11**) and 1896670 (**3.12**).

3.3.   Result and Discussion

3.3.1.   *Synthesis and characterization of Si(II)/NHC supported Cu⁺ complexes (3.1, 3.2, 3.4, 3.5) coordinating with symmetric arenes (C₆Me₆, C₆H₆):*

A simple synthetic protocol was designed to generate the desired copper cations. To check the credentials of **2.9** as a ligand, we commenced our investigation by probing the reaction of **2.9** with $AgSbF_6$ in the presence of hexamethylbenzene with the assumption that it would furnish [(η^6 -C₆Me₆)Cu]⁺ analogous to Hayton's results. Gratifyingly, the abstraction of bromide ions from a dichloromethane solution of **2.9** with $AgSbF_6$ in the presence of hexamethylbenzene results in the formation of [{PhC(NtBu)₂SiN(SiMe₃)₂}Cu(η^6 -C₆Me₆)]⁺[SbF₆]⁻ (**3.1**) (Scheme 3.1).

The molecular structure of **3.1** is shown in Figure 3.1, which revealed the η^6 mode of the arene ring. The Si atom adopts a distorted tetrahedral geometry with a Si→Cu bond length of 2.219(1) Å, which is in good accordance with that in **2.9** [2.222(2) Å].[9] The Cu–C(arene) bond lengths varies from 2.310(4) to 2.449(5) Å, reflecting a slightly unsymmetrical binding of the Cu with respect to the ring. The C–C bond lengths in the arene ring are
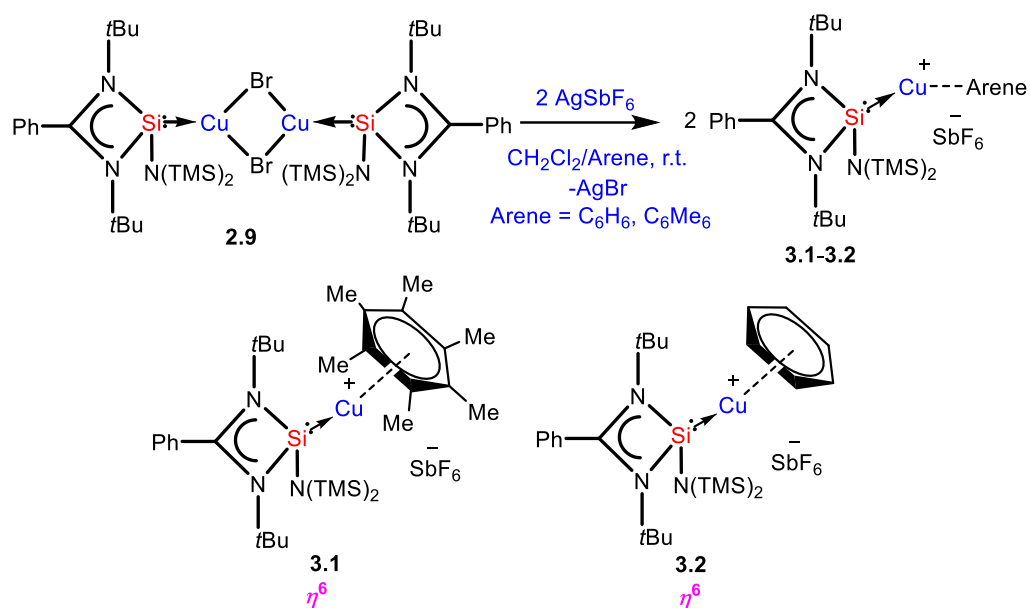
Scheme 3.1. *Syntheses of complexes **3.1** and **3.2***
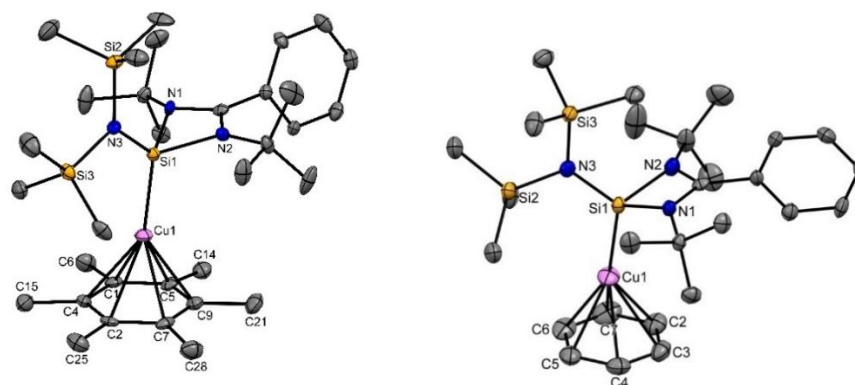
Figure 3.1. *The molecular structure of **3.1** (left) and **3.2** (right) (ellipsoids are shown at the probability level of 50%). Counter anion SbF_6^- and hydrogen atoms are omitted for clarity. Selected bond lengths (Å) of **3.1**: Si1-Cu1 2.219(1), Si1-N1 1.837(3), Si1-N2 1.834(3), Cu1-C1 2.449(5), Cu1-C2 2.372(4), Cu1-C4 2.443(5), Cu1-C5 2.407(4), Cu1-C7 2.318(4), Cu1-C9 2.310(4), C1-C4 1.408(6), C4-C2 1.414(5), C2-C7 1.420(6), C7-C9 1.410(6), C9-C5 1.409(6), C5-C1 1.414(6). **3.2**: N2-Si1 1.844(4), N1-Si1 1.847(5), N3-Si1 1.737(5), Cu1-Si1 2.231(2), Cu1-C2 2.454(7), Cu1-C3 2.477(8), Cu1-C4 2.413(9), Cu1-C5 2.359(9), Cu1-C6 2.342(9), Cu1-C7 2.379(8), C2-C3 1.38(1), C3-C4 1.39(1), C4-C5 1.39(1), C5-C6 1.39(1), C6-C7 1.40(1), C7-C2 1.40(1).*

more or less the same ranging from 1.408(6) to 1.420(6) Å. The distance between the Cu atom and the centroid of the arene ring is 1.920 Å.

Next, we turned our endeavours towards our primary objective of isolating [Cu(η^6-C$_6$H$_6$)]$^+$. A similar synthetic protocol was adopted to access [{PhC(NtBu)$_2$SiN(SiMe$_3$)$_2$}Cu(η^6-C$_6$H$_6$)]$^+$ [SbF$_6$]$^-$ (**3.2**). Complex **3.2** crystallizes in the monoclinic space group *P*2$_1$/*n*. The molecular structure of **3.2** (Figure 3.1) reveals the η^6 coordination mode of benzene to the Cu center. The Cu–C$_{benzene}$ bond distances range from 2.342(9) to 2.477(8) Å, with an average of 2.404 Å, which is longer than those reported for [Cu(η^6-C$_6$Me$_6$)]$^+$.[6] Similarly, the distance between the Cu atom and the centroid of the benzene ring (Cu–C$_{centroid}$ 1.960 Å) in **3.2** is slightly longer than those in Hayton's [Cu(η^6-C$_6$Me$_6$)]$^+$ complexes (**3.IIIa** and **3.IIIb**: 1.800(3) and 1.775(6) Å),[6] but significantly shorter than those reported for the tethered Cu(arene) complexes such as Cu(I)-cyclophanes or 9,10-anthracene derived endo-cyclic Cu(I) complexes (~2.5–3.0 Å).[4] The [SbF$_6$] anion in the asymmetric unit shows no significant bonding interaction with the Cu$^+$ atom and the closest approach between the F atom and the Cu center (Cu⋯F) is 4.96(1) Å, which rules out any possibility of interaction between them. The average C–C bond length of the C$_6$H$_6$ ligand in **3.2** is 1.39 Å (range 1.38(1)–1.40(1) Å) (C–C$_{C6H6(nonbound)}$: 1.40 Å; C–C$_{Me6C6(non-bound)}$: 1.41 Å). The Si(II) atom assumes a distorted tetrahedral geometry with a Si(II)-Cu bond length of 2.231(2) Å, which is similar to that in **2.9** and **3.1**.

All analytical and spectroscopic data of **3.1** and **3.2** are consistent with the proposed structures. The binding of benzene to the Cu atom in **3.2** resulted in a slight downfield shift of the C$_6$H$_6$ protons (δ 7.46 ppm). The appearance of two signals for the trimethylsilyl groups in ^{1}H (δ 0.24 and 0.39 ppm) as well as ^{29}Si NMR (δ 7.21 and 7.65 ppm) of **3.2** indicates that they are not equivalent and the diastereotopicity arises from the bulky substituents around the Si(II) atom. The Si(II) center resonates at δ 4.41 ppm, which is marginally upfield relative to that in **2.9** (δ 5.72 ppm)[9] in the ^{29}Si NMR spectrum.

To extend the analogous chemistry with N-heterocyclic carbenes, we reacted the previously reported IPr·CuBr (**3.3**)[11] with AgSbF$_6$ in the presence of hexamethylbenzene and benzene, which afforded [IPr·Cu(η^3-C$_6$Me$_6$)]$^+$[SbF$_6$]$^-$ (**3.4**) and [IPr·Cu(η^2-C$_6$H$_6$)]$^+$[SbF$_6$]$^-$ (**3.5**), respectively (Scheme 3.2). Single crystal X-ray
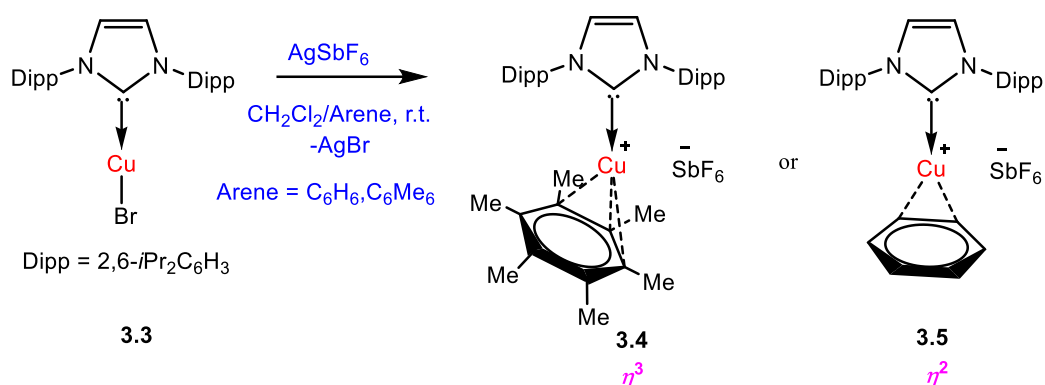
Scheme 3.2. *Syntheses of complexes **3.4** and **3.5***

studies of **3.4** and **3.5** indicated η^3 and η^2 coordination[12] of the Cu atom with the arene rings, respectively (Figure 3.2). The assignment of hapticity for the complexes having low hapticities (η^1– η^3) has always been a tough job. Therefore, we adopted the method developed by Alvarez and co-workers to calculate the hapticity (Table 3.A.1, see Appendix for the deduction of hapticities in **3.4** and **3.5**). The C_{IPr}–Cu bond lengths in **3.4** and **3.5** are 1.890(3) and 1.886(5) Å, respectively. The Cu–C_{arene} bond lengths in **3.4** range from 2.114(4) to 2.319(4) Å, and from 2.129(6) to 2.217(5) Å for **3.5**. The methyl protons of the C_6Me_6 ring appear at δ 1.8 ppm with an integration of 18 protons.
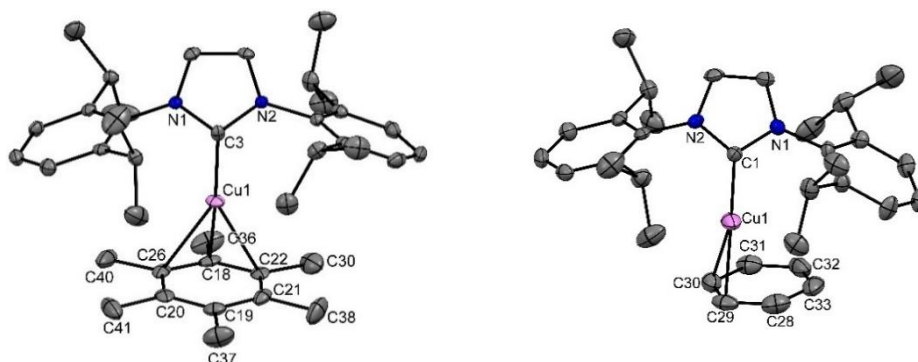
Figure 3.2. *Molecular structure of **3.4** (left) and **3.5** (right) (ellipsoids are shown at the probability level of 50%). Counter anion SbF_6^- and hydrogen atoms are omitted for clarity. Selected bond lengths (Å) **3.4**: N1-C3 1.353(4), N2-C3 1.356(4), Cu1-C3 1.890(3), Cu1-C18 2.114(4), Cu1-C22 2.289(4), Cu1-*

C26 2.319(4); Cu1-C21 2.678(4), Cu1-C20 2.715(4), Cu1-C19 2.894(4). **3.5**: *C1-N1 1.356(7), C1-N2 1.349(6), C1-Cu1 1.886(5), Cu1-C29 2.129(6); Cu1-C30 2.217(5), Cu1-C28 2.456(6), Cu1-C31 2.621(5), Cu1-C33 2.813(6), Cu1-C32 2.892(6).*

3.3.2. *Synthesis and characterization of Si(II)/NHC supported Cu⁺ complexes (**3.6, 3.7, 3.8, 3.9**) coordinating with asymmetric arenes (toluene, m-xylene):*

After this achievement, we wanted to check the coordination pattern with asymmetric arenes by using **2.9** and **3.3**. For this purpose, we followed the similar synthetic protocol for toluene and *m*-xylene with **2.9** which afforded
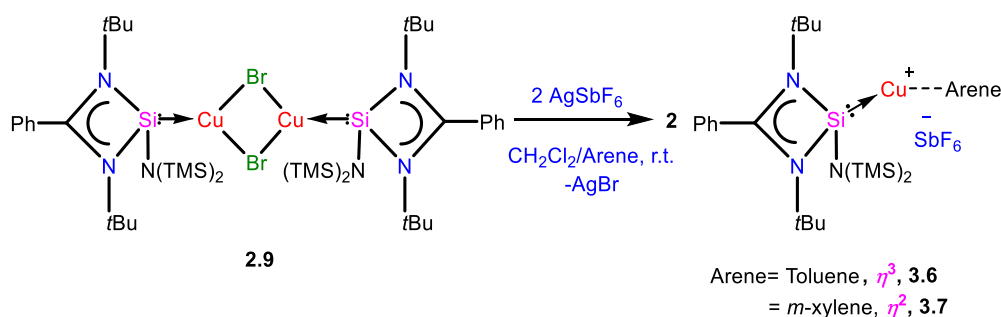
Scheme 3.3. *Syntheses of complexes **3.6** and **3.7**.*

[{PhC(N*t*Bu)$_2$SiN(SiMe$_3$)$_2$}Cu(η^3-C$_7$H$_9$)]$^+$[SbF$_6$]$^-$ (**3.6**) and [{PhC(N*t*Bu)$_2$SiN(SiMe$_3$)$_2$}Cu(η^2-Me$_2$C$_4$H$_4$)]$^+$[SbF$_6$]$^-$ (**3.7**) respectively, but unlike benzene, they adopt η^3 and η^2 binding mode, respectively (Scheme 3.3). The coordination of the arene ring to the Cu centre is accompanied by the ^{1}H NMR spectrum of **3.6** displaying a peak for three methyl protons of toluene at δ 2.51 ppm which is slightly upfield shifted when compared to that in the free toluene (2.36 ppm). The six protons of the methyl group of *m*-xylene were observed at δ 2.28 ppm as a singlet (for free *m*-xylene at 2.40 ppm) in the ^{1}H NMR spectrum of **3.7**. The ^{29}Si NMR spectra of **3.6** and **3.7** display resonances at 2.28 ppm and 2.80 ppm, respectively, which correspond to the central Si(II) atom and are slightly upfield shifted in comparison to that of **2.9** (5.72 ppm).[9]

3.6 and **3.7** crystallize in orthorhombic *P*2$_1$2$_1$2$_1$ and monoclinic *Pn* space groups, respectively. The molecular structures of **3.6** and **3.7** (Figure 3.3) unveil the η^3 and η^2 binding mode of the toluene and *m*-xylene rings, respectively (Table 3A.1, see Appendix for the deduction of hapticities in **3.6** and **3.7**).[12] The central Si(II) atom
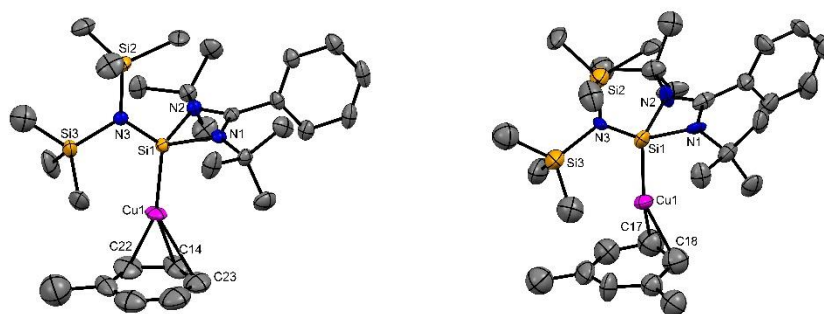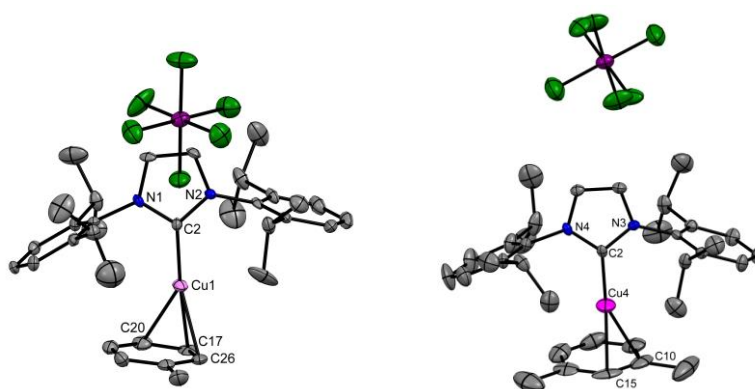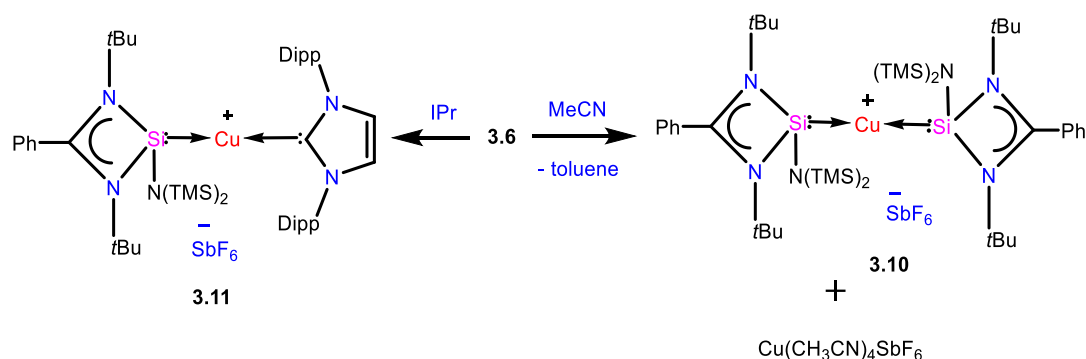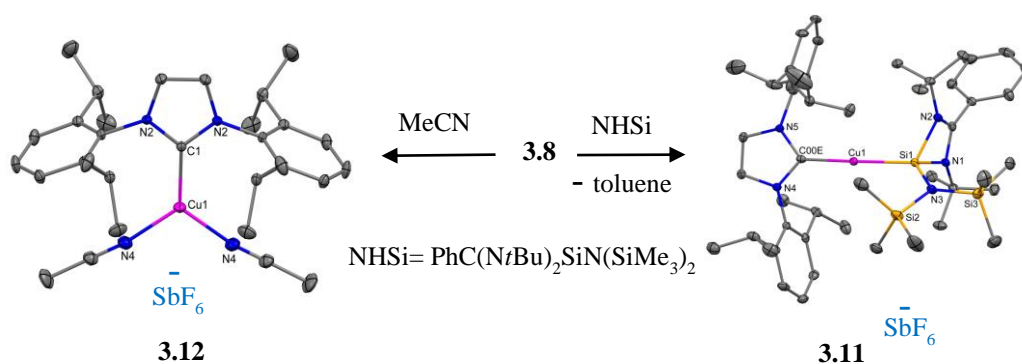
Figure 3.3*. The molecular structures of **3.6** (left) and **3.7** (right) (ellipsoids are shown at the probability level of 30%). Hydrogen atoms and SbF$_6$ anion are omitted for clarity. Selected bond lengths (Å): (**3.6**) Si1-Cu1 2.234(2), Si1-N3 1.704(6), Cu1-C14 2.230(1), Cu1-C22 2.330(1), Cu1-C23 2.426(1), Cu1-C15 2.64(1), Cu1-C24 2.697(2), Cu1-C27 2.828(2). (**3.7**) Si1-Cu1 2.244(8), Si1-N3 1.721(2), Cu1-C18 2.161(5), Cu1-C17 2.195(5), Cu1-C2 2.573(4), Cu1-C6 2.678(3), Cu1-C9 2.827(4), Cu1-C29 2.957(3).*

is four coordinate in both the cases and adopts a distorted tetrahedral geometry with the Si - Cu bond distances of 2.234(2) Å (**3.6**) and 2.244(8) Å (**3.7**), which are slightly longer than those in **2.9** [2.222(2) Å].[9]
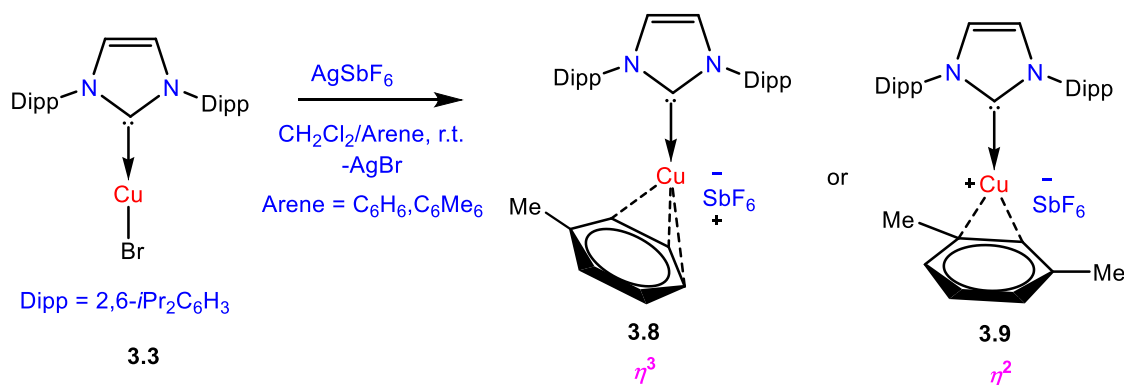
Scheme 3.4*. Syntheses of complexes **3.8** and **3.9**.*

Furthermore, we treated the IPr·CuBr (**3.3**) adduct[11] with AgSbF$_6$ in the presence of toluene and *m*-xylene, respectively, which resulted in the corresponding [IPr·Cu(η^3-C$_7$H$_8$)]$^+$[SbF$_6$]$^-$ (**3.8**) and [IPr·Cu(η^2-Me$_2$C$_6$H$_4$)]+[SbF$_6$]$^-$ (**3.9**) complexes (Scheme 3.4). The ^{1}H NMR spectra of **3.8** and **3.9** further supported the coordination of the respective arenes to the copper centre. **3.8** and **3.9** crystallize in the monoclinic *Cc* and orthorhombic *Pbca* space groups, respectively (Figure

3.4). The Cu–C$_{IPr}$ distance of **3.8** is 1.882(1) Å and matched well with the C$_{IPr}$–Cu bond length of [IPr·Cu(η^3-C$_6$H$_6$)]$^+$[SbF$_6$]$^-$ (1.890(3) Å) and [IPr·Cu(η^3-Me$_6$C$_6$)]$^+$[SbF$_6$]$^-$ (1.886(5) Å), respectively. The Cu–C$_{arene}$ bond distances and the hapticity calculations of **3.8** and **3.9** indicate the η^3 and η^2 binding mode of toluene and *m*-xylene to the Cu centre, respectively (Table 3A.1, see Appendix for the deduction of hapticities in **3.8** and **3.9**).[12] We attempted to isolate such coordination complexes with bigger arene systems (naphthalene, biphenyl, styrene, etc.) but unfortunately it did not work, and instead led to the formation of **3.10** most of the time.

Figure 3.4. *The molecular structures of **3.8** (left) and **3.9** (right) (ellipsoids are shown at the probability level of 30%). Hydrogen atoms are omitted for clarity. Selected bond lengths (Å): (5) C2–Cu1 1.882(1), Cu1–C17 2.064(2), Cu1–C20 2.314(2), Cu1–C26 2.316(1), Cu1–C13 2.746(1), Cu1–C21 2.827(9), and Cu1–C15 3.001(1).*

3.3.3. Reactivity of *3.6* and *3.8* with MeCN, NHC and NHSi:

It is well known that σ-donor ligands bind more strongly than π-donor ligands. Therefore, displacement reactions of arene rings with σ-donor ligands such as MeCN, NHC and NHSi with **3.6** and **3.8** were performed. Upon reaction of **3.6** with MeCN, the formation of a dimeric copper complex **3.10** along with Cu(CH$_3$CN)$_4$SbF$_6$ salt was noted (Scheme 3.5). **3.10** was spectroscopically characterized but the single crystal X-ray data are not sufficiently good to discuss the structural parameters. An analogous reaction of **3.8** afforded a tricoordinate copper cation **3.12,** where two acetonitrile molecules were coordinated to the Cu center (Scheme 3.6). The Cu–C$_{IPr}$ bond distance is elongated to 1.926(5) Å in **3.12**. The arene

Scheme 3.5. *Reaction of **3.6** with acetonitrile and IPr.*

Scheme 3.6. *Reaction of **3.8** with MeCN and NHSi. The molecular structures of **3.11** (right) and **3.12** (left) (ellipsoids are shown at the probability level of 30%). Hydrogen atoms and the SbF6 anion are omitted for clarity. Selected bond lengths (Å) and bond angles (deg) for **3.11**: C1–Cu1 1.939(4), Cu1–Si1 2.271(1); and C1–Cu1–Si1 178.6(1). **3.12**: C1–Cu1 1.926(5), C1–N2 1.361(4), Cu1–N4 1.976(4); N4–Cu1–N4 111.11(19), N4–Cu1–C1 124.38(10), C4–C3–N4 179.7(5), and C3–N4–Cu1 168.6(3).*

displacement reaction of **3.6** with IPr or **3.8** with NHSi afforded an identical complex, **3.11**, where a dicoordinate copper cation is bound to one silylene and one carbene ligand. This is a rare example of a mixed tetrelylene coinage metal cation. Note that, both the Cu–C$_{IPr}$ [1.939(4) Å] and Cu–Si [2.271(1) Å] bond lengths have been increased compared to their parent bond lengths.

3.3.4. *Theoretical investigation of **3.1**, **3.2**, **3.4**, and **3.5***:

In order to understand the different hapticities observed experimentally, the geometries of **3.1**, **3.2**, **3.4**, and **3.5** have been optimized at the B3LYP-D3 level of

theory together with the experimental values (Table 3.2). It can be seen that the experimental Cu–L (L= Si, C) distances are reproduced within 0.02 Å and the Cu–arene ones within 0.1 Å. The η^6 coordination in the silylene complexes is well reproduced by our calculations. The hapticities for other cases for which η^1, η^2 and η^3 coordinations can be hard to distinguish are deduced from the values of the distance ratios of the three shortest Cu–C$_{arene}$ distances (d$_1$ < d$_2$ < d$_3$), ρ_1 (d$_2$/d$_1$) and ρ_2 (d$_3$/d$_1$).[12] For the carbene complexes, the calculated hapticity is η^3 for **3.4** and η^2 for **3.5**, as indicated by the corresponding values of ρ_1 and ρ_2. It is worth mentioning here that carbene complexes evolve to η^3/η^2 when starting the optimization from an η^3 geometry, whereas silylene complexes behave conversely.

We have performed an NBO analysis of the benzene complexes **3.2** and **3.5** to try to rationalize their different behavior in terms of arene coordination. Second order perturbation analysis revealed that bonding between Cu and the carbene ligand is a donor–acceptor interaction from the carbene lone pair to an empty Cu orbital (nC→nCu*, E= 109.1 kcal mol^{-1}). Cu–silylene donor–acceptor interactions in **3.2**, however, are not clearly determined because the complex could not be decomposed into the same fragments as in **3.5**. On the other hand, the coordination of the benzene ring to the metal atom is associated with donor–acceptor interactions involving a mixture of s and p benzene orbitals (98 and 84 kcal mol^{-1} in **3.2** and **3.5**, respectively). Moreover, for the carbene complex there is π-back donation towards the benzene ring (nCu→πC–C*, E= 19.3 kcal mol^{-1}). Another relevant result is that the atomic charge on the donor atoms is -0.06 for C$_{IPr}$ in **3.5**, but +1.26 for the Si atom in **3.2**. These values are consistent with the zero-valent nature of the carbenoid carbon atom and the formal positive charge of the Si atom in the zwitterionic Lewis structure of the ligand (Scheme 3.7), calculated to be
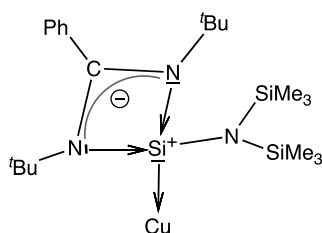
Scheme 3.7. *Zwitterionic form of the silylene ligand*

+1.18 for the free ligand. The calculated charge on Si in **3.2** is thus the result of a formal positive charge increased by σ donation, partially compensated by π back-donation from Cu. The presence of H···H attractive interactions,[13] involving the arene's hydrogen atoms on one side, and those of the *i*Pr and SiMe3 groups of the carbene and silylene ligands on the other side, might also have some effect on the different stabilities of the η^6 coordination in the two cases. The optimized

Table 3.2. *Optimized geometrical parameters of the four molecules under study. The dispersion-corrected B3LYP-D3 method and the 6-31G* basis set for N and Cu and 6-311+G*. for H and C were employed. The numbers given in parentheses are the Cu-arene distance ratios ρ_1 and ρ_2.*

Molecule	Hepticity (ρ_1, ρ_2)		Cu-L (Å)	shortest Cu-C$_{arene}$ (Å)
3.1	exp.	η^6	2.219	2.310
	calcd.	η^6	2.206	2.298
3.2	exp.	η^6	2.231	2.342
	calcd.	η^6	2.209	2.272
3.4	exp.	η^3 (1.05, 1.09)	1.890	2.114
	calcd.	η^3 (1.08, 1.13)	1.886	2.078
3.5	exp.	η^2 (1.04, 1.15)	1.886	2.129
	exp.	η^2 (1.01, 1.33)	1.887	2.105

complexes present numerous dihydrogen contacts between the arene and the silylene ligand at distances in the range of 2.3–2.5 Å (consistent with C···C distances of 3.5–3.9 Å in the crystal structures). Such intramolecular interactions have been shown to stabilize otherwise unstable systems, as for example in the case of molecules with very long C–C bonds[14] or the cis form of a substituted azobenzene.[15]

We have performed NCI (non-covalent interaction) calculations[16] (Figure 3.A.1, see Appendix), observing regions of attractive non-covalent interactions between the hydrogen atoms of the benzene and the methyl groups of the silylene in **3.2** (also in the hexamethylbenzene complex **3.1**) and between the benzene

Table 3.3. *Energy decomposition analysis (EDA) into electrostatic (ΔE_{elect}), dispersion (ΔE_{disp}), polarization (ΔE_{pol}), charge transfer (ΔE_{CT}) and Pauli repulsion (ΔE_{Pauli}) terms for compounds 3.2, 3.5 and 3.5', corrected for the BSSE. The interaction is defined between the C_6H_6 ring and the Cu(IPr) and Cu(silylene) fragments, respectively; energies in kcal/mol.*

Cpd.	ΔE_{int}	ΔE_{elect}	ΔE_{disp}	ΔE_{pol}	ΔE_{CT}	ΔE_{Pauli}		
						Total	$C_6H_6 \cdot L$	$C_6H_6 \cdot Cu$
3.2 (η^6)	- 23.3	- 51.7	- 15.4	- 25.0	- 27.5	96.4	10.6	85,8
3.5' (η^6)	- 17.4	- 70.6	- 22.0	- 27.0	- 32.8	134.9	37.5	97,4
3.5 (η^2)	- 38.9	- 36.4	- 15.0	- 19.7	- 23.0	55.4	7.2	48,2

and the carbene ^{i}Pr groups in **3.5**. Indeed, AIM analysis of **3.2** discloses a bond path between the H atoms of the coordinated C_2H_2 moiety of benzene and those of the ^{i}Pr groups of the carbene, with an electron density at a bond critical point of 0.003 au, similar to previously reported dihydrogen interactions.[17]

To further test the relative influence of steric repulsions and non-covalent interactions on the hapticity of the coordinated arenes we have carried out energy decomposition analysis (EDA) for **3.2** and **3.5** (Table 3.3), as well as for the hypothetical complex **3.5´** in which the benzene is forced to be coordinated in an η^6 mode. In this constrained model complex, which is not a minimum of the potential energy surface, the Cu–C$_{arene}$ distances were set to those of **3.2**. In general, the interaction energy and its decomposition was evaluated between two molecular fragments: the C_6H_6 ring and the Cu(IPr) and Cu(silylene) fragments, respectively. It can be seen that the results for **3.5´** indicate a much stronger Pauli repulsion between the two ligands than in **3.2**, which is relieved by its slippage to a η^2 coordination. Even if slippage also reduces the stabilizing components, the balance yields a more favorable interaction energy due to the dramatic decrease of the Pauli repulsion term. EDA analysis of the interaction between benzene and the complementary ligands in the absence of the Cu centre for the three compounds in Table 3.3 allows us to estimate a Pauli term that calibrates the part of the steric repulsion that comes from benzene–ligand interactions, and we can also roughly estimate the benzene–Cu repulsion as the difference between the total and the benzene–ligand Pauli terms. The

important Pauli repulsion between the η^6-C_6H_6 molecule and the Cu ion can be attributed to the interaction between the occupied $\pi(e_{1g})$ orbitals of benzene and the d_{xz} and d_{yz} orbitals of Cu. Hence, the smaller repulsion in η^6-**3.2** compared to η^6-**3.5′** must also be attributed to the longer Cu–Si/C$_{carbene}$ distance in the former case (2.21 Å in **3.2** *vs.* 1.89 Å in **3.5′**). Clearly, slippage of the benzene ring from the η^6 coordination in **3.5′** to the η^2 mode in **3.5** results in a significant decrease in both the benzene–carbene and benzene–copper Pauli repulsions, and explains the preference for the η^2 mode in the latter, in contrast with the preference for the η^6 coordination in **3.2**.

The dispersion interaction contributes signifcantly to the bonding between the C_6H_6 ring and the CuL fragments (L= {PhC(NtBu)$_2$SiN(SiMe$_3$)$_2$} and IPr for **3.2** and **3.5**, respectively), and outweighs in both cases the benzene–ligand steric repulsions, contributing some 5–8 kcal mol^{-1} to the bonding between the benzene and the CuL fragment. It must be noted that the dispersion contribution is similar in the two cases and therefore has a negligible effect on the hapticity.

3.3.5. *Theoretical investigation of* **3.6**, **3.7**, **3.8**, and **3.9**:

We have carried out quantum mechanical calculations at the M06/def2-TZVPP//BP86/def2-SVP level of theory to explore the bonding interaction between the silylene/IPr and Cu-centre as well as the arene ring in complexes **3.6**, **3.7**, **3.8** and **3.9** (The optimization using metaGGA functional M06 and GGA functional BP86 with D3BJ dispersion correction by Grimme (BP86-D3-BJ) also leads to the Z2/Z3-coordination of the arene ring.) The NBO charge analysis (Table 3.A.5, see Appendix) of the complexes **3.6** and **3.7** shows that the N(SiMe$_3$)$_2$ (-0.53 *e*) and (Ph)C(Nt-Bu)$_2$ (-0.35 to -0.36 *e*) ligands possess negative group charges. The positive charge is mainly located on the Si(II)-centre (1.43 *e*), Cu (0.27–0.29 *e*) and the arene ligand (0.16–0.189 *e*). Thus, a high positive charge on Si and a low positive charge on the Cu-centre indicate a strong Si(II)→Cu donor acceptor character, which is commonly observed in silylene complexes.[7a,7e,7f,18]
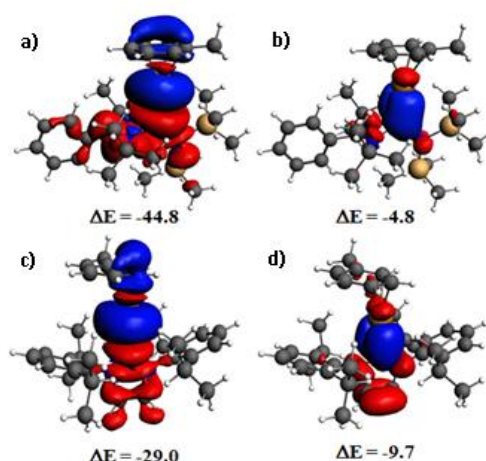
*Figure 3.5. Plots of deformation densities (BP86/TZ2P) for **a**) donation from Si(II)→ sp-hybrid orbital on Cu; **b**) backdonation from d-orbital of Cu →Si-N π**-MO of silylene in **3.6**; **c**) donation from NHC →sp-hybrid orbital on Cu and **d**) back donation from d-orbital of Cu →π**-MO of NHC in **3.8**. The direction of charge flow is from red to blue. The isosurface value for the plot is 0.0003. The associated energy (ΔE) is given in kcal mol^{-1}.*

The NBO analyses of complexes **3.6** and **3.7** suggest that five d-orbitals of Cu^{+} ([1]S, 3d[10]4s[0]) are occupied, and one of the vacant sp-hybrid orbital (79.6% s and 18.4% p) accepts the lone pair from silylene to form the Si(II)→Cu bond. The NBO charge analysis (Table 3.A.5, see Appendix) indicates significant differences in charge distribution on the carbene complexes **3.8** and **3.9** compared to that on **3.6** and **3.7**. The Cu-centre in **3.8** (0.51–0.51 *e*) has a more positive charge than that in **3.6**. The group charge on the NHC ligand is positive (0.33 *e* and 0.32 *e*) which indicates the IPr→Cu donor–acceptor bond in the complexes **3.8** and **3.9**.[19] The NBO analysis further confirms that the five d-orbitals of Cu^{+} ([1]S, 3d[10]4s[0]) are occupied in the complexes **3.8** and **3.9** and one of the vacant sp-hybrid orbital (80.4% s and 14.9% p) accepts the lone pair from the NHC to form the IPr→Cu bond. The nature of bonding between silylene/NHC and the Cu-centre as well as the arene ring and the Cu-centre was further analysed by the EDA-NOCV method and the results of the toluene complexes **3.6** and **3.8** are discussed here (Table 3.4).

The analysis of Si(II)→Cu in **3.6** by the EDA-NOCV method (Table 3.4) indicates that the electrostatic interaction (ΔE$_{elstat}$= 64.6%) is higher than the covalent interaction (σ-type lone pair on silylene to the vacant sp-hybrid orbital on Cu accounts to 64.2% of the total covalent interaction) (Figure 3.5a, -44.8 kcal mol^{-1}). The back donation from the filled d-

orbitals on Cu to the Si–N σ*-molecular orbital (MO) of silylene contributes to 6.9% of the total orbital interaction (Figure 3.5b, -4.8 kcal mol^{-1}). Similar to **3.6**, the IPr→Cu bond in **3.8** (Table 3.4) also has a significant contribution from electrostatic interaction (ΔE_{elstat}= 69.1%).

*Table 3.4. The EDA-NOCV results (BP86/TZ2P) in **3.6** and **3.8**. (a) For the interaction of L^{1}L^{2}Si fragment with Cu(Tol)$^+$ and (b) L^{1}L^{2}SiCu$^+$ fragment with Tol in complex **3.6**. (c) The NHC (IPr) fragment with Cu(Tol)$^+$ and (d) NHCCu$^+$ fragment with Tol in complex **3.8**. L^1 = N(SiMe$_3$)$_2$, L^2 = (Ph)C(Nt-Bu)$_2$, Tol = C$_6$H$_5$(CH$_3$). Energies are in kcal/mol.*

Parameter	(a)	(b)	(c)	(d)
ΔE_{int}	-94.8	-27.2	-94.6	-37.2
ΔE_{Pauli}	102.2	76.1	109.5	69.9
$\Delta E_{elstat}{}^a$	-127.3 (64.6%)	-58.4 (56.4%)	-141.1 (69.1%)	-57.4 (53.6%)
$\Delta E_{orb}{}^a$	-69.8 (35.4%)	-45.0 (43.6%)	-63.0 (30.9%)	-49.7 (46.4%)
$\Delta E_{Tol \rightarrow Cu}{}^b$	--	-22.5 (50.0%)	--	-24.7 (49.7%)
$\Delta E_{Cu \rightarrow Tol}{}^b$	--	-8.7 (19.3%)	--	-11.5 (23.1%)
$\Delta E_{Silylene/NHC \rightarrow Cu}{}^b$	-44.8 (64.2%)	--	-29.0 (46.0%)	--
$\Delta E_{Cu \rightarrow Silylene/NHC}{}^b$	-4.8 (6.9%)	--	-9.7 (15.4%)	--
$\Delta E_{rest}{}^{b,c}$	-20.2	-13.8	-24.3	-13.5
$\Delta E_{prep}{}^d$	7.9	3.5	3.2	4.5

^{a}*Values in parentheses give the percentage contribution to the total attractive interactions, ΔE_{orb} + ΔE_{elstat}.* ^{b}*Values in parentheses give the percentage contribution to the orbital interactions, ΔE_{orb}.* $^c\Delta E_{rest} = \Delta E_{orb} - (\Delta E_{M \rightarrow L} + \Delta E_{L \rightarrow M})$. $^d\Delta E_{prep}$ and De represent the preparatory and dissociation energy respectively.*

3.3.6. Catalytic Studies:

To explore the catalytic activity of our newly synthesized complexes, **3.6** and **3.8**, we have studied the CuAAC reaction, which has been widely used for the synthesis of 1,2,3-triazoles.[20] 1,2,3-triazoles are interesting molecule with extensive application in drug development and bio-conjugation.[20c] Unlike, NHC-Cu(I) complexes, which have ample literature precedence in CuAAC catalysis,[21] there is only one report of CuAAC reaction with NHSi–Cu(I) multinuclear complexes (**1.72a** and **1.72b**, Chart 3.2) by Stalke et al,[22] however, the methodology is limited to only benzyl azide (5 examples).
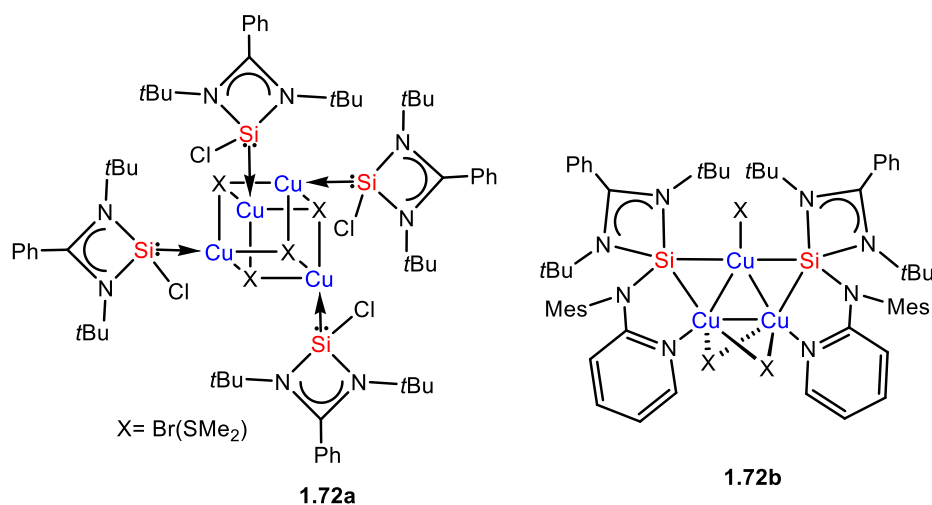
Chart 3.2. *Reported Si(II)-Cu(I) catalysts for the click chemistry.*

Moreover, there is no report of monocoordinated Si(II)-Cu complex for CuAAC reactions. Therefore, we have used **3.6** as a catalyst for different azides and alkynes at ambient conditions (Scheme 3.8), which afforded the desired trizoles in good to excellent yields. Higher yield is observed for aromatic alkynes (**3.13a, 3.13b, 3.13e, 3.13f, 3.13i, 3.13j**) than aliphatic ones (Scheme 3.8). Aromatic azides bearing electron donating groups afford better yields (**3.13i** and **3.13j**) than electron withdrawing ones (**3.13k** and **3.13l**) (Scheme 3.8). Replacement of benzyl azide with naphthylmethyl moiety has little effect in the yield except in the case of **3.13g** (Scheme 3.8). It is to be noted here that the exploitation of naphthylmethyl azide in homogeneous click chemistry is not known, and the formation of triazole with naphthylmethyl group is only accessed in heterogeneous manner.[23] The drop of yield for trimethylsilyl alkynes (**3.13d** and **3.13h**, Scheme 3.8) was also noted with Stalke's multinuclear Si(II)-Cu catalyst. In fact, the performance of **3.6** is better than Stalke's catalysts in terms of catalyst loading (0.5 mol% vs 1 mol%) and reaction time.
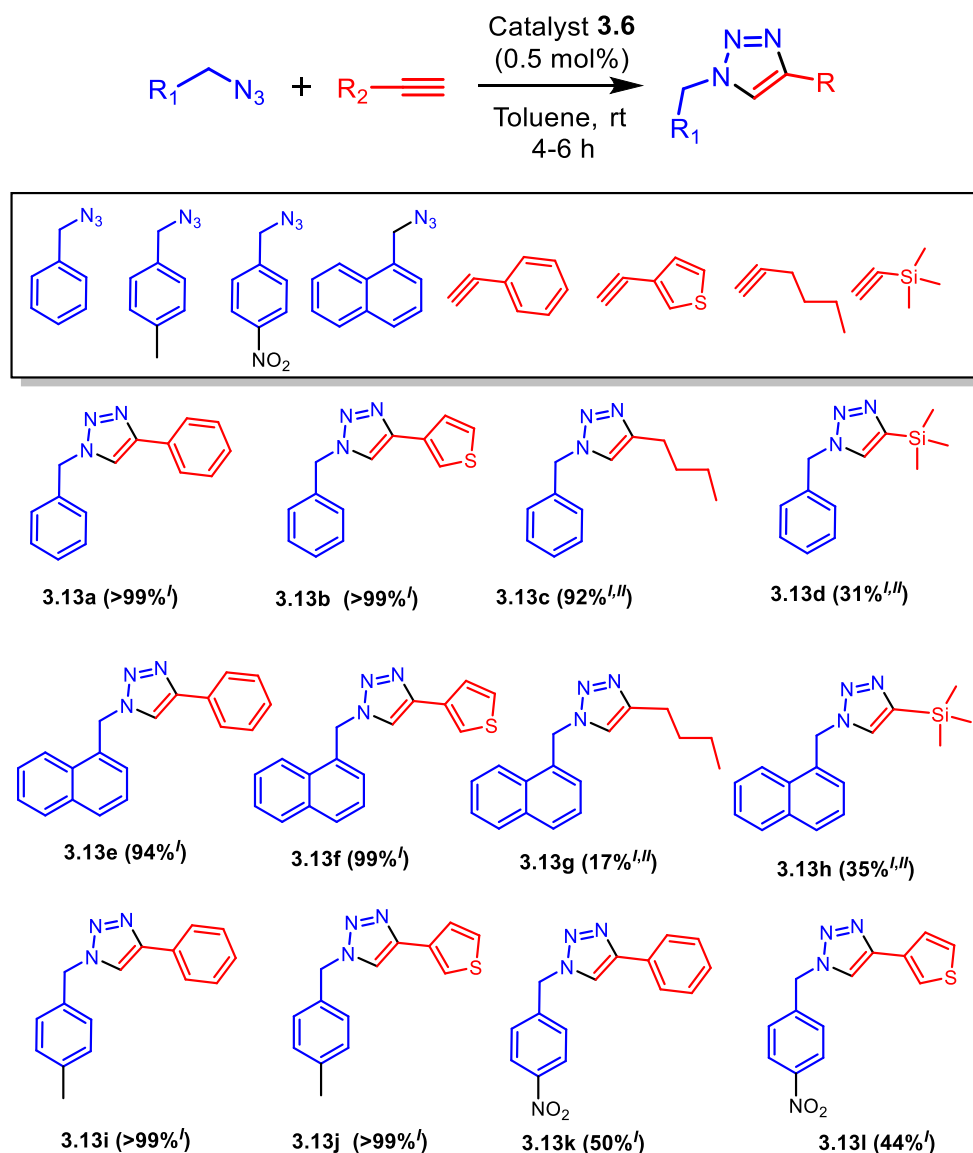
Scheme 3.8. *General reaction scheme and substrate scope for triazole synthesis using **3.6**. [I]Reaction condition: azide (0.2 mmol), alkyne (0.2 mmol), toluene (2 mL) at room temperature. [II]Heating at 50 °C. ^{1}H NMR spectroscopy was used to determine the conversion yield of the products.*

3.4.   Conclusions

This study was undertaken to synthesize the first monocoordinated copper(I)-silylene/IPr complexes coordinating with symmetrical arenes (benzene and hexamethyl benzene) as well as with unsymmetrical arenes (toluene and *m*-xylene). It was observed that silylene supported copper cation was found to be bound with both benzene and hexamethylbenzene in an η^6 mode whereas with

toluene and *m*-xylene it forms η^3 and η^2 coordination mode, respectively. Hence, we have isolated the first elusive $[Cu(\eta^6\text{-}C_6H_6)]^+$ moiety stabilized by silylene, which is otherwise only been observed in the gas phase. DFT calculation of $[Cu(\eta^6\text{-}C_6H_6)]^+$ revealed that the positive charge on silylene favors back-donation from the Cu atom, thus relieving the repulsions between the benzene π-system and the Cu d-electrons. Although, the weak bonding between copper and free arene is the synthetic obstacle, it constitutes a major driving force for the catalysis reaction by easy substitution of an arene with the substrates. Hence we have carried out the click reaction for the synthesis of a series of triazoles by using Si(II) supported copper-toluene cationic complex. Low catalyst loading and less reaction time is the important feature of the catalyst. We observed that 0.5 mol% catalyst loading is sufficient for different types of azides and alkynes under ambient conditions, which afforded the desired triazoles in good to excellent yields.

3.5. References

1. (a) Herrero-Gómez, E.; Nieto-Oberhuber, C.; López, S.; Benet-Buchholz, J.; Echavarren, A. M. *Angew. Chem.* **2006**, *118*, 5581–5585; *Angew. Chem., Int. Ed.* **2006**, *45*, 5455–5459. (b) Lavallo, V.; Frey, G. D.; Kousar, S.; Donnadieu, B.; Bertrand, G. *Proc. Natl. Acad. Sci. U. S. A.* **2007**, *104*, 13569–13573. (c) Shelly, K.; Finster, D. C.; Lee, Y. J.; Scheidt, W. R.; Reed, C. A. *J. Am. Chem. Soc.* **1985**, *107*, 5955-5959.

2. (a) Dines, M. B.; Bird, P. H. *J. Chem. Soc. Chem. Commun.* **1973**, 12. (b) Conry, R. R. *Chem. Commun.* **1998**, 555–556. (c) Conry, R. R.; Striejewske, W. S.; Tipton, A. A. *Inorg. Chem.* **1999**, *38*, 2833–2843. (d) Lee, A. M.; Na, S. J.; Kwon, H. Y.; Lee, B. Y.; Kang, S. O. Organometallics **2004**, *23*, 5382–5385. (e) Turnerla, R. W.; Amma, E. L. *J. Am. Chem. Soc.* **1966**, *88*, 1877–1882.

3. Meyer, F.; Khan, F. A.; Armentrout, P. B. *J. Am. Chem. Soc.* **1995**, *117*, 9740–9748.

4. (a) Mascal, M.; Kerdelhu, J.-L.; Blake, A. J.; Cooke, P. A. *Angew. Chem.* **1999**, *111*, 2094-2096; *Angew. Chem., Int. Ed.* **1999**, *38*, 1968–1971. (b) Xu, F.-B.; Li, Q.-S.; Wu, L.-Z.; Leng, X.-B.; Li, Z.-C.; Zeng, X.-S.; Chow, Y. L.; Zhang, Z.-Z. *Organometallics* **2003**, *22*, 633–640.

5. Zhang, S.-L.; Liu, L.; Fu, Y.; Guo, Q.-X. *J. Mol. Struct.* **2005**, *757*, 37–46.

6. Wright, A. M.; Irving, B. J.; Wu, G. A.; Meijer, J. H. M.; Hayton, T. W. *Angew. Chem.* **2015**, *127*, 3131-3134; *Angew. Chem., Int. Ed.* **2015**, *54*, 3088–3091.

7. (a) Someya, C. I.; Haberberger, M.; Wang, W.; Enthaler, S.; Inoue, S. *Chem. Lett.* **2013**, *42*, 286–288. (b) Brück, A.; Gallego, D.; Wang, W.; Irran, E.; Driess, M.; Hartwig, J. F. *Angew. Chem.* **2012**, *124*, 11645-11649; *Angew. Chem., Int. Ed.* **2012**, *51*, 11478–11482. (c) Alvarez-Rodriguez, L.; Cabeza, J. A.; Garcia-Alvarez, P.; Polo, P. *Coord. Chem. Rev.* **2015**, *300*, 1–28. (d) Blom, B.; Stoelzel, M.; Driess, M. *Chem. Eur. J.* **2013**, *19*, 40 – 62. (e) Khan, S.; Ahirwar, S. K.; Pal, S.; Parvin, N.; Kathewad, N. *Organometallics* **2015**, *34*, 5401-5406. (f) Khan, S.; Pal, S.; Kathewad, N.; Purushothaman, I.; De, S.; Parameswaran, P. *Chem. Commun.* **2016**, *52*, 3880-3882. (g) Wang, W.; Inoue, S.; Enthaler, S.; Driess, M. *Angew. Chem.* **2012**, *124*, 6271–6275; *Angew. Chem., Int. Ed.* **2012**, *51*, 6167- 6171. (h) Wang, W.; Inoue, S.; Irran, E.; Driess, M. *Angew. Chem.,* **2012**, *124*, 3751–3754; *Angew. Chem., Int. Ed.* **2012**, *51*, 3691–3694. (i) Wang, W.; Inoue, S.; Yao, S.; Driess, M. *J. Am. Chem. Soc.* **2010**, *132*, 15890–15892. (j) Gallego, D.; Brück, A.; Irran, E.; Meier, F.; Kaupp, M.; Driess, M.; Hartwig, J. F. *J. Am. Chem. Soc.* **2013**, *135*, 15617–15626.

8. Sen, S. S.; Hey, J.; Herbst-Irmer, R.; Roesky, H. W.; Stalke, D. *J. Am. Chem. Soc.* **2011**, *133*, 12311-12316.

9. Parvin, N.; Dasgupta, R.; Pal, S.; Sen, S. S.; Khan, S. *Dalton Trans.* **2017**, *46*, 6528–6532.

10. Parvin, N.; Pal, S.; Khan, S.; Das, S.; Pati, S. K.; Roesky, H. W. *Inorg. Chem*. **2017**, *56*, 1706–1712.

11. Díez-González, S.; Escudero-Adán, E. C.; Benet-Buchholz, J.; Stevens, E. D.; Slawin, A. M. Z.; Nolan, S. P. *Dalton Trans.* **2010**, *39*, 7595–7606.

12. Falceto, A.; Carmona, E.; Alvarez, S. *Organometallics* **2014**, *33*, 6660-6668.

13. Echeverría, J.; Aullón, G.; Danovich, D.; Shaik, S.; Alvarez, S. *Nature Chem.* **2011**, *3*, 323-330.

14. Schreiner, P. R.; Chernish, L. V.; Gunchenko, P. A.; Tikhonchuk, E. Y.; Hausmann, H.; Serafin, M.; Schlecht, S.; Dahl, J. E. P.; Carlson, R. M. K.; Fokin, A. A. *Nature* **2011**, *477*, 308-311.

15. Schweighauser, L.; Strauss, M. A.; Bellotto, S.; Wegner, H. A. *Angew. Chem.* **2015**, *127*, 13636-13639; *Angew. Chem., Int. Ed.* **2015**, *54*, 13436-13439.

16. Johnson, E. R.; Keinan, S.; Mori-Sánchez, P.; Contreras-García, J.; Cohen, A. J.; Yang, W. *J. Am. Chem. Soc.* **2010**, *132*, 6498-6506.

17. Echeverría, J.; Aullón, G.; Alvarez, S. *Int. J. Quantum Chem, DOI: 10.1002/qua.25432.*

18. (*a*) Blom, B.; Enthaler, S.; Inoue, S.; Irran, E.; Driess, M. *J. Am. Chem. Soc.* **2013**, *135*, 6703–6713. (*b*) Gallego, D.; Brück, A.; Irran, E.; Meier, F.; Kaupp, M.; Driess, M.; Hartwig, J. F.; *J. Am. Chem. Soc.* **2013**, *135*, 15617–15626.

19. (a) Petz, W.; Neumüller, B.; Klein, S.; Frenking, G. *Organometallics* **2011**, *30*, 3330–3339. (b) Boehme, C.; Frenking, G. *Organometallics*, **1998**, *17*, 5801–5809.

20. (a) Schulze, B.; Schubert, *U. S. Chem. Soc. Rev.* **2014**, *43*, 2522–2571. (b) Finn, M. G.; Fokin, V. V. *Chem. Soc. Rev.* **2010**, *39*, 1231–1232. (c) Nair, D.P.; Podgórski, M.; Chatani, S.; Gong, T.; Xi, W.; Fenoli, C.R.; Bowman, C.N. *Chem. Mater.* **2014**, *26*, 724.

21. (a) Dı́ez-Gonzalez, S.; Nolan, S. P. *Angew. Chem., Int. Ed.* **2008**, *47*, 8881–8884. (b) Haldón, E.; Nicasio, M. C.; Pérez, P. J. *Org. Biomol. Chem.* **2015**, *13*, 9528–9550.

22. Paesch, A. N.; Kreyenschmidt, A.-K.; Herbst-Irmer, R.; Stalke, D. *Inorg. Chem.* **2019**, *58*, 7000–7009.

23. Moghaddam, F. M.; Saberi, V.; Kalhora, S.; Ayati, S. E. *RSC Adv.* **2016**, *6*, 80234–80243 and references therein.

*****

Chapter 4

Ligand on Demand: Carbene/Silylene/Germylene supported Nearly Naked Au(I)-Arene Complexes and Their Applications in Glycosidation

---

4.1. Introduction

Development of new ligands to regulate the reactivity is of fundamental interest in transition metal catalysis. Of late, N-heterocyclic silylenes are emerging as a new class of steering ligands. Silylene transition metal complexes have been explored as catalysts for the borylation of benzene,[1] Sonogashira coupling,[2] Kumada-Corriu coupling,[3] cyclotrimerization of alkynes,[4] the hydrosilylation of ketones,[5] amination of arenes,[6] and the reduction of amides to amines,[7] thanks to pioneering works from the groups of Driess and Hartwig. Usually, the transition metals involved in these aforementioned reactions are Mn, Fe, Ni, Co, Rh, Ir, Pd, Pt etc.[8]

In recent years, great progress has been made in efficient Au catalyzed transformation.[9] It has been proposed that the true catalysts are the cationic Au(I) complexes [LAu+], which are prepared *in situ* from the gold halide precursors.[9f] The naked Au(I) cation, [LAu+] is very unstable due to high Lewis acidic nature and hence not isolable. It is postulated that when the naked Au(I) cation is generated *in situ* in the reaction mixture, it activates the alkynes/alkenes towards a range of nucleophiles.[9g] A closest related

4.Ia R= Cy, Ar= toluene, η^1
4.Ib R= Cy, Ar= *p*-xylene, η^2
4.Ic R= *t*Bu, Ar= toluene, η^2
4.Id R= *t*Bu, Ar= *p*-xylene, η^2

4.II
η^2
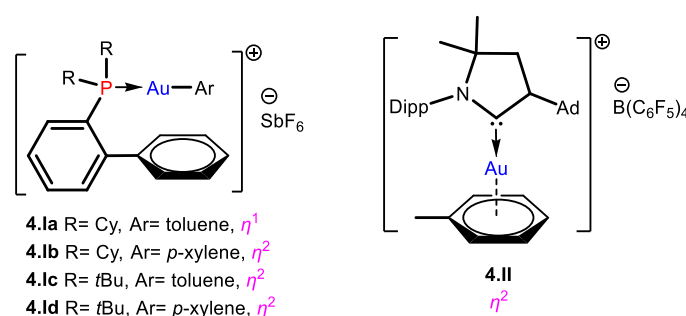
Chart 4.1. *Reported examples of [Au-C_6H_6]+ cationic complexes.*

complex of the naked Au cation, could be the [Au-(arene)]+ complexes as the binding of gold with arene is significantly weaker than alkyne/alkene (bond dissociation enthalpies of [Au-(C_2H_2)]+, [Au-(C_2H_4)]+ and [Au-(C_6H_6)]+ were -64.9, -72.9 and -3.9 kcal mol^{-1}).[10-15] Till date only two well-defined [Au(I)-arene]+ (arene = xylene and toluene) complexes are reported (**4.I** and **4.II**, Chart 4.1). While Echavarren and coworkers used phosphines as ligands,[16] the group of Bertrand and Straub utilized different carbene ligands to stabilize [Au(I)-toluene]+ cationic complexes.[17] Bertrand's complex was further used as a catalyst to generate allene cross coupling products.[17a]

It is apparent that although silylenes have excelled in TM chemistry, it has surprisingly not been used as a ligand in homogeneous Au(I) catalysis. Recently, we have shown the potential of amidinato silylene [{PhC(NtBu)$_2$}Si{N(SiMe$_3$)$_2$}][18] (NHSi) as a ligand in the isolation of unprecedented copper-η^6-benzene [{PhC(NtBu)$_2$}Si{N(SiMe$_3$)$_2$}]Cu-η^6-(C$_6$H$_6$)][SbF$_6$][19a] and other arene complexes.[19b] The latter was shown to catalyze click reaction.[19b] Given our recent interests in silylene-Au chemistry,[20,21] we have embarked into the synthesis of a well-defined [Au-arene]$^+$ complex using silylene as a σ-donor ligand. Gratifyingly, the halide abstraction from [{PhC(NtBu)$_2$}Si{N(SiMe$_3$)$_2$}]AuCl (**4.1**) in the presence of benzene led to the hitherto elusive [silylene-Au···benzene]$^+$ complex, [{PhC(NtBu)$_2$}Si{N(SiMe$_3$)$_2$}Au···η^1(benzene)][SbF$_6$] (**4.2**). Analogous reaction with related N-heterocyclic germylene as well as IPr (1,3-bis(2,6-diisopropylphenyl)imidazole-2-ylidene) was also performed resulting in
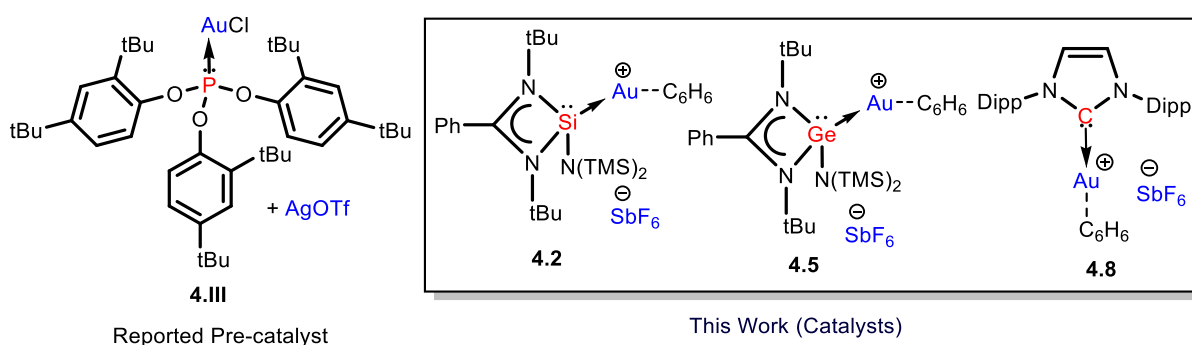
Chart 4.2. *Our previously reported precatalyst (**4.III**) for glycosidation and new catalysts (**4.2**, **4.5** and **4.8**) used in this work.*

[{PhC(NtBu)$_2$}Ge{N(SiMe$_3$)$_2$}Au···(benzene)][SbF$_6$] (**4.5**) and [IPrAu···η^2(benzene)][SbF$_6$] (**4.8**). To explore the potential of **4.2**, **4.5**, and **4.8** as catalysts they were probed for the glycoside synthesis. Recently, there is an increase in the use of Au catalysts for the synthesis of oligosaccharides,[22] however, the ligands are limited to only phosphines/phosphites and the catalysts are usually not well-defined and generated *in situ.* For example, we have previously reported oligosaccharide synthesis by using (2,4-(tBu)$_2$C$_6$H$_3$O)$_3$PAuCl/AgOTf as a pre-catalyst (**4.III**, Chart 4.2).[23] Hence, there is a scope for exploring new neutral σ-donor like NHCs or silylenes in the Au catalysed glycosidation reactions. As NHCs, silylenes or germylenes have not been explored as ligands in the Au

catalyzed synthesis of disaccharides and polysaccharides, we report for the first time the use of well-defined nearly naked NHC and silylene stabilized [Au(I)-benzene]$^+$ complexes for such synthesis. Moreover, due to their well-defined structures, it would be convenient to understand the mechanism of the catalytic cycle. Further, practical application of the above catalysts was achieved by the synthesis of the branched pentamannan core of the HIV-gp120 envelope under mild conditions.

4.2. Experimental Section

4.2.1. General Remarks

All experiments were carried out under an atmosphere of dry argon or in vaccuo using standard Schlenk technique and in a dinitrogen filled MBRAUN MB 150-G1 glovebox. The solvents used were purified by MBRAUN solvent purification system MB SPS-800. The starting materials **4.1** and **4.7** were prepared as reported in the literature. All other chemicals purchased from Aldrich were used without further purification. ^{1}H, ^{13}C, ^{31}P, ^{19}F and ^{29}Si NMR spectra were recorded in Bruker 400 MHz spectrometer, using CDCl$_3$ as solvent with external standards SiMe$_4$ (^{1}H, ^{13}C and ^{29}Si), 85% H$_3$PO$_4$ (^{31}P) and CHF$_3$ (^{19}F). Concentrated solution of the samples in CDCl$_3$ were sealed off in a NMR tube for measurement. All the heteronuclear NMRs are proton decoupled. Mass spectra were recorded using AB Sciex, 4800 plus MALDI TOF/TOF and HRMS ESI-TOF mass analyzer.

4.2.2. Synthesis of **4.2**-**4.20**

Synthesis of 4.2

AgSbF$_6$ (0.171 g, 0.5 mmol) was dissolved in DCM and added to the solution of **4.1** (0.325 g, 0.5 mmol) in benzene. Immediately AgCl was precipitated out. After overnight stirring, AgCl was separated out from the reaction mixture by filtration and reduced the volume to 15 mL and kept it at 0 °C. Colorless hexagonal shaped crystals suitable for X-ray analysis was observed after one day. Yield: 0.354 g (75%). Mp: 145 °C (decomposed). ^{1}H NMR (400.31 MHz, CDCl$_3$): δ 0.28 (*s*, 9H, Si*Me$_3$*), 0.43 (*s*, 9H, Si*Me$_3$*), 1.18 (*s*, 18H, C*Me$_3$*), 7.23-7.30 (*m*, 1H, Ph), 7.35-7.44 (*m*, 2H, Ph), 7.48 (*s*, 6H, C$_6$*H$_6$*) 7.52-7.69 (*m*, 2H, Ph) ppm. ^{13}C NMR {^{1}H} (100.67 MHz, CDCl$_3$): δ 3.61 (Si*Me$_3$*), 5.38 (Si*Me$_3$*), 30.65 (C*Me$_3$*), 54.40 (*C*Me$_3$), 126.06, 126.24, 127.20, 127.39, 127.99, 128.68, 130.59 (Ph-*C*), 172.45 (N*C*N) ppm. ^{29}Si {^{1}H} NMR (79.495 MHz, CDCl$_3$, 298 K): δ 9.45 (*Si*Me$_3$), 8.39 (*Si*Me$_3$), -6.44

(*Si*N(SiMe$_3$)$_2$) ppm. MALDI: *m/z* [C$_{27}$H$_{47}$N$_3$Si$_3$Au]$^+$: 616.05 [M-C$_6$H$_6$]$^+$. Anal Calcd: C, 35.56; H, 5.33; N, 4.44. Found: C, 35.23; H, 5.15; N, 4.57.

Synthesis of 4.3

AgSbF$_6$ (0.171 g, 0.5 mmol) was dissolved in DCM and added to the solution of **4.1** (0.350g, 0.5 mmol) in *m*-xylene. Immediately AgCl was precipitated out. After overnight stirring, AgCl was separated out from the reaction mixture by filtration and reduced the volume to 15 mL and kept it at 0 °C. Colorless block shaped crystals suitable for X-ray analysis was observed after one day. Yield: 0.329 g (68%). Mp: 148 °C (decomposed). ^{1}H NMR (400.31 MHz, CDCl$_3$): δ 0.25 (*s*, 9H, Si*Me$_3$*), 0.35 (*s*, 9H, Si*Me$_3$*), 1.14 (*s*, 18H, C*Me$_3$*), 2.40 (*s*, 6H, C$_6$H$_4$(C*H$_3$*)$_2$, 7.21-7.30 (*m*, 4H, Ph), 7.35-7.45 (*m*, 3H, Ph), 7.47-7.54 (*s*, 1H, C$_6$*H$_6$*) 7.57-7.64 (*m*, 1H, Ph) ppm. ^{13}C {^{1}H} NMR (100.67 MHz, CDCl$_3$): δ 3.39 (Si*Me$_3$*), 4.93 (Si*Me$_3$*), 20.47 (C$_6$H$_4$(*C*H$_3$)$_2$), 30.40 (C*Me$_3$*), 54.24 (*C*Me$_3$), 122.14, 125.89, 125.99, 127.08, 127.52, 128.12, 130.12, 130.40, (Ph-*C*), 172.38 (N*C*N) ppm. ^{29}Si {^{1}H} NMR (79.495 MHz, CDCl$_3$, 298 K): δ 9.34 (*Si*Me$_3$), 8.47 (*Si*Me$_3$), -8.85 (*Si*N(SiMe$_3$)$_2$). MALDI: *m/z* [C$_{27}$H$_{47}$N$_3$Si$_3$Au]$^+$: 616.05 [M-C$_6$H$_4$(CH$_3$)$_2$]$^+$. Anal Calcd: C, 37.00; H, 5.59; N, 4.32. Found: C, 36.73; H, 5.42; N, 4.40.

Synthesis of 4.4

30 mL toluene was added into the mixture of 0.232 g (0.5 mmol) of germylene [{PhC(N*t*Bu)$_2$}Ge{N(SiMe$_3$)$_2$}] and 0.147 g (0.5 mmol) of AuCl.SMe$_2$ in a 100 mL schlenk flask. After overnight stirring at room temperature, the reaction mixture was dried completely and filtered in DCM through frit and crystalized in DCM/pentane mixture. Colorless crystals suitable for X-ray analysis was observed at 0 °C. Yield: 0.290 g (83%). Mp: >240 °C. ^{1}H NMR (400.31 MHz, CDCl$_3$): δ 0.34 (*s*, 9H, Si*Me$_3$*), 0.53 (*s*, 9H, Si*Me$_3$*), 1.20 (*s*, 18H, C*Me$_3$*), 7.35-7.37 (*d*, J= 7.1 Hz, 2H, Ph), 7.44-7.55 (*m*, 3H, Ph) ppm. ^{13}C NMR {^{1}H} (100.67 MHz, CDCl$_3$): δ 3.65 (Si*Me$_3$*), 5.14 (Si*Me$_3$*), 30.82 (C*Me$_3$*), 54.17 (*C*Me$_3$), 126.60, 126.88, 127.17, 127.23, 129.57, 130.79 (Ph-*C*), 168.95 (N*C*N) ppm. MALDI: *m/z* [C$_{21}$H$_{41}$N$_3$Si$_2$GeAuClNa]$^+$: 720.08 [M+Na]$^+$. Anal Calcd: C, 36.20; H, 5.93; N, 6.03. Found: C, 36.25; H, 5.95; N, 6.07.

Synthesis of 4.5

AgSbF$_6$ (0.171 g, 0.5 mmol) was dissolved in DCM and added to the solution of **4.4** (0.348 g, 0.5 mmol) in benzene. Immediately AgCl was precipitated out. After overnight stirring,

AgCl was separated out from the reaction mixture by filtration and reduced the volume to 15 mL and kept it at 0 °C. Colorless block shaped crystals suitable for X-ray analysis was observed after one day. Yield: 0.340 g (69%). Mp: 210 °C (decomposed). ^{1}H NMR (400.31 MHz, CDCl$_3$): δ 0.39 (*s*, 9H, Si*Me$_3$*), 0.56 (*s*, 9H, Si*Me$_3$*), 1.23 (*s*, 18H, C*Me$_3$*), 7.18-7.24 (*m*, 1H, Ph), 7.36-7.41 (*m*, 5H, Ph), 7.45-7.62 (*m*, 5H, Ph) ppm. ^{13}C NMR {^{1}H} (100.67 MHz, CDCl$_3$): δ 4.69 (Si*Me$_3$*), 6.38 (Si*Me$_3$*), 32.00 (C*Me$_3$*), 55.36 (*C*Me$_3$), 127.02, 128.03, 128.41, 128.70, 128.77, 131.30, (Ph-*C*), 170.74 (N*C*N) ppm. MALDI: *m/z* [C$_{28}$H$_{50}$N$_3$Si$_2$GeAu]$^+$: 661.97 [M-C$_6$H$_6$]$^+$. Anal Calcd: C, 33.96; H, 5.09; N, 4.24. Found: C, 33.88; H, 5.15; N, 4.21.

Synthesis of 4.6

AgSbF$_6$ (0.171 g, 0.5 mmol) was dissolved in DCM and added to the solution of **4.4** (0.348 g, 0.5 mmol) in toluene. Immediately AgCl was precipitated out. After overnight stirring, AgCl was separated out from the reaction mixture by filtration and reduced the volume to 15 mL and kept it at 0 °C. Colorless block shaped crystals suitable for X-ray analysis was observed after one day. Yield: 0.360 g (72%). Mp: 212 °C (decomposed). ^{1}H NMR (400.31 MHz, CDCl$_3$): δ 0.29 (*s*, 9H, Si*Me$_3$*), 0.46 (*s*, 9H, Si*Me$_3$*), 1.24 (*s*, 18H, C*Me$_3$*), 2.70 (*s*, 3H, C*H$_{3,\text{toluene}}$*), 7.04-7.10 (*m*, 1H, Ph), 7.15-7.18 (*m*, 2H, Ph), 7.28-7.34 (*m*, 1H, Ph), 7.36-7.62 (*m*, 6H, Ph) ppm. ^{13}C NMR {^{1}H} (100.67 MHz, CDCl$_3$): δ 4.77 (Si*Me$_3$*), 6.36 (Si*Me$_3$*), 21.64 (*C*H$_{3,\text{toluene}}$), 32.09 (C*Me$_3$*), 55.64 (*C*Me$_3$), 125.49, 127.76, 128.06, 128.30, 128.41, 129.23, 129.39, 129.92, 131.01, 131.42 (Ph-*C*), 138.06 (N*C*N) ppm. MALDI: *m/z* [C$_{29}$H$_{52}$N$_3$Si$_2$GeAu]$^+$: 662.25 [M-C$_6$H$_5$CH$_3$]$^+$. Anal Calcd: C, 34.68; H, 5.22; N, 4.18. Found: C, 34.65; H, 5.25; N, 4.11.

Synthesis of 4.8

AgSbF$_6$ (0.171 g, 0.5 mmol) was dissolved in DCM and added to the solution of **4.7** (0.310 g, 0.5 mmol) in benzene. Immediately AgCl was precipitaed out. After overnight stirring, AgCl was separated out from the reaction mixture by filtration and reduced the volume to 10 mL and kept it at 0 °C. Colorless block shaped crystals suitable for X-ray analysis was observed after one day. Yield: 0.330 g (71%). Mp: 230 °C (decomposed). ^{1}H NMR (400.31 MHz, CDCl$_3$): δ 0.76 (d, 12H, *J*= 6.9 Hz, CH(C*H$_3$*)$_2$), 0.96 (d, 12H, *J*= 6.9 Hz, CH(C*H$_3$*)$_2$), 2.16-2.23 (m, 4H, C*H*(CH$_3$)$_2$), 6.97 (m, 1H, Ph), 7.04 (m, 4H, *J*= 7.8 Hz Ph), 7.22-7.28 (m, 4H, Ph), 7.39 (t, 2H, *J*= 7.8 Hz, C$_6$*H$_6$*) ppm. ^{13}C NMR {^{1}H} (100.67 MHz,

CDCl$_3$): δ 24.05, 24.25, 24.56, 28.63, 124.35, 125.08, 130.78, 133.95, 145.08, 184.36 ppm. MALDI: *m/z* [C$_{33}$H$_{40}$N$_2$Au]$^+$: 585.31 [M-C$_6$H$_6$]$^+$. Anal Calcd: C, 44.66; H, 4.96; N, 3.06. Found: C, 44.52; H, 4.51; N, 3.07.

Synthesis of 4.9

30 mL toluene was added into 0.420 g of silylene [{PhC(N*t*Bu)$_2$}Si{N(SiMe$_3$)$_2$}] (1 mmol) in a 100 mL schlenk flask and CoCp(CO)$_2$ (0.133 mL, 1mmol) was added into the reaction mixture. After overnight stirring at room temperature, the reaction mixture was dried completely and 15 mL pentane was added into the reaction mixture and kept it at -30 °C. Red colored crystals suitable for X-ray analysis was observed after two days. Yield: 0.390 g (66%). Mp: 190 °C. ^{1}H NMR (400.31 MHz, CDCl$_3$): δ 0.46 (*s*, 9H, Si*Me$_3$*), 0.76 (*s*, 9H, Si*Me$_3$*), 1.25 (*s*, 18H, C*Me$_3$*), 4.87 (*s*, 5H, *Cp*), 6.91-6.97 (*m*, 3H, Ph), 7.06 (*br*, 1H, Ph), 7.30 (*br*, 1H, Ph) ppm. ^{29}Si {^{1}H} NMR (79.495 MHz, CDCl$_3$, 298 K): δ 0.84 (*Si*Me$_3$), 4.90 (*Si*Me$_3$), 50.64 (*Si*N(SiMe$_3$)$_2$) ppm. MALDI: *m/z* [C$_{28}$H$_{49}$N$_3$Si$_3$OCo]$^+$: 587.20 [M+H]$^+$, 508.21 [M-Cp+2H]$^+$. IR ν_{CO} (solid): 1873 cm^{-1}. Anal Calcd: C, 57.30; H, 8.42; N, 7.16. Found: C, 57.38; H, 8.45; N, 7.21.

Synthesis of 4.10

20 mL hexane was added into 0.646 g (1 mmol) of tris(2,4-di-tert-butylphenyl)phosphite in a 100 mL schlenk flask and CoCp(CO)$_2$ (0.133 mL, 1 mmol) was added into the reaction mixture and was refluxed for 5 days. After filtration, kept the reaction mixture at -30 °C. Red colored crystals suitable for X-ray analysis was observed after two days. Yield: 0.570g (70%). Mp: 174-176 °C. ^{1}H NMR (400.31 MHz, CDCl$_3$): δ 1.30 (*s*, 36H, C*Me$_3$*), 1.53 (*s*, 36H, C*Me$_3$*), 4.64 (*s*, 5H, *Cp*), 7.05 (*d*, *J*= 8.6 Hz, 3H, Ph), 7.36 (*s*, 3H, Ph), 7.68 (*d*, *J*= 8.6 Hz, 3H, Ph) ppm. ^{31}P {^{1}H} NMR (161.976 MHz, CDCl3, 298K): δ 155.41 ppm. MALDI: *m/z* [C$_{49}$H$_{71}$PO4Co]$^+$: 834.12 [M-2H]$^+$, 755.18 [M-Cp-H]$^+$. IR ν_{CO} (solid): 1956 cm^{-1}. Anal Calcd: C, 72.30; H, 8.79. Found: C, 72.28; H, 8.81.

General procedure for the glycosylation:
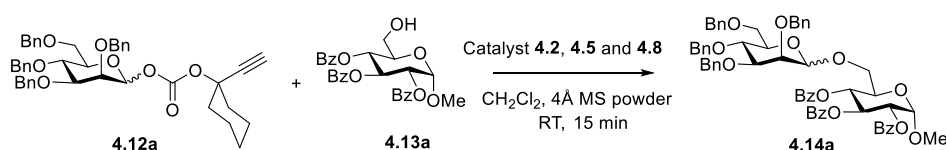
Silylene-Au complex (**4.2**) (0.014 g, 0.0145 mmol) was added to a solution of donor **4.12a** (0.100 g, 0.145 mmol) and acceptor **4.13a** (0.073 g, 0.145 mmol) in anhydrous CH_2Cl_2 (4 mL) containing 4Å MS powder (0.200 g) and stirred at 25 ^{0}C for 15 min, concentrated *in vacuo*, and resulting residue was purified by column chromatography (*n*-hexane/EtOAc) to afford disaccharide **4.14a** (0.113 g, 75%) as a thick syrup.

Similar procedure was adopted for the synthesis of **4.14b, 4.14c, 4.14d, 4.14e, 4.14f, 4.18** and **4.20** in case of other Au-complexes (**4.5** and **4.8**) also.

Synthesis of 4.19

To a solution of compound **4.18** (0.350 g, 0.241 mmol, 1 eq), methanol-CH_2Cl_2 (1:1) (4 mL), a 1 M solution of NaOMe in MeOH (1 mL), was added and stirred for 1 h. The NaOMe was quenched by Amberlite IR-120, filtered, and concentrated in vacuo and the resulting residue was purified by column chromatography (*n*-hexane/EtOAc) to afford trisaccharide di-ol **4.19** (0.275 g, 92%) as a thick syrup

Compound Characterization Data

Compound 4.12a

Mishra, B.; Neralkar, M.; Hotha, S. *Angew. Chem., Int. Ed.* **2016**, *55*, 7786-7791.

Compound 4.12b

1-*O*-(((1-ethynylcyclohexyl)oxy)carbonyl)-2-*O*-benzoyl-3,4,6-tri-*O*-benzyl α/β-D-mannopyranoside [α:β (1.0:3.0)]: Syrup; $[α]^{25}_D$ (CHCl₃, *c* 1.0): +13.8; IR (cm^{-1}, CHCl₃): 3250, 2935, 1730, 1625, 1455, 1260, 1130, 1080, 915, 705; ¹H NMR (400.31 MHz, CDCl₃): δ 1.19 – 1.27 (m, 2H), 1.40 – 1.45 (m, 4H), 1.50 – 1.60 (m, 6H), 1.67 – 1.73 (m, 2H), 1.78 – 1.86 (m, 2H), 1.88 – 2.01 (m, 2H), 2.03 – 2.15 (m, 2H), 2.38 (s, 1H), 2.41 (s, 1H), 3.67 – 3.73 (m, 2H), 3.76 – 3.91 (m, 7H), 4.03 – 4.25 (m, 1H), 4.50 – 4.67 (m, 8H), 4.73 – 5.35 (m, 5H), 5.38 – 6.34 (m, 3H), 7.12 – 7.19 (m, 14H), 7.27 – 7.34 (m, 16H), 7.38 – 7.43 (m, 4H), 7.52 – 7.57 (m, 2H), 7.99 – 8.01 (m, 4H); ¹³C {¹H} NMR (100.67 MHz, CDCl₃): δ 22.3, 22.4, 22.5, 22.5, 24.9, 25.0, 36.4, 36.7, 36.7, 36.8, 68.1, 68.2, 72.5, 72.7, 73.4, 73.6, 73.6, 75.0, 75.1, 75.2, 75.2, 75.3, 75.6, 76.4, 77.2, 77.4, 78.2, 78.4, 79.8, 79.8, 82.5, 82.5, 93.5, 95.5, 127.7 – 128.0 (12C), 128.1 (6C), 128.4 – 128.5 (16C), 129.5, 129.7, 130.0 (4C), 133.3 (2C), 137.6, 137.9 (2C), 138.0 (2C), 138.1, 151.0, 151.3, 165.1, 165.5; HRMS (ESI-MS): *m/z* [C₄₃H₄₄O₉Na]⁺: 727.2874 [M+Na]⁺.

Compound 4.12c

Mishra, B.; Neralkar, M.; Hotha, S. *Angew. Chem., Int. Ed.* **2016**, *55*, 7786-7791.

Compound 4.12d

1-*O*-(((1-ethynylcyclohexyl)oxy)carbonyl)-2,3,5-tri-*O*-benzyl α-D-arabinoside: Syrup; $[\alpha]^{25}_D$ (CHCl$_3$, *c* 1.0): +33.2; IR (cm^{-1}, CHCl$_3$): 3020, 1746, 1518, 1215, 1049, 740, 669; ^{1}H NMR (400.31 MHz, CDCl$_3$): δ 1.39 (m, 1H), 1.54 – 1.65 (m, 1H), 1.65 – 1.79 (m, 4H), 1.92 – 2.00 (m, 2H), 2.22 – 2.36 (m, 2H), 2.71 (s, 1H), 3.69 (d, J = 4.9 Hz, 2H), 4.08 (dd, J = 5.8, 2.0 Hz, 1H), 4.23 (d, J = 2.8 Hz, 1H), 4.47 (q, J = 5.0 Hz, 1H), 4.53 – 4.60 (m, 3H), 4.61 (d, J = 2.1 Hz, 2H), 4.70 (d, J = 11.9 Hz, 1H), 6.25 (s, 1H), 7.29 – 7.43 (m, 15H); ^{13}C {^{1}H} NMR (100.67 MHz, CDCl$_3$): δ 22.6, 22.6, 25.0, 36.7, 37.0, 69.4, 72.1, 72.1, 73.5, 75.2, 78.0, 82.9, 83.4, 83.4, 87.0, 103.2, 127.7, 127.8, 127.8, 127.8, 127.8, 127.8, 128.1, 128.1, 128.1, 128.4, 128.4, 128.4, 128.4, 128.5, 128.5, 137.2, 137.7, 138.0, 151.4; HRMS (ESI-MS): *m/z* [C$_{35}$H$_{38}$O$_7$Na]$^+$: 593.2518 [M+Na]$^+$.

Compound 4.12e

Sureshkumar, G.; Hotha, S. *Glycoconjugate. Journal,* **2012**, *29*, 221-230.

Compound 4.12f

Thadke, S. A.; Mishra, B.; Hotha, S. *Org. Lett.* **2013**, *15*, 2466-2469.

Compound 4.13a

Tiwari, V.; Badavath, V. N.; Singh, A. K.; Kandasamy, J. *Tetrahedron Lett.* **2018**, *59*, 2511–2514.

Compound 4.14a

Methyl 2,3,4-tri-*O*-benzoyl-6-*O*-(2,3,4,6-tetra-*O*-benzyl α/β-D-mannopyranosyl) α-D-glucopyranoside [α:β (3.0:1.0)]: Syrup; $[\alpha]^{25}_D$ (CHCl$_3$, *c* 1.0): +44.7; IR (cm^{-1}, CHCl$_3$): 3021, 2931, 1730, 1503, 1455, 1271, 1215, 1101, 919, 748, 699; ^{1}H NMR (400.31 MHz, CDCl$_3$): δ 3.37 (s, 3H), 3.43 (s, 3H), 3.48 – 3.57 (m, 2H), 3.59 – 3.74 (m, 7H), 3.80 – 4.02 (m, 5H), 4.03 – 4.26 (m, 3H), 4.29 – 4.42 (m, 3H), 4.42 – 4.67 (m, 9H), 4.68 – 5.09 (m, 7H), 5.14 – 5.37 (m, 4H), 5.48 – 5.66 (m, 2H), 6.00 – 6.25 (m, 2H), 7.14 – 7.20 (m, 4H), 7.20 – 7.41 (m, 50H), 7.41 – 7.56 (m, 4H), 7.83 – 8.01 (m, 12H); ^{13}C {^{1}H} NMR (100.67 MHz, CDCl$_3$): δ 55.5, 55.6, 66.3, 68.2, 68.7, 69.0, 69.1, 69.5, 69.6, 69.9, 70.7, 70.7, 71.5, 72.1, 72.2, 72.2, 72.3, 72.7, 73.3, 73.5, 74.0, 74.2, 74.8, 74.9, 74.9, 75.1, 75.2, 76.1, 80.0, 82.2, 97.0, 97.1, 98.3, 102.4, 127.5 – 128.2 (24C), 128.3 – 128.5 (28C), 129.0, 129.2, 129.2, 129.2, 129.4, 129.4, 129.8 – 130.0 (12C), 133.2, 133.2, 133.4, 133.5, 133.5, 133.6, 138.3, 138.4, 138.5, 138.5,

138.6, 138.7, 138.8, 139.0, 165.2, 165.2, 165.5, 165.9, 165.9, 166.0; HRMS (ESI-MS): *m/z* [$C_{62}H_{60}O_{14}Na$]$^+$: 1051.3875 [M+Na]$^+$.

Compound 4.14b

Methyl 2,3,4-tri-*O*-benzoyl-6-*O*-(2-*O*-benzoyl-3,4,6-tri-*O*-benzyl α-D-mannopyranosyl) α-D-glucopyranoside: Mp: 64 °C; [α]^{25}$_D$ (CHCl$_3$, *c* 1.0): +42.3; IR (cm^{-1}, CHCl$_3$): 3021, 1727, 1453, 1267, 1103, 1099, 1028, 745, 669; ^{1}H NMR (400.31 MHz, CDCl$_3$): δ 3.45 (s, 3H), 3.67 (dd, J = 11.0, 2.8 Hz, 1H), 3.74 (dd, J = 10.8, 2.9 Hz, 1H), 3.83 (dd, J = 10.8, 3.7 Hz, 1H), 3.87 (d, J = 8.7 Hz, 1H), 4.01 (dd, J = 11.0, 5.3 Hz, 1H), 4.09 – 4.19 (m, 2H), 4.31 (ddd, J = 9.8, 4.9, 3.0 Hz, 1H), 4.48 (d, J = 12.0 Hz, 1H), 4.56 (dd, J = 15.4, 11.2 Hz, 2H), 4.70 (d, J = 12.0 Hz, 1H), 4.75 (d, J = 11.4 Hz, 1H), 4.94 (d, J = 10.9 Hz, 1H), 5.07 (d, J = 1.4 Hz, 1H), 5.28 (d, J = 3.6 Hz, 1H), 5.37 (dd, J = 10.2, 3.6 Hz, 1H), 5.57 – 5.72 (m, 2H), 6.23 (t, J = 9.9 Hz, 1H), 7.22 – 7.43 (m, 23H), 7.43 – 7.59 (m, 4H), 7.94 (m, 2H), 7.99 – 8.07 (m, 4H), 8.12 (m, 2H); ^{13}C {^{1}H} NMR (100.67 MHz, CDCl$_3$): δ 55.7, 66.5, 68.3, 69.0, 69.1, 69.8, 70.7, 71.7, 71.9, 72.3, 73.5, 74.3, 75.3, 78.1, 97.1, 98.1, 127.6, 127.6, 127.6, 127.7, 127.7, 128.1, 128.1, 128.3, 128.3, 128.4, 128.4, 128.4, 128.4, 128.4, 128.5, 128.5, 128.5, 128.5, 128.6, 128.6, 128.6, 128.6, 129.1, 129.2, 129.4, 129.8, 129.8, 129.8, 130.0, 130.1, 130.1, 130.1, 130.1, 130.1, 133.3, 133.3, 133.5, 133.5, 138.2, 138.6, 138.7, 165.4, 165.7, 166.0, 166.0; HRMS (ESI-MS): *m/z* [$C_{62}H_{58}O_{15}Na$]$^+$: 1065.3690 [M+Na]$^+$.

Compound 4.14c

Methyl 2,3,4-tri-*O*-benzoyl-6-*O*-(2,3,4,6-tetra-*O*-benzoyl α-D-mannopyranosyl) α-D-glucopyranoside: Mp: 72 °C; [α]^{25}$_D$ (CHCl$_3$, *c* 1.0): +2.9; IR (cm^{-1}, CHCl$_3$): 3045, 2910, 1720, 1625, 1228, 1035, 970; ^{1}H NMR (400.31 MHz, CDCl$_3$): δ 3.61 (s, 3H), 3.78 (d, *J* = 10.7 Hz, 1H), 4.09 (dd, *J* = 10.7, 6.1 Hz, 1H), 4.34 – 4.40 (m, 2H), 4.51 – 4.55 (m, 1H), 4.62 (dd, *J* = 11.9,1.7 Hz, 1H), 5.15 (s, 1H), 5.26 (dd, *J* = 10.2, 3.7 Hz, 1H), 5.33 (d, *J* = 3.6 Hz, 1H), 5.58 (td, *J* = 9.9, 1.6 Hz, 1H), 5.76 (dd, *J* = 3.1, 1.7 Hz, 1H), 5.98 (dd, *J* = 10.1, 3.2 Hz, 1H), 6.08 (t, *J* = 10.1 Hz, 1H), 6.21 (t, *J* = 9.9 Hz, 1H), 7.26 – 7.31 (m, 3H), 7.34 (m, 3H), 7.39 – 7.43 (m, 6H), 7.45 – 7.49 (m, 5H), 7.52 – 7.55 (m, 2H), 7.58 – 7.63 (m, 2H), 7.84 – 7.87 (m, 2H), 7.92 – 7.94 (m, 2H), 7.97 – 8.04 (m, 6H), 8.06 – 8.11 (m, 4H); ^{13}C {^{1}H} NMR (100.67 MHz, CDCl$_3$): δ 55.8, 62.9, 66.6, 67.1, 68.5, 69.1, 69.6, 70.2, 70.5, 70.7, 72.3, 97.1, 97.6, 128.4 (4C), 128.5 (2C), 128.6 (6C), 128.7(2C), 128.9, 129.2, 129.3 (3C), 129.4, 129.5, 129.9 (6C), 130.0 (6C), 130.1 (2C), 133.1, 133.2, 133.2, 133.4, 133.5, 133.6, 133.6, 165.5, 165.5, 165.5, 165.7, 165.9, 165.9, 166.2; HRMS (ESI-MS): *m/z* [$C_{62}H_{52}O_{18}Na$]$^+$: 1107.3046 [M+Na]$^+$.

Compound 4.14d

Methyl 2,3,4-tri-*O*-benzoyl-6-*O*-(2,3,5-tri-*O*-benzyl α/β-D-arabinofuranosyl) α-D-glucopyranoside [α:β (1.4:1.0)]: [α]^{25}$_D$ (CHCl$_3$, *c* 0.5): +74.8; IR (cm^{-1}, CHCl$_3$): 2920, 1724, 1452, 1258, 1102, 1024, 801, 704; ^{1}H NMR (400.31 MHz, CDCl$_3$): δ 3.36 (s, 3H), 3.44 (s, 3H), 3.50 – 3.52 (m, 4H), 3.61 (dd, *J* = 11.6, 5.8 Hz, 1H), 3.66 (dd, *J* = 11.1, 3.1 Hz, 1H), 3.85 – 3.99 (m, 3H), 3.99 – 4.12 (m, 4H), 4.18 – 4.23 (m, 3H), 4.41 – 4.51 (m, 7H), 4.52 – 4.61 (m, 3H), 4.65 (d, *J* = 11.8 Hz, 1H), 4.82 (d, *J* = 11.7 Hz, 1H), 5.05 – 5.07 (m, 2H), 5.18 – 5.27 (m, 4H), 5.54 (dd, *J* = 10.2, 9.4 Hz, 1H), 5.63 (t, *J* = 9.8 Hz, 1H), 6.12 (td, *J* = 9.6, 1.0 Hz, 2H), 7.24 – 7.54 (m, 48H), 7.80 – 8.02 (m, 12H); ^{13}C {^{1}H} NMR (100.67 MHz, CDCl$_3$): δ 55.5, 55.6, 65.6, 66.0, 68.5, 69.0, 69.2, 69.5, 69.6, 70.6, 70.7, 72.0, 72.0, 72.1, 72.1, 72.2, 72.3, 72.4, 73.3, 73.3, 80.4, 80.5, 83.2, 83.3, 84.2, 88.4, 96.8, 96.9, 101.3, 106.1, 127.5 – 127.9 (15C), 128.2 – 128.3 (15C), 128.4 (12C), 129.0, 129.1 (2C), 129.3 (2C), 129.4, 129.7 (4C), 129.8 (2C), 129.9 (6C), 133.0, 133.0, 133.2, 133.3, 133.3, 133.4, 137.6, 138.0, 138.0, 138.1, 138.1, 138.2, 165.1, 165.3, 165.8, 165.8, 165.8, 165.9; HRMS (ESI-MS): *m/z* [C$_{54}$H$_{52}$O$_{13}$Na]$^+$: 947.3989 [M+Na]$^+$.

Compound 4.14e

Methyl 2,3,4-tri-*O*-benzoyl-6-*O*-(2-*O*-benzoyl-3,4,6-tri-*O*-benzyl α-D-mannopyranosyl) α-D-glucopyranoside: See (**4.14b**).

Compound 4.14f

Methyl 2,3,4-tri-*O*-benzoyl-6-*O*-(2-*O*-benzoyl-3,5-tri-*O*-benzyl β-D-ribofuranosyl) α-D-glucopyranoside: Mp: 92 °C; [α]^{25}$_D$ (CHCl$_3$, *c* 1.0): +56.4; IR (cm^{-1}, CHCl$_3$): 3020, 1729, 1514, 1272, 1215, 1105, 742, 669; ^{1}H NMR (400.31 MHz, CDCl$_3$): δ 3.33 (s, 3H), 3.44 (dd, J = 10.4, 6.1 Hz, 1H), 3.51 – 3.65 (m, 2H), 3.85 (d, J = 11.3 Hz, 1H), 4.07 – 4.16 (m, 2H), 4.19 – 4.25 (m, 1H), 4.27 (d, J = 11.5 Hz, 1H), 4.40 – 4.41(m, 2H), 4.48 (d, J = 11.4 Hz, 1H), 5.07 – 5.15 (m, 2H), 5.14 – 5.22 (m, 1H), 5.37 – 5.50 (m, 2H), 6.05 (t, J = 9.8 Hz, 1H), 7.05 – 7.46 (m, 22H), 7.76 – 7.80 (m, 2H), 7.81 – 7.85 (m, 2H), 7.87 – 7.91 (m, 2H), 7.95 – 7.99 (m, 2H); ^{13}C {^{1}H} NMR (100.67 MHz, CDCl$_3$): δ 55.6, 66.6, 68.9, 69.8, 70.6, 71.2, 72.2, 73.0, 73.3, 74.3, 78.0, 80.8, 96.9, 105.9, 127.6, 127.7, 127.7, 127.8, 128.0, 128.0, 128.3, 128.3, 128.3, 128.3, 128.4, 128.4, 128.4, 128.4, 128.5, 128.5, 128.5, 128.5, 129.1, 129.1, 129.3, 129.7, 129.7, 129.7, 129.9, 129.9, 129.9, 129.9, 130.0, 130.0, 133.1, 133.3, 133.4, 133.4, 137.6, 138.2, 165.3, 165.5, 165.9, 165.9; HRMS (ESI-MS): *m/z* [C$_{54}$H$_{50}$O$_{14}$Na]$^+$: 945.3099 [M+Na]$^+$.

Compound 4.17

Methyl 2,4-di-*O*-benzyl-α-D-mannopyranoside: Syrup; [α]$^{25}_D$ (CHCl$_3$, *c* 0.5): +14.0; IR (cm^{-1}, CHCl$_3$): 3568, 3017, 2925, 910, 738, 564; ^{1}H NMR (400.31 MHz, CDCl$_3$): δ 2.48 (s, 2H), 3.30 (s, 3H), 3.58 (ddd, *J* = 9.8, 4.4, 2.8 Hz, 1H), 3.68 (t, *J* = 9.5 Hz, 1H), 3.71 (dd, *J* = 3.7, 1.6 Hz, 1H), 3.77 (dd, *J* = 11.9, 4.4 Hz, 1H), 3.84 (dd, *J* = 11.8, 2.9 Hz, 1H), 3.98 (dd, *J* = 9.2, 3.7 Hz, 1H), 4.59 (d, *J* = 11.8 Hz, 1H), 4.65 (d, *J* = 11.1 Hz, 1H), 4.70 (d, *J* = 11.8 Hz, 1H), 4.73 (d, *J* = 1.6 Hz, 1H), 4.88 (d, *J* = 11.2 Hz, 1H), 7.29 – 7.36 (m, 10H); ^{13}C {^{1}H} NMR (100.67 MHz, CDCl$_3$): δ 54.9, 62.3, 71.3, 71.8, 73.2, 74.9, 76.4, 78.4, 98.3, 127.9, 128.0, 128.0, 128.1, 128.1, 128.2, 128.5, 128.5, 128.7, 128.7, 137.7, 138.4; HRMS (ESI-MS): *m/z* [C$_{21}$H$_{26}$O$_6$Na]$^+$: 397.1635 [M+Na]$^+$.

Compound 4.18

Methyl 2,4-di-*O*-benzyl-3,6-di-*O*-(2-*O*-benzoyl-3,4,6-tri-*O*-benzyl-α-D-mannopyranosyl)-α-D-mannopyranoside: syrup; [α]$^{25}_D$ (CHCl$_3$, *c* 0.5): +12.4; IR (cm^{-1}, CHCl$_3$): 3265, 3025, 2955, 1725, 917, 730, 571; ^{1}H NMR (400.31 MHz, CDCl$_3$): δ 3.22 (s, 3H), 3.65 – 3.71 (m, 3H), 3.73 – 3.85 (m, 5H), 3.87 – 3.96 (m, 2H), 4.02 – 4.10 (m, 4H), 4.13 – 4.19 (m, 2H), 4.47 (s, 1H), 4.49 – 4.50 (m, 3H), 4.51 – 4.56 (m, 3H), 4.65 – 4.68 (m, 4H), 4.71 – 4.76 (m, 3H), 4.80 (d, *J* = 11.0 Hz, 1H), 4.87 – 4.92 (m, 2H), 5.10 (d, *J* = 1.8 Hz, 1H), 5.33 (d, *J* = 1.7 Hz, 1H), 5.73 (t, *J* = 2.9 Hz, 1H), 5.77 (t, *J* = 2.6 Hz, 1H), 7.16 – 7.40 (m, 44H), 7.52 – 7.56 (m, 2H), 8.02 – 8.04 (m, 2H), 8.07 – 8.09 (m, 2H); ^{13}C {^{1}H} NMR (101.67 MHz, CDCl$_3$): δ 54.9, 66.6, 68.8, 68.8, 69.1, 69.2, 69.5, 71.1, 71.2, 71.7, 71.9, 72.5, 72.5, 73.5, 73.6, 74.3, 74.5, 75.1, 75.1, 75.3, 77.6, 77.6, 78.3, 78.7, 98.3, 98.3, 99.8, 127.5, 127.6 (5C), 127.7 (2C), 127.8 (4C), 127.9 (4C), 128.0 (4C), 128.1 (4C), 128.3 (2C), 128.4 (10C), 128.5 (6C), 128.6 (2C), 130.0, 130.1 (5C), 133.2, 133.2, 138.0, 138.0, 138.0, 138.3, 138.6, 138.6, 138.7, 138.8, 165.6, 165.6; HRMS (ESI-MS): *m/z* [C$_{89}$H$_{90}$O$_{18}$Na]$^+$: 1469.6021 [M+Na]$^+$.

Compound 4.19

Methyl 2,4-di-*O*-benzyl-3,6-di-*O*-(3,4,6-tri-*O*-benzyl-α-D-mannopyranosyl)-α-D-mannopyranoside: syrup; [α]$^{25}_D$ (CHCl$_3$, *c* 1.0): +46.1; IR (cm^{-1}, CHCl$_3$): 3554, 3275, 3037, 2963, 925, 716, 552; ^{1}H NMR (400.31 MHz, CDCl$_3$): δ 2.37 (s, 2H), 3.23 (s, 3H), 3.58 – 3.73 (m, 6H), 3.75 – 3.93 (m, 8H), 3.93 – 4.03 (m, 2H), 4.08 – 4.14 (m, 2H), 4.44 – 4.57 (m, 7H), 4.57 – 4.62 (m, 5H), 4.62 – 4.70 (m, 3H), 4.83 (t, *J* = 10.7 Hz, 2H), 5.07 (d, *J* = 1.8 Hz, 1H), 5.21 (d, *J* = 1.7 Hz, 1H), 7.12 – 7.34 (m, 40H); ^{13}C {^{1}H} NMR (101.67 MHz, CDCl$_3$): δ 54.9, 66.2, 68.2, 68.8, 68.9, 69.5, 71.3, 71.6, 71.6, 72.1, 72.2, 72.4, 73.5, 73.7, 74.4, 74.6, 75.0, 75.1, 75.1, 75.2, 77.9, 79.1, 79.7, 80.2, 98.3, 99.8, 101.6, 127.6, 127.7 (8C), 127.8 (2C),

127.9 (5C), 128.0 (6C), 128.1 (2C), 128.4 (8C), 128.5 (2C), 128.6 (6C), 138.0, 138.0, 138.2, 138.4, 138.4, 138.4, 138.6, 138.7; HRMS (ESI-MS): *m/z* $[C_{75}H_{82}O_{16}Na]^+$: 1261.5495 $[M+Na]^+$.

Compound 4.20

Methyl 2,4-di-*O*-benzyl-3,6-di-*O*-(2-*O*-(2,3,4,6-tetra-*O*-benzoyl α-Dmannopyranosyl) - 3,4,6-tri-O-benzyl α-D-mannopyranosyl)-α-D-mannopyranoside: syrup; $[\alpha]^{25}_D$ (CHCl$_3$, *c* 0.5): +8.4; IR (cm^{-1}, CHCl$_3$): 3272, 3045, 2964, 1720, 1130, 945, 730, 583; ^{1}H NMR (400.31 MHz, CDCl$_3$): δ 3.25 (s, 3H), 3.55 – 3.75 (m, 6H), 3.78 – 3.86 (m, 2H), 3.86 – 3.95 (m, 3H), 3.99 – 4.04 (m, 5H), 4.11 – 4.18 (m, 2H), 4.29 (dt, *J* = 12.4, 2.5 Hz, 1H), 4.36 – 4.46 (m, 3H), 4.47 – 4.60 (m, 9H), 4.61 – 4.63 (m, 3H), 4.65 – 4.68 (m, 3H), 4.70 – 4.75 (m, 1H), 4.80 (s, 1H), 4.92 (t, *J* = 10.5 Hz, 2H), 5.04 (d, *J* = 2.5 Hz, 1H), 5.13 (d, *J* = 2.5 Hz, 1H), 5.21 (d, *J* = 2.5 Hz, 1H), 5.34 (d, *J* = 2.5 Hz, 1H), 5.86 (d, *J* = 2.8 Hz, 1H), 5.89 – 5.98 (m, 3H), 6.13 (td, *J* = 10.1, 2.0 Hz, 1H), 6.19 (td, *J* = 10.1, 2.0 Hz, 1H), 6.88 – 7.06 (m, 5H), 7.06 – 7.23 (m, 15H), 7.28 – 7.33 (m, 26H), 7.35 – 7.46 (m, 14H), 7.51 – 7.64 (m, 4H), 7.83 – 7.91 (m, 8H), 8.04 – 8.06 (m, 4H), 8.12 – 8.14 (m, 4H); ^{13}C {^{1}H} NMR (101.67 MHz, CDCl$_3$): δ 54.9, 62.7, 62.7, 66.4, 66.7, 66.9, 69.2, 69.2, 69.4, 69.6, 70.3, 70.3, 70.5, 70.6, 71.7, 71.9, 71.9, 72.2, 72.6, 72.7, 73.2, 73.4, 74.7, 74.8, 74.9, 74.9, 75.1, 75.4, 77.1, 77.4, 77.9, 78.7, 79.4, 79.7, 98.3, 99.5, 99.5, 99.8, 101.1, 127.1 (2C), 127.4 (2C), 127.5 – 127.7 (14C), 127.9 (2C), 128.0 (4C), 128.3 (4C), 128.4 (12C), 128.5 (12C), 128.7 (4C), 129.1, 129.2, 129.4, 129.5, 129.7, 129.7, 129.9 – 130.0 (16C), 130.1, 130.2, 133.0, 133.1, 133.1, 133.1, 133.4, 133.4, 133.4, 133.4, 138.2, 138.3, 138.3, 138.3, 138.5, 138.5, 138.7, 138.8, 165.2, 165.2, 165.4, 165.5, 165.5, 165.6, 166.2, 166.3; HRMS (ESI-MS): *m/z* $[C_{143}H_{134}O_{34}Na]^+$: 2418.8691 $[M+Na]^+$.

4.2.3   X-ray crystallographic Details

Single crystals of suitable size, coated with paraffin oil was mounted for all the complexes. Crystal data for all the complexes were collected on a Bruker Smart Apex Duo diffractometer at 100 K using Mo Kα radiation (λ = 0.71073 Å). Collected data were integrated by using SAINT and then absorption correction was done by multi-scan method using SADABS program. All the structures were solved by direct methods and refined by full-matrix least-squares methods against F^2 (SHELXL-2014/6). Crystallographic Information File (CIF) for the structures has been deposited to the Cambridge Crystallographic Data Centre as supplementary publication nos. 1819357

(**4.2**), 1819358 (**4.3**), 1990445 (**4.4**), 1954430 (**4.8**), 1990448 (**4.9**), 1990449 (**4.10**). These CIF can be obtained free of charge from The Cambridge Crystallographic Data Centre via www.ccdc.cam.ac.uk/data_request/cif.

4.2.3. Computational Methodology

Geometry optimizations were performed using GGA DFT functional BP86[1] with def2-SVP2[2] basis set using Gaussian 09[3] software. Single point calculations were carried out using meta-GGA functional M06[4] with def2-TZVPP[2] level of theory on the optimized geometries. Solvent effects were incorporated in single point calculations using PCM model[5] by incorporating dichloromethane solvent (DCM). ΔE and $\Delta E^{\#}$ represent reaction enthalpy and enthalpy of activation respectively calculated by adding electronic energy at the M06/PCM/def2-TZVPP level of theory and zero point energy at the BP86/def2-SVP level of theory. ΔG and $\Delta G^{\#}$ represent the Gibbs free energy of reaction and Gibbs free energy of activation respectively, calculated by adding electronic energy at the M06/PCM/def2-TZVPP level of theory and the thermal correction to Gibbs free energy at 298.15 K and 1 atm at the BP86/def2-SVP level of theory. The population analysis was performed by natural bond orbital (NBO)[6] method at M06/PCM/def2-TZVPP//BP86/def2-SVP level of theory.

4.3.   Result and Discussion

4.3.1. Synthesis and characterization of *4.2*- *4.6* and *4.8*

To put the idea into practice, complex **4.1** was reacted with $AgSbF_6$ in a mixture of CH_2Cl_2 and benzene, which afforded the formation of **4.2** (Scheme 4.1). Analogous reaction with *m*-xylene instead of benzene resulted in the formation of **4.3**. The ^{1}H NMR spectrum of **4.2** clearly shows a peak for the six protons at δ 7.48 ppm, which can be assigned for the coordinated C_6H_6. Complex **4.3** shows a peak at δ 2.40 ppm for the six protons, which could be assigned for the two methyl substituents in the aryl ring. Upon coordination, these characteristic peaks of **4.2** and **4.3** are slightly downfield shifted with respect to the uncoordinated molecules (uncoordinated C_6H_6 and $1,3-(CH_3)_2(C_6H_4)$ appear at 7.36 and 2.27 ppm, respectively). The ^{29}Si NMR spectra of **4.2** and **4.3** resonate at δ -6.44 and -8.85 ppm, respectively, which is shifted upfield as compared to **4.1** (8.76 ppm).

The crystals of **4.2** and **4.3**, suitable for X-ray crystallography, were grown in CH_2Cl_2/arene mixture at 0 °C and crystallize in the monoclinic space group, $P2_1/n$ and
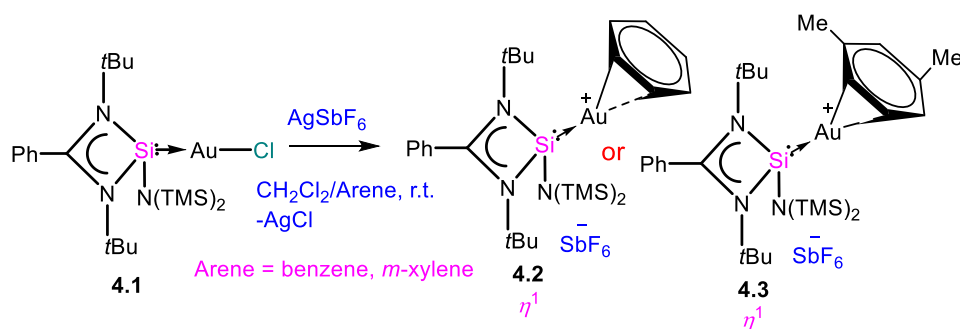
Scheme 4.1. *Syntheses of* **4.2** *and* **4.3.**

$P2_1/c$, respectively. The X-ray structure analysis of **4.2** shows that the Si(II) center is tetracoordinate (Figure. 4.1) and exhibits a distorted tetrahedral geometry. However, the Au(I) centre shows η^1 interaction with the shortest Au-C8 (benzene ring) distance of 2.371(5) Å in **4.2** along with a secondary interaction to C20 (2.605(7)) Å. The Si–Au distance of 2.276(2) Å is close to that in **4.1** (2.265(1) Å)[20] and the theoretically predicted Si(II)–Au(I) bond length of 2.329 Å.[24] The molecular structure of **4.3** (Figure 4.A.1, see
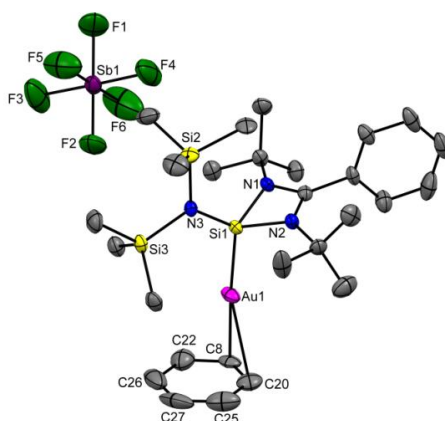
Figure 4.1. *The molecular structure of* **4.2** *(ellipsoid are shown at the probability level of 30%). Counter anion SbF_6^-, and hydrogen atoms are omitted for clarity. Selected bond length (Å) and bond angles (deg); N1-Si1 1.815(4), N2-Si1 1.822(4)], N3-Si1 1.706(4), Si1-Au1 2.276(2), Au1-C8 2.371(5), Au1-C20 2.605(7); N1-Si1-Au1 112.1(1), N2-Si1-Au1 110.6(2), N3-Si1-Au1 119.9(1), Si1-Au1-C8 173.9(1), Si1-Au1-C20 151.2(1).*

Appendix) also shows η^1 coordination of Au centre to the *m*-xylene ring. Although X-ray diffraction on a single crystal unambiguously established the connectivity of **4.3**, we refrain from a discussion of bonding parameters because of the disorder in the molecule. The assignment of hapticity number for the complexes having low hapticities (η^1-η^3) has been done by using a method proposed by Alvarez and co-workers to deduce the hapticity of the metal-arene complexes (Table 4.A.3, see Appendix).[25]

Subsequently, we have used an analogous germylene [{PhC(N*t*Bu)$_2$}Ge{N(SiMe$_3$)$_2$}][26a] to prepare the gold(I) complex (**4.4**). Abstraction of chloride ion from the latter with AgSbF$_6$ in the presence of benzene or toluene afforded the expected complexes **4.5** and **4.6,** respectively (Scheme 4.2). Complexes **4.4**-**4.6** were characterized by routine NMR techniques, mass and elemental analysis. **4.4** crystallizes in monoclinic space group, *P*2$_1$/*c* and the important bond lengths and angles are given in the legend of Scheme 4.2. The molecular structure of **4.4** discloses a linear geometry at Au(I) centre with

4.4

4.5, arene = benzene
4.6, arene = toluene
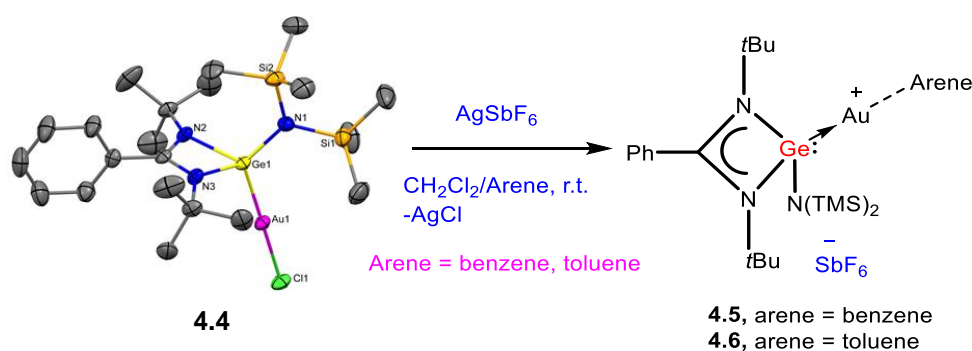
Scheme 4.2. *Syntheses of* **4.5** *and* **4.6**. *The molecular structure of* **4.4** *(ellipsoid are shown at the probability level of 30%). Hydrogen atoms are omitted for clarity. Selected bond length (Å) and bond angles (deg); N1-Ge1 1.833(4), N2-Ge1 1.946(3), N3-Ge1 1.941(4), Ge1-Au1 2.327(5), Au1-Cl 2.311(1); N1-Ge1-Au1 122.4(1), N2-Ge1-Au1 115.0(1), N3-Ge1-Au1 114.2(1), Ge1-Au1-Cl1 179.4(3).*

Ge-Au-Cl bond angle of 179.4° which is matching well with the reported Ge(II)→AuCl complex ({PhC(N*t*Bu)$_2$}Ge(AuCl)(*t*Bu), 177.41(3)°).[26b] Unfortunately, crystals suitable for X-ray analysis could not be obtained for **4.5** and **4.6** even after several attempts.

Next, we have substituted silylene/germylene with N-heterocyclic carbene (IPr) to compare the ligand properties. For this purpose, we treated IPrAuCl (**4.7**)[27a] with AgSbF$_6$
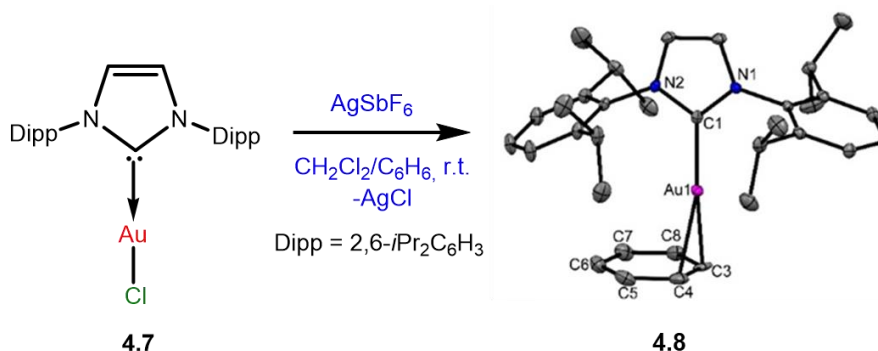
Scheme 4.3. *Synthesis and the molecular structure of* **4.8** *(ellipsoids are shown at the probability level of 30%). Hydrogen atoms and SbF6 anion are omitted for clarity. Selected bond lengths (Å) and bond angles (deg): C1-Au1 1.991(3), Au1-C3 2.293(3), Au1-C4 2.346(3); C1-Au1-C4 159.6(1).*

in CH_2Cl_2/benzene mixture to afford the colorless crystals of **4.8** (Scheme 4.3). The latter crystallizes in the monoclinic space group $P2_1$/c. The C1 and Au1 bond distance is of 1.991(3) Å (Scheme 4.3). The Au-$C_{benzene}$ bond distances [(2.293(3), 2.346(3), 2.885(4), 2.961(3), 3.363(4), 3.396(4) Å)] indicate the η^2 binding mode of **4.8** (see Appendix, Table 4.A.3), which is in agreement with the calculations given by Alvarez and coworkers.[25]

4.3.2. Electronic and Steric Properties

With all these well-defined Au(I) complexes in hand, we have wished to probe them as catalysts. Before that, we sought to understand their donor strength. So, we have reacted NHSi and [(tBu)$_2$C$_6$H$_3$O)]$_3$P with CpCo(CO)$_2$ in toluene/n-hexane at room temperature and at 68 °C (5 days), respectively, which afforded corresponding complexes, NHSiCoCp(CO) (**4.9**) and ((tBu)$_2$C$_6$H$_3$O)$_3$PCoCp(CO) (**4.10**) (Scheme 4.4). The analogous NHC complex was previously known.[27b] The carbonyl stretching frequency (ν_{CO}) for **4.9** and **4.10**, was found 1873 cm^{-1} and 1956 cm^{-1}, respectively. The relative comparison of electron donating abilities of NHSi, IPr [IPrCoCp(CO) (1921 cm^{-1})],[27b] and [(tBu)$_2$C$_6$H$_3$O)]$_3$P gives the order of NHSi > IPr > [(tBu)$_2$C$_6$H$_3$O)]$_3$P as per their carbonyl stretching frequencies in **4.9**, **4.10** and IPrCoCp(CO).[27b] The steric bulk of **4.1** was also calculated, which is found to be the most

bulky ($V_{bur}\% = 54$) than the other two ligands [$V_{bur}\% = 45.5$ for **4.7** and 37.8 for [(tBu)$_2$C$_6$H$_3$O)]$_3$PAuCl] (Chart 4.3).[27c]

(a) CpCo(CO)$_2$ $\xrightarrow[\text{[($t$Bu)$_2C_6H_3$O)]$_3$P @ 68 °C, 5 days}]{\text{NHSi @ rt, 12 hrs}}$ NHSiCoCp(CO) (**4.9**) or [(tBu)$_2$C$_6$H$_3$O)]$_3$PCoCp(CO) (**4.10**)

-CO

(b)

4.9

4.10

(c)

4.9, ν_{CO} = 1873 cm⁻¹

4.10, ν_{CO} = 1956 cm⁻¹
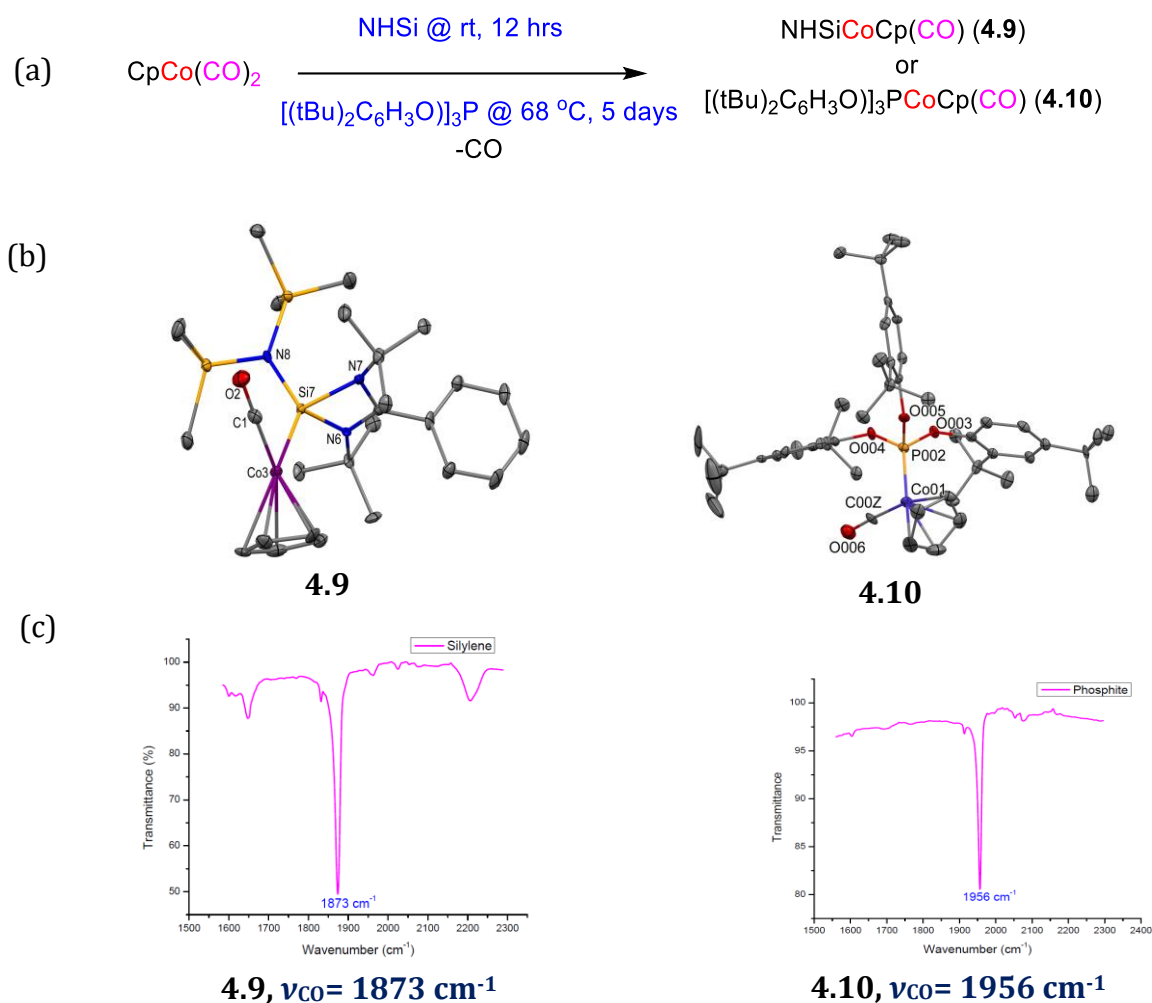
Donor strength: NHSi > IPr > [(tBu)$_2$C$_6$H$_3$O)]$_3$P

Scheme 4.4. *(a) Synthesis of NHSiCoCp(CO) (**4.9**) and ((tBu)$_2$C$_6$H$_3$O)$_3$PCoCp(CO) (**4.10**); (b) Molecular structures of **4.9** and **4.10**; (b) IR spectra (ν_{CO}) of **4.9** and **4.10** for the comparison of their electronic properties with IPr (IPrCoCp(CO), ν_{CO}= 1921 cm⁻¹).[27b]*

4.3.3. Catalytic Studies

Glycosidation is one of the fundamental reactions that facilitates synthesis of glycoconjugates and oligosaccharides. This process usually involves a full protected glycosyl donor, which generates an oxocarbenium ion upon activation and a glycosyl

acceptor that frequently contains a lone alcohol. Despite several methods, syntheses of oligosaccharides and glycoconjugates is still a challenging task.[28-29]Recent introduction of gold-catalyzed glycosidations using alkynyl glycosides brought a new dimension to the
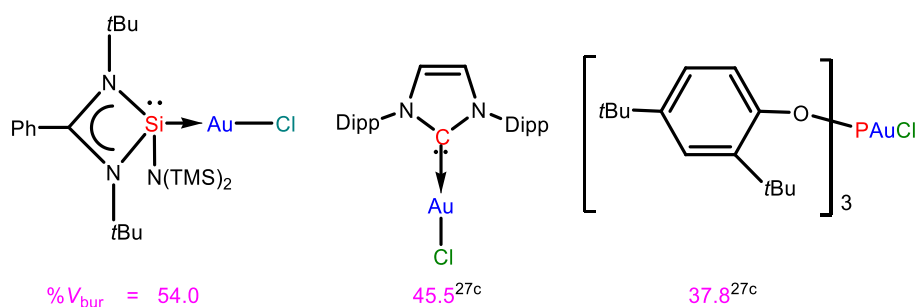
Chart 4.3. % V_{bur} of the ligands used in this catalysis. Percent buried volumes were calculated with the SambVca 2.0 web tool (https://www.molnac.unisa.it/OMtools/sambvca2.0/).

already burgeoning influence of transition metal catalysis on glycosidations.[22] The activation of alkynyl glycosides was attributed to the alkynophilicity as well as the oxophilicity of the gold catalysts.[30] One of the perceived and major problems in the synthesis of oligosaccharides is the oxophilicity of the Lewis acid as the interglycosidic bond is susceptible for the hydrolysis.[31-34] Recently, the ethynylcyclohexyl carbonate glycosyl donors are activated by the synergistic action of [Au]- and [Ag]- catalysts exploiting salient features of $(2,4-(tBu)_2C_6H_3O)_3PAuCl/AgOTf$ catalytic system wherein the active catalyst is not well understood yet.[23]

In this premise, the gold complexes (**4.2, 4.5** and **4.8**) have been envisioned to be excellent for the synthesis of glycosides due to their interesting donor properties. Among the various alkynyl glycosyl donors, more reactive alkynyl glycosyl carbonate donors and alkynyl 1,2-orthoesters were selected for the initial explorations.

Glycosyl alkynyl carbonates are the recent addition to the slew of emerging catalytic protocols available in the arsenal for the synthesis of oligosaccharides and glycoconjugates. Our explorations begun by subjecting the mannopyranosyl carbonate donor **4.12a** to the glycosidation with a model glycosyl acceptor **4.13a**. The reaction was

carried out in the presence of AgSbF$_6$ and Au-phosphite catalyst (**4.11**) as reported earlier[23] and compared with **4.2, 4.5** and **4.8** (Scheme 4.5). Gratifyingly, in all the catalytic systems, formation of the disaccharide **4.14a** was noticed in very high yields with subtle changes in the overall yield. Glycosidation in the presence of catalyst **4.2** gave 84% yield
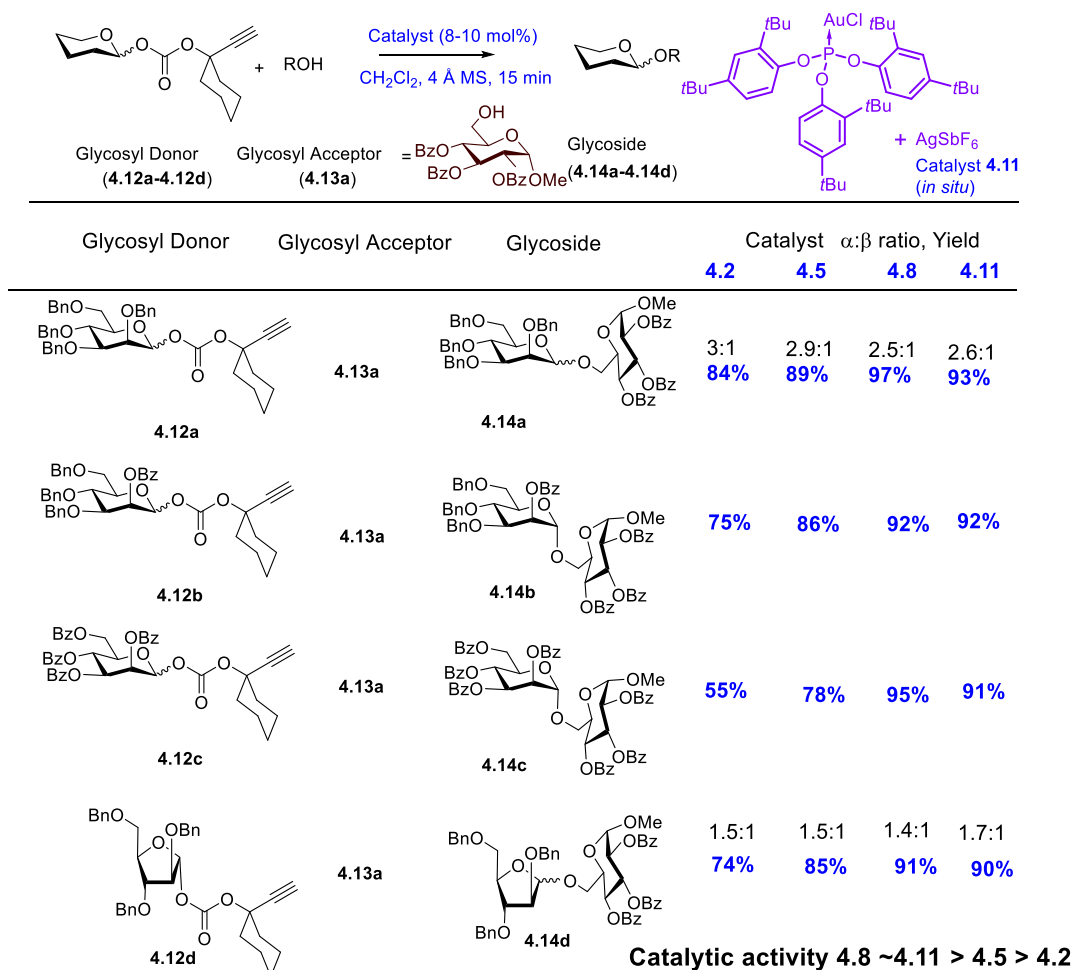
Scheme 4.5. *Activation of glycosyl carbonate donors utilizing catalysts **4.2, 4.5, 4.8** and **4.11**.*

whereas catalysts **4.5, 4.8** and **4.11** resulted in 89-97% yield. In all the cases, the 1.2-*trans* anomer was noticed to be dominating. Similar results were noticed while employing these reaction conditions with the super-armed donor **4.12b** or disarmed **4.12c** to obtain **4.14b** or **4.14c,** respectively. Furthermore, the arabinofuranosyl carbonate **4.12d** also

underwent the glycosylation smoothly with the glycosyl acceptor **4.13a** to afford **4.14d** in 74%, 85%, 91% and 90% with the catalysts **4.2**, **4.5, 4.8** and **4.11,** respectively.

Table 4.1. *Attempts of disaccharide synthesis using carbonate donors with different catalysts.*[a]

Entry	Catalyst	Mol %	Yield (%)
1	**4.1**	10	-
2	TfOH	10	10
3	AgSbF$_6$	10	-
4	[Et$_3$O]+ [SbCl$_6$]-	10	20
5	PPh$_3$AuCl/AgSbF$_6$	10	75
7	**4.1**/AgSbF$_6$ (*in situ*) (DCM+benzene)	10	55
8	[IPr$_2$Au]$^+$[SbF$_6$]$^-$	10	-

[a]*Reagents and conditions: **4.12c** (1 eq.), **4.13a** (1 eq.), Catalyst, DCM, room temperature, 12 h.*
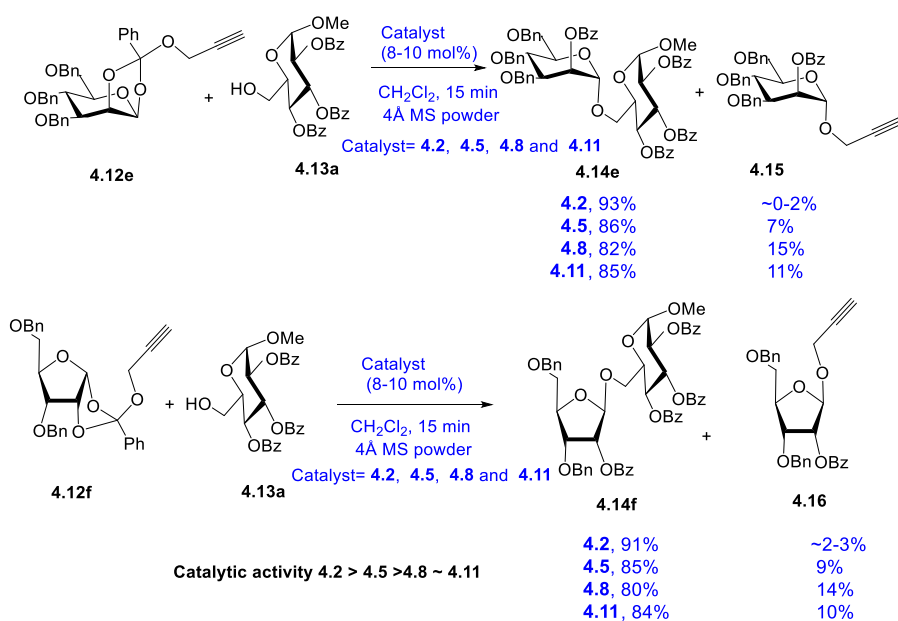
Scheme 4.6. *Propargyl 1,2-O-orthoesters activation by **4.2**, **4.5**, **4.8** and **4.11**.*

Table 4.2. *Attempts of disaccharide synthesis using orthoester donors with different catalysts.*[b]

Entry	Catalyst	Mol %	Yield (%)
1	AgSbF$_6$	10	30% (**4.14f**), 10% (**4.16**)
2	PPh$_3$AuCl/AgSbF$_6$	10	65% (**4.14f**), 30% (**4.16**)
3	AuBr$_3$	10	55% (**4.14f**), 15% (**4.16**)
4	**4.1**/AgSbF$_6$ *(in situ)* (DCM)	10	76% (**4.14f**), 20% (**4.16**)
5	**4.1**/AgSbF$_6$ *(in situ)* (DCM+benzene)	10	90% (**4.14f**), 2% (**4.16**)
6	[IPr$_2$Au]$^+$[SbF$_6$]$^-$	10	-

[b]*Reagents and conditions:* **4.12f** *(1 eq.),* **4.13a** *(1 eq.), Catalyst, DCM, room temperature,12 h.*

Overall, catalytic performance of **4.8** is superior than the rests which can be attributed to its stronger alkynophilicity. Furthermore, we screened various catalysts including **4.1** (Table 4.1) and found them inefficient for this catalytic reaction including TfOH.[23] We have also carried out the in situ reaction of **4.1**/AgSbF$_6$ in CH$_2$Cl$_2$ to see the effect of the weakly coordinated arene on the catalytic efficiency and found that the presence of the arene is vital for the better catalytic yield (Table 4.1). This could be attributed to the extra stability provided by the η-coordination of arene to Au(I), which reduces the decay of the gold catalyst.[9f]

Alkynyl 1,2-orthoesters are very good donors due to their long shelf stability and high reactivity. Synthesis of the heneicosafuranosyl arabinogalactan of *Mycobacterium tuberculosis* cell wall clearly exemplifies the utility of orthoester chemistry for the oligosaccharide synthesis.[35] The moderate alkynophilicity is ideal for the activation of

1,2-O-orthoester. Hence, **4.2** was treated with propargyl 1,2-O-orthoesters **4.12e** and **4.12f** as glycosyl donors and glucosyl acceptor **4.13a** (Scheme 4.6). Usually, alkynyl ortho esters upon activation result in the desired glycoside **4.14e** as well as a small quantity of propargyl glycosides **4.15**. To our satisfaction, **4.2** produced the disaccharide **4.14e** with almost negligible amount of propargyl mannoside **4.15** (~0–2%). Similarly, furanosyl donor **4.12f** also underwent the glycosylation in the presence of the acceptor **4.13a** and catalyst **4.2** to give disaccharide **4.14f** almost exclusively. Conversely, **4.5**, **4.8** and **4.11** led to **4.14e** and **4.14f** with a small amount of **4.15** and **4.16**, respectively. We screened several other catalysts as well and found **4.2** as the most efficient for this reaction (Table 4.2). Similar to carbonate donors, the reaction of ortho ester donors was also performed by the *in situ* generated catalyst [**4.1**/AgSbF$_6$ in CH$_2$Cl$_2$ (Table 4.2)], which led to the same observation like the carbonate donors.

4.3.4. Theoretical Investigations

We have carried out quantum mechanical calculations to explore the mechanism of model glycosidation reaction[36,37] between alkynyl glycosyl carbonate A (glycosyl donor), and an acceptor B (ROH) catalyzed by N-heterocyclic carbene/silylene supported Au(I)-benzene complexes **4.8** and **4.2** at the M06/PCM/def2-TZVPP//BP86/def2-SVP level of theory by considering DCM as solvent. The overall reaction is highly exothermic (scheme 4.A.1, see Appendix), ΔE = -32.6 kcal/mol) and exergonic (ΔG = -31.4 kcal/mol). We have calculated different reaction pathways for glycosidation reaction. Herein, we explain the most feasible mechanism of the glycosidation reaction catalyzed by N-heterocyclic carbene supported Au(I)-benzene complex **4.8** (Scheme 4.7). The optimized geometries (BP86/def2-SVP) and important geometrical parameters of reactants, products, intermediates, and transition states are given in supporting information (Figures 4.A.4 to 4.A.6, see Appendix).
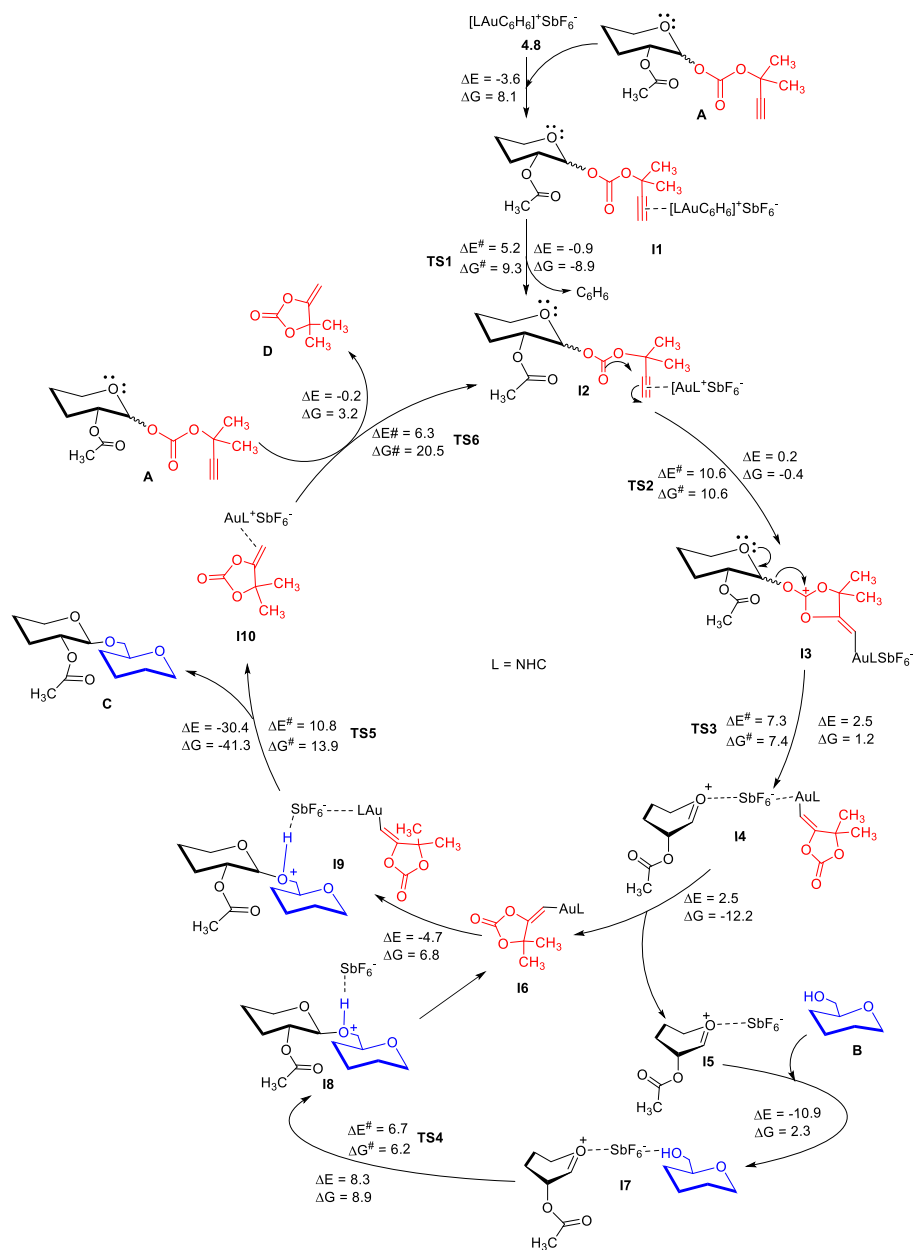
Scheme 4.7. *The mechanism for glycosidation reaction by remote activation in the presence of **4.8**. ΔE and ΔE# (in kcal/mol) represent reaction enthalpy and enthalpy of activation, respectively at the M06/PCM/def2-TZVPP//BP86/def2-SVP level of theory. ΔG and ΔG# (in kcal/mol) represent the Gibbs free energy of reaction and Gibbs free energy of activation respectively, at the same level of theory at 298.15 K and 1 atm. The curly bond here represents the equatorial substitution.*
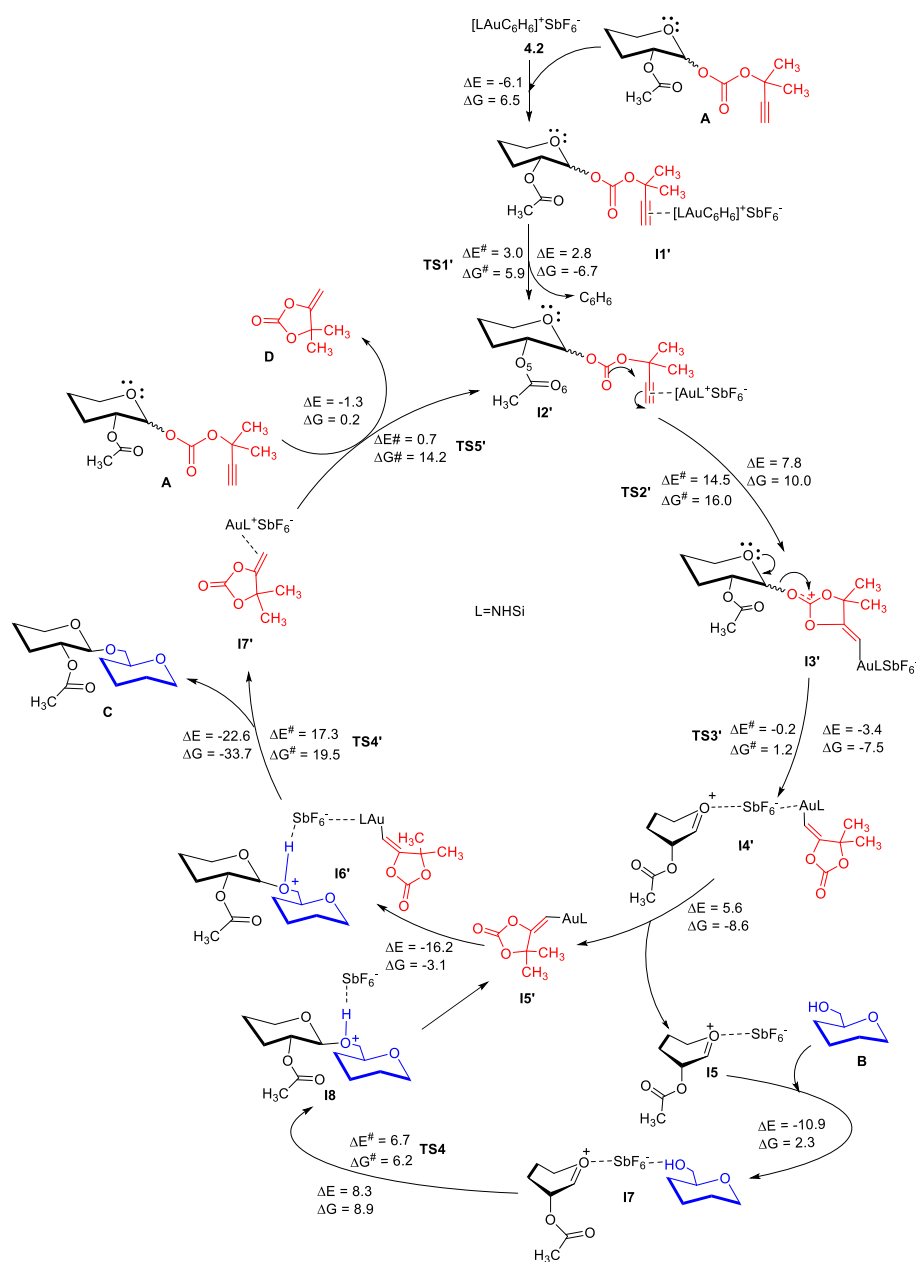
Scheme 4.8. *Feasible mechanism for glycosidation reaction by remote activation in the presence of **4.2**. ΔE and ΔE# (in kcal/mol) represent reaction enthalpy and enthalpy of activation respectively at the M06/PCM/def2-TZVPP//BP86/def2-SVP level of theory. ΔG and ΔG# (in kcal/mol) represent the Gibbs free energy of reaction and Gibbs free energy of activation respectively, at same level of theory at 298.15 K and 1 atm.*

The first step of the reaction involves the interaction of gold catalyst **4.8** with alkynyl glycosyl carbonate **A** to form a weakly bound complex **I1**, where the carbonyl oxygen of

the carbonate group has a slight bonding interaction with hydrogen atoms of the benzene ring coordinated to Au (O$\cdots$H distance = 2.487 Å). The reaction energy and Gibbs free energy for this step are found to be -3.6 kcal/mol and 8.1 kcal/mol, respectively. In the next step, the alkynyl group replaces the arene ring in **I1** to form Au-alkyne complex **I2**. The formation of **I2** is exothermic by 0.9 kcal/mol, and exergonic by 8.9 kcal/mol and corresponding energy barrier is low ($\Delta E^{\#}$ = 5.2 kcal/mol and $\Delta G^{\#}$ = 9.3 kcal/mol). The metal coordination stabilizes the π^{*}-MO (LUMO+1, E = -2.09 eV, Figure 4.7) centered on C≡C bond in **I2** as compared to the corresponding MO on **A** (LUMO+1, E = -0.54 eV, Figure 4.7). This facilitates the intramolecular nucleophilic addition of the lone pair on carbonyl oxygen to π^{*}-MO of **I2** resulting the vinylgold complex **I3**. The reaction energy for the generation of **I3** is only slightly endothermic (0.2 kcal/mol) and exergonic (-0.4 kcal/mol) and the corresponding energy barrier is not very high ($\Delta E^{\#}$ = 10.6 kcal/mol and $\Delta G^{\#}$ = 10.6 kcal/mol). In the next step, the glycosidic bond undergoes cleavage to form the intermediate **I4**, which is also facilitated by the donation of lone pair of electrons on pyranose oxygen to σ^{*}- orbital glycosidic bond. The formation of **I4** is slightly endergonic process (1.2 kcal/mol) and endothermic (2.5 kcal/mol), and the corresponding change in free energybarrier is 7.4 kcal/mol. The bound complex **I4** is then separated into two
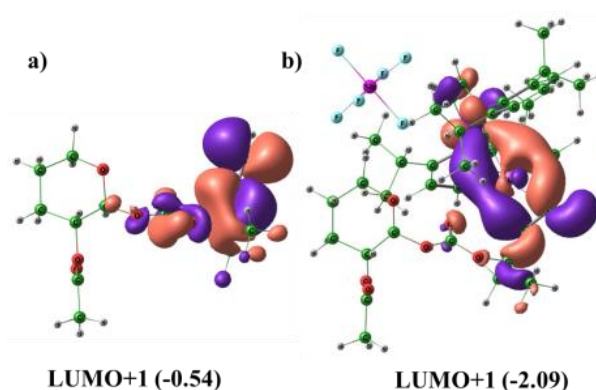
Figure 4.4. The low lying π^{*} -molecular orbitals centered on C≡C in a) A and b) I2 at the M06/PCM/def2-TZVPP//BP86/def2-SVP level of theory. Eigen values (eV) are given in parenthesis.

intermediates viz. oxocarbenium ion **I5** and the cyclic carbonate vinyl gold complex **I6**. The oxocarbenium ion **I5** is now susceptible to interact with nucleophiles such as the aglycone (ROH) molecule (**B**) leading to new complex **I7**. The nucleophilic attack of alcohol oxygen atom O_{OH}, which is a part of aglycone moiety in **I7** on to the anomeric carbon of the oxocarbenium ion, produces a new intermediate **I8**. The corresponding energy values are given in Scheme 4.7. Subsequently, **I8** interacts with the vinyl gold complex **I6** to from a weakly bound complex **I9.** Note that the natural charge on C_{AuL} is -0.64 e, whereas that in the other carbon atom of C=C is slightly positive (0.20 e). Hence, this promotes the electrophilic addition of positively charged H_{SbF6-} (0.55 e) to electron rich C_{AuL}. This results in the cleavage of Au–C_{AuL} σ bond, leading to the formation of Au-alkene π complex **I10** and the disaccharide molecule **C**. The product formation step is highly exothermic as well as exergonic (ΔE = -30.4 kcal/mol and ΔG = -41.3 kcal/mol). The alkynyl group in alkynyl glycosyl carbonate **A** now competes with the alkene in **I10** to coordinate with Au(I) and leads to the formation of **I2**, and thus the catalytic cycle continues. This step is exothermic by -0.2 kcal/mol, and endergonic by 3.2 kcal/mol and the corresponding kinetic energy barrier is $\Delta E^{\#}$ = 6.3 kcal/mol, and $\Delta G^{\#}$ = 20.5 kcal/mol.The reaction mechanism for the glycosidation reaction catalyzed by silylene-supported gold-benzene complex **4.2** is given in Scheme 4.8. The extent of elongation of C≡C bond length in **I2** (1.257 Å) is larger than that in **I2′** (1.244 Å). Hence, the C≡C in NHC supported Au(I)-alkyne complex (**I1**) is more activated by the donation of π electrons from an alkyne to Au as well as a greater back donation from Au→alkyne in comparison with Au(I)-alkyne complex supported by silylene (**I2′**). The activation of alkyne, and thereby formation of intermediate **I3** is more favorable in the case of reaction catalyzed by **4.8**. The barrier for the formation of similar intermediate **I3′**, catalyzed by **4.2** is highly energy demanding. Both step-wise, as well as the concerted mechanism, indicate that the energy barrier for the product formation step is high in the case of reaction catalyzed by **4.2**. The DFT studies on the glycosidation reaction between glycosyl carbonate **A** and an aglycone molecule **B** (ROH) catalyzed by N-heterocyclic carbene/silylene supported Au(1)-benzene complexes **4.8** and **4.2**, indicate that the NHC supported complex **4.8** is better catalyst than **4.2**.

As observed in almost all the homogeneous gold catalytic reactions, there is decay of cationic gold(I) to gold(0) (known as stage 3 in the catalytic cycle),[9f] we have also isolated

the deactivated catalyst (L_2Au^+) (L= IPr) during the column chromatography (See Appendix, Figure 4A.2). We performed a model reaction with it to test the efficiency but it did not work (Table 4.1 and 4.2).

Furthermore, the utility of the present catalytic glycosylation protocol using catalyst **4.2, 4.5** and **4.8** has been investigated by synthesizing a pentamannan core of the HIV1-gp120[38-40] surface high mannan (Scheme 4.9). Easily accessible methyl mannopyranoside[41] **4.17** was subjected to the glycosylation with glycosyl donor **4.12b** in the presence of 10 mol% of the catalysts to notice the formation of the trisaccharide **4.18** in 78-83% yield within 15 min. Saponification under Zemplén conditions afforded again a diol **4.19** which was further reacted with 2.2 equivalents of the glycosyl donor **4.12c** to isolate the desired pentamannan **4.20** in 72-80% yield within 15 min. Successful synthesis of pentamannan **4.20** in a highly convergent manner utilizing **4.2, 4.5** and **4.8** establishes the potential of thus identified catalytic glycosidation protocol.
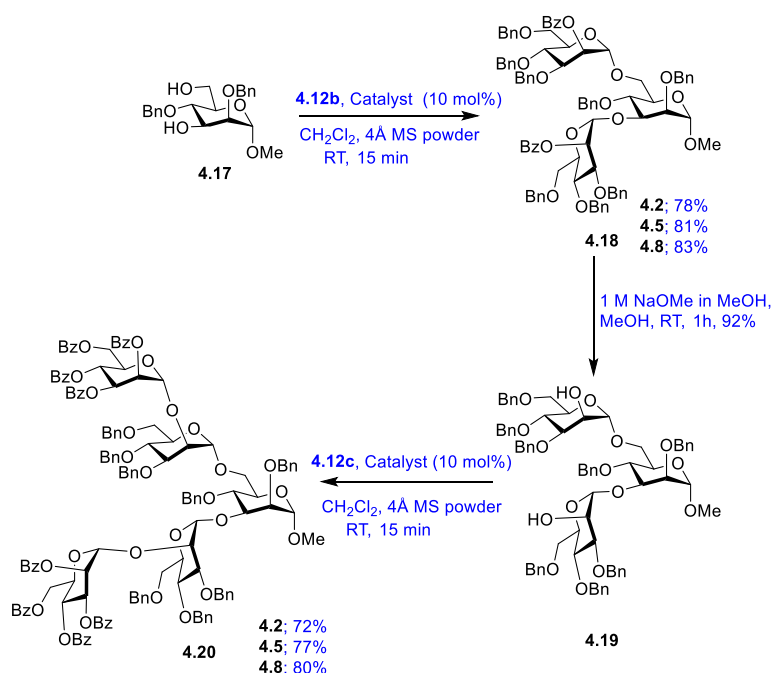
Scheme 4.9. *Synthesis of pentamannan core of the HIV1-gp120 using catalyst* **4.2, 4.5** *and* **4.8.**

4.4. Conclusion

In this study, we have synthesized a series of Au cations supported by silylene, germylene and N-heterocyclic carbene ligands (**4.2, 4.5** and **4.8**) featuring Au⋯benzene interaction. Consequently, we have tested them for the first time as catalysts in the glycoside synthesis and benchmarked their efficiencies with the existing protocols. The silylene-gold complex (**4.2**) was shown to be superior over **4.5** and **4.8** for the activation of propargyl 1,2-orthoester donors. It should be noted here that the current protocol for the activation of 1,2-orthoesters involve the use of Au(III) salts which always resulted a significant amount of side product. Our methodology of using donor stabilized Au(I) cation for this activation overcomes the said lacuna. When it comes for the activation of carbonate donors, **4.8** is the most efficient. To delineate the role of the arenes, we have compared the catalytic efficiency of **4.2** with the *in situ* generated catalyst (**4.1**+AgSbF$_6$ in DCM) and observed that the presence of benzene affords better efficiency than the *in situ* generated catalyst. The reason can be attributed to the weak arene-Au(I) interaction which reduces the decay of the catalyst. DFT calculations were performed to understand the mechanism of the glycosidation reaction. Finally successful synthesis of pentamannan **4.20** in a highly convergent manner utilizing **4.2, 4.5** and **4.8** establishes the potential of thus identified catalytic glycosidation protocol. Our findings will spur further interest to synthesize newer Au(I) complexes with a variety of neutral donor ligands and explore them in several other unexplored organic transformations.

4.5. References

1. Hyper- Brück, A.; Gallego, D.; Wang, W.; Irran, E.; Driess M.; Hartwig, J. F. *Angew. Chem., Int. Ed*. **2012**, *51*, 11478–11482.

2. Gallego, D.; Brück, A.; Irran, E.; Meier, F.; Kaupp, M.; Driess, M.; Hartwig, J. F. *J. Am. Chem. Soc.* **2013**, *135*, 15617 – 15626.

3. Tan, G.; Enthaler, S.; Inoue, S.; Blom, B.; Driess, M. *Angew. Chem., Int. Ed.* **2015**, *54*, 2214 – 2218.

4. Wang, W.; Inoue, S.; Enthaler, S.; Driess, M. *Angew. Chem., Int. Ed.* **2012**, *51*, 6167 – 6171

5. (*a*) Metsänen, T. T.; Gallego, D.; Szilvási, T.; Driess, M.; Oestreich, M. *Chem. Sci.* **2015**, *6*, 7143 – 7149. (*b*) B. Blom, S. Enthaler, S. Inoue, E. Irran and M. Driess, *J. Am. Chem. Soc.* **2013**, *135*, 6703 – 6713.

6. Zhou, Y.-P.; Raoufmoghaddam, S.; Szilvási, T.; Driess, M. *Angew. Chem., Int. Ed.* **2016**, *55*, 12868 –12872.

7. Stoelzel, M.; Präsang, C.; Blom, B.; Driess, M. *Aust. J. Chem.* **2013**, *66*, 1163 – 1170.

8. Driess, M.; Zhou, Y. *Angew. Chem., Int. Ed.* **2019**, *58*, 3715-3728.

9. (*a*) Hashmi, A. S. K. *Chem. Rev.* **2007**, *107*, 3180-3211. (*b*) Arcadi, A. *Chem. Rev.* **2008**, *108*, 3266-3325. (*c*) Jimenez-Nunez, E.; Echavarren, A. M. *Chem. Rev.* **2008**, *108*, 3326-3350. (*d*) Gorin, D. J.; Sherry, B. D.; Toste, F. D. *Chem. Rev.* **2008**, *108*, 3351-3378. (*e*) Benitez, D.; Shapiro, N. D.; Tkatchouk, E.; Wang, Y.; Goddard, W. A.; Toste, F. D. *Nat. Chem.* **2009**, *1*, 482-486. (*f*) Wang, W.; Hammond, G. B.; Xu, B. *J. Am. Chem. Soc.* **2012**, *134*, 5697–5705. (*g*) Fürstner, A.; Davies, P. W. *Angew. Chem., Int. Ed.* **2007**, *46*, 3410–3449. (*h*) Petuskova, J.; Bruns, H.; Alcarazo, M. *Angew. Chem., Int. Ed.* **2011**, *50*, 3799– 3802.

10. Stringer, K. L.; Citir, M.; Metz, R. B. *J. Phys. Chem. A* **2004**, *108*, 6996-7002.

11. Sievers, M. R.; Jarvis, L. M.; Armentrout, P. B. *J. Am. Chem. Soc.* **1998**, *120*, 1891-1899.

12. Schröder, D.; Schwarz, H.; Hrušák, J.; Pyykkö, P. *Inorg. Chem.* **1998**, *37*, 624-632.

13. Hertwig, R. H.; Koch, W.; Schröder, D.; Schwarz, H.; Hrušák, J.; Schwerdtfeger, P. *J. Phys. Chem.* **1996**, *100*, 12253-12260.

14. Schröder, D.; Hrusak, J.; Hertwig, R. H.; Koch, W.; Schwerdtfeger, P.; Schwarz, H. *Organometallics* **1995**, *14*, 312-316.

15. Nechaev, M. S.; Rayón, V. M.; Frenking, G. *J. Phys. Chem. A* **2004**, *108*, 3134-3142.

16. Herrero-Gómez, E.; Nieto-Oberhuber, C.; López, S.; Benet-Buchholz, J.; Echavarren, A. M. A. M. *Angew. Chem., Int. Ed.* **2006**, *45*, 5455–5459.

17. (*a*) Lavallo, V.; Frey, G. D.; Kousar, S.; Donnadieu, B.; Bertrand, G. *Proc. Natl. Acad. Sci. U. S. A.* **2007**, *104*, 13569–13573. (*b*) Weber, S. G.; Rominger, F.; Straub, F. B. *Eur. J. Inorg. Chem.* **2012**, 2863–2867.

18. Sen, S. S.; Hey, J.; Herbst-Irmer, R.; Roesky, H. W.; Stalke, D. *J. Am. Chem. Soc.* **2011**, *133*, 12311–12316.

19. (*a*) Parvin, N.; Pal, S.; Echeverría, J.; Alvarez, S.; Khan, S. *Chem. Sci.* **2018**, *9*, 4333-4337. (*b*) N. Parvin, J. Hossain, A. George, P. Parameswaran and S. Khan, *Chem. Commun.*, **2020**, *56*, 273–276.

20. Khan, S.; Ahirwar, S. K.; Pal, S.; Parvin, N.; Kathewad, N. Organometallics **2015**, *34*, 5401-5406.

21. Khan, S.; Pal, S.; Kathewad, N.; Purushothaman, I.; Deb, S.; Parameswaran, P. *Chem. Commun.* **2016**, *52*, 3880-3882.

22. (*a*) Peng P.; Schmidt, R. R. *J. Am. Chem. Soc.* **2015**, *137*, 12653-12659. (*b*) Adhikari, S.; Baryal, K. N.; Zhu, D. Y.; Li, X. H.; Zhu, J. L. *ACS Catal.* **2013**, *3*, 57-60. (*c*) Palo-Nieto, C.; Sau, A.; Galan, M. C. *J. Am. Chem. Soc.* **2017**, *139*, 14041–14044.

23. Mishra, B.; Neralkar, M.; Hotha, S. *Angew. Chem., Int. Ed.* **2016**, *55*, 7786-7791.

24. Boehme, C.; Frenking, G. *Organometallics* **1998**, *17*, 5801– 5809.

25. Falceto, A.; Carmona, E.; Alvarez, S. *Organometallics* **2014**, *33*, 6660-6668.

26. (*a*) Samuel, P. P.; Singh, A. P.; Sarish, S. P.; Matussek, J.; Objartel, I.; Roesky, H. W.; Stalke, D. *Inorg. Chem.*, **2013**, *52*, 1544–1549. (*b*) Álvarez-Rodríguez, L.; Cabeza, J. A.; García-Álvarez, P.; Polo, D. *Organometallics* **2015**, *34*, 5479-5484.

27. (*a*) Frémont, P. de; Scott, S. M.; Steves, E. D.; Nolan S. P. *Organometallics* **2005**, *24*, 2411-2418. (*b*) Simms, R. W.; Drewitt, M. J.; Baird, M. C. *Organometallics* **2002**, *21*, 2958-2963. (*c*) Clavier, H.; Nolan, S. P. *Chem. Commun.*, **2010**, *46*, 841–861.

28. (*a*) Seeberger, P. H.; Werz, D. B. *Nature* **2007**, *446*, 1046-1051. (*b*) Zhu, X.; Schmidt, R. R. *Angew. Chem., Int. Ed.* **2009**, *48*, 1900-1934.

29. Adhikari, S.; Li, X.; Zhu, J. *J. Carbohydrate Chem.* **2013**, *32*, 336-359.

30. Hotha, S.; Kashyap, S. *J. Am. Chem. Soc.* **2006**, *110*, 9620-9621.

31. Kayastha, A. K.; Hotha, S. *Beilstein J. Org. Chem.* **2013**, *9*, 2147–2155.

32. Kayastha, A. K.; Hotha, S. *Chem. Commun.* **2012**, *48*, 7161–7163.

33. Kayastha, A. K.; Hotha, S. *Tetrahedron Lett.* **2010**, *51*, 5269-5272.

34. Sureshkumar, G.; Hotha, S. *Tetrahedron Lett.* **2007**, *48*, 6564-6568.

35. Thadke, S. A.; Mishra, B.; Islam, M.; Pasari, S.; Manmode, S.; Rao, B. V.; Neralkar, M.; Shinde, G. P.; Walke, G.; Hotha, S. *Nature Commun.* **2017**, *8*, 14019.

36. See computational details in ESI for detailed citations.

37. See computational details in ESI for detailed explanation.

38. Bewley, C. A.; Kiyonaka, S.; Hamachi, I. *J. Mol. Biol.* **2002**, *322*, 881–889.

39. Barrientos, L. G.; Gronenborn, A. M. *Med. Chem.* **2005**, *5*, 21–31.

40. Lam, S. N.; Gervay-Hague, J. *J. Org. Chem.* **2005**, *70*, 8772–8779.

41. Neralkar, M.; Mishra, B.; Hotha, S. *J. Org. Chem.* **2017**, *82*, 11494-11504.

*****

Chapter 5

C-N Cross-Coupling Reactions of Bulky Primary Anilines with Aryl Halides Using Pd/NHSi System

---

5.1. Introduction:

The Pd-catalyzed cross-coupling reactions of amines and aryl halides, known as Buchwald-Hartwig amination reactions for the formation of C-N bonds,[1] has materialized as a general tool for the preparation of aromatic amines with extensive applications in basic science and applied chemistry e.g. pharmaceuticals, synthesis of natural products, material science, and catalysis.[2] At the beginning of the 20th century, Goldberg[3] and Ullmann[4] used copper-mediated processes, whereas, Migita and co-workers introduced palladium complexes for the $C(sp^2)$-N bond formation in 1983.[5] Along with other drawbacks, limited substrate scope is the general obstacle for both the methods. Hence in 1995, Stephen L. Buchwald and John F. Hartwig overcame the difficulties and promoted a new general efficient protocol for the C-N bond formation by using Pd salts (Scheme 5.1).[6] Cooperative efforts of both the groups and other scientists open a new era in organic chemistry.
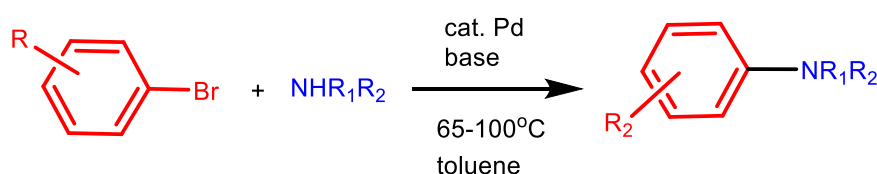
Scheme 5.1. *General scheme of C-N cross-coupling reaction.*

Development of new ligands to regulate the reactivity, selectivity and efficiency is of fundamental interest in transition metal catalysis. For the C-N cross-coupling reactions, electron-rich ligands are more efficient for stabilizing active metals, ligands replacement from the metal centre, or to promptly activate the bond. From the last few decades, phosphines and NHCs are the dominating ligands in homogeneous catalysis due to the strong σ-donating property. It is well evident from the literature that various kind of phosphine ligands[7] bearing alkyl groups, aryl groups, specially BINAP,[8,9] dppf, DPEPhos,[8,10] Xantphos,[11] dppp,[8] CyPF-t-Bu,[12] BippyPhos,[13] MorDalPhos[14] as well as various NHCs[15] have nurtured the rapid development of Buchwald-Hartwig amination reactions.

N-heterocyclic silylenes (NHSis), the lighter analogue of NHCs, are well known for strong σ-donor and π-acceptor ability and can be a good candidate with transition metals for various organic transformation reactions. A similar phenomenon is also demonstrated theoretically by Szilvási and co-workers where they showed that silylenes have the ability to compete with the well-known carbenes and phosphines ligands.[16] In 2010, Driess group investigated σ-donor strengths of a series of *β*-diketiminato silylenes by examining the CO stretching frequency of the corresponding isoelectronic $Ni(CO)_3$ complexes and observed that some of them are strong σ-donor than phosphines and NHCs.[17] Very recently, our group reported a similar observation of benzamidinato silylene.[21c] Hence NHSis are widely used as ligands for transition metals after 1977, when Welz and Schmid isolated the first NHSi-iron complex.[18] The emerging NHSi-TM complexes have the propensity to perform as an efficient catalystic system in various catalytic reactions by using Mn, Fe, Ni, Co, Rh, Ir, Pd, Pt, Cu, Au etc.[19] Several research groups including Driess and Hartwig, Roesky, Fürstner and our group have added new feathers for the exploration of the versatility of silylene in catalysis, for example, the Suzuki cross-coupling,[20a] Heck coupling,[20b] cyclotrimerization of alkynes,[20c] borylation of benzene,[20d] Sonogashira coupling,[20e] Kumada-Corriu coupling,[20f] ketones hydrosilylation,[20g,h,i] amide reduction,[20j] amination of arenes,[20k] click reaction,[21b] disaccharide and polysaccharide formation[21c] etc. The NHSi-Pd complexes are employed in the C-C cross-coupling reaction i.e. Suzuki coupling[20a] and Heck coupling[20b] by Fürstner and Roesky group, respectively. However they have never been introduced in C-N cross-coupling reactions. Although in

1.70a L= Br
1.70b L= CO
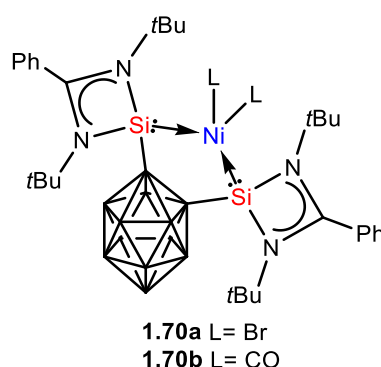
Chart 5.1. *Reported example of C-N cross-coupling reactions by silylene*

2016, Driess and coworkers reported the C-N cross-coupling reactions of aryl halides and secondary amines by using ortho-carborane stabilized bis(silylene)-Ni complexes (**1.70a** and **1.70b**) as a precatalyst (Chart 5.1).[20k]

Recently, our group utilized the NHSi [{PhC(NtBu)$_2$}Si{N(SiMe$_3$)$_2$}] for the isolation of unrivaled Cu(I)-η^6-benzene,[21a] Cu(I)-η^3-toluene and Cu(I)-η^2-m-xylene complexes.[21b] Further, we have employed the NHSi-Cu-toluene complex for the click reaction as a potent catalyst for various alkynes and azides. In 2020, we have synthesized amidinato silylene/germylene supported Au(I)-benzene complexes and exploited them as catalysts for the isolation of a series of disaccharides and branched pentamer which is the core of the HIV-gp120 envelope.[21c,22] Functionalized amidinato silylene [PhC(NtBu)$_2$SiN(PPh$_2$)(2,6-iPr$_2$-C$_6$H$_3$)] (**1.35**), containing two coordinating sites Si(II) and P(III), is well established by our group and reported to form a coordination complex with Au(I).[23] Due to two different coordinating sites, we became interested in examining the unrivalled silylene **1.35** as a ligand in homogeneous catalysis. Herein, we examine, C-N cross-coupling reactions by utilizing **1.35** as a ligand with Pd(dba)$_2$ metal salt *insitu* for enormously bulky primary anilines with bulky aryl bromide containing Me and fluoro substituents by a conventional method as well as under the microwave technique (10-15 min). Recent studies on C-N cross-coupling reactions by Buchwald and co-workers motivated us to develop new ligands for sterically hindered groups with a broad substrate scope.[24] We believe that these studies will be worthwhile because of the lack of general studies on these bulky class of substrates where the yields are very low ($\sim$30–70%) (*vide infra*).[25b,d,e]

5.2. Experimental Section

5.2.1. General Remarks

All experiments were carried out under an inert gas atmosphere of dinitrogen using standard Schlenk techniques and in a dinitrogen filled MBRAUN MB 150-G1 glove box. The solvents used were purified by a MBRAUN solvent purification system MB SPS-800. Compound **1.35**,[23] 2,6-dibenzhydryl-4-methylaniline,[26a] and 2,6-bis(bis(4-(tert-butyl)phenyl)methyl)-4-methylaniline[26b] were prepared by literature methods. All chemicals purchased from Aldrich were used without further purification. ^{1}H, ^{13}C, ^{19}F, ^{31}P and ^{29}Si NMR spectra were recorded in C$_6$D$_6$, and CDCl$_3$ using Bruker 400 MHz

spectrometer with external standard $SiMe_4$ for ^1H, ^{13}C and ^{29}Si, trifluorotoluene for ^{19}F and 85% H_3PO_4 for ^{31}P. Mass spectra were recorded using AB Sciex, 4800 plus MALDI TOF/TOF.

5.2.2. Synthesis of **5.1a-5.1p**

10 mL toluene was added into the mixture of ligand **1.35** (SiNP) (0.012 mmol) and Pd(dba)$_2$ (0.012 mmol) in a 100 mL Schlenk flask and stirred it at room temperature for 1 hour. 0.625 mmol of aryl halide, 1.7 mmol of NaO*t*Bu and 0.625 mmol of bulky primary aniline were added into this and stirred the whole thing for 20 h at 100°C under reflux condition. All the additions have done in an inert atmosphere. Then cool it at room temperature and extracted in *n*-hexane. Sodium sulphate was added into this as a drying agent. The resulting solution was dried in *vaccuo* and purified by column chromatography (*n*-hexane) to afford the expected product. Products obtained as solids or liquids were dried under high vaccum. Analytical thin layer chromatography was performed on pre-coated silica plates. All the compounds were characterized by NMR spectroscopy and mass spectrometry. All the heteronuclear NMRs are proton decoupled.

Synthesis of 5.1a: Yield: 90%. ^1H NMR (400 MHz, CDCl$_3$, 298K): δ 1.15 (*d*, 12H, *J*= 6.9 Hz, CH*Me$_2$*), 2.00 (*s*, 6H, C*H$_3$*), 2.27 (*s*, 3H, C*H$_3$*), 3.13-3.30 (*m*, 2H, C*H*Me$_2$), 4.74 (*s*, 1H, N*H*), 6.80 (*s*, 2H, Ph), 7.14 (*s*, 3H, Ph) ppm. ^{13}C {^1H} NMR (100.613 MHz, CDCl$_3$, 298 K): δ 19.38, 20.54, 23.56, 28.08, 123.34, 124.27, 126.43, 129.18, 130.15, 139.28, 140.55, 143.47 ppm. IR: 533.81, 577.20, 731.69, 780.97, 852.46, 928.26, 1017.77, 1255.55, 1333.53, 1443.94, 1550.35, 1735.56, 1909.62, 1953.86, 2169.04, 2312.00, 2374.66, 2508.72, 2729.27, 2862.27, 2919.57, 2955.92, 3183.63, 3429.21, 3589.26, 3643.10, 3742.38, 3819.10, 3878.31cm^{-1}. MALDI *m/z* (C$_{21}$H$_{29}$N): 295.35 [M]$^+$.

Synthesis of 5.1b: Yield: 86%. ^1H NMR (400 MHz, CDCl$_3$, 298K): δ 1.16 (*d*, 12H, *J*= 6.9 Hz, CH*Me$_2$*), 2.02 (*s*, 6H, C*H$_3$*), 3.14-3.24 (*m*, 2H, C*H*Me$_2$), 4.83 (*s*, 1H, N*H*), 6.76 (*t*, 1H, *J*= 7.4 Hz, Ph), 6.97 (*d*, 2H, *J*= 7.4 Hz, Ph), 7.12-7.21 (*m*, 3H, Ph) ppm. ^{13}C {^1H} NMR (100.613 MHz, CDCl$_3$, 298 K): δ 19.48, 23.59, 28.18, 29.85, 119.72, 123.37, 124.95, 125.75, 129.64, 138.92, 143.26, 144.28. IR: 535.63, 602.89, 691.83, 757.97, 793.90, 1053.22, 1103.00, 1271.51, 1332.19, 1464.77, 1591.38, 1727.82, 2866.78, 2959.94, 3432.34, 3589.63, 3740.76, 3817.29, 3874.09. MALDI *m/z* (C$_{20}$H$_{27}$N): 281.46 [M]$^+$.

Synthesis of 5.1c: Yield: 85%. ^{1}H NMR (400 MHz, CDCl$_3$, 298K): δ 1.44 (*s*, 6H, C*H$_3$*), 2.12 (*s*, 3H, C*H$_3$*), 2.24 (*s*, 3H, C*H$_3$*), 4.11 (*s*, 1H, N*H*), 5.51 (*s*, 2H, CH*Ph$_2$*), 6.47 (*s*, 2H, Ph), 6.70 (*m*, 2H, Ph), 6.90 (*d*, 8H, *J*= 6.7 Hz, Ph), 7.16-7.26 (*m*, 12H, Ph) ppm. ^{13}C {^{1}H} NMR (100.613 MHz, CDCl$_3$, 298 K): δ 18.45, 20.46, 21.41, 52.23, 125.88, 126.18, 128.18, 128.95, 129.10, 129.48, 129.55, 131.71, 137.52, 138.47, 138.73, 143.58 ppm. IR: 595.74, 694.18, 752.53, 851.91, 1020.51, 1071.63, 1237.80, 1325.84, 1446.17, 1488.73, 1557.17, 1736.40, 1942.62, 2143.88, 2316.21, 2583.05, 2758.31, 2856.32, 2919.38, 3186.00, 3258.51, 3350.17, 3398.37, 3585.87, 3636.74, 3736.20, 3821.16 cm^{-1}. MALDI *m/z* (C$_{42}$H$_{39}$N): 557.54 [M]$^+$.

Synthesis of 5.1d: Yield: <99%. ^{1}H NMR (400 MHz, CDCl$_3$, 298K): δ 1.46 (*s*, 6H, C*H$_3$*), 2.14 (*s*, 3H, C*H$_3$*), 4.19 (*s*, 1H, N*H*), 5.52 (*s*, 2H, CH*Ph$_2$*), 6.50 (*s*, 2H, Ph), 6.68-6.77 (*m*, 1H, Ph), 6.91 (*d*, 9H, *J*= 7.1 Hz, Ph), 7.15-7.30 (*m*, 13H, Ph) ppm. ^{13}C {^{1}H} NMR (100.613 MHz, CDCl$_3$, 298 K): δ 18.49, 21.43, 29.71, 52.30, 119.57, 125.46, 126.23, 128.22, 128.98, 129.04, 129.46, 132.27, 137.20, 138.97, 141.29, 143.54 ppm. IR: 532.96, 604.82, 693.23, 756.50, 1027.61, 1077.09, 1313.78, 1450.76, 1589.27, 1740.30, 1949.17, 2174.77, 2311.57, 2504.20, 2573.87, 2852.40, 2918.80, 3019.72, 3194.85, 3302.45, 3346.31, 3395.82, 3749.77, 3823.04, 3877.35 cm^{-1}. MALDI *m/z* (C$_{41}$H$_{37}$N): 543.41 [M]$^+$.

Synthesis of 5.1e: Yield: <99%. ^{1}H NMR (400 MHz, CDCl$_3$, 298K): δ 1.52 (*s*, 6H, C*H$_3$*), 2.16 (*s*, 3H, C*H$_3$*), 2.26 (*s*, 3H, C*H$_3$*), 2.35 (*s*, 12H, C*H$_3$*), 4.20 (*s*, 1H, N*H*), 5.48 (*s*, 2H, CH*Ph$_2$*), 6.54 (*s*, 2H, Ph), 6.73 (*s*, 2H, Ph), 6.81 (*d*, 8H, *J*= 8.0 Hz, Ph), 7.06 (*d*, 8H, *J*= 7.8 MHz, Ph) ppm. ^{13}C {^{1}H} NMR (100.613 MHz, CDCl$_3$, 298 K): δ 18.62, 20.53, 21.12, 21.50, 51.43, 126.08, 128.89, 128.99, 129.36, 129.58, 131.63, 135.52, 137.67, 138.79, 139.07, 140.94 ppm. IR: 576.82, 642.36, 719.48, 763.32, 806.25, 857.08, 1013.07, 1176.37, 1236.28, 1323.68, 1492.56, 1551.06, 1744.27, 1862.61, 1944.70, 2106.97, 2159.58, 2311.81, 2387.28, 2502.67, 2626.63, 2761.74, 2856.85, 2922.44, 3001.10, 3093.44, 3209.86, 3266.43, 3373.97, 3465.55, 3549.43, 3594.90, 3660.68, 3740.17, 3827.76, 3876.83, 3922.28 cm^{-1}. MALDI *m/z* (C$_{46}$H$_{47}$N): 613.46 [M]$^+$.

Synthesis of 5.1f: Yield: 96%. ^{1}H NMR (400 MHz, CDCl$_3$, 298K): δ 1.49 (*s*, 6H, C*H$_3$*), 2.15 (*s*, 3H, C*H$_3$*), 2.33 (*s*, 12H, C*H$_3$*), 4.24 (*s*, 1H, N*H*), 5.45 (*s*, 2H, CH*Ph$_2$*), 6.52 (*s*, 2H, Ph), 6.66-6.73 (*m*, 1H, Ph), 6.78 (*d*, 8H, *J*= 7.7 Hz, Ph), 6.90 (*d*, 2H, *J*= 7.2 Hz, Ph), 7.04 (*d*, 8H, *J*= 7.5 Hz, Ph) ppm. ^{13}C {^{1}H} NMR (100.613 MHz, CDCl$_3$, 298 K): δ 18.67, 21.13, 21.47, 29.80, 51.50, 119.49, 125.61, 128.93, 129.02, 129.34, 132.20, 135.58, 137.31, 139.30, 140.88,

141.61 ppm. IR: 570.92, 653.90, 763.45, 812.37, 1027.45, 1100.34, 1183.57, 1241.20, 1310.13, 1459.05, 1506.36, 1564.24, 1743.54, 2311.25, 2503.46, 2857.22, 2922.99, 3095.22, 3184.95, 3275.82, 3401.41, 3627.54, 3748.52, 3811.92, 3866.13. MALDI *m/z* ($C_{45}H_{45}N$): 599.47 [M]+.

Synthesis of 5.1g: Yield: <99%. ^{1}H NMR (400 MHz, CDCl$_3$, 298K): δ 1.22-1.31 (*s*, 6H, C*H$_3$*), 2.11 (*s*, 3H, C*H$_3$*), 2.19 (*s*, 3H, C*H$_3$*), 4.03 (*s*, 1H, N*H*), 5.34 (*s*, 2H, CH*Ph$_2$*), 6.45 (*s*, 2H, Ph), 6.62 (*s*, 2H, Ph), 6.79 (*dd*, 8H, *J*= 8.3, 1.9 Hz, Ph), 7.20 (*dd*, 8H, *J*= 8.3, 1.9 Hz, Ph) ppm. ^{13}C {^{1}H} NMR (100.613 MHz, CDCl$_3$, 298 K): δ 18.26, 20.56, 21.47, 31.49, 34.50, 51.54, 125.01, 125.85, 128.67, 128.83, 129.16, 129.40, 131.28, 137.42, 138.58, 138.80, 140.69, 148.79 ppm. IR: 569.37, 647.57, 704.41, 752.86, 837.38, 1015.04, 1191.94, 1262.10, 1320.56, 1463.98, 1739.53, 1906.59, 2198.35, 2308.86, 2388.29, 2498.65, 2630.11, 2748.93, 2858.92, 2950.28, 3190.62, 3303.06, 3385.92, 3622.22, 3739.42, 3824.25, 3920.60 cm-1. MALDI *m/z* ($C_{58}H_{71}N$): 782.71 [M]+.

Synthesis of 5.1h: Yield: 98%. ^{1}H NMR (400 MHz, CDCl$_3$, 298K): δ 1.30 (*s*, 36H, C*H$_3$*), 1.58 (*s*, 6H, C*H$_3$*), 2.24 (*s*, 3H, C*H$_3$*), 4.94 (*s*, 1H, N*H*), 5.59 (*s*, 2H, CH*Ph$_2$*), 6.55-6.62 (*m*, 1H, Ph), 6.72-6.76 (*m*, 1H, Ph) 6.82 (*s*, 2H, Ph), 6.92 (*d*, 8H, *J*= 7.7, Ph), 6.97-7.03 (*m*, 1H, Ph), 7.23 (*d*, 8H, *J*= 7.9 Hz, Ph) ppm. ^{13}C {^{1}H} NMR (100.613 MHz, CDCl$_3$, 298 K): δ 21.70, 31.38, 34.33, 50.68, 124.99, 128.89, 129.57, 134.02, 136.31, 140.37, 144.41, 148.70 ppm. IR: 581.23, 701.66, 814.29, 1032.41, 1103.41, 1268.23, 1461.19, 1506.28, 1549.94, 1744.58, 1953.60, 2153.86, 2311.28, 2504.18, 2735.88, 2857.95, 2956.94, 3189.25, 3270.88, 3397.91, 3561.36, 3613.32, 3740.79, 3822.98 cm-1. MALDI *m/z* ($C_{57}H_{69}N$): 767.83 [M]+.

Synthesis of 5.1i: Yield: 96%. ^{1}H NMR (400 MHz, CDCl$_3$, 298K): δ 1.18 (*d*, 12H, *J*= 6.9 Hz, CH*Me$_2$*), 3.16-3.26 (*m*, 2H, C*H*Me$_2$), 5.34 (*s*, 1H, N*H*), 6.20-6.24 (*m*, 1H, Ph), 6.63-6.69 (*m*, 1H, Ph), 6.85-6.89 (*m*, 1H, Ph), 7.05-7.10 (*m*, 1H, Ph), 7.26-7.29 (*m*, 2H, Ph), 7.33-7.37 (*m*, 1H, Ph) ppm. ^{13}C {^{1}H} NMR (100.613 MHz, CDCl$_3$, 298 K): δ 14.22, 23.94, 28.29, 29.80, 113.20, 114.58, 114.76, 117.06, 117.13, 124.00, 124.49, 127.69, 128.21, 134.22, 136.46, 136.57, 147.83, 149.94, 152.31 ppm. ^{19}F {^{1}H} NMR (376.66 MHz, CDCl3, 298 K): δ -137.41 ppm. IR: 540.90, 628.41, 740.92, 792.32, 884.51, 926.81, 1042.01, 1099.90, 1186.82, 1248.72, 1326.35, 1453.59, 1507.40, 1618.17, 2869.22, 2961.36, 3062.03, 3430.30, 3741.76. MALDI *m/z* ($C_{18}H_{22}FN$): 271.81 [M]+.

Synthesis of 5.1j: Yield: 97%. MALDI *m/z* ($C_{20}H_{21}NF_6$): ^{1}H NMR (400 MHz, CDCl3, 298K): δ 1.17 (*d*, 12H, *J*= 6.9 Hz, CH*Me2*), 3.06-3.16 (*m*, 2H, C*H*Me2), 5.53 (*s*, 1H, N*H*), 6.85 (*s*, 2H, Ph), 7.19 (*s*, 1H, Ph), 7.28-7.29 (*m*, 2H, Ph), 7.37-7.41 (*m*, 1H, Ph) ppm. ^{13}C {^{1}H} NMR (100.613 MHz, CDCl3, 298 K): δ 23.79, 28.35, 29.71, 124.40, 128.50, 132.35, 132.70, 147.40, 148.93 ppm. ^{19}F {^{1}H} NMR (376.66 MHz, CDCl3, 298 K): δ -63.21 ppm. IR: 557.08, 607.46, 678.38, 765.31, 802.11, 863.79, 954.87, 998.10, 1127.70, 1271.60, 1325.65, 1413.29, 1508.51, 1618.34, 2858.95, 2924.11, 2959.93, 3434.07, 3749.64, 3823.28, 3871.33 cm^{-1}. MALDI *m/z* ($C_{20}H_{21}NF_6$): 392.27 [M+3H]+.

Synthesis of 5.1k: Yield: 98%. ^{1}H NMR (400 MHz, CDCl3, 298K): δ 2.19 (*s*, 3H, C*H3*), 2.00 (*s*, 6H, C*H3*), 4.73 (*s*, 1H, N*H*), 5.60 (*s*, 2H, CH*Ph2*), 6.28-6.41 (*m*, 1H, Ph), 6.59-6.68 (*m*, 1H, Ph), 6.72 (*s*, 1H, Ph), 6.79-6.87 (*m*, 1H, Ph), 6.92-7.04 (*m*, 9H, Ph), 7.14-7.23 (*m*, 12H, Ph) ppm. ^{13}C {^{1}H} NMR (100.613 MHz, CDCl3, 298 K): δ 21.75, 51.82, 112.92, 114.75, 114.93, 117.32, 117.38, 124.60, 126.21, 128.33, 129.38, 129.89, 134.12, 136.64, 143.34, 144.22 ppm. ^{19}F {^{1}H} NMR (376.66 MHz, CDCl3, 298 K): δ -136.75 ppm. IR: 599.53, 693.92, 749.86, 918.07, 988.97, 1076.82, 1179.62, 1237.97, 1318.79, 1451.56, 1499.61, 1550.28, 1614.10, 1742.19, 1947.85, 2045.31, 2113.38, 2315.38, 2386.43, 2505.94, 2505.94, 2855.29, 2920.92, 3011.10, 3178.20, 3286.89, 3365.16, 3599.01, 3746.70, 3819.21, 3873.51, 3930.08 cm^{-1}. MALDI *m/z* ($C_{39}H_{32}FN$): 533.45[M]+.

Synthesis of 5.1l: Yield: 95%. ^{1}H NMR (400 MHz, CDCl3, 298K): δ 2.20 (*s*, 3H, C*H3*), 4.82 (*s*, 1H, N*H*), 5.45 (*s*, 2H, CH*Ph2*), 6.64 (*s*, 2H, Ph), 6.70 (*s*, 2H, Ph), 6.90-6.92 (*m*, 8H, Ph), 7.09-7.24 (*m*, 15H, Ph) ppm. ^{13}C {^{1}H} NMR (100.613 MHz, CDCl3, 298 K): δ 21.72, 52.12, 126.48, 128.42, 129.16, 130.09, 132.92, 137.65, 142.70, 143,94, 147.98 ppm. ^{19}F{^{1}H} NMR (376.66 MHz, CDCl3, 298 K): δ -63.08 ppm. IR: 532.63, 606.08, 690.81, 794.29, 864.48, 1014.90, 1086.78, 1171.37, 1264.95, 1375.55, 1461.97, 1615.62, 1741.62, 1952.16, 2313.02, 2500.20, 2647.44, 2862.87, 2961.68, 3744.08, 3822.81. MALDI *m/z* ($C_{41}H_{31}NF_6$): 651.35 [M]+.

Synthesis of 5.1m: Yield: 96%. ^{1}H NMR (400 MHz, CDCl3, 298K): δ 2.20 (*s*, 3H, C*H3*), 2.31 (*s*, 12H, C*H3*), 4.80 (*s*, 1H, N*H*), 5.53 (*s*, 2H, CH*Ph2*), 6.75 (*s*, 2H, Ph), 6.85-6.87 (*m*, 9H, Ph), 7.02-7.04 (*m*, 11H, Ph) ppm. ^{13}C {^{1}H} NMR (100.613 MHz, CDCl3, 298 K): δ 21.03, 21.69, 50.92, 113.01, 114.61, 114.78, 124.48, 128.30, 128.91, 129.15, 129.60, 130.13, 133.99, 135.58, 140.58, 144.28. ^{19}F {^{1}H} NMR (376.66 MHz, CDCl3, 298 K): δ -136.78 ppm. IR: 532.42, 577.27, 736.52, 801.54, 1019.88, 1090.36, 1181.41, 1239.85, 1320.15, 1455.83,

1505.25, 1561.00, 1616.97, 1745.94, 2311.20, 2495.22, 2859.17, 2917.49, 3003.42, 3097.32, 3378.39, 3585.36, 3636.57, 3733.41, 3824.53, 3871.19, 3924.77. MALDI *m/z* ($C_{43}H_{40}FN$): 590.57 [M+H]$^+$.

Synthesis of 5.1n: Yield: 95%. ^{1}H NMR (400 MHz, CDCl$_3$, 298K): δ 2.24 (*s*, 3H, C*H$_3$*), 2.32 (*s*, 12H, C*H$_3$*), 4.90 (*s*, 1H, N*H*), 5.40 (*s*, 2H, CH*Ph$_2$*), 6.66 (*s*, 2H, Ph), 6.75 (*s*, 2H, Ph), 6.82 (*d*, 8H, *J*= 8.0 Hz, Ph), 7.04 (*d*, 8H, *J*= 7.9 Hz, Ph), 7.15 (*s*, 1H, Ph) ppm. ^{13}C {^{1}H} NMR (100.613 MHz, CDCl$_3$, 298 K): δ 20.97, 21.73, 51.32, 128.99, 129.07, 129.91, 132.87, 135.89, 137.44, 139.93, 144.08, 148.12. ^{19}F {^{1}H} NMR (376.66 MHz, CDCl3, 298 K): δ -63.16 ppm. IR: 526.51, 569.71, 678.26, 715.06, 812.82, 865.62, 955.96, 1036.59, 1137.27, 1271.05, 1324.24, 1382.45, 1465.20, 1511.38, 1555.17, 1618.84, 1741.08, 1905.66, 2312.81, 2377.52, 2503.46, 2726.58, 2856.81, 2925.46, 3638.56, 3746.83, 3821.34, 3872.02. MALDI *m/z* ($C_{45}H_{39}NF_6$): 707.44 [M]$^+$.

Synthesis of 5.1o: Yield: 80%. ^{1}H NMR (400 MHz, CDCl$_3$, 298K): δ 1.27 (*s*, 36H, C*H$_3$*), 2.21 (*s*, 3H, C*H$_3$*), 2.19 (*s*, 3H, C*H$_3$*), 4.92 (*s*, 1H, N*H*), 5.57 (*s*, 2H, CH*Ph$_2$*), 6.80 (*s*, 2H, Ph), 6.89 (*s*, 10H, *J*= 7.4 Hz, Ph), 6.79 (*dd*, 8H, *J*= 8.3, 1.9 Hz, Ph), 7.20 (*d*, 10H, *J*= 7.4 Hz, Ph) ppm. ^{13}C {^{1}H} NMR (100.613 MHz, CDCl$_3$, 298 K): δ 21.78, 31.47, 34.41, 50.75, 125.08, 128.98, 129.65, 134.09, 136.40, 140.45, 144.50, 148.78. ^{19}F {^{1}H} NMR (376.66 MHz, CDCl3, 298 K): δ -137.14 ppm. IR: 533.61, 580.25, 640.80, 693.74, 742.41, 832.65, 1019.57, 1102.38, 1187.87, 1248.26, 1314.29, 1457.69, 1504.47, 1558.63, 1620.92, 1745.82, 1946.77, 2048.58, 2255.97, 2309.57, 2498.02, 2642.08, 2730.95, 2861.04, 2947.75, 3174.04, 3305.75, 3374.14, 3426.75, 3632.74, 3738.95, 3813.12, 3876.44, 3921.02 cm^{-1}. MALDI: *m/z* ($C_{55}H_{67}NF$): 758.68 [M]$^+$.

Synthesis of 5.1p: Yield: 97%. ^{1}H NMR (400 MHz, CDCl$_3$, 298K): δ 2.24 (*s*, 3H, C*H$_3$*), 2.32 (*s*, 12H, C*H$_3$*), 4.90 (*s*, 1H, N*H*), 5.40 (*s*, 2H, CH*Ph$_2$*), 6.66 (*s*, 2H, Ph), 6.75 (*s*, 2H, Ph), 6.82 (*d*, 8H, *J*= 8.0 Hz, Ph), 7.04 (*d*, 8H, *J*= 7.9 Hz, Ph), 7.15 (*s*, 1H, Ph) ppm. ^{13}C {^{1}H} NMR (100.613 MHz, CDCl$_3$, 298 K): δ 21.83, 31.41, 34.43, 51.16, 125.25, 128.81, 130.12, 132.98, 137.50, 139.96, 144.14, 148.40, 149.12 ppm. ^{19}F {^{1}H} NMR (376.66 MHz, CDCl3, 298 K): δ -63.03 ppm. IR: 575.03, 692.23, 821.26, 952.39, 1028.92, 1125.43, 1172.52, 1270.56, 1370.91, 1464.61, 1509.87, 1622.09, 1744.72, 1952.65, 2159.68, 2308.71, 2570.51, 2863.66, 2957.59, 3208.97, 3618.41, 3739.77, 3821.47, 3867.90. MALDI *m/z* ($C_{57}H_{63}NF_6$): 876.86 [M]$^+$.

5.2.3. X-ray Crystallography Details

Single crystals of suitable size, coated with paraffin oil was mounted for all the complexes. Crystal data for all the complexes were collected on a Bruker Smart Apex Duo diffractometer at 100 K using Mo Kα radiation (λ = 0.71073 Å). Collected data were integrated by using SAINT and then absorption correction was done by multi-scan method using SADABS program All the structures were solved by direct methods and refined by full-matrix least-squares methods against F^2 (SHELXL-2014/6).

5.3. Result and Discussions

We investigated the performance of **1.35**/Pd(dba)$_2$ system *insitu* for C-N cross-coupling reactions of sterically bulky 2,6-bis [bis(4-methylphenyl)methyl]-4-methylaniline and mesityl bromide as a model reaction. We examined the consequences of various reaction parameters such as mol% of Pd(dba)$_2$, mol% of ligand **1.35**, and reaction time. The results of our screening experiments disclosed that the best result was acquired by using 2 mol % of **1.35** with 2 mol% of Pd(dba)$_2$ at 100°C (Table 5.1, entry 4). The full conversion was obtained within 20h. We have used toluene as a solvent and NaO*t*Bu was used as a base in the reaction mixture. Pd(PPh$_3$)$_4$ as a Pd salt is also effective like Pd(dba)$_2$. Blank test experiment (without Pd(dba)$_2$) gives no product conversion, even after refluxing for 4 days with 5 mol% of **1.35** (Table 5.1, entry 5). On the other hand the amination reaction without **1.35** gives a 10-15% yield of the coupling product (Table 5.1, entry 6).

To understand the steric protection of the ligand **1.35**, we have calculated the buried volume (%V$_{bur}$)[27] by using a previously reported **1.35**-AuCl complex.[23] %V$_{bur}$= 52.4% of **1.35** indicates that the ligand is highly sterically protected than many well-known phosphines e.g. DPEphos (%Vbur=45.3%), Xantphos (%Vbur=46.8%) and IPr carbene (%Vbur=44.5%). To understand the catalytic efficiency of **1.35**, we have examined and compared it with previously reported ligands e.g. NHSi,[28] GeNP,[29] SnNP[29] (GeNP and SnNP are the higher analogs of **1.35**) along with previously reported phosphines PNP[30] and DPEphos under the optimized reaction conditions (Chart 5.2). We have screened above-mentioned ligands with Pd(dba)$_2$ for synthesizing three coupling products

Table 5.1. *Screening of the reaction conditions for the coupling of 2,6-bis[bis(4-methylphenyl)methyl]-4-methylaniline and mesityl bromide using* **1.35** *and Pd(dba)₂.[a]*
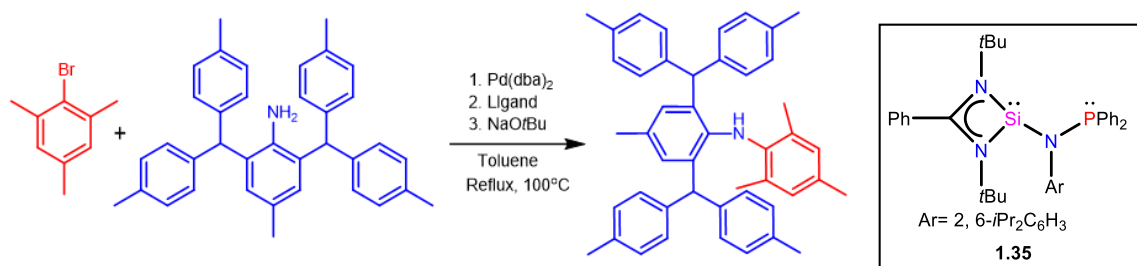
Entry	Mol % Pd(dba)$_2$	Mol % **1.35**	Time (h)	Isolated Yield (%)[b]
1	1	1	12	75
2	1	1	20	90
3	2	2	12	85
4	**2**	**2**	**20**	**> 99**
5[c]	-	5	96	0
6 [d]	5	-	96	10

[a]*Reaction conditions: Aryl amine = 2,6-bis[bis(4-methylphenyl)methyl]-4-methylaniline, (1 equiv.), aryl bromide = mesityl bromide (1 equiv.), Pd(dba)₂/*1.35* system, sodium tert-butoxide (2.8 equiv.). [b] Isolated yields (average of two runs). [c] Blank reaction without Pd source. [d] Blank reaction with only Pd source.*

N-(2,6-bis(di-p-tolylmethyl)-4-methylphenyl)-2,4,6-trimethylaniline (**5.1e**), 2,6-bis(bis(4-(tert-butyl)phenyl)methyl)-N-mesityl-4-methylaniline (**5.1g**), 2,6-bis(bis(4-(tert-butyl)phenyl)methyl)-N-(3,5-bis(trifluoromethyl)phenyl)-4-methylaniline (**5.1p**), summarized in Table 5.2. It was observed that ligand **1.35** (93->99%) proves its better potentiality as a ligand over NHSi (55-63%), PNP (80-92%), DPEphos (80-91%) ligands and reason can be attributed to the presence of two strong donor sites in **1.35**. Alongside, the higher analogues of **1.35,** i.e., GeNP and SnNP gave a considerably lower yield of C-N coupled products (GeNP: 68-74% and SnNP: 54-66%), which is probably due to the weak
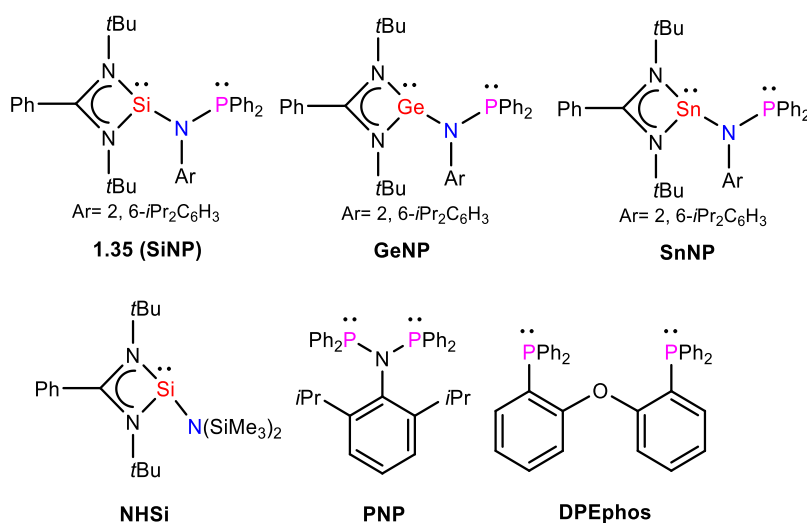
Chart 5.2. *List of selected ligands used to compare catalytic efficiency for coupling reactions.*

Table 5.2. *Screening of various ligands for the coupling products **5.1e**, **5.1g**, and **5.1p**.[a,b]*

1.35 (NHSi) : >99%	
NHSi[c] : 60%	
GeNP[d] : 70%	
SnNP[e] : 63%	
PNP[f] : 87%	
DPEphos[g] : 91%	

1.35 (NHSi) : >99%	
NHSi[c] : 63%	
GeNP[d] : 76%	
SnNP[e] : 61%	
PNP[f] : 92%	
DPEphos[g] : 88%	

1.35 (NHSi) : 93%	
NHSi[c] : 55%	
GeNP[d] : 66%	
SnNP[e] : 56%	
PNP[f] : 80%	
DPEphos[g] : 82%	

[a]*Reaction conditions: Aryl amine = 2,6-bis[bis(4-methylphenyl)methyl]-4-methylaniline, (1 equiv.), aryl bromide = mesityl bromide (1 equiv.), $Pd(dba)_2$/**1.35** (2 mol%)(dba = dibenzylideneacetone), sodium tert-butoxide (2.8 equiv.), reflux for 20h.* [b] *Isolated yields (average of two runs).* [c]*NHSi= [{PhC(NtBu)2}Si{N(SiMe3)2}],* [d]*GeNP= [PhC(NtBu)$_2$GeN(PPh$_2$)(2,6-iPr$_2$-C$_6$H$_3$)],* [e] *SnNP= [PhC(NtBu)$_2$SnN(PPh$_2$)(2,6-iPr$_2$-C$_6$H$_3$)],* [f]*PNP [(Ph$_2$P)$_2$N(2,6-iPr$_2$-C$_6$H$_3$)],* [g]*DPEphos= O[C$_6$H$_4$P(C$_6$H$_5$)$_2$]$_2$.*

σ-donation property of Ge(II) and Sn(II) as compared to Si(II). The above results confirm that **1.35** is dominant over other ligands.

Nowadays, microwave-assisted organic synthesis (MAOS)[31] brings a revolution in catalysis. Normally transition metal-catalyzed homogeneous reactions demanded to prolong reaction time, and the MW irradiation technique accelerated the reaction by producing a high yield very fast than the normal condition. Sometimes it showed higher selectivity as well as decreased the amount of by-products and increased the lifetime of the catalyst.[32,33] In this study we have also optimized C-N cross-coupling reactions under the MW irradiation technique and as expected the reaction is completed very fast with low catalyst loading (1 mol%) than the conventional method. 60 mins are sufficient to complete the reaction using 1 mol% of **1.35** and 1 mol% of Pd(dba)$_2$ in toluene (Table 5.3, entry 2). The **1.35**/Pd(dba)$_2$ system loading of 2 mol% yielded more than 99% within 10-15 minutes (Table 5.3, entry 3). Here also we have done blank tests and the results are similar to the conventional method (Table 5.3, entry 4 and 5).

Table 5.3. *Screening of the microwave-assisted reaction conditions for the coupling of 2,6-bis[bis(4-methylphenyl)methyl]-4-methylaniline and mesityl bromide using* **1.35** *and Pd(dba)$_2$.[a]*

Entry	Mol % Pd(dba)$_2$	Mol % 1.35	Temp (°C)	Time (min)	Isolated Yield (%)[b]
1	1	1	150	30	82
2	1	1	**150**	**60**	**> 99**
3	2	2	150	15	> 99
4[c]	-	5	150	60	0
5 [d]	5	-	150	96	20

[a]*Reaction conditions: Aryl amine = 2,6-bis[bis(4-methylphenyl)methyl]-4-methylaniline, (1 equiv.), aryl bromide = mesityl bromide (1 equiv.), Pd(dba)$_2$/***1.35*** system, sodium tert-butoxide (2.8 equiv.).* [b] *Isolated yields (average of two runs).* [c] *Blank reaction without Pd source.* [d] *Blank reaction with only Pd source.*

Fortunately, ligand **1.35** is found to be highly productive to give a magnificent isolated yield of secondary amines using various primary amines and aryl halide with different

steric and electronic properties. Normally, bulky substituents on the amine as well as aryl halide substrates inhibit the reaction rate which reflects in the catalytic performance of the catalyst to give lower yields. In this study, we gradually increased the steric bulk at the ortho position of the aryl ring of primary amines from $CHMe_2$ to $CHPh_2$ to $CH(C_6H_5Me)_2$ to $CH(C_6H_5tBu)_2$, and results of the coupled products are summarized in Table 5.4. Ligand **1.35**/Pd(dba)$_2$ system was executed as the outstanding catalyst for a series of extremely sterically hindered primary amines with electron donating bulky aryl bromide to give the coupling products **5.1a**–**5.1h** (85% – >99%) (Table 5.4a). Notably, **5.1c** and **5.1d** were found to give excellent product conversion (85% and >99%, respectively) compared to the previous reports by Jones and co-workers (78% and 70% respectively) using [(IPr)Pd(Im)] catalyst.[25e,f] Subsequently, we have examined **1.35**-Pd(dba)$_2$ for electron-withdrawing fluoride and -CF_3 substituted aryl bromides with bulky primary amines which afforded excellent yields of coupled products **5.1i**-**5.1p** (95%-98%) (Table 5.4b). Phosphines like PNP gave poor yield (70%)[29] for **5.1i** as

---

Table 5.4. *Substrate scope of Pd(dba)$_2$/**1.35** Catalyzed amination reactions of sterically bulky primary amines with electron-donating and electron-withdrawing aryl bromides.*[a,b]

a) Scope of Electron donating aryl bromides:

5.1a (90%)   **5.1b** (86%)   **5.1c** (85%)   **5.1d** (>99%)

5.1e (>99%)   **5.1f** (96%)   **5.1g** (>99%)   **5.1h** (98%)
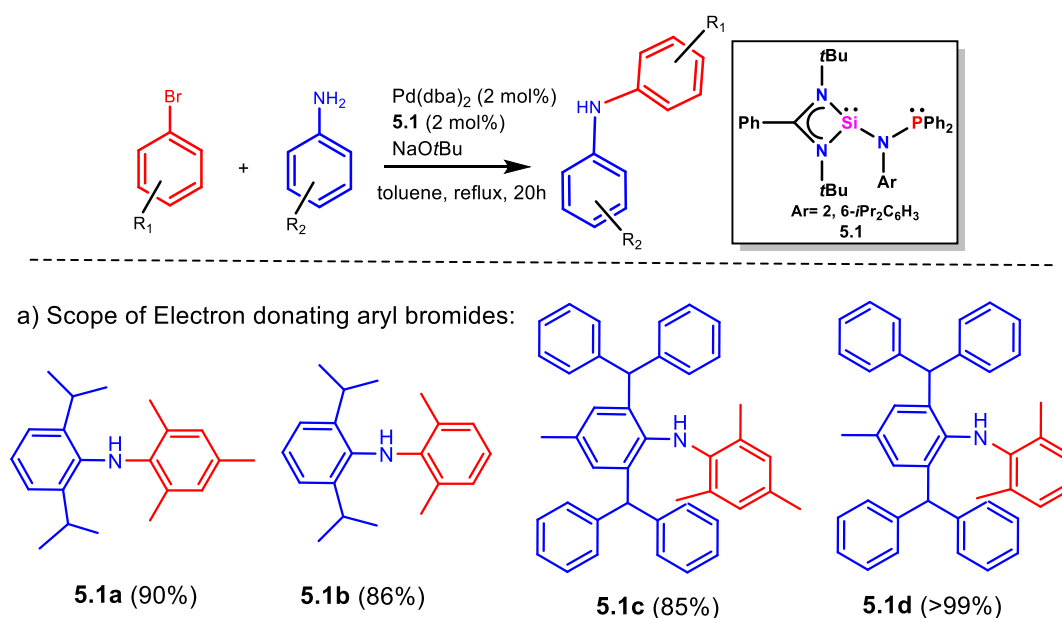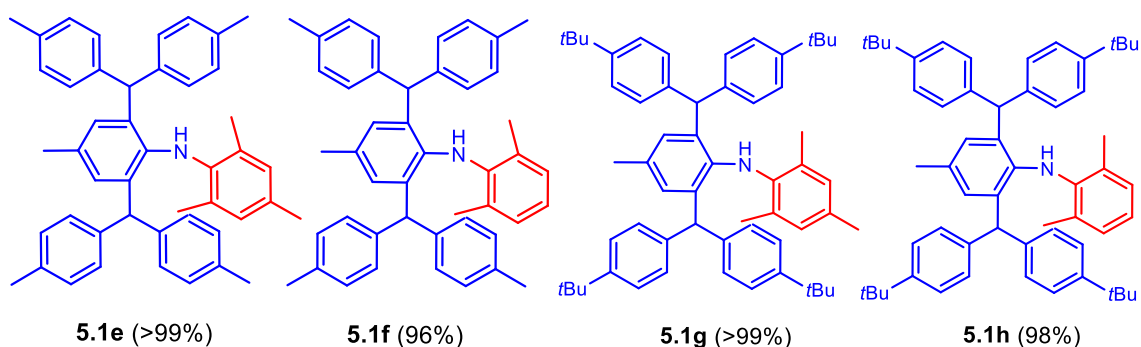
b) Scope of Electron withdrawing aryl bromides:

5.1i (96%)   **5.1j** (97%)   **5.1k** (98%)   **5.1l** (95%)

5.1m (96%)   **5.1n** (95%)   **5.1o** (80%)   **5.1p** (97%)
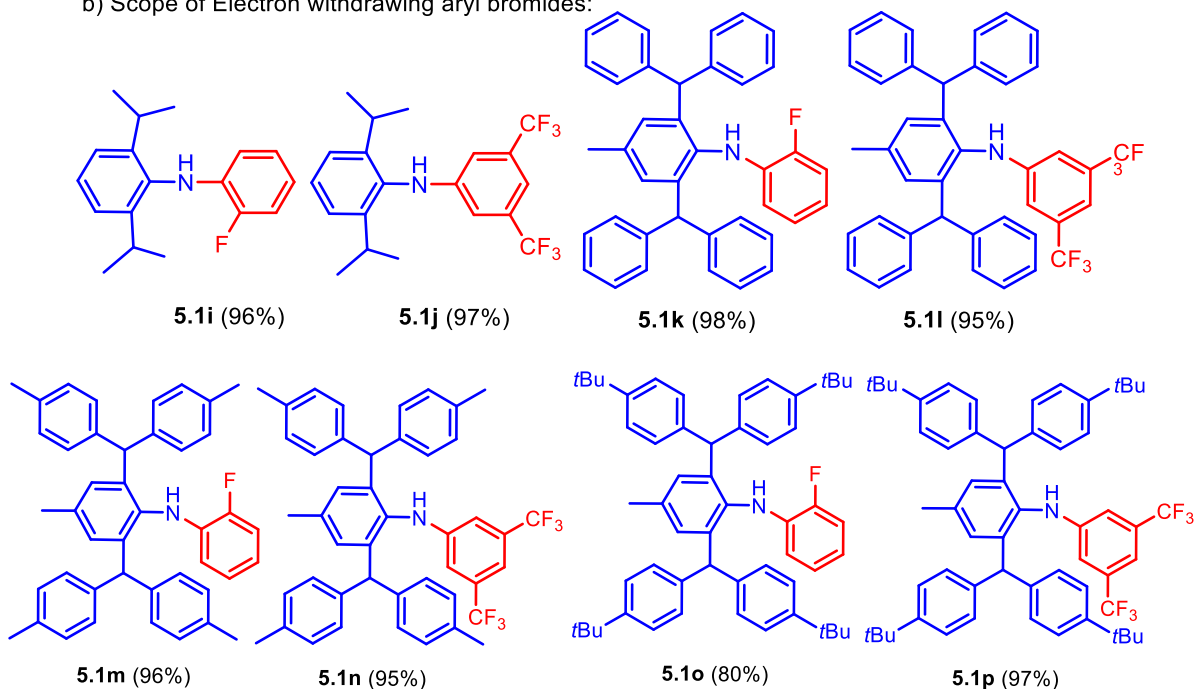
*[a]Reaction conditions: Aryl amine (1 equiv.), aryl bromide (1 equiv.), Pd(dba)$_2$ (2 mol %), ligand **1** (2 mol %), sodium tert-butoxide (2.8 equiv.),* toluene, *reflux at 100°C, 20 h. [b]Isolated yields (average of two runs).*

---

compared to **1.35**-Pd(dba)$_2$ system (96%). Similarly, the formation of the amination products containing bulky aryl group as well as electron-withdrawing aryl group with -CF$_3$ substituent is very challenging. The previous report of Jones and co-workers proved it by observing only 32% yield of **5.1l** using IPr carbene ligand,[25e] whereas, our ligand **1.35** with Pd salt efficiently yielded 95% for the same. Few coupling products are also confirmed by single-crystal X-ray studies (Figure 5.1).
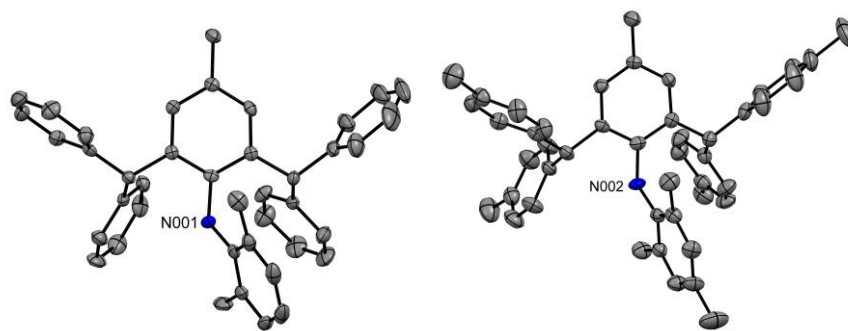
Figure 5.1. *Molecular structure of 2,6-dibenzhydryl-N-(2,6-dimethylphenyl)-4-methylaniline (**5.1d**) (left) and N-(2,6-bis(di-p-tolylmethyl)-4-methylphenyl)-2,4,6-trimethylaniline (**5.1e**) (right) with anisotropic displacement parameters depicted at the 50% probability level. Hydrogen atoms are not shown for clarity.*

5.4. Theoretical Calculations

We have evaluated energetics for the Pd-catalyzed N-arylation of amine reaction using the Gaussian09.[34] The newly designed bidentate ligand (L) coordinated to Pd without any modification was employed in the calculation. Geometry optimizations were carried out in the gas phase using the B3LYP functional with the LANL2DZ effective core potential and the associated double-ζ basis set for Pd and the 6-31G* basis set for all other atoms (B3LYP-I level). Single-point energies were calculated, in which the 6-31G* basis was replaced by the larger 6-311+G**(B3LYP-II level). The LANL2DZ basis set for Pd was used in calculations whenever it was applicable. The reported free energies were obtained from the B3LYP-II energies by adding thermal and entropic corrections (B3LYP-I level) as well as dispersion and continuum solvation corrections. The catalytic cycle involves three key steps: (a) oxidative addition, (b) transmetalation, and (c) reductive elimination, was investigated. The energy profile diagram is shown in Figure 5.2. The overall reaction is found to be highly exoergic (about 40 kcal/mol). In the first step, the oxidative addition of aryl halide to Pd-L (**I**) occurs via **TS-1**. This step is found to be exoergic by 41.1 kcal/mol and requires a marginal activation barrier of 2.0 kcal/mol. The subsequent dissociative transmetalation step involves halide ion exchange with tert-butoxide of base followed by deprotonation and coordination of aryl amine to Pd complex (**III**). The transmetalation step is endoergic by 5 kcal/mol. In the final step, reductive elimination occurs via **TS-2** to furnish N-arylated amine. The activation barrier for the reductive
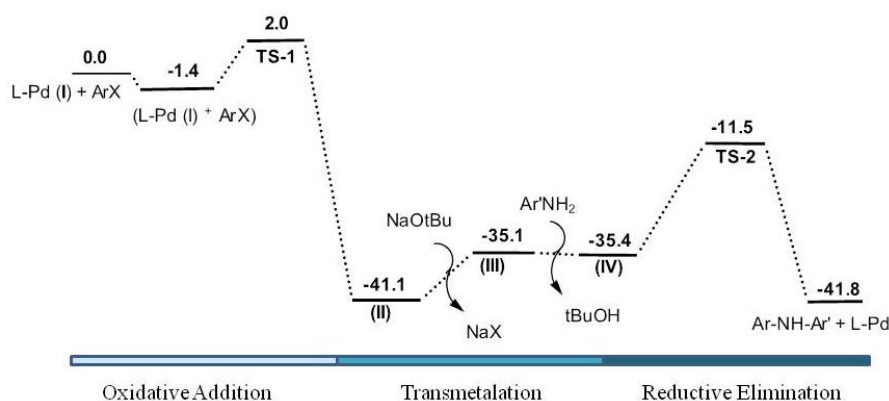
Figure 5.2. *Reaction Profile diagram for the Pd-L(**I**) -catalyzed N-arylation of aniline.*

elimination step is 24.0 kcal/mol, which is likely to be the rate-limiting step for this reaction. After establishing energetics for the reaction mechanism, we have analyzed the donor-acceptor properties of newly designed ligand (L) in Pd-L (**I**) complex using natural bond orbital (NBO) analysis. The Pd····Si and Pd····P distances in Pd-L are 2.31 and 2.36 Å, respectively. Although the Pd····Si and Pd····P distances in Pd-L are in comparable range, the calculated bond order (BO) for the Pd····Si (BO: 0.65) is slightly higher than that of Pd····P (BO: 0.42) suggesting relatively stronger interaction between Pd····Si as compared to Pd····P (Table 5.5). The delocalization energies obtained from the NBO analysis also corroborates the strong interaction between Pd and Si in Pd–L (**I**) complex. The cumulative delocalization energies for $n(\text{Si}) \rightarrow d(\text{Pd})$ and $n(\text{P}) \rightarrow d(\text{Pd})$ donation are 122 and 77 kcal/mol, respectively. The HOMO of Pd-L (**I**) exhibiting the Pd····Si and Pd····P bonding interactions is shown in Figure 5.3. The difference in the interaction between Pd····Si and Pd····P is more distinct in the Pd complexes **II**, **III,** and **IV** as well as in the transition states **TS-1** and **TS-2**. The Pd····Si and Pd····P bond distances and corresponding bond order in Pd-complexes and transition state provided in the Supplementary Information. In all, our calculations show that interaction between Pd····Si is noticeably higher than Pd····P in Pd-L complexes and could be a major factor responsible for the stabilization of Pd species in the catalytic cycle.

Table 5.5. *Selected bond distances (in Å) and bond order of Pd complexes and transition states.*

Pd complexes	Pd⋯Si Distances	Bond Order	Pd⋯P Distances	Bond Order
I	2.31	0.65	2.36	0.42
TS-1	2.30	0.61	2.54	0.28
II	2.30	0.69	2.43	0.44
III	2.30	0.65	2.49	0.35
IV	2.36	0.62	2.47	0.36
TS-2	2.33	0.63	3.07	0.14
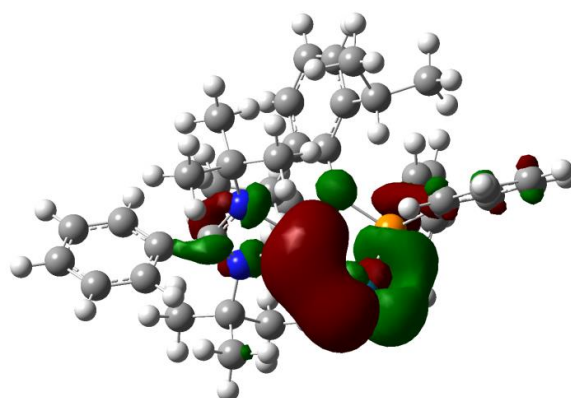
Figure 5.3. *HOMO of Pd-L (I) showing Pd⋯Si (Red) and Pd⋯P (green) interactions.*

5.5. Conclusion

In summary, we have thoroughly investigated the use of **1.35**/Pd(dba)$_2$ system in Buchwald-Hartwig amination reactions. The C-N cross-coupling reactions of the extremely sterically bulky primary anilines with electron-donating and electron-withdrawing bulky aryl bromides are very challenging and our ligand **1.35** with Pd(dba)$_2$ imparts outstanding performance (~90-99%), even better than many reported phosphines and carbenes. The remarkable potential of the **1.35** may be elucidated due to the presence of two strong donor sites, Si(II) and P(III). The theoretical calculation also revealed that the strong Si-Pd bond plays a key role in the catalytic process.

5.6.   References

1. For selected reviews, see: (a) Hartwig, J. F. *Angew. Chem. Int. Ed.* **1998**, *37*, 2046 – 2067. (b) Yang, B. H.; Buchwald, S. L. *J. Organomet. Chem.* **1999**, 576, 125 – 146. (c) Lundgren, R. J.; Stradiotto, M. *Chem. Eur. J.* **2012**, *18*, 9758 – 9769. (d) Surry, D. S.; Buchwald, S. L. *Chem. Sci.* **2011**, *2*, 27 – 50. (e) Wolfe, J. P.; Wagaw, S.; Marcoux, J.-F.; Buchwald, S. L. *Acc. Chem. Res.* **1998**, *31*, 805 – 818. (f) Palladium- Catalyzed Amination of Aryl Halides and Related Reactions: Hartwig, J. F. Handbook of Organopalladium Chemistry for Organic Synthesis, *Wiley-Interscience*, *New York*, **2003**. (g) Heravi, M. M.; Kheilkordi, Z.; Zadsirjan, V.; Haydari, M.; Malmir, M. *J. Organomet. Chem.* **2018**, *861*, 17 – 104.

2. (a) Ruiz-Castillo, P.; Buchwald, S. L. *Chem. Rev.* **2016**, *116*, 12564 – 12649. (b) Buchwald, S. L.; Mauger, C.; Mignani, G.; Scholz, U. *Adv. Synth. Catal.* **2006**, *348*, 23 – 39. (c) Torborg, C.; Beller, M. *Adv. Synth. Catal.* **2009**, *351*, 3027 – 3043. (d) Schlummer, B.; Scholz, U. *Adv. Synth. Catal.* **2004**, *346*, 1599 –1626. (e) Corbet, J.-P.; Mignani, G. *Chem. Rev.* **2006**, *106*, 2651 – 2710. (f) Dorel, R.; Grugel, C. P.; Haydl, A. M. *Angew. Chem. Int. Ed.* **2019**, *58*, 2–14.

3. Goldberg, I. *Chem. Ber.* **1906**, *39*, 1691 – 1692.

4. Ullmann, F. *Chem. Ber.* **1903**, *36*, 2382 – 2384.

5. Kosugi, M.; Kameyama, M.; Migita, T. *Chem. Lett.* **1983**, *12*, 927 – 928.

6. (a) Guram, A. S.; Buchwald, S. L. *J. Am. Chem. Soc.* **1994**, *116*, 7901 – 7902. (b) Paul, F.; Patt, J.; Hartwig, J. F. *J. Am. Chem. Soc.* **1994**, *116*, 5969 – 5970. (c) Louie, J.; Hartwig, J. F. *Tetrahedron Lett.* **1995**, *36*, 3609 –3612. (d) Guram, A. S.; Rennels, R. A.; Buchwald, S. L. *Angew. Chem. Int. Ed. Engl.* **1995**, *34*, 1348 – 1350; *Angew. Chem.* **1995**, *107*, 1456 – 1459.

7. (a) Díez-González, S.; Marion, N.; Nolan, S. P. *Chem. Rev.* **2009**, *109*, 3612–3676. (b) Fortman, G. C.; Nolan, S. P. *Chem. Soc. Rev.* **2011**, *40*, 5151–5169. (c) Kantchev, E. A. B.; O'Brien, C. J.; Organ, M. G. *Angew. Chem., Int. Ed.* **2007**, *46*, 2768–2813.

8. Wolfe, J. P.; Wagaw, S.; Marcoux, J.-F.; Buchwald, S. L. *Acc. Chem. Res.* **1998**, *31* (12), 805–818.

9. Wolfe, J. P.; Buchwald, S. L. *J. Org. Chem*. **2000**, *65*, 1144–1157.

10. Mann, G.; Hartwig, J. F.; Driver, M. S.; Fernández-Rivas, C. *J. Am. Chem. Soc.* **1998**, *120*, 827–828.

11. Yin, J.; Buchwald, S. L. *Org. Lett.* **2000**, *2*, 1101–1104. (b) Artamkina, G. A.; Sergeev, A. G.; Beletskaya, I. P. *Tetrahedron Lett.* **2001**, *42*, 4381–4384.

12. Hartwig, J. F. *Acc. Chem. Res.* **2008**, *41*, 1534–1544.

13. Crawford, S. M.; Lavery, C. B.; Stradiotto, M. *Chem. - Eur. J.* **2013**, *19*, 16760–16771.

14. Tardiff, B. J.; McDonald, R.; Ferguson, M. J.; Stradiotto, M. *J. Org. Chem.* **2012**, *77*, 1056–1071.

15. Marion, N.; Ecarnot, E. C.; Navarro, O.; Amoroso, D.; Bell, A.; Nolan, S. P. *J. Org. Chem.* **2006**, *71*, 3816–3821. (b) Fortman G. C.; S. P. Nolan, *Chem. Soc. Rev.*, **2011**, *40*, 5151–5169. (c) Li, Y.-J.; Zhang, J.-L.; Li, X.-J.; Geng, Y.; Xu, X.-H.; Jin, Z. *J. Org. Chem.*, **2013**, *737*, 12–20.

16. Benedek, Z.; Szilvási, T. *RSC Adv.* **2015**, *5*, 5077–5086.

17. Meltzer, A.; Inoue, S.; Präsang, C.; Driess, M. *J. Am. Chem. Soc.* **2010**, *132*, 3038–3046.

18. Schmid, G.; Welz, E. *Angew. Chem.*, **1977**, *89*, 823; *Angew. Chem., Int. Ed. Engl.,* **1977**, *16*, 785.

19. (a) Raoufmoghaddam, S.; Zhou, Y. –P.; Wang, Y.; Driess, M. *J. Organomet. Chem.* **2017**, *829*, 2-10. (b) Blom, B.; Gallego, D.; Driess, M. *Inorg. Chem. Front.,* **2014**, *1*, 134–148. (c) Zhou, Y.-P.; Driess, M. *Angew. Chem. Int. Ed.* **2019**, *58*, 3715 – 3728.

20. (a) Fürstner, A.; Krause, H.; Lehmann, C. W. *Chem. Commun.,* **2001**, 2372-2373. (b) Zhang, M.; Liu, X.; Shi, C.; Ren, C.; Ding, Y.; Roesky, H. W. *Z. Anorg. Allg. Chem.* **2008**, *634*, 1755-1758. (c) Wang, W.; Inoue, S.; Enthaler, S.; Driess, M. *Angew. Chem., Int. Ed.* **2012**, *51*, 6167-6171. (d) Brűck, A.; Gallego, D.; Wang, W.; Irran, E.; Driess, M.; Hartwig, J. F. *Angew. Chem., Int. Ed.* **2012**, *51*, 11478 –11482. (e) Gallego, D.; Brück, A.; Irran, E.; Meier, F.; Kaupp, M.; Driess, M.; Hartwig, J. F. *J. Am. Chem. Soc.* **2013**, *135*, 15617-15626. (f) Blom, B.; Enthaler, S.; Inoue, S.; Irran, E.; Driess, M. *J. Am. Chem. Soc.* **2013**, *135*, 6703-6713. (g) Metsänen, T. T.; Gallego, D.; Szilvási, T.; Driess, M.; Oestreich, M. *Chem. Sci.* **2015**, *6*, 7143-7149. (h) Gallego, D.; Inoue, S.; Blom, B.; Driess, M. *Organometallics* **2014**, *33*, 6885–6897. (i) Stoelzel, M.; Praesang, C.; Blom, B.; Driess, M. *Aust. J. Chem.* **2013**, *66*, 1163-1170. (j) Tan, G.; Enthaler, S.; Inoue, S.; Blom, B.; Driess, M. *Angew. Chem., Int. Ed*. **2015**, *54*, 2214 –2218. (k) Zhou, Y.-P.; Raoufmoghaddam, S.; Szilvási, T.; Driess, M. *Angew. Chem., Int. Ed.* **2016**, *55*, 12868 – 12872.

21. (a) Parvin, N.; Pal, S.; Echeverría, J.; Alvarez, S.; Khan, S. *Chem. Sci.* **2018**, *9*, 4333-4337. (b) Parvin, N.; Hossain, J.; George, A.; Parameswaran, P.; Khan, S. *Chem. Commun.*,

2020, *56*, 273–276. (c) Parvin, N.; Mishra, B.; George, A.; Neralkar, M.; Hossain, J.; Parameswaran, P.; Hotha, S.; Khan, S. *Chem. Commun.*, **2020**, *56*, 7625-7628.

22. Khan, S.; Ahirwar, S. K.; Pal, S.; Parvin, N.; Kathewad, N. *Organometallics* **2015**, *34*, 5401-5406.

23. Khan, S.; Pal, S.; Kathewad, N.; Purushothaman, I.; Deb, S.; Parameswaran, P. *Chem. Commun.* **2016**, *52*, 3880-3882.

24. Castillo, P. R.; Blackmond, D. G.; Buchwald, S. L. *J. Am. Chem. Soc.,* **2015**, *137*, 3085–3092.

25. (a) Rodriguez, S.; Qu, B.; Haddad, N.; Reeves, D. C.; Tang, W.; Lee, H.; Krishnamurthy, D.; Senanayake, C. H. *Adv. Synth. Catal.*, **2011**, *353*, 533–537. (b) Hill, L. L.; Moore, L. R.; Huang, R.; Craciun, R.; Vincent, A. J.; Dixon, D. A.; Chou, J.; Woltermann, C. J.; Shaughnessy, K. H. *J. Org. Chem.,* **2006**, *71*, 5117–5125. (c) Raders, S. M.; Moore, J. N.; Parks, J. K.; Miller, A. D.; Leißing, T. M.; Kelley, S. P.; Rogers, R. D.; Shaughnessy, K. H. *J. Org. Chem.,* **2013**, *78*, 4649–4664. (d) Hadlington, T. J.; Li, J.; Jones, C.; *Can. J. Chem.,* **2014**, *92*, 427–433. (e) Hicks, J.; Hadlington, T. J.; Schenk, C.; Li, J.; Jones, C. *Organometallics* **2013**, *32*, 323–329

26. (a) Berthon-Gelloz, G.; Siegler, M. A.; Spek, A. L.; Tinant, B.; Reek, J. N. H.; Marko, I. E. *Dalton Trans.,* **2010,** *39*, 1444–1446. (b)Weber, S. G.; Loos, C.; Rominger, F.; Straub, B. F. *doi: http://dx.doi.org/10.3998/ark.5550190.0013.317.*

27. Clavier, H.; Nolan, S. P. *Chem. Commun.*, **2010**, *46*, 841–861.

28. Sen, S. S.; Hey, J.; Herbst-Irmer, R.; Roesky, H. W.; Stalke, D. *J. Am. Chem. Soc* **2011**, *133*, 12311–12316.

29. Parvin, N.; Pal, S.; Rojisha, V. C.; De, S.; Parameswaran, P.; Khan, S. *Chemistry Select*, **2016** ,*1*, 1991–1995.

30. Kathewad, N.; Anagha M.C., Parvin, N.; Parambath, S.; Parameswaran, P.; Khan, S. *Dalton Transactions*, **2019**, *48*, 2730-2734.

31. For some recent reviews on microwave-assisted reactions, see: a) Caddick, S. *Tetrahedron* **1995**, *51*, 10403–10432. b) Lidström, P.; Tierney, J. P.; Wathey, B.; Westman, J. *Tetrahedron* **2001**, *57*, 9225. c) Lew, A.; Krutzik, P. O.; Hart, M. E.; Chamberlain, A. R. *J. Comb. Chem.* **2002**, *4*, 95–105. d) Loupy, A. *Microwaves in Organic Synthesis*, Wiley-VCH, Weinheim, **2002**. e) Hayes, B. L. *Microwave Synthesis: Chemistry at the Speed of Light*, CEM Publishing, Matthews, NC, **2002**. f) Blackwell, H. E. *Org. Biomol. Chem.* **2003**, *1*, 1251. g) Adam, D. *Nature* **2003**, *421*, 571–572. h) Kappe, C. O.;

Stadler, A. *Microwaves in Organic and Medicinal Chemistry*, Wiley-VCH, Weinheim, **2005**. i) Appukkuttan, P.; Eycken, E. V. der *Top. Curr. Chem.* **2006**, *266*, 1–44. j) Loupy A. *Microwaves in Organic Synthesis*, 2nd ed., Wiley-VCH, Weinheim, **2006**. k) Kappe, C. O.; Dallinger, D. *Nat. Rev. Drug Discov.* **2006**, *5*, 51c. m) Ravichandran, S.; Karthikeyan, E. *Int. J. ChemTech Res.* **2011**, *3*, 466-470.

32. a) Loupy, A.; Petit, A.; Hamelin, J.; Texier, B. F.; Jacquault, P.; Mathe, D. *Synthesis* **1998**, *5*, 1213–1234. b) Larhed, M.; Moberg, C.; Hallberg, A. *Acc. Chem. Res.* **2002**, *35*, 717-727. c) Kappe, C. O. *Curr. Opin. Chem. Biol.* **2002**, *6*, 314–320. d) Hayes, B. L. *Aldrichimica Acta* **2004**, *37*, 66. e) Nilsson, P.; Olofsson, K.; Larhed, M. *Top. Curr. Chem.* **2006**, *266*, 103–144. f) Appukkuttan, P.; Eycken, E. V. der *Eur. J. Org. Chem.* **2008**, 1133–1155. g) Hajipour, A. R.; Rafiee, F. *J. Iran. Chem. Soc* **2015**, *12*, 1163–1169.

33. Kappe, C. O. *Angew. Chem., Int. Ed.* **2004**, *43*, 6250.

34. M. J. Frisch. et al. *GAUSSIAN 09 (Revision B.01)* Gaussian, Inc. Wallingford CT, **2009**.

*****

Summary

In the overall conclusion, I can state that the fundamental objective of my doctoral research was to introduce transition metals especially coinage metals (Cu and Au) and Pd in silylene chemistry in a better perspective and to explore their remarkable catalytic applications in homogeneous catalysis. Alongside, stabilization of elusive double bonded compound between Si and E (E= O, S, and Se) atom is another challenging part. Owing to have a lone pair of electrons at the E centre, they tend to undergo complexation reaction with Lewis acids of composition Si=E→LA (E=O, S, and Se). Particularly for O atom, we stabilized Si/Ge=O moiety via Lewis acid-base adduct formation. Hence we have isolated and characterized a series of Si=E→LA complexes **2.4**-**2.7**, **3.3** and **3.4**. The thesis deals with the design, systhesis, and thorough experimental investigations of a number of nearly naked Si(II)-coinage metal (Cu(I) and Au(I)) cationic complexes where the Cu(I) and Au(I) centres are weakly bound with arene ring such as benzene, hexamethyl benzene, toluene, and *m*-xylene. In this context, it is important to mention that we have successfully isolated and characterized the first elusive $[Cu(\eta^6-C_6H_6)]^+$ moiety stabilized by silylene, which is otherwise only been observed in the gas phase. The synthetic difficulties to isolate weakly bound Cu(I)/Au(I)-free arene constitutes a major thrust for the catalysis reaction by easy substitution of an arene with the substrates. Hence, we employed the above mentioned Si(II) supported Cu(I)/Au(I)-arene cationic complexes as catalysts in click reaction and in glycosidation reaction, respectively. Low catalyst loading with less reaction time is the important feature of Si(II)-Cu(I)-toluene catalyst to synthesize triazoles for a series of azides and alkynes. Conversely, well-defined [Au-arene]$^+$ complexes using N-heterocyclic silylene, germylene, and carbene as a σ-donor ligand were probed first time for disaccharide synthesis and observed the superiority of Si(II)-Au(I) catalyst over Au(III) salt, even better than NHC- and phosphite-Au(I) complexes for the activation of propargyl 1,2-orthoester donors. Further isolation of branched pentamer which is the core of the HIV-gp120 envelope is the practical aspect of newly developed cationic Au(I) catalysts. Eventually, we examined the potential application of a modified bidentate ligand (SiNP) bearing Si(II) and P(III) coordination site with Pd(dba)$_2$ salt for Buchwald-Hartwig amination reactions for a series of extremely bulky primary anilines with electron-donating and withdrawing bulky aryl

bromide by the conventional method as well as under the microwave technique (10-15 min) and found outstanding catalytic performance (~90-99%). Amination reaction of such bulky class of substrates are scarce.

Hence, the study related to coordination and catalytic application of NHSi-TM complexes is still in the early stage and 'miles to go' before it reaches to mankind.
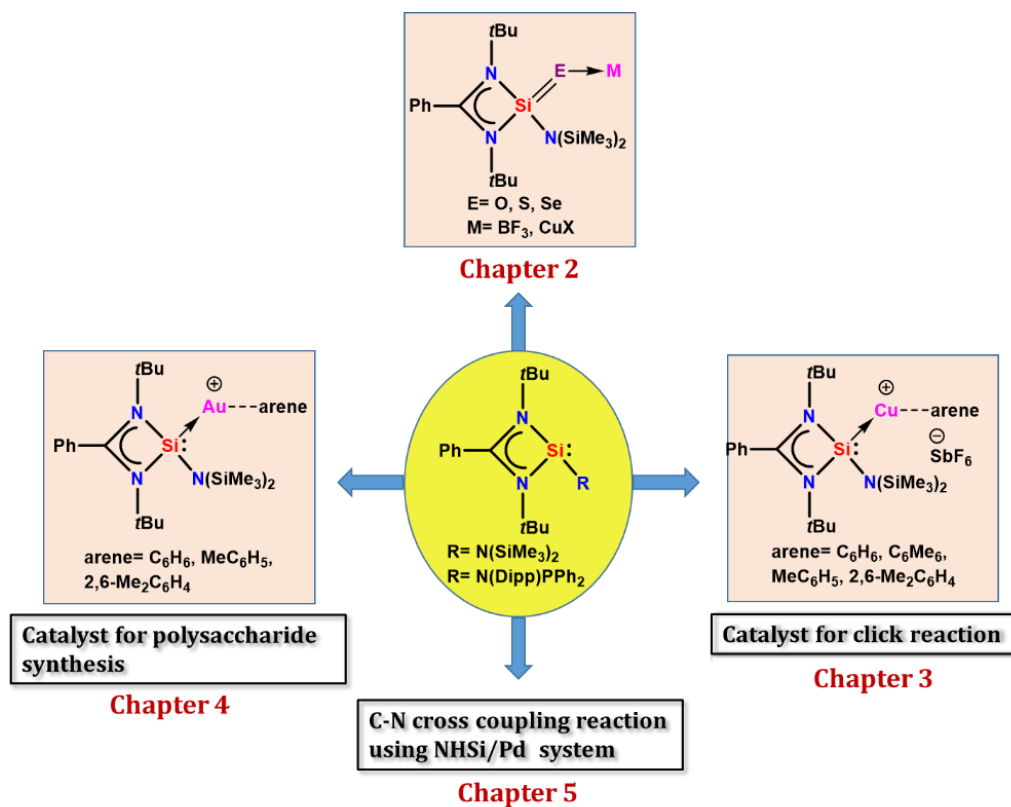
Schematic representation of my doctoral research

*****

Appendix

Appendix of Chapter 2A

Table 2A.A.1. *Crystallographic details for **2A.2, 2A.3, 2A.4** and **2A.5**.*

	2A.2	2A.3	2A.4	2A.5
Chemical formula	$C_{21}H_{41}N_3Si_3S$	$C_{21}H_{41}N_3Si_3Se$	$C_{21}H_{41}N_3Si_3SCuCl$	$C_{21}H_{41}N_3Si_3SCuBr$
Formula weight	451.90 g/mol	498.80 g/mol	550.89 g/mol	595.35 g/mol
Temperature	100(2) K	100(2) K	100(2) K	100(2) K
Wavelength	0.71073 Å	0.71073 Å	0.71073 Å	0.71073 Å
Crystal system	monoclinic	triclinic	orthorhombic	monoclinic
Space group	*P2₁/c*	*P -1*	*Pbca*	*P2₁/c*
Unit cell dimentions	a = 18.757(5) Å	a = 13.8646(18) Å	a = 17.7574(18) Å	a = 19.1905(6) Å
	b = 8.662(2) Å	b = 13.9873(17) Å	b = 16.0785(17) Å	b = 9.1326(3) Å
	c = 17.853(5) Å	c = 13.9873(17) Å	c = 19.521(2) Å	c = 18.2543(6) Å
	α = 90°	α = 89.90°	α = 90°	α = 90°
	β = 114.688(7)°	β = 81.020(2)°	β = 90°	β = 92.758(2) °
	γ = 90°	γ = 81.020(2)°	γ = 90°	γ = 90°
Volume	2635.3(12) Å³	2645.7(6) Å³	5573.4(10) Å³	3195.53(18) Å³
Z	4	4	8	4
Density	1.139 g/cm³	1.252 g/cm³	1.313 g/cm³	1.237 g/cm³
Absorption coefficient	0.271 mm⁻¹	1.567 mm⁻¹	1.097 mm⁻¹	2.124 mm⁻¹
F(000)	984	1056	2336	1240
Theta range for data collection	2.286 to 25.250°	2.27 to 28.20°	2.294 to 25.248°	2.234 to 25.242°
Index ranges	-22<=h<=22	-16<=h<=16	-20<=h<=21	-23<=h<=23
	-10<=k<=9	-16<=k<=16	-19<=k<=14	-10<=k<=10
	-21<=l<=21	-16<=l<=16	-23<=l<=21	-21<=l<=2

Reflections collected	28503	61047	39019	123182
Independent reflections	4783 [R(int) = 0.2260]	9576 [R(int)= 0.0744]	5043 [R(int)= 0.2298]	5768 [R(int) = 0.0617]
Coverage of independent reflections	100%	99%	99%	100%
Data/ restraints/ parameters	4783/ 0/ 265	9576/ 0/ 529	5043/ 18/ 283	5768/ 0/ 283
Goodness-of-fit on F2	1.050	1.016	1.064	1.031
Δ/ σ max	0.000	0.001	0.000	0.013
Final R indices	2529 data; [$I>2\sigma(I)$] R_1 = 0.0867, wR_2 = 0.1166	7122 data; [$I>2\sigma(I)$] R_1 = 0.0377, wR_2 = 0.0667	2656 data; [$I>2\sigma(I)$] R_1 = 0.0744, wR_2 = 0.1019	5341 data; [$I>2\sigma(I)$] R_1 = 0.0357, wR_2 = 0.0690
	all data, R_1 = 0.1941, wR_2 = 0.1486	all data, R_1 = 0.0670, wR_2 = 0.0755	all data, R_1 = 0.1813, wR_2 = 0.1281	all data, R_1 = 0.0425, wR_2 = 0.0718
Largest diff. peak and hole	0.554 and -0.450 eÅ^{-3}	0.368 and -0.330 eÅ^{-3}	0.842 and -0.619 eÅ^{-3}	1.255 and -0.388 eÅ^{-3}
R. M. S deviation from mean	0.102 eÅ^{-3}	0.075 eÅ^{-3}	0.114 eÅ^{-3}	0.061 eÅ^{-3}

Table 2A.A.2. *Crystallographic details for **2A.6, 2A.7, 2A.8** and **2A.9**.*

	2A.6	2A.7	2A.8	2A.9
Chemical formula	$C_{21}H_{41}N_3Si_3SeCuCl$	$C_{21}H_{41}N_3Si_3SeCuBr$	$C_{49}H_{90}Cl_2Cu_2N_6Si_6$	$C_{49}H_{89}Br_2Cu_2N_6Si_6$
Formula weight	597.79 g/mol	642.25 g/mol	1129.78 g/mol	1217.70 g/mol

Temperature	100(2) K	100(2) K	100(2) K	100(2) K
Wavelength	0.71073 Å	0.71073 Å	0.71073 Å	0.71073 Å
Crystal system	orthorhombic	orthorhombic	triclinic	triclinic
Space group	*Pbca*	*Pbca*	*P-1*	*P-1*
Unit cell dimentions	a = 17.993(2) Å	a = 18.1256(19) Å	a = 11.0995(16) Å	a = 11.0391(10) Å
	b = 15.7923(16) Å	b = 15.6375(16) Å	b = 16.235(2) Å	b = 16.2036(16) Å
	c = 19.676(2) Å	c = 19.893(2) Å	c = 17.997(3) Å	c = 18.0379(16) Å
	α = 90°	α = 90°	α = 84.770(4)°	α = 85.486(2)°
	β = 90°	β = 90°	β = 72.241(4)°	β = 72.999(2) °
	γ = 90°	γ = 90°	γ = 74.247(4)°	γ = 75.928(2)°
Volume	5590.9(10) Å^3	5638.4(10) Å^3	2972.4(8) Å^3	2992.8(5) Å^3
Z	8	8	2	2
Density	1.420 g/cm^3	1.513 g/cm^3	1.262 g/cm^3	1.351 g/cm^3
Absorption coefficient	2.321 mm^{-1}	3.624 mm^{-1}	0.963 mm^{-1}	2.202 mm^{-1}
F(000)	2480	2624	1204	1274
Theta range for data collection	2.264 to 25.243°	2.247 to 25.250°	2.377 to 25.249°	2.114 to 25.250°
Index ranges	-21<=h<=21 -18<=k<=18 -23<=l<=23	-21<=h<=21 -18<=k<=18 -23<=l<=23	-13<=h<=13 -19<=k<=19 -21<=l<=21	-13<=h<=13 -19<=k<=19 -21<=l<=21
Reflections collected	74361	128051	59699	64740
Independent reflections	5056 [R(int) = 0.0902]	5105 [R(int) = 0.1942]	10781 [R(int)= 0.1502]	10828 [R(int) = 0.1600]
Coverage of independent reflections	100%	100%	99.9%	99.9%
Data/ restraints/ parameters	5056/ 0/ 283	5105/ 6/ 283	10781/ 6/ 611	10828/ 18/ 610

Nasrina Parvin

Goodness-of-fit on F2	1.050	1.349	1.171	1.061
Δ/ σ max	0.001	0.001	0.002	0.001
Final R indices	3951 data; $[I>2\sigma(I)]$ R_1 = 0.0322, wR_2 = 0.0567	4019 data; $[I>2\sigma(I)]$ R_1 = 0.0793, wR_2 = 0.1042	6422 data; $[I>2\sigma(I)]$ R_1 = 0.0543, wR_2 = 0.0857	6450 data; $[I>2\sigma(I)]$ R_1 = 0.0650, wR_2 = 0.1310
	all data, R_1 = 0.0556, wR_2 = 0.0638	all data, R_1 = 0.1116, wR_2 = 0.1137	all data, R_1 = 0.1263, wR_2 = 0.0996	all data, R_1 = 0.1368, wR_2 = 0.1546
Largest diff. peak and hole	0.399 and -0.358 e$Å^{-3}$	0.732 and -0.599 e$Å^{-3}$	0.586 and -0.575 e$Å^{-3}$	1.843 and -0.766 e$Å^{-3}$
R. M. S deviation from mean	0.080 e$Å^{-3}$	0.162 e$Å^{-3}$	0.099 e$Å^{-3}$	0.135 e$Å^{-3}$

Table 2A.A.3. *Crystallographic details for* **2A.11, 2A.13** *and* **2A.14.**

	2B.11	2B.13	2B.14
Chemical formula	$C_{83} H_{64} N_2 S$	$C_{76} H_{64} N_2 S\ Br\ Cu$	$C_{76} H_{64} N_2 Se\ Br\ Cu$
Formula weight	1037.35 g/mol	1180.80 g/mol	1227.70 g/mol
Temperature	100(2) K	100(2) K	100(2) K
Wavelength	0.71073 Å	0.71073 Å	0.71073 Å
Crystal system	triclinic	monoclinic	monoclinic
Space group	P -1	$P2_1/c$	$P2_1/c$
Unit cell dimentions	a = 12.601(6) Å	a = 20.9505(9) Å	a = 21.191(12) Å
	b = 15.542(7) Å	b = 12.6441(6) Å	b = 12.807(7) Å
	c = 16.027(7) Å	c = 24.9325(10) Å	c = 25.044(14) Å

Nasrina Parvin

	$\alpha = 74.564(10)°$	$\alpha = 90°$	$\alpha = 90°$
	$\beta = 70.050(10)°$	$\beta = 99.889(3)°$	$\beta = 99.715(10)°$
	$\gamma = 81.531(11)°$	$\gamma = 90°$	$\gamma = 90°$
Volume	2839(2) Å³	6506.5(5) Å³	6699(6) Å³
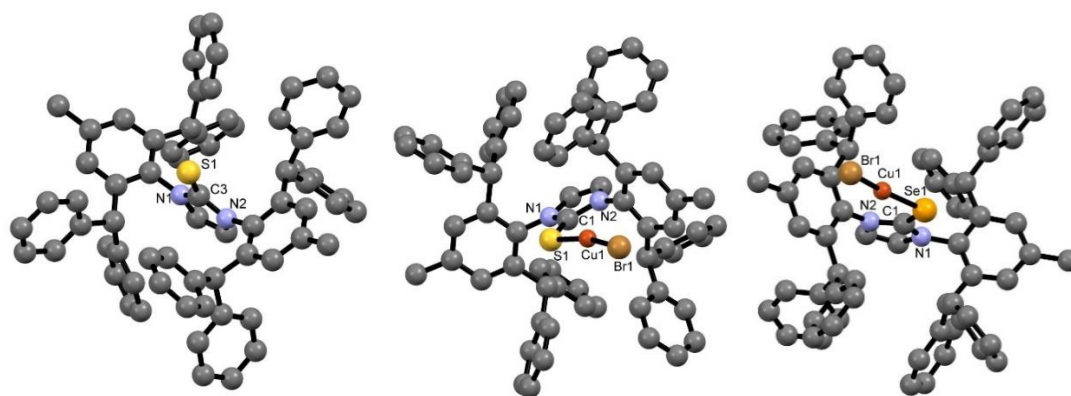
Figure 2A.A.1. *Molecular structure of **2A.11, 2A.13,** and **2A.14**. Hydrogen atoms are not shown for clarity.*
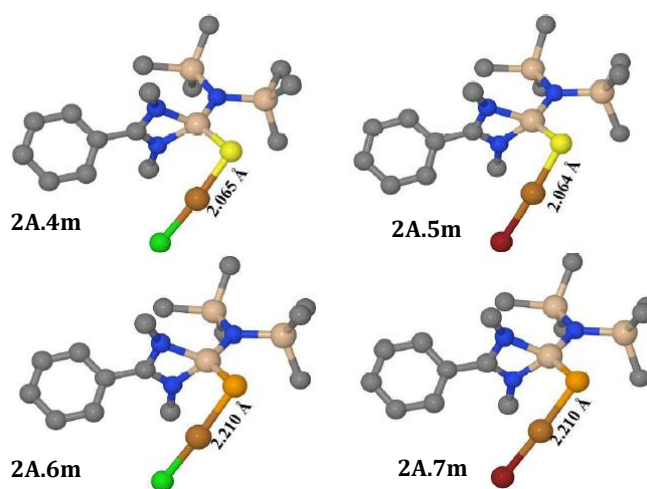
Figure 2A.A.2. *Geometry optimized structures of complexes between Si-chalcogenones and CuX (X=Cl, Br) (**2A.4m-2A.7m**).*
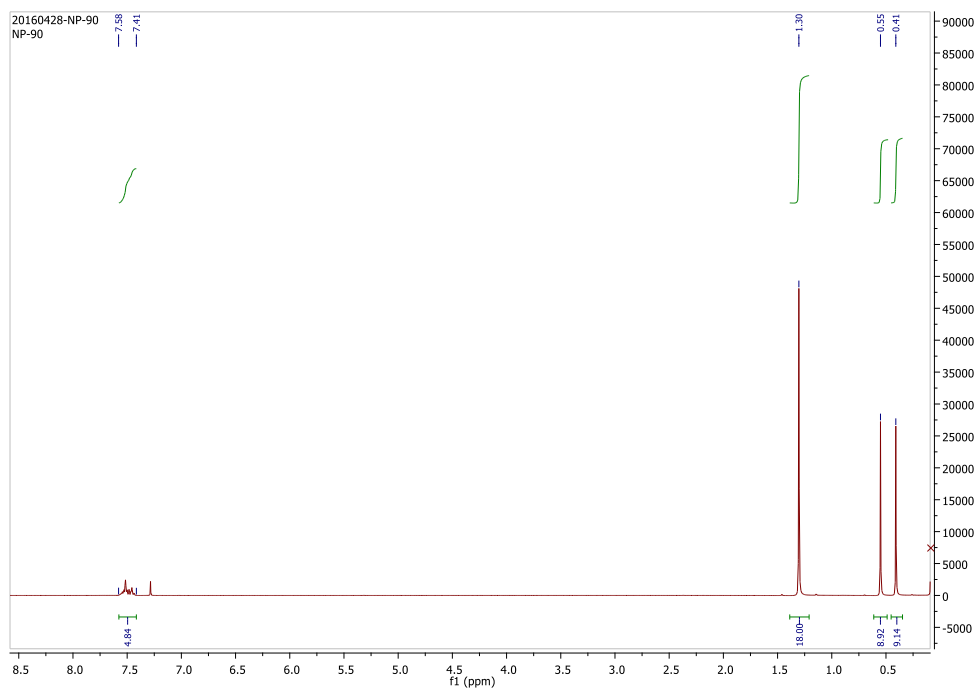
Figure 2A.A.3. *^{1}H NMR of* ***2A.2***
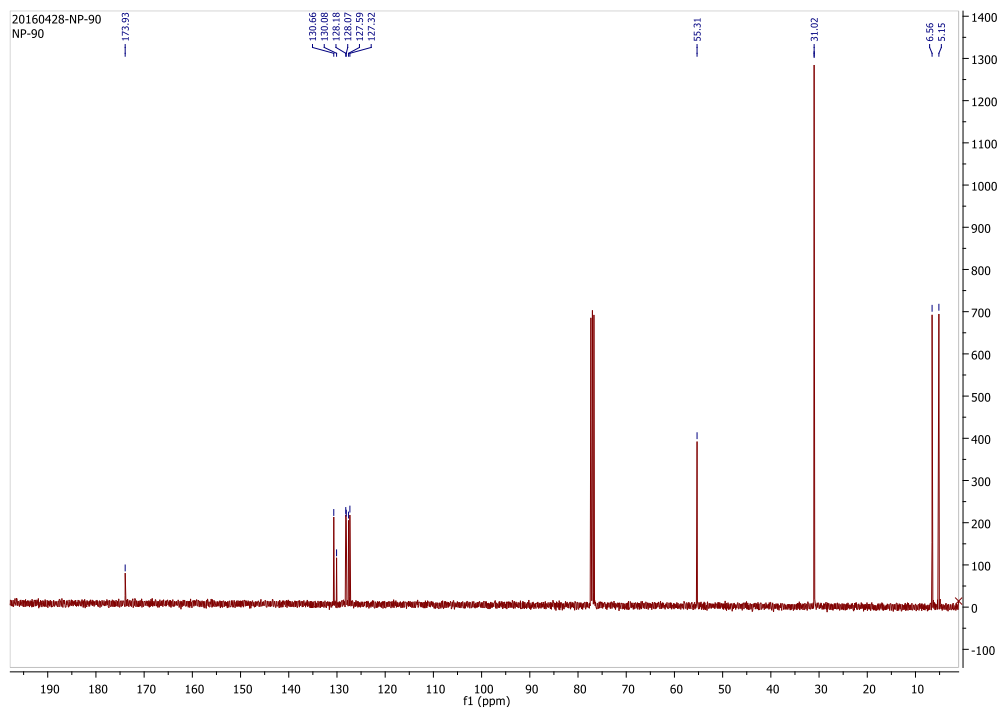
Figure 2A.A.4. *^{13}C NMR of* ***2A.2***
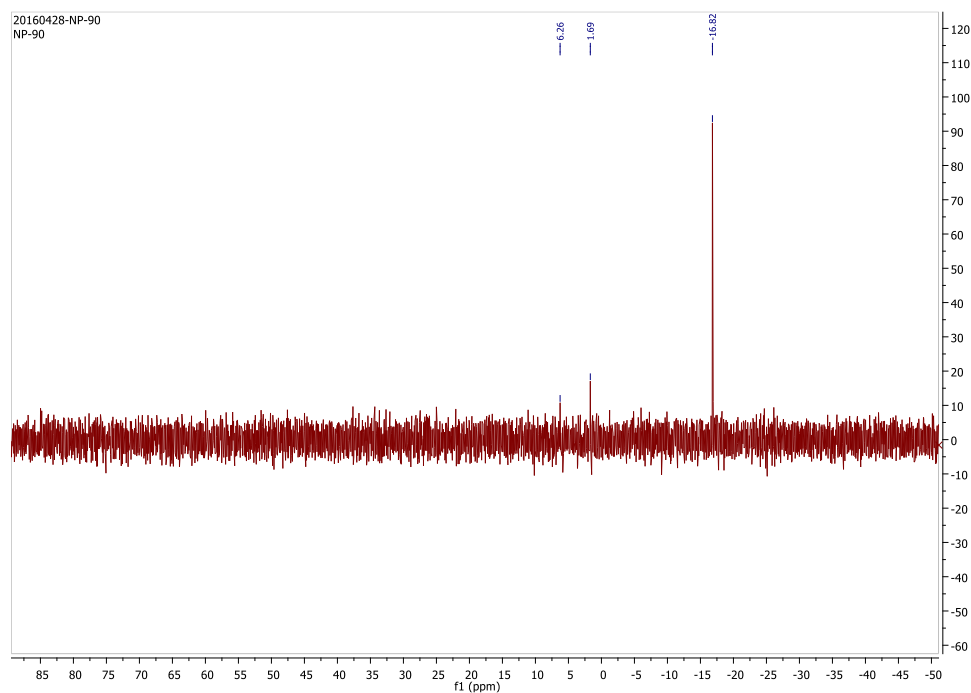
Figure 2A.A.5. *^{29}Si NMR of* **2A.2**
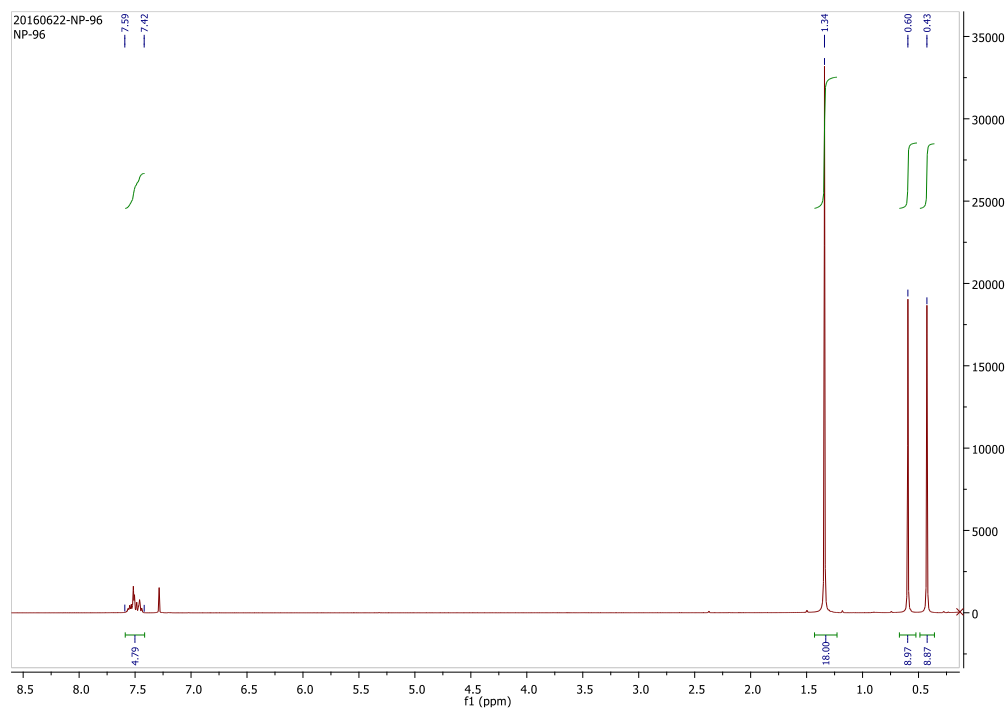
Figure 2A.A.6. *^1H NMR of* **2A.3**
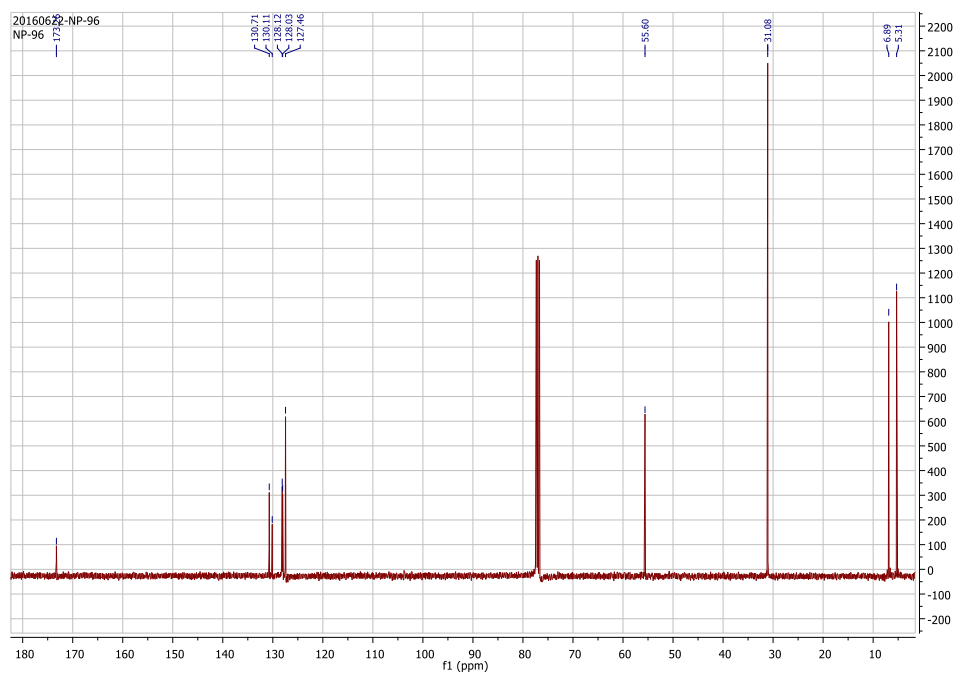
Figure 2A.A.7. *^{13}C NMR of **2A.3***
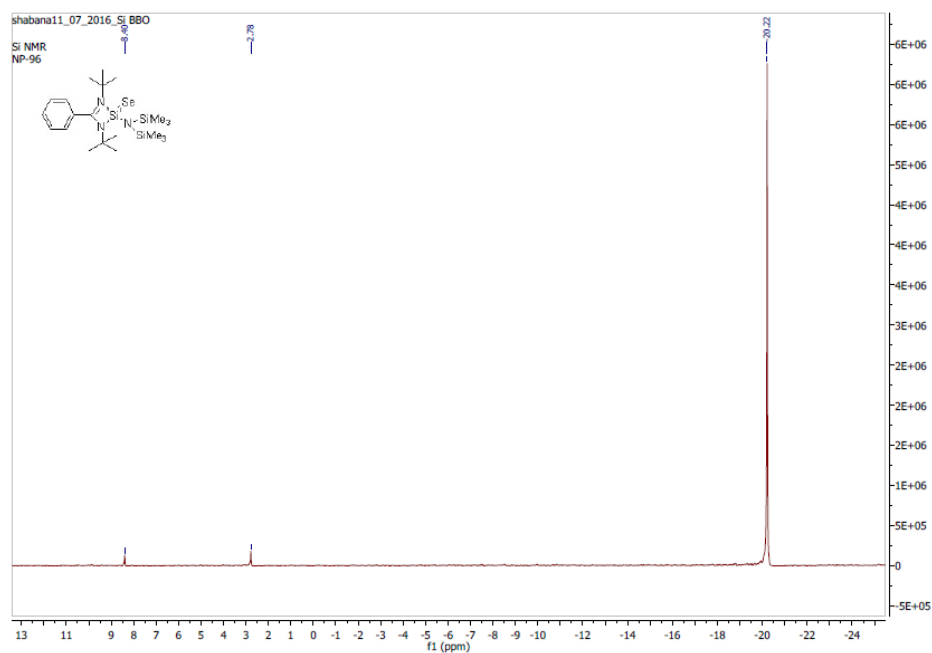
Figure 2A.A.8. *^{29}Si NMR of **2A.3***
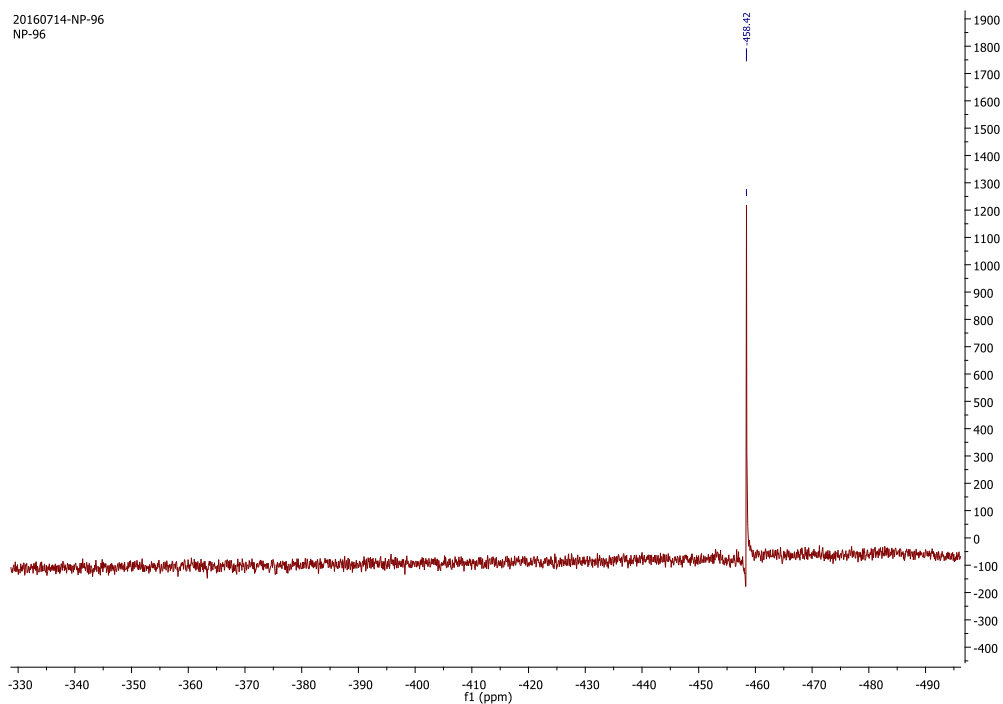
Figure 2A.A.9. *^{77}Se NMR of* **2A.3**
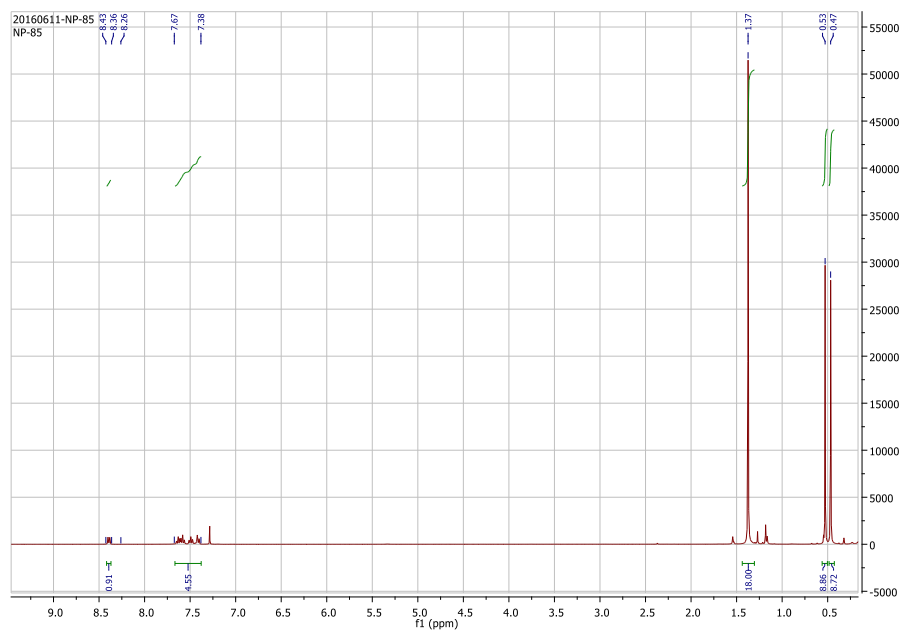
Figure 2A.A.10. *^{1}H NMR of* **2A.4**
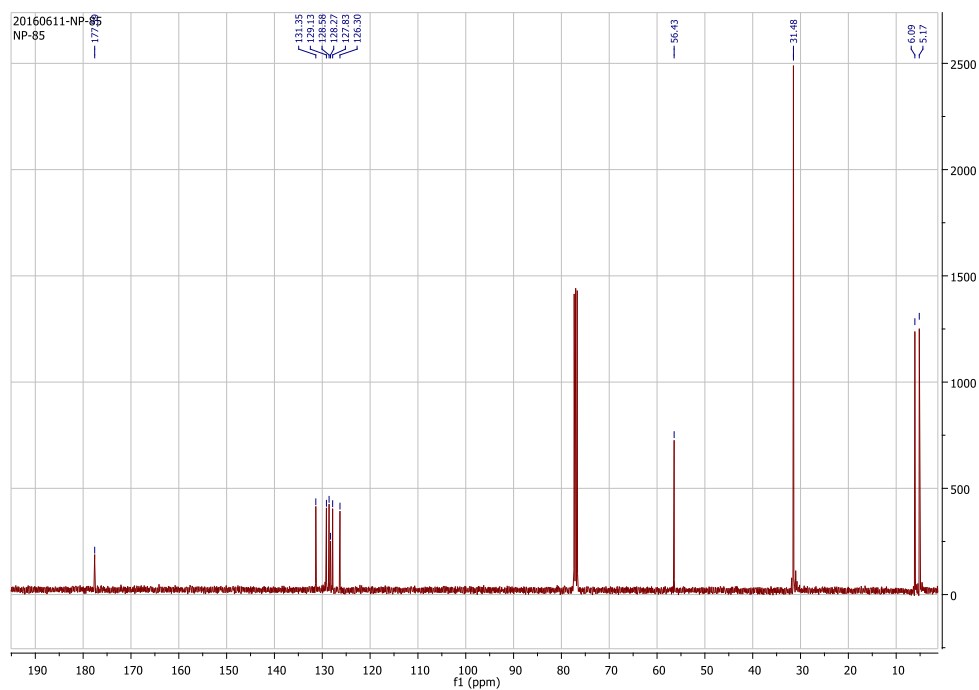
Figure 2A.A.11. *^{13}C NMR of* **2A.4**
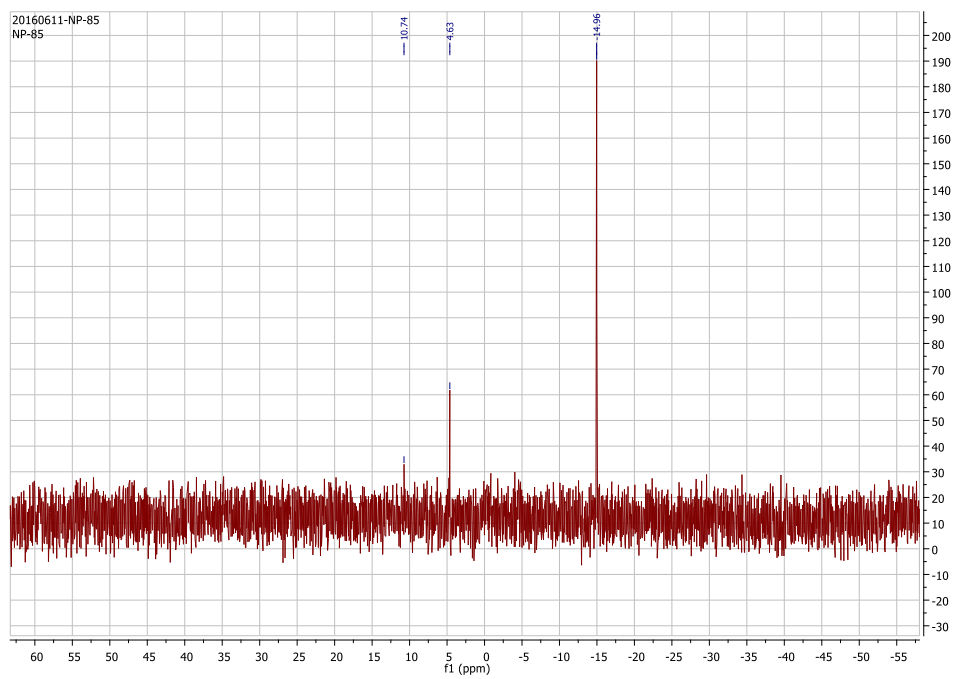
Figure 2A.A.12. *^{29}Si NMR of* **2A.4**
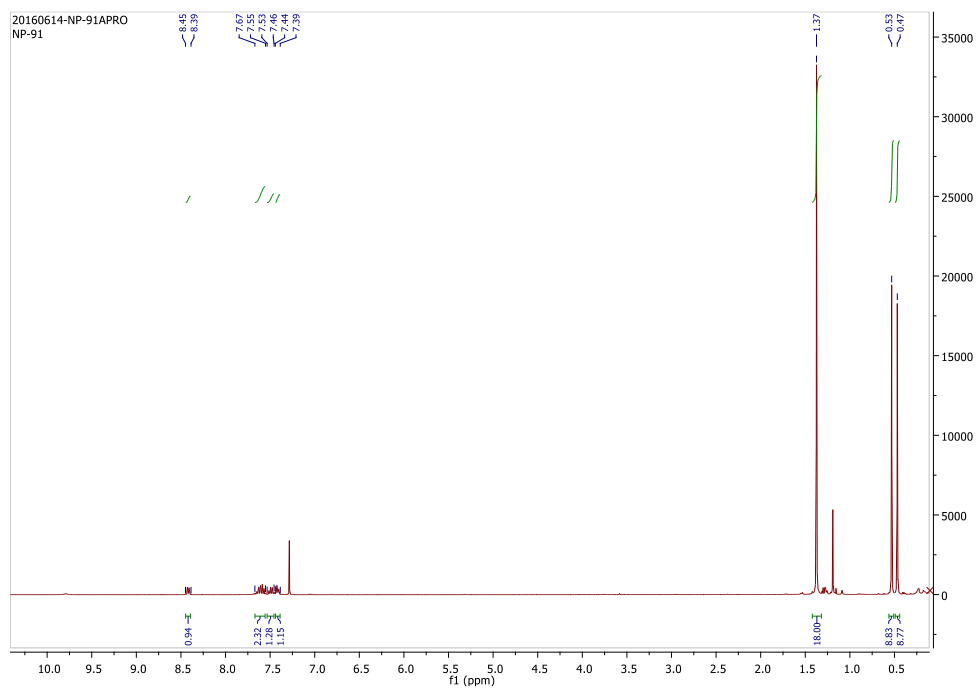
Figure 2A.A.13. *^{1}H NMR of* **2A.5**
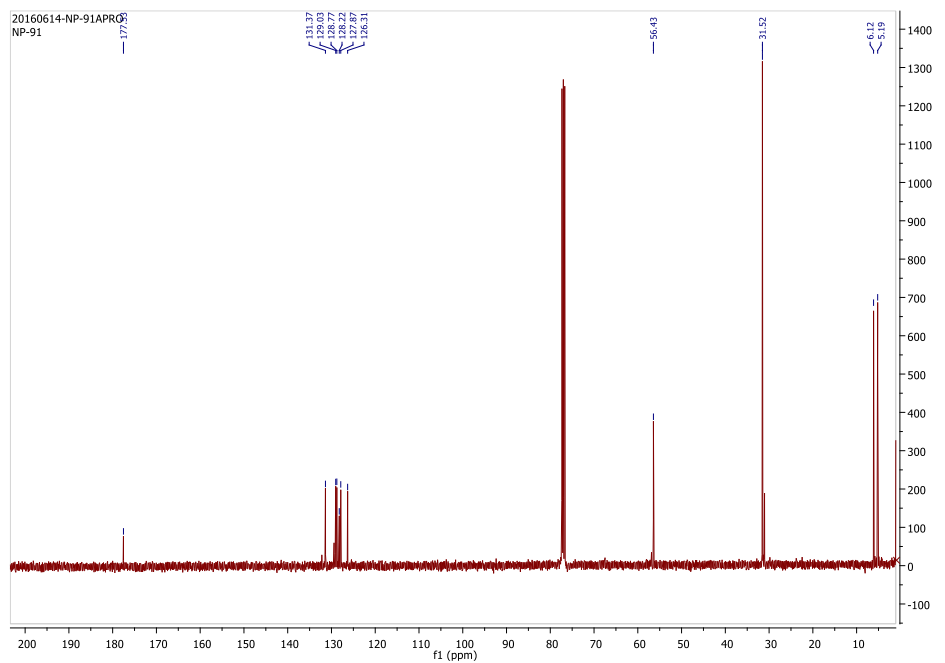
Figure 2A.A.14. *^{13}C NMR of* **2A.5**
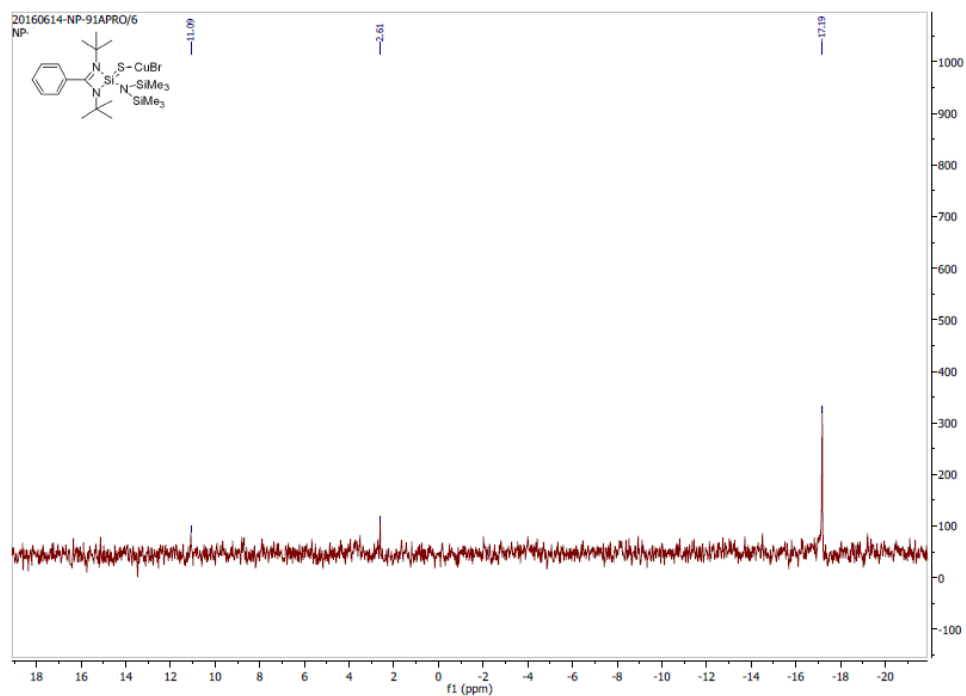
Figure 2A.A.15. *^{29}Si NMR of* **2A.5**
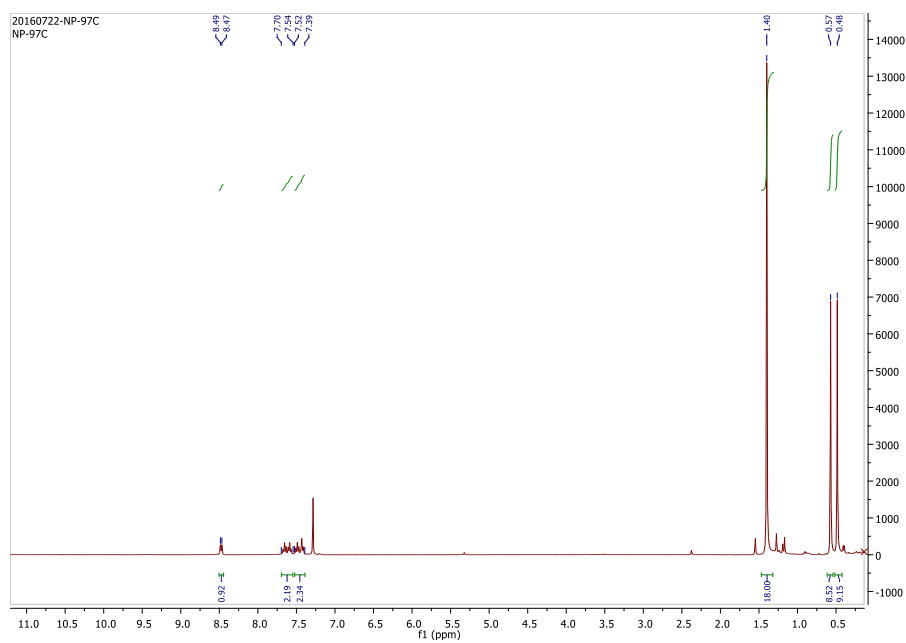
Figure 2A.A.16. *^{1}H NMR of* **2A.6**
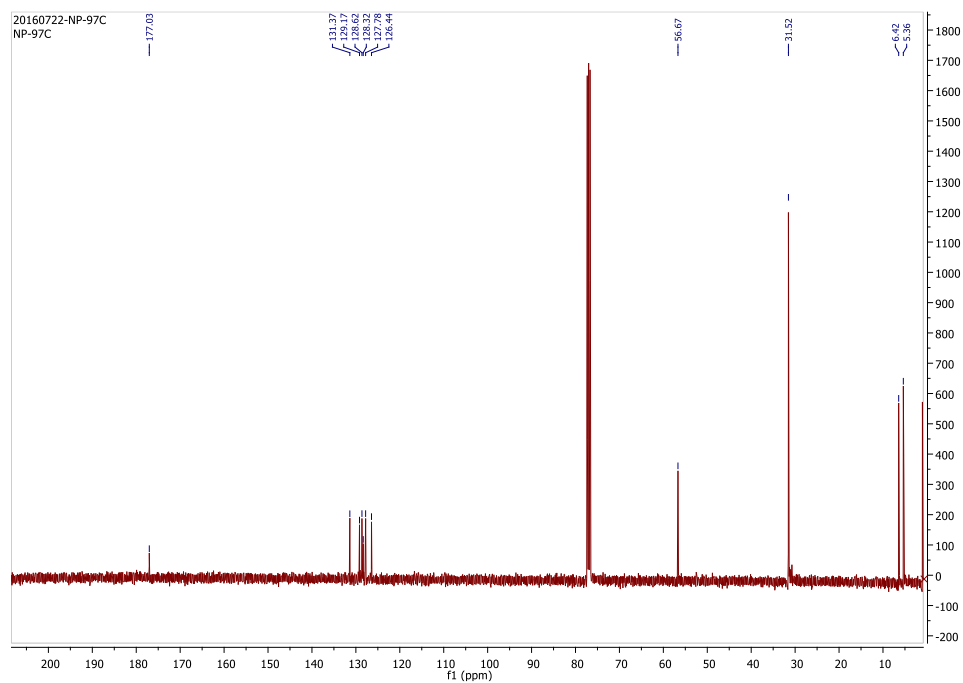
Figure 2A.A.17. *^{13}C NMR of* **2A.6**
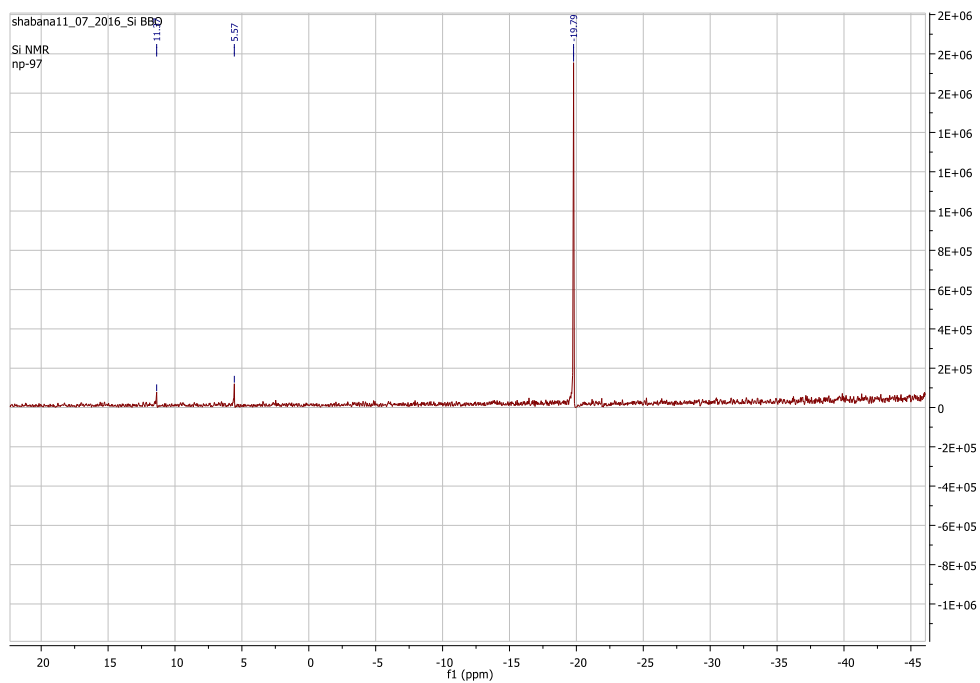
Figure 2A.A.18. *^{29}Si NMR of* **2A.6**
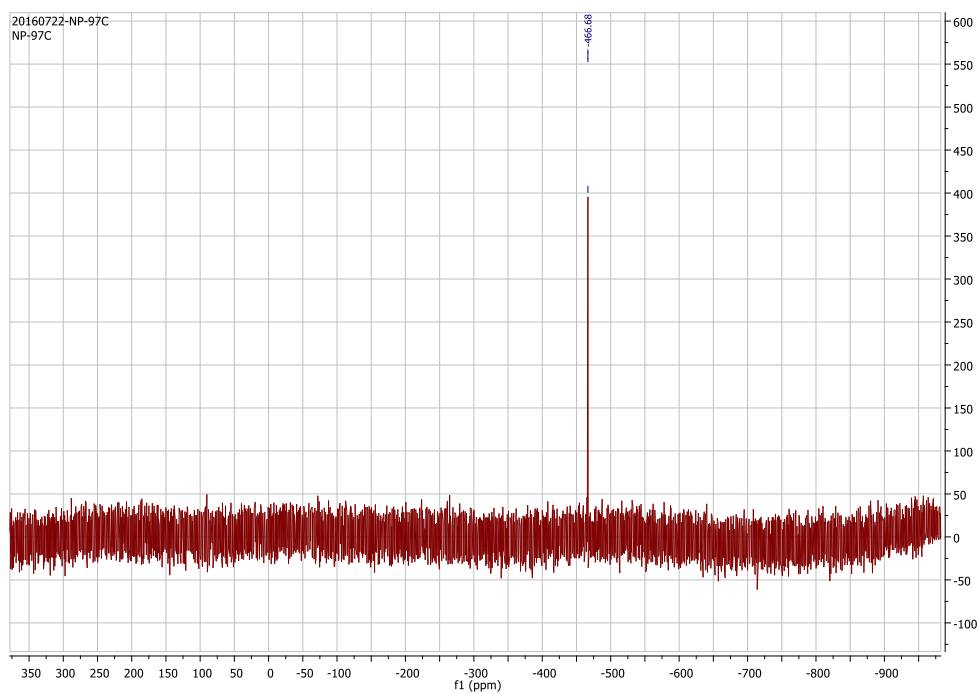
Figure 2A.A.19. *^{77}Se NMR of* **2A.6**
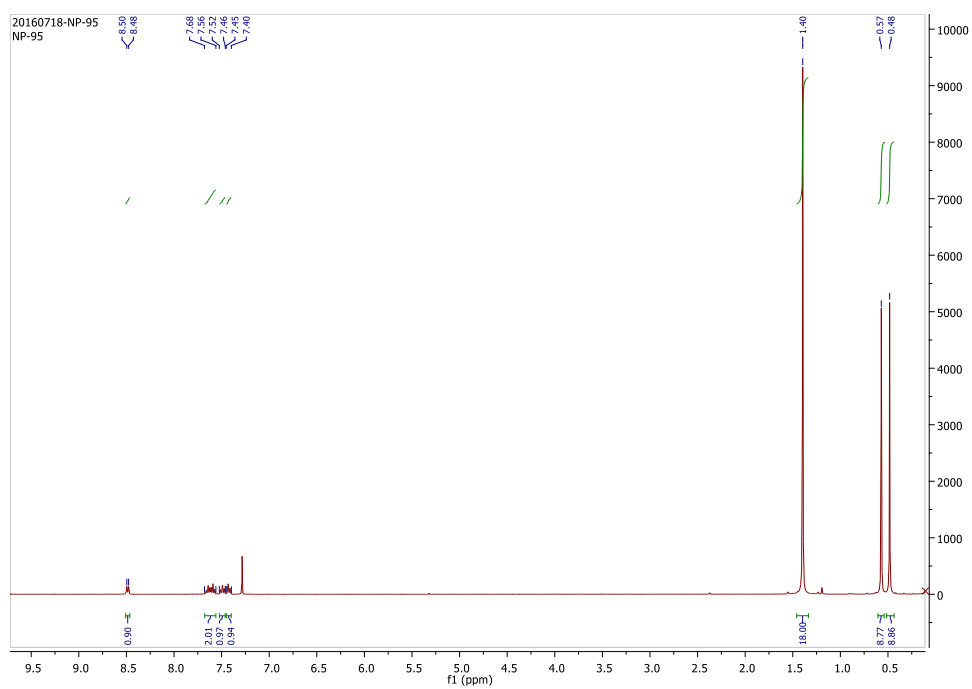
Figure 2A.A.20. *^{1}H NMR of* **2A.7**
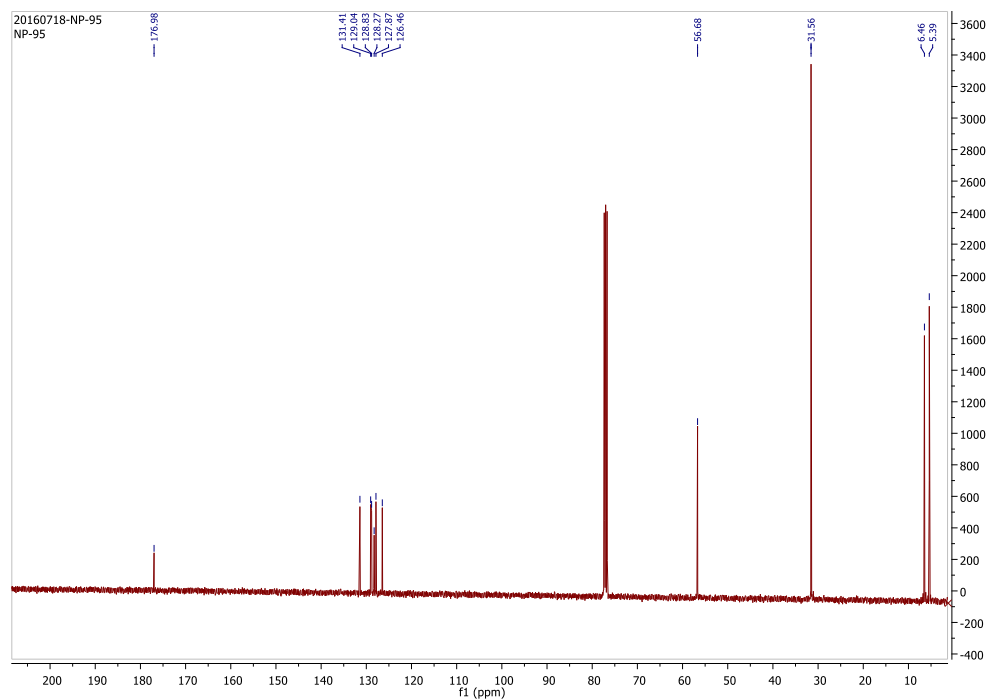
Figure 2A.A.21. *¹³C NMR of* **2A.7**
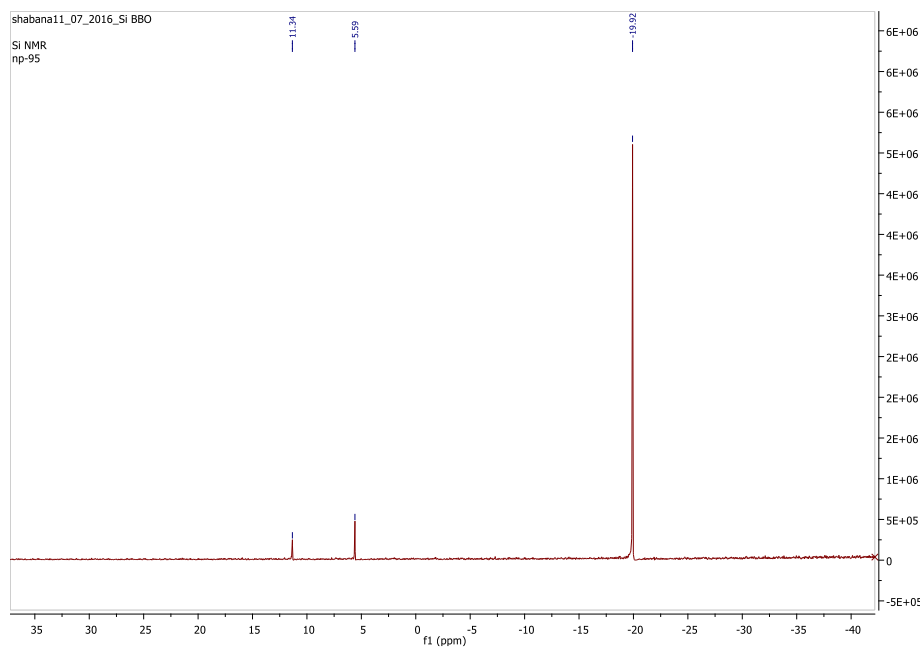
Figure 2A.A.22. *²⁹Si NMR of* **2A.7**
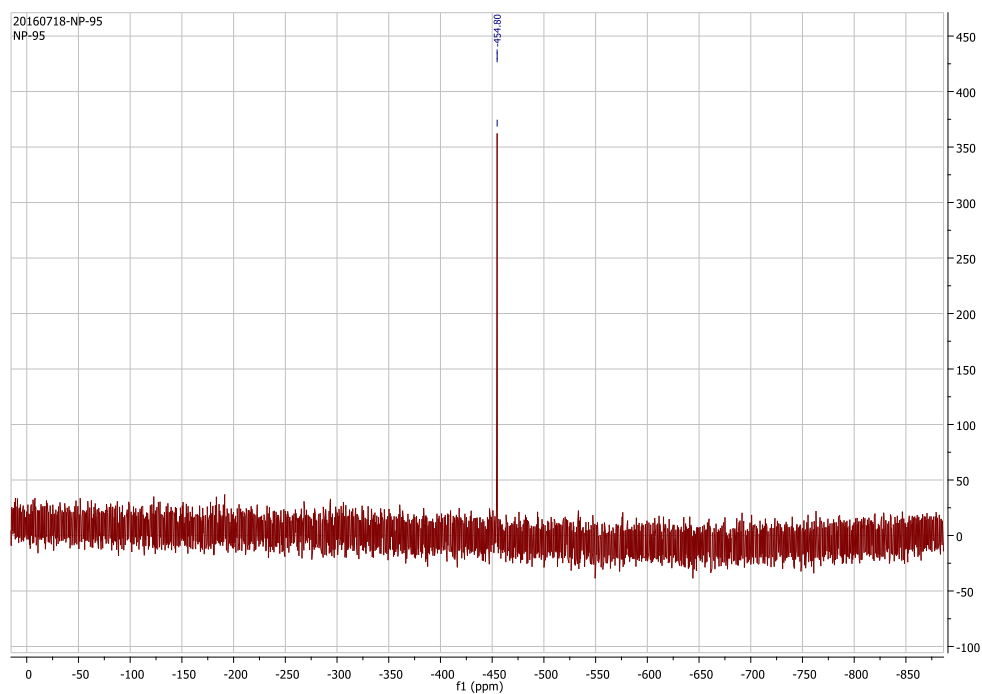
Figure 2A.A.23. *^{77}Se NMR of* **2A.7**
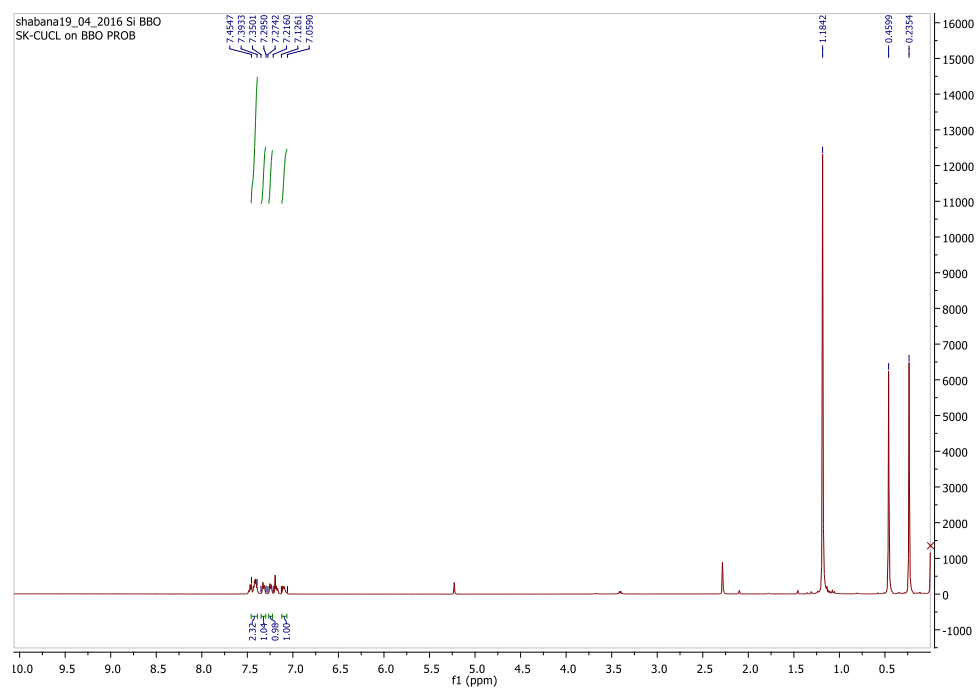
Figure 2A.A.24. *^{1}H NMR of* **2A.8**
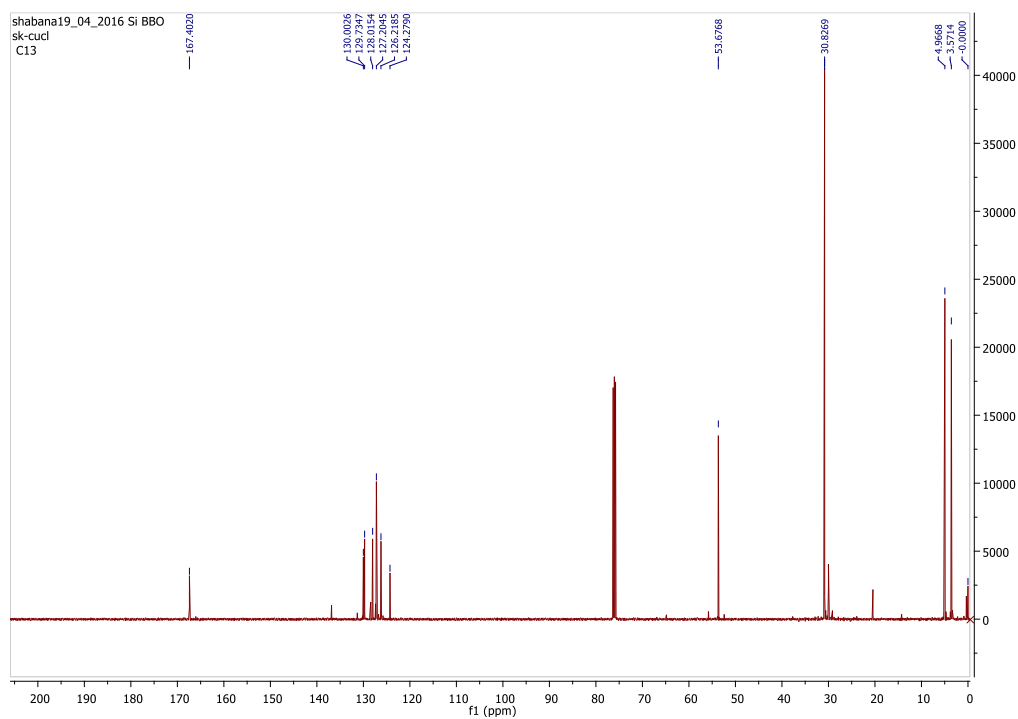
Figure 2A.A.25. *^{13}C NMR of* **2A.8**
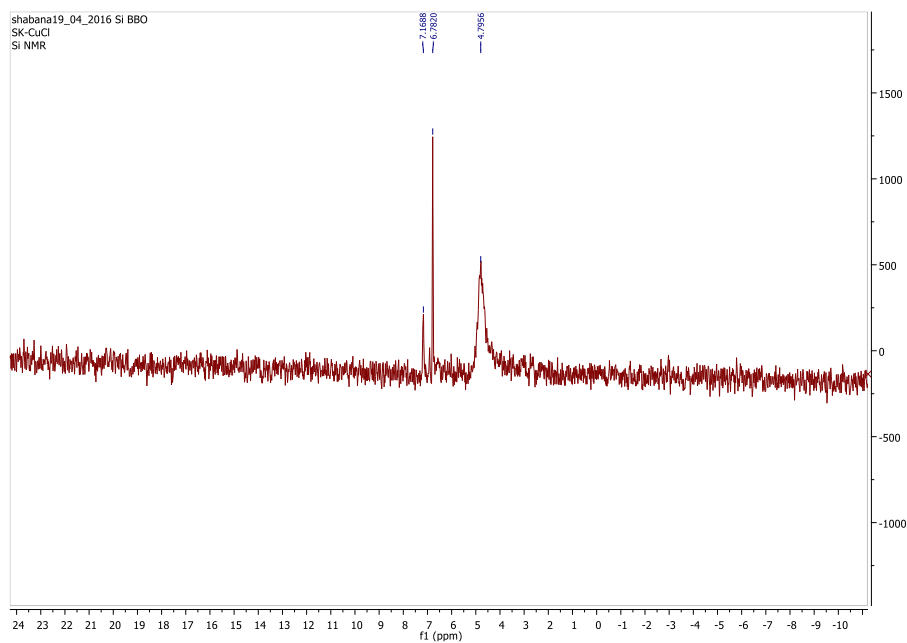
Figure 2A.A.26. *^{29}Si NMR of* **2A.8**
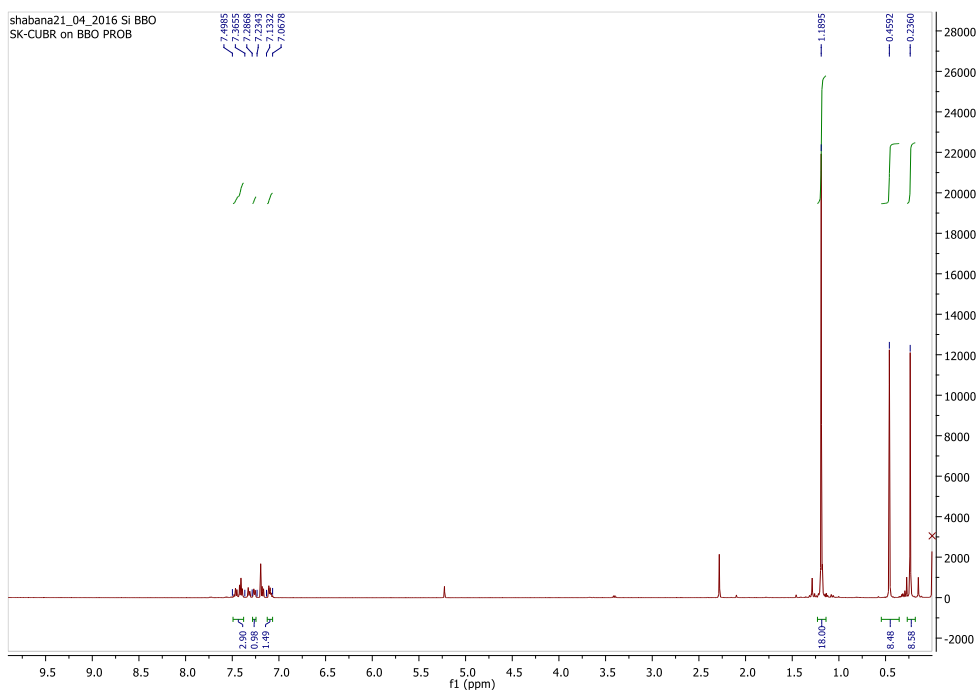
Figure 2A.A.27. *¹H NMR of* **2A.9**
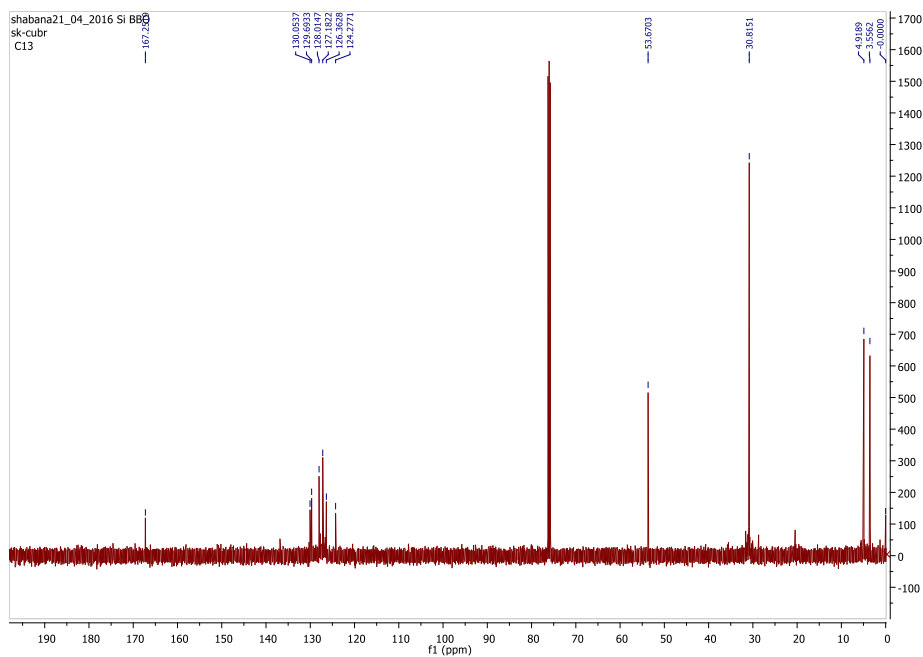
Figure 2A.A.28. *¹³C NMR of* **2A.9**
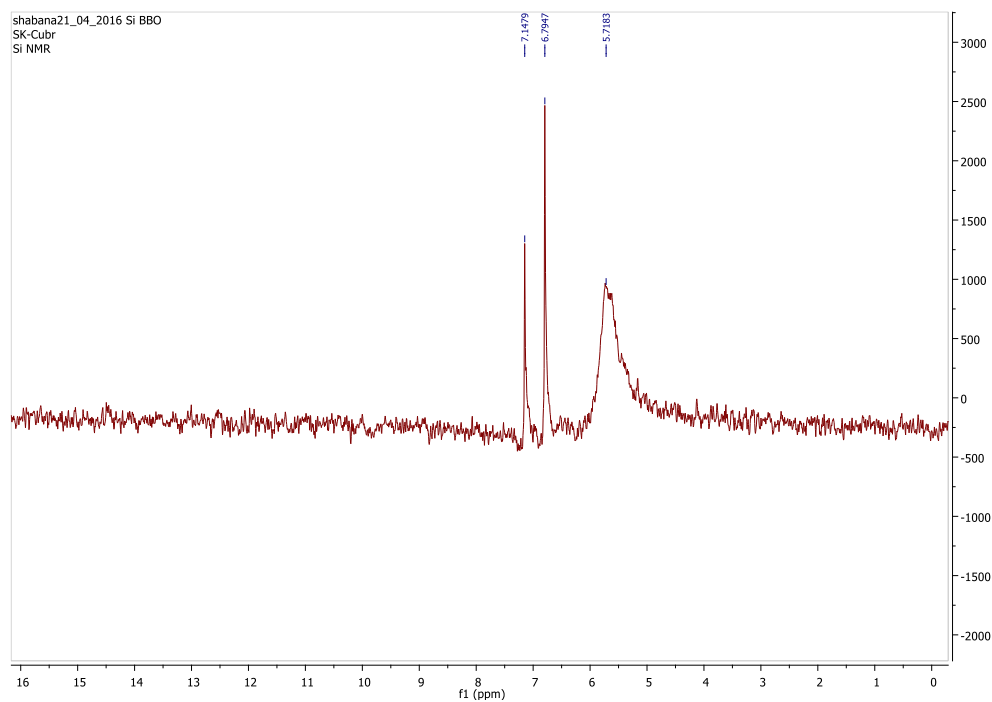
Figure 2A.A.29. ^{29}Si NMR of **2A.9**
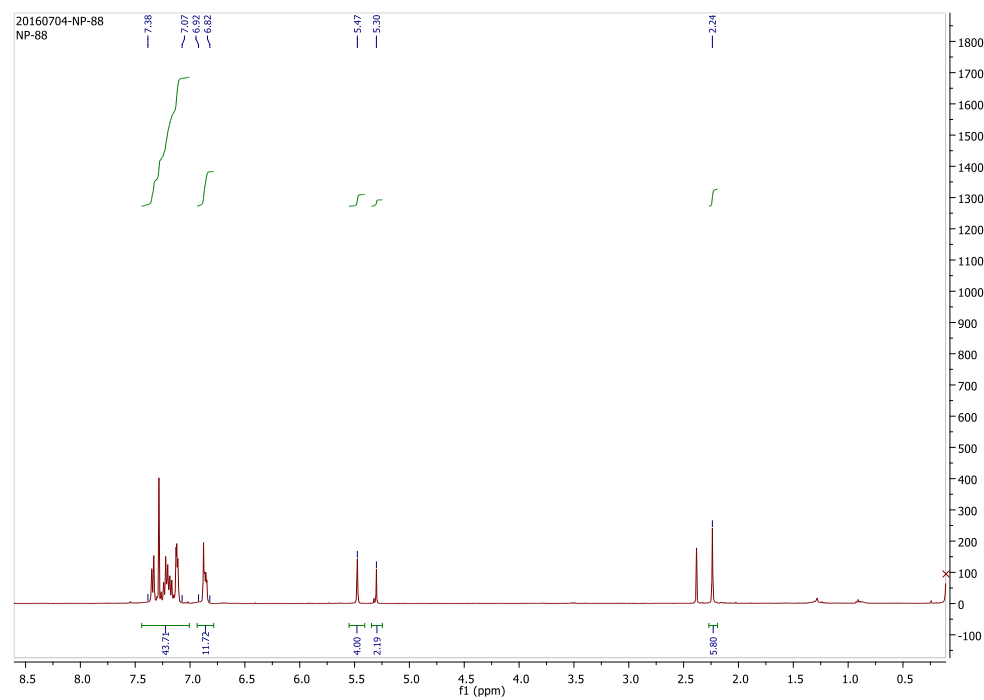
Figure 2A.A.30. ^{1}H NMR of **2A.11**
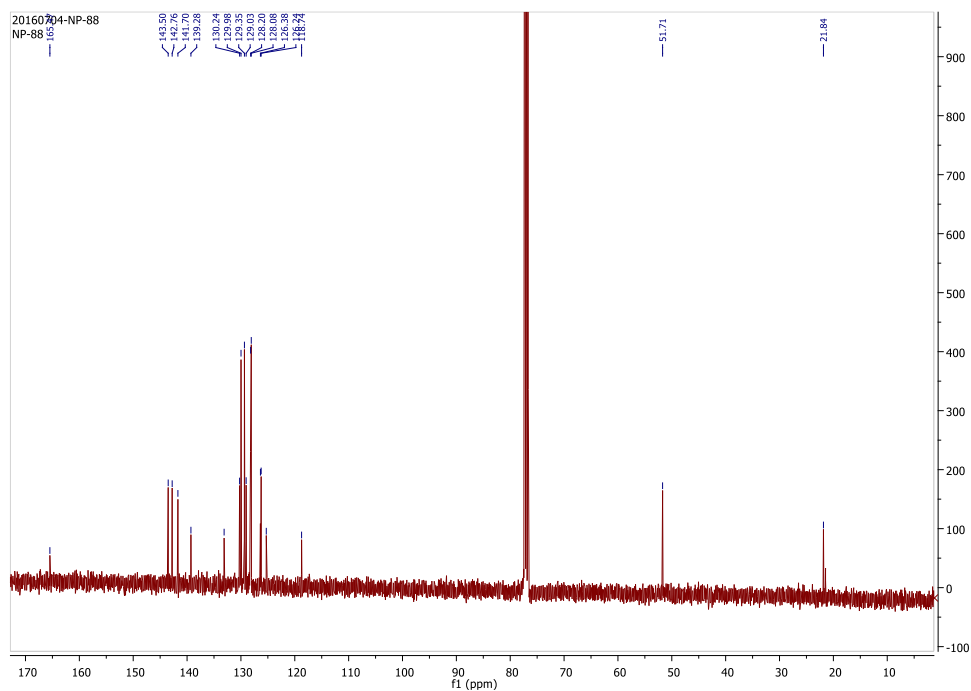
Figure 2A.A.31. *¹³C NMR of* **2A.11**
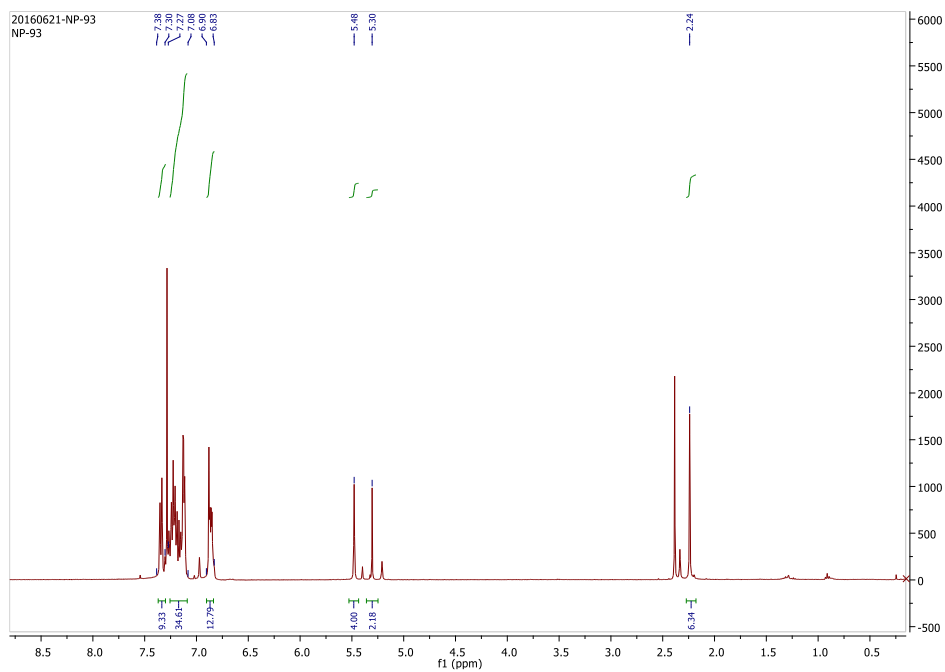
Figure 2A.A.32. *¹H NMR of* **2A.13**
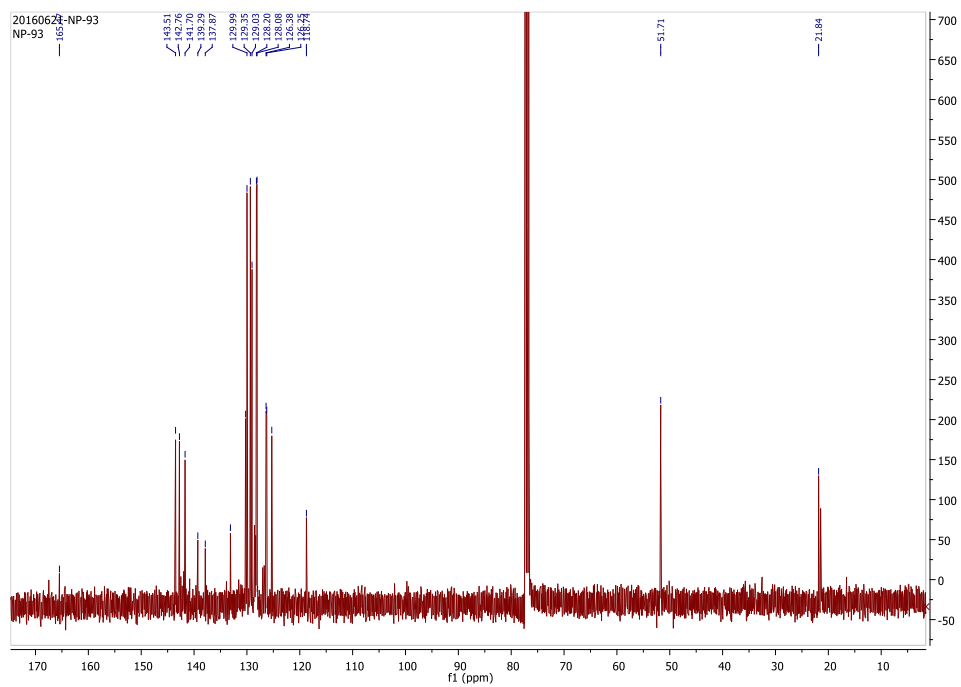
Figure 2A.A.33. *¹³C NMR of* **2A.13**
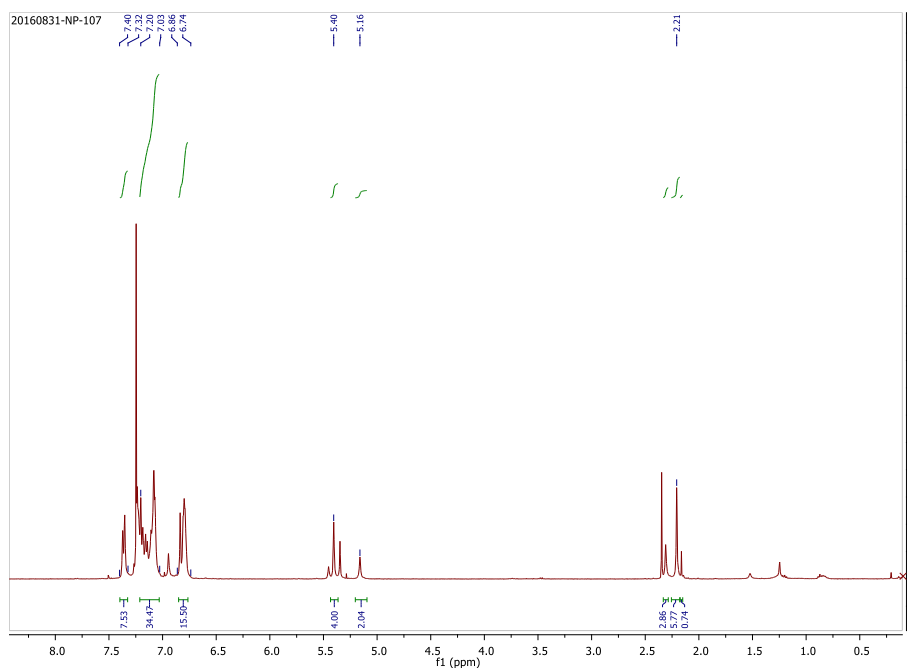
Figure 2A.A.34. *¹H NMR of* **2A.14**
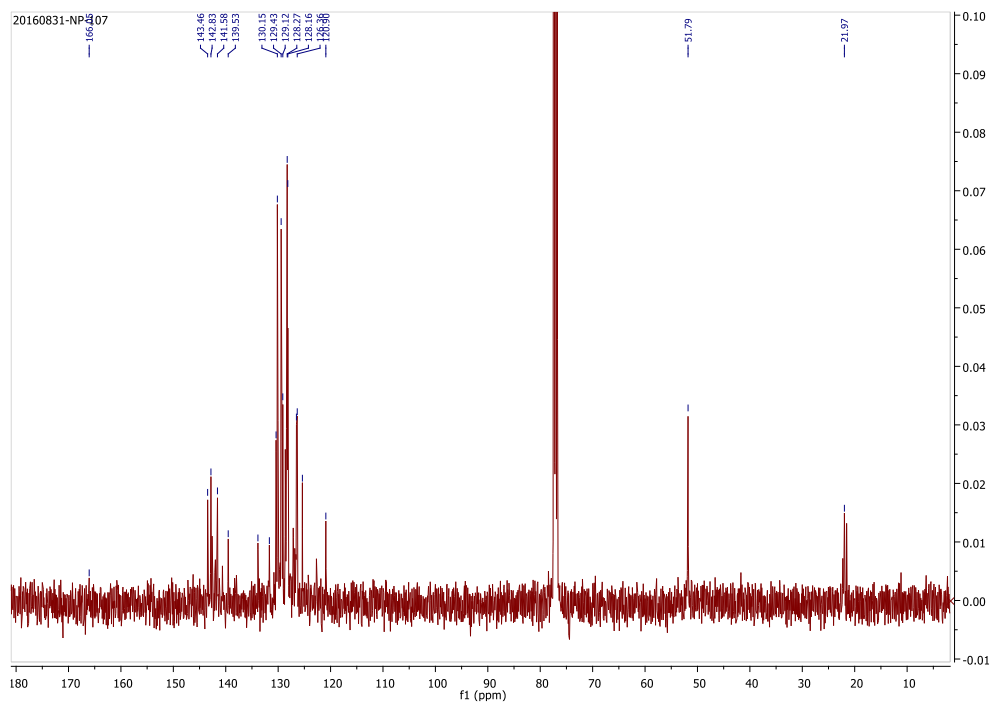
Figure 2A.A.35. ^{13}C *NMR of* **2A.14**
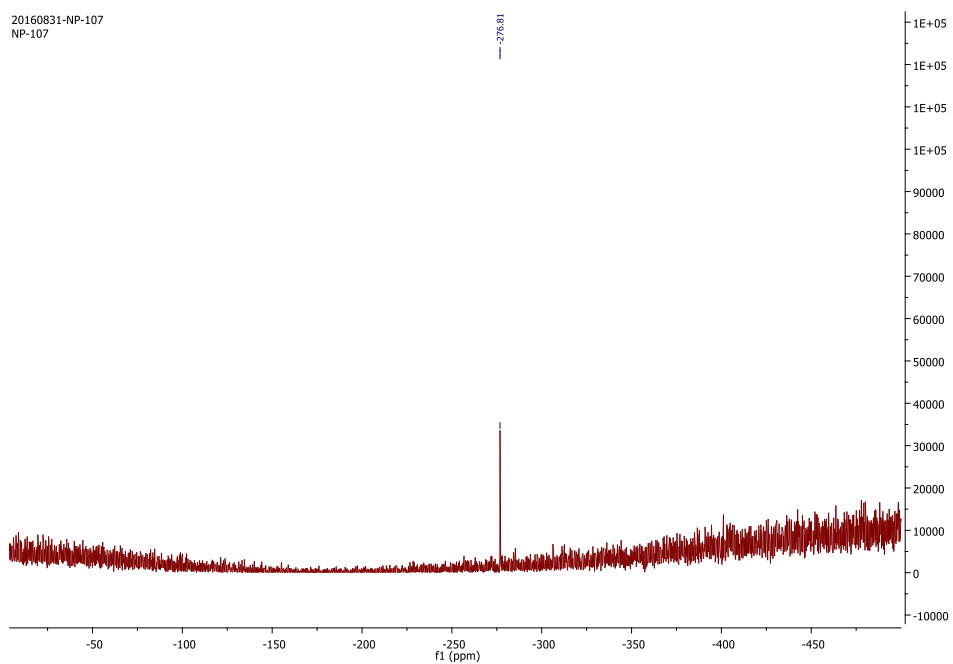
Figure 2A.A.36. ^{77}Se *NMR of* **2A.14**
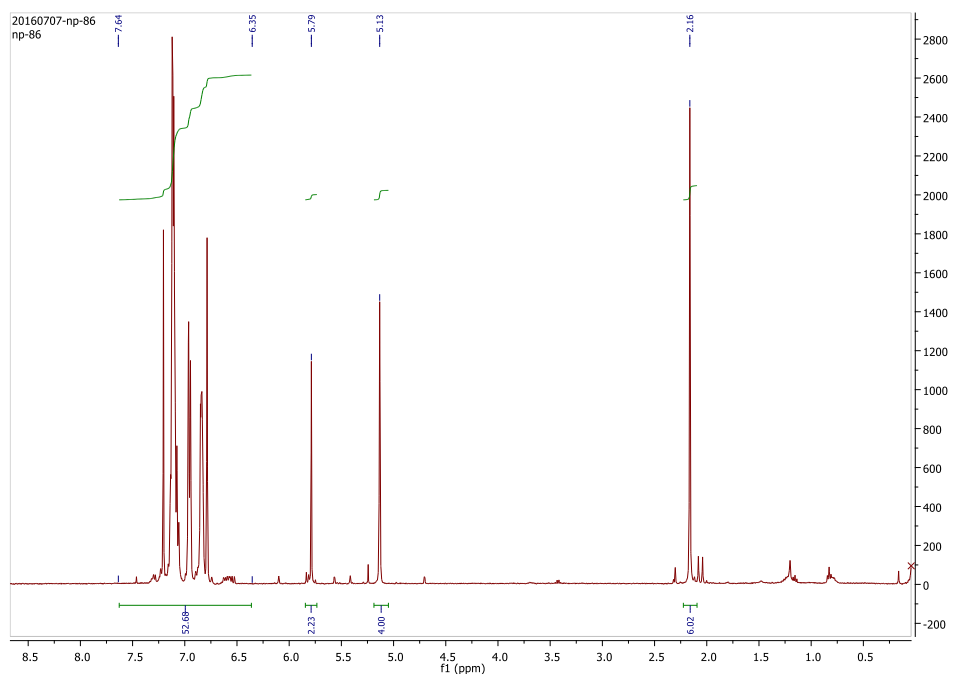
Figure 2A.A.37. *¹H NMR of* **2A.15**
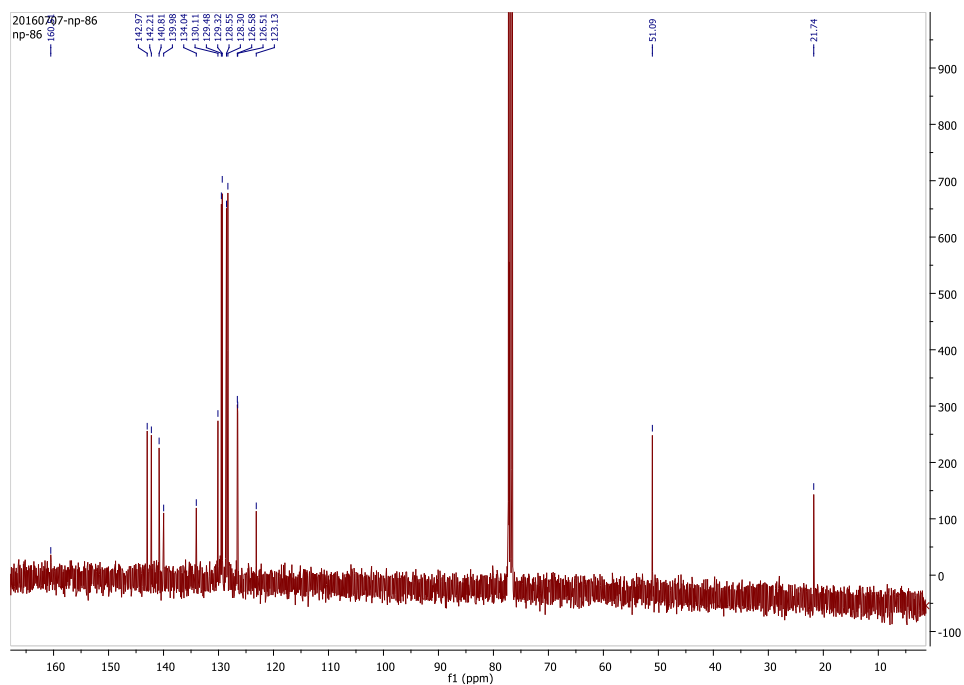
Figure 2A.A.38. *¹³C NMR of* **2A.15**

Appendix of Chapter 2B

Table 2B.A.1. *Crystallographic details for **2B.2**, **2B.3** and **2B.4**.*

	2B.2	2B.3	2B.4
Chemical formula	$C_{21}H_{41}BF_3N_3OSi_3$	$C_{21}H_{41}BF_3GeN_3OSi_2$	$C_{21}H_{41}F_2N_3Si_3$
Formula weight	503.65	548.15	457.84
Temperature	100(2)	100(2)	100(2)
Wavelength	0.71073	0.71073	0.71073
Crystal system	monoclinic	monoclinic	monoclinic
Space group	*Pn*	*Pn*	*P21/c*
Unit cell dimentions	*a*=8.803(3) Å	*a*=8.726(3) Å	*a*=18.681(7) Å
	b=17.123(6) Å	*b*=17.121(6) Å	*b*=8.385(3) Å
	c=18.354(6) Å	*c*=18.523(6) Å	*c*=18.595(7) Å
	α=90°	α=90°	α=90°
	β=95.252(7)°	β=95.199(6)°	β=116.752(9)°
	γ=90°	γ=90°	γ=90°
Volume	2754.8(15) Å³	2756.0(15) Å³	2600.9(17) Å³
Z	4	4	4
Density (calculated)	1.214 g/cm³	1.321 g/cm³	1.169 g/cm³
Absorption coefficient	0.210 mm⁻¹	1.237 mm⁻¹	0.209 mm⁻¹
F(000)	1080	1152	992
Theta range for data collection	2.23 to 25.25°	2.20 to 25.24°	2.194 to 25.25°
Reflections collected	94426	73281	75811
Independent reflections	9989 [R(int)= 0.2249]	9988 [R(int)= 0.2156]	4704 [R(int)= 0.0996]

Coverage of independent reflections	100%	99.9%	100%
Data/ restraints/ parameters	9989/ 2/ 601	9988/ 2/ 601	4704/ 0/ 274
Goodness-of-fit on F2	1.021	1.007	1.003
Δ/ σ max	0.034	0.009	0.003
Final R indices	6147 data; [I>2σ(I)] R_1= 0.0699, wR_2= 0.1293	6532 data; [I>2σ(I)] R_1= 0.0705, wR_2= 0.1296	3533 data; [I>2σ(I)] R_1= 0.0411, wR_2= 0.0871
	all data, R_1= 0.1472, wR_2= 0.1595	all data, R_1= 0.1320, wR_2= 0.1555	all data, R_1= 0.0681, wR_2= 0.0997
Largest diff. peak and hole	0.464 and -0.490 eÅ^{-3}	0.903 and -0.956 eÅ^{-3}	0.277 and -0.267eÅ^{-3}
R. M. S deviation from mean	0.085 eÅ^{-3}	0.113 eÅ^{-3}	0.051 eÅ^{-3}

Figure 2B.A.1. *Optimized geometries and important geometrical parameters of a) BF$_3$ coordinated sila- and germa acetamide* **2B.2** *and* **2B.3**. *b) sila- and gema-acetamide without BF$_3$* **2B.2'** *and* **2B.3'**. *Distances are given in Å and angles are in (°). Hydrogens are omitted for clarity.*

a)

b)
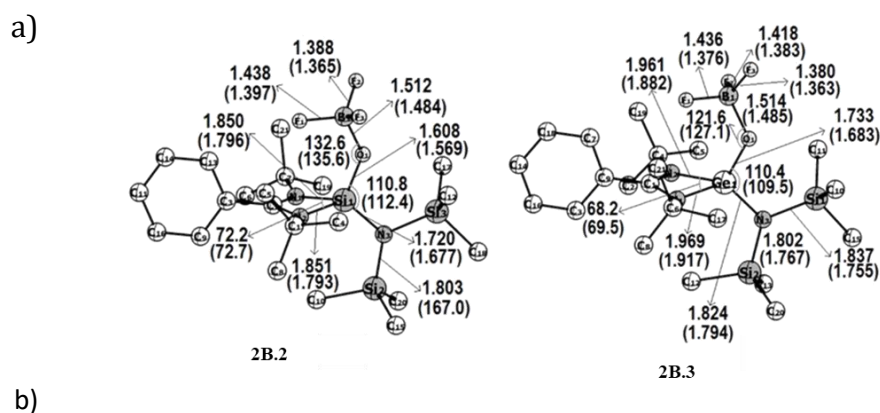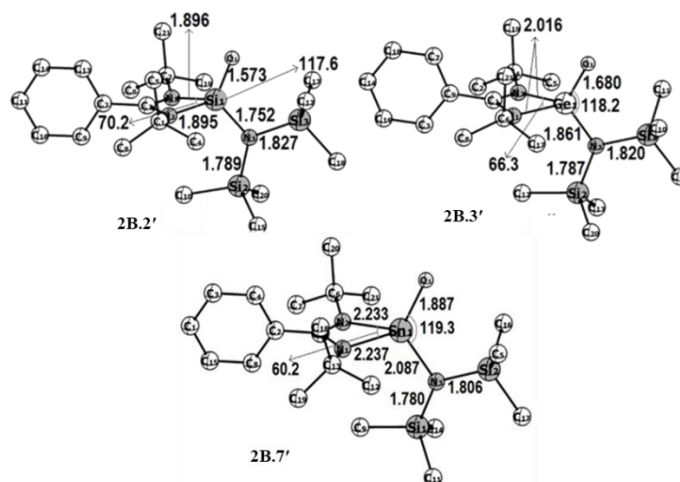
Table 2B.A.2. *Second order perturbation interactions and bond occupancy of the selected bonds in* **2B.2**, **2B.3**, **2B.2'** *and* **2B.3'** *given by the natural population analysis calculated at the M06/def2-TZVPP//BP86/def2-SVP level of theory.*

	Charge			WBI
	Si1	**O**	**B**	**Si1–O**
2.2	2.45	-1.17	1.34	0.70
2.2'	2.32	-1.29	-	1.07
	Ge	**O**	**B**	**Ge-O**
2.3	2.32	-1.13	1.33	0.70
2.3'	2.19	-1.23	-	1.09

Table 2B.A.3. *Second order perturbation interactions and bond occupancy of the selected bonds in **2B.2**, **2B.3**, **2B.2**′ and **2B.3**′ given by the natural population analysis calculated at the M06/def2-TZVPP//BP86/def2-SVP level of theory.*

2B.2			2B.3		
Donor	**Acceptor**	**Energy (kcal/ mol)**	**Donor**	**Acceptor**	**Energy (kcal/ mol)**
LP(2) O	BD*(1) Si-N1	10.7	**LP(1) O**	BD*(1) Ge1-N1	6.37
LP(2) O	BD*(1) Si-N2	7.00	**LP(2)O**	BD*(1) Ge1-N1	4.26
LP(2) O	BD*(1) F2-B14	7.01	**LP(2) O**	BD*(1) F2-B	7.68
LP(1) O	BD*(1) Si-N1	2.50	**LP(2) O**	BD*(1) Ge1-N2	10.47
LP(1) O	BD*(1) Si-N2	5.74	**LP(1) O**	BD*(1) Ge1-N2	1.14
LP(1) O	BD*(1) F1-B	5.38	**LP(1) O**	BD*(1) F1-B	3.00
2B.3′			**2B.4′**		
Donor	**Acceptor**	**Energy (kcal/ mol)**	**Donor**	**Acceptor**	**Energy (kcal/ mol)**
BD (2) Si1–O	BD*(1) Si1–N2	20.6	**BD (2)Ge1–O**	BD*(1)Ge1–N2	30.2
BD (2) Si1–O	BD*(1) Si1–N1	18.0	**BD (2)Ge1–O**	BD*(1)Ge1–N1	14.7
BD (3) Si1–O	BD*(1) Si1–N3	16.7	**BD (3)Ge1–O**	BD*(1)Ge1–N3	15.2
LP (1) O1	RY (1) Si1	10.9	**LP (1) O4**	RY (1)Ge1	6.9

Table 2B.A.4. EDA-NOCV data of all the bonding possibilities of *2B.2'* and *2B.3'* at the BP86/TZ2P level of theory. Energies are given in kcal/mol.

		ΔE_{int}	ΔE_{Pauli}	ΔE_{Elstat}	ΔE_{Orb}
2B.2'	**A**	-264.7	337.6	-309.2	-293.2
	B	-225.2	417.9	-170.7	-472.4
	C	-241.7	309.3	-150.5	-400.5
2B.3'	**A**	-232.0	285.9	-280.1	-237.8
	B	-181.6	313.2	-128.1	-366.7
	C	-203.4	253.9	-128.5	-328.8

Table 2B.A.5. EDA-NOCV results of the best possible bonding representation (*A* in Scheme S1) of *2B.2'* and *2B.3'* at the BP86/TZ2P level of theory. Energies are given in kcal/mol.

	ΔE_{int}	ΔE_{Pauli}	ΔE_{Elstat}	ΔE_{Orb}	[a]ΔE_1	[b]ΔE_2	[b]ΔE_3	[b,c]ΔE_{rest}	ΔE_{prep}	$-D_e$
2B.2'	-264.7	337.6	-309.2, 51.3%	-293.2, 48.6%	-196.9, 67.1%	-35.3, 12.0%	-32.4, 11.0%	-28.6, 9.7%	101	-163.7
2B.3'	-232.0	285.9	-280.1, 54.1%	-237.8, 45.9%	-161.9, 68.1%	-28.7, 12.1%	-23.2, 9.7%	-24.0, 10.1%	114.6	-117.4

[a]*Values in parenthesis give the percentage contribution to the total attractive interaction* $\Delta E_{Elstat} + \Delta E_{Orb}$.
[b]*Values in paranthesis give the percentage contribution to the total orbital interaction* ΔE_{Orb}. [c]$\Delta E_{rest} = \Delta E_{Orb} - (\Delta E_1 + \Delta E_2)$.

Figure 2B.A.2. *Plots of α-NOCV pair of orbitals ψ_{-n}, ψ_n with their eigen values in the parenthesis, the associated deformation densities $\Delta\rho_n$ and the associated orbital stabilization energies ΔE of* **2B.2'** *(in kcal/mol) at the BP86/TZ2P level of theory. The isosurface value for the NOCV plots is 0.03 and for the deformation densities is given in the paranthesis.*

Ψ_{-1} (-0.79)	Ψ_1 (0.79)	$\Delta_{\rho1}$ ($\Delta E_1 = -196.9$) (Isosurface value = 0.002)
Ψ_{-2} (-0.24)	Ψ_2 (0.24)	$\Delta_{\rho2}$ ($\Delta E_2 = -35.3$) (Isosurface value = 0.001)
Ψ_{-3} (-0.22)	Ψ_3 (0.22)	$\Delta_{\rho3}$ ($\Delta E_3 = -32.4$) (Isosurface value = 0.001)
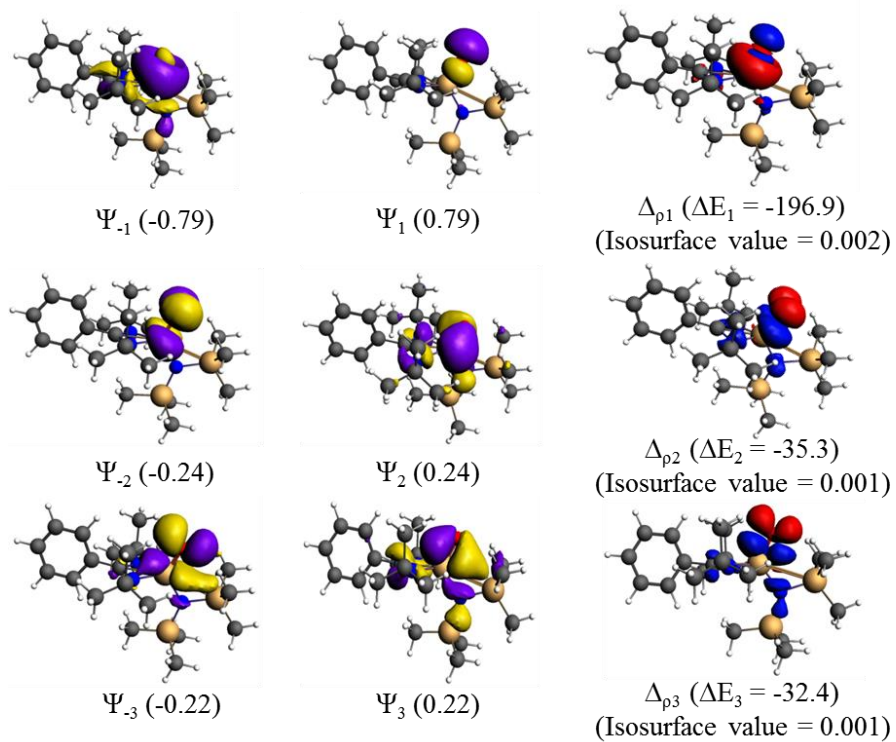
Figure 2B.A.3. *Plot of electrostatic potential (kcal/mol) on the molecular van der Waals surfaces of* ***2B.2′*** *and* ***2B.3′*** *at the M06/def2-TZVPP//BP86/def2-SVP level of theory. The global minima and global maxima are given in italics*
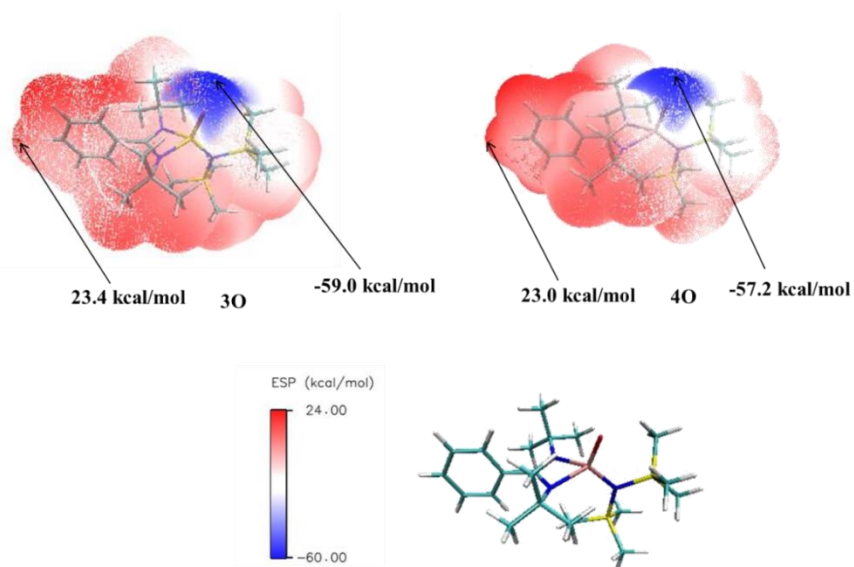
Table 2B.A.6*. Molecular electrostatic potential values on the molecular of oxygen atom in* ***2B.2′****,* ***2B.3′****,* ***2B.2*** *and* ***2B.3*** *calculated at the M06/def2-TZVPP//BP86/def2-SVP level of theory.*

	ESP (kcal/mol)		ESP (kcal/mol)
2B.2′	-52.9	**2B.3′**	-51.7
2B.2	-32.9	**2B.3**	-35.3

Table 2B.A.7. *Reaction energy for the formation of* ***2B.2*** *and* ***2B.3*** *from the reaction of* ***2B.2′*** *and* ***2B.3′*** *with BF₃ and the reaction energy for the formation of hypothetical compounds* ***2B.2′****,* ***2B.3′*** *and* ***2B.7′*** *calculated at the M06/def2-TZVPP//BP86/def2-SVP level of theory*

Reaction	Reaction Energy (kcal/mol)
2B.2′ + BF₃ → 2B.2	-40.3

2B.3′ + BF$_3$ → 2B.3	-40.8
1.14b + O → 2B.2′	-149.6
2B.1 + O → 2B.3′	-99.5
2B.6 + O → 2B.6′	-68.5

Figure 2B.A.4. *Plots of α-NOCV pair of orbitals ψ_{-n}, ψ_n with their eigen values in the parenthesis, the associated deformation densities $\Delta\rho_n$ and the associated orbital stabilization energies ΔE of **3′** (in kcal/mol) at the BP86/TZ2P level of theory. The isosurface value for the NOCV plots is 0.03 and for the deformation densities is given in the paranthesis.*
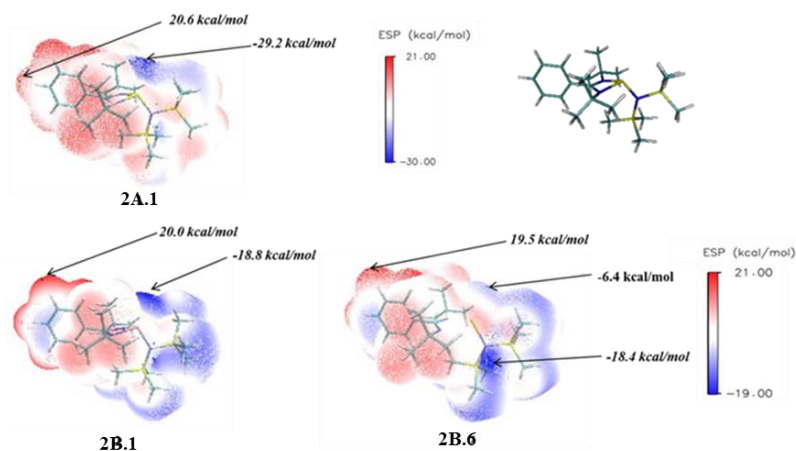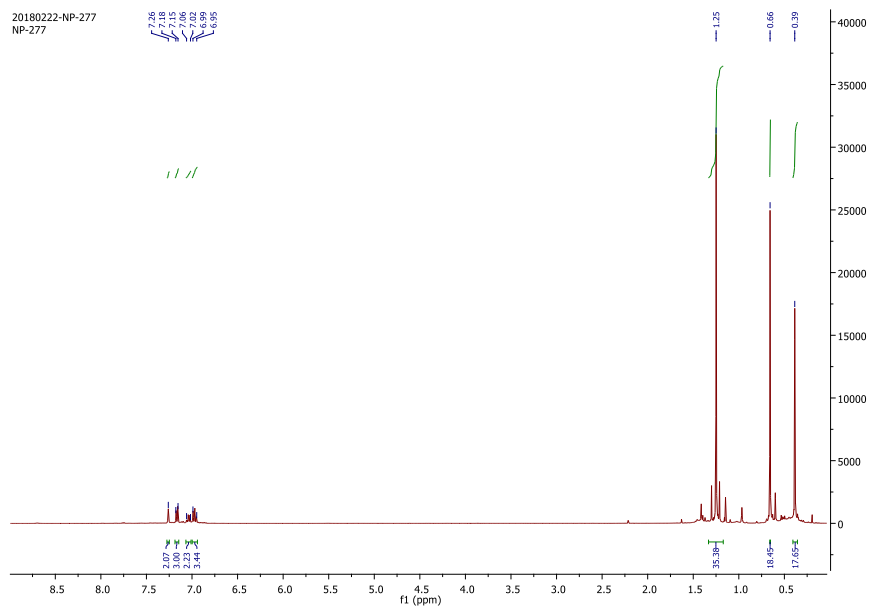
Figure 2B.A.5. *^{1}H NMR (C_6D_6) of **2B.2** and **2B.4***
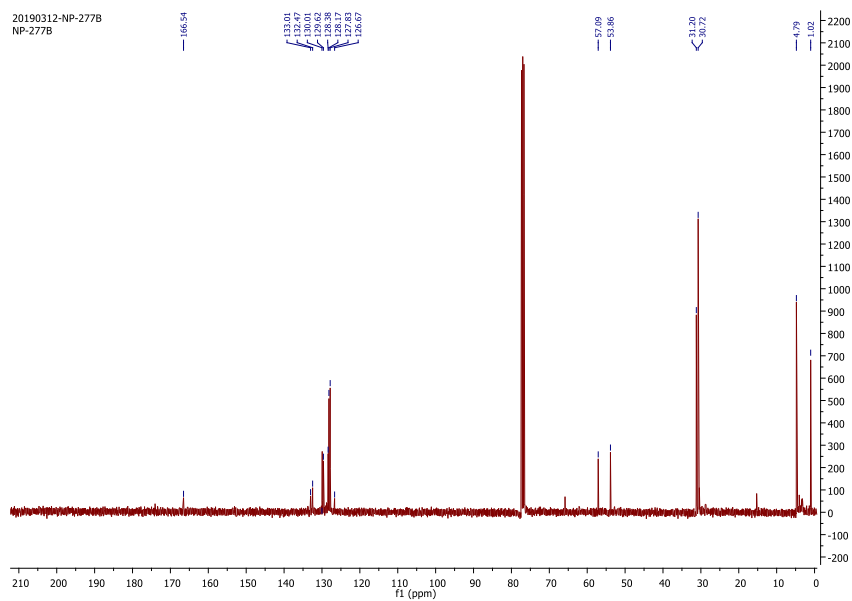
Figure 2B.A.6. *^{13}C NMR (C_6D_6) of **2B.2** and **2B.4***
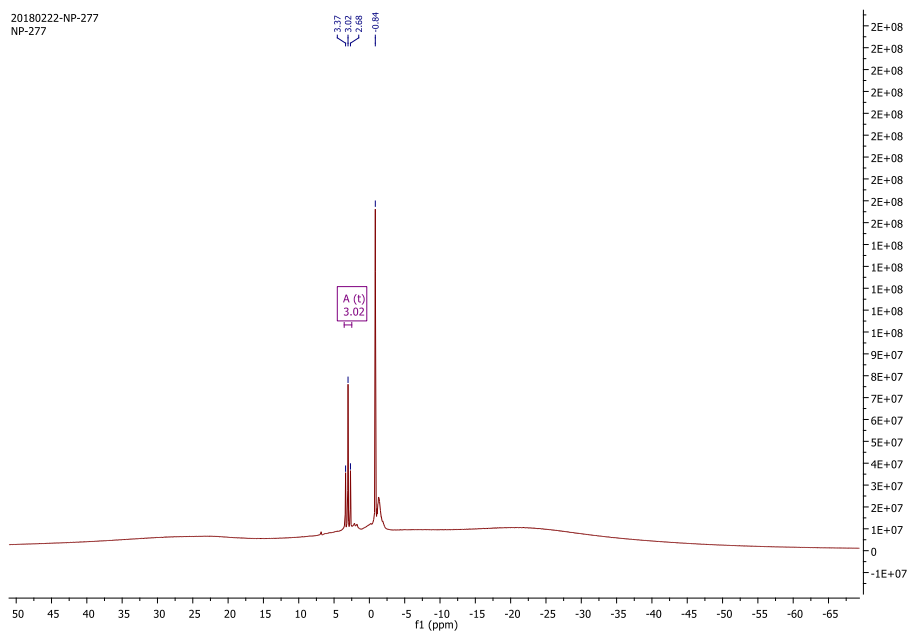
Figure 2B.A.7. *^{11}B NMR (C_6D_6) of* ***2B.2*** *and* ***2B.4***
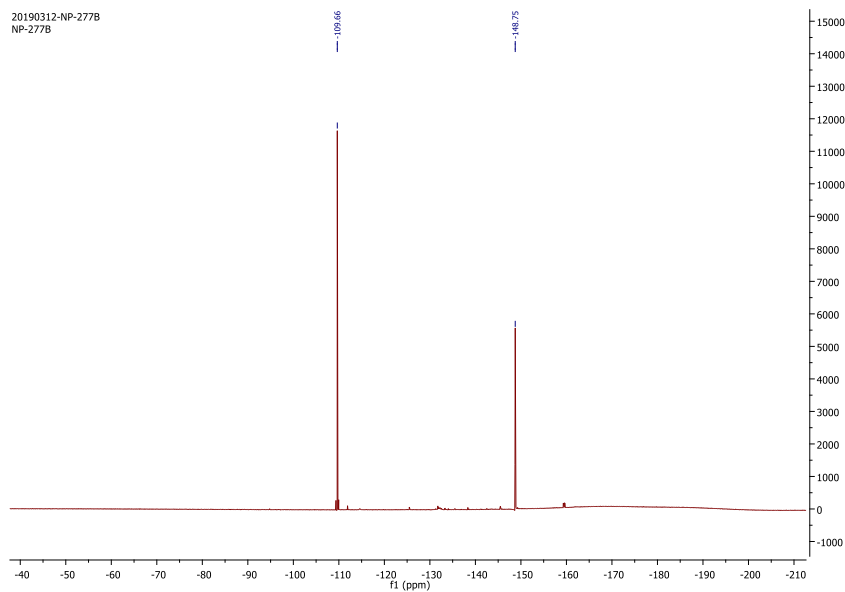
Figure 2B.A.8. *^{19}F NMR (C_6D_6) of* ***2B.2*** *and* ***2B.4***
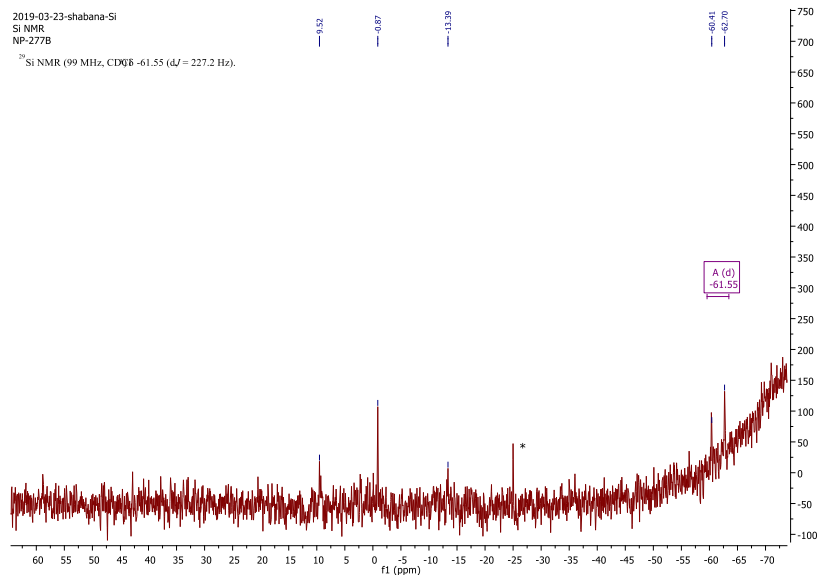
Figure 2B.A.9. ^{29}Si *NMR (C_6D_6) of* *2B.2* *and* *2B.4* *(*= grease peak)*
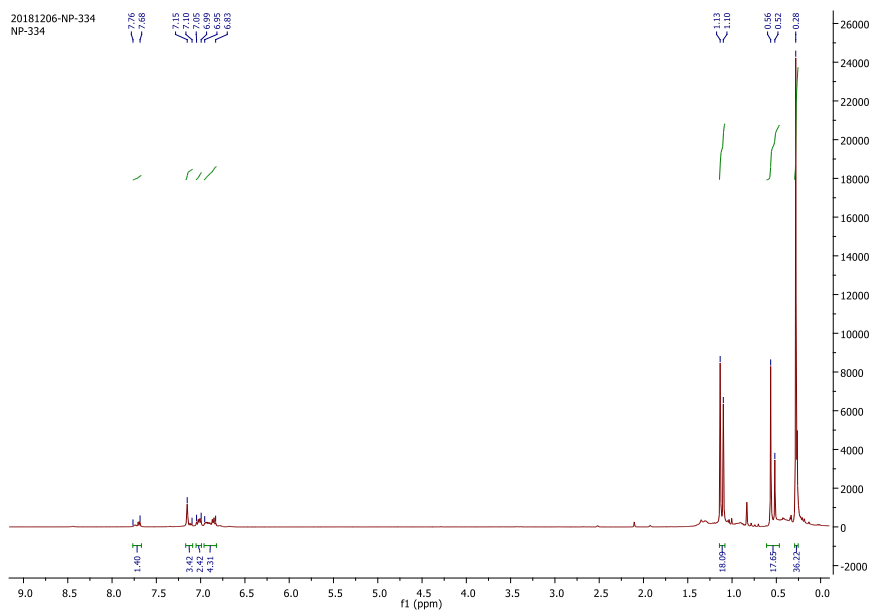
Figure 2B.A.10. ^1H *NMR (C_6D_6) of* *2B.3* *and* *2B.5*
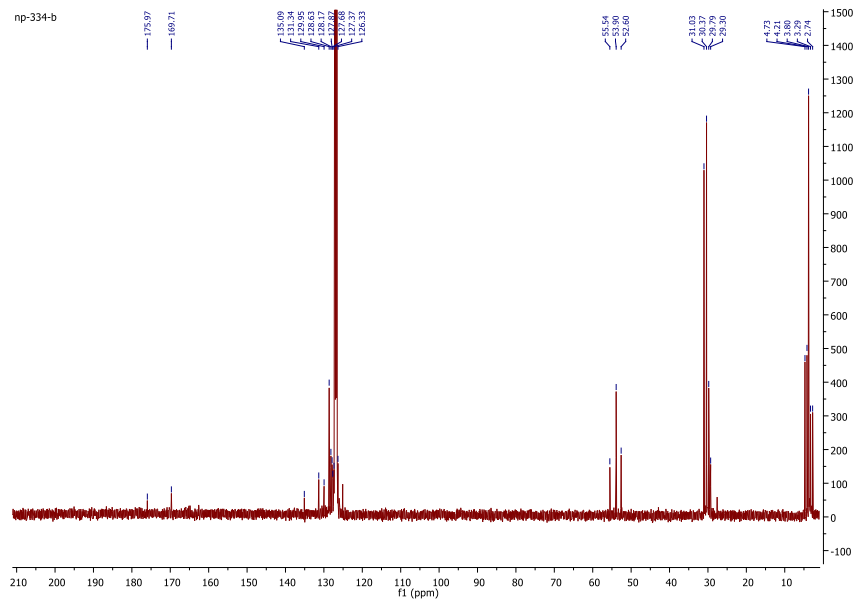
Figure 2B.A.11. *^{13}C NMR (C_6D_6) of **2B.3** and **2B.5***
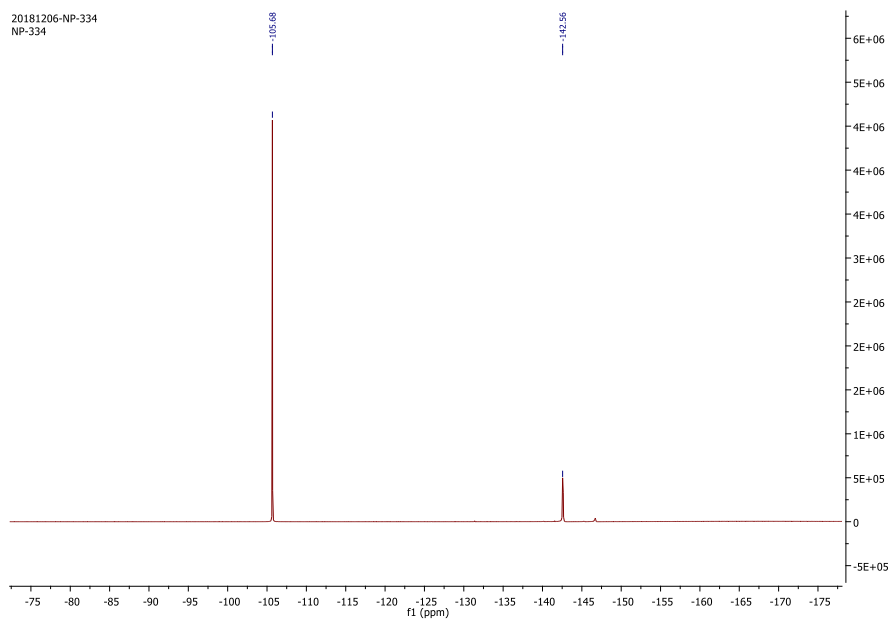
Figure 2B.A.12. *^{19}F NMR (C_6D_6) of **2B.3** and **2B.5***

2019-03-24-shabana-Si
Si NMR
NP-334

—11.40
—4.21
—2.33

*

65 60 55 50 45 40 35 30 25 20 15 10 5 0 -5 -10 -15 -20 -25 -30 -35 -40 -45 -50
f1 (ppm)
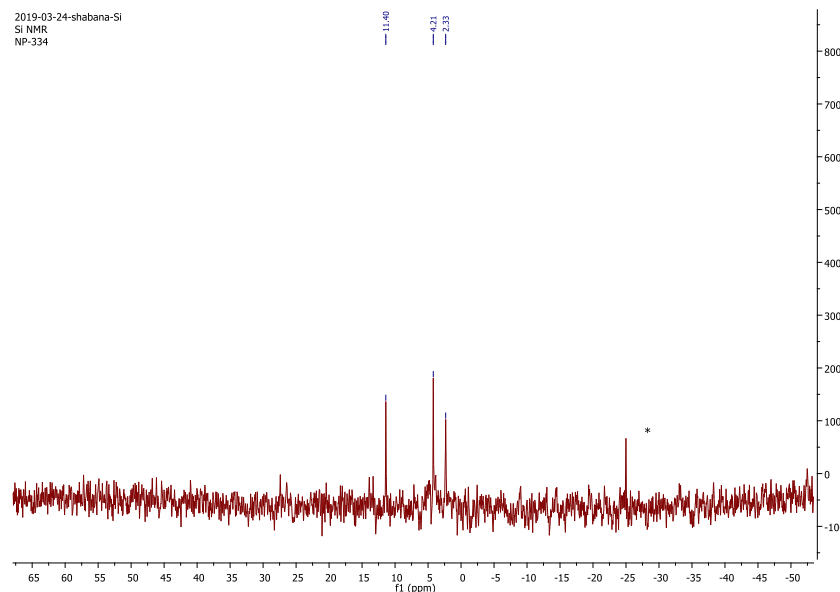
Figure 2B.A.13. *^{29}Si NMR (C$_6$D$_6$) of* ***2B.3*** *and* ***2B.5*** *(*= grease peak)*

20190316-NP-334C
NP-334C

-0.01
-0.10
-0.19
-0.27
-0.84

^{11}B NMR (128 MHz, CD$_6$) δ -0.14 (dd, J = 22.4, 11.2 Hz).

A (dd)
-0.14

20 15 10 5 0 -5 -10 -15 -20 -25 -30
f1 (ppm)
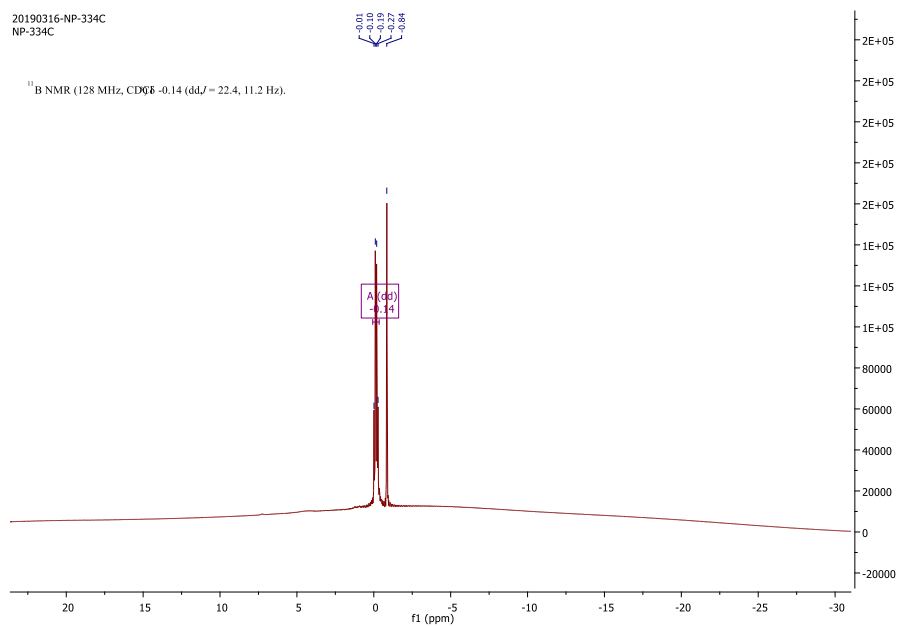
Figure 2B.A.14. *^{11}B NMR (C$_6$D$_6$) of* ***2B.3*** *and* ***2B.5***
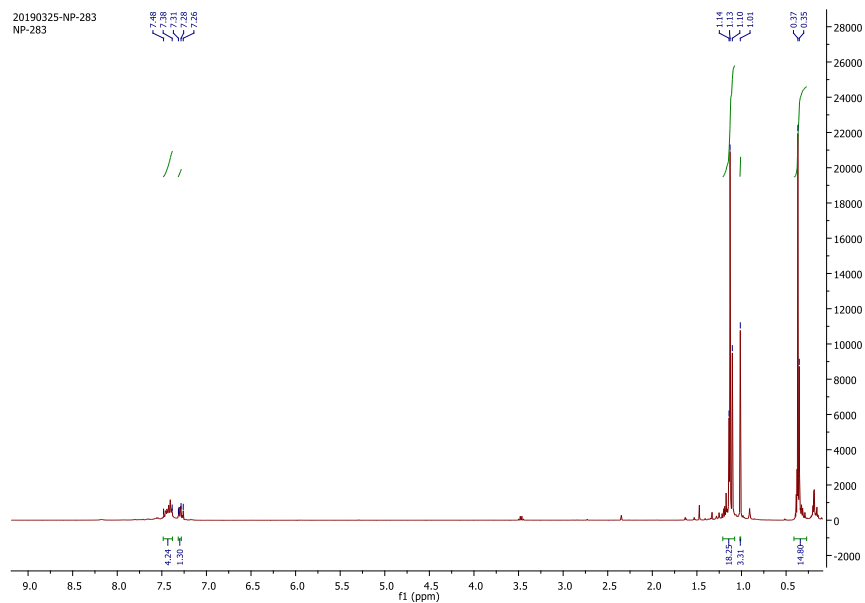
Figure 2B.A.15. *^{1}H NMR (C_6D_6) of **2B.7***
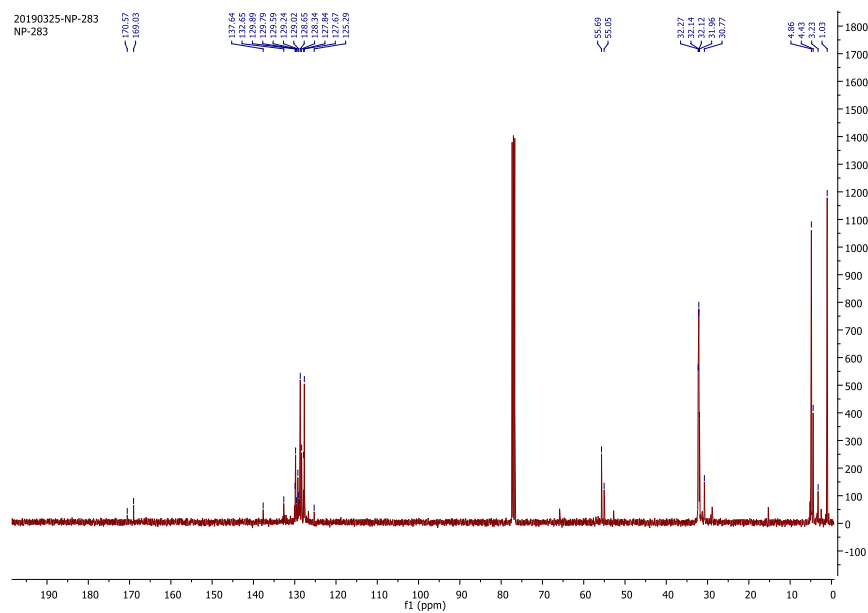
Figure 2B.A.16. *^{13}C NMR (C_6D_6) of **2B.7***
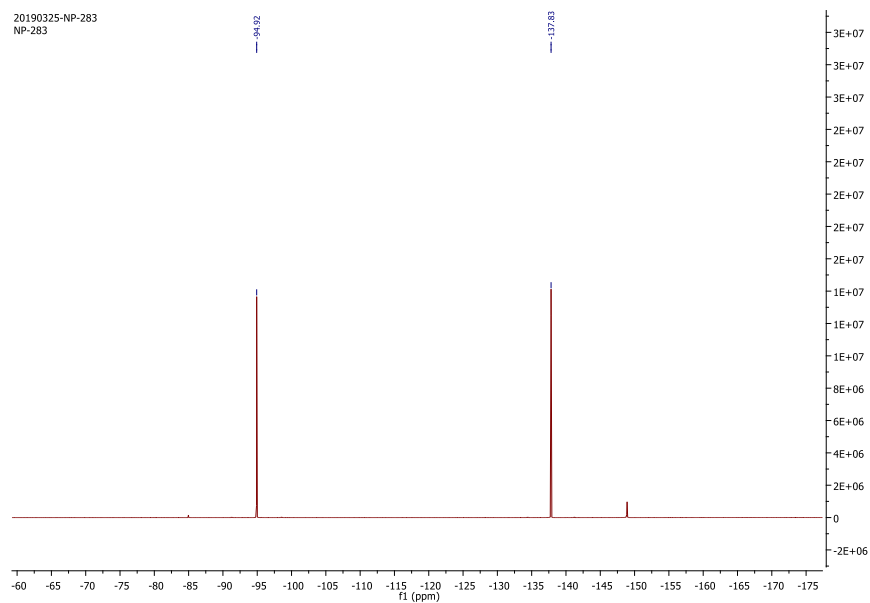
Figure 2B.A.17. ^{19}F NMR (C_6D_6) of **2B.7**
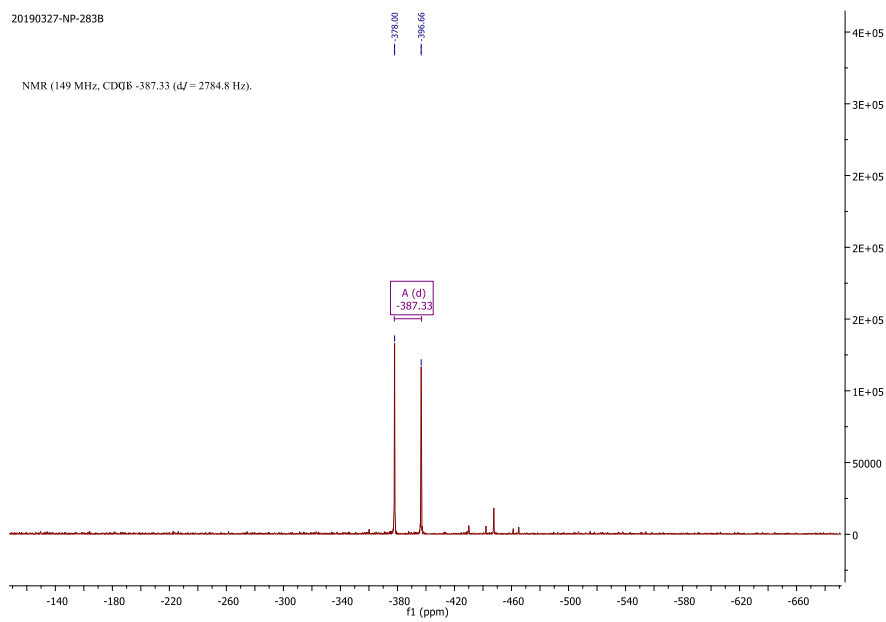
Figure 2B.A.18. ^{119}Sn NMR (C_6D_6) of **2B.7**
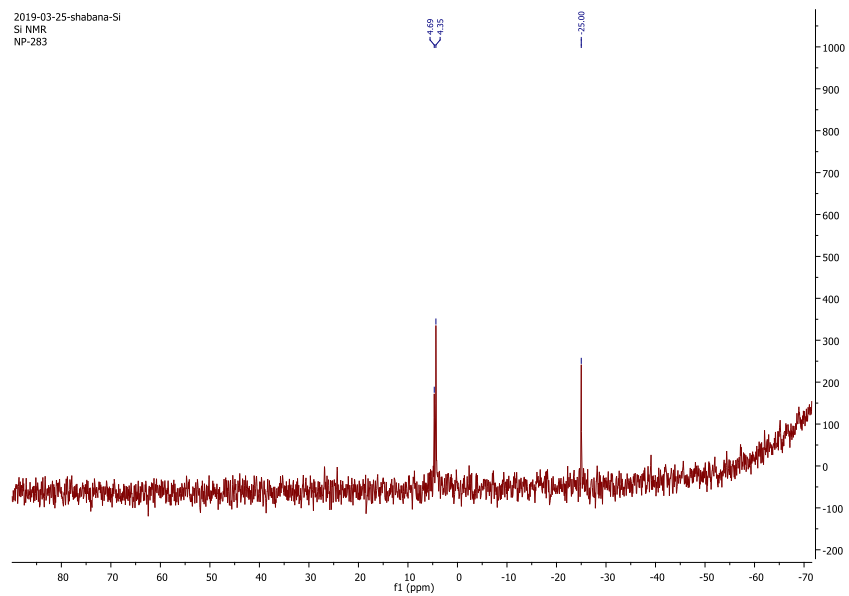
Figure 2B.A.19. *^{11}B NMR (C_6D_6) of* ***2B.7***

Appendix of Chapter 3

Table 3.A.1. *Hapticity calculation of **3.4**, **3.5**, **3.6**, **3.7**, **3.8** and **3.9** by comparing the three shortest M–C (metal-arene) distances, $d_1 < d_2 < d_3$, via the distance ratios ρ_1 and ρ_2.[b]*

	M-C[a] d_1, d_2, d_3	Distance ratio ρ_1	Distance ratio ρ_2	η
3.4	2.11, 2.29, 2.32	1.085	1.099	3
3.5	2.13, 2.22, 2.46	1.042	1.155	2
3.6	2.23, 2.33, 2.43	1.044	1.089	3
3.7	2.16, 2.19, 2.57	1.013	1.189	2
3.8	2.06, 2.31, 2.32	1.121	1.126	3
3.9	2.19, 2.22, 2.42	1.013	1.105	2

[a]$M = Cu$, $d_1 < d_2 < d_3$, $\rho_1 = d_2/d_1$, $\rho_2 = d_3/d_1$, if $\rho_1 \approx \rho_2 \approx 1$ then η^1, if $d_1 \approx d_2 < d_3$, we expect $\rho_2 > \rho_1 \approx 1$ then η^2, and if $\rho_1 \approx \rho_2 \approx 1$ then η^3. [b] *Falceto, A., Carmona, E. & Alvarez, S. Electronic and Structural Effects of Low-Hapticity Coordination of Arene Rings to Transition Metals. Organometallics **2014**, 33, 6660–6668.*

*Table 3.A.2. Crystallographic data for **3.1**, **3.2**, **3.4** and **3.5**.*

	3.1	3.2	3.3	3.4
Chemical formula	$C_{33}H_{59}CuF_6N_3SbSi_3$	$C_{36}H_{56}CuF_6N_3SbSi_3$	$C_{40}H_{56}Cl_2CuF_6N_2Sb$	$C_{33}H_{42}CuF_6N_2$ Sb
Formula weight	881.39	914.39	935.08	766.00
Temperature	100(2)	100(2)	100(2)	100(2)
Wavelength	0.71073	0.71073	0.71073	0.71073
Crystal system	monoclinic	monoclinic	monoclinic	monoclinic
Space group	*P 2₁/c*	*P 2₁/n*	*P 2₁/n*	*P 2₁/c*
Unit cell dimentions	a=13.605(4) Å	a=14.617(7) Å	a=10.469(3) Å	a=13.3555(16) Å

	b=14.057(4) Å	b=14.759(7) Å	b=20.541(5) Å	b=13.9173(16) Å
	c=21.790(8) Å	c=21.243(10) Å	c=20.041(5) Å	c=18.181(2) Å
	α=90°	α= 90°	α= 90°	α=90°
	β=107.833(9)°	β= 107.874(10)°	β=104.289(7)°	β=102.245(3)°
	γ=90°	γ=90°	γ=90°	γ=90°
Volume	3967(2) Å^3	4361(4) Å^3	4176.4(18) Å^3	3302.4(7) Å^3
Z	4	4	4	4
Density (calculated)	1.476 g/cm^3	1.393 g/cm^3	1.487 g/cm^3	1.541 g/cm^3
Absorption coefficient	1.363 mm^{-1}	1.242 mm^{-1}	1.341 mm^{-1}	1.521 mm^{-1}
F(000)	1816	1876	1912	1552
Theta range for data collection	2.44 to 25.25°	2.44 to 25.25°	2.24 to 25.25	2.26 to 25.25°
Index ranges	-16<=h<=16 -16<=k<=16 -26<=l<=26	-17<=h<=17 -17<=k<=17 -25<=l<=25	-12<=h<=12 -24<=k<=24 -24<=l<=24	-16<=h<=16 -16<=k<=16 -21<=l<=21
Reflections collected	182758	77830	142079	104497
Independent reflections	7182[R(int)=0.1797]	7893[R(int)=0.1631]	7557[R(int)=0.1114]	5981[R(int)=0.1502]
Coverage of independent reflections	99.9%	99.9%	99.9%	99.9%
Function minimized	$\Sigma\ w(Fo^2 - Fc^2)^2$	$\Sigma\ w(Fo^2 - Fc^2)^2$	$\Sigma\ w(Fo^2 - Fc^2)^2$	$\Sigma\ w(Fo^2 - Fc^2)^2$
Data/ restraints/ parameters	7182/ 0/ 442	7893/ 18/ 451	7557/ 0/ 483	5981/ 0/ 396
Goodness-of-fit on F2	1.094	1.009	1.034	1.027

Nasrina Parvin

Δ/ σ max	0.012	0.001	0.001	0.001
Final R indices	4904 data; [I>2σ(I)] R_1= 0.0382, wR_2= 0.0642	5006 data; [I>2σ(I)] R_1= 0.0586, wR_2= 0.1179	5835 data; [I>2σ(I)] R_1= 0.0362, wR_2= 0.0760	4129 data; [I>2σ(I)] R_1= 0.0516, wR_2= 0.0932
	all data, R_1= 0.0834, wR_2= 0.0772	all data, R_1= 0.1162, wR_2= 0.1441	all data, R_1= 0.0587, wR_2= 0.0861	all data, R_1= 0.0958, wR_2= 0.1086
Largest diff. peak and hole	0.817 and -0.657 e$Å^{-3}$	1.218 and -0.860 e$Å^{-3}$	1.309 and -0.601 e$Å^{-3}$	1.001 and -0.937 e$Å^{-3}$
R. M. S deviation from mean	0.111 e$Å^{-3}$	0.127 e$Å^{-3}$	0.091 e$Å^{-3}$	0.108 e$Å^{-3}$

Table 3.A.3. *Crystallographic data for* **3.6**, **3.7**, *and* **3.8**.

	3.6	3.7	3.8
Chemical formula	$C_{28}H_{49}CuF_6N_3SbSi_3$	$C_{29}H_{51}CuF_6N_3SbSi_3$	$C_{34}H_{44}CuF_6N_2Sb$
Formula weight	811.26	825.29	780.00
Temperature	100(2)	100(2)	100(2)
Wavelength	0.71073	0.71073	0.71073
Crystal system	orthorhombic	monoclinic	monoclinic
Space group	$P2_12_12_1$	*P*n	*Cc*
Unit cell dimentions	a=11.762(6) Å	a=9.226(7) Å	a=24.087(2) Å
	b=14.725(7) Å	b=11.541(9) Å	b=9.1915(9) Å
	c=21.300(9)Å	c=18.052(14) Å	c=19.165(3) Å
	α=90°	α=90°	α=90°

Nasrina Parvin

	$\beta=90°$	$\beta=98.414(18)°$	$\beta=124.966(2)°$
	$\gamma=90°$	$\gamma=90°$	$\gamma=90°$
Volume	3689(3) Å³	1901(2) Å³	3477.2(7) Å³
Z	4	2	4
Density (calculated)	1.461 g/cm³	1.442 g/cm³	1.490 g/cm³
Absorption coefficient	1.458 mm⁻¹	1.416 mm⁻¹	1.446 mm⁻¹
F(000)	1656	844	1584
Theta range for data collection	2.22 to 25.25°	2.23 to 24.00°	2.20 to 25.25°
Reflections collected	81475	39863	43896
Independent reflections	6657[R(int)=0.0983]	5967[R(int)=0.2784]	6285[R(int)=0.1028]
Coverage of independent reflections	99.9%	99.9%	100%
Data/ restraints/ parameters	6657/ 24/ 392	5967/ 98/ 403	6285/ 8/ 406
Goodness-of-fit on F2	1.049	1.012	1.003
Δ/ σ max	0.001	0.023	0.004
Final R indices	5034 data; [I>2σ(I)] R_1= 0.0442, wR_2= 0.0931	2797 data; [I>2σ(I)] R_1= 0.0841, wR₂= 0.1605	4635 data; [I>2σ(I)] R_1= 0.0449, wR_2= 0.0735
	all data, R_1= 0.0748, wR_2= 0.1065	all data, R_1= 0.2138, wR_2= 0.2103	all data, R_1= 0.0840, wR_2= 0.0860
Largest diff. peak and hole	0.567 and -0.420 eÅ⁻³	0.959 and -0.528 eÅ⁻³	0.724 and -0.446 eÅ⁻³

Nasrina Parvin

R. M. S deviation from mean	0.073 eÅ^{-3}	0.111 eÅ^{-3}	0.085 eÅ^{-3}

Table 3.A.4. *Crystallographic data for **3.9**, **3.11**, and **3.12**.*

	3.9	3.11	3.12
Chemical formula	$C_{35}H_{46}CuF_6N_2Sb$	$C_{49}H_{79}Cl_2CuF_6N_5SbSi_3$	$C_{38}H_{50}CuF_6N_4Sb$
Formula weight	794.03	1192.63	862.11
Temperature	100(2)	100(2)	100(2)
Wavelength	0.71073	0.71073	0.71073
Crystal system	orthorhombic	monoclinic	orthorhombic
Space group	*Pbca*	*P2₁/n*	*Pnma*
Unit cell dimentions	a=18.355(3) Å	a= 21.510(7) Å	a=13.623(5) Å
	b=18.334(3) Å	b= 12.624(4) Å	b=14.768(5) Å
	c=42.496(6) Å	c= 21.590(7) Å	c=20.118(7) Å
	α= 90°	α=90°	α=90°
	β=90°	β= 96.299(9)°	β=90°
	γ=90°	γ=90°	γ=90°
Volume	14301(4) Å³	5827(3) Å³	4047(2) Å³
Z	18	4	4
Density (calculated)	1.660 g/cm³	1.359 g/cm³	1.415 g/cm³
Absorption coefficient	1.583 mm^{-1}	1.037 mm^{-1}	1.251 mm^{-1}
F(000)	7272	2472	1760
Theta range for data collection	2.22 to 25.25	2.15 to 25.25°	2.27 to 25.24°

Reflections collected	177708	109049	139751
Independent reflections	12935 [R(int)= 0.1740]	10536 [R(int)= 0.0648]	3812 [R(int)= 0.1906]
Coverage of independent reflections	99.9%	99.9%	99.9%
Data/ restraints/ parameters	12935/ 0/ 831	10536/ 0/ 624	3812/ 0/ 250
Goodness-of-fit on F2	1.039	1.047	1.001
Δ/ σ max	0.002	0.058	0.001
Final R indices	7894 data; [I>2σ(I)] R_1= 0.0479, wR_2= 0.0681	8198 data; [I>2σ(I)] R_1= 0.0531, wR_2= 0.1267	2659 data; [I>2σ(I)] R_1= 0.0394, wR_2= 0.0588
	all data, R_1= 0.1107, wR_2= 0.0848	all data, R_1= 0.0745, wR_2= 0.1449	all data, R_1= 0.0787, wR_2= 0.0712
Largest diff. peak and hole	0.941 and -0.950 eÅ^{-3}	1.180 and -1.616 eÅ^{-3}	0.751 and -0.651 eÅ^{-3}
R. M. S deviation from mean	0.100 eÅ^{-3}	0.138 eÅ^{-3}	0.092 eÅ^{-3}

Table 3.A.5. *Charges by natural population analysis (M06/def2-TZVPP//BP86/def2-SVP) on atoms and groups of atoms in the optimized geometry of complexes* **3.5** *and* **3.6** *($L^1L^2SiCu(L)^+$) as well as* **3.7** *and* **3.8** *(NHCCu(L)$^+$), where L^1 = N(SiMe$_3$)$_2$, L^2 = (Ph)C(Nt-Bu)$_2$, NHC = N-heterocyclic carbene with (i-Pr)$_2$Ph substituent on each N and L = Tol (C$_6$H$_5$(CH$_3$)) and m-Xyl (1,3 C$_6$H$_4$(CH$_3$)$_2$).*

$L^1L^2SiCu(L)^+$	L^1	L^2	Si	Cu	L
3.5	-0.53	-0.36	1.43	0.27	0.18

3.6	-0.53	-0.35	1.43	0.29	0.16
NHCCu(L)⁺	NHC	C7	Cu	L	--
3.7	0.33	0.10	0.52	0.16	--
3.8	0.32	0.10	0.51	0.17	--

Figure 3.A.1. *NCI plots of* **3.1**, **3.2**, **3.4** *and* **3.5**.

3.1

3.2

3.4

3.5

20170927-NP-166
NP-166

7.5540
7.4215
7.3634
7.3071
5.2511
2.3454
1.0601
0.2753
0.2046

4.34
1.23
18.00
17.95
8.99
8.84
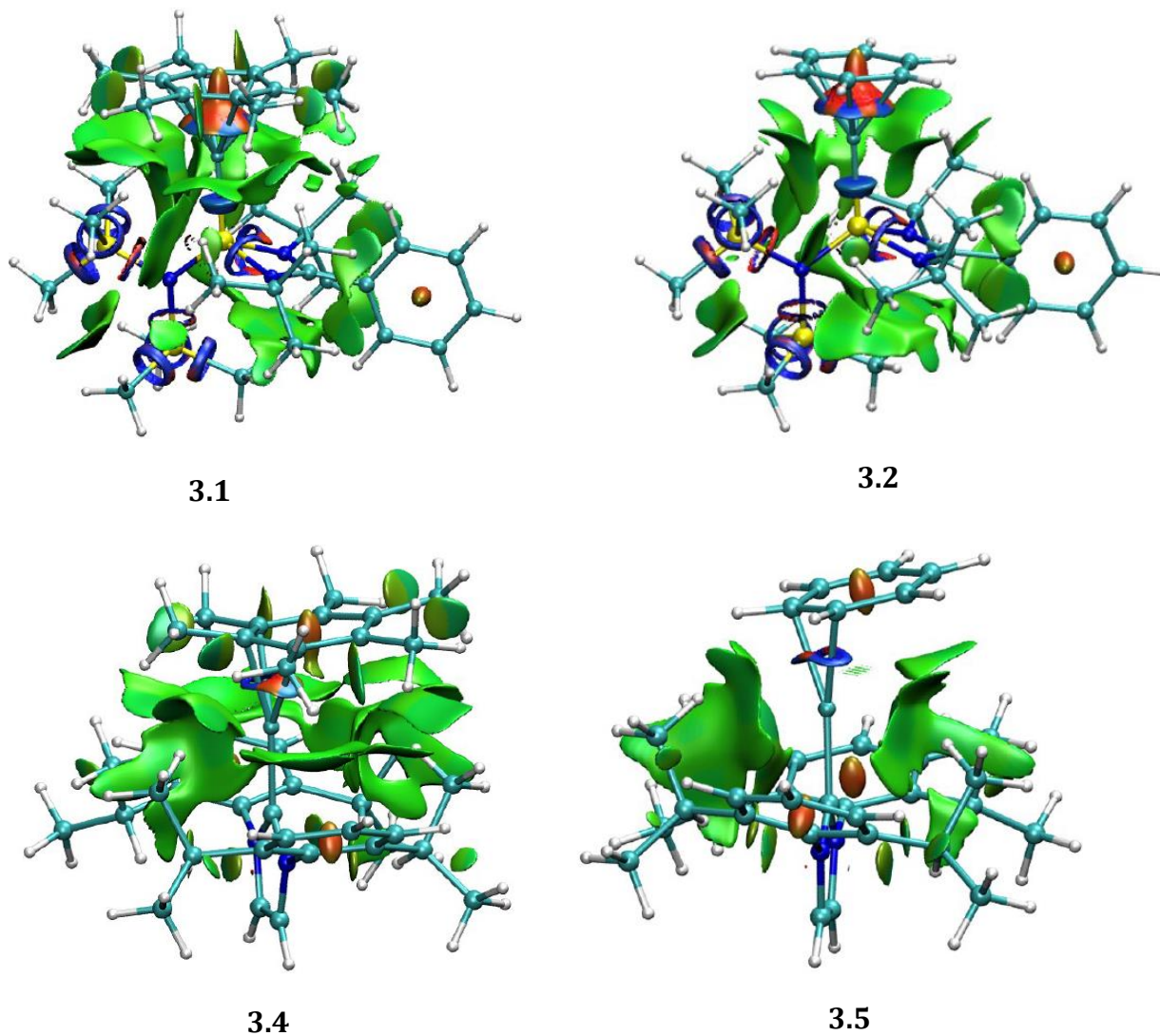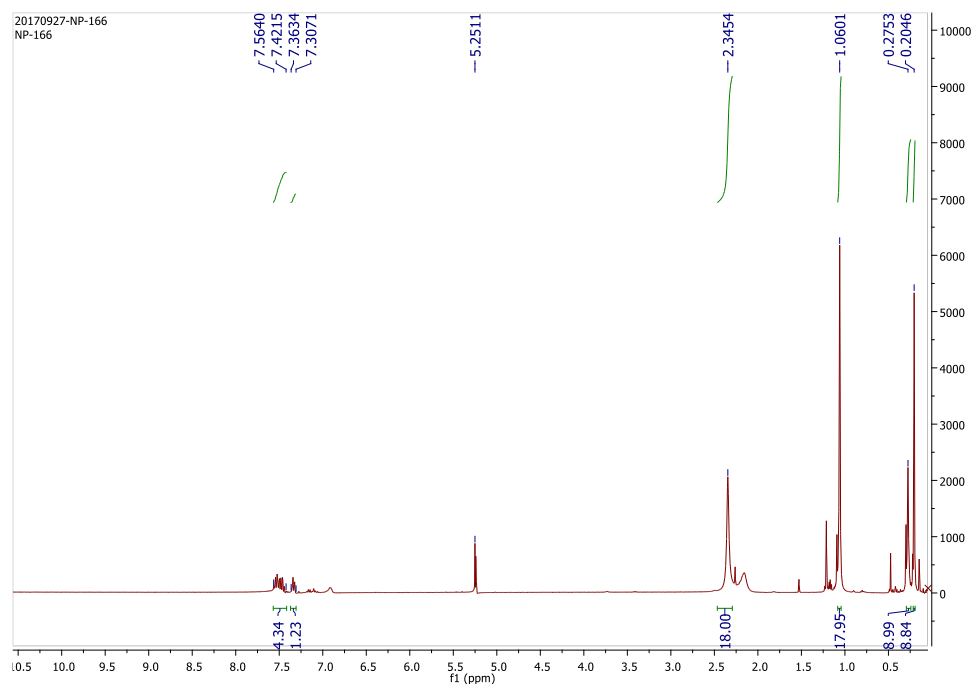
Figure 3.A.2 ¹H NMR (CDCl₃) of **3.1**

20170927-NP-166
NP-166

131.3187
130.5607
129.8948
128.8666
128.4703
127.9234
126.1089
54.6081
31.5396
17.5889
5.1536
4.5999
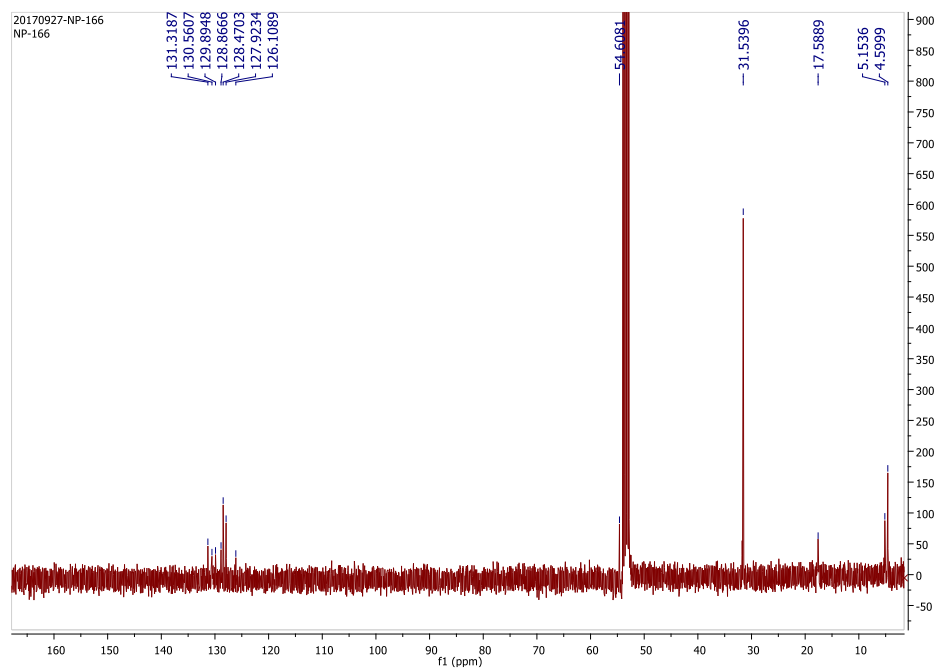
Figure 3.A.3 ¹³C NMR (CDCl₃) of **3.1**
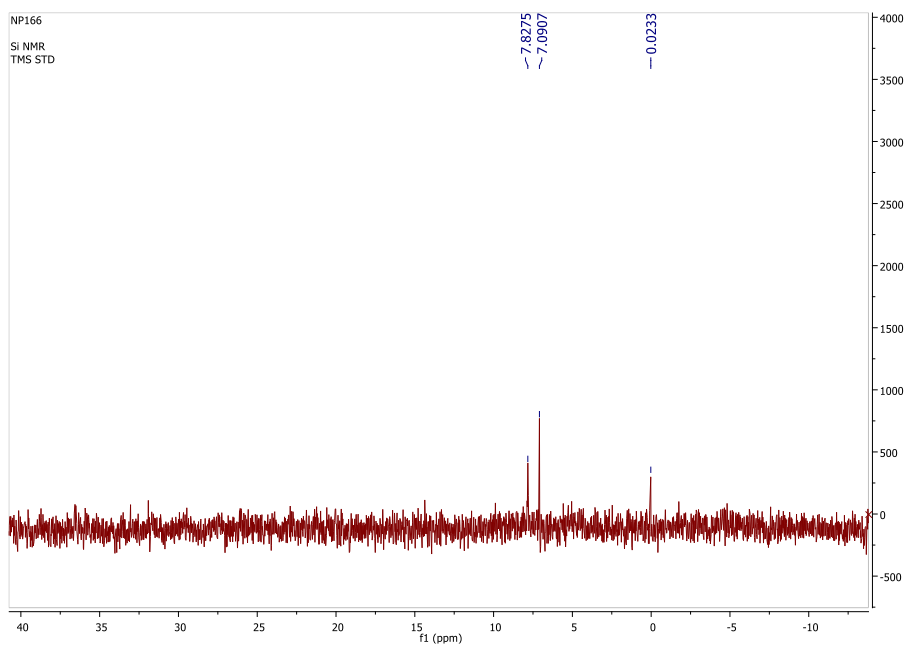
Figure 3.A.4 ^{29}*Si NMR (CDCl$_3$) of* **3.1**
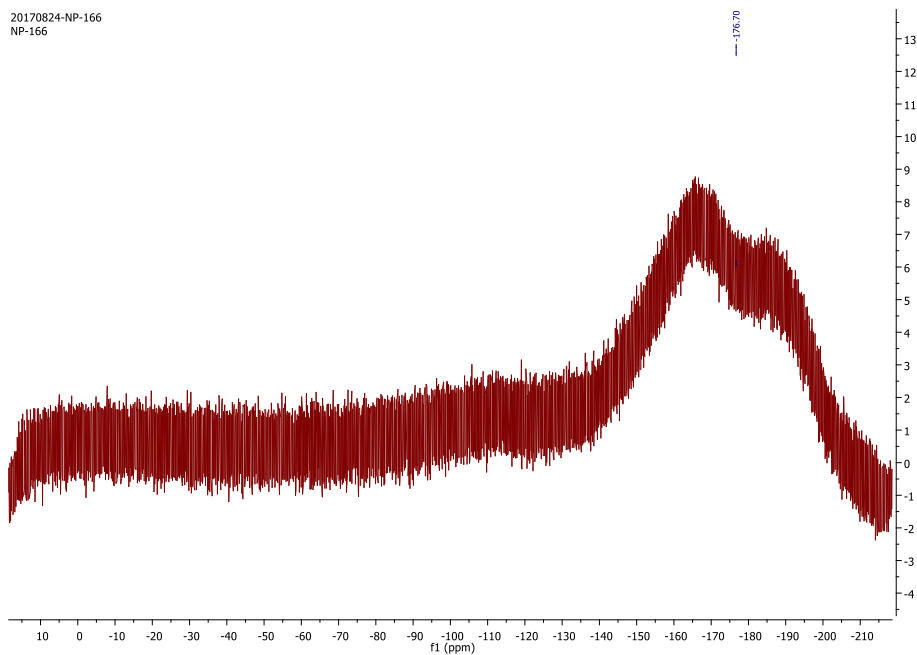
Figure 3.A.5 ^{19}*F NMR (CDCl$_3$) of* **3.1**
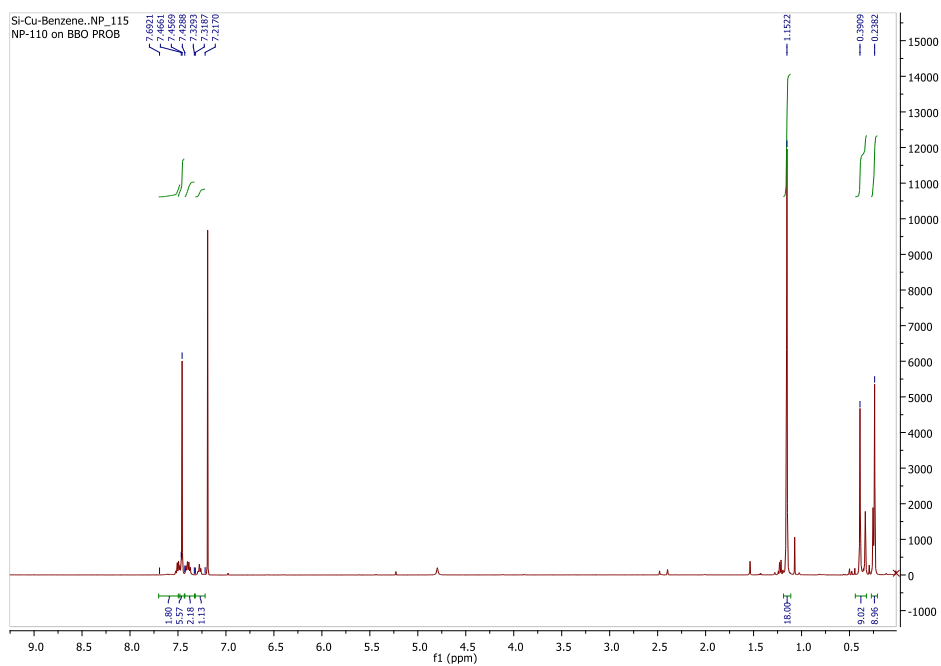
Figure 3.A.6 *^{1}H NMR (CDCl$_3$) of **3.2***
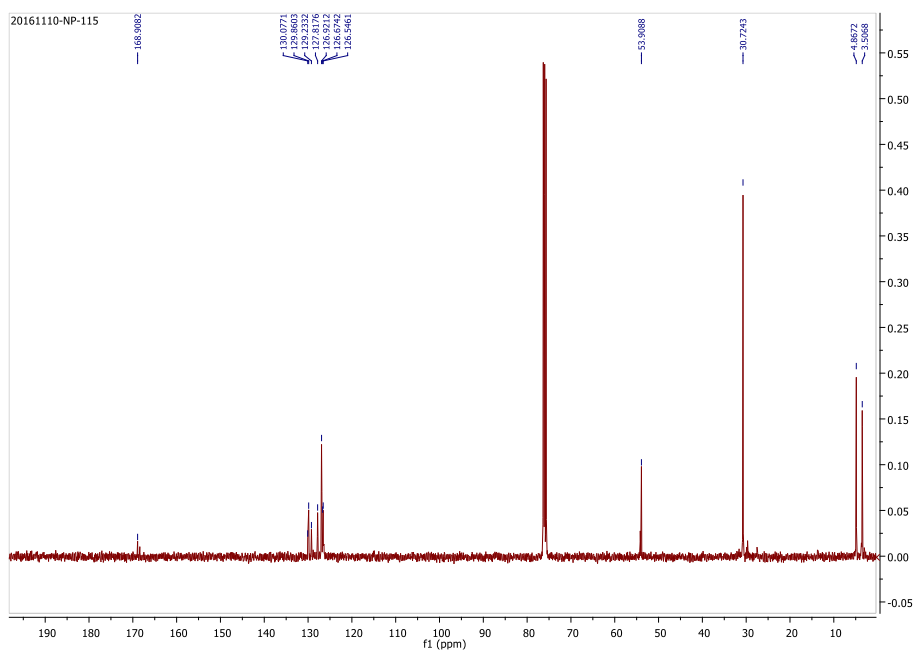
Figure 3.A.7 *^{13}C NMR (CDCl$_3$) of **3.2***
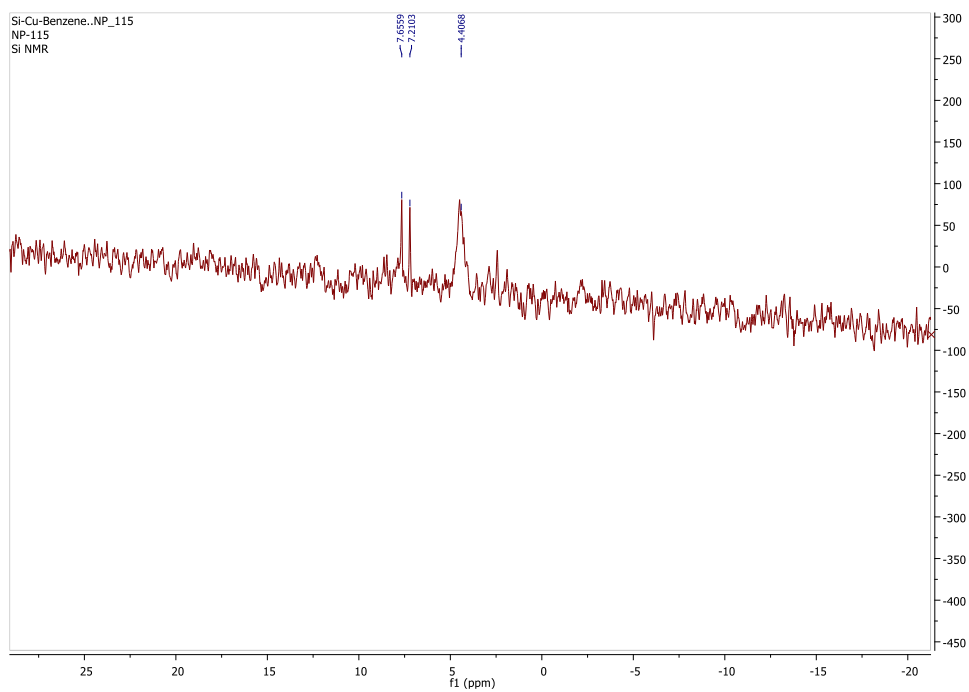
Figure 3.A.8 *^{29}Si NMR (CDCl$_3$) of **3.2***
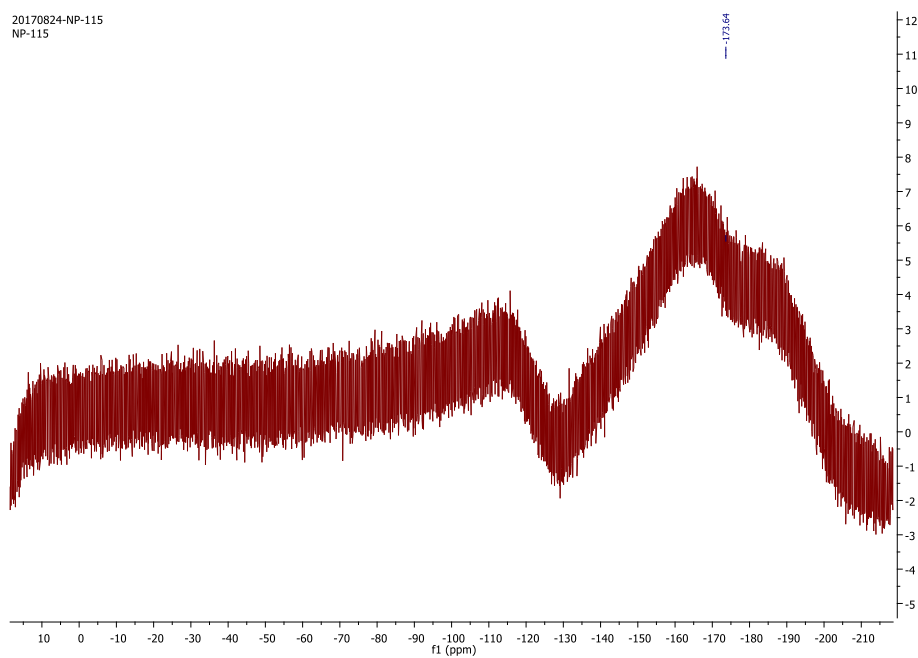
Figure 3.A.9 *^{19}F NMR (CDCl$_3$) of **3.2***

20170308-NP-165
NP-165

^{1}H NMR (400 MHz, CDCl$_3$) δ 7.52 (t, J = 7.8 Hz, 1H), 7.29 (d, J = 7.8 Hz, 1H), 1.10 (dd, J = 9.7, 6.9 Hz, 1H).

C (t)
7.52

B (d)
7.29

A (dd)
1.10
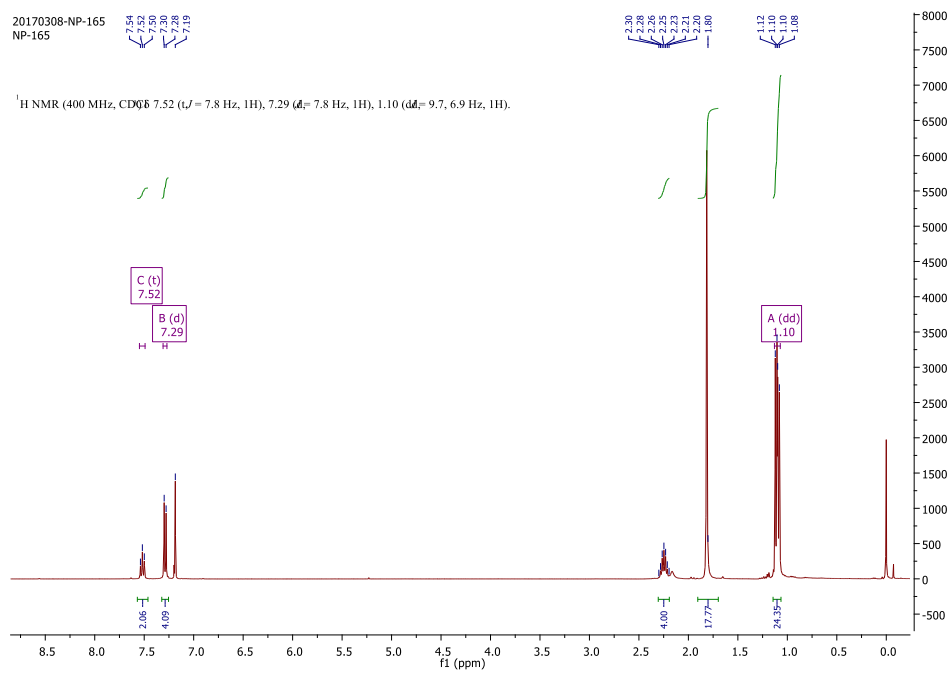
Figure 3.A.10 *^{1}H NMR (CDCl$_3$) of* ***3.4***

20170308-NP-165
NP-165
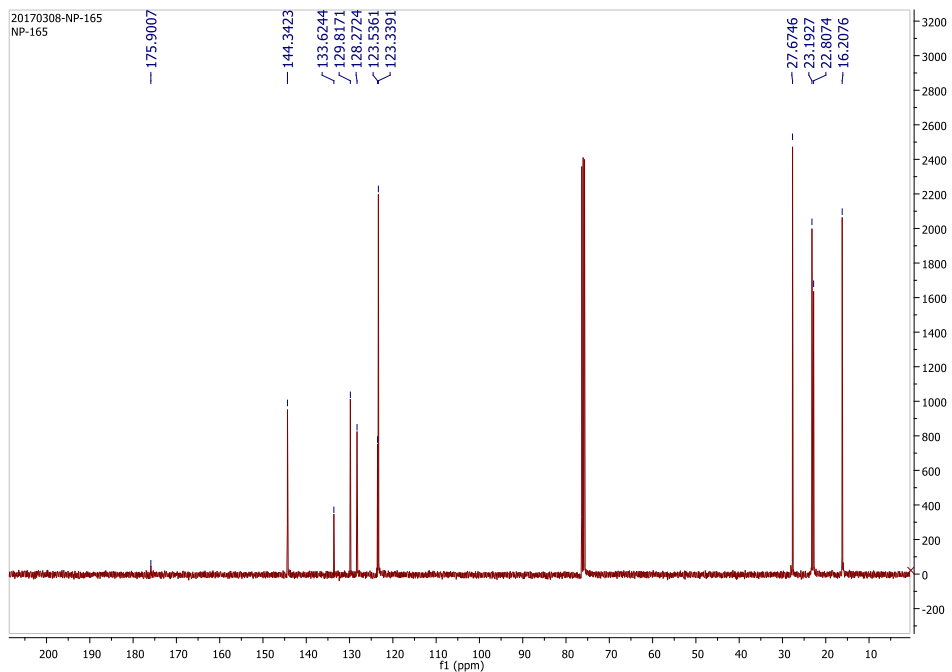
Figure 3.A.11 *^{13}C NMR (CDCl$_3$) of* ***3.4***
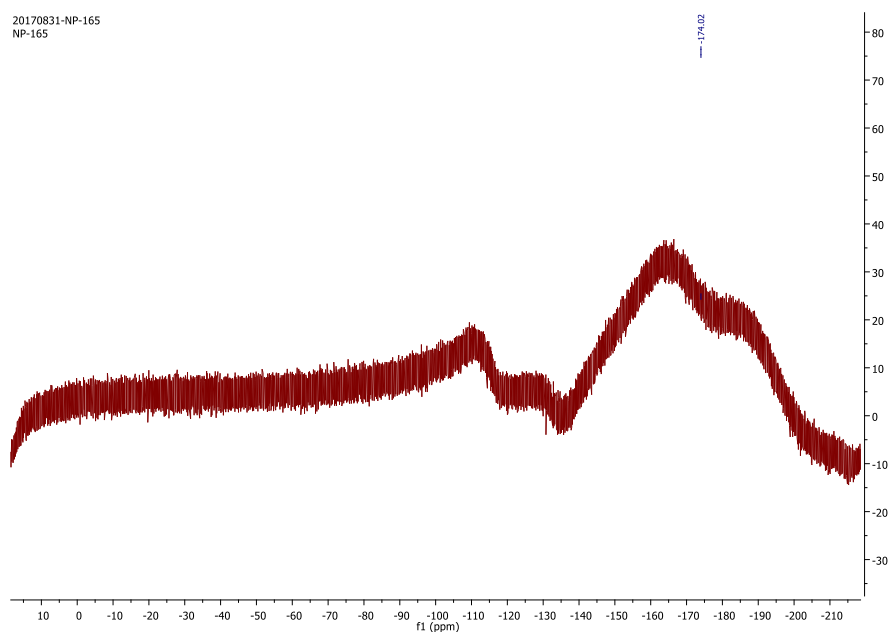
Figure 3.A.12 ^{19}F NMR (CDCl$_3$) of **3.4**
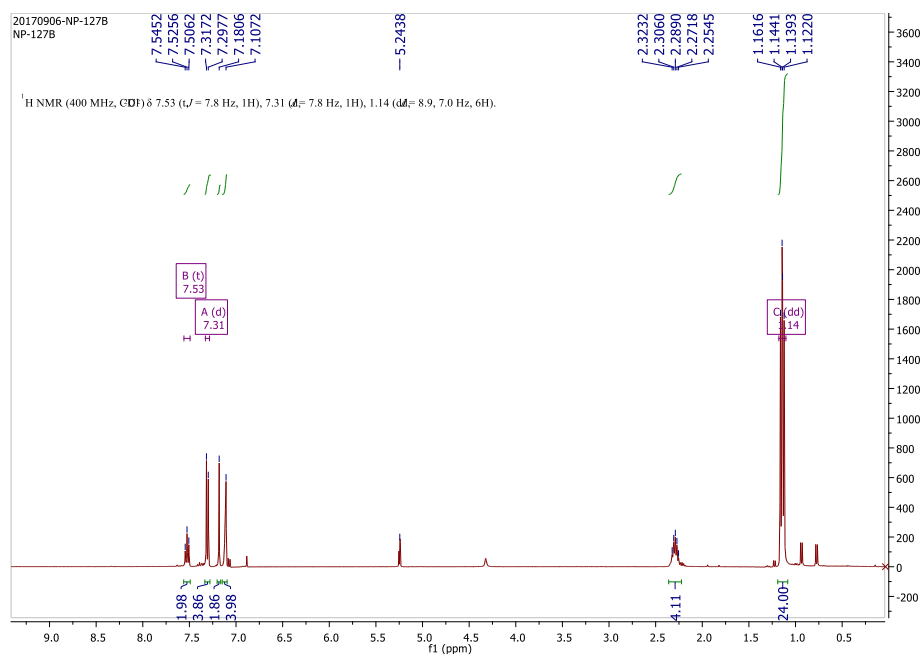
Figure 3.A.13 ^{1}H NMR (CDCl$_3$) of **3.5**
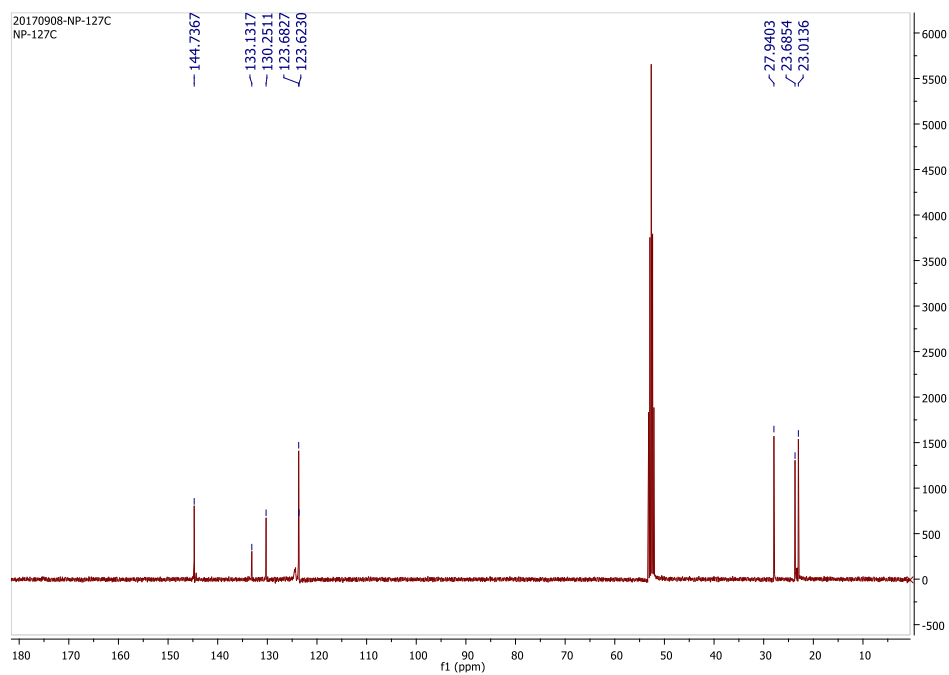
Figure 3.A.14 *¹³C NMR (CDCl₃) of **3.5***
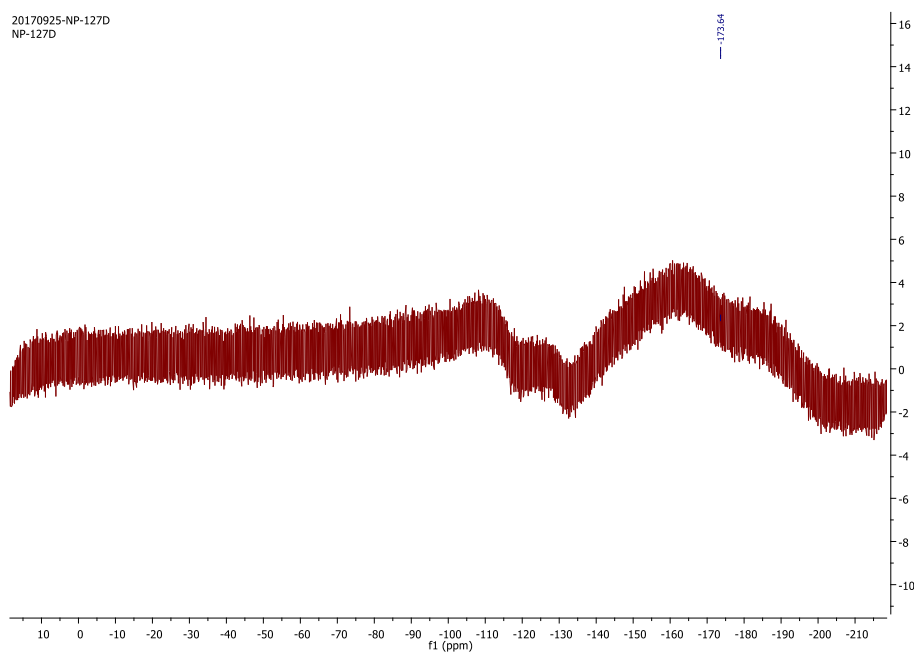
Figure 3.A.15 *¹⁹F NMR (CDCl₃) of **3.5***
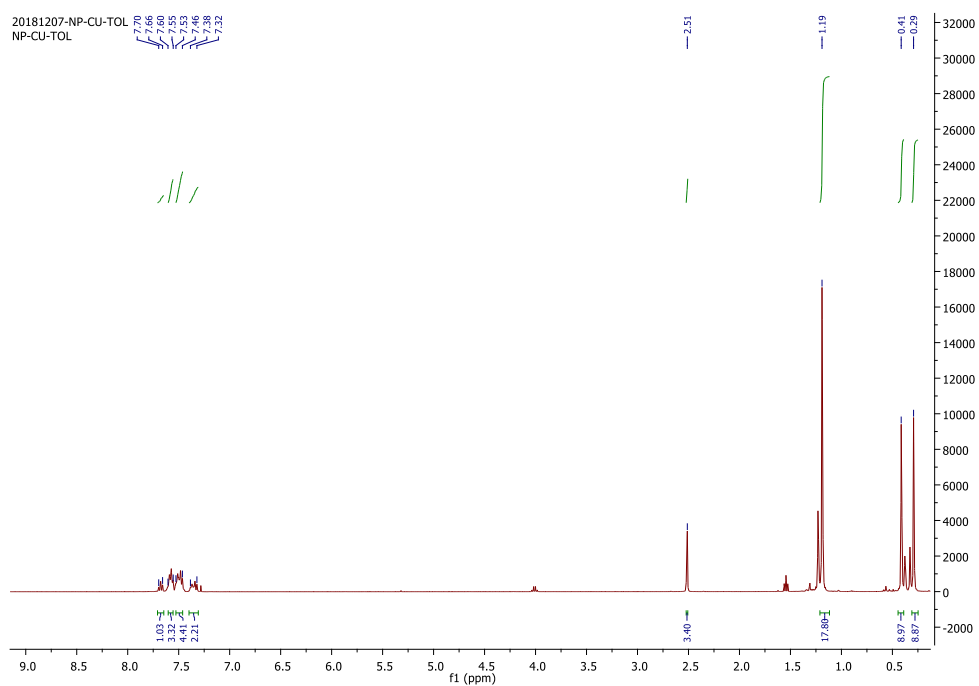
Figure 3.A.16 *¹H NMR (CDCl₃) of* **3.6**
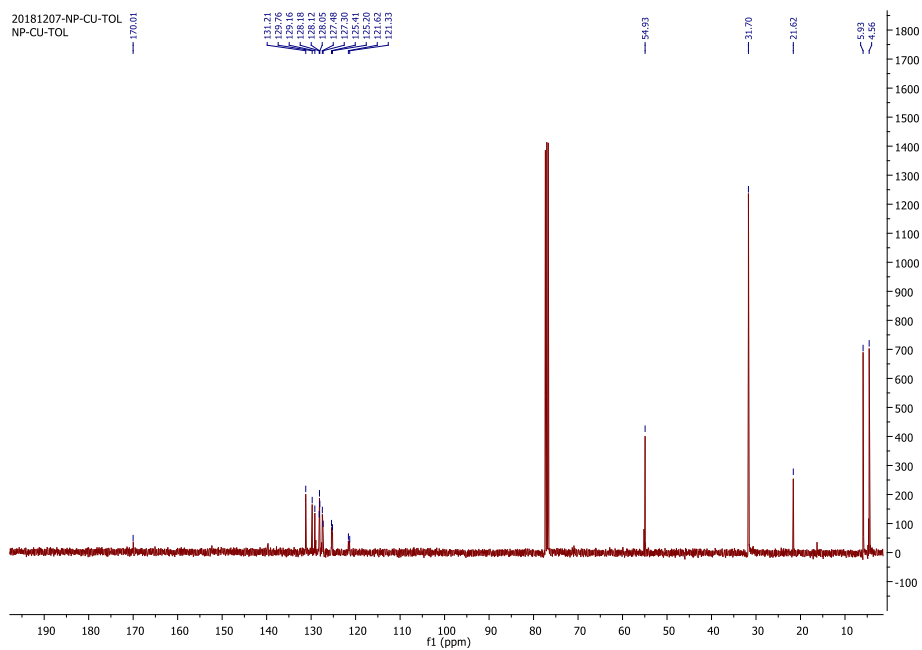
Figure 3.A.17 *¹³C NMR (CDCl₃) of* **3.6**

20181218-shabana-Si
Si NMR
NP-110E
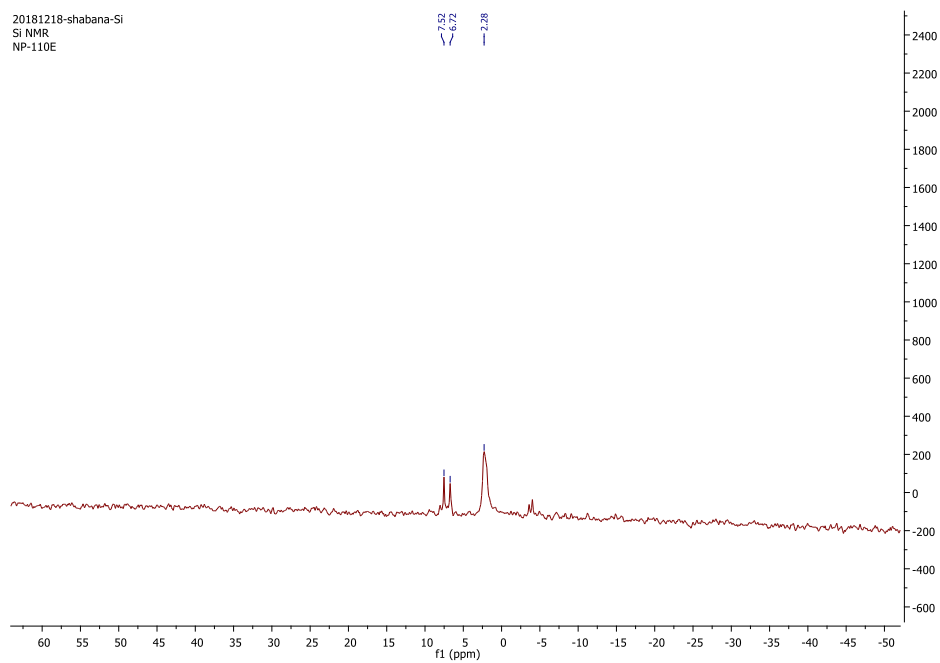
Figure 3.A.18 ²⁹*Si NMR (CDCl₃) of* **3.6**

20181207-NP-CU-TOL
NP-CU-TOL
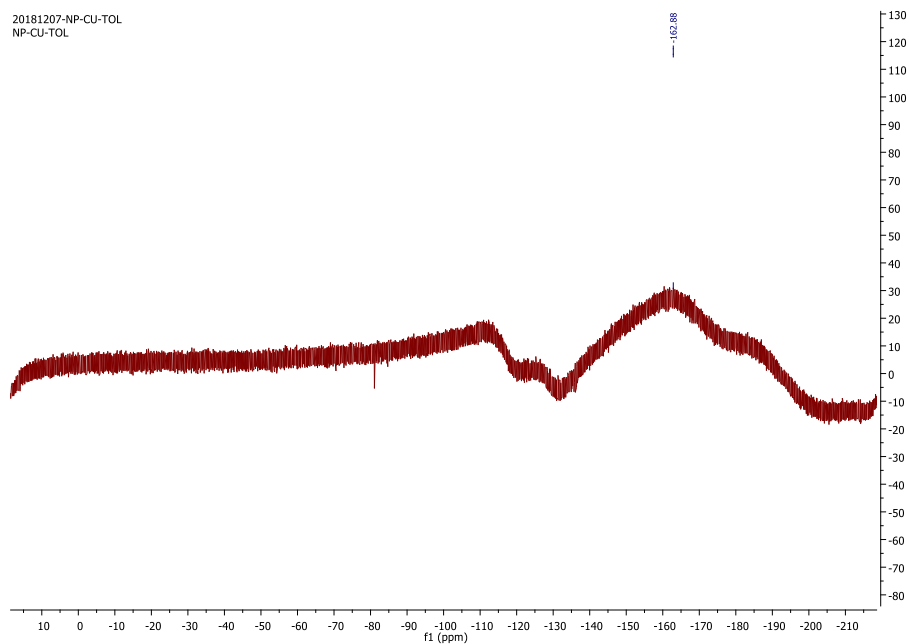
Figure 3.A.19 ¹⁹*F NMR (CDCl₃) of* **3.6**
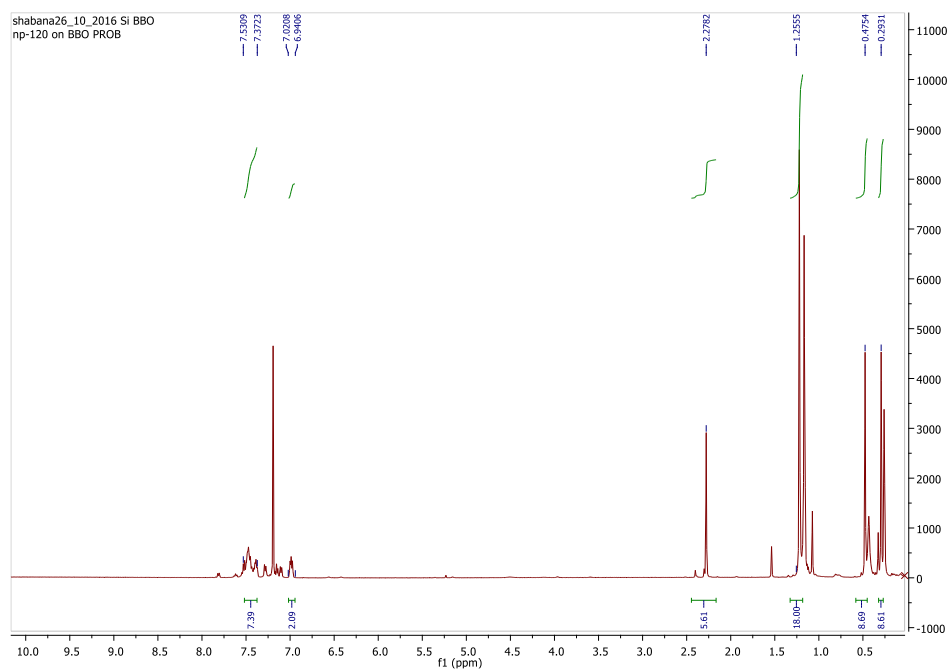
Figure 3.A.20 ^{1}H NMR (CDCl$_3$) of **3.7**
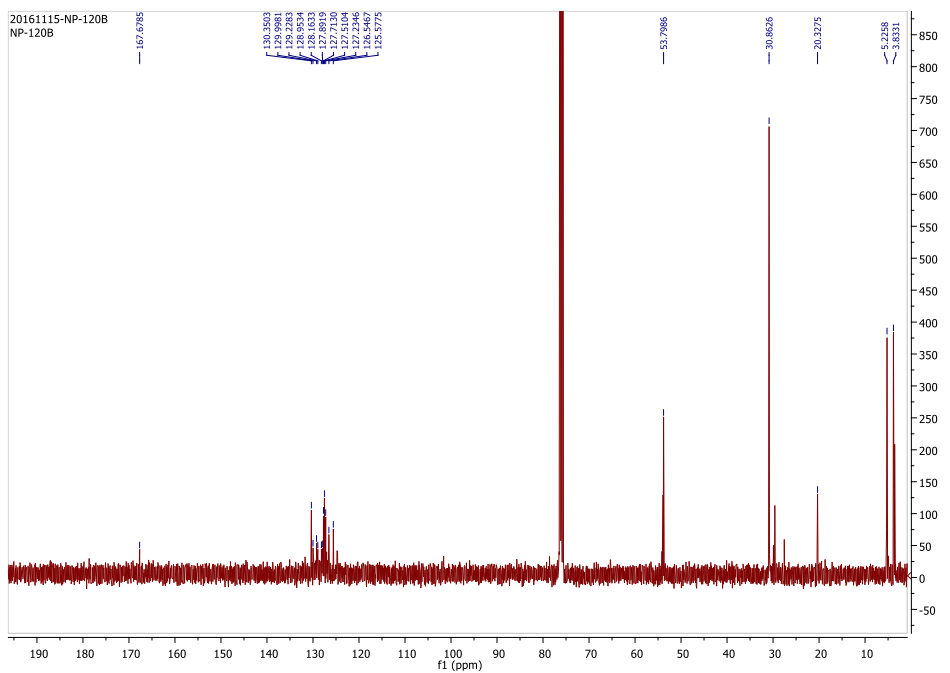
Figure 3.A.21 ^{13}C NMR (CDCl$_3$) of **3.7**
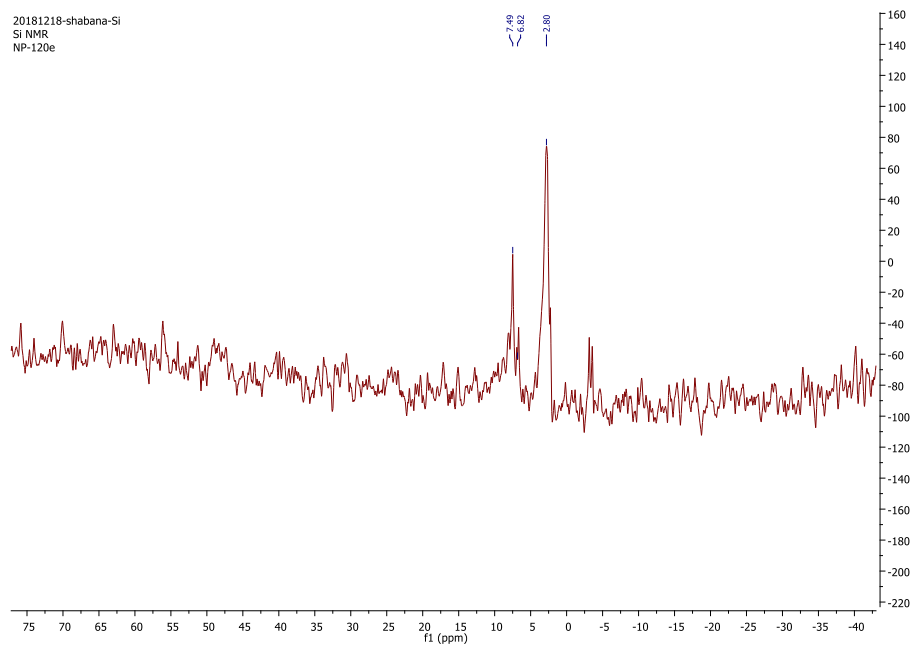
Figure 3.A.22 *²⁹Si NMR (CDCl₃) of* **3.7**
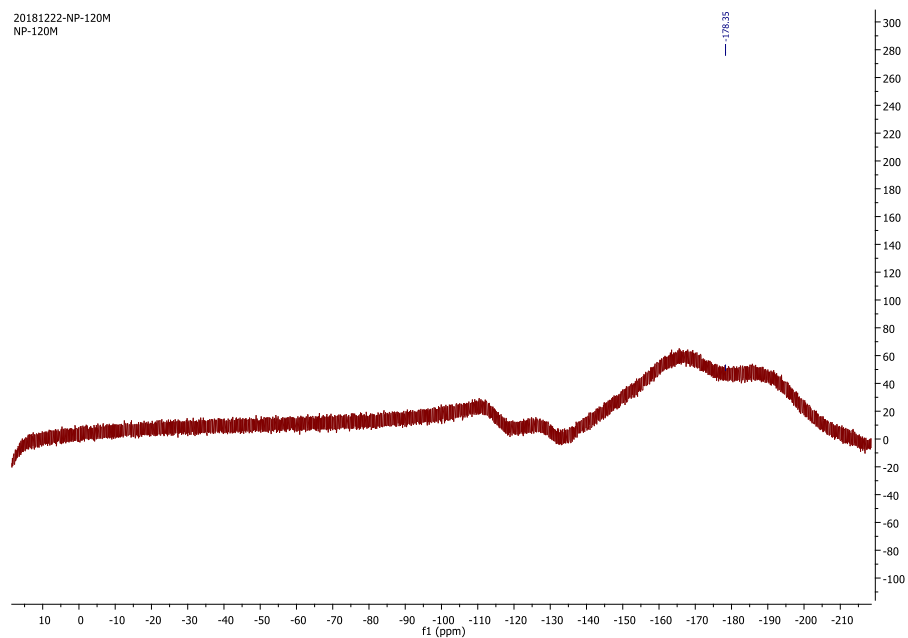
Figure 3.A.23 *¹⁹F NMR (CDCl₃) of* **3.7**
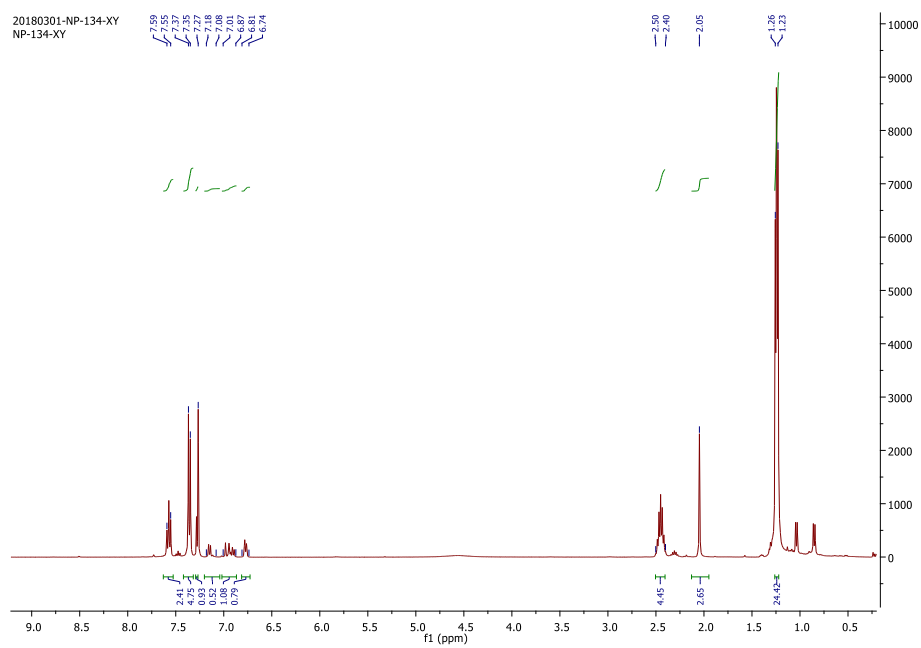
Figure 3.A.24 *^{1}H NMR (CDCl$_3$) of* **3.8**
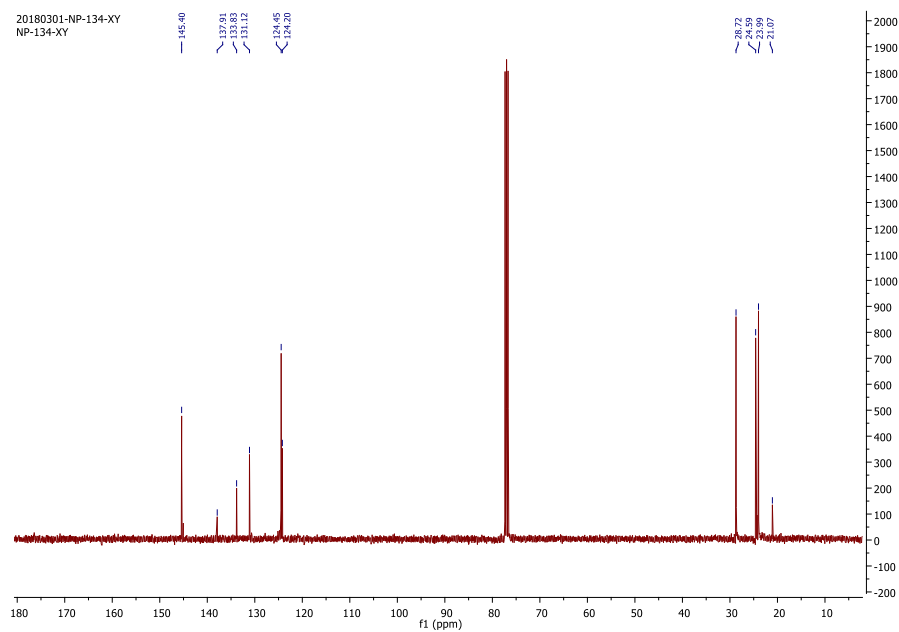
Figure 3.A.25 *^{13}C NMR (CDCl$_3$) of* **3.8**
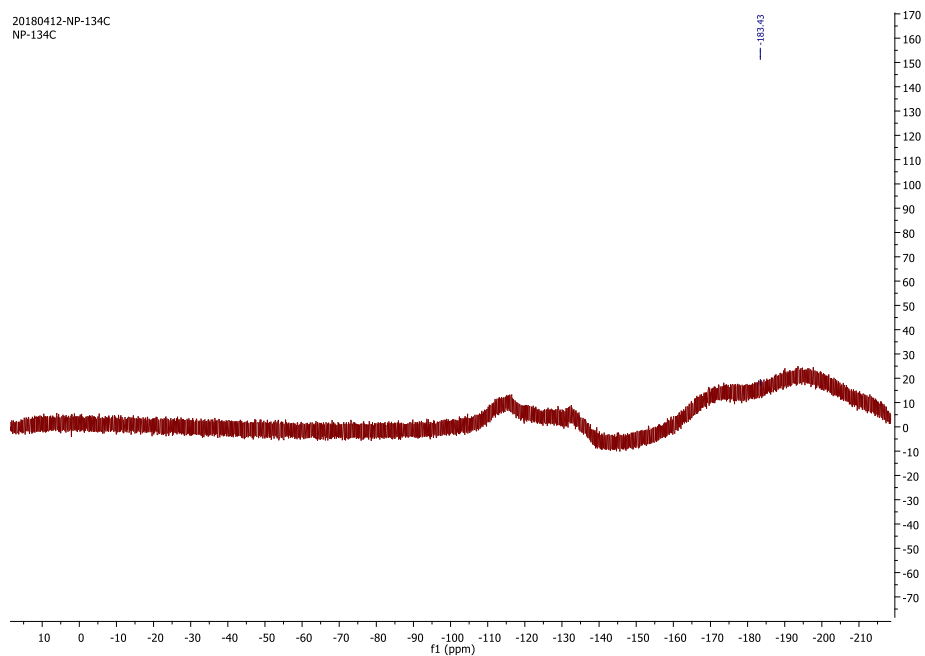
Figure 3.A.26 *¹⁹F NMR (CDCl₃) of* **3.8**
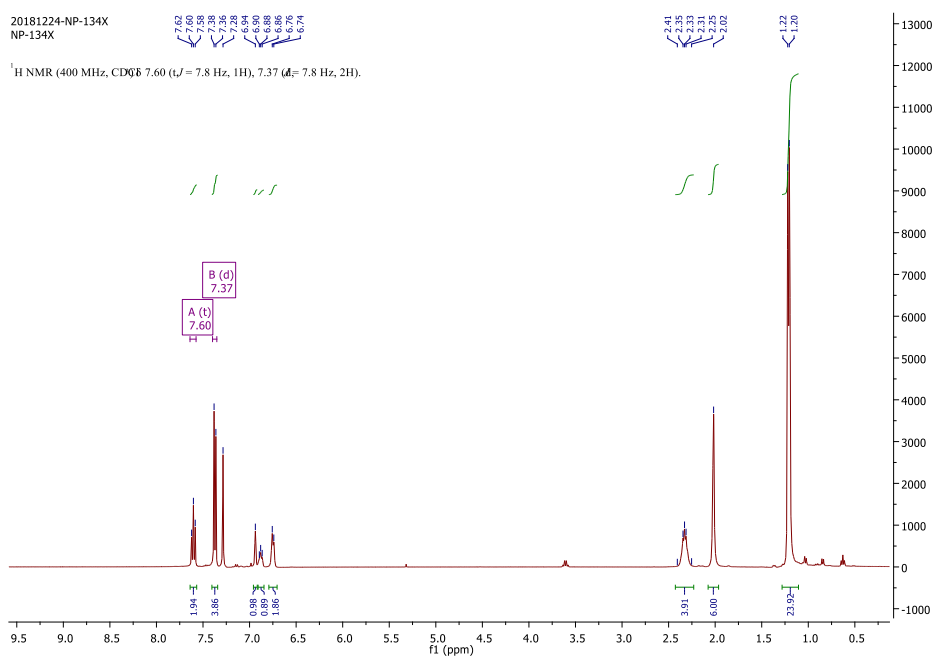
Figure 3.A.27 *¹H NMR (CDCl₃) of* **3.9**
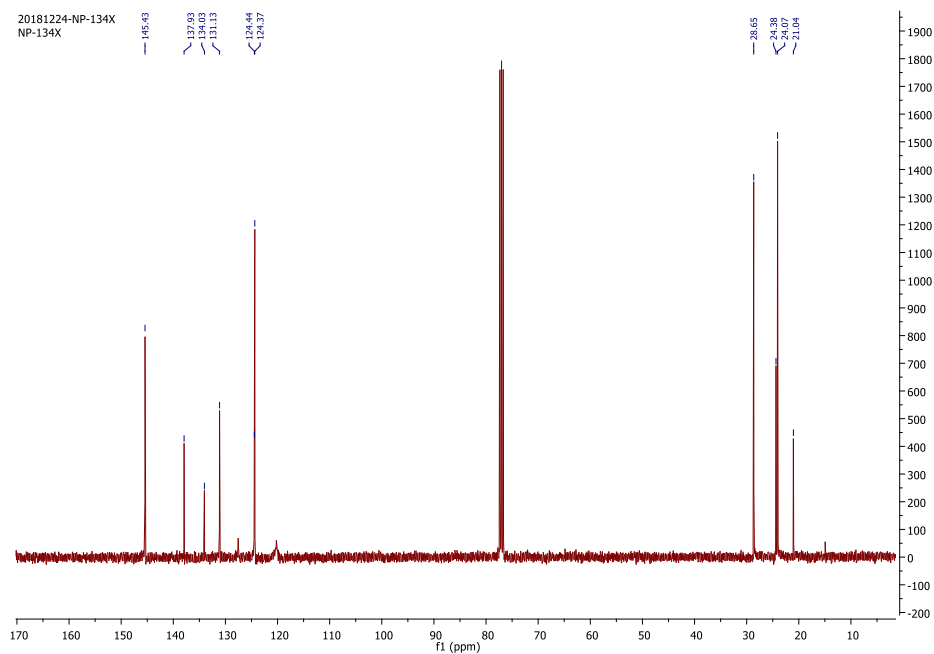
Figure 3.A.28 *^{13}C NMR (CDCl$_3$) of* **3.9**
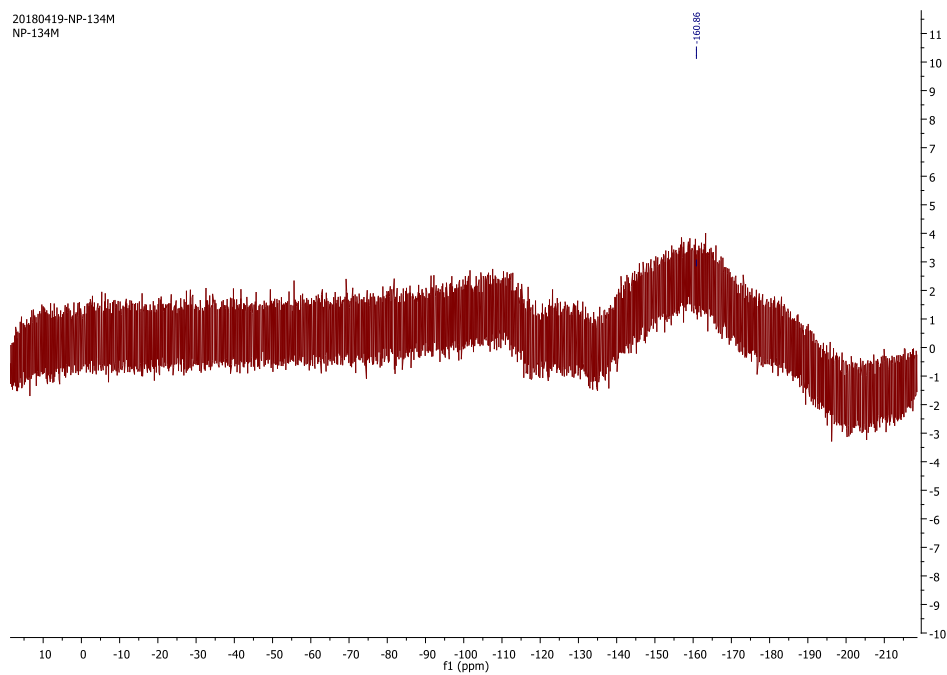
Figure 3.A.29 *^{19}F NMR (CDCl$_3$) of* **3.9**
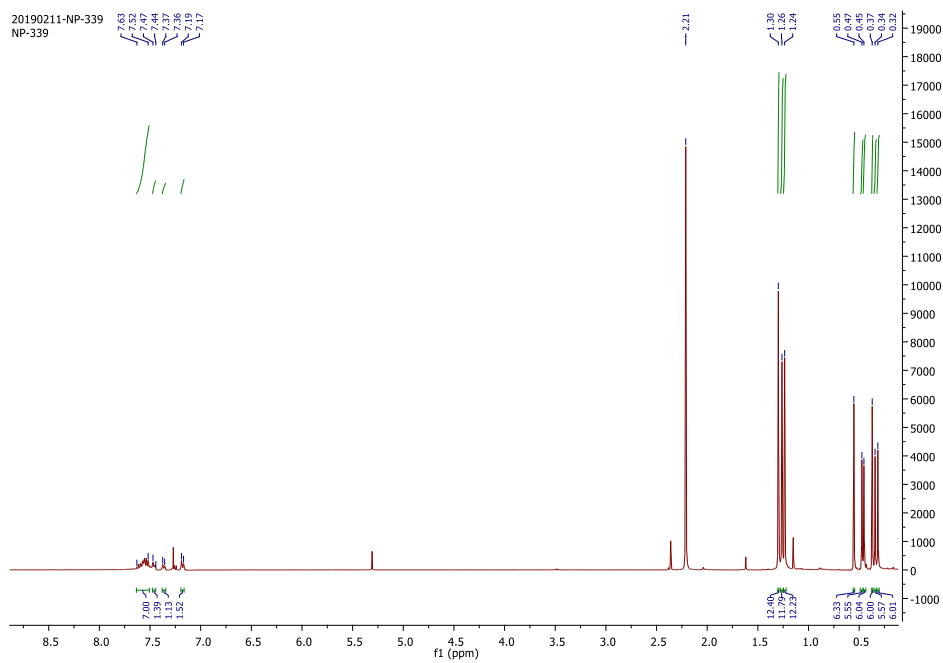
Figure 3.A.30 *^{1}H NMR (CDCl$_3$) of **3.10***
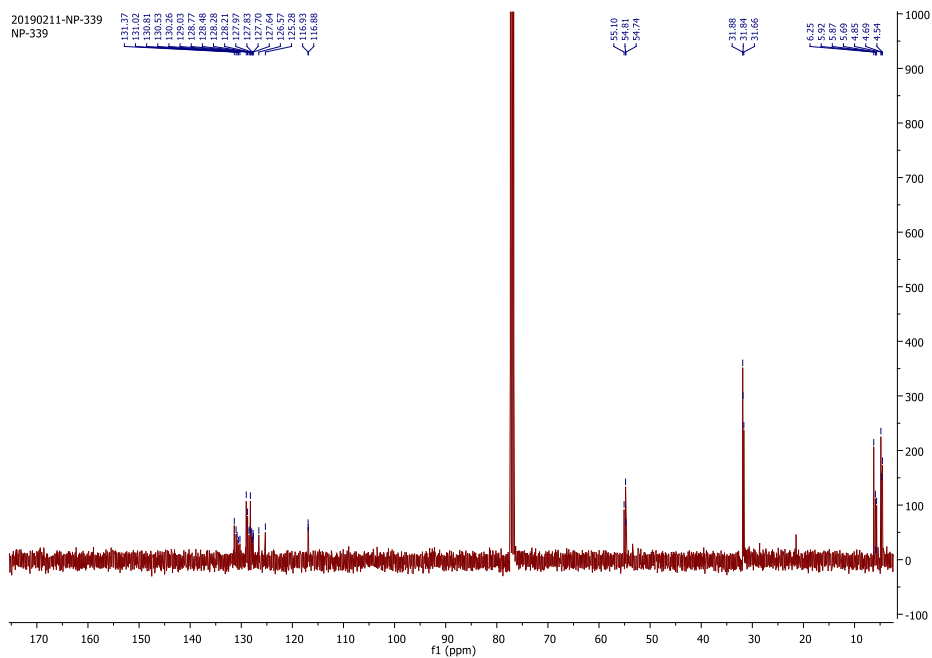
Figure 3.A.31 *^{13}C NMR (CDCl$_3$) of **3.10***

20190207-shabana-Si
Si NMR
np-339

²⁹Si NMR (99 MHz, CDCl₃) δ 10.22 (d, J = 20.8 Hz), 7.09 (d, J = 21.3 Hz).

B (d)
10.22

A (d)
7.09
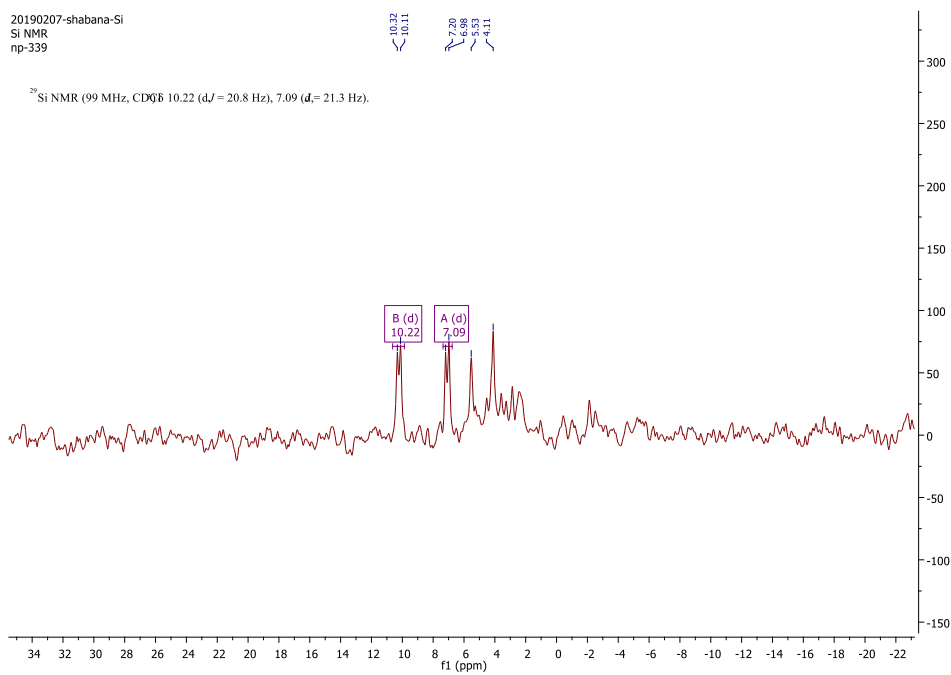
Figure 3.A.32 *²⁹Si NMR (CDCl₃) of* **3.10**

20190130-NP-354
NP-354

¹H NMR (400 MHz, CDCl₃) δ 1.35 (d, J = 6.8 Hz, 1H), 1.22 (d, J = 6.8 Hz, 1H).

B (d)
1.35

A (d)
1.22
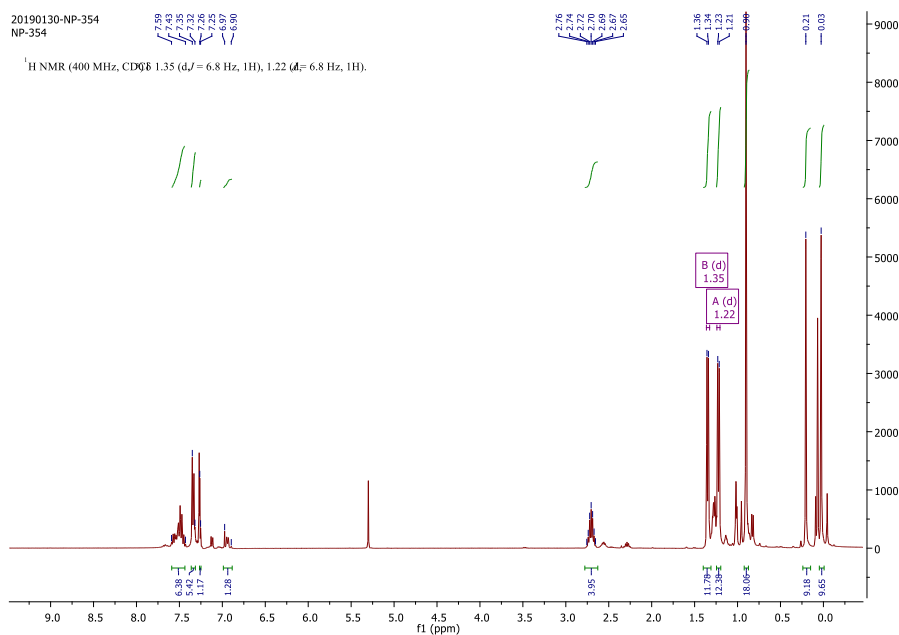
Figure 3.A.33 *¹H NMR (CDCl₃) of* **3.11**
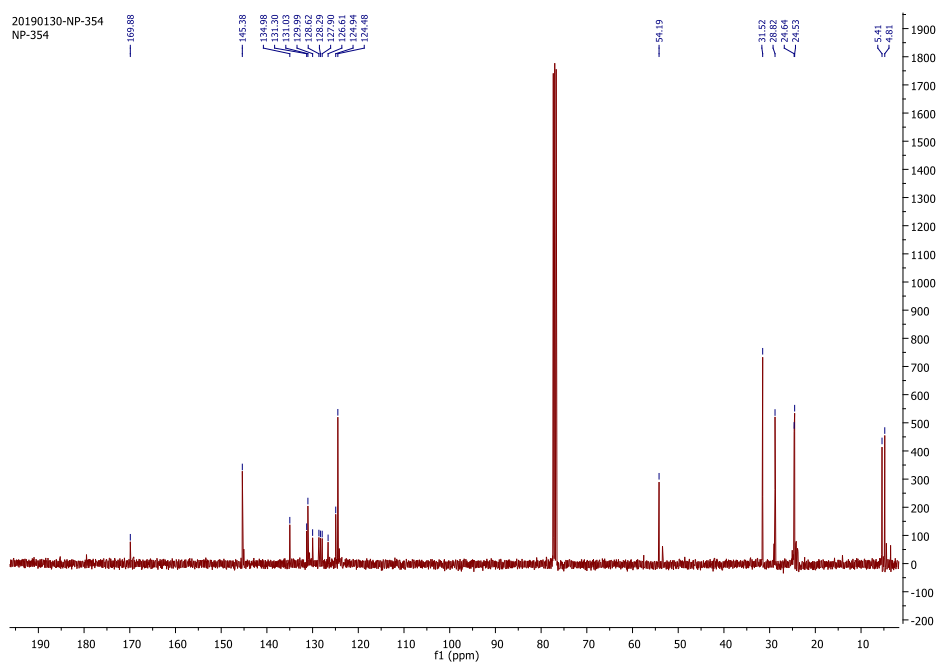
Figure 3.A.34 *¹³C NMR (CDCl₃) of* **3.11**
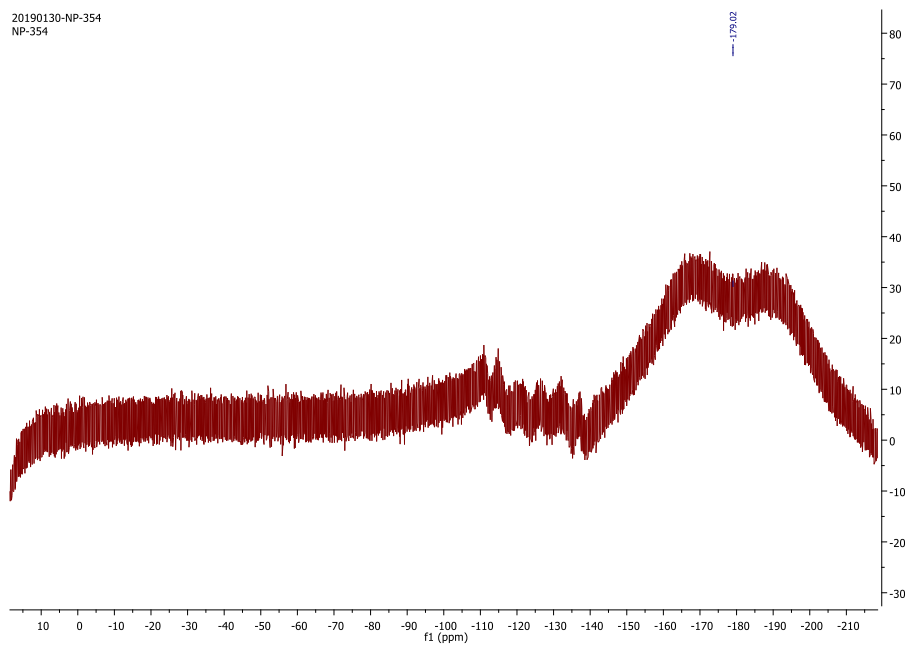
Figure 3.A.35 *¹⁹F NMR (CDCl₃) of* **3.11**
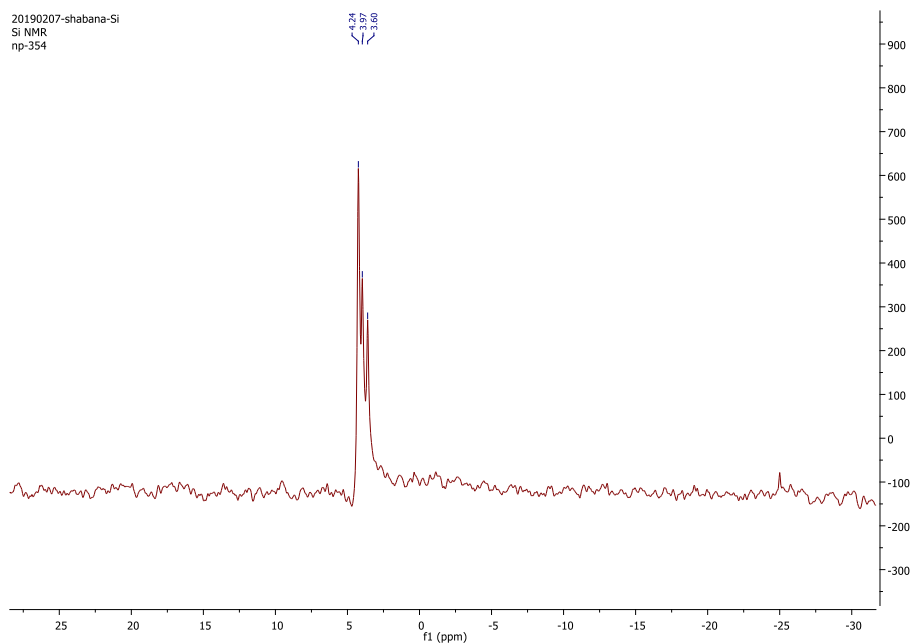
Figure 3.A.36 *^{29}Si NMR (CDCl$_3$) of **3.11***
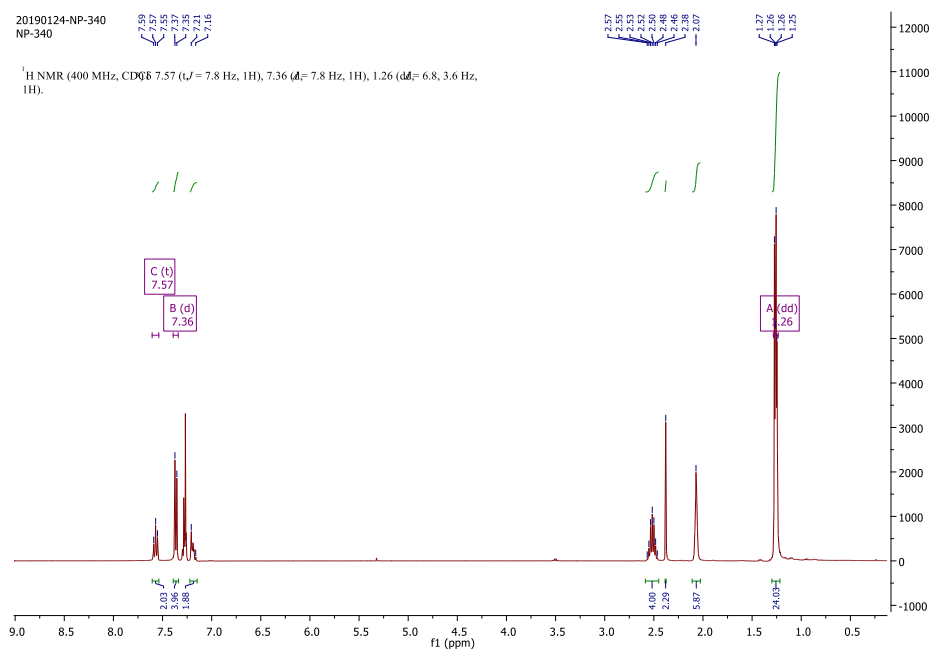
Figure 3.A.37 *^{1}H NMR (CDCl$_3$) of **3.12***
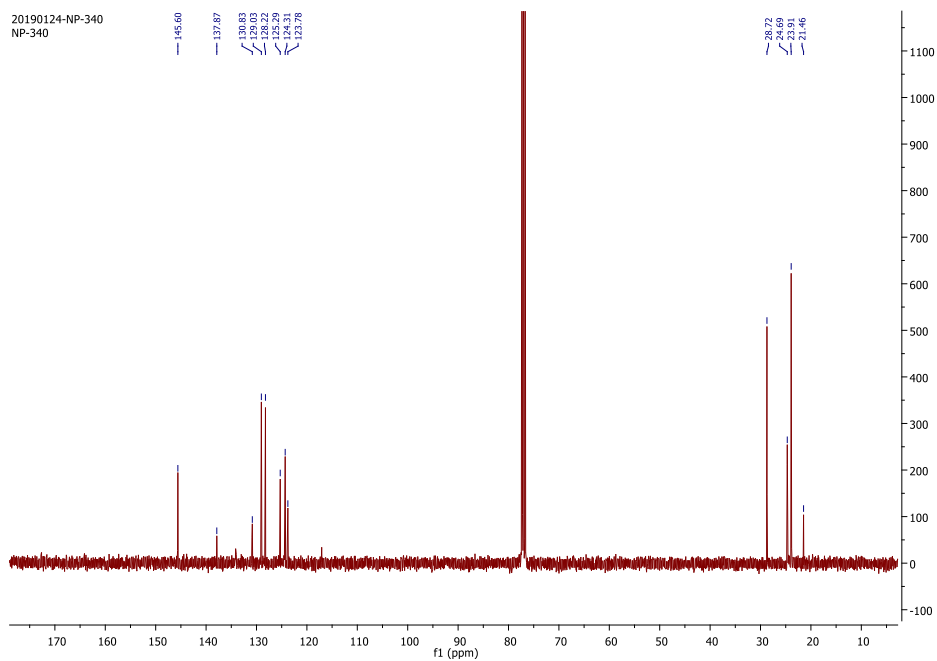
Figure 3.A.38 *¹³C NMR (CDCl₃) of **3.12***
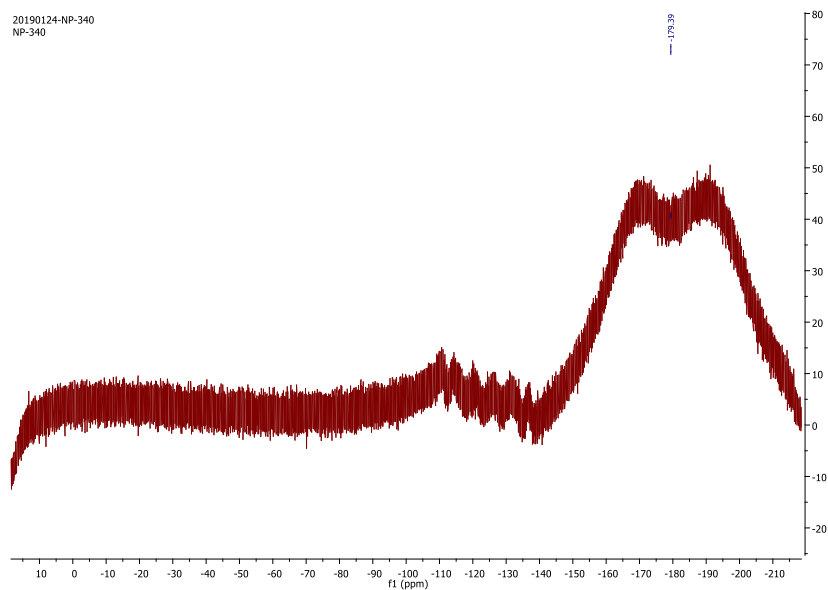
Figure 3.A.39 *¹⁹F NMR (CDCl₃) of **3.12***

Appendix of Chapter 4
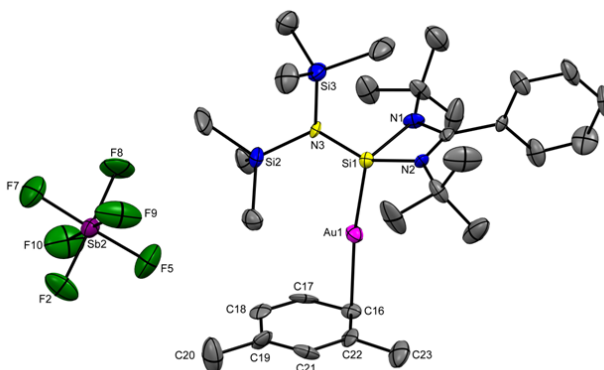
Figure 4.A.1 *The molecular structure of* **4.3** *(ellipsoid are shown at the probability level of 50%). Hydrogen atoms are omitted for clarity.*
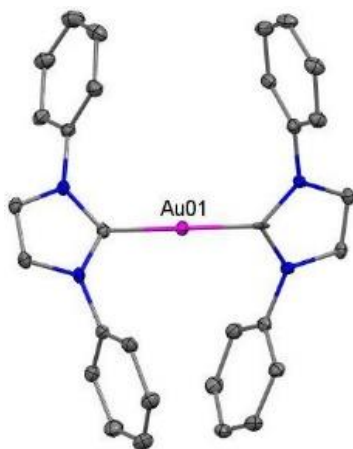
Figure 4.A.2. *The molecular structure of the deactivated catalyst of* **4.8** *(ellipsoids are shown at the probability level of 30%). Hydrogen atoms, iPr groups and SbF$_6$ anion are omitted for clarity.*
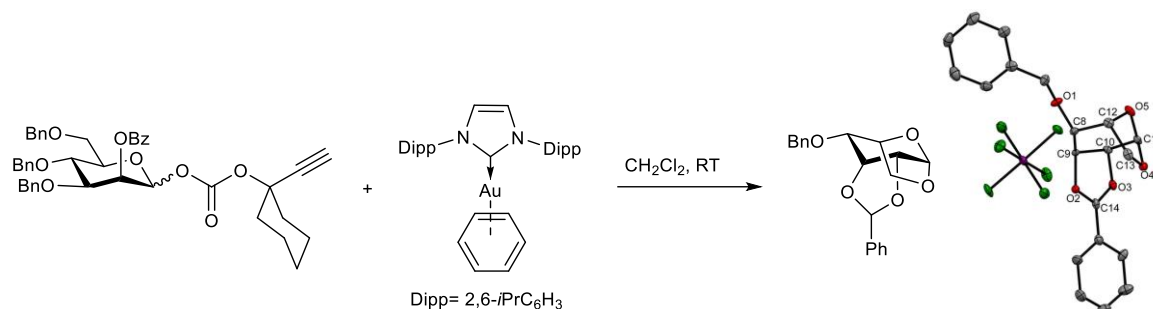
Figure 4.A.3. *The molecular structure of rearranged intermediate (ellipsoid are shown at the probability level of 50%). Hydrogen atoms are omitted for clarity.*

Table 4.A.1. *Crystallographic data for* **4.2**, **4.3** *and* **4.4**

	4.2	**4.3**	**4.4**
Chemical formula	$C_{27}H_{47}AuF_6N_3SbSi_3$	$C_{29}H_{51}AuF_6N_3SbSi_3$	$C_{21}H_{39}AuClGeN_3Si_2$
Formula weight	930.66	958.71	694.74
Temperature	100(2)	100(2)	100(2)
Wavelength	0.71073	0.71073	0.71073
Crystal system	monoclinic	monoclinic	monoclinic
Space group	$P2_1/n$	$P2_1/c$	$P2_1/c$
Unit cell dimentions	a=11.831(7) Å	a=22.214(7) Å	a=8.9235(5)Å
	b=21.434(14) Å	b=18.276(6) Å	b=18.5223(13)Å
	c=14.563(10) Å	c=18.686(6) Å	c=17.8450(12) Å
	α= 90°	α=90°	α= 90°
	β= 98.575(18)°	β=93.012(7)°	β= 101.332(2)°
	γ=90°	γ=90°	γ=90°
Volume	3652(4) Å³	7576(4) Å³	2892.0(3)Å³
Z	4	8	4

Nasrina Parvin

Density (calculated)	1.693 g/cm^3	1.681 g/cm^3	1.596 g/cm^3
Absorption coefficient	4.903 mm^{-1}	4.729 mm^{-1}	6.294 mm^{-1}
F(000)	1824	3776	1368
Theta range for data collection	2.28 to 25.25°	2.23 to 25.16°	2.20 to 25.25°
Index ranges	-14<=h<=14 -25<=k<=25 -17<=l<=17	-26<=h<=26 -21<=k<=21 -22<=l<=22	-10<=h<=10 -22<=k<=22 -21<=l<=21
Reflections collected	87805	104634	81573
Independent reflections	6620 [R(int)= 0.1276]	13512 [R(int)= 0.2456]	5233 [R(int)= 0.0618]
Coverage of independent reflections	99.9%	99.4%	100%
Function minimized	$\Sigma\ w(Fo^2 - Fc^2)^2$	$\Sigma\ w(Fo^2 - Fc^2)^2$	$\Sigma\ w(Fo^2 - Fc^2)^2$
Data/ restraints/ parameters	6620/ 0/ 382	13512/ 108/ 849	5233/ 0/ 274
Goodness-of-fit on F2	1.015	1.078	1.119
Δ/ σ max	0.001	0.001	0.002
Final R indices	4974 data; [$I>2\sigma(I)$] $R1=$ 0.0363, $wR2=$ 0.0622	7556 data; [$I>2\sigma(I)$] $R1=$ 0.0800, $wR2=$ 0.1492	4144 data; [$I>2\sigma(I)$] $R1=$ 0.0280, $wR2=$ 0.0597
	all data, $R1=$ 0.0649, $wR2=$ 0.0708	all data, $R1=$ 0.1724, $wR2=$ 0.1766	all data, $R1=$ 0.0457, $wR2=$ 0.0668
Largest diff. peak and hole	0.946 and -0.912 eÅ^{-3}	2.265 and -1.323 eÅ^{-3}	0.501 and -0.787 eÅ^{-3}
R. M. S deviation from mean	0.132 eÅ^{-3}	0.252 eÅ^{-3}	0.145 eÅ^{-3}

Table 4.A.2. *Crystallographic data for* **4.8**, **4.9** *and* **4.10**.

	8	9	10
Chemical formula	$C_{33}H_{42}AuF_6N_2Sb$	$C_{27}H_{46}CoN_3OSi_3$	$C_{55}H_{75}CoO_4P$
Formula weight	899.40	571.87	890.05
Temperature	100(2)	100(2)	100(2)
Wavelength	0.71073	0.71073	0.71073
Crystal system	monoclinic	triclinic	triclinic
Space group	*P2₁/c*	*P-1*	*P-1*
Unit cell dimentions	*a*=13.4432(9) Å	*a*= 9.741(9) Å	*a*=12.132(3) Å
	b=14.6762(9) Å	*b*=17.157(15) Å	*b*=13.703(5) Å
	c=17.3789(8) Å	*c*=18.969(15)Å	*c*=17.467(6) Å
	α= 90°	*α*=102.473(13)°	*α*=112.033(7)°
	β= 100.2060(10)°	*β*=91.56(2)°	*β*=104.987(7)°
	γ=90°	*γ*=91.73(2)°	*γ*=92.737(8)°
Volume	3374.5(3) Å³	3092(5) Å³	2565.8(14) Å³
Z	4	4	2
Density (calculated)	1.770 g/cm³	1.228 g/cm³	1.152 g/cm³
Absorption coefficient	5.201 mm⁻¹	0.695 mm⁻¹	0.408 mm⁻¹
F(000)	1752	1224	958
Theta range for data collection	2.25 to 25.25°	2.20 to 25.25	2.19 to 25.25
Index ranges	-16<=*h*<=16 -17<=*k*<=17 -20<=*l*<=20	-11<=*h*<=11 -20<=*k*<=20 -22<=*l*<=22	-12<=*h*<=13 -16<=*k*<=16 -20<=*l*<=20
Reflections collected	108354	85325	19606
Independent reflections	6111 [R(int)= 0.0432]	11186 [R(int)= 0.1194]	8546 [R(int)= 0.1786]
Coverage of independent reflections	99.9%	99.8%	91.9%
Function minimized	*Σ w(Fo² - Fc²)²*	*Σ w(Fo² - Fc²)²*	*Σ w(Fo² - Fc²)²*

Data/ restraints/ parameters	6111/ 0/ 396	11186/0/655	8546/0/552
Goodness-of-fit on F2	1.037	1.696	1.050
Δ/σ max	0.002	0.042	0.000
Final R indices	5485 data; $[I>2\sigma(I)]$ $R_1=$ 0.0201, $wR_2=$ 0.0401	8239 data; $[I>2\sigma(I)]$ $R_1=$ 0.1474, $wR_2=$ 0.3961	3619 data; $[I>2\sigma(I)]$ $R_1=$ 0.1149, $wR_2=$ 0.2600
	all data, $R_1=$ 0.0251, $wR2=$ 0.0420	all data, $R_1=$ 0.1738, $wR_2=$ 0.4128	all data, $R_1=$ 0.2596, $wR_2=$ 0.3260
Largest diff. peak and hole	2.132 and -1.629 eÅ^{-3}	7.657 and -1.648 eÅ^{-3}	0.618 and -0.793 eÅ^{-3}
R. M. S deviation from mean	0.082 eÅ^{-3}	0.257 eÅ^{-3}	0.112 eÅ^{-3}

Table 4.A.3. Deduction of hapticities in 4.2, 4.3 and 4.8.

Complex	M-C^a d$_1$, d$_2$, d$_3$	*Distance ratio* ρ_1	*Distance ratio* ρ_2	η
4.2	2.37, 2.60, 2.77	1.09	1.16	1
4.3	2.31, 2.73, 2.78	1.18	1.20	1
4.8	2.29, 2.34, 2.88	1.02	1.25	2
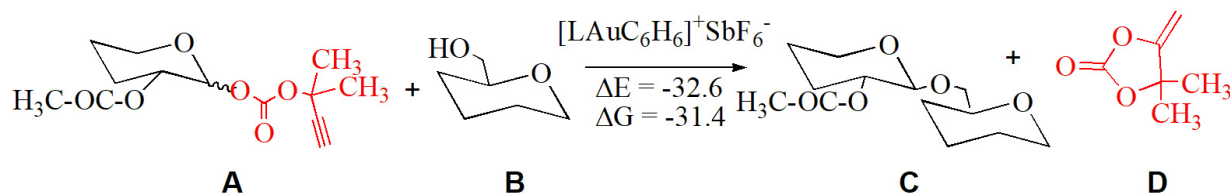
Scheme 4.A.1. *Overall glycosidation reaction at M06/PCM/def2-TZVPP//BP86/def2-SVP level of theory.*
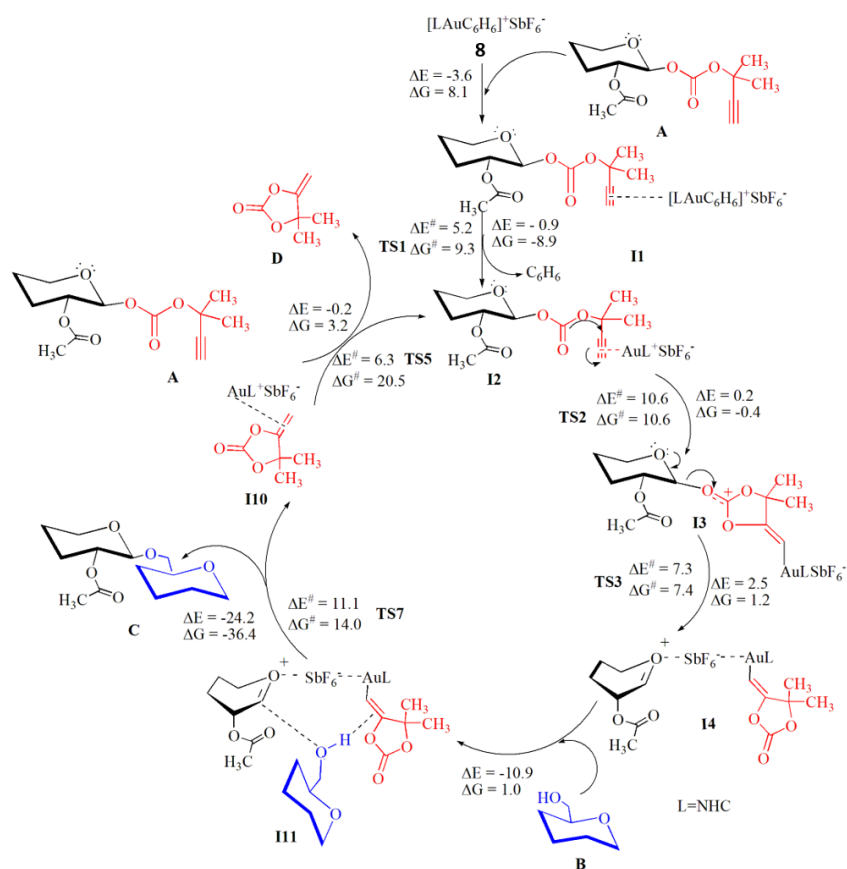
Scheme 4.A.2. *Mechanism for glycosidation reaction by remote activation using* **4.8** *through intermediate* **I11**. *Energies are given in kcal/mol. ΔE and ΔE# (in kcal/mol) represent reaction enthalpy and enthalpy of activation respectively at the M06/PCM/def2-TZVPP//BP86/def2-SVP level of theory. ΔG and ΔG# (in kcal/mol) represent the Gibbs free energy of reaction and Gibbs free energy of activation respectively, at same level of theory at 298.15 K and 1 atm.*
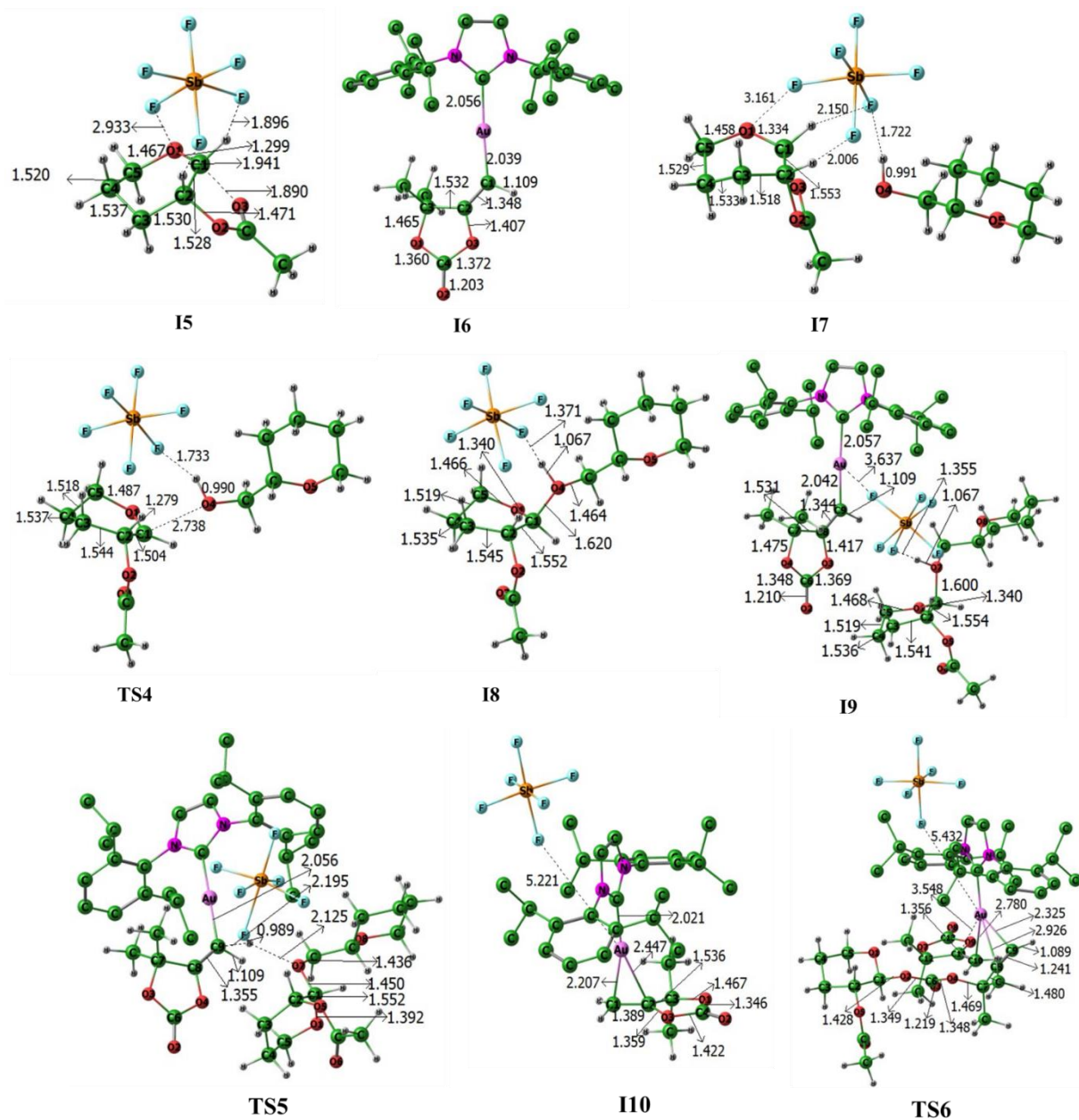
Figure 4.A.4. *Optimized geometries and important geometrical parameters of intermediates, transition states and products at the BP86/def2-SVP level of theory. Distances are given in angstroms and angles in degrees.*
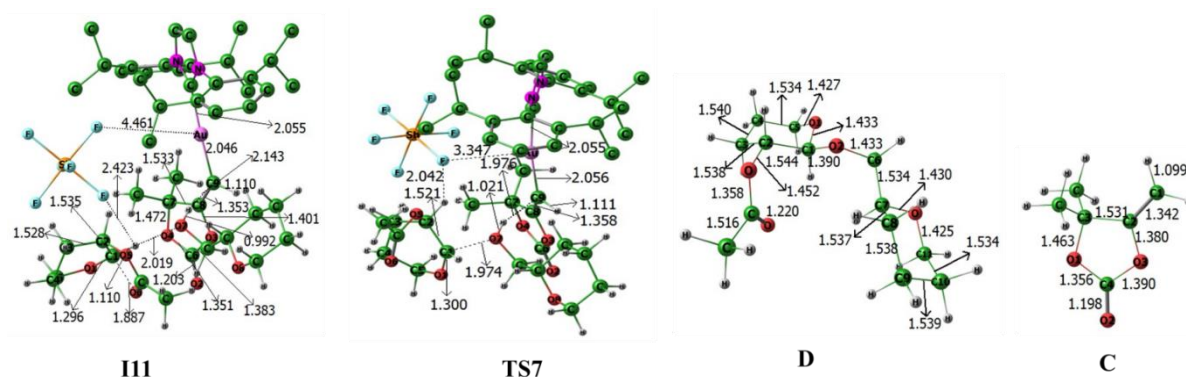
Figure 4.A.5. *Optimized geometries and important geometrical parameters of intermediates, transition states and products at the BP86/def2-SVP level of theory. Distances are given in angstroms and angles in degrees.*
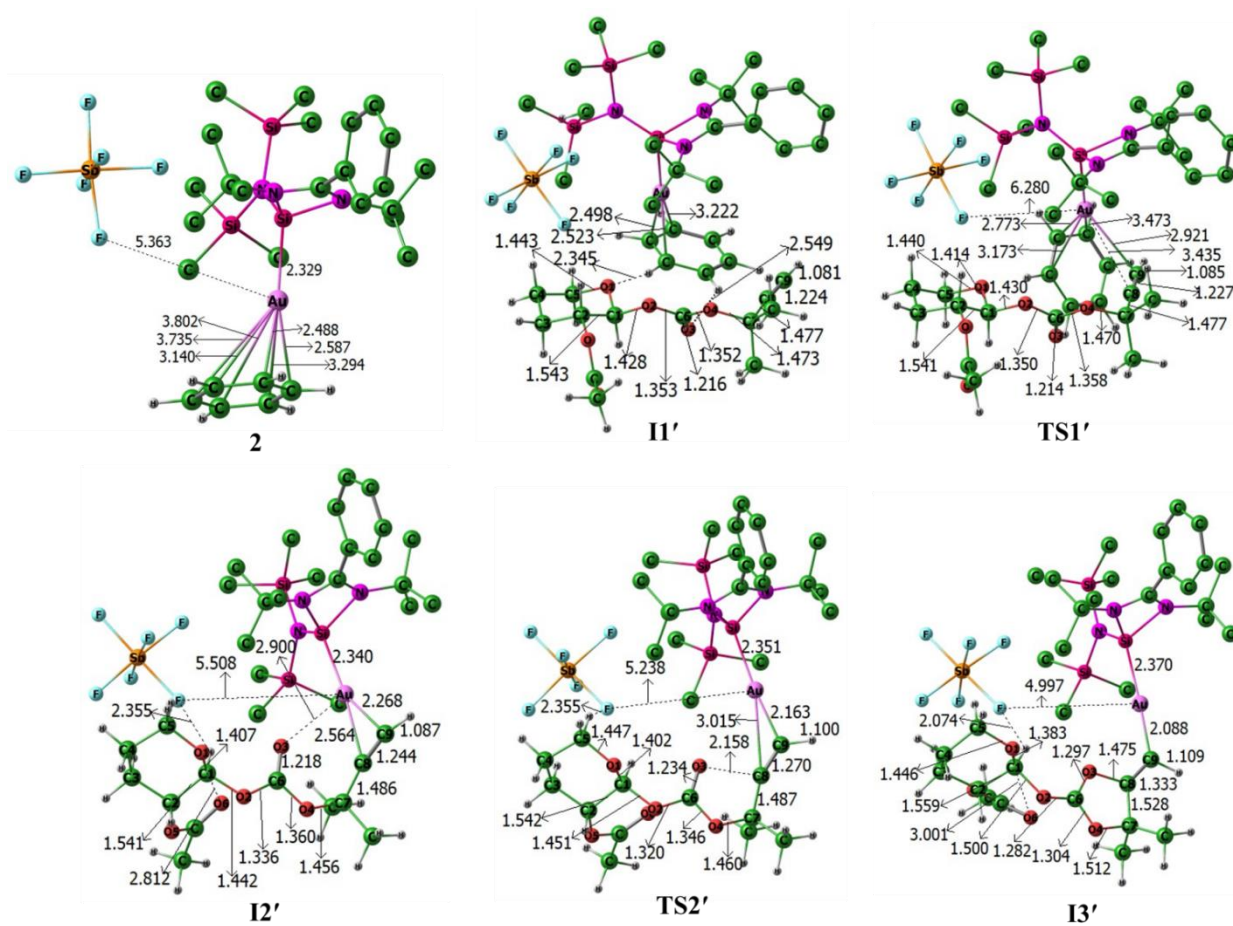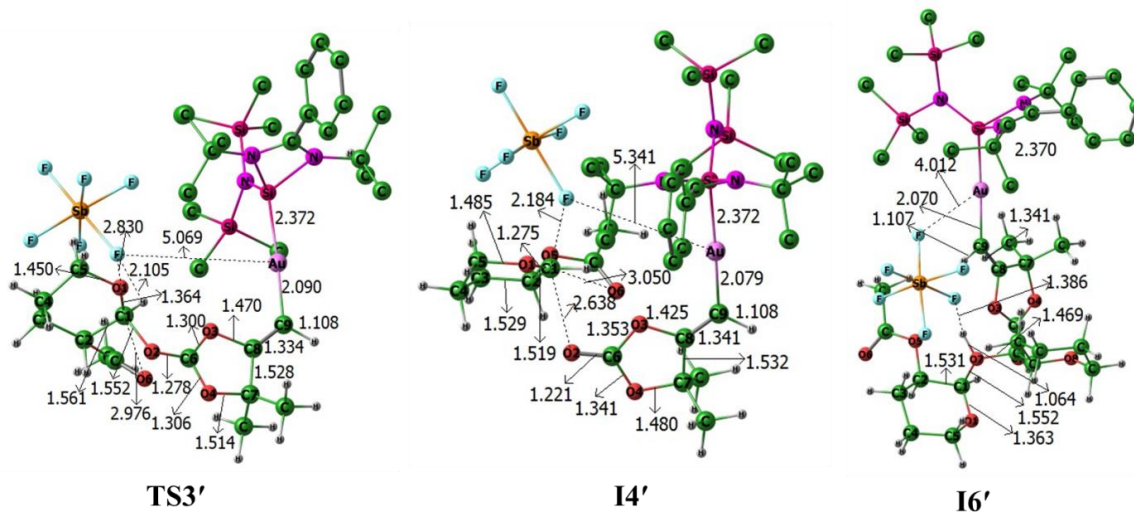
Figure 4.A.6. *Optimized geometries and important geometrical parameters of intermediates and transition states at the BP86/def2-SVP level of theory. Distances are given in angstroms and angles in degrees.*
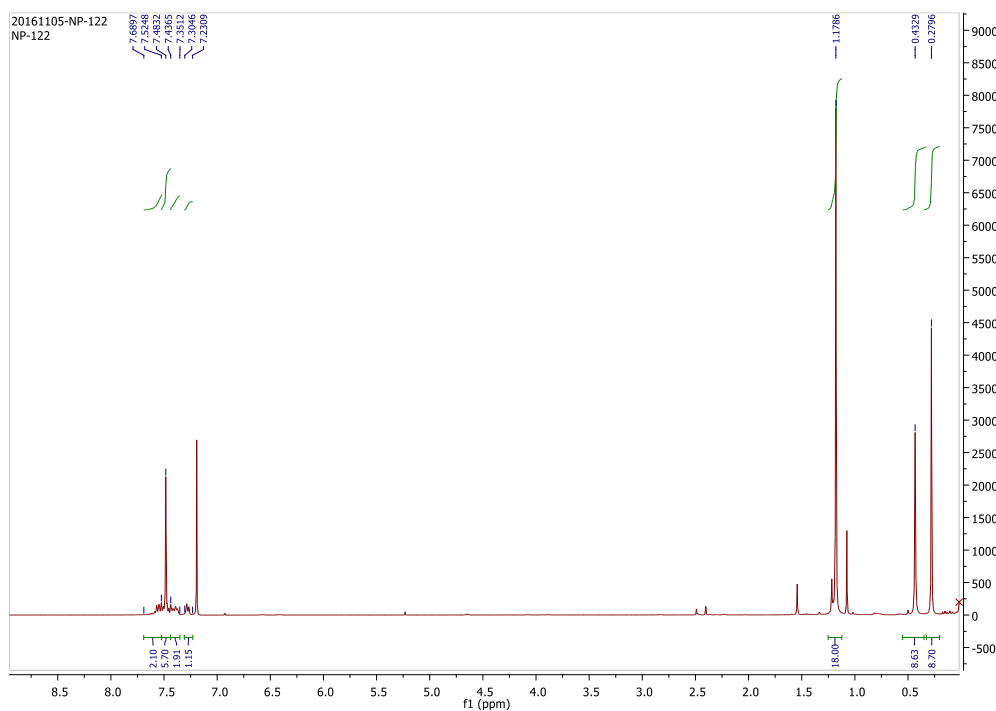
Figure 4.A.7. *^{1}H NMR spectrum (400.31 MHz, CDCl$_3$) of compound **4.2***
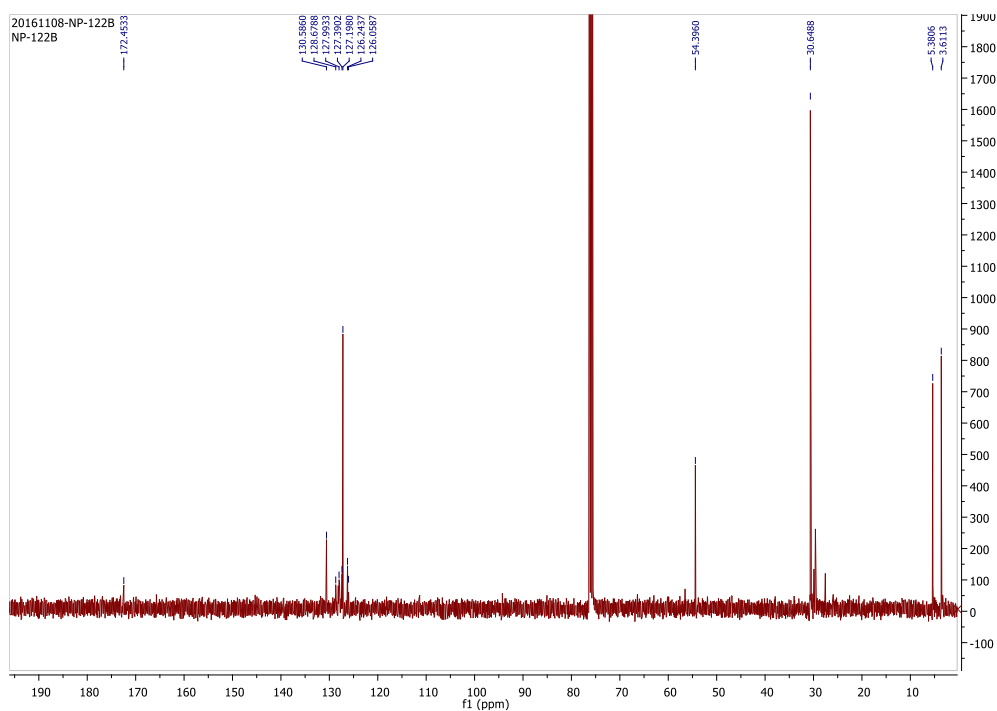
Figure 4.A.8. *^{13}C NMR Spectrum (100.67 MHz, CDCl$_3$) of compound **4.2***
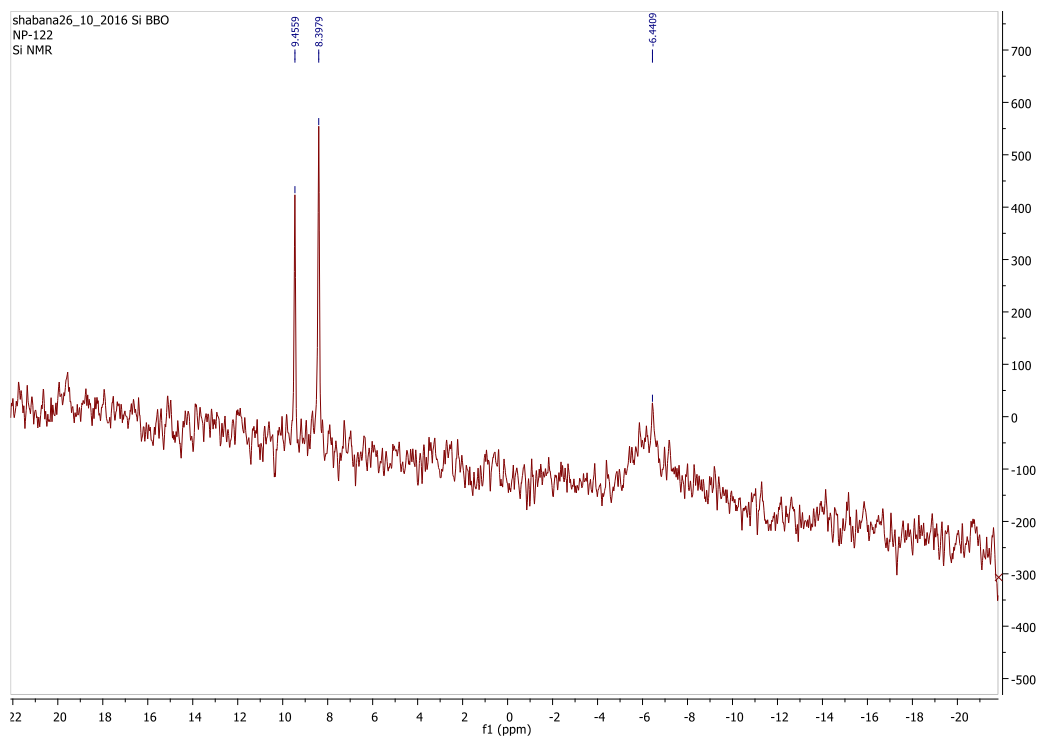
Figure 4.A.9. *^{29}Si NMR Spectrum (79.495 MHz, CDCl$_3$) of **4.2***
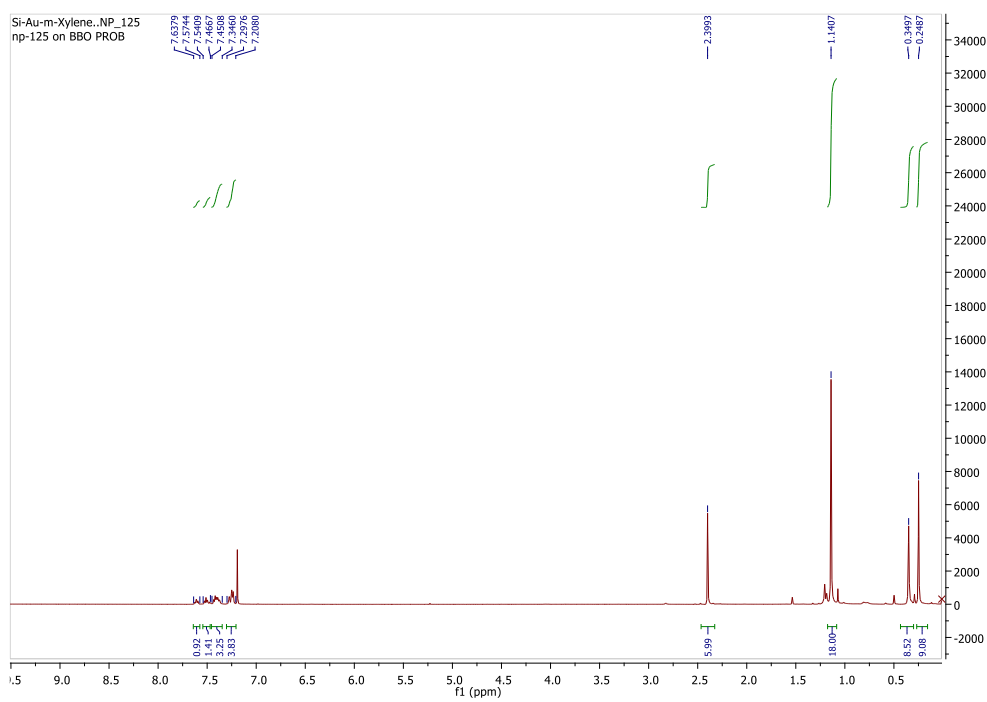
Figure 4.A.10. *^{1}H NMR spectrum (400.31 MHz, CDCl[3]) of compound* **4.3**
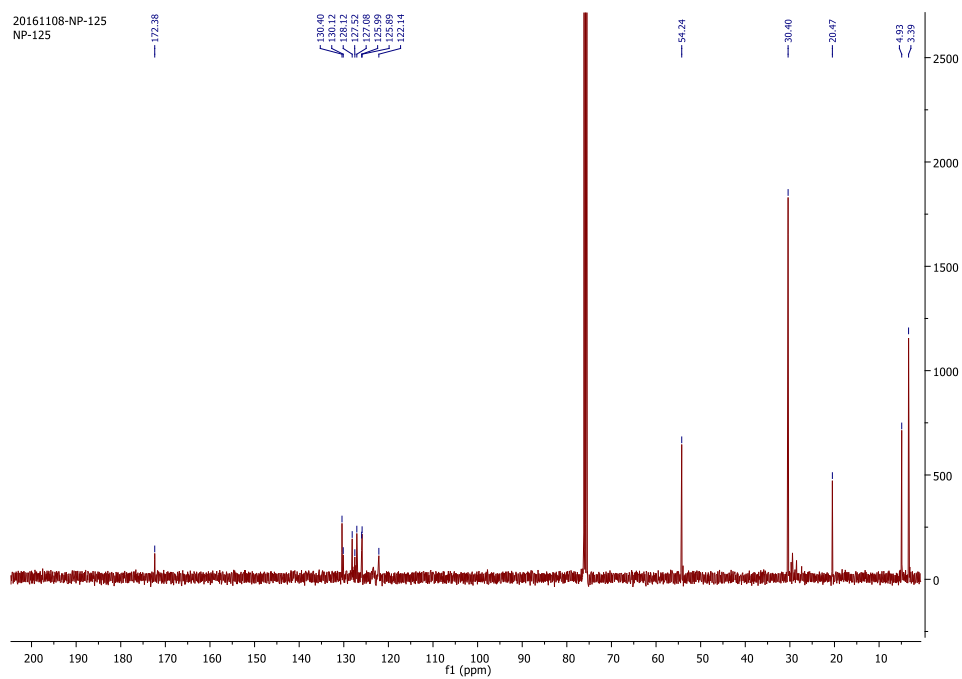
Figure 4.A.11. *^{13}C NMR Spectrum (100.67 MHz, CDCl[3]) of compound* **4.3**

Figure 4.A.12. *^{29}Si NMR Spectrum (79.495 MHz, CDCl$_3$) of* **4.3**

Figure 4.A.13. *^1H NMR spectrum (400.31 MHz, CDCl$_3$) of compound* **4.4**

20200306-NP-449

168.95

130.79
129.57
127.23
127.16
126.88
126.60

54.17

30.82

5.14
3.65
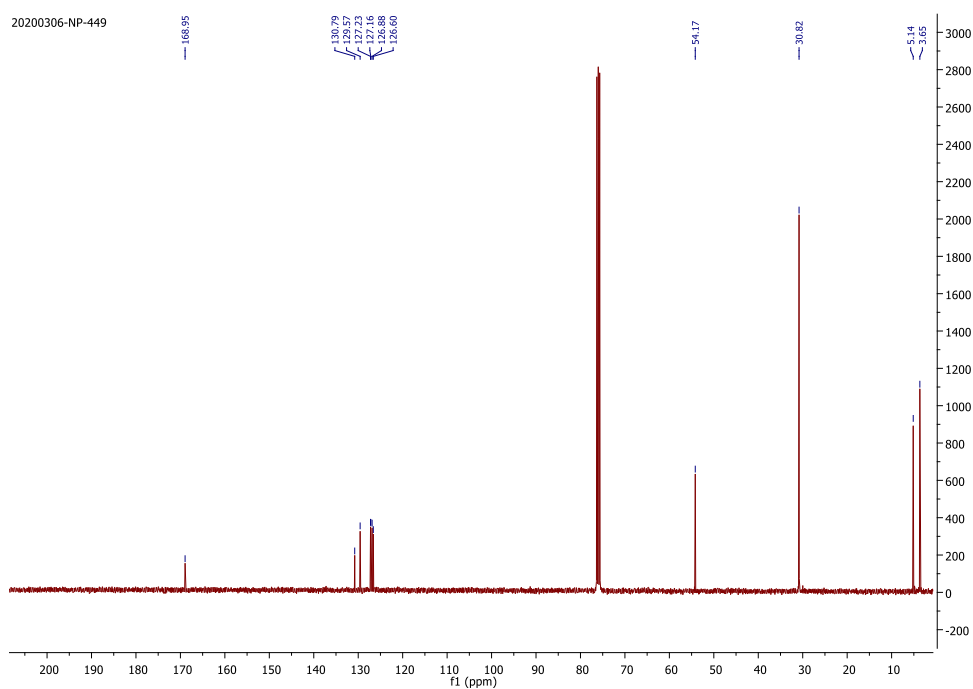
Figure 4.A.14. *¹³C NMR Spectrum (100.67 MHz, CDCl₃) of compound **4.4***

20200309-NP-455

7.62
7.45
7.41
7.36
7.24
7.18

1.23

0.56
0.39

5.07
4.72
1.42

18.47

9.06
9.18
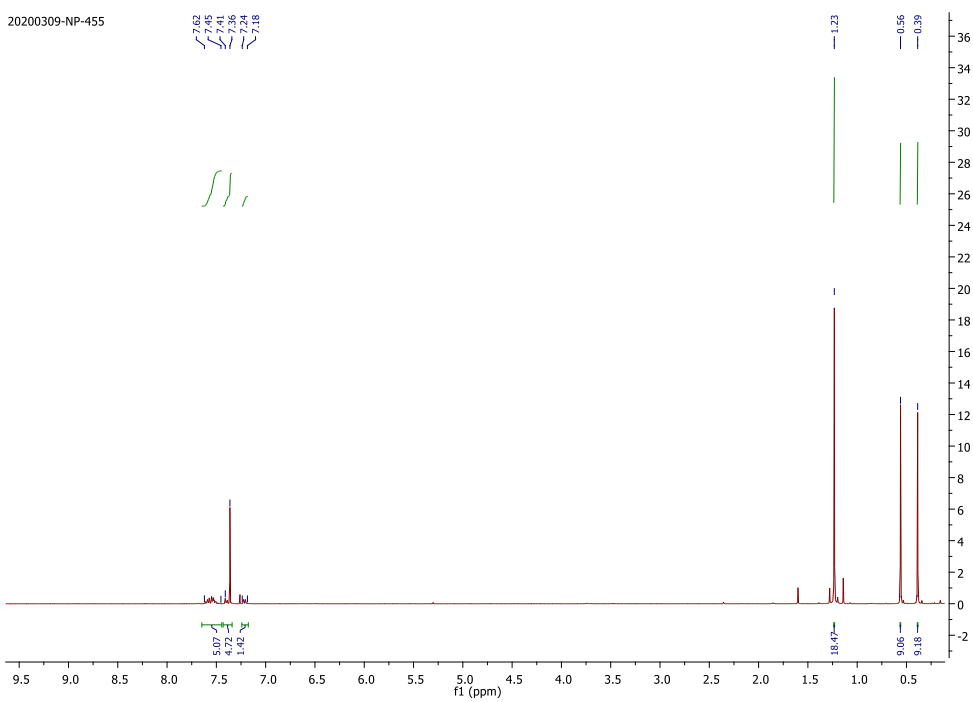
Figure 4.A.15. *¹H NMR spectrum (400.31 MHz, CDCl₃) of compound **4.5***
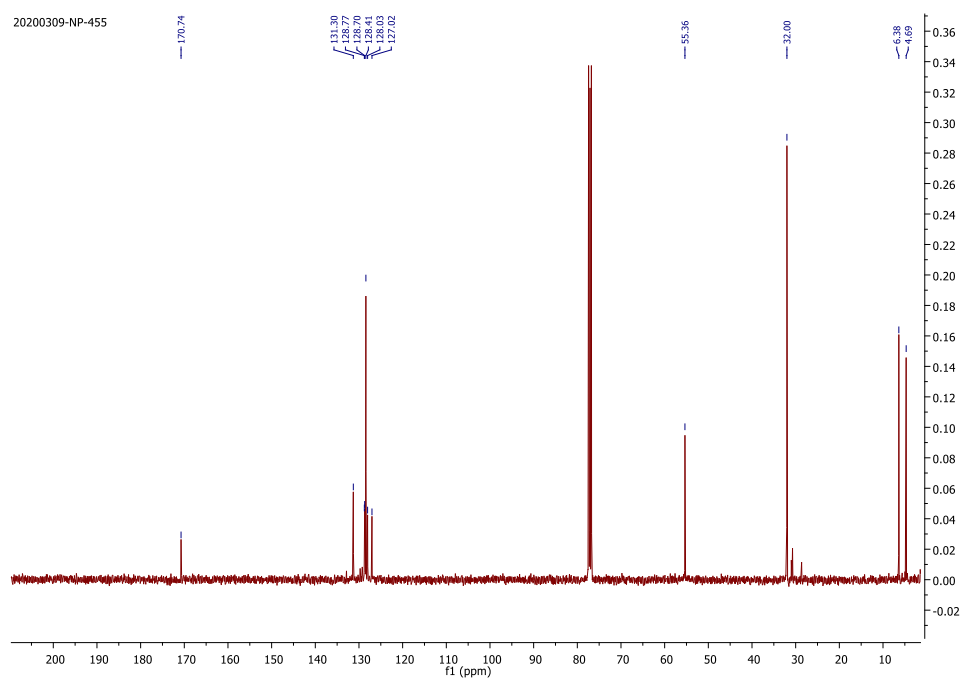
Figure 4.A.16. *¹³C NMR Spectrum (100.67 MHz, CDCl₃) of compound **4.5***
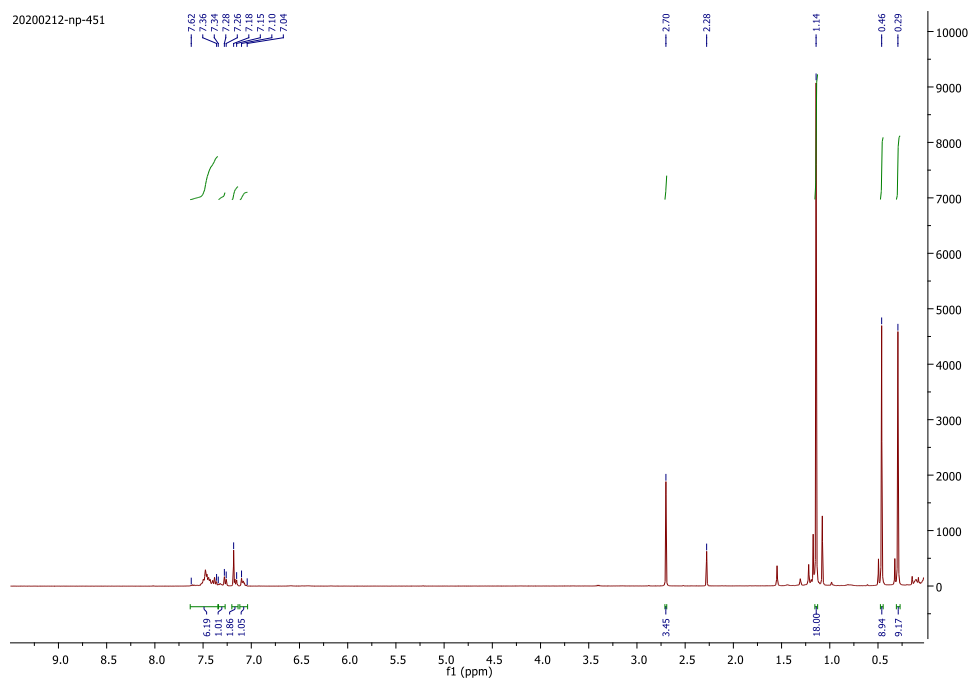
Figure 4.A.17. *¹H NMR spectrum (400.31 MHz, CDCl₃) of compound **4.6***
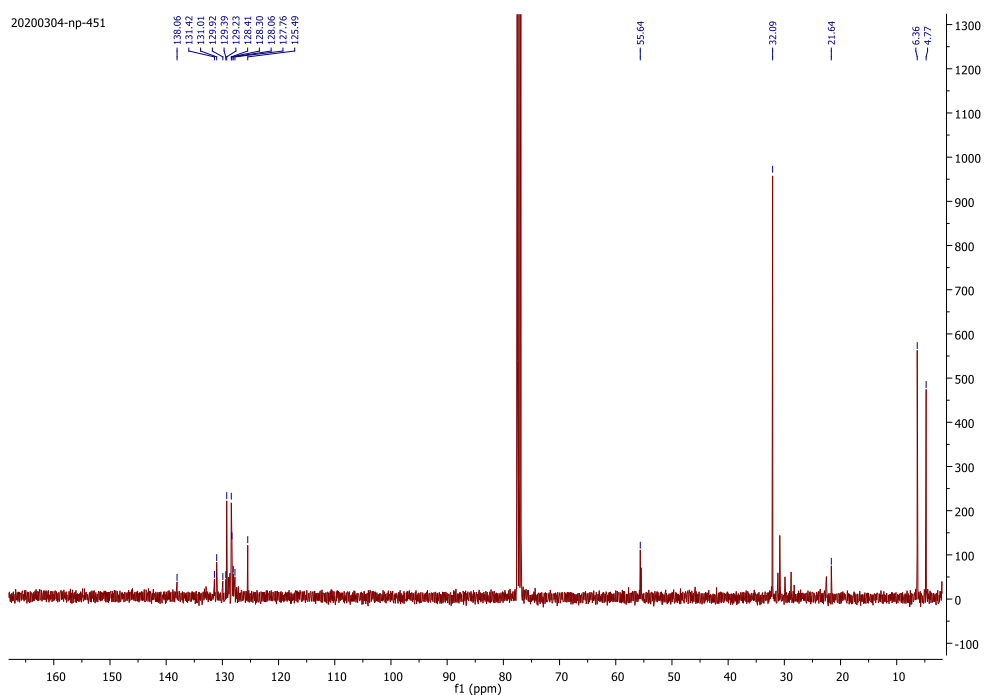
Figure 4.A.18. *^{13}C NMR Spectrum (100.67 MHz, CDCl$_3$) of compound **4.6***

^{1}H NMR (400 MHz, CDCl$_3$): 7.39 (t, J = 7.8 Hz, 1H), 7.04 (d, J = 7.8 Hz, 1H), 0.96 (d, J = 6.9 Hz, 1H), 0.76 (d, J = 6.9 Hz, 1H).
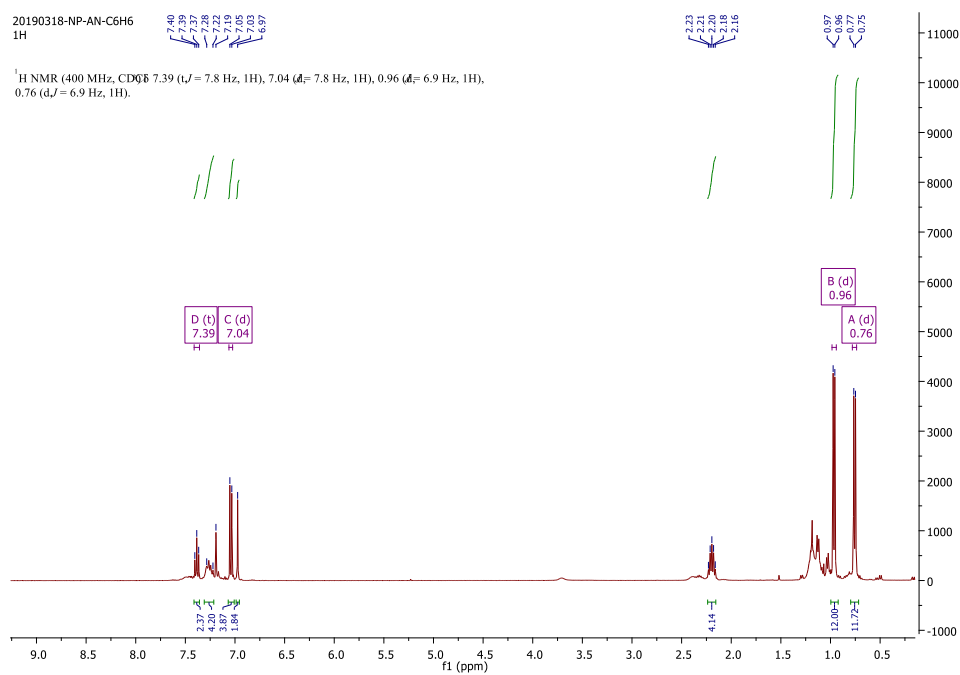
Figure 4.A.19. *^{1}H NMR spectrum (400.31 MHz, CDCl$_3$) of compound **4.8***
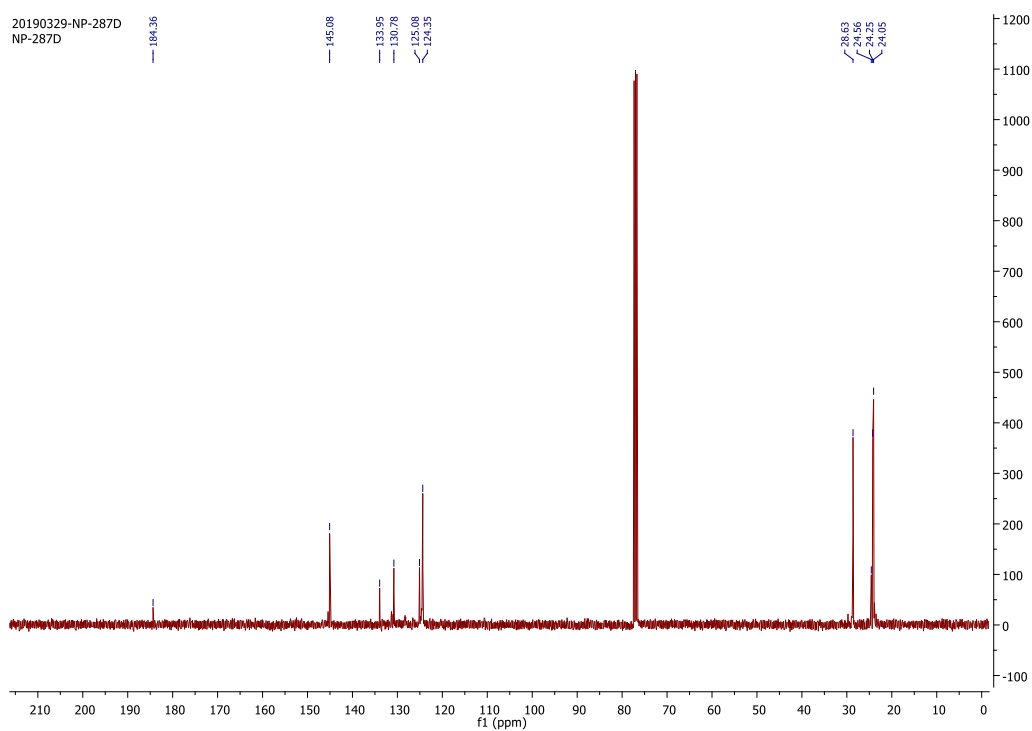
Figure 4.A.20. ^{13}C *NMR Spectrum (100.67 MHz, CDCl$_3$) of compound* **4.8**
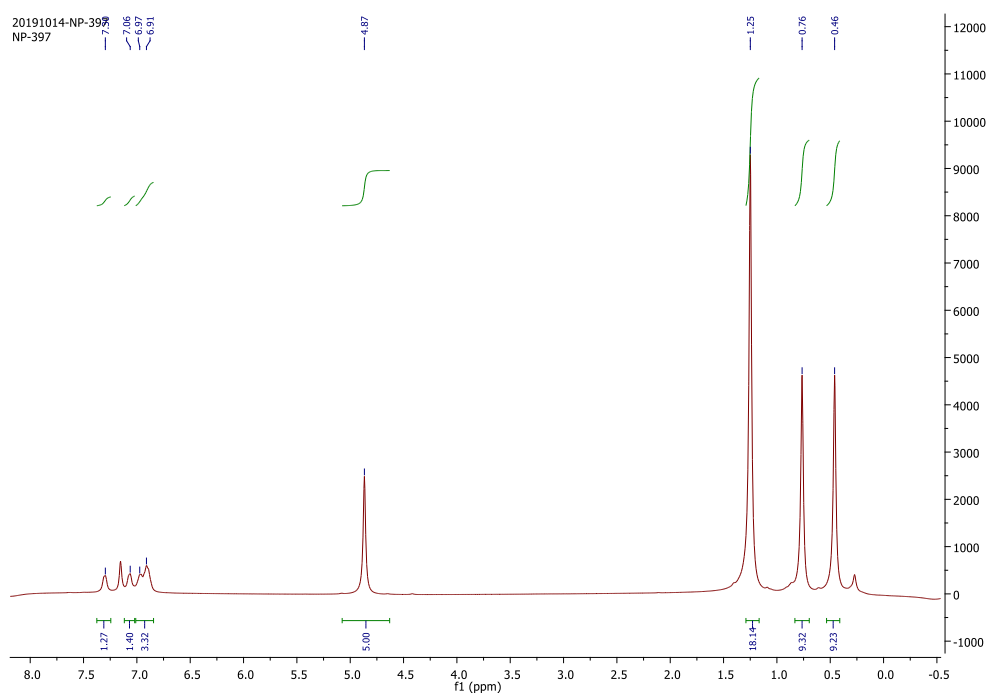
Figure 4.A.21. ^{1}H *NMR spectrum (400.31 MHz, CDCl$_3$) of compound* **4.9**
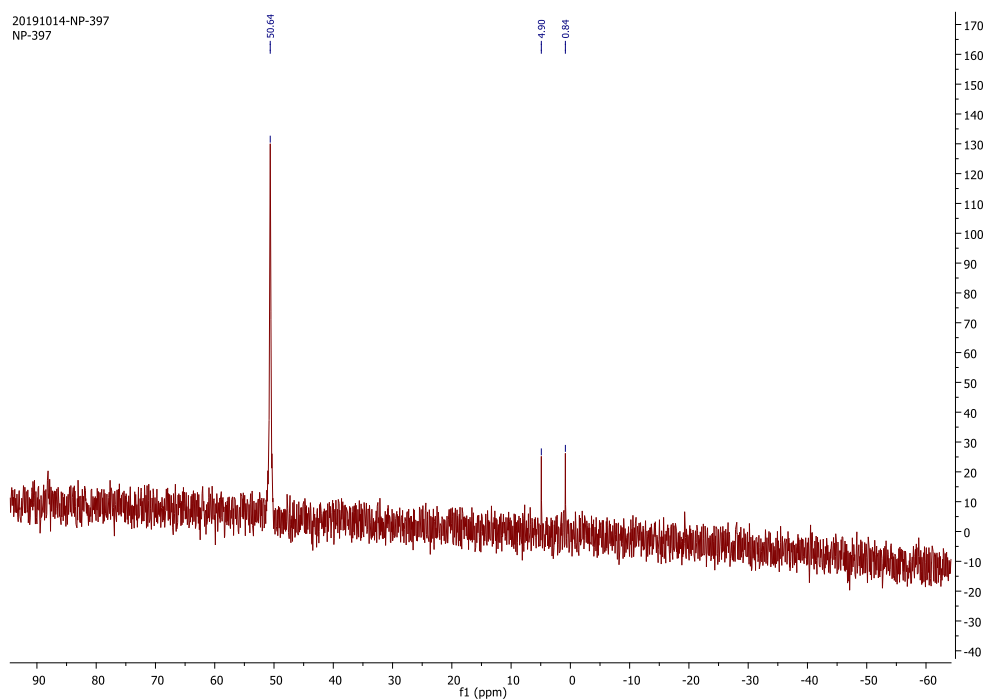
Figure 4.A.22. *²⁹Si NMR Spectrum (79.495 MHz, CDCl₃) of* **4.9**

¹H NMR (400 MHz, CDCl₃) δ 7.68 (d, *J* = 8.6 Hz, 1H), 7.05 (d, *J* = 8.6 Hz, 1H).
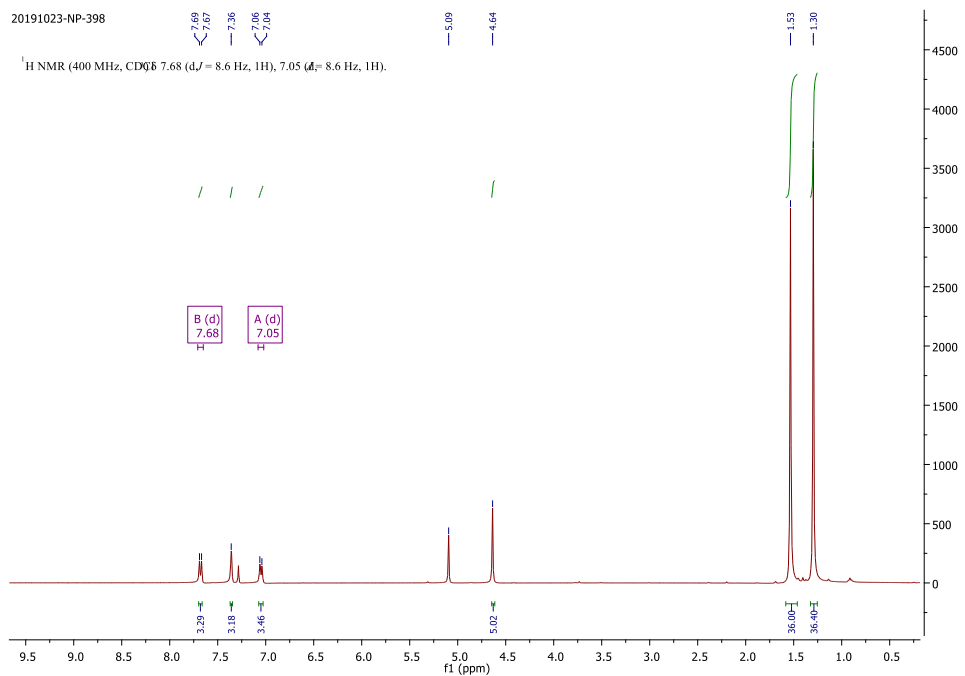
Figure 4.A.23. *¹H NMR spectrum (400.31 MHz, CDCl₃) of compound* **4.10**

20191023-NP-398

155.41
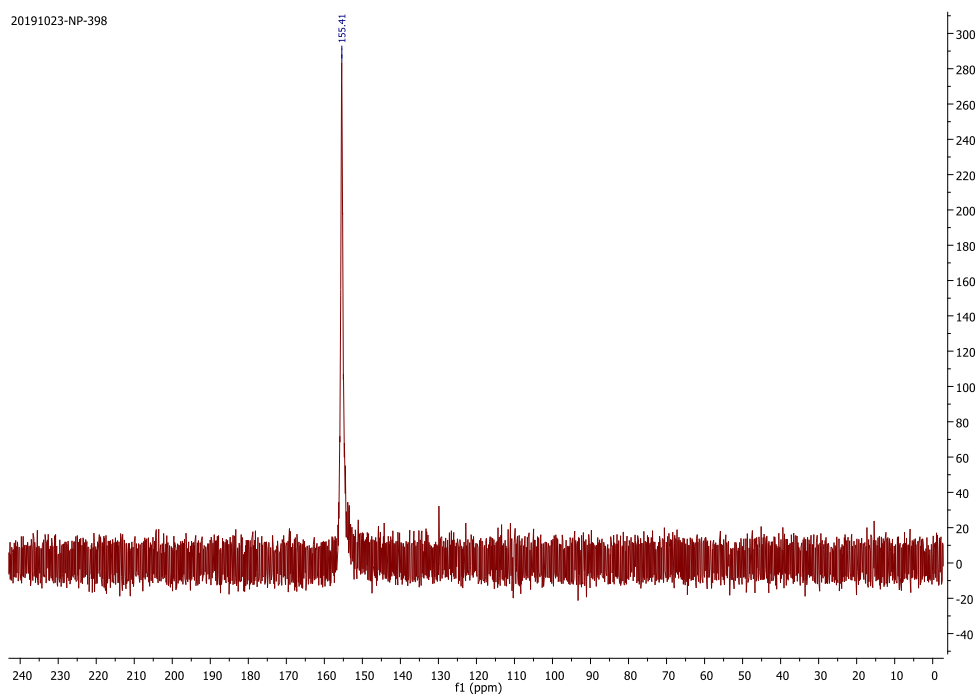
Figure 4.A.24. ^{31}P *NMR spectrum (161.976 MHz, CDCl$_3$) of* **4.10**

Appendix of Chapter 5
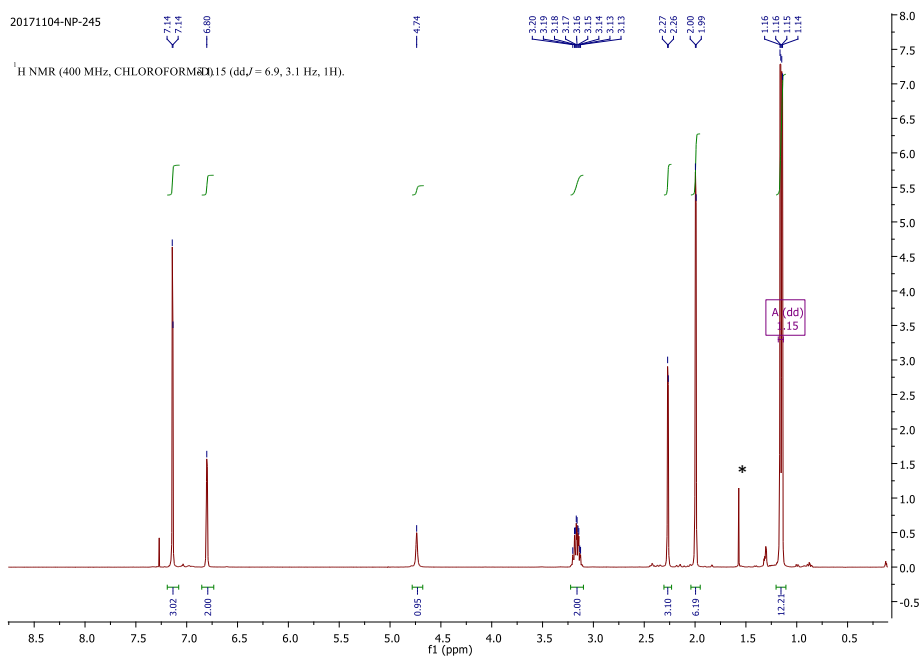
Figure 5.A.1. ¹H NMR of 5.1a (= H₂O)*

Figure 5.A.2. ¹³C NMR of 5.1a

20180529-NP-199

^{1}H NMR (400 MHz, CHLOROFORM-D) 6.97 (d, *J* = 7.4 Hz, 1H), 6.76 (t, *J* = 7.4 Hz, 1H), 1.16 (d, *J* = 6.9 Hz, 1H).

C (t)
6.76

B (d)
6.97

A (d)
1.16
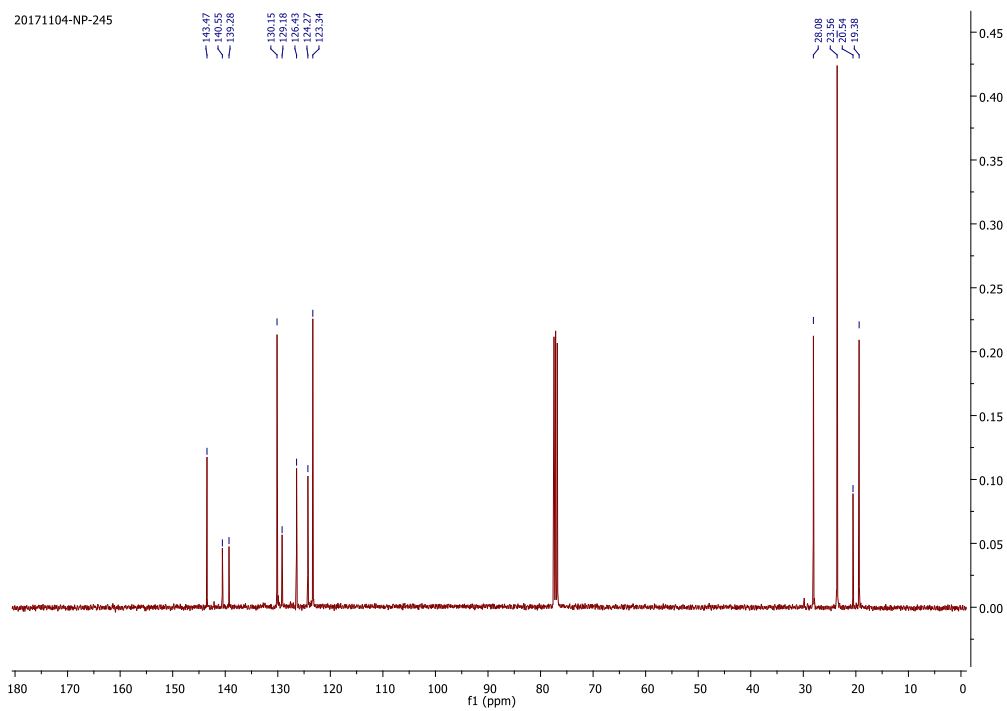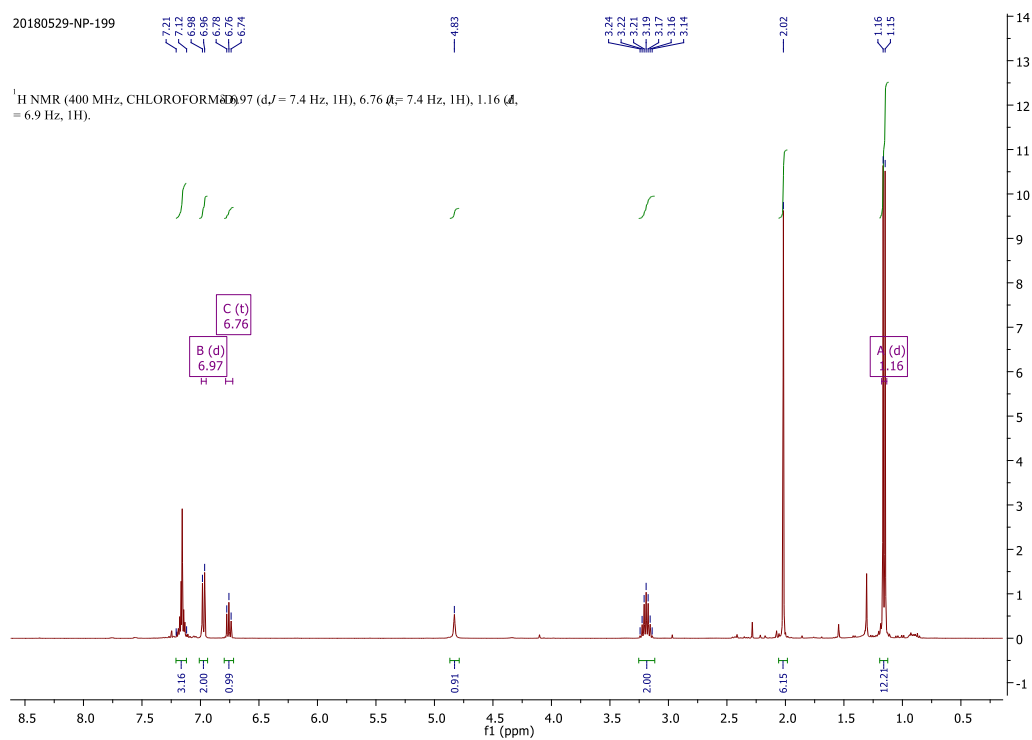
Figure 5.A.3. *^{1}H NMR of* ***5.1b***

20180529-NP-199
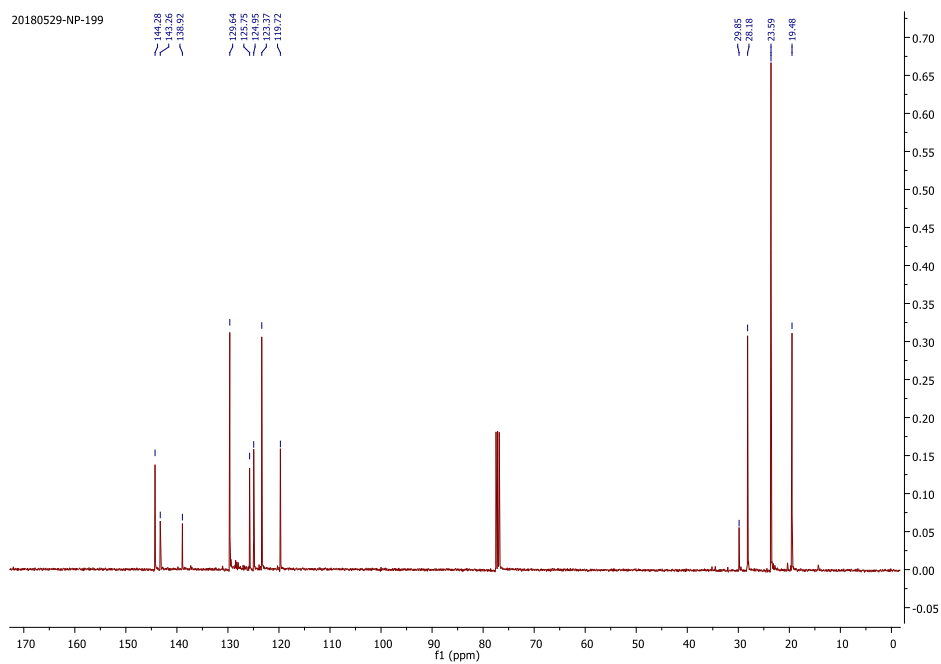
Figure 5.A.4. *^{13}C NMR of* ***5.1b***
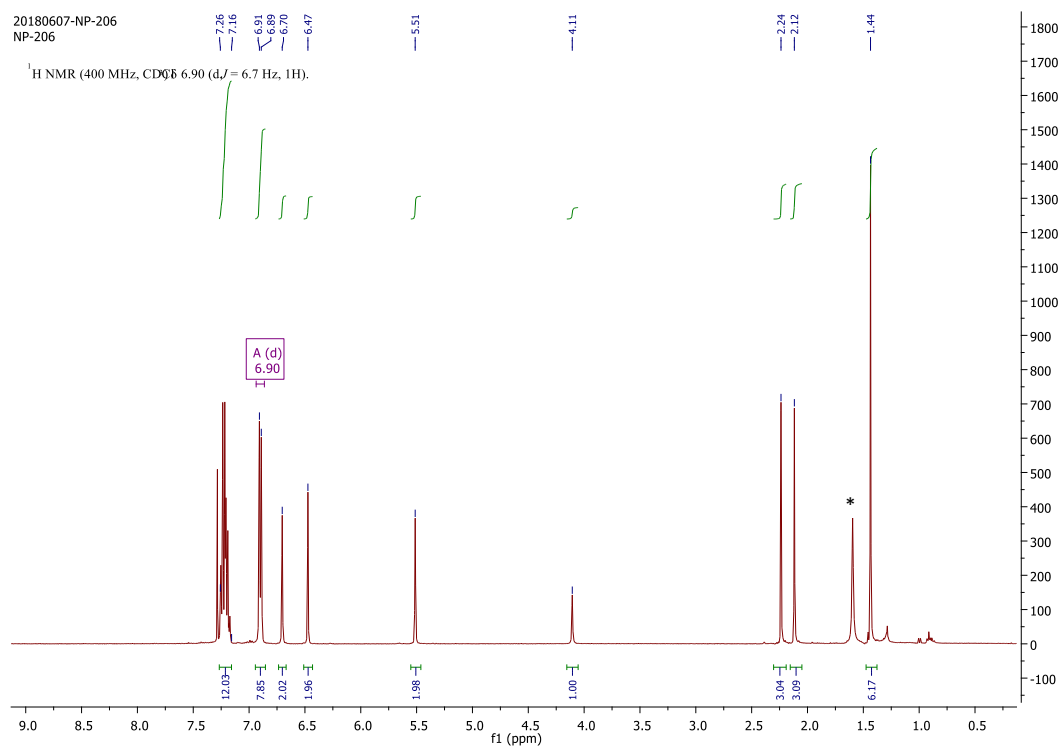
Figure 5.A.5. *^{1}H NMR of **5.1c** (*=H$_2$O)*
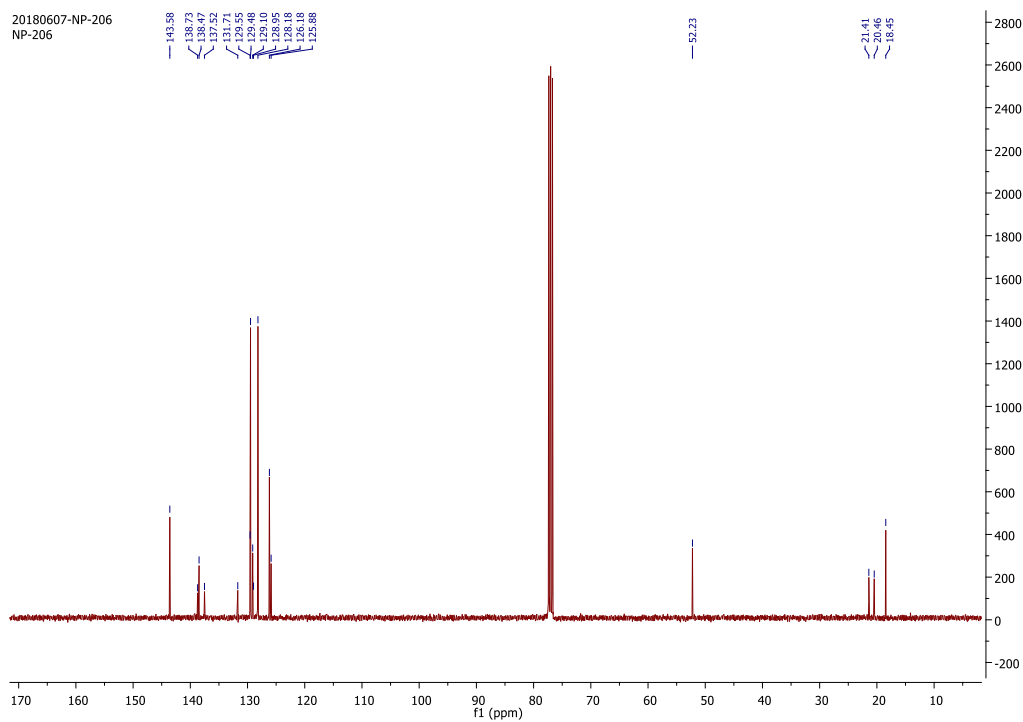
Figure 5.A.6. *^{13}C NMR of **5.1c***
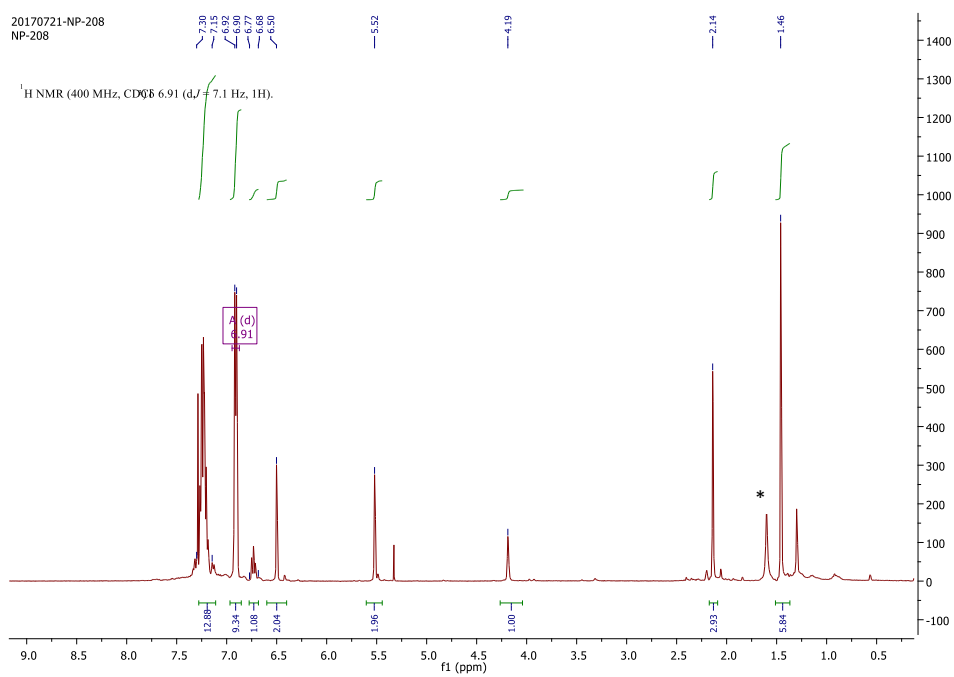
Figure 5.A.7. *¹H NMR of* **5.1d** *(*= H₂O)*
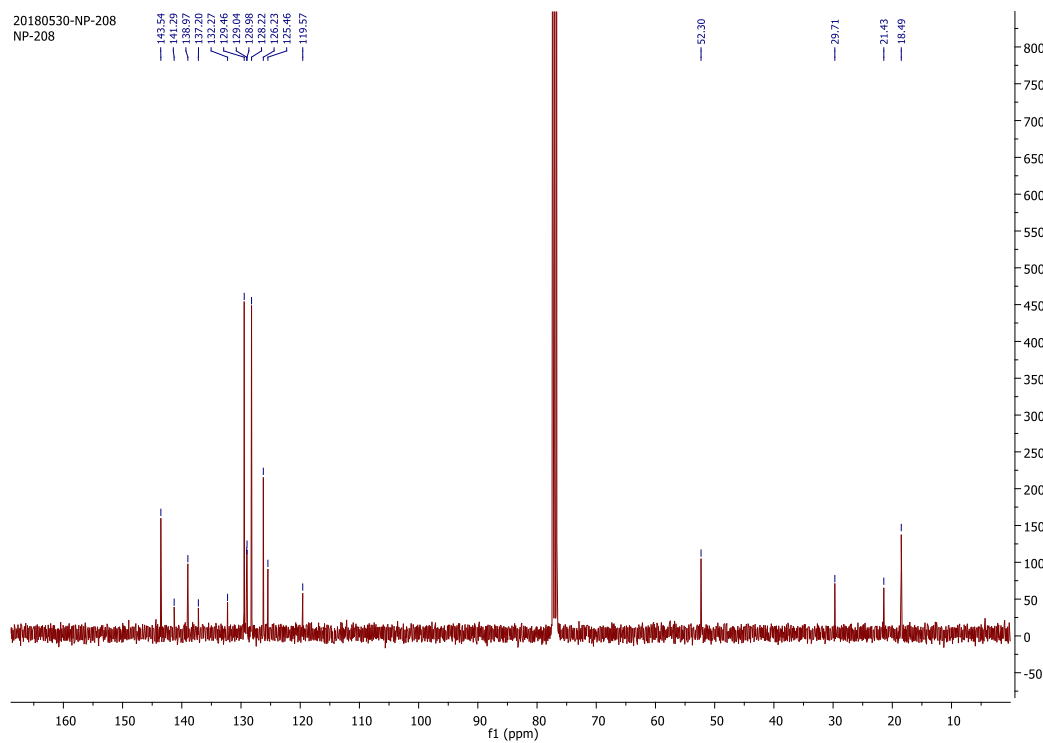
Figure 5.A.8. *¹³C NMR of* **5.1d**
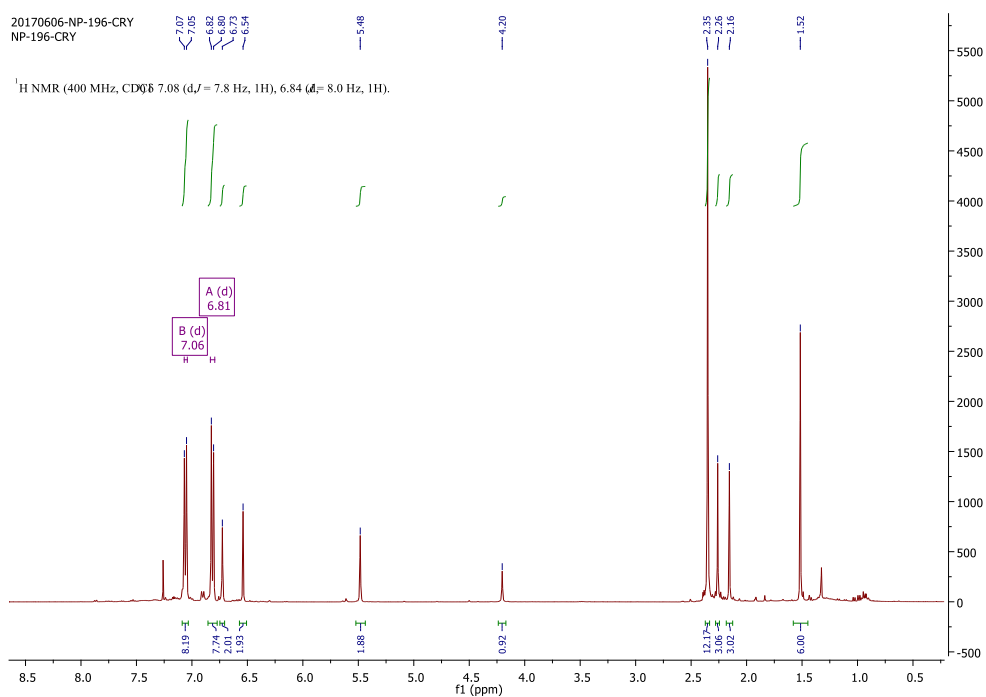
Figure 5.A.9. *¹H NMR of **5.1e***
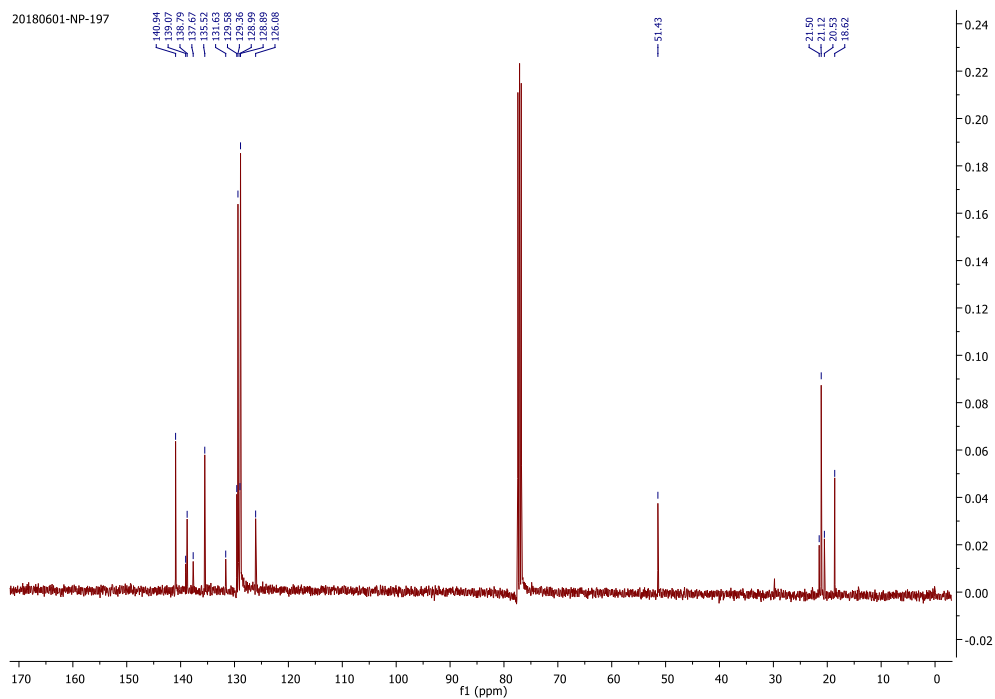
Figure 5.A.10. *¹³C NMR of **5.1e***
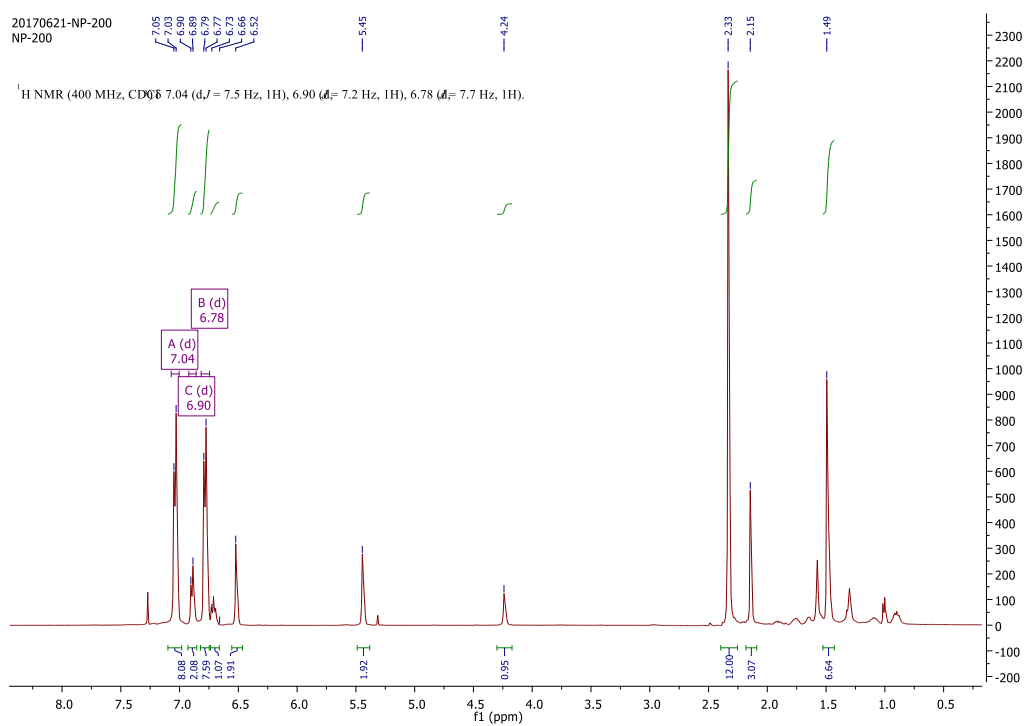
Figure 5.A.11. *¹H NMR of* **5.1f**
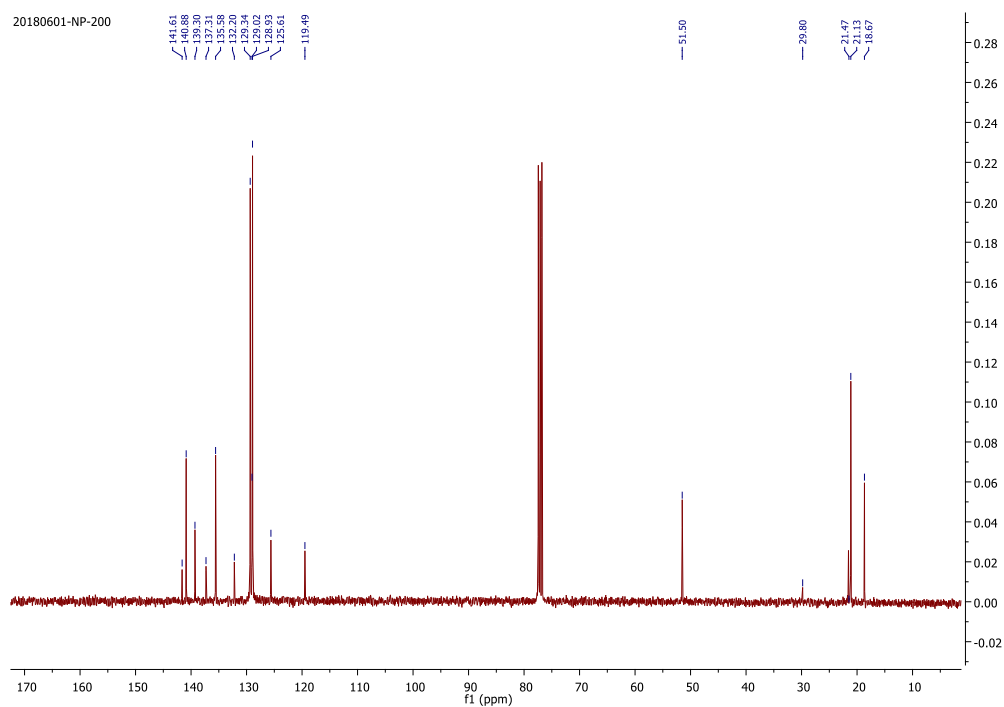
Figure 5.A.12. *¹³C NMR of* **5.1f**

20171024-NP-234

H NMR (400 MHz, CHLOROFORM-D) 7.20 (dd, *J* = 8.3, 1.9 Hz, 1H), 6.79 (dd, *J* = 8.3, 1.9 Hz, 1H).

Figure 5.A.13. *¹H NMR of* **5.1g**

20171024-NP-234

Figure 5.A.14. *¹³C NMR of* **5.1g**

7.24
7.22
7.03
6.97
6.93
6.91
6.82
6.76
6.72
6.62
6.55
5.59
4.94
2.24
1.58
1.30

20180605-NP-238
NP-238

¹H NMR (400 MHz, CDCl₃) δ 7.23 (d, J = 7.9 Hz, 1H), 6.92 (d, J = 7.7 Hz, 1H).

B (d)
7.23

A (d)
6.92

8.23
1.37
8.30
2.13
1.13
1.14
2.10
1.00
3.39
6.41
36.42

Figure 5.A.15. *¹H NMR of **5.1h***

20180605-NP-238
NP-238

148.70
144.41
140.37
136.31
134.02
129.57
128.89
124.99
50.68
34.33
31.38
21.70

Figure 5.A.16. *¹³C NMR of **5.1h***
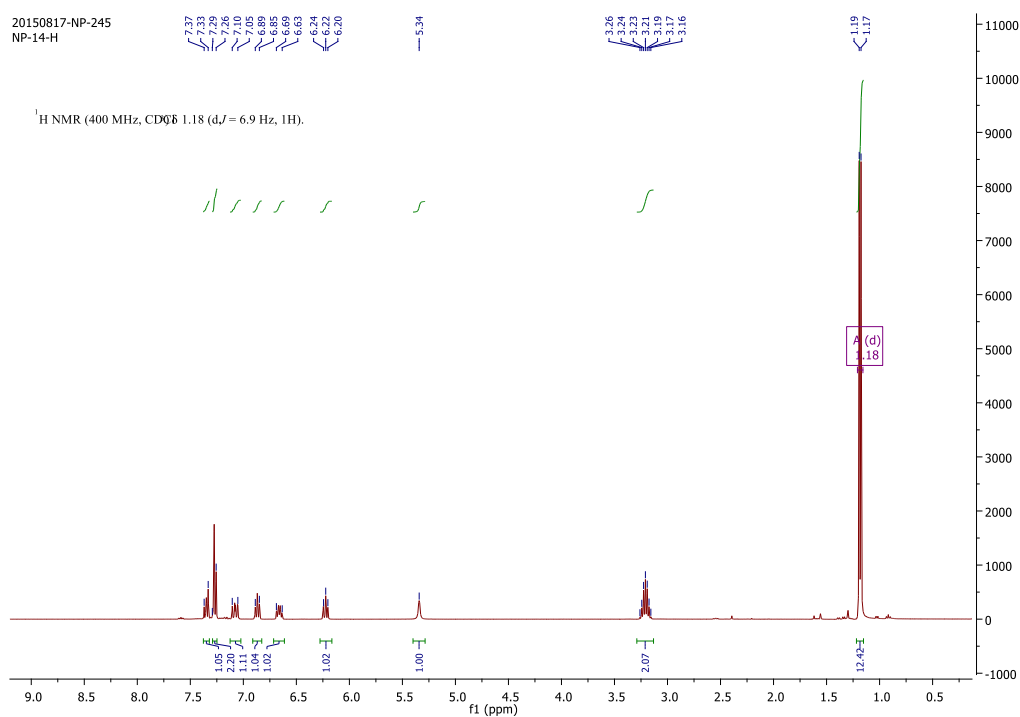
Figure 5.A.17. *¹H NMR of* **5.1i**
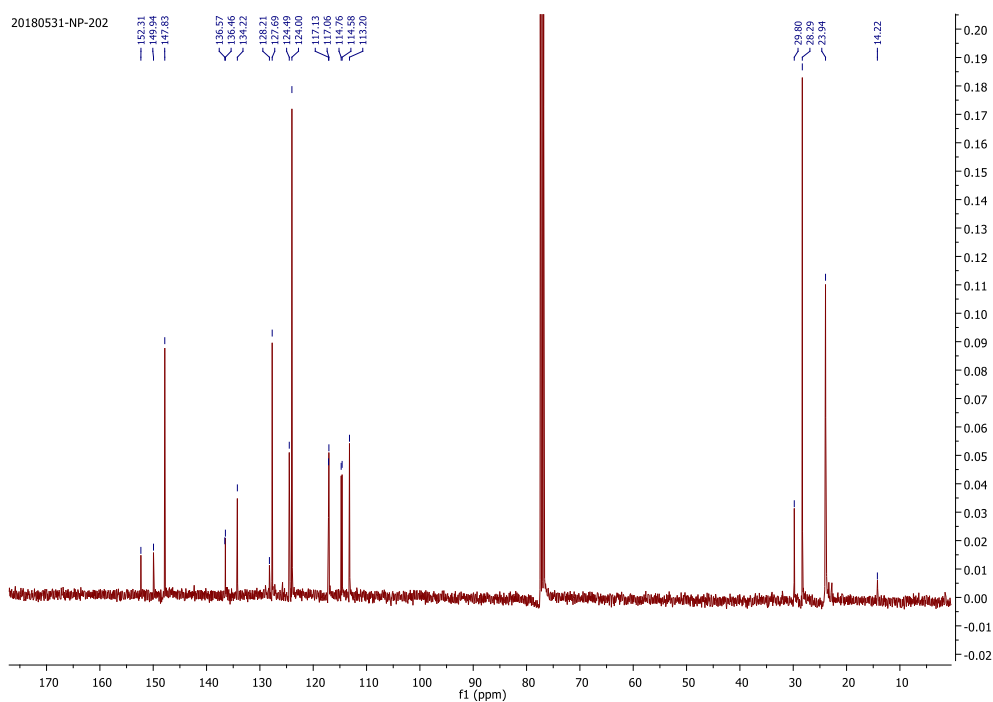
Figure 5.A.18. *¹³C NMR of* **5.1i**
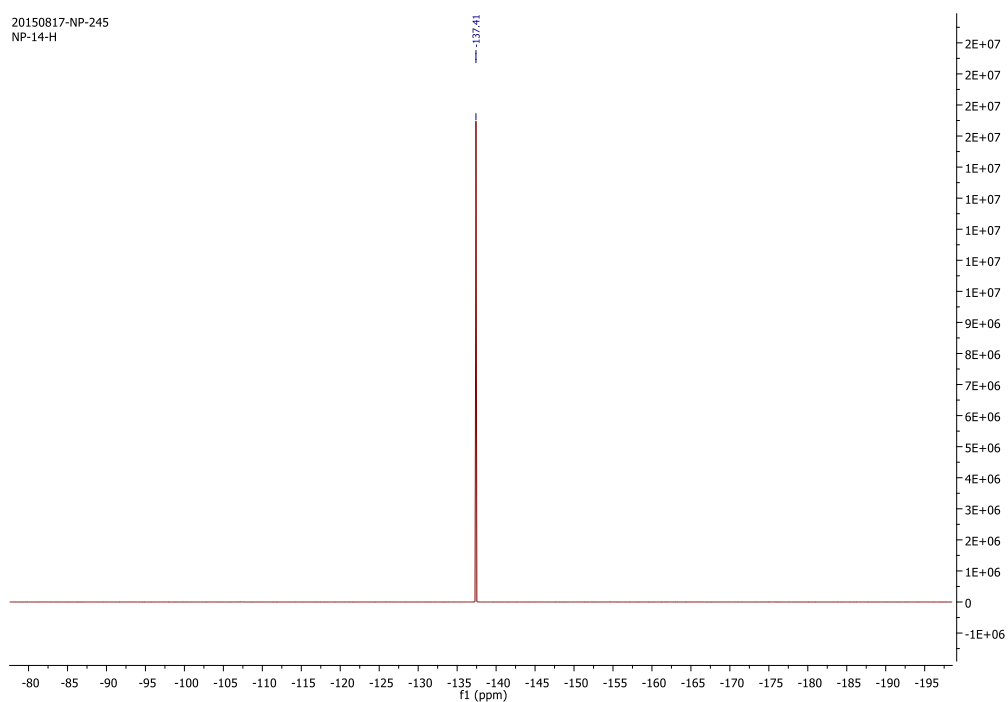
Figure 5.A.19. *^{19}F NMR of* **5.1i**
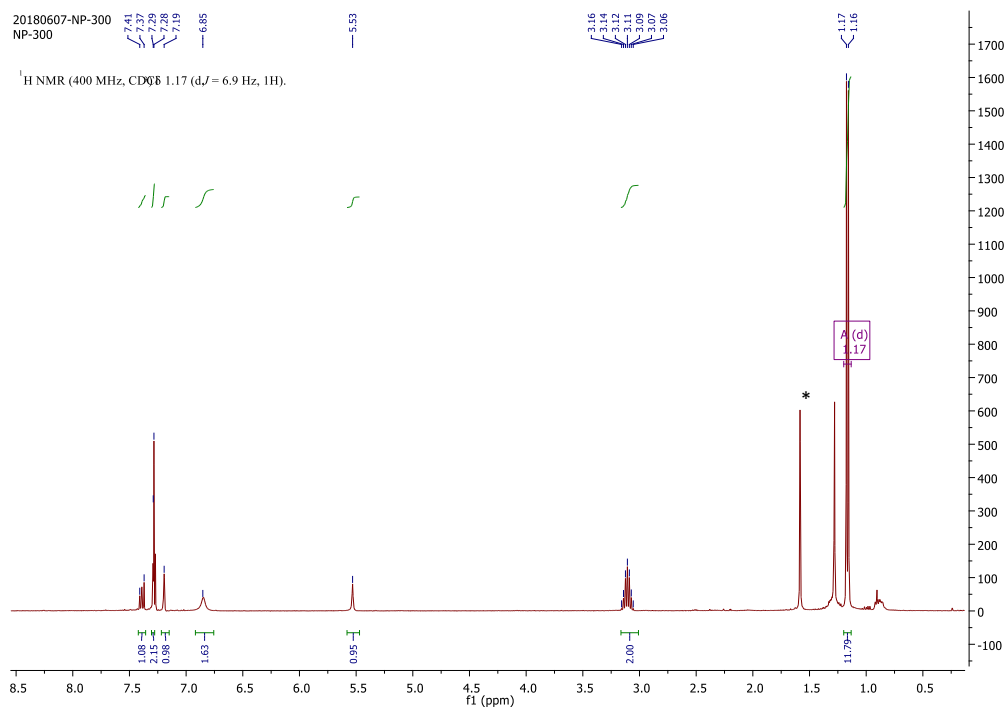
Figure 5.A.20. *^1H NMR of* **5.1j** *(*= H$_2$O)*
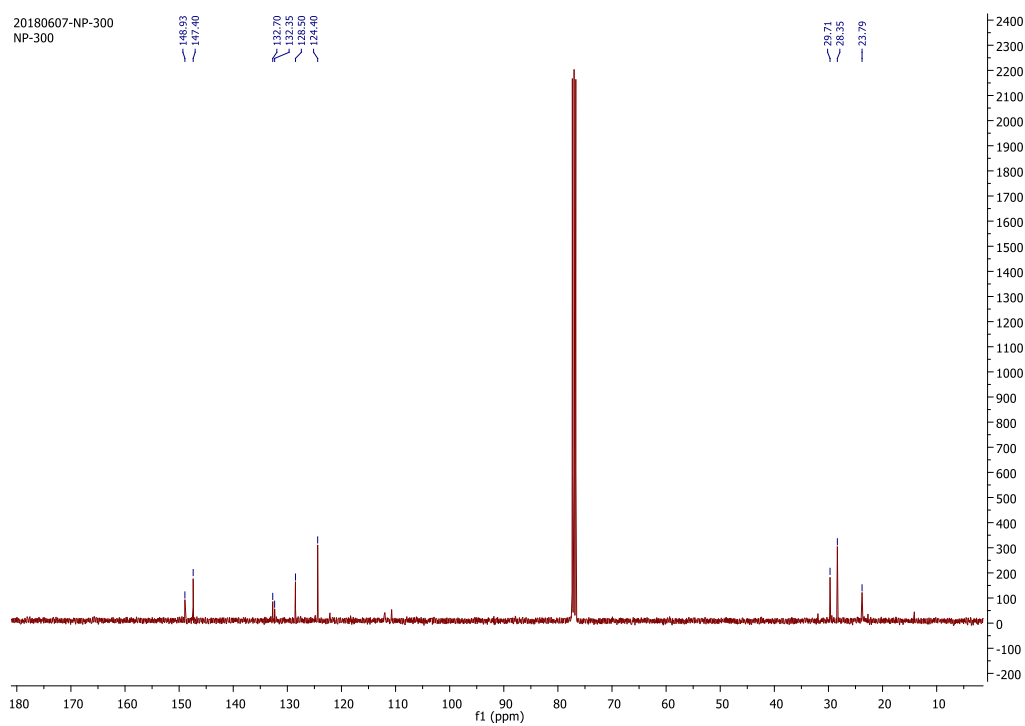
Figure 5.A.21. *13C NMR of* **5.1j**
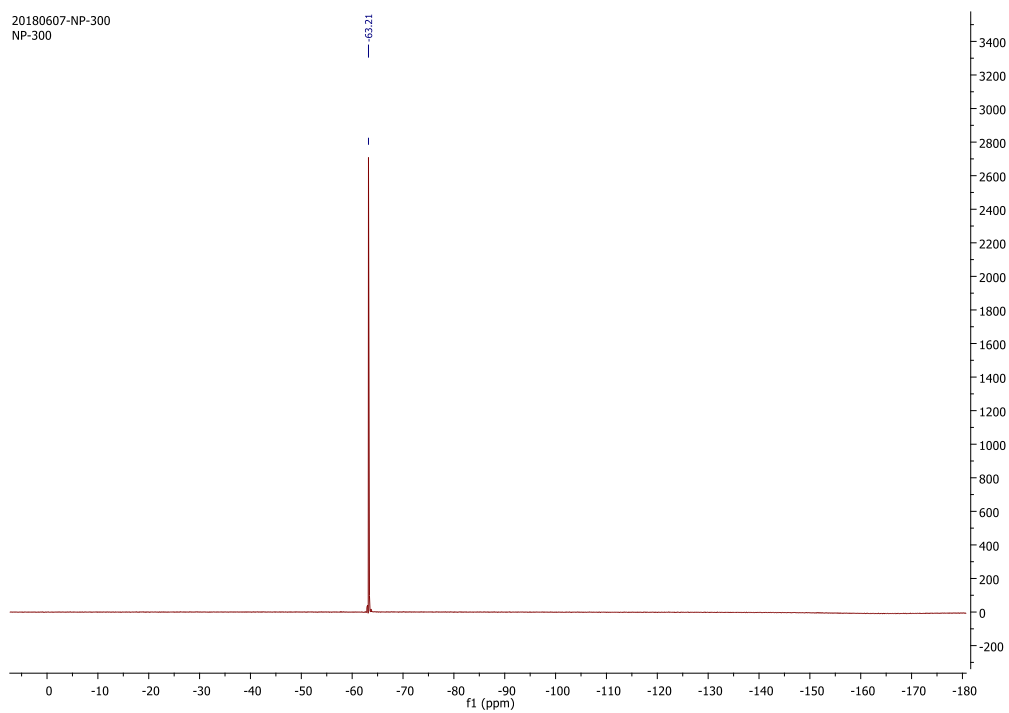
Figure 5.A.22. *19F NMR of* **5.1j**
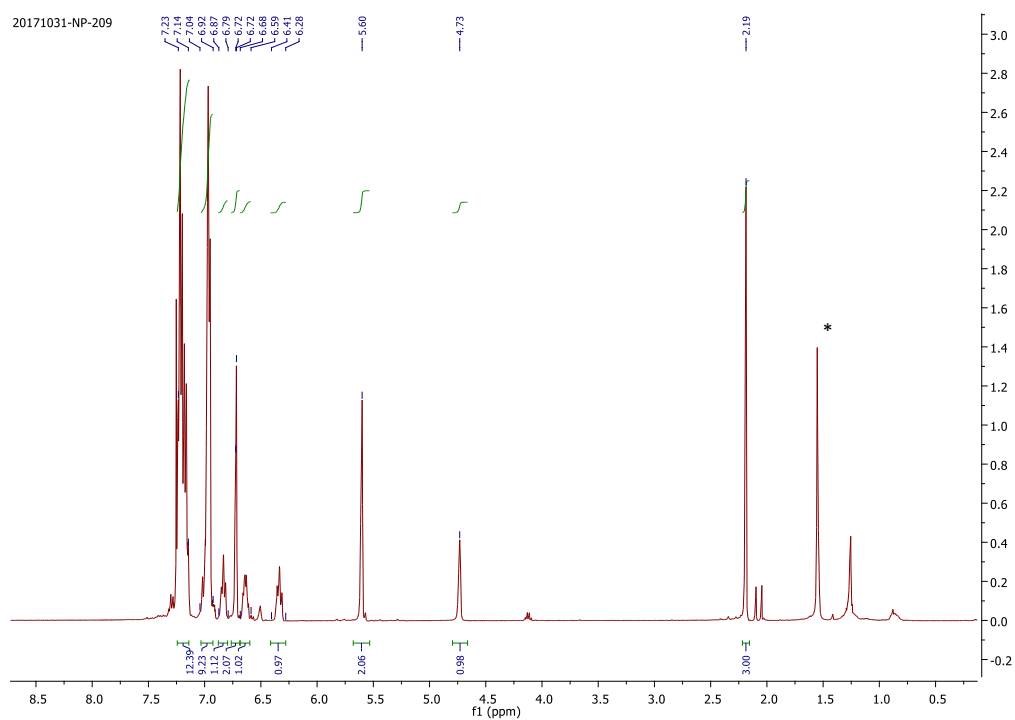
Figure 5.A.23. *^1H NMR of **5.1k** (*= H_2O)*
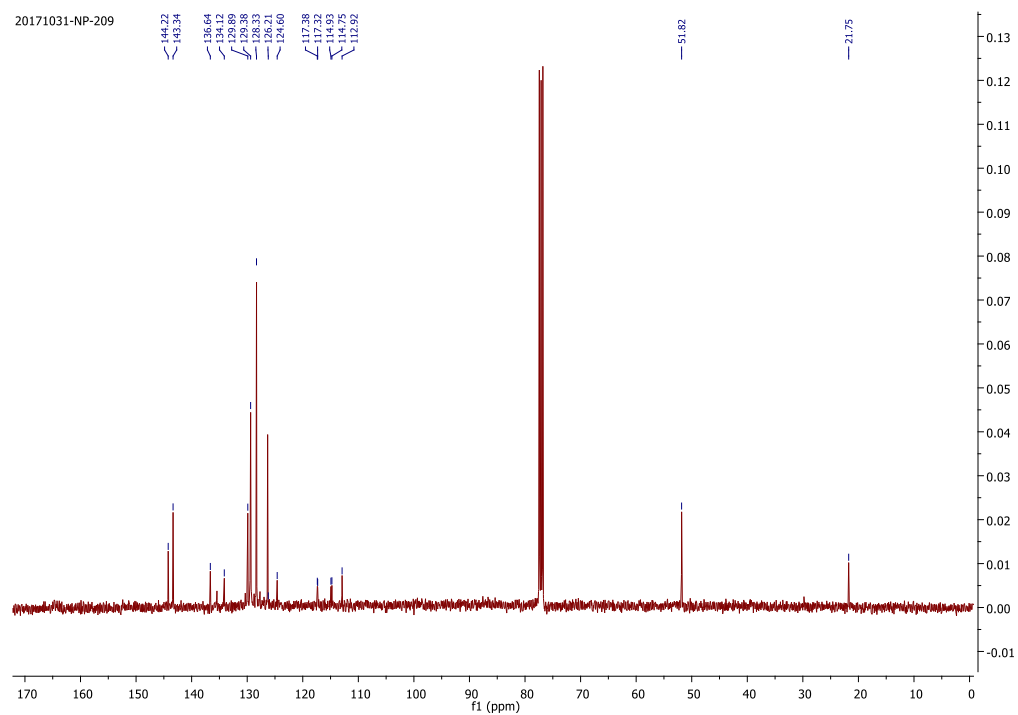
Figure 5.A.24. *^{13}C NMR of **5.1k***
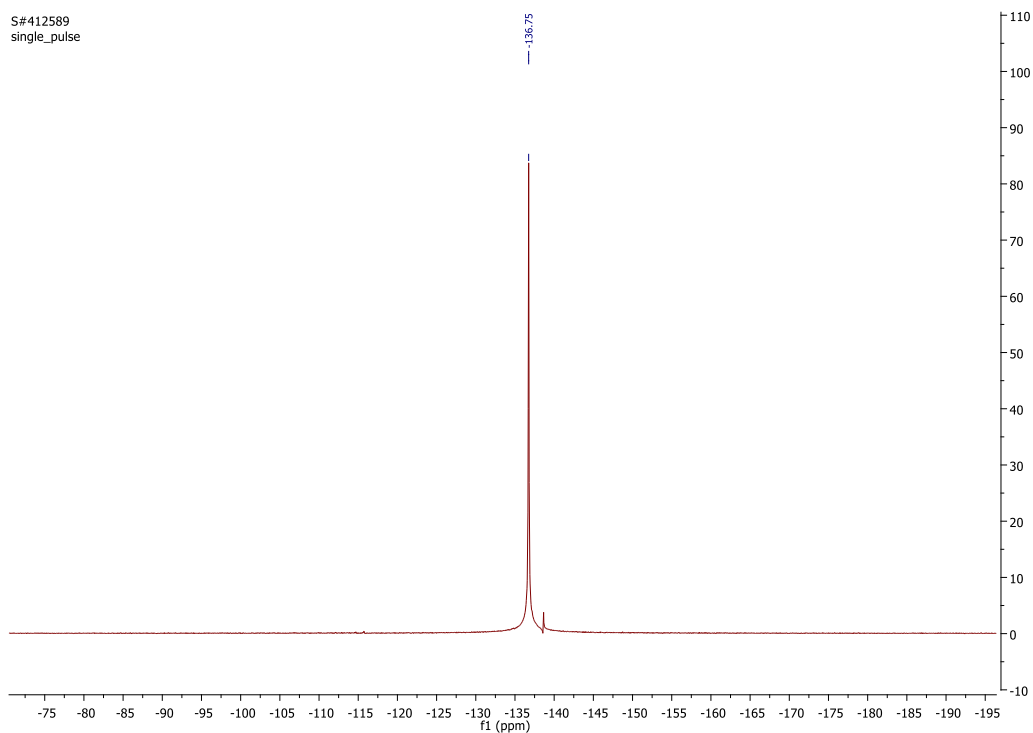
Figure 5.A.25. ^{19}F NMR of 5.1k
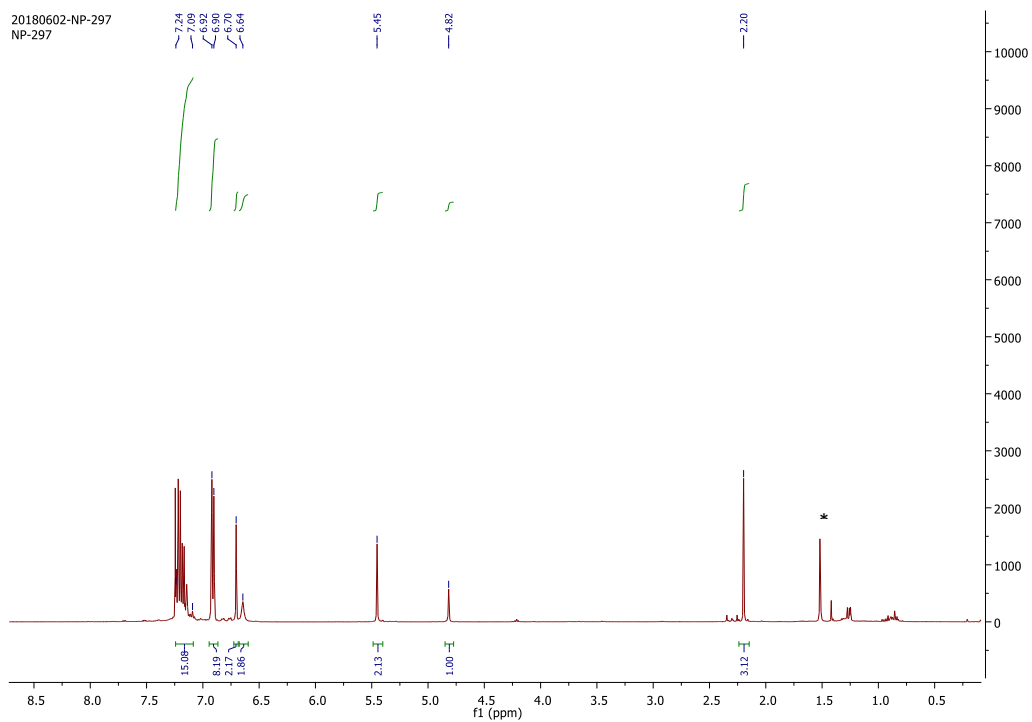
Figure 5.A.26. ^1H NMR of 5.1l (*= H_2O)
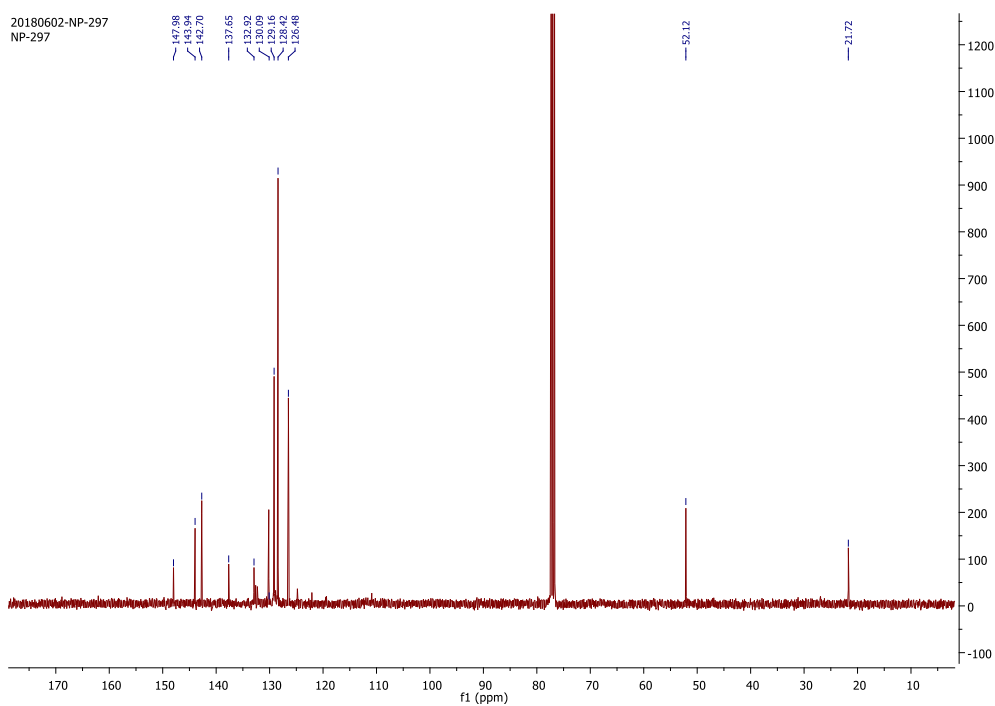
Figure 5.A.27. *^{13}C NMR of* **5.1l**
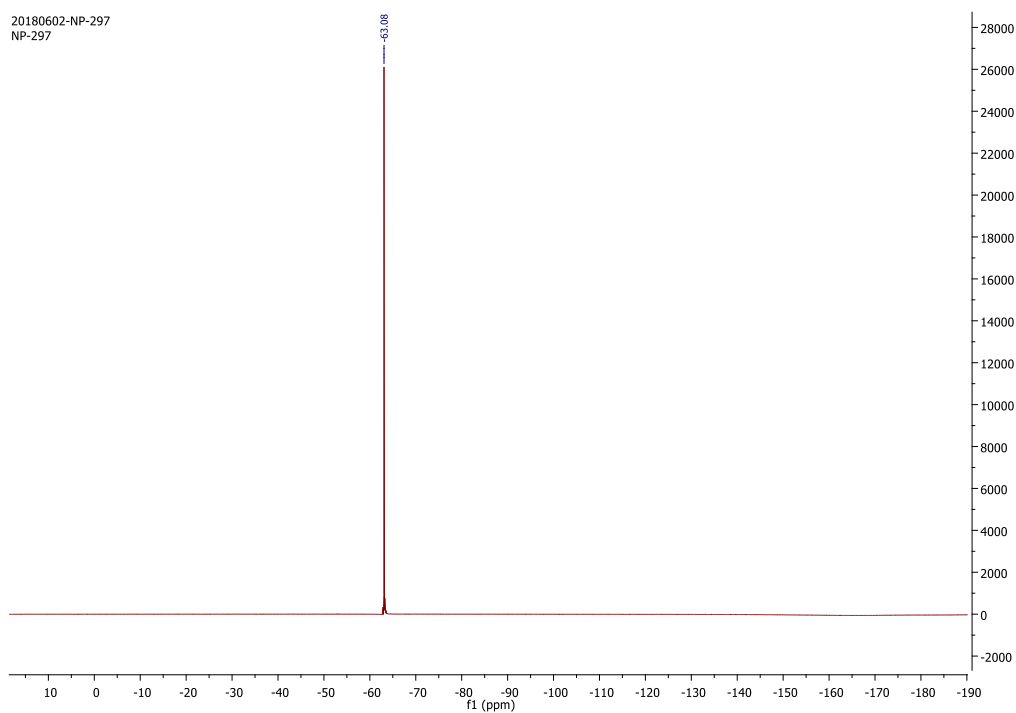
Figure 5.A.28. *^{19}F NMR of* **5.1l**
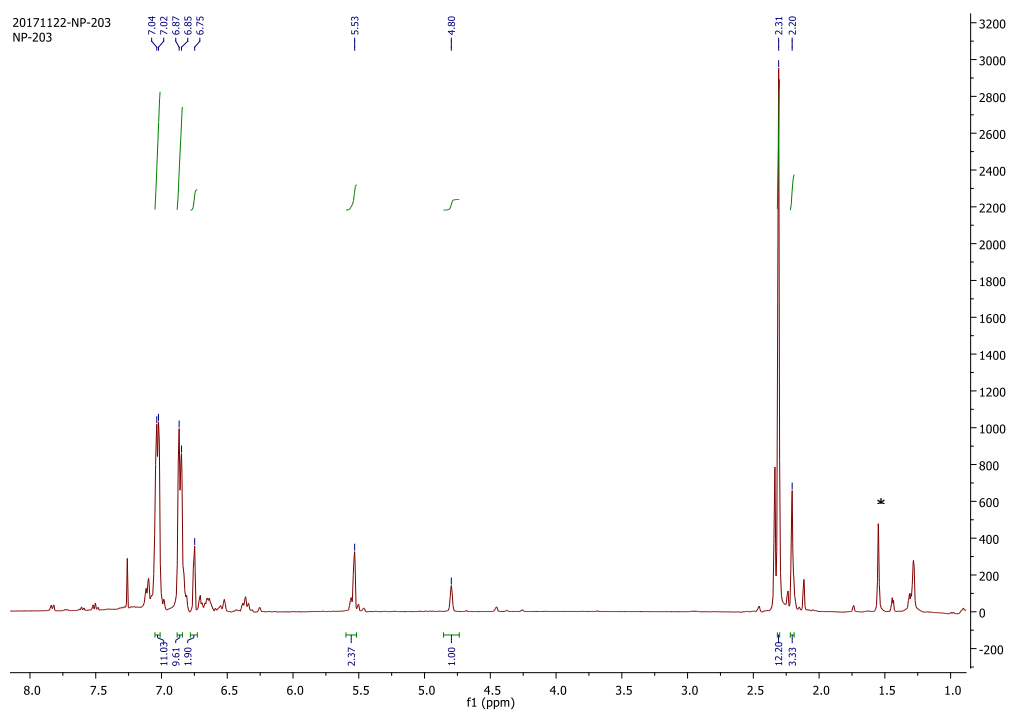
Figure 5.A.29. *¹H NMR of **5.1m** (*= H₂O)*
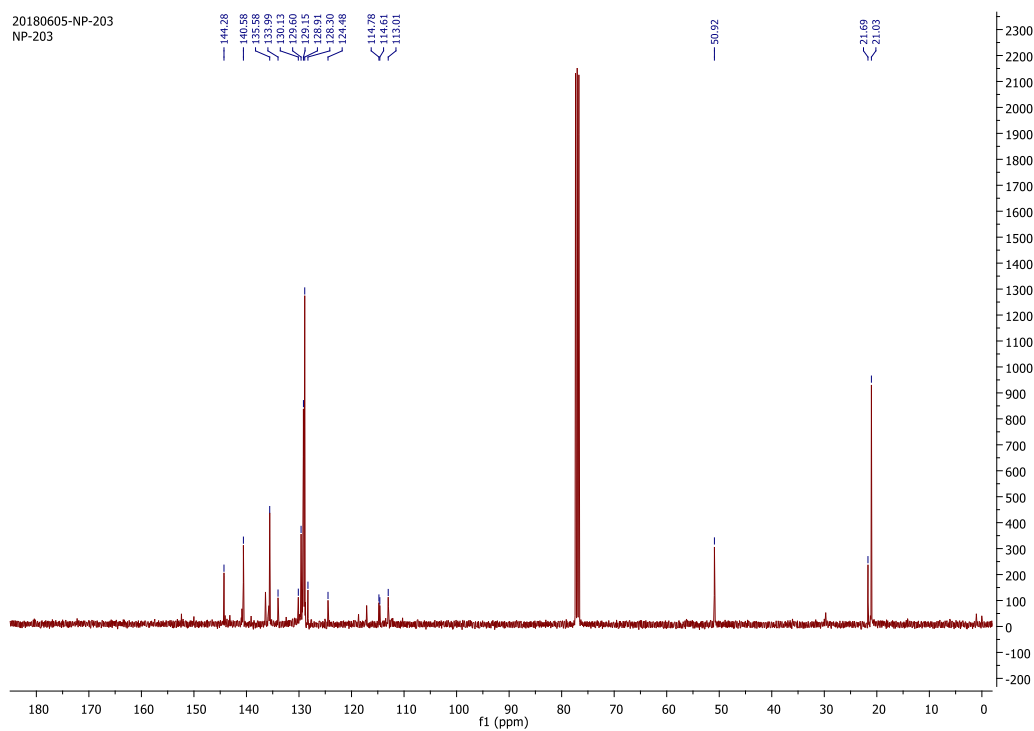
Figure 5.A.30. *¹³C NMR of **5.1m***

20180605-NP-238
NP-238

−136.78
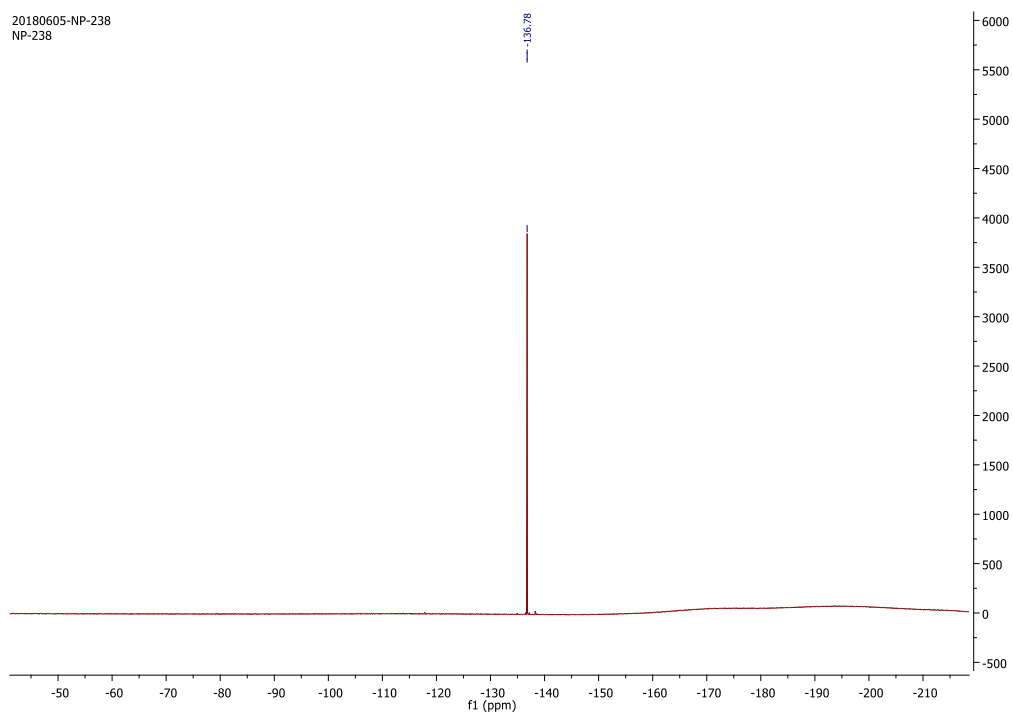
Figure 5.A.31. ¹⁹F NMR of 5.1m

20180528-NP-294
NP-294

7.15
7.05
7.03
6.83
6.81
6.75
6.66

5.40

4.90

2.32
2.24

¹H NMR (400 MHz, CDCl₃) δ 7.04 (d, J = 7.9 Hz, 1H), 6.82 (d, J = 8.0 Hz, 1H).

B (d)
7.04

A (d)
6.82

1.09
8.09
7.76
1.92
1.76

2.00

1.00

12.03
3.08

f1 (ppm)
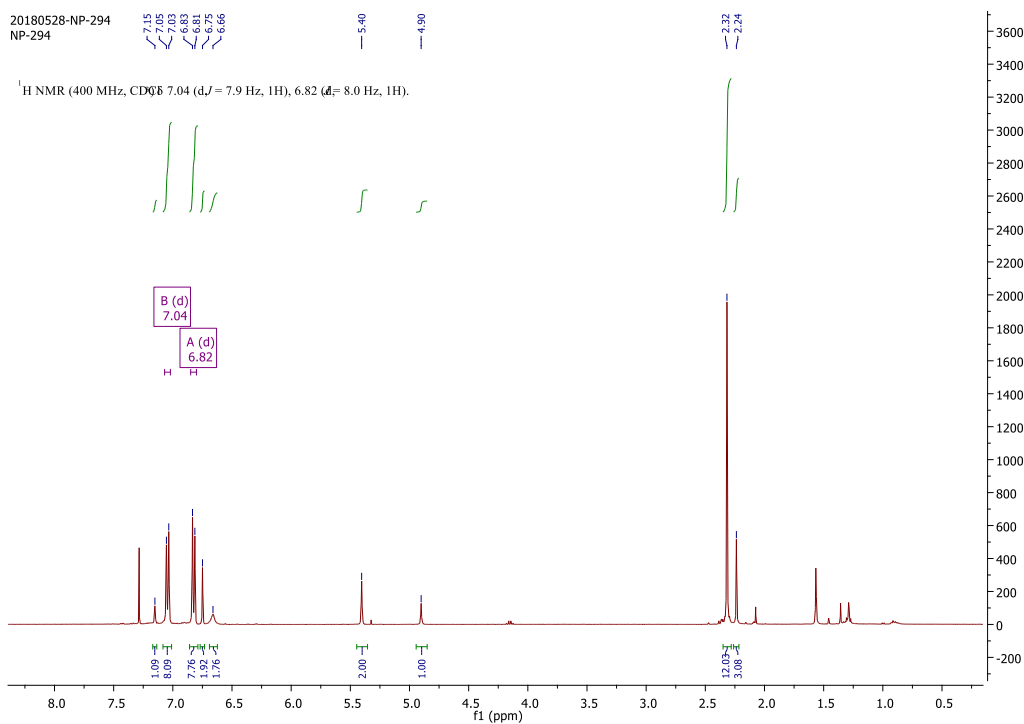
Figure 5.A.32. ¹H NMR of 5.1n

Nasrina Parvin

275
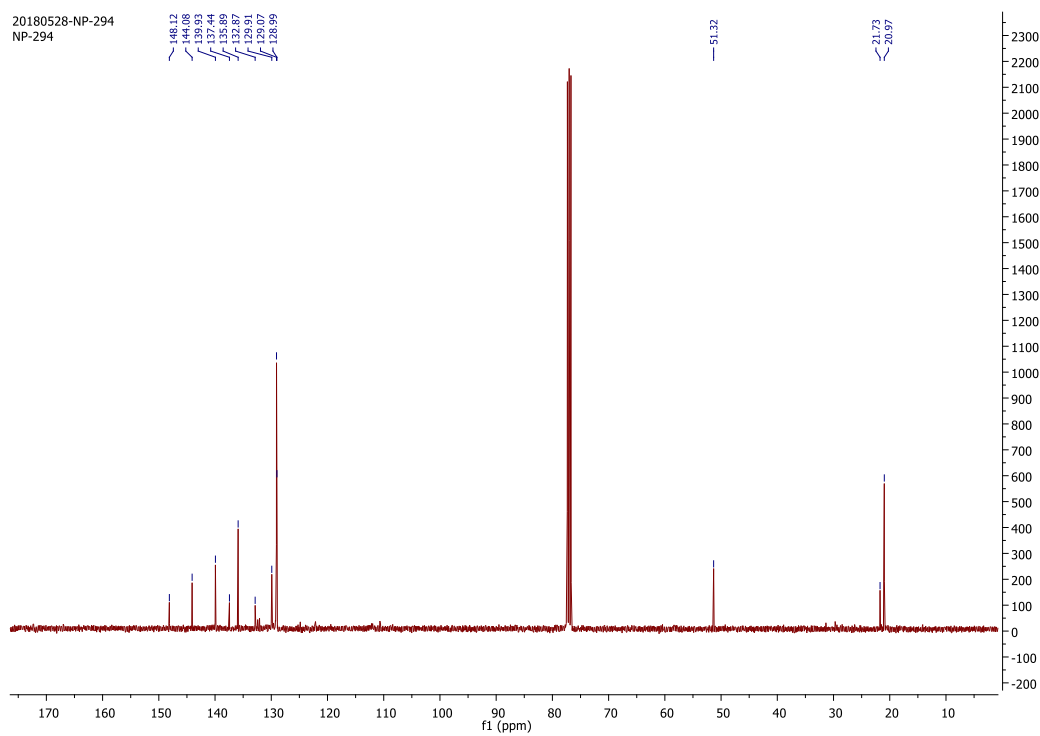
Figure 5.A.33. *¹³C NMR of* **5.1n**
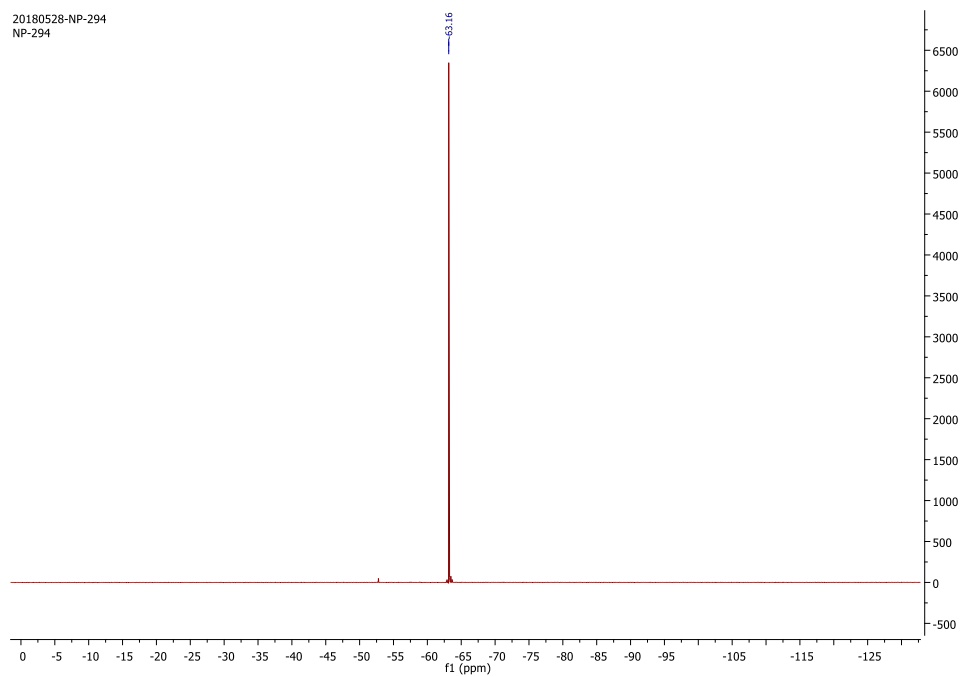
Figure 5.A.34. *¹⁹F NMR of* **5.1n**

20171106-NP-234B

^{1}H NMR (400 MHz, CHLOROFORM-D) 7.20 (d, J = 7.4 Hz, 1H), 6.89 (d, J = 7.4 Hz, 1H).

B (d)
7.20

A (d)
6.89
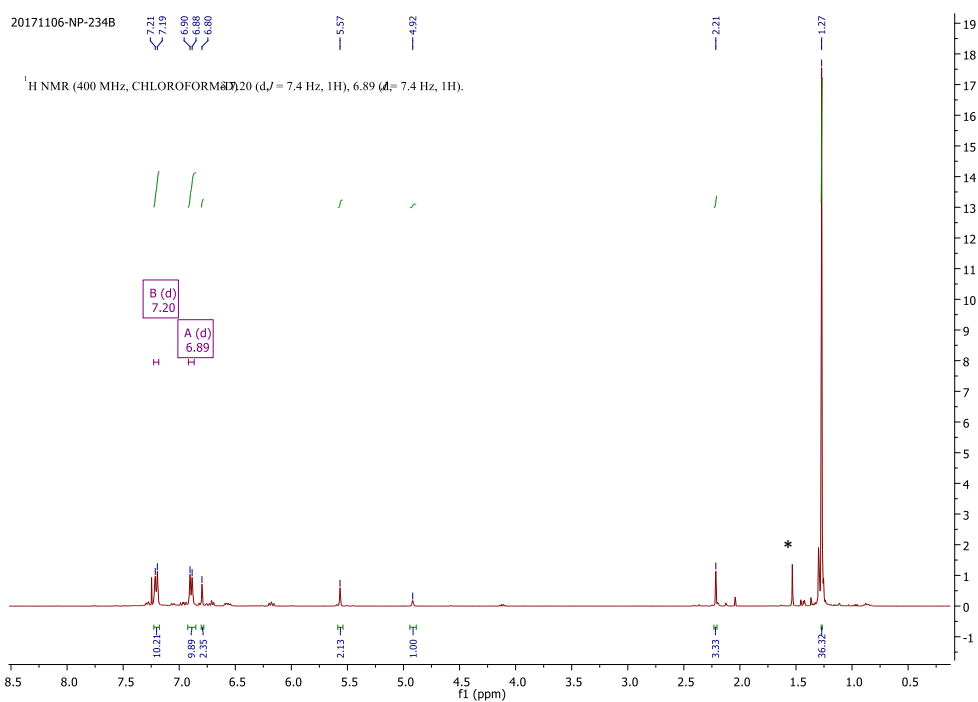
Figure 5.A.35. ^{1}H NMR of **5.1o** (*= H$_2$O peak)

20171106-NP-234B
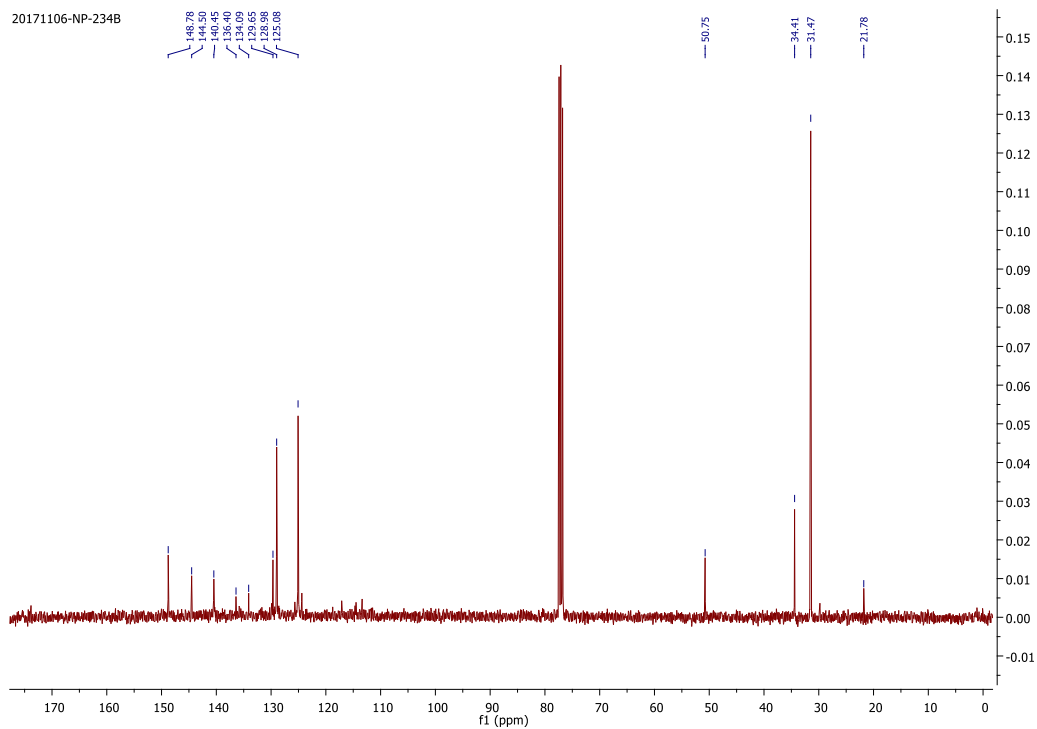
Figure 5.A.36. ^{13}C NMR of **5.1o**

S#341426
single_pulse

−137.14
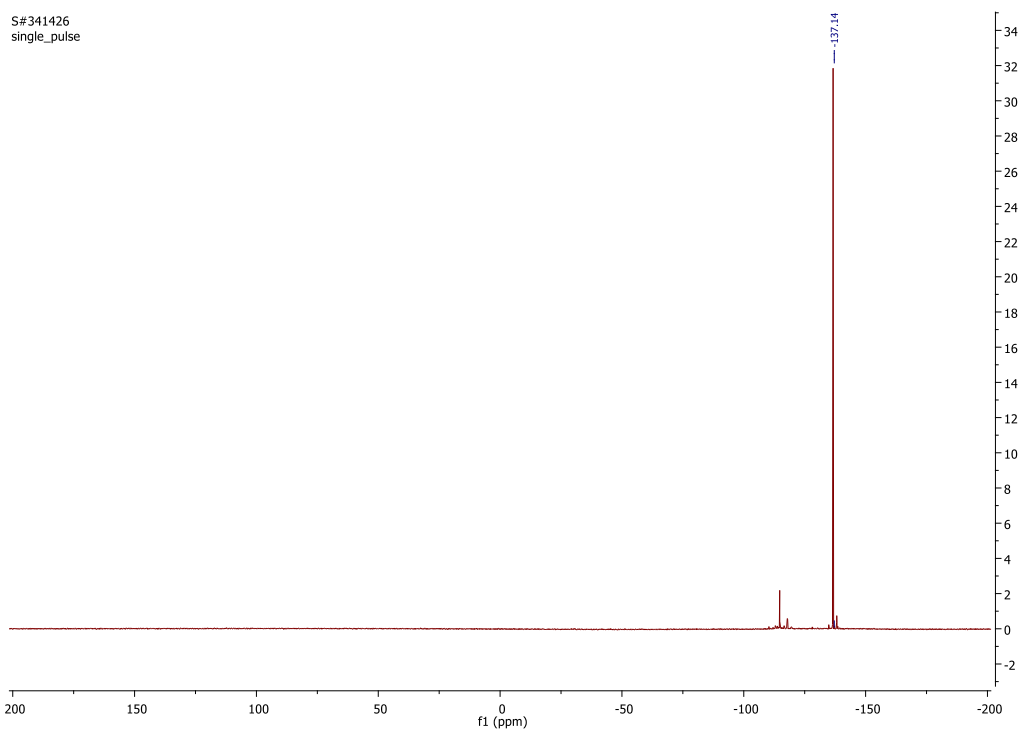
Figure 5.A.37. *¹⁹F NMR of **5.1o***

20180518-NP-289

7.23
7.21
7.11
6.85
6.83
6.78
6.70

5.42

5.00

2.23

1.27

¹H NMR (400 MHz, CHLOROFORM-D) 7.22 (d, J = 8.2 Hz, 1H), 6.84 (d, J = 8.3 Hz, 1H).

B (d)	A (d)
7.22	6.84
H	H

8.08
1.03
8.34
2.10
1.81
2.08
1.00
3.09
36.50
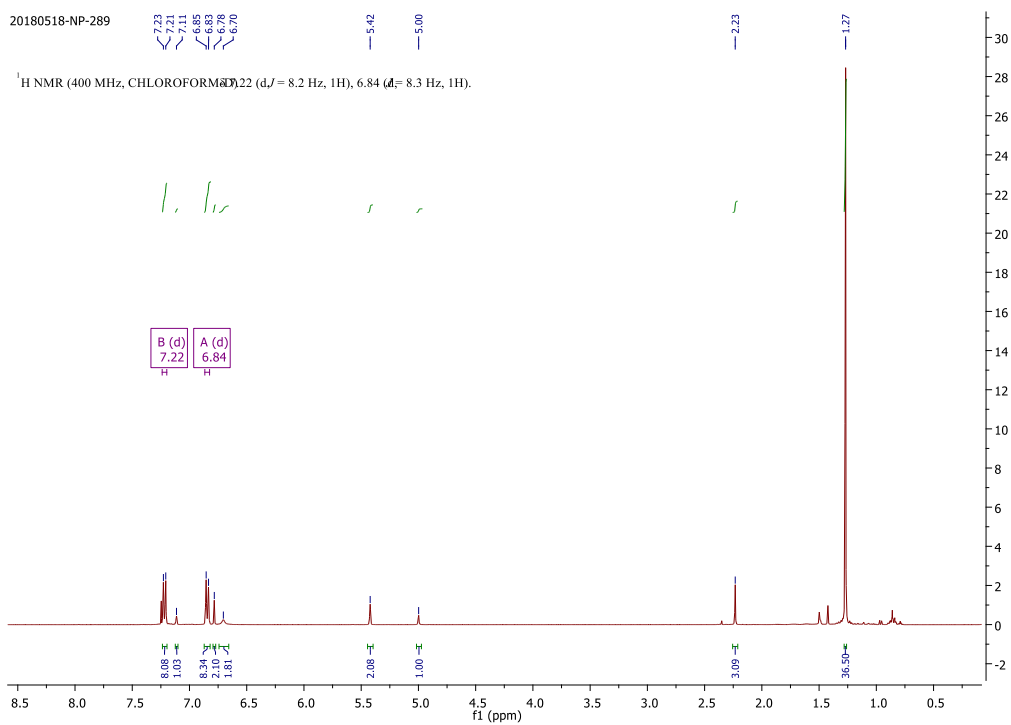
Figure 5.A.38. *¹H NMR of **5.1p***
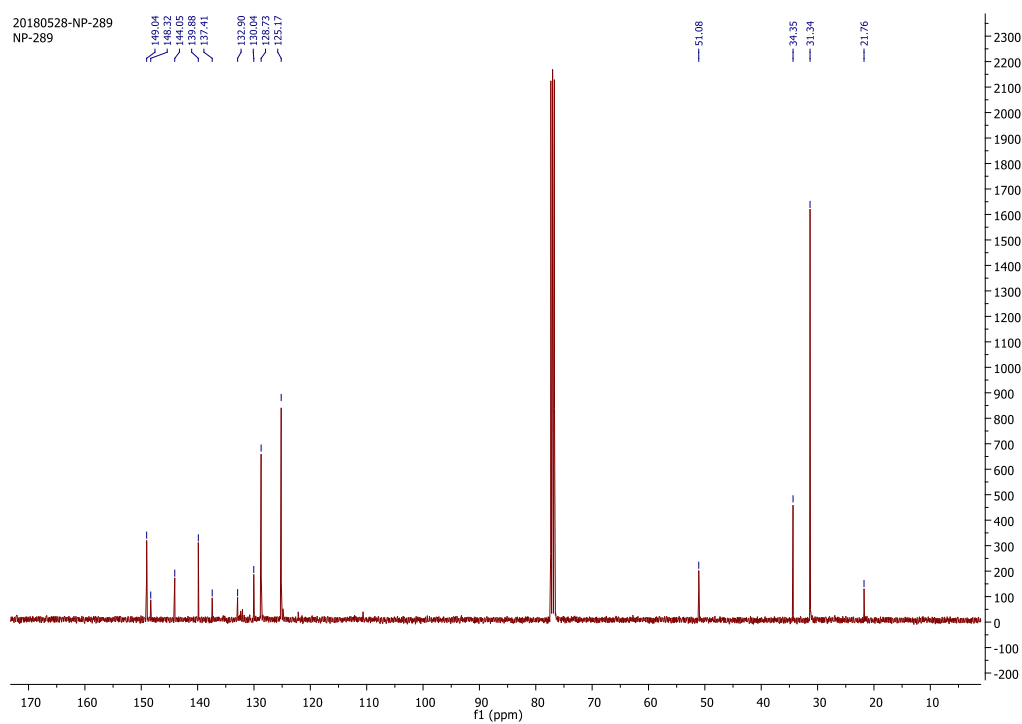
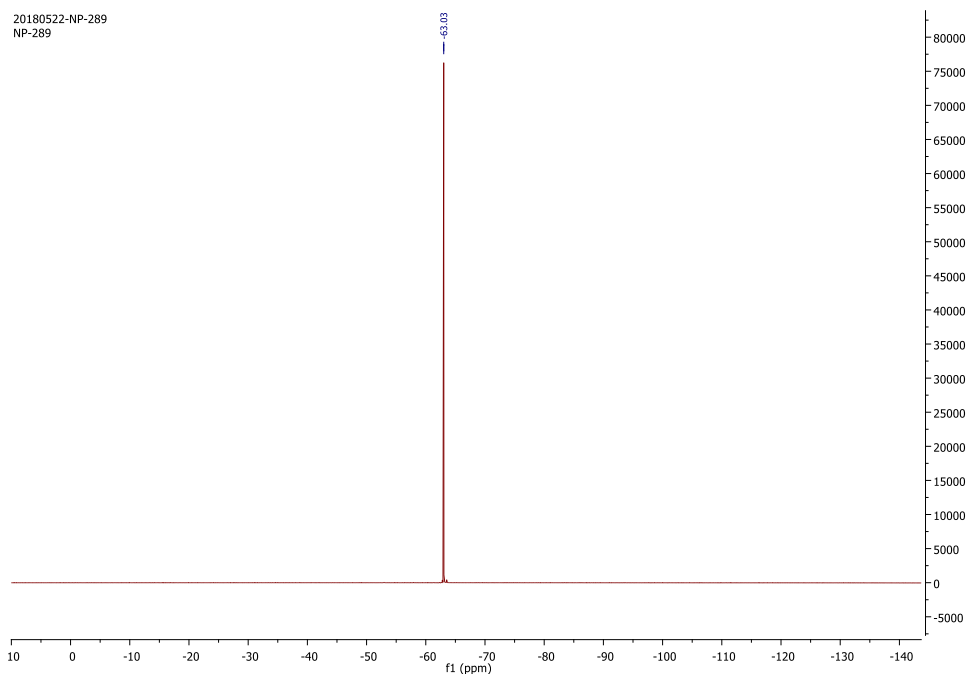***Figure 5.A.39.*** *¹³C NMR of* **5.1p**

Figure 5.A.40. *¹⁹F NMR of* **5.1p**

*****

Rights and Permissions

1. **Chapter 2:**

Reprint of **Parvin, N.**; Pal, S.; Khan, S.;* Das, S.; Pati, S. K.;* Roesky, H. W.* Unique Approach to Copper(I) Silylene Chalcogenone Complexes, *Inorganic Chemistry* **2017** , *56*, 1706–1712.

Copyright 2017: American Chemical Society
The dissertation author is the main author for this article.

Reprint of **Parvin, N.**; Dasgupta, R.; Pal, S.; Sen, S. S.;* Khan, S.* Strikingly Diverse Reactivity of Structurally Identical Silylene and Stannylene, *Dalton Transaction* **2017**, *46*, 6528-6532.
Copyright 2017: Royal Society of Chemistry
The dissertation author is the main author for this article.

2. **Chapter 3:**

Reprint of **Parvin, N.**; Pal, S.; Echeverría, J.; Alvarez, S.;* Khan, S.* Taming Monomeric [Cu(η^6-C$_6$H$_6$)]$^+$ Complex with Silylene, *Chemical Science* **2018**, *9,* 4333-4337.
Copyright 2018: Royal Society of Chemistry
The dissertation author is the main author for this article.

Parvin, N.; Hossain, J.; George, A., Parameswaran, P.;* Khan, S.* N-heterocyclic Silylene Stabilized Monocordinated Copper(I)–Arene Cationic Complexes and Their Application in Click Chemistry, *Chem. Comm.* **2020,** *56*, 273-276.
Copyright 2020: Royal Society of Chemistry
The dissertation author is the main author for this article.

3. **Chapter 4:**

Parvin, N.; Mishra, B.; George, A.; Neralkar, M.; Hossain, J;. Parameswaran, P.;* Hotha, S.;* Khan, S.* N-Heterocyclic Silylene/Germylene Ligands in Au(I) Catalysis, *Chem. Comm.* **2020**, *56*, 7625-7628.
Copyright 2020: Royal Society of Chemistry
The dissertation author is the main author for this article.

Copyright Clearance Center　　**RightsLink®**　　Home　?　Help　　✉ Email Support　　👤 Sign in　　👤 Create Account

ACS Publications
Most Trusted. Most Cited. Most Read.

Unique Approach to Copper(I) Silylene Chalcogenone Complexes

Author: Nasrina Parvin, Shiv Pal, Shabana Khan, et al

Publication: Inorganic Chemistry

Publisher: American Chemical Society

Date: Feb 1, 2017

Copyright © 2017, American Chemical Society

PERMISSION/LICENSE IS GRANTED FOR YOUR ORDER AT NO CHARGE

This type of permission/license, instead of the standard Terms & Conditions, is sent to you because no fee is being charged for your order. Please note the following:

- Permission is granted for your request in both print and electronic formats, and translations.
- If figures and/or tables were requested, they may be adapted or used in part.
- Please print this page for your records and send a copy of it to your publisher/graduate school.
- Appropriate credit for the requested material should be given as follows: "Reprinted (adapted) with permission from (COMPLETE REFERENCE CITATION). Copyright (YEAR) American Chemical Society." Insert appropriate information in place of the capitalized words.
- One-time permission is granted only for the use specified in your request. No additional uses are granted (such as derivative works or other editions). For any other uses, please submit a new request.

BACK　　　　　　　　　　　　　　　　　　　　　　　　　　CLOSE WINDOW